SYNTHESIS AND MODELLING OF HIGH Tg COPOLYMERS THROUGH SUSPENSION COPOLYMERIZATION WITH BIFUNCTIONAL INITIATORS

By

MARCO AURELIO VILLALOBOS

A Thesis

Submitted to the School of Graduate Studies

in Partial Fulfilment of the Requirements

for the Degree

Doctor of Philosophy

McMaster University

December 1992

SYNTHESIS AND MODELLING OF HIGH Tg COPOLYMERS THROUGH SUSPENSION COPOLYMERIZATION WITH BIFUNCTIONAL INITIATORS

DOCTOR OF PHILOSOPHY (1993)
(Chemical Engineering)

McMASTER UNIVERSITY
Hamilton, Ontario

TITLE: Synthesis and Modelling of High Tg Copolymers Through Suspension Copolymerization with Bifunctional Initiators

AUTHOR: Marco Aurelio Villalobos, M. of Eng. (McMaster University)
B. of Sc. (Universidad Nacional Autónoma de México)

SUPERVISORS: Dr. Archie E. Hamielec, and Dr. Philip E. Wood

NUMBER OF PAGES: xviii, 394

ABSTRACT

In this thesis, the copolymerization theory has been extended to account for the unique phenomenon of multiple initiation/propagation/termination cycles, experienced by copolymer chains in free radical copolymerization with bifunctional initiators. A comprehensive model for the most general free radical copolymerization scheme, involving simultaneous and competitive statistical and donor-acceptor propagation mechanisms, has been developed. The effects of multiple chain recombination during bifunctionally initiated batch free radical copolymerization, on copolymer microstructure and compositional drift, have been evaluated. As a result, the concepts of effective instantaneous copolymer composition, and number of segments per copolymer chain have been introduced as an addition to the copolymerization theory.

The ability to control the segment composition of the multi-segment copolymers formed during bifunctionally initiated free radical copolymerization, has been the basis for the design and synthesis of four different high T_g engineering copolymers. Styrene/α-methylstyrene (T_g~115°C), styrene/N-phenylmaleimide (T_g~215°C), and α-methylstyrene/N-phenylmaleimide copolymers (T_g~260°C), as well as styrene/α-methylstyrene/n-phenylmaleimide terpolymers (T_g~220°C), have been synthesized in bulk and suspension, and fully characterized. The performance of these four copolymer systems in suspension polymerization with bifunctional initiators has been evaluated at pilot plant scale, to assess the technical feasibility for their commercial production.

In addition, a novel route for the synthesis of suspension expandable polystyrene with bifunctional initiators, in a highly productive simultaneous polymerization/impregnation stage, has been developed and fully tested in pilot plant scale.

From the comprehensive kinetic and micro-structure models proposed in this thesis, two computer simulation programs (BIPEN and BICOP), have been developed. Both programs, predicting the most important phenomena of the polymerization processes studied herein, have been used as a product design tool, throughout this thesis, with very good results.

ACKNOWLEDGMENT

The author wishes to express his gratitude:

To his supervisors, Dr. Archie Hamielec, and Dr. Philip Wood, for their valuable help and guidance during the development of this work, but most of all for the friendship that they have offered me throughout my entire stay at McMaster University.

To the Department of Chemical Engineering at McMaster University, CONACYT (México), and the Research and Development Group of Industrias Resistol, S.A. (México), for the financial support received.

To PRODESA (México), PlastiFab LTD (Calgary), and NESTE OY (Finland), for giving me the opportunity to prove that I have learned something after all these years in school, and for providing me with a nice alternative to avoid TA.

To Shiping, Hidetaka, Paul, Tuyu and other polymer people, with whom I have coincided during my years at Mac, for showing me every day, with the most amazing technical discussions, that my decision to come to McMaster University was the best.

To Peter and Ausra, Paul and Julie, and John and Diane, for having taken some time to show me how beautiful Canada is.

Finally, to Lucyanne, Cecilia, Agustin, Daniel and the rest of the Latinamerican gang, for being always there (or somewhere else) when I needed them.

To all of you: Mil Gracias

MARCO

TABLE OF CONTENTS

Table of Contents (Continued)

Table of Contents (Continued) Page

Table of Contents (Continued)

LIST OF FIGURES

List of Figures (Continued)

List of Figures (Continued)

List of Figures (Continued)

List of Figures (Continued)

List of Figures (Continued)

List of Figures (Continued)

List of Figures (Continued)

LIST OF TABLES

CHAPTER 1

INTRODUCTION

In this chapter the general problem motivating this study is introduced. With an understanding of this problem, a potential strategy for its solution emerges, allowing a statement of the general objectives of this thesis. The sequential research approach followed to achieve these objectives, and ultimately to arrive at a solution to the problem, is explained in detail.

1.1 Suspension Polymerization

The term "suspension polymerization" defines a process in which a monomer, or a mixture of monomers, relatively insoluble in water, is dispersed in water by means of agitation into liquid droplets and, upon polymerization, the resultant polymer is obtained as a dispersed solid phase suspended in an aqueous continuous phase. Oil soluble initiators are used and the polymerization proceeds with the same reaction mechanisms as with bulk or solution polymerization [Hamielec et.al. (1967)].

Suspension polymerization has certain advantages, over bulk or solution processes in that polymer synthesis occurs with relatively high heat transfer rates and the slurry formed can be effectively agitated and pumped with conventional equipment [Church (1966)].

The suspension polymerization process has some negatives compared to bulk processes in that the polymer must be separated from the water phase and dried. In addition, the water phase which is contaminated with recipe ingredients must be disposed of, and the agents used to disperse and prevent coalescence of polymer particles are adsorbed to some degree on the polymer surface contaminating the final product.

Most of the complications encountered with suspension polymerization are primarily due to the difficulty in controlling coalescence of the polymer particles, sometimes causing the formation of large, unworkable polymeric masses with consequent inability of the system to transfer adequately the heat of polymerization to a cooling source [Grulke (1985)].

The proper selection and formulation of the stabiliser (suspending agent) is instrumental in the control of particle size. Stabilisers can be either a water-soluble polymer or a finely divided inorganic powder. Water-soluble non-ionic polymers provide steric stabilization to the particles, whereas inorganic powders confer a combination of electrostatic-mechanical stabilization [Roger et.al.(1984), Tanaka (1985)]. The range of particle size of suspension resins varies from 0.1 to 2.5 mm.

Although several inverse suspension polymerization resins of some commercial importance have been developed to date, in this thesis the term suspension polymerization will refer exclusively to processes using water as continuous phase.

1.2 Current State of Suspension Polymerization Processes

In the last decade most manufacturers of suspension polymers and copolymers have had to compete with an increasing number of continuous processes, developed as the most cost effective processes for the production of commodity polymer products previously produced by batch suspension polymerization. For example, the production of crystal polystyrene (PS), high impact polystyrene (HIPS), and styrene-acrylonitrile copolymer (SAN), has changed from nearly 90% suspension at the beginning of the 1980's to approximately 25% at the beginning of 1990.[1]

The productivity limitations involved in any batch process, such as suspension polymerization, along with the fact that in this type of polymerization more than 50% of the reactor capacity is occupied by the

dispersion-cooling medium (water), compared to the high production rates achieved in continuous processes, have been the major reasons for these changes. In addition, the ever increasing prices of monomers and the relatively low increases in the resins selling prices, have narrowed considerably the utility margins in the production of suspension polymer commodities. During the first half of the 1980's, for instance, the manufacturing costs of the aforementioned polymers accounted only for 40 to 50% of the price of the final product. Since the beginning of the oil crisis of 1986, the cost of monomer alone accounts for nearly 85% of the total price of the product.[2] As a result, the utility margins for these suspension polymers have shrunk from c.a. 50% to merely 6 to 8% in less than five years. In other words, batch suspension polymerization processes are no longer competitive for the production of commodity resins.

It is obvious that with such low utility margins the profitability depends mostly on the volume of sales. This is a clear disadvantage for suspension polymer manufacturers.

The only alternatives for suspension polymer manufacturers are, therefore, change or diversification. Change deals with development or adoption of new process technology, and involves a long term-high cost modification or replacement of both existing polymerization plants and product technology, to move on to more productive processes (in continuous, emulsion, or otherwise).

Diversification, on the other hand, deals only with the development or adoption of new product technology using the same process technology. Clearly, the new suspension polymer products must be of the low volume-high value added type, and able to be scaled-up for commercial production in existing facilities.

The relative ease of implementation and control linked to suspension polymerization processes make this option more attractive than the former for some manufacturers.

Since one of the main parameters establishing the added value of a given polymer is its performance in high temperature applications, suspension polymer manufacturers willing to diversify have turned their attention in recent years to the development of high deformation temperature engineering thermoplastics.

To fully understand the implications of following such an alternative, let us first define the different types of polymers in terms of their application temperature

1.3 Engineering and High Performance Polymers

In general, according to their limiting application temperature, polymers may be classified as: Commodities, Engineering Polymers, and High Performance Polymers.

Polymer commodities have a glass transition temperature (T_g) below 100°C. Therefore, their use is limited to applications below this temperature. Some thermoplastic elastomers and general commodity resins, such as most styrenic resins, acrylics, polyolefins, polyurethanes, poly(vinyl chloride), and related chlorinated polyolefins, loose their mechanical properties below 100°C. Certain acrylonitrile-butadiene-styrene polymers (ABS) maintain mechanical properties in the vicinity of 100°C, and are considered engineering polymers for specific applications.

Engineering Polymers are thermoplastics that maintain dimensional stability and most mechanical properties above 100°C and below 0°C. This definition encompasses plastics which can be formed into functional parts that can bear loads in temperature environments commonly experienced by the traditional engineering materials: wood, metals, glass, and ceramics. Generic resins falling within this scope include polycarbonates (PC), polyamides (nylons) (PA), polyethylene-therephthalate (PET), and some others.[3]

High Performance polymers are defined as materials that retain mechanical properties for thousands of hours at 230 °C, hundreds of hours at 300 °C, minutes at 540 °C, or seconds up to 760 °C. These temperatures may be encountered during the manufacture or use of the product.[4] Polyimides (PI), polyetherimides (PEI), polyetherketones (PEK), liquid crystal polymers (LCP), and polysulfones (PSU), are examples of this type of materials.

Figure 1.1, below, shows schematically the increase in performance of many commercial resins as their glass transition temperature (T_g) increases. In this figure, the higher the resin is in the pyramid, the higher the market price and the lower its production volume.

Figure 1.1

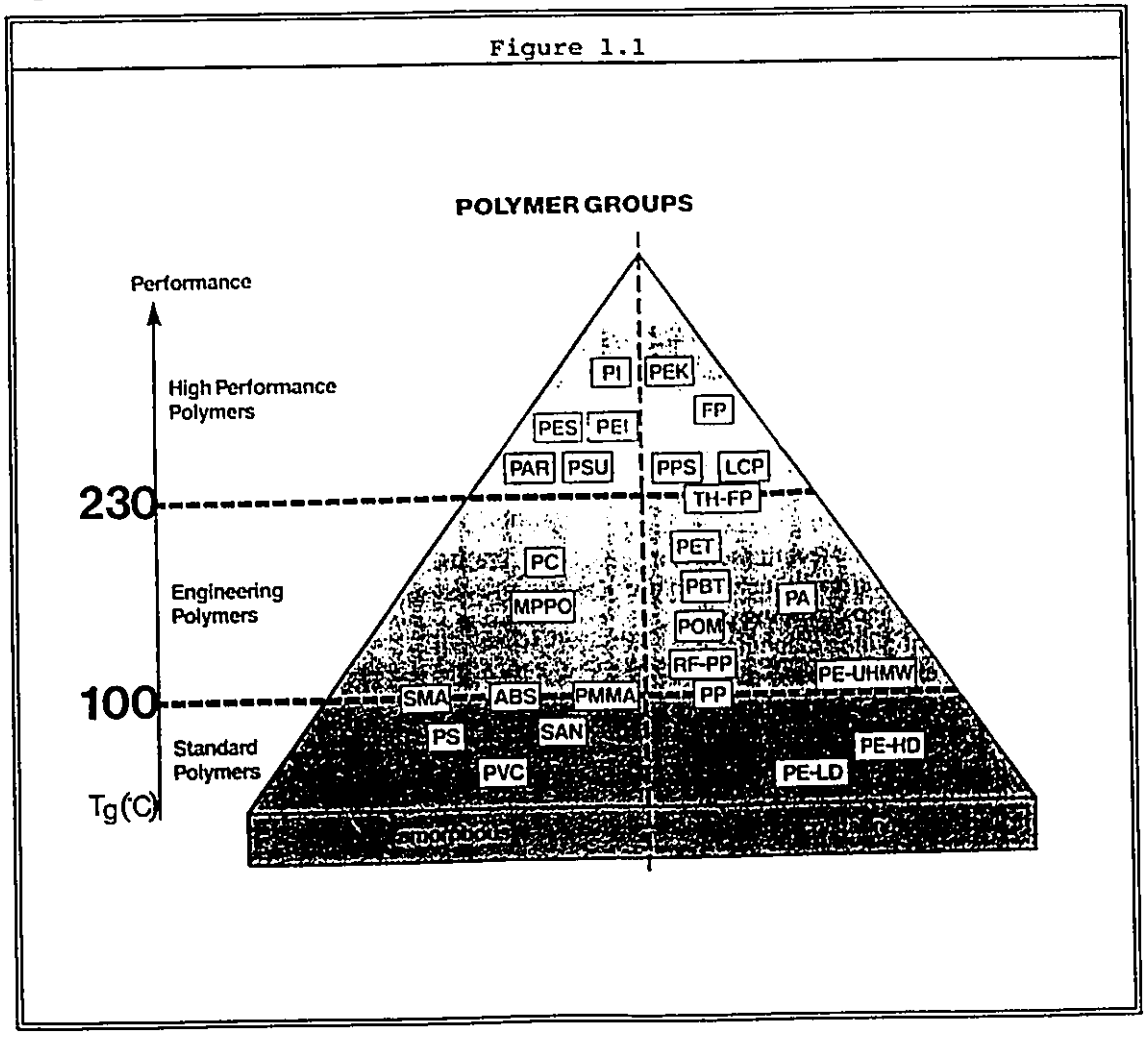

Figure. 1.1. Classification of polymers according to their thermal behaviour (from ref. 3).

The applications of heat resistant polymers self-explain their very high prices and their rapidly growing markets. Such applications include:[4]

a) Electronic and microelectronic components (circuit boards, mouldings, flexible cables, insulators, coatings).

b) Gaskets, sealants and tubing.

c) Binding system in brake shoes, abrasive wheels, and cutting disks.

d) Structural resins (adhesives, composites, foams, and mouldings) for advanced aircraft and space vehicles.

e) Engine components (fan blades, flaps, ducting, rods).

f) Nuclear reactor components (coolants, insulation, structural parts).

g) Conveyor belts for treating and drying materials.

h) Filters and pipes for chemical processing and energy generators.

i) Fire-resistant materials (protective clothing, parachutes).

j) Automotive components (wrist pins, pistons).

k) Industrial machinery and cookware coatings.

Figure 1.2 (a), below, shows the distribution of high temperature polymers by type and application. In figure 1.2 (b) the advantageous perspectives of market growth, for these materials in this decade, is shown.[2]

A recent worldwide survey carried out by Kline & Company, forecasts that the world market for high-temperature polymers will grow at over 8% per year, reaching nearly US $5 billion by 1998 up from $2.3 billion in 1988. The survey demonstrates that opportunities for high-temperature thermoplastics are still emerging from aerospace and electrical/electronics applications. The survey also showed a very strong shift in research and development towards modifying existing polymer systems, rather than developing new ones. This has happened because the number of licensing agreements and joint ventures regarding globalisation, as well as technology acquisitions has slowed down, after a very active period in the late 1980's.[2]

Figure 1.2

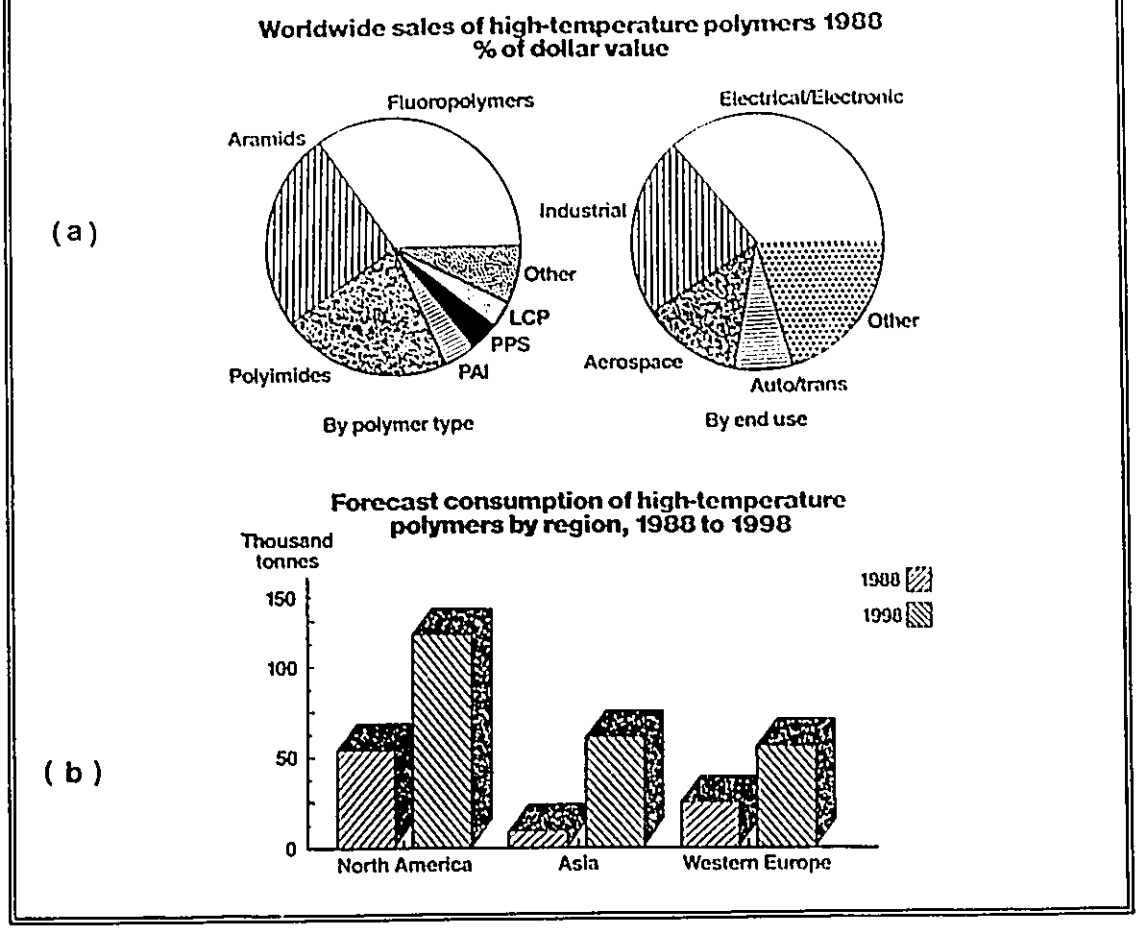

Figure. 1.2. (a) Current market participation of high-temperature polymers by product and application. (b) Growing market trends for high-temperature polymers in this decade (from ref. 2).

1.4 Constraints in the Design of Suspension Polymers

It seems obvious, with a glance at figures 1.1 and 1.2, that the development of this type of Engineering or High Performance suspension polymers would solve the so-called competitiveness problem stated above. However, multiple practical constraints arise in the design and development of suspension polymers. Such constraints may be listed as follows:

a) As a general rule step-growth polymerization resins cannot be synthesised by this technique. First the monomers employed bear polar reactive groups which make them partially to totally water soluble. Secondly, in this type of polymerization high molecular weights are achieved only at very high conversions. Due to this fact, the system is extremely difficult to stabilize as polymer particles contain low molecular weight polymer and low viscosity fluid for most of the polymerization time. In addition, for many systems, the condensation product is water, and the presence of large amounts of water in the continuous medium displaces the equilibrium towards depolymerization, slowing down the overall reaction, or triggering hydrolysis reactions. Moreover, water has a negative effect on most of the catalysts employed in this type of polymerization.

b) Anionic, or cationic polymerization cannot be done using this technique. Living anions or cations are killed through reactions with water (H+ or OH-) ions.

c) Semicontinuous suspension copolymerization processes are difficult to stabilize and control. Although there are several commercial semicontinuous processes for production of diverse grades of SAN, disruptions in the particle-water interface, caused by the addition of low viscosity monomer during the course of the reaction, causes serious suspension stability problems. The stability problems are partially overcome by using an excess of suspending agent.

d) Stabilisers have a restricted temperature range of application. Most of the steric and inorganic stabilisers used in suspension polymerization are only effective at temperatures below 150 °C. The lack of effectiveness of stabilisers at high temperatures is due to a combination of changes in the conformation at the interface, solubility of the stabiliser, viscosity of the disperse medium, and heat transfer rates through the interface.

e) Polymerizations proceeding at too high a rate are extremely unstable. The breakup-coalescence dynamics controlling the stability of the suspension involves a certain minimum time for interfacial events to take place. When the reaction rate is too high the events leading to coalescence accelerate whereas those leading to breakup remain at the same rate, the net effect being high suspension instability.

As a result of all of the above constraints, the development of new high Tg suspension products is limited to batch (or semicontinuous) processes using free radical copolymerization at moderate temperatures.

Due to this fact a compromise must be established in the product design since higher T_g's of the product may require higher temperatures for their syntheses. In order to achieve high conversions, and owing to the glassy effect, the polymerization temperature must be above the T_g of the product, otherwise a limiting conversion will be reached at the point where the T_g of the polymer-monomer mix reaches the reaction temperature [Horie et.al. (1968)].

Since the limiting polymerization temperature is around 150°C the product must be designed to have a T_g below this temperature or a limiting conversion must be acceptable when the T_g of the product is above 150°C.

Since the limiting conversion can be accommodated by product devolatilization, or by the use of solvents in the formulations, as T_g depressors of the polymerization mix, with the subsequent elimination of the solvent by devolatilization, the compromise in this regard depends on whether or not devolatilization is acceptable in the process.

In a previous study, the author has demonstrated that the optimal route for the synthesis of commercial suspension polystyrene (crystal and expandable) is achieved with a combination of high temperature (100 - 130°C) and bifunctional initiation [Villalobos (1989)]. This synthesis is optimal inasmuch as the best balance between productivity, suspension stability, and product properties is achieved.

The amount of knowledge in the suspension homopolymer design, generated through such study now permits the approach of the new high T_g suspension polymer design as a modification of suspension polystyrene resins via the new optimal route. That is, the High T_g copolymers to be synthesized through this research project will be styrene based copolymers made using high temperature suspension polymerization with bifunctional initiators.

Having provided an adequate background in the above, the general problem to be approached in this thesis can be now stated.

1.5 Statement of the Problem

This thesis deals with the development of a synthesis technology for High Deformation Temperature Engineering Suspension Copolymers, as the best competitive alternative for current suspension polymer manufacturers, from two perspectives: 1) The evaluation of the effectiveness of bifunctional initiators in bulk and suspension syntheses; and 2) The development of a comprehensive general kinetic model for free radical copolymerization with bifunctional initiators, to simulate the main copolymerization characteristics of the selected systems, as a function of the synthesis conditions, and to be used as the main tool in their optimization and scale-up to commercial production.

Although it seems a little odd to justify a Ph.D. research project on merely economic bases, there is a general worldwide trend towards greater financial support for universities by industry. This has reduced the gap between fundamental and applied research and has made possible the investigation of interesting industrial problems, like the one considered in this thesis.

In this research, in addition, a strong theoretical core is developed as a means to understand and facilitate the commercial implementation of a new synthesis technology for high-temperature polymers.

The comonomer systems chosen for this study are:

a) Styrene/α-Methylstyrene.

b) Styrene/N-Phenylmaleimide.

c) α-Methylstyrene/N-Phenylmaleimide.

d) Styrene/α-Methylstyrene/N-Phenylmaleimide.

With the following bifunctional initiators:

A) 1,4-bis(*tert*-butyl peroxycarbo)cyclohexane.

B) 1,1-di(*tert*-butyl peroxy)cyclohexane.

The bases for the selection of these comonomers and bifunctional initiators are explained in detail in Chapter 2 of this thesis, along with a justification for their employment as the best means to approach the synthesis of novel high T_g copolymers.

1.6 Objectives of the Project

Two main hypotheses comprise the essence of this research project:

1. High deformation temperature copolymers of styrene/α-methylstyrene, styrene/N-phenylmaleimide, α-methylstyrene/N-phenylmaleimide, and styrene/α-methylstyrene/N-phenylmaleimide can be synthesized, to obtain high molecular weight engineering polymers at competitive rates, by using bifunctional initiators.
2. Adequate polymerization conditions can be found to synthesize these copolymers up to high yields through a suspension polymerization process which can be scaled-up to commercial production levels.

The general objectives of this project, necessary to prove these hypotheses, can be summarized as follows:

a) Consolidate the knowledge developed during the author's Master of Engineering research on Suspension Polymerization Through Bifunctional Initiators, to optimize the synthesis technology of novel suspension copolymers.

b) Evaluate bifunctional initiators for the bulk and suspension synthesis of the proposed binary copolymers and terpolymer.

c) Develop a kinetic model to simulate conversion history, copolymerization rate, heat generation rate, molecular weight distribution development, copolymer composition development, and copolymer microstructure, in free radical copolymerization through bifunctional initiators, which comprises the unique features of the systems studied.

d) Evaluate the feasibility to scale-up the optimized copolymer systems by comparing their behaviour in suspension polymerization to that of suspension polystyrene.

1.7 Structure of the Project

The general structure of this research project, designed to achieve the above objectives, can be described as follows:

The project comprises two main independent stages:

Stage 1: Consolidation of Master's results.

Stage 2: Synthesis and modelling of high T_g copolymers through suspension polymerization with bifunctional initiators.

Stage 1, was designed to complement the results obtained during the development of the Master's project (objective a) [see Villalobos (1989)]. This stage is not related to the synthesis of high T_g copolymers, but to the optimization of suspension expandable polystyrene with bifunctional initiators. As such, this stage may appear out of place in this thesis, however, it gives the parameters required to compare the suspension behaviour of the new copolymer systems to optimized suspension polystyrene.

This stage, comprises three different studies: i) the effect of n-pentane concentration ($[C_5]$), and conversion of n-pentane addition (X_{ad}) on polymerization rate (R_p), and molecular weight distribution (MWD) in monofunctionally and bifunctionally initiated bulk polystyrene; ii) The

effect of $X_{wi}(C_5)$ on suspension stability and particle size distribution (PSD) in bifunctionally initiated suspension polystyrene; and iii) the evaluation of different suspending agents for the suspension polymerization of styrene with bifunctional initiators, in the presence of n-pentane.

The detailed structure of this stage can be seen in figure 1.3, below. In this figure, the main parts of the stage are on top, and the order of execution of the studies is from top to bottom. Studies at the same level in the figure are carried out simultaneously.

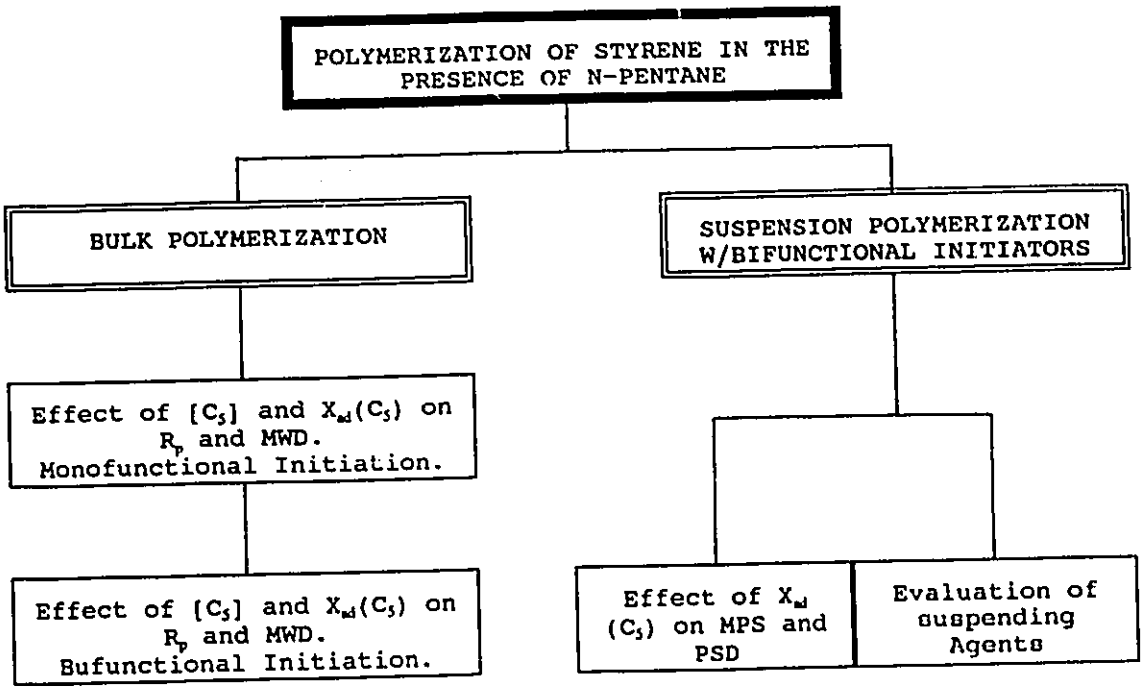

Figure 1.3. Detailed structure of Stage 1 of this research project.

Stage 2, comprises the bulk of this research project and was designed to achieve the objectives b, c, and d, stated above.

This stage is subdivided in three major simultaneous and interrelated parts: I) experimental investigation of the effect of the synthesis conditions on the kinetics of the copolymer systems selected; II) characterization of the products; and III) development of the kinetic model and simulation program.

The studies to be performed in the experimental part can be classified as follows: i) effect of the polymerization temperature (T_p), bifunctional initiator concentration ([I]), and comonomer composition (f) on monomer conversion (X), copolymerization rate (R_p), molecular weight distribution (MWD), copolymer composition (F), and glass transition temperature (T_g), for the bulk copolymer synthesis of the selected systems; and ii) effect of f, and R_p on suspension stability, mean particle size (MPS) and particle size distribution (PSD), in the bifunctionally initiated suspension copolymerization of the selected systems.

Within each study of this part, two different experimental phases are contemplated: A broad exploratory phase, to gain understanding on the main trends of the system and to generate results that permit the adequate evaluation and adjustment of the model parameters. An optimization phase, designed in a narrow range of manipulated variables with the aid of the adjusted simulation program, to minimize the number of experiments.

The obtaining of valuable experimental results requires the appropriate characterization of both the bulk copolymers synthesized and the suspension particles obtained (part II of this stage). The following analytical techniques have been used for the complete characterization of the samples; Gravimetry (Gv), to quantify monomer conversion, Gel Permeation Chromatography (GPC) to evaluate MWD, Nuclear Magnetic Resonance (NMR) to characterize both copolymer composition and microstructure, Differential Scanning Calorimetry (DSC) to evaluate R_p during copolymerization and T_g of the products, and Sieving (Sv), to evaluate MPS and PSD of the suspension particles.

The development of the kinetic model and simulation program (part III) must follow the next steps: proposal of the elementary reaction scheme and mechanism of copolymerization; derivation of the kinetic equations; establishment of a valid numerical solution strategy; evaluation and adjustment of parameters from experimental data; and evaluation of the predicting capabilities.

Figure 1.4, below, shows the detailed structure of the stage 2 of this project. In this figure, the main parts of this stage are at the top, and the order of execution of the different studies proposed are from top to bottom. Activities at the same level are to be carried out simultaneously.

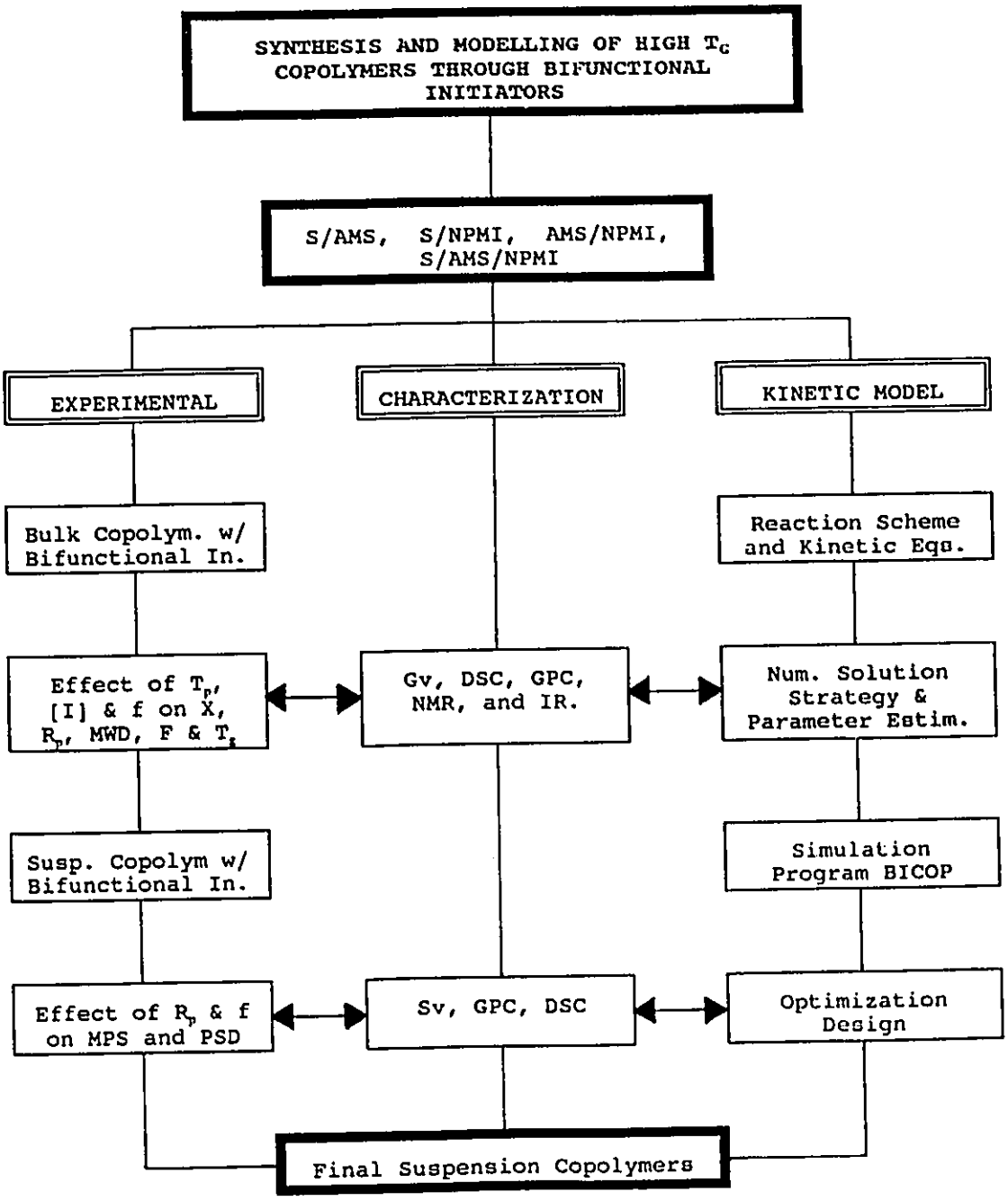

Figure 1.4. Detailed structure of Stage 2. of this research project.

1.8 Thesis Structure

The remainder of this thesis has been structured as follows:

Chapter 2, gives a complete literature review of all the topics of interest for this research. The theoretical support and published data for modelling considerations, experimental design, and model parameter evaluation, are contained within this chapter.

In Chapter 3, the consolidation of the Master's results is pursued through the comparative study of monofunctionally and bifunctionally initiated suspension polymerization of styrene in the presence of n-pentane. As mentioned before, this study complements previous work on optimization of EPS processes, and is only related to the scope of this thesis in that it gives the comparison parameters for the evaluation of the suspension behaviour of the copolymer systems to be synthesized.

The complete derivation of a general kinetic model for copolymerization through bifunctional initiators, considering the unique features of statistical and donor-acceptor copolymerization, is given in Chapter 4, along with the bases for its numerical solution on which the simulation program is developed. This chapter, as mentioned above, comprises the theoretical core of this thesis.

Chapter 5 through 7 show the experimental studies and results on the synthesis and characterization of styrene/α-methylstyrene, styrene/N-phenylmaleimide, and α-methylstyrene/N-phenylmaleimide copolymers with bifunctional initiators, respectively. The application of the simulation program to reproduce the experimental results and assist in the experimental design is emphasized throughout these chapters.

Chapter 8 gives the experimental results for the synthesis and characterization of styrene/α-methylstyrene/N-phenylmaleimide terpolymers. In this chapter, the kinetic model and simulation program are extended to deal with a ternary system, and its application to the system at hand is evaluated.

In Chapter 9, the most interesting results for each system are summarized, along with the general conclusions of this thesis. In this chapter the main contributions to the field, emerging from these studies, are given as well.

The rest of the thesis comprises a complete list of the references consulted and quoted throughout the text, along with two Appendices dealing with the detailed derivation of key equations appearing in the text.

CHAPTER 2

THEORETICAL BACKGROUND

In this chapter, a literature survey is included to place into context the most relevant theoretical background concerning this study. Direct implications of some of the concepts explained herein on the research in this thesis are highlighted throughout the chapter. Bases for the selection of the monomers and bifunctional initiators used in this study are explained in detail.

2.1 Heat Resistant Polymers

2.1.1 Glass and Melting Transitions in Polymers

Any liquid which may be cooled without the incidence of crystallization experiences a second-order transition and solidifies to a glass over a fairly narrow temperature range which is characteristic of the substance [Fox and Flory (1950)]. The temperature at which this transformation takes place is usually referred to as the glass transition temperature (T_g). For polymers, This point is often designated as the "brittle temperature" inasmuch as the polymer changes from a highly viscous liquid, or rubbery solid, to a brittle solid which will tolerate little deformation without fracture at all lower temperatures ($T<T_g$).

Polymers exhibit mechanical properties commonly associated with solids when in either of two different states: crystalline and glassy state. The high degree of microstructural regularity necessary for crystallization is hard to achieve with large molecules, as a result, very few polymers are able to crystallize. Even for polymers which do crystallize, the degree of crystallinity is always less than 100% [Flory (1956)].

Consequently, in any polymer system, there is a fraction of polymer which is amorphous even at temperatures well below the freezing point. This amorphous polymer will be in the glassy state whenever the temperature is sufficiently low.

Hiemenz (1984), describes the thermal behaviour of polymers in terms of the observed changes in the specific volume of the system as follows: Let us fix our attention on figure 2.1, below. In this figure, line ABDG shows the behaviour upon freezing of a typical low molecular weight compound. For these compounds a sharp first-order transition occurs at a single temperature, the melting point T_m. The slopes of AB and DG measure the coefficients of thermal expansion of liquid and solid, respectively, which shows a discontinuity at the melting point.

Figure 2.1

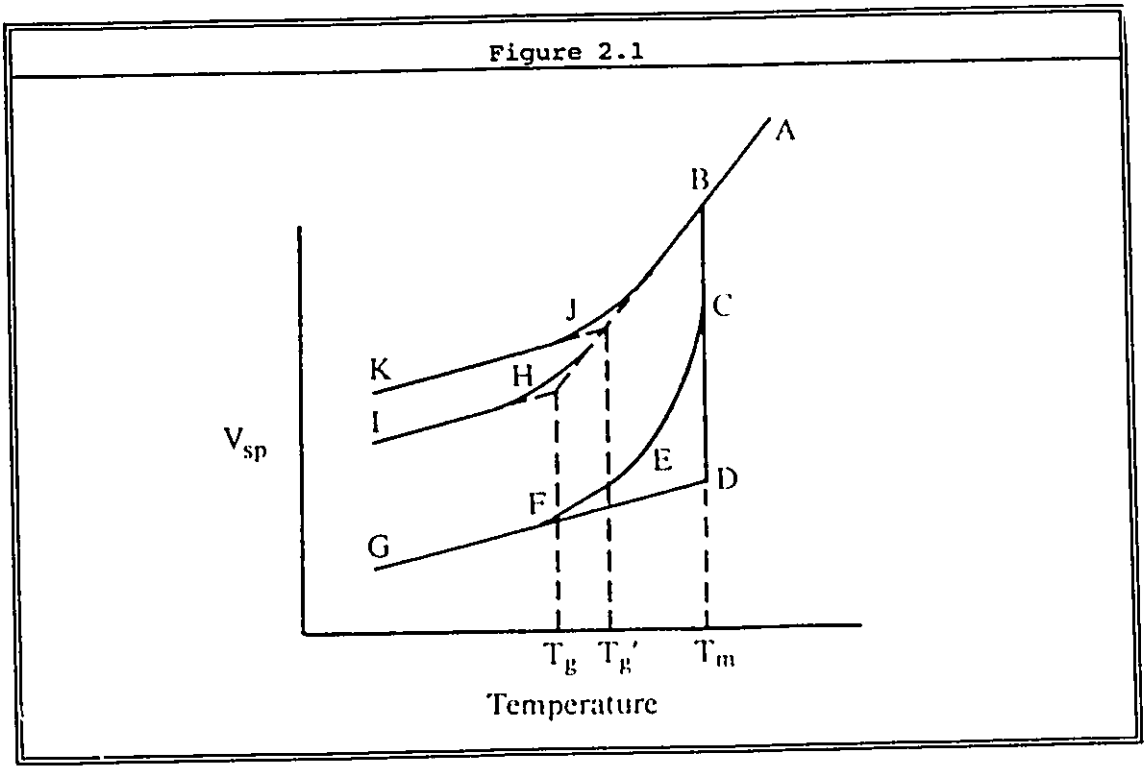

Figure 2.1. Schematic representation of possible changes in the specific volume of a polymer with temperature. See text for description of lettered curves. (From Hiemenz (1984)).

For polymers, a different behaviour without discontinuity at T_m, given by the pattern ABHI, is observed. Line AB, characterizing the

liquid state of the system, changes slope at T_g to become HI. In fact, the change of slope occurs over a range of temperatures, as shown in the figure. Extrapolation of the two lines permits T_g to be defined by this method. Line HI represents the region of the glassy state of the system and the threshold for its appearance is the glass transition temperature (T_g). In the region BH, the polymer system exhibits the behaviour of a supercooled liquid.

The line ABJK is a displaced variation of ABHI in which the glass state JK is offset from HI due to a higher cooling rate. Note how T_g has also been displaced appearing at a higher temperature (T_g'). Evidently, then, the T_g of the system is dependent amongst other things on the thermal history of the sample, and its punctual value must be considered as the extrapolation of the observed behaviour at zero cooling (or heating) rate.

The line ABCEFG in figure 2.1, characterizes the behaviour of a partly crystalline, partly amorphous polymer. At T_m crystallization begins and a discontinuity in specific volume is observed. Such discontinuity, however, is not as sharp as for low molecular weight compounds due to the amorphous fraction of the polymer. Region EF reflects the supercooling of this fraction.

As in the absence of crystallization the change in slope between EF and FG occurs at T_g. The onset point in this case, however, becomes harder to detect as the fraction of crystalline polymer increases.

2.1.2 Models for Glass Transition in Polymers

The glass transition temperature can be used as an indicator for predicting the lower-bound flexible temperatures of a rubber or to estimate the heat distortion temperature of a glassy polymer. It can also be employed to predict upper bound temperatures at which the creep of a polymeric product will become significant under loading [Lee (1989)]. Owing to this, success in the estimation of T_g for novel polymers is a useful tool in new product development.

It is not uncommon to find newly synthesized polymers which cannot be processed by extrusion or injection moulding due to their high T_g, or to find commercial polymers which have T_g too low to fully capitalize on their thermal stability. Both of these problems can be partially overcome if the T_g of the expected product can be predicted in advance. As a first step, thorough understanding of the phenomena involved during the glass transition is necessary to develop predictive models.

As the temperature of a supercooled polymeric liquid approaches T_g, the relaxation time for structural reorganization increases rapidly until at T_g it becomes much longer than the time scale of the experiment [O'Reilly (1962), Allegra (1978)]. Such an increase in the relaxation time can be observed from the variation of thermodynamic properties other than the specific volume (V), such as enthalpy (H), entropy (S), free energy (F), diffusion coefficient (D), and dynamic shear modulus (γ).

For all these first-order properties, no discontinuity is observed at the transition point, however, their first temperature derivatives, such as the thermal expansion coefficient (α), and the heat capacity (C), exhibit abrupt changes (discontinuities) at the onset of the transition. Due to this fact the glass transition temperature is referred to as a "second order transition" [Fox and Flory (1950), Gibbs and DiMarzio (1958)].

The fundamental mechanistic problem of the phenomena related to the glass transition temperature, therefore, consists in establishing the dependence of the structural relaxation time on these properties.

Early attempts at describing the glass transition phenomenon were based on the development of the free volume theory. The assumption of a very large structural relaxation time at T_g suggests that in the glassy state the free volume remains nearly constant, therefore, the relationship between T_g, and T and P, could be given in terms of the free volume dependence on these properties.

The evolution of the early ideas on free volume [Doolittle (1951), Bondi (1954)] by Cohen and Turnbull (1959), and later by Flory et.al. (1964) led to the development of the well known free volume equation:

$$V_F = \alpha V_m (T - T_0)$$

where α and V_m are the thermal expansion coefficient and molecular volume mean values over the relevant temperature range, and T_0 may be chosen as the temperature where $V_F=0$. Similarly, if β is the isothermal compressibility:

$$V_F = \alpha V_m (T - T_0) - \beta V_p \Delta P$$

where V_p is a similar mean molecular volume for the pressure increment ΔP.

Ryong-Joon and Tonelli (1978) approach glass transition modelling by demonstrating that, due to the dependence of the properties of glassy materials on the past history imposed on the samples, the glass state cannot be described by means of the free volume concept alone, since free volume does not automatically give information on the degree of relaxation of other properties. They state that if only a single-order parameter is frozen in at T_g, as is assumed in the simple free volume theory, the dependence of T_g on pressure, given by

$$dT_g/dP = T_g V \Delta\alpha / \Delta C_p$$

and

$$dT_g/dP = \Delta\beta / \Delta\alpha$$

where Δ denotes the difference between the properties of the liquid and the glass, and C_p is the isobaric specific heat, only shows marginal agreement with experimental data. Thus, the inadequacy of assuming a single structural feature (single order parameter) to be frozen at T_g, is clear.

The need for a second order parameter or a second structural element becoming immobilized in polymeric glasses to model the phenomenon becomes obvious.

In the same study, Ryong-Joon and Tonelli, following the ideas on rotational isomeric states (RIS) introduced by Flory [Flory (1969)], calculate the conformational specific heat of various polymers and compare them with experimental values of ΔC_p, thereby assessing the importance of the polymer conformation as an order parameter describing the glassy state.

By following this procedure, they found that roughly 10 to 20% of the total change in C_p observed at T_g is due to changes in the conformation of the polymer chains, with the remaining 80 to 90% due to changes in free volume.

Recently, Allegra et.al.(1990) extended the lattice models introduced first by Gibbs and DiMarzio [Gibbs and DiMarzio (1958)] to explain the glass transition phenomenon in terms of the freezing of rotational oscillations in the polymer chains.

Their Space-Filling Model is based on evidence that backbone oscillations around the rotational minima suffer a discontinuous decrease upon cooling of the amorphous polymer at the lower limit of the glass transition temperature.

Based on the agreement of their model with experimental data, they strongly state that across T_g any chain of the system merely changes from a multitude of elementary configurations to a single one, in contrast to previous findings that two different discontinuities, one in the number of RIS states and another in the amplitude of the oscillations, exist at T_g.

The discontinuity in the structural mobility of the polymer chains at T_g is shown below in figure 2.2. Note in this figure the changes in specific volume across T_g brought about by the inability of the polymer chains in the glassy state to change their configuration through free torsion movements.

Figure 2.2

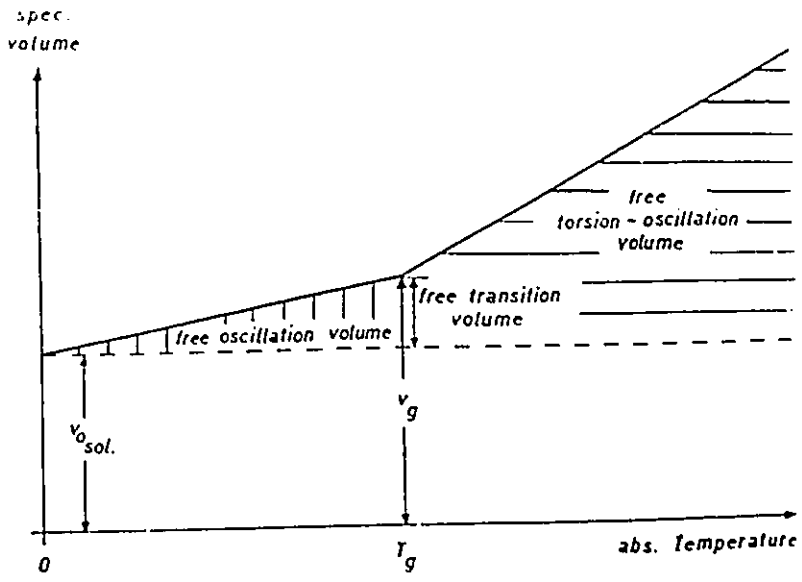

Figure 2.2. Schematic representation of the discontinuity in the polymer chain mobility at the glass transition. (From Ueberreiter and Kanig (1952)).

2.1.3 Effect of Polymer Molecular Weight on T_g

The lack of more reliable analytical techniques in the 1950's to characterize the molecular mobility of monomeric and polymeric substances forced polymer chemists to employ the macroscopic viscosity as an inverse measure of this property. Fox and Flory (1948) observed that the second order transition of monomeric compounds generally occurs at a viscosity of about 10^{12} poise.

For polymers, however, the viscosity depends not only on the segmental mobility but also on intersegment interactions. Since interactions increase rapidly with molecular weight, viscosities well above 10^{12} poises at T_g should be expected if the molecular weight is large.

On the basis of this, the second order transition might be expected to be independent of the molecular weight except in the range where it affects the configuration of the polymer in the liquid state.

Fox and Flory (1950) determined the T_g of narrow molecular weight distribution polystyrene (PS) samples, previously fractionated, by measuring the specific volume of the samples at different temperatures. The molecular weight of the PS fractions was determined previously by viscosity measurements. They found that the T_g of the samples reached an asymptotic value of 100°C at about M_n = 30,000. Below this point, they found that T_g decreases linearly with $1/M_n$ according to

$$T_g = 100 - 1.7\times10^5/M_n$$

The specific volume at T_g (V_g) was found to follow

$$V_g = 0.943 + 2.4\times10^{-4}T_g$$

with the specific volume below T_g varying according to

$$V = V_g - 2.5\times10^{-4}T \qquad (T \leq T_g)$$

This equation demonstrates the important observation that the specific volume below T_g is nearly independent of the molecular weight. Figure 2.3 below shows Fox and Flory's experimental results based on this iso-free volume concept at T_g.

These findings were later corroborated by Gibbs and DiMarzio (1958) who applied an extension of the Meyer-Flory-Huggins lattice model [Flory (1953)] to demonstrate from thermodynamic principles that the theoretical second order transition (T_2) corresponds to the onset of the T_g when approached from above.

Figure 2.3

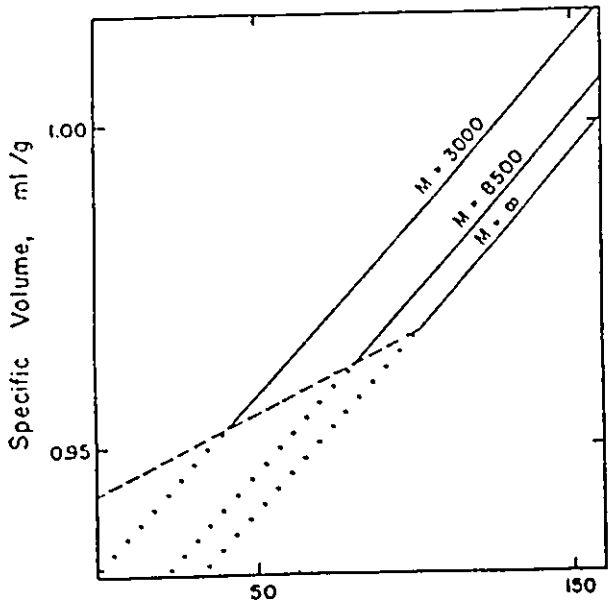

Figure 2.3 Specific volume-temperature relations for various polystyrene fractions (∞ = MW > 30000). (——) Equilibrium curves; (···) non attainable portions of equilibrium curves; (---) v-T curve for PS in the glassy state. (From Fox and Flory (1950).

Ueberreiter and Kanig (1952) approached the problem considering the chain end groups acting as plasticizer. They considered that the end groups have a greater expansion coefficient according to an improved mobility due to their position and, based on the concentration of end groups obtained an empirical correlation for the dependence of T_g on the degree of polymerization (P_n) for PS as

$$1/T_g = 0.002768 + 0.004954/P_n$$

They also pointed out that the difference between the specific volumes at T_g and 0°K, $V_g - V_{(0)sol.}$, is a constant equal to 0.0646, and

explain that this volume difference is the space which, in the amorphous solid, is available for oscillations at the transition temperature. The oscillations in the solid body cause a certain enlargement of the structure necessary for the torsion oscillations at the transition point. Such enlargement is independent of the degree of polymerization. This means that the end groups as well as middle groups in starting the torsion oscillation motion which causes a rearrangement of the groups, need the same minimum volume for this displacement.

Following similar arguments Fox and Loshaek (1955) arrived at the general expression:

$$1/T_g = 1/T_{g(\infty)} + K/T^2_{g(\infty)}M_n$$

Here the constant $K = (m + m_e)[\Delta\alpha T_{g(\infty)} + \Delta V_0]/(\alpha_\infty - B)$; where m is the weight of the monomer unit and m_e is the combined weight of the two chain ends, the subindex (∞) represents the value of the property for very large polymer molecules, and B is a constant dependent on the polymer system.

Fox and Flory (1954) point out the difficulty to visualize the physical significance of the "free torsion oscillation volume" as defined by Ueberreiter and Kanig, since their definition requires that its extrapolated value be negative for the equilibrium (liquid) polymer below T_g. They also confirmed their previous prediction that the viscosity-temperature coefficient (E_T) for a glass forming polymer should go through a maximum at T_g and fall to a low value at lower temperatures. They also give a revised form of their empirical relationships for PS as

$$T_g = T_{g(\infty)} - 1.1\times10^5/M_n \qquad \text{(iso-free volume)}$$

and

$$T_g = 373 - 1.0\times10^5/M_n \qquad \text{(constant } E_T \text{ at } T_g\text{)}$$

which show better agreement with their earlier experimental data.

Kanig (1963) explains the iso-free volume concept from thermodynamic principles and arrives at a very complex equation describing the T_g dependence on molecular weight.

Using the same iso-free volume concept, Richardson and Savill (1977) fit specific volume data for anionic polystyrene of narrow molecular weight distribution to a general equation of the form $V=A+BT+CT^2+(a+bT+cT^2)/M_n$. Employing multiple regression analysis they found the constants to be: 1) for V_g: A=0.9498, B=1.962x10^{-4}, C=1.683x10^{-7}, a=3.157, b=0, c=3.229x10^{-2}; and 2) for V_l A=0.9199, B=5.098x10^{-4}, C=2.354x10^{-7}, a=32.46, b=0.1017, c=0.

In their experiments they found a low value for the $T_{g(\infty)}$ = 93.4°C which is explained in terms of the careful annealing of their samples in the vicinity of T_g. Since the linear equations described earlier fit well the data for dV/dT and give physical meaning to the parameters, this empirical "sophistication" seems completely useless.

Using thermodynamics concepts on the effect of the polymer composition on the glass transition temperature, Couchman (1979) arrives at expressions identical to the Fox-Flory and Ueberreiter-Kanig equations. He conceives the polymer system as mixtures of chain ends and high polymer chains, with different energies of conformation.

Consequently if both states associated with the transition have identical entropy the following relation can be derived:

$$T_g = \frac{(n-2)\Delta C_p^0 T_g^0 + 2\Delta C_p^e T_g^e}{(n-2)\Delta C_p^0 + 2\Delta C_p^0}$$

Here superscript 0 and e refer to high polymer and chain ends respectively, and n is the degree of polymerization or (number average chain length). If $\Delta C_p^0/\Delta C_p^e = 1$ the above equation reduces to the Fox-Flory equation.

2.1.4 Effect of Copolymer Composition on T_g

Copolymerization has been widely used to combine or enhance the desired properties of separate homopolymer systems. In light of the fact that glass transition temperature is an important property in determining the final application of a given polymer, it is no wonder that a substantial amount of research has been devoted to find suitable expressions to explain or predict the thermal behaviour of copolymers and polymer blends.

Fox (1956), derived from simple assumptions the first relationship for the dependence of the glass temperature on composition for a copolymer or a plasticized polymer as:

$$\frac{1}{T_g} = \frac{w_1}{T_{g1}} + \frac{w_2}{T_{g2}}$$

For a plasticized polymer T_{g1} and T_{g2} represent the glass temperatures of the pure polymer and pure diluent, and w_1 and w_2 are their respective weight fractions in the mixture. For a copolymer, w_1 and w_2 refer to the weight fraction of the comonomers chemically bound in the copolymer, whereas T_{g1} and T_{g2} refer to the glass temperatures of the two corresponding homopolymers.

It is remarkable that the T_g of several statistical (random) copolymers is well represented by this model. Unfortunately, experience often shows that many copolymers do not follow this simple additive rule.

Williams et.al.(1955) in an attempt to generalize the free volume concept for different polymer systems came up with the following expression:

$$V_f = 0.025 + 4.8\times10^{-4}(T - T_g)$$

In this relation 0.025 is the free volume at T_g, and the additional term expresses the increase in free volume due to the expansion of the polymer as the temperature is raised from T_g to T.

Starting from this relation, Kelly and Bueche (1961) derived an equation for the T_g of a polymer diluent system as

$$T_{gmix} = [4.8x10^{-4}cT_g+\alpha_s(1-c)T_g']/[4.8x10^{-4}c+\alpha_s(1-c)]$$

Where, c is the volume fraction of the polymer in the mix, T_g is the glass temperature of the pure polymer, α_s and T_g' are the thermal expansion coefficient and glass transition temperature of the diluent, respectively.

Couchman and Karasz (1978), obtained a generalized form of Kelly and Buecher's model from classical thermodynamic principles by treating the glass transition as a second order transition and using the characteristic continuity and discontinuity conditions, as described in the previous section, of such phenomena. By doing this, they arrived at the expression:

$$T_g = \frac{\phi_1^0\Delta\alpha_1T_{g1} + \phi_2^0\Delta\alpha_2T_{g2}}{\phi_1^0\Delta\alpha_1 + \phi_2^0\Delta\alpha_2}$$

Here, the volume fractions ϕ are defined in terms of the molar volumes V evaluated at their respective T_g, and the transition isobaric volume expansivity increments $\Delta\alpha$ are derived from the definition:

$$\alpha_i \equiv 1/V_i(\delta V_i/\delta T)_P$$

The above equation is also of the same form as the general model for the T_g-copolymer composition relationship given previously by Gordon and Taylor (1952), with the difference that the latter expressed the copolymer composition by weight rather than volume fractions as

$$T_g = K(T_{gB} - T_g)c_B/c_A + T_{gA}$$

Here the subindex A and B refer to the pure homopolymers, and the constant $K=\Delta\alpha_h/\Delta\alpha_l$.

Illers (1963), fit this model successfully to experimental data of T_g vs composition for several copolymer pairs such as ethylacrylate/styrene (EA/S), butylacrylate/styrene (BA/S), styrene/acrylamide (S/AAm), styrene/methylmethacrylate (S/MMA), methylacrylate/methylmethacrylate (MA/MMA), styrene/methylacrylate (S/MA), styrene/acrylic acid (S/AA), and methylmethacrylate/acrylonitrile (MMA/AN) among others.

Figures 2.4 a and b, below, show Illers' experimental results for T_g vs copolymer composition for the systems styrene/mathylacrylate (S/MAc) and styrene/methylmethacrylate (S/MMA), respectively.

Note, in these figures, that for the system S/MAc the ratio $\Delta\alpha_s/\Delta\alpha_{MA}$ remains nearly constant throughout the copolymer composition range and, consequently, a linear increase in T_g between T_{gMA} and T_{gS} is observed. For the system S/MMA the $\Delta\alpha_{MMA}$ decreases at certain copolymer compositions. As a result, a minimum in the copolymer T_g, well below the T_{gS}, is observed.

Evidently, the complex molecular interactions between dissimilar chemical structures comprising the copolymer chains, play a substantial role in the packing of such chains near the glass transition, and therefore in their free volume and mobility, which are in turn responsible for the thermal behaviour of the copolymer.

Such complex behaviour has been more recently attributed to the copolymer microstructure and sequence distribution since both are related to the mobility of the copolymer chains.

As a general rule the T_g of the copolymer is believed to be closely associated with the distribution of diads (AA, AB, and BB linkages in the A-B copolymer) with the difference between authors being the weighing factors used.

Figure 2.4

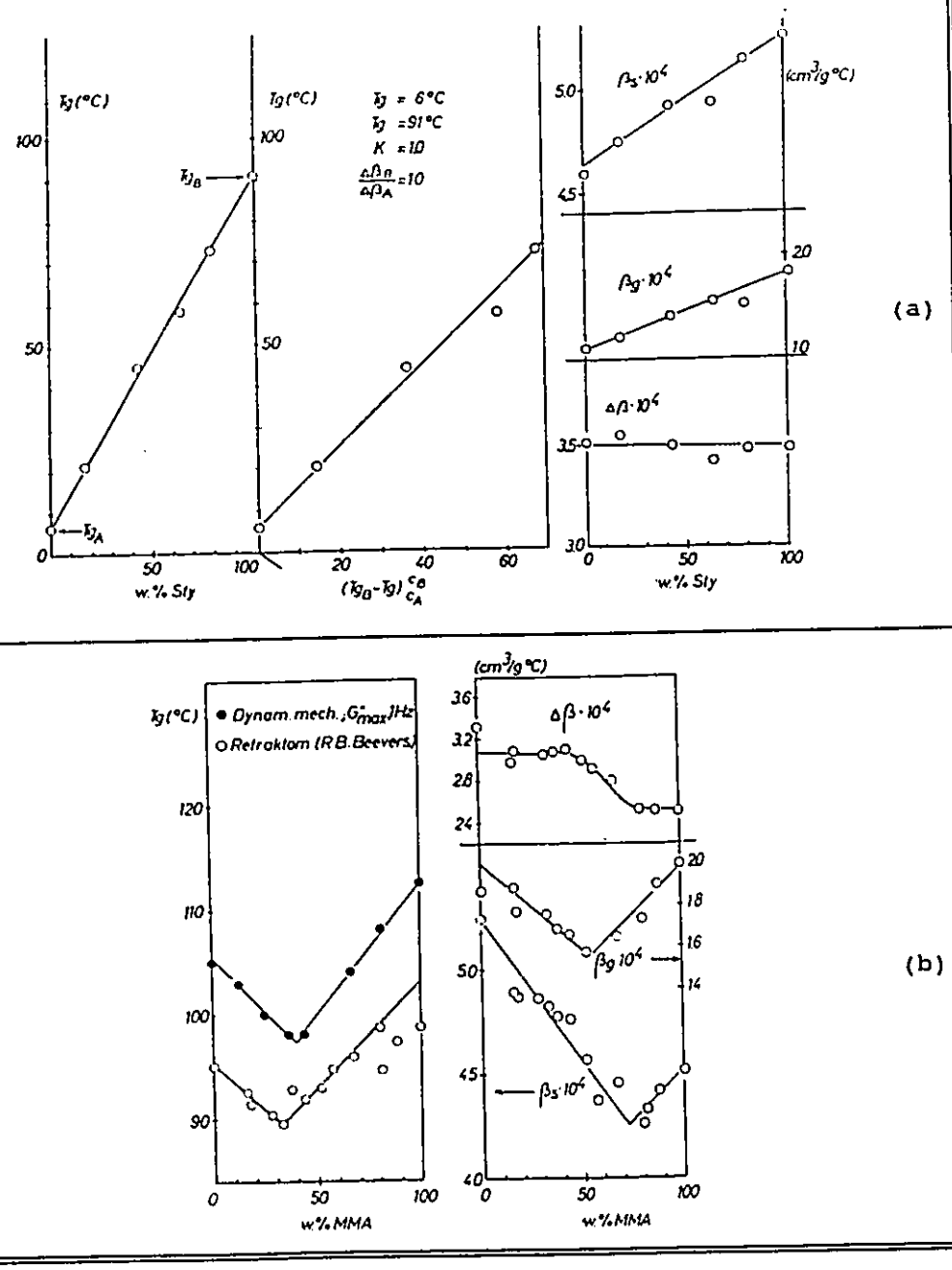

Figure 2.4. Glass transition temperature and thermal expansion coefficients of solid (β_s), glass (β_g) and difference ($\Delta\beta$) as a function of copolymer composition for the systems (A/B): (a) MAc/S; and (b) S/MMA. (From Illers (1963)).

Barton (1970), Johnston (1973), and Couchman (1982) based on the diad composition approach derived the following models, respectively:

Barton's Model

$$T_g = \Sigma n'_{ij} T_{gij} \qquad \text{where } n' = n_{ij}\alpha_{ij}/\Sigma n_{ij}\alpha_{ij}$$

Johnston's Model

$$1/T_g = \Sigma (M_i/\Sigma n_i M_i) * n_{ij} (1/T_{gij})$$

Couchman's Model

$$\log(T_g) = \Sigma n_{ij}\Delta C_{pij} * \log(T_{gij}) / (\Sigma n_{ij}\Delta C_{pij})$$

Where M_i, n_i are the molecular weight and the molar fraction of monomer i, T_{gij}, n_{ij} are the glass transition temperature of the ideal copolymer built only with the structural diad ij and the molar fraction of the diad ij in the actual copolymer, respectively, α_{ij} is the number of rotable bonds in the diad ij, to which a heat capacity increment ΔC_{pij} is associated at the glass transition temperature.

It is noteworthy that these equations, although derived for binary copolymers , hold for multicomponent systems.

Bruckner (1981), shows that in general, block copolymers exhibit two different T_g's corresponding approximately to those of the parent homopolymers comprising the blocks. When the T_g values of the block copolymer differ significantly from those of the homopolymers, this indicates a change in morphology due to an evolution in the miscibility of the two phases.

This is the case of the thermoplastic elastomers (TPE), in which block copolymers bearing hard (glassy) and soft (rubbery) segments have a thermal behaviour hardly related to the parent homopolymers. This is due to micro-phase separation with glassy domain formation (crystallinity regions) which confer the product with a glassy thermal behaviour, which makes them processable through extrusion or injection moulding, combined with the mechanical properties of elastomers.

Recently, Guillot (1990) assessed the applicability of the above models in T_g simulation of different copolymer systems characterized by differential scanning calorimetry (DSC). He claims that it is possible to predict with accuracy, from a kinetic investigation of the polymerization process, the glass transition of a complex mixture of random copolymers, at least when compatibility is poor.

In such cases, DSC analysis seems to show that any copolymer chain behaves as an isolated molecule, so that a theoretical DSC thermogram can be derived from the computed heat capacity of the instantaneous copolymers generated by the polymerization process, in close agreement to experimental data. In particular, it explains the shape of the thermograms and the spreading of the glass transition temperature range, which depends on the complexity of the copolymer chains mixed. A complete description of the differential scanning calorimetry technique can be found in Vankrevelen (1976).

2.1.5 Polymer Structure-T_g Relationship

In the above sections the physical factors affecting the T_g of a polymer, such as molecular weight and molecular weight distribution, close packing (crystallinity), molecular interactions and composition, have been discussed. Along with these, a number of chemical factors determining the steric structure of the polymer play an instrumental role in the thermal behaviour of the polymer. The chemical factors which influence heat resistance include primary bond strength, secondary or Van der Waals bonding forces, hydrogen bonding, resonance stabilization, mechanism of bond cleavage, molecular symmetry, rigid intrachain structure, and degrees of branching and crosslinking.

The primary bond strength is the single most important factor contributing to heat resistance [Hergenrother (1991)]. The bond dissociation energy of a carbon-carbon single bond is ~350 kJ/mol, and carbon-carbon double bond is ~610 kJ/mol.

Resonance stabilization in aromatic systems adds 164-287 kJ/mol to the latter [Cottrell (1958)]. As a result, aromatic and heterocyclic rings are widely used in thermally stable polymers. The nitrogen-nitrogen bond dissociation energy is relatively low, ~160kJ/mol, and would not be expected to form part of thermally stable polymers. However, owing to resonance stabilization, the N-N bond in heterocyclic rings exhibits higher thermal stability.

Secondary or Van der Waals forces provide additional strength and thermal stability. Dipole-dipole interaction and hydrogen bonding contribute 25-41 kJ/mol toward molecular stability and affect the cohesion energy density, which influences stiffness, T_g, melting point, and solubility.

Allegra (1968), and Allegra and Immirzi (1969) give a complete statistical-mechanical treatment of the neighbour interactions in polymer chains, accounting for all rotational states, as a means to calculate the conformational averages of a free polymer chain. From their model, the interaction energy contributing to the stiffness of the polymer chains, and therefore to their thermal stability, can be estimated.

Polar chemical groups participating in strong intermolecular association, such as -CO-, and $-SO_2-$, are often contained in heat resistant polymers. In addition, polymers containing electron withdrawing moieties (acceptors), like -CO-, as connecting groups are generally more stable than those containing electron-donating groups (donors), like -O-.

Fryd (1984), explains the role of the formation of charge-transfer complexes (CTC) on the observed T_g of the resulting polymer. He suggests that CTC formation between strong donor/acceptor pairs (diamine and dianhydride, respectively) increases greatly the interchain interaction forces, and proposes CTC formation as a main cause for the high T_g's observed in polyimides. He observed that the presence of a bridging group within dianhydride repeating units affects the T_g more profoundly than its presence within diamine repeating units.

According to Fryd's study, the presence of bridging groups such as -O- and -CO- within dianhydride units largely reduces their electron affinity, and therefore reduces the interchain interaction forces of the CTC present.

Assuming that Fryd's observations are correct, then, the T_g of polymers forming charge-transfer complexes (donor/acceptor pairs) will primarily be a function of the electron affinity of the acceptor.

The mechanism of bond cleavage also influences thermal stability [Thomas and Kendrick (1969)]. The thermal decomposition of a heat resistant polymer is very complex. Most aromatic heterocyclic polymers and polymers formed by step-growth polymerization undergo degradation via random scission along the chain , eliminating fragments that eventually break down further.

Zhu (1991), and Gloor et.al.(1992), have recently modelled the effects of chemically induced random scission on the molecular weight and molecular weight distribution of polyolefins. They found that due to the higher probability of larger polymer chains to undergoing scission, the molecular weight distribution, of broad MWD polymers, narrows considerably under controlled extent of scission. Moreover, even a small degree of chain cleavage serves to destroy the structural integrity and, consequently, affects the thermal behaviour of the polymer.

Molecular symmetry or stereo-regularity of the chemical structure arises when moieties are joined in the same position in each repeat unit. Williams and Flory (1969) show that the conformations accessible to a vinyl polymer chain $H-(CH_2CHR)_x-CH_3$, in which R is a large group such as C_6H_5 (i.e. polystyrene, poly(α-methylstyrene), etc), are severely limited by steric interactions. The effect of these non-bonded interactions on the conformations of the polymer chain depend on the stereochemical configurations of the succession of asymmetric centres CHR. The over-all stereochemical configuration of a vinyl polymer chain may be described by the sequence of meso (m) and racemic (r) dyads $-CHR-CH_2-CHR-$.

The chemical bonding in each polymer molecule comprised by a single, or mix of isomers is identical, apart from the geometrical differences. Then, from a thermodynamic point of view, the isomers differ from one another only through differences in the non-bonded interactions associated with the various conformations of each isomer. As a general rule, the presence of isomers in the same polymer chain lowers the T_g due to an increase in the number of rotational states.

Experimental evidence shows that isotactic, and syndiotactic conformations, with respect to the asymmetric groups, and cis conformations, with respect to the symmetric groups in the polymer chain, confer higher thermal stability than atactic and trans conformations, respectively, owing to the aforementioned stereo-chemical restrictions.

Yoon et.al.(1975), describe in detail the conformational characteristics of polystyrene. Figure 2.5, below, shows the stereochemical structure of the isotactic polystyrene chain in the all trans conformation.

Figure 2.5

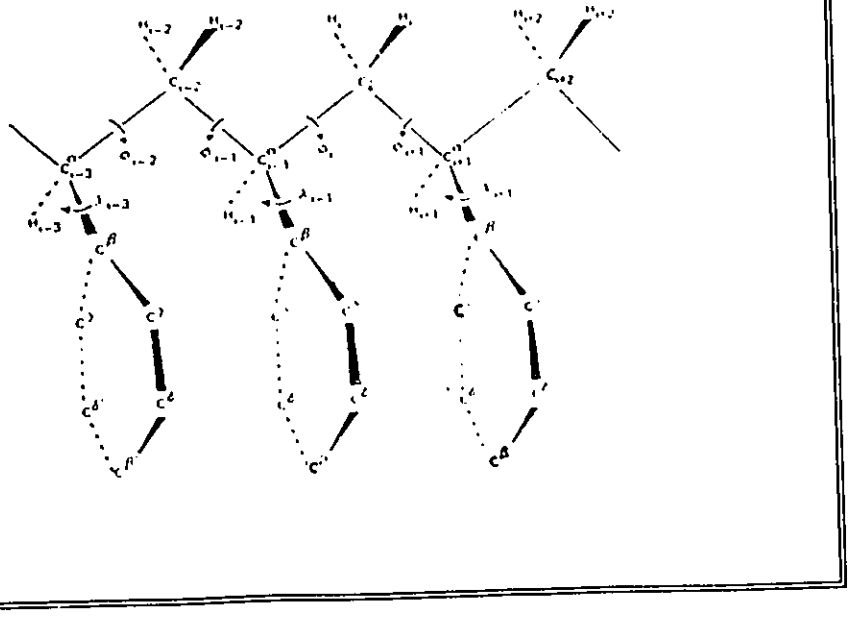

Figure 2.5. Portion of the isotactic polystyrene chain in the all-trans configuration. (From Joon et.al.(1975)).

In this figure, it can be seen that the phenyl substituent is confined to orientations such that its plane is approximately perpendicular to the plane defined by the skeletal bonds flanking the carbon C^{α} to which it is attached. Similar steric interactions affect the rotation χ of the phenyl group in each of the preferred conformations. Repulsions between one of the ortho CH groups of phenyl and one of the H atoms of the neighbouring CH_2 group, and between the ortho CH and an atom H or group pendent to the adjoining C^{α} are responsible for the limited rotation. The rotation, then, is confined to a range $\chi \pm 20°$, given by the bond angles. As a result, increased stiffness is conferred to the isotactic polystyrene chain and a higher T_g is expected in comparison to an atactic structure in which no such strong rotational restrictions exist.

The rigid intrachain structure refers to the position of the substituents in the aromatic or heterocyclic rings. Although para-oriented polymers have the highest thermal stability and T_g, they have the lowest solubility and processability. Allegra (1978), approaches the problem of polymer viscoelasticity by assessing the elasticity of the individual polymer chains upon different modes of motion. He shows that the configurational statistics of macromolecular chains define not only the elasticity of individual polymer chains but also the macroscopic elasticity observed.

The degree of crosslinking also affects the thermal behaviour of the polymer. Higher degree of crosslinking improves heat resistance primarily because, upon energy increase, more bonds must be cleaved in the same vicinity for the polymer to exhibit a change in its stereo-chemical conformation characteristics [Hergenrother (1991)]. Crystalline regions in a polymer serve as functional crosslinks imparting stiffness to the polymer chain by restricting the number of rotational states in a highly ordered system. Large amount of experimental evidence, mostly from the behaviour of polyolefins, seems to demonstrate that branching negatively affects thermal stability.

2.1.6 Polymers with High Heat Resistance

According to the polymer performance pyramid shown above in figure 1.1, and restricting the search to amorphous polymers, given the scope of this thesis, the highest heat resistant polymers are those comprised within the generic polyimides (PI), polyetherimides (PEI), and polyethersulfones (PES). On the basis of all that has been explained above on the factors governing the thermal behaviour of polymers, the structural characteristics of these compounds corroborate the requirements for heat resistance, and give the bases for the selection of monomers used in this thesis project, which will be explained below.

Polyimides are condensation polymers derived from bifunctional carboxylic acid anhydrides and primary diamines. They contain the imide structure -CO-NR-CO- as a linear or heterocyclic unit along the main chain of the polymer backbone:

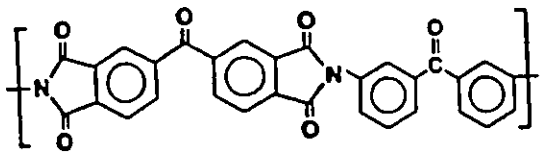

Aromatic, heterocyclic polyimides exhibit outstanding mechanical properties and an excellent thermal and oxidative stability, and currently are of major commercial and industrial importance. At present, these materials are widely used in place of metals and glass in high performance applications throughout the electrical, electronics, automotive, aerospace, and packaging industries.

Polyimides are considered specialty plastics because of their outstanding high performance engineering properties. As such, they are priced well above commodity polymers such as polyethylene and polystyrene [Verbicky Jr. (1991)].

As suggested by Fryd (1984), the strong interchain interactions caused by the formation of a donor/acceptor complex between dianhydride

and diamine groups is primarily responsible for the large T_g exhibited by these compounds. Depending on the particular substituents on both the dianhydride and the diamine units the T_g of these polymers varies within the range of 300 - 410°C, [Lee (1989)].

In the condensation of bisphenols with dinitrobisimides, through nucleophilic aromatic substitution, the polymer chains are generated by the formation of successive aromatic ether bonds. This mechanism is quite different from that of the condensation of polyimides, and the polymers derived from this synthesis route are known as polyetherimides.

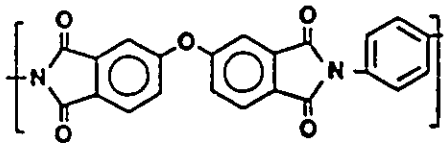

It has been stated above, that flexible units along the main polymer chain, such as ether -O- groups, increase the freedom of chain motion and, as a result, tend to lower the T_g. A lower T_g reduces the final use temperature as well as the temperature required for processing the polymer in the melt. In this regard, polyetherimides are unique, because they still show very high thermal stability, T_g in the range of 250 to 400 °C, with higher processability in conventional equipment than common polyimides [Lee (1989), Verbicky Jr. (1991)].

Polyethersulfones are high polymers containing sulfone groups and aromatic nuclei in the main polymer chain, connected by ether oxygens. Among these compounds those derived from dihydric phenols and 4,4'-dichlorodiphenylsulfone have achieved commercial application.

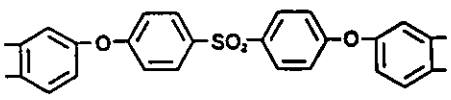

Polyethersulfones are clear, rigid tough thermoplastics with glass transition temperatures of 180-250°C. Chain rigidity is derived from the relatively inflexible and immobile phenyl and SO_2 groups, and toughness from the connecting ether oxygens. These groups also impart the thermal stability and chemical inertness that characterize these resins. In addition, the good thermal oxidative stability allows the usual range of thermoplastic processing operations in spite of the high melt temperatures encountered. These properties make possible continuous use in the 150-200°C range [Hergenrother (1991)].

2.1.7 Selection of Monomers for this Research

In the previous sections it has been implicitly shown that one of the most effective ways to increase the heat distortion temperature of styrenic polymers is by the addition of suitable comonomers which increase the backbone stiffness. For the past few years, the most common monomers employed to accomplish this have been maleic anhydride, α-methylstyrene, and maleimides [Priddy et.al.(1990)].

Based on this and all that has been previously detailed in this section (2.1), and considering the main objectives of this research along with the general constraints in suspension polymers design, explained in chapter 1, the monomers selected for suspension polystyrene modification to obtain high T_g copolymers are α-methylstyrene (AMS), and N-phenylmaleimide (NPMI).

α-Methylstyrene due to the methyl substituent in the α-carbon of the styrene molecule, upon polymerization, limits considerably the rotation of this carbon throughout the polymer chain, and consequently limits as well the rotation of the β-carbon, conferring stiffness to the polymer chain.

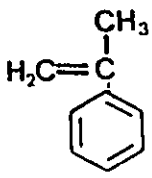

The T_g of pure, high molecular weight (M_n > 20,000), poly(α-methylstyrene) varies in the range of 170-180°C depending on the synthesis route and conditions [Malhotra et.al.(1978)]. The variation of T_g of poly(α-methylstyrene) with M_n seems to obey the following relationship:

$$T_{g(AMS)} = 453 - 3.1x10^5/M_n \qquad (°K)$$

As a result, T_g's in the range 100-180°C must be expected for the copolymer styrene-αmethylstyrene, depending on the copolymer composition and chain microstructure [Priddy et.al.(1990)]. This characteristic, makes the copolymer suitable, in principle, for suspension synthesis.

In spite of the difference in structure of N-phenylmaleimide with other imides used in condensation polymerization, described above, the possibility of using this compound in free radical polymerization, owing to its carbon-carbon double bond, makes it extremely attractive for polystyrene modification.

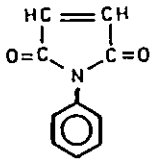

Two main features are worth noting from the NPMI structure: the first is the very restricted mobility of the aromatic group due to the proximity of the carbonyl, CO, groups, and the second is the completely hindered rotation of the carbons bearing the double bond, due to their attachment to the heterocyclic ring, upon polymerization. These structural features are responsible for the extremely high T_g exhibited by pure poly(N-phenylmaleimide) of 335-350°C depending on the synthesis route [Fles et.al. (1989)].

In addition, NPMI is a very strong electron acceptor which combined with the moderate donor effect of styrene allows the formation of charge-transfer (donor-acceptor) complexes (CTC) whose interchain interactions contribute positively to increase the T_g of the copolymer. Moreover, the strong tendency towards alternation, which will be described later, promoted by polymerization of donor-acceptor complexes along with the fact that NPMI does homopolymerize by free radical mechanisms allows one to obtain copolymers with T_g's in the range of 100-340°C depending on the copolymer composition and microstructure.

The above upper temperature limit, as explained in Chapter 1, is well beyond the capabilities of suspension syntheses. However, this suggests that only small amounts of NPMI used as comonomer with styrene are necessary to confer the copolymer with high thermal stability in the desired functional range for suspension synthesis. This possibility along with the fact that NPMI does not hydrolyses in water (as CTC forming maleic anhydride -MA- does) makes the system S-NPMI suitable for suspension synthesis.

Even though the T_g's expected for the free radical copolymers of AMS-NPMI are very high (180-340°C) for traditional suspension copolymerization, the synthesis of these heat resistant copolymers, along with the synthesis of the high T_g terpolymer of S-AMS-NPMI are also attempted in this research project to show the complete span of products that can be obtained from the monomers selected.

2.1.8 Selection of Bifunctional Initiators

Two complex problems, which bases will be explained in detail in the remainder of this chapter, arise in the free radical copolymerization of the proposed systems. The first one is related to the low ceiling temperature of α-methylstyrene, and the second one is related to the possible small concentration of N-phenylmaleimide in the comonomer mix, and consequently in the copolymer.

The solution of both of these problems, are attempted in this research through the use of bifunctional initiators which justifies their employment and selection.

The ceiling temperature of α-methylstyrene is only 61°C, above this temperature AMS does not homopolymerize [McCormick (1957)]. If free radical copolymerization of AMS with styrene is attempted above this temperature reversible propagation steps in the reactions involving this monomer will be present. As a result, lower copolymerization rates along with lower molecular weights will be obtained as the concentration of AMS increases in the copolymerization mix [O'Driscoll and Dickson (1968)].

In order to overcome this limitation, recently, low temperature emulsion or anionic solution polymerization processes have been preferably employed to obtain high T_g copolymers of AMS of high molecular weight. However, Malhotra et.al.(1978.b), have demonstrated that even S/AMS copolymers obtained through these routes are very susceptible to thermal degradation.

This thermal degradation process has been found to consist of two steps; first random thermal scission of the chains form shorter chain segments which then depolymerize into volatile products. It has also been found that long sequences of AMS units in the copolymer chains are more prone to undergo random scission than styrene sequences. This low thermal stability has made this copolymer, so far, not very attractive for commercial production.

It has been demonstrated that the use of bifunctional initiators allows one to simultaneously obtain high reaction rates and high molecular weights, which is not possible to achieve with traditional monofunctional initiation [Choi et.al. (1988), Villalobos (1989)]. Therefore, the use of bifunctional initiators in this copolymerization system must permit, in theory, one to obtain high copolymer of S-AMS at competitive rates.

In monofunctionally initiated batch free radical copolymerization in which the comonomer pair forms a donor-acceptor complex (CTC), such as in the S-NPMI case, if one of the comonomers is in low concentration, the

following succession of events will take place: 1) The CTC forms readily in the comonomer mix; 2) Since the CTC is generally more reactive than any of the monomers comprising it, the propagation reactions will consume rapidly the lower concentration monomer complexed in the CTC; 3) Once the low concentration monomer is depleted, or nearly depleted from the mix, the monomer in higher concentration will nearly homopolymerize until it is consumed. As a result a blend of alternating copolymer and homopolymer or copolymer of very low concentration of one comonomer is obtained, instead of the desired copolymer, with the consequent phase separation problems [Villalobos et.al.(1992)].

Traditionally, this problem is dealt with by carrying out a semicontinuous copolymerization, which allows one to obtain copolymer with the desired composition throughout the reaction coordinate, by the implementation of a suitable conversion dependent monomer feed policy [Hamielec et.al.(1987)].

Since, as stated above, batch operation is preferred in suspension processes owing to stability problems, the use of bifunctional initiators gives a novel alternative to overcome this problem.

Due to the sequential decomposition of the two peroxide groups in the bifunctional initiator a fraction of the polymer molecules formed in the early stages of the reaction will undergo a random number of re-initiation/propagation/termination cycles, throughout the conversion range, which allows the chemical binding of the alternating and low concentration copolymer or homopolymer, in multi-block structures [Villalobos et.al.(1992)]. This not only overcomes the phase separation problem, but also opens the possibility of combining the properties of the different blocks to confer the copolymer with high thermal and mechanical properties.

The comprehensive description and modelling of the mechanisms and phenomena involved in statistical and donor-acceptor free radical copolymerization with bifunctional initiators, constitutes the core and main theoretical contribution of this thesis, and is given in chapter 4.

In previous work Villalobos (1989) optimized the suspension polystyrene synthesis through bifunctional initiators. From the three different symmetric bifunctional initiators evaluated, two of them: 1,4-bis(terbutyl peroxycarbo)cyclohexane, and 1,1-di(terbutyl peroxy) cyclohexane, showed the best relationship between reaction rate and molecular weight in the upper temperature limit of the range of suspension operability.

Since this thesis deals with the modification of this optimized system, and since the use of bifunctional initiators has been justified, the same two bifunctional initiator types will be employed in this work. Their chemical structures are given below. The physical properties of these initiators can be found in Villalobos (1989).

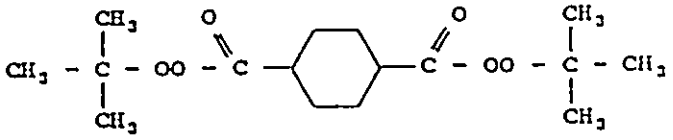

1,4-bis(terbutyl peroxycarbo)cyclohexane

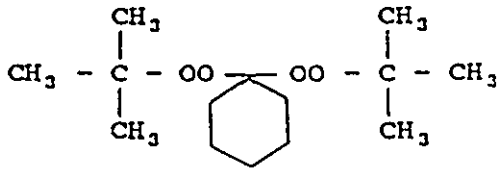

1,1-di(t-butyl peroxy)cyclohexane

2.2 Free Radical Copolymerization Kinetics

2.2.1 Models for Copolymerization Kinetics

Since the amount of work done to date in this field is enormous, the discussion presented in this section has been limited to the most outstanding work related to the development of the kinetic copolymerization theory for linear systems, including the two particular cases of copolymerization with depropagation, and donor-acceptor copolymerization, since only these kind of systems are considered within

the scope of this thesis. Recent and complete comprehensive studies on free radical copolymerization for non-linear systems can be found in Tobita (1990) and Zhu (1991).

The pioneering work of Alfrey and Goldfinger (1944), and Mayo and Lewis (1944), in developing a comprehensive kinetic theory for linear binary copolymerization led to what nowadays is known as the terminal model. The elementary set of reactions considered in this scheme may be written as:

Initiation

$$\begin{array}{lcccll} & & I & \rightarrow & 2R^{\bullet}_{in} & (K_{i1}) \\ R^{\bullet}_{in} & + & M_1 & \rightarrow & R^{\bullet}_{1,1} & (K_1) \\ R^{\bullet}_{in} & + & M_2 & \rightarrow & R^{\bullet}_{1,2} & (K_2) \end{array}$$

Propagation

$$\begin{array}{lcccll} R^{\bullet}_{r,1} & + & M_1 & \rightarrow & R^{\bullet}_{r+1,1} & (K_{11}) \\ R^{\bullet}_{r,1} & + & M_2 & \rightarrow & R^{\bullet}_{r+1,2} & (K_{12}) \\ R^{\bullet}_{r,2} & + & M_1 & \rightarrow & R^{\bullet}_{r+1,1} & (K_{21}) \\ R^{\bullet}_{r,2} & + & M_2 & \rightarrow & R^{\bullet}_{r+1,2} & (K_{22}) \end{array}$$

Termination

$$\begin{array}{lcclcll} R^{\bullet}_{r,1} & + & R^{\bullet}_{s,1} & \rightarrow & P_{r+s} \quad \text{or} \quad P_r + P_s & & (K_{t11}) \\ R^{\bullet}_{r,1} & + & R^{\bullet}_{s,2} & \rightarrow & P_{r+s} \quad \text{or} \quad P_r + P_s & & (K_{t12}) \\ R^{\bullet}_{r,2} & + & R^{\bullet}_{s,2} & \rightarrow & P_{r+s} \quad \text{or} \quad P_r + P_s & & (K_{t22}) \end{array}$$

A simple ratio between the kinetic equations for the consumption of monomer 1 (M_1), and monomer 2 (M_2), neglecting consumption through initiation reactions yields the first form of the instantaneous copolymer composition equation, as:

$$\frac{d[M_1]}{d[M_2]} = \frac{K_{11}[R^{\bullet}_{r,1}][M_1] + K_{21}[R^{\bullet}_{r,2}][M_1]}{K_{12}[R^{\bullet}_{r,1}][M_2] + K_{22}[R^{\bullet}_{r,2}][M_2]} \qquad (2.1)$$

Alfrey and Goldfinger (1944) defined the copolymerization reactivity ratios as $r_1=K_{11}/K_{12}$ and $r_2=K_{22}/K_{21}$. These parameters depend on the specific monomer pair used and their product gives information on the statistical microstructure in random copolymers.

The smaller the r_1r_2 product (i.e. $r_1 \to 0$, $r_2 \to 0$) the higher the tendency toward alternation of the M_1, M_2 units in the copolymer chain. When $r_1r_2 \to 1$ a more random distribution of the monomer units along the chain is obtained, and $r_1r_2 >> 1$ shows tendency towards the formation of large sequences or blocks of the same unit. In addition, it can be shown that in large random copolymer chains the number of M_1 units followed by M_2 units is statistically equal to the number of M_2 units followed by M_1 units. This suggests that $K_{12}[R_{r,1}][M_2] \approx K_{21}[R_{r,2}][M_1]$.

By introducing this equality into eq. (2.1) along with the reactivity ratios the so-called instantaneous copolymer composition equation is obtained as:

$$\frac{F_1}{F_2} = \frac{d[M_1]}{d[M_2]} = \frac{1 + r_1[M_1]/[M_2]}{1 + r_2[M_2]/[M_1]} \qquad (2.2)$$

Mayo and Lewis (1944), were amongst the earliest workers to clarify the relationship between copolymer and comonomer compositions. They defined F_i as the mole fraction of the ith component bound in the polymer and f_i as the mole fraction of the ith component in the comonomer mixture, thus, deriving the equation that relates the composition of the copolymer formed to the instantaneous composition of the feedstock and to the parameters r_1 and r_2, which characterize the specific system, as:

$$F_1 = \frac{r_1f_1^2 + f_1f_2}{r_1f_1^2 + 2f_1f_2 + r_2f_2^2} \qquad (2.3)$$

Equation 2.3 is commonly referred to as the Lewis-Mayo equation. Figure 2.6, below, shows the instantaneous copolymer composition as a function of the comonomer composition, for various values of r_1 and r_2. In this figure it can be noted that batch operation at any point of the given curves departing from the $F_1=f_1$ curve will cause the preferential consumption of the more reactive monomer over the less reactive, changing

the instantaneous composition of the feedstock, and consequently displacing the copolymer composition with conversion in the direction of the arrows.

This phenomenon is referred to as compositional drift, and is responsible for the complex mix of birth conversion dependent compositions of the copolymer chains comprising the final product. In turn, the extent of the compositional drift along with the monomer characteristics (i.e. structure, polarity, etc.) may be responsible for phase separation problems and poor mechanical properties of the product.

Figure 2.6

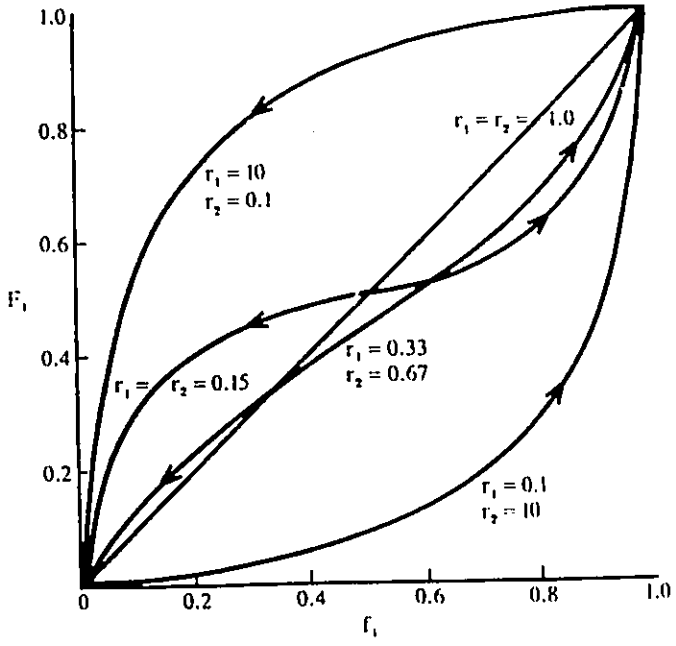

Figure 2.6. Instantaneous mol fraction of monomer units 1 in copolymer (F_1) and feedstock (f_1) for different values of the reactivity ratios r_1 and r_2. (From Hiemenz (1984)).

The points at which the instantaneous copolymer composition curve intercepts the $F_1=f_1$ curve are known as azeotropes, or azeotropic compositions. Operation at this points does not produce compositional drift because the feedstock composition does not change since the monomer are consumed at a rate proportional to their mol fraction in the mix. As shown in figure 2.6 not all comonomer pairs show an azeotropic composition. Also, the larger the differences in reactivity ratios the more pronounced the compositional drift observed.

Given the fact that the behaviour of several copolymer systems were not well explained by the terminal model, and being clear that the terminal model neglects the effect of the copolymer composition near the active chain end, a great deal of work was done in the 1960's to improve the existing theory.

Ham (1960), generalized Alfrey's penultimate effect extension to the copolymerization theory [Alfrey and Goldfinger (1944.b)], to account for penultimate and further chain end composition effects. He established that for the condition in copolymerization where $r_1 = K_{1111}/K_{1112}$ differed substantially from $r_1' = K_{2111}/K_{2112}$ the copolymer composition equation is given by:

$$n - 1 = \frac{[r_1"x(r_1'x + 1)/(r_1"x + 1)](r_1x + 1)}{[r_1"x(r_1'x + 1)/(r_1"x + 1)] + 1} \qquad (2.4)$$

where (n-1) is the ratio F_1/F_2, $x=f_1/f_2$, and $r_1"=K_{211}/K_{212}$.

Through proper manipulation of eq. (2.4) ultimate, penultimate, and third last unit effects may be accounted for in the model.

Even though, as in Ham's model, many compositional effects can be considered, and the respective models elaborated by the inclusion of the proper set of elementary reactions, a problem arises for the evaluation of the rate constants employed in these models. This is due to the impossibility in practice to distinguish between the different reactions involved for a single radical type (i.e. R_{1111} vs R_{2111}, etc).

The solution of such models, therefore, becomes a numerical or statistical problem, which the large number of parameters amplifies. The physical meaning of the values obtained for such parameters, however, is often unclear.

As a very good contribution to copolymerization theory, Meyer and Lowry (1965) derived the equation relating comonomer composition to monomer conversion, by integrating the Lewis-Mayo equation for isothermal synthesis, as:

$$X = 1 - (f_1/f_{10})^{\alpha} [(1-f_1)/(1-f_{10})]^{\beta} [(f_{10}-\delta)/(f_1-\delta)]^{\gamma} \qquad (2.5)$$

where: $\alpha = r_2/(1-r_2)$; $\beta = r_1/(1-r_1)$; $\gamma = [(1-r_1r_2)/((1-r_1)(1-r_2))]$; and $\delta = [(1-r_2)/(2-r_1-r_2)]$.

The simultaneous solution of eqs. (2.3) and (2.5) permits the calculation of the compositional drift path of a given copolymer system when the initial feedstock composition (f_{10}) and the reactivity ratios are known.

Different refinements of the copolymerization theory were introduced earlier on to solve the troublesome aspect of the reactivity ratios on the fact that they needed to be determined and reported as a pair. The ideal case of specifying one or two general parameters for each monomer which would correctly represent its contribution to all reactivity ratios was approached by Price and Alfrey (1947). Based on polarity and resonance considerations the Price-Alfrey approach begins by defining three parameters -P, Q, and e- for each of the comonomers in a reaction system. Since, as shown below, the parameter P is eliminated from the theory, the Price-Alfrey system is known as the Q-e scheme for copolymerization.

For the reaction of radical i with monomer j, Price and alfrey assume that the cross-propagation rate constant can be expressed as:

$$K_{ij} = P_iQ_j\exp(-e_ie_j) \qquad (2.6)$$

In this equation P and Q are parameters that describe the reactivity of the radical and monomer of the designated species, and the values of e measure the polarity of the two components without distinguishing between monomer and radical. With this, the definition of the reactivity ratios can be written as:

$$r_1 = (Q_1/Q_2)\exp[-e_1(e_1-e_2)]; \quad \text{and} \quad r_2 = (Q_2/Q_1)\exp[-e_2(e_2-e_1)]$$

And combining the above expressions:

$$r_1 r_2 = \exp[-(e_1-e_2)^2] \tag{2.7}$$

The main advantage of this scheme is that each monomer is characterized by its own values for Q and e, which are assumed to be independent of the nature of the comonomer. Thus, if Q and e values were available for all monomers, this could be combined to generate the parameters r_1 and r_2 for any comonomer pair, which define copolymer composition and microstructure. Values of Q and e for a large number of monomers may be found in Price (1962), and Ham (1964). It should be pointed out here that the Q-e scheme is only semi-quantitative in its success. However it is very useful in providing some orientation to a new system before carrying out an experimental investigation.

Odian (1981) summarizes further developments of the linear copolymerization theory, including the development of the terpolymerization equations, and the sequence length probability equations to estimate the microstructural features of copolymer systems [Mayo and Lewis (1944), Ring (1967)].

The most substantial advances in recent years on the binary and multi-component linear copolymerization kinetics were brought about by the development of the pseudo-kinetic rate constant method, which reduces the treatment of the copolymerization equations to that for homopolymerization [Hamielec and MacGregor (1983), Hamielec et.al. (1987)].

This method considers a general and complete elementary reaction scheme, given below, based on the terminal model, and it is applicable whenever the terminal model is valid and the number-average chain length is larger than a few hundred [Tobita (1990)].

Initiation

$$\begin{array}{lcll} & I & \rightarrow & 2R^{\bullet}_{in} \quad (K_d) \\ R^{\bullet}_{in} + & M_1 & \rightarrow & R^{\bullet}_{1,1} \quad (K_i) \\ R^{\bullet}_{in} + & M_2 & \rightarrow & R^{\bullet}_{1,2} \quad (K_i) \end{array}$$

Propagation

$$\begin{array}{llcll} R^{\bullet}_{r,1} + & M_1 & \rightarrow & R^{\bullet}_{r+1,1} & (K_{11}) \\ R^{\bullet}_{r,1} + & M_2 & \rightarrow & R^{\bullet}_{r+1,2} & (K_{12}) \\ R^{\bullet}_{r,2} + & M_1 & \rightarrow & R^{\bullet}_{r+1,1} & (K_{21}) \\ R^{\bullet}_{r,2} + & M_2 & \rightarrow & R^{\bullet}_{r+1,2} & (K_{22}) \end{array}$$

Termination by Combination

$$\begin{array}{llcll} R^{\bullet}_{r,1} + & R^{\bullet}_{s,1} & \rightarrow & P_{r+s} & (K_{tc11}) \\ R^{\bullet}_{r,1} + & R^{\bullet}_{s,2} & \rightarrow & P_{r+s} & (K_{tc12}) \\ R^{\bullet}_{r,2} + & R^{\bullet}_{s,2} & \rightarrow & P_{r+s} & (K_{tc22}) \end{array}$$

Termination by Disproportionation

$$\begin{array}{llcllll} R^{\bullet}_{r,1} + & R^{\bullet}_{s,1} & \rightarrow & P_r + & P_s & (K_{td11}) \\ R^{\bullet}_{r,1} + & R^{\bullet}_{s,2} & \rightarrow & P_r + & P_s & (K_{td12}) \\ R^{\bullet}_{r,2} + & R^{\bullet}_{s,2} & \rightarrow & P_r + & P_s & (K_{td22}) \end{array}$$

Transfer to Monomer

$$\begin{array}{llcllll} R^{\bullet}_{r,1} + & M_1 & \rightarrow & P_r + & R^{\bullet}_{1,1} & (K_{fm11}) \\ R^{\bullet}_{r,1} + & M_2 & \rightarrow & P_r + & R^{\bullet}_{1,2} & (K_{fm12}) \\ R^{\bullet}_{r,2} + & M_1 & \rightarrow & P_r + & R^{\bullet}_{1,1} & (K_{fm21}) \\ R^{\bullet}_{r,2} + & M_2 & \rightarrow & P_r + & R^{\bullet}_{1,2} & (K_{fm22}) \end{array}$$

Transfer to Small Molecule

$$\begin{array}{llcllll} R^{\bullet}_{r,1} + & T & \rightarrow & P_r + & T^{\bullet} & (K_{fT1}) \\ R^{\bullet}_{r,2} + & T & \rightarrow & P_r + & T^{\bullet} & (K_{fT2}) \end{array}$$

Based on the pseudo-kinetic rate constant method and the above reaction scheme, the propagation rate for polymerization, given by:

$$R_p = K_p[M][R^\bullet] \tag{2.8}$$

will be applicable to binary copolymerization if the propagation rate constant K_p is defined as:

$$K_p = (K_{11}f_1 + K_{12}f_2)\Phi_1 + (K_{21}f_1 + K_{22}f_2)\Phi_2 \tag{2.9a}$$

or extending the concept to multicomponent polymerization, by:

$$K_p = \Sigma K_{ij}\Phi_i f_j \qquad (i,j=1 \text{ to } N) \tag{2.9b}$$

where $f_i=[M_i]/[M]$, $[M]=\Sigma[M_i]$, $\Phi_i=[R_i]/[R^\circ]$, $[R_i]=\Sigma[R_{r,i}]$ $(r\geq 1)$, $[R^\circ]=\Sigma[R_i]$, and N=number of components.

The same concept applies to termination and transfer rate equations if the pseudo-kinetic rate constants are defined as:

Combination:

$$K_{tc} = \Sigma K_{tcij}\Phi_i\Phi_j \tag{2.10}$$

Disproportionation:

$$K_{td} = \Sigma K_{tdij}\Phi_i\Phi_j \tag{2.11}$$

Transfer to monomer:

$$K_{fm} = \Sigma K_{fij}\Phi_i f_j \tag{2.12}$$

Transfer to small molecule:

$$K_{fT} = \Sigma K_{fTi}\Phi_i \tag{2.13}$$

By defining these pseudo-kinetic rate constants, the set of equations obtained through the mass balances for each copolymer species, may be solved to compute conversion history, average molecular weights and copolymer composition, with the same degree of difficulty as the solution for the homopolymerization equations [Tobita (1990)]. Recently, Tobita and Hamielec (1991) have defined valid pseudo kinetic rate constants for the penultimate model.

2.2.2 Copolymerization with Depropagation

Dainton and Ivin (1948), found that certain polymerization reactions, such as the homopolymerization of α-methylstyrene (AMS), do not occur above a temperature known as the ceiling temperature (T_c). The ceiling temperature phenomenon is due to a reversal of the propagation reaction (i.e. depropagation). Thus, for any polymerization in which the propagation step is:

$$R_i^{\bullet} + M \leftrightarrow R_{i+1}^{\bullet} \qquad (K_p, K_{dp})$$

there is a T_c above which the rate of depropagation is greater than the rate of propagation and therefore above which reaction will not proceed.

From both kinetic and equilibrium thermodynamic principles T_c was defined as:

$$T_c = \Delta H/(\Delta S^{\circ} + R \ln[m]) \qquad (2.14)$$

where ΔH and ΔS° are the heat and standard entropy of polymerization, respectively, and [m] is the monomer equilibrium concentration.
For most monomers, however, this temperature is higher than their decomposition temperature. As a result no depropagation is observed upon polymerization of such monomers, even at temperatures approaching decomposition.

McCormick (1957) through anionic solution polymerization of α-methylstyrene in tetrahydrofuran, measured the monomer equilibrium concentration as a function of the initial monomer concentration and established that the ceiling temperature is dependent only upon the monomer concentration while the rate of depropagation is not. He also found that for α-methylstyrene the ceiling temperature is 61°C. By fitting his data to Dainton and Ivin's relationship he found that for AMS monomer ΔH_p=-6.96 Kcal/mol, and $\Delta S_p°$=-24.8 cal/mol-K.

Following basically the same procedure, Worsfold and Bywater (1957) arrived at the values ΔH_p=-8.02 Kcal/mol, and $\Delta S_p°$=-28.75 cal/mol-K for the same AMS monomer.

Ham (1960,b), expanded the copolymerization theory for systems involving α-methylstyrene. He gave mathematical evidence that copolymers containing in excess of about 75 mole-% α-methylstyrene cannot be obtained due to inability of AMS to add to a sequence of three AMS units. As a result in eq. (2.4) above r_1=0 (i.e. K_{1111}=0) and the instantaneous copolymer composition equation becomes:

$$n - 1 = \frac{r_1^{*}x(2r_1'x + 1)}{(r_1^{*}x + 1)(r_1'x + 1)} \qquad (2.15)$$

The system α-methylstyrene/acrylonitrile follows this equation when $r_1' = K_{2111}/K_{2112} = 0.04$, and $r_1^{*} = K_{211}/K_{212} = 0.13$. Recall $n-1=F_1/F_2$, and $x=f_1/f_2$.

Ivin and Spensley (1967) established that monomer showing the greatest tendency toward reversible propagation are those with the lowest heats of polymerization (0-10 Kcal/mol). They showed that for α-methylstyrene the low heat of polymerization is the result of the steric strain in the polymer chains. They found that for the cationic bulk polymerization of AMS-S at -20°C, the reactivity ratios are $r_1 = 0.14\pm0.06$ and $r_2 = 10.1\pm1.5$, which demonstrates the low probability of formation of dyads and triads of AMS units, even at very low temperatures.

O'Driscoll and Gasparro (1967) showed that Lowry's case II copolymerization treatment, which considers the penultimate effect for the propagation reaction, describes better the free radical copolymerization kinetics of styrene/α-methylstyrene, below and above the T_c of AMS, than Ham's model. Lowry's case I, assumes that both the sequences $-M_1M_2M_2^\circ$ and $-M_2M_2M_2^\circ$ may depropagate, whereas Lowry's case II assumes that only $-M_2M_2M_2^\circ$ sequences are subject to reversible propagation steps [Lowry (1960)].

In Lowry's case II , the thermodynamic reversible nature of the propagation reaction is considered, and an implicit allowance for the influence of temperature variation on copolymer composition may be derived as:

$$\frac{m_2}{m_1} = \frac{\beta\gamma - 1 + [1/(1-\beta)]^2}{((r_1[M_1]/[M_2]) + 1)\,(\beta\gamma + [\beta/(1-\beta)])} \qquad (2.16)$$

Here:

$$\beta = (1+K[M_2]+K[M_1]/r_2) - (1+K[M_2]+(K/r_2)[M_1]^2 - 4K[M_2])^{1/2}/2 \qquad (2.17)$$

and

$$\gamma = (K[M_2] + (K/r_2)[M_1] - \beta)/(K[M_2]) \qquad (2.18)$$

Thus, the solution of these equations require exclusively the knowledge of the two usual reactivity ratios r_1 and r_2, and the equilibrium constant (K) for the reaction:

$$-M_2\text{-}M_2^\bullet + M_2 \leftrightarrow -M_2\text{-}M_2\text{-}M_2^\bullet \qquad (K)$$

which can be calculated from equilibrium monomer concentration experiments or from heat and entropy of polymerization data, according to eq.(2.14), above.

From these equations, O'Driscoll and Gasparro's experimental data for the variation of the copolymer composition with monomer feed of the S/AMS system was accurately fit, for a range of polymerization temperatures varying between 0-100°C. They obtained values of $r_1 = 1.3$, $r_2 = 0.3$, and K = 1.32, 0.095, and 0.015 at 0, 60, and 100°C, respectively.

Figure 2.7, below, shows their results for instantaneous copolymer composition at different temperatures. Note how the copolymer composition for a given comonomer mix seems to be independent of the polymerization temperature for most of the composition range, inasmuch as the reactivity ratios do not change sensibly over these temperatures.

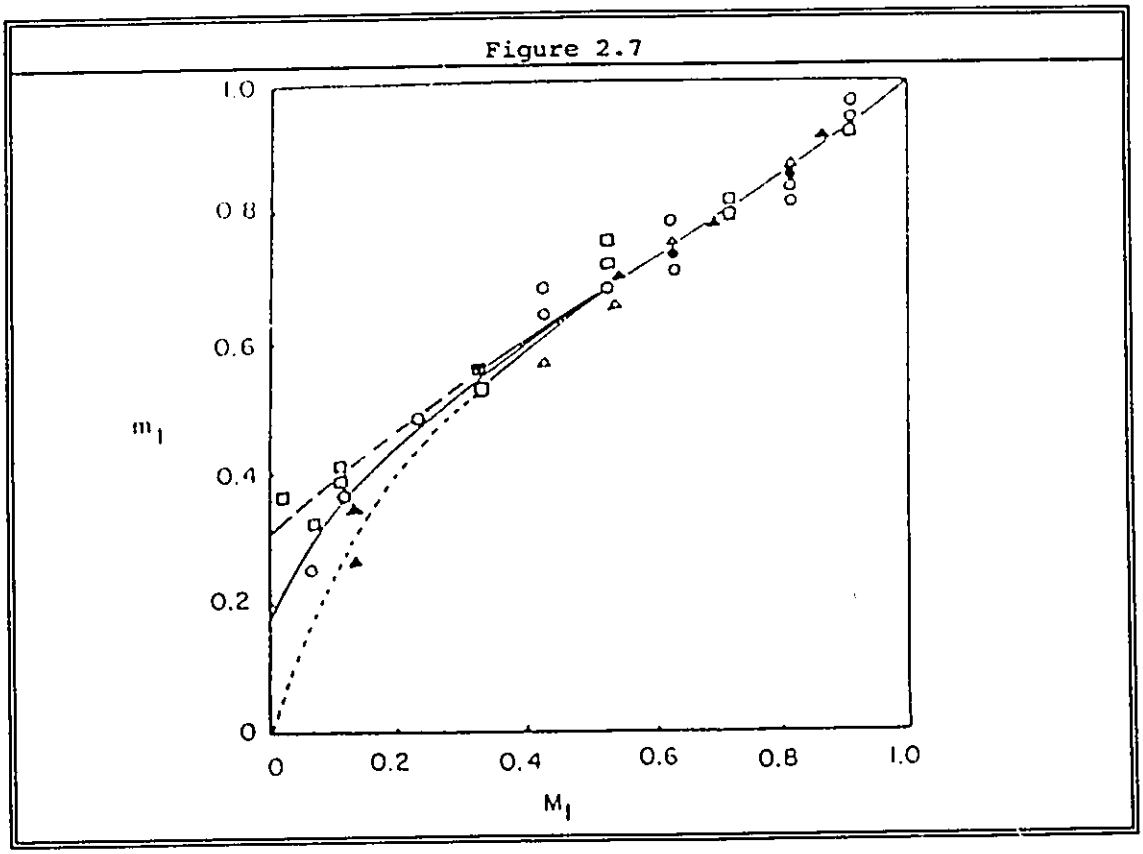

Figure 2.7. Variation of copolymer composition with monomer feed for the system S/AMS (M_1/M_2). Experimental points at 0, 60 and 100°C (○, △, □). Solution of eqs. (2.16) - (2.18) at 0 (···); 60 (——); and 100°C (---). (From O'Driscoll and Gasparro (1967)).

The strong retarding effect in the copolymerization of S/AMS, brought about by the reversible propagation steps of the reactions involving dyads of AMS, was studied by O'Driscoll and Dickson (1968). They derived a quantitative expression to account for the difference in reaction rate of pure styrene polymerization relative to the copolymerization rate with AMS, as:

$$R_{p(rel)} = \frac{K_{21}[M_1]\left(\left(r_1/[M_2]\right)[M_1]\left(\gamma+\left(1/1-\beta\right)\right)+2\gamma+\left(\left(3-2\beta\right)/\left(1-\beta\right)^2\right)\right)}{K_{11}[M_1]_{bulk}\left(A'^2+\left(K_{t12}/K_{t11}\right)A'B'+\left(K_{t22}/K_{t11}\right)B'^2\right)^{1/2}} \qquad (2.19)$$

Here: $\beta=[(m_2)_{n+1}]/[(m_2)_n]$, $\gamma=[(m_2)_1]/[(m_2)_2]$, or in general $[(m_1)_n]$ are the concentration of growing chains ending with n units of comonomer i, and $A'=(K_{21}[M_1]/K_{12}[M_2])(\gamma+1/(1-\beta))+(\beta^2/(1-\beta))$, $B'=(1+\beta+\gamma)$ account for the relative contribution of growing radicals of different length to the termination rate. Knowing the two homopolymerization rate constants and the reactivity ratios (given above) eq. (2.19) was fit to experimental data, using β and γ as parameters, and assuming $K_{t11} = 10^7$, $K_{t22} = 10^{10}$, K_{t12} as a weighed function of the previous two, and the ratio $K_{21}/K_{12} = 3$ based on orbital theory considerations. The best fit solution compared with experimental data is shown below in figure 2.8.

Figure 2.8

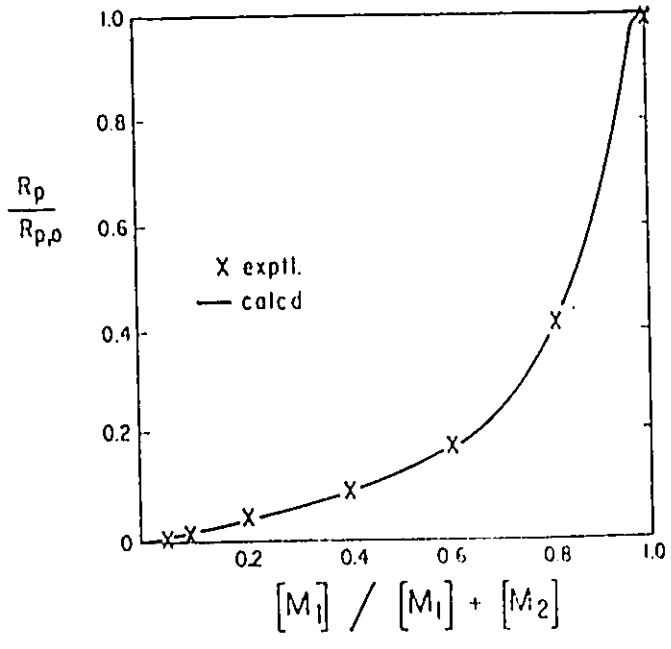

Figure 2.8. Rate of copolymerization (R_p) of S/AMS (M_1/M_2) relative to the styrene homopolymerization rate ($R_{p,0}$). (From O'Driscoll and Dickson (1968)).

The main conclusions of the results obtained through the solution of eq. (2.19) are that for pure AMS initiated polymerization near the ceiling temperature produces mostly low molecular weight free radicals (mainly dimers and trimers), which rapidly diffuse together and terminate, forming oligomers. When styrene is added, some radical chains may grow to higher molecular weight and produce polymer, however, in addition to the retarding effect created by the AMS reversible propagation reactions, low molecular weight copolymer should be expected.

Baldwin and Reed (1968) demonstrated that all the compounds from a series of substituted α-methylstyrenes of the general form $CH_2=C(C_6H_5)-CH_2-Y$ (with Y=H, OH, $O-CH_3$, and $O-CO-CH_3$) were inactive in homopolymerization at 60°C, but copolymerized with styrene with a retarding effect. They attribute the retarding effect of these compounds to the low energy of the radicals ending in AMS units. They claim that resonance effects associated with the phenyl group and steric hindrance caused by the two bulky substituents of the α-carbon bearing the free radical, are chiefly responsible for the low rate of addition of another monomer unit to the propagating chain. They concluded that since these monomers do not undergo homopolymerization under free radical initiation, radicals of substituted AMS do not add to a monomer molecule of the same type (i.e. $K_{22}=0$)

Johnston and Rudin (1971) compiled a set of previously reported reactivity ratios for S/AMS, obtained from experimental data using several estimation methods all of them based on terminal model equations. From these values they computed the joint 95% confidence limits of r_1, r_2 at different temperatures, using non-linear least squares. At 60°C values of $r_1=1.124$ and $r_2=0.627$, and at 90°C values of $r_1=.788$ and $r_2=0.297$ were obtained.

More importantly, based on model fits for the system styrene/α-methylstyrene they concluded that the conventional copolymer equation predicts copolymer composition more accurately than models which assume reversible polymerization of AMS.

The best fit to the Lowry's case II produced r_1=0.50 and r_2=1.25, but the mean deviations between experimental and predicted copolymer compositions are much larger than for the terminal model. Moreover, even with the refinements introduced by Lowry's case I, no reductions in the mean deviations were achieved. Therefore, the system S/AMS may be well represented by the terminal model which reduces the number of constants to be evaluated and avoids the calculation of the equilibrium constant for the reversible propagation steps.

Kang et.al.(1972) derived a method for calculating instantaneous copolymer composition for a multi-component system with reversibility of the propagation steps. Based on a probability approach using the terminal model and allowing for reversibility of all M_iM_j diads (referred to as diad model) they successfully predicted the copolymer composition for the system acrylonitrile/methyl methacrylate/α-methylstyrene employing a large number of parameters and assumptions.

Fischer (1972) was amongst the first researchers in attempting free radical copolymerization of styrene/α-methylstyrene above the ceiling temperature of AMS. In bulk copolymerization initiated with AIBN in the range of 60 to 150°C he corroborated that the amount of AMS bound in the copolymer is a weak function of the polymerization temperature. However, in disagreement with O'Driscoll and Gasparro's results, he found that the reactivity ratios, specially that for AMS, vary considerably with temperature. In addition, he found substantially different values for the equilibrium constant of the reversible propagation step based on the terminal model with depropagation of the diads of AMS from which he modified the Mayo-Lewis equation of instantaneous copolymer composition.

Some useful data for the present project is given in his list of rate constants for this system, at different temperatures between 90 and 150°C. Figure 2.9, below, summarizes the most remarkable results of Fischer's model for S/AMS copolymer composition. Note in this figure that K_{11} is equivalent to 1/K in O'Driscoll's model.

Figure 2.9

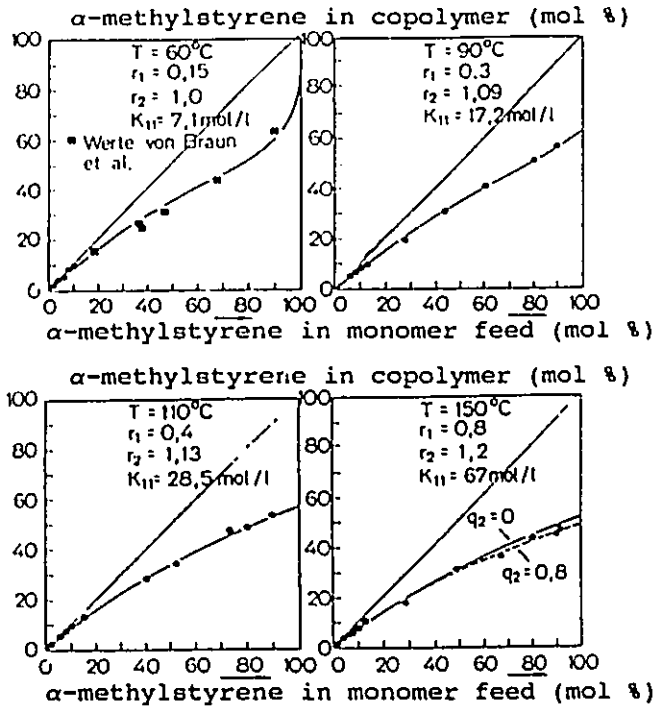

Figure 2.9. Instantaneous copolymer composition in AMS/S (M_1/M_2) copolymerization above T_c. (From Fischer (1972)).

Free radical copolymerization of styrene/α-methylstyrene in toluene and dimethyl phthalate solutions at 60°C was studied in detail by Rudin and Chiang (1974). Based on the observation that the polymerization rate is proportional to the square root of the solution viscosity, $\eta^{1/2}$, for fixed [M] and [I], they derived an expression for the copolymerization rate relative to the homopolymerization rate of pure styrene, as:

$$\frac{R_{p0}}{R_{p1}} = \frac{[I]_0^{1/2} K_{11} [M_1] \{ (r_1[M_1]/K_{11}) + (r_2[M_2]/K_{22}) \}_1 (K_{t0})^{1/2} (\eta_0)^{1/2}}{[I]_1^{1/2} (K_{t11})^{1/2} (r_1[M_1]^2 + 2[M_1][M_2] + r_2[M_2]^2)_1 (\eta_1)^{1/2}} \qquad (2.20)$$

Where the subscript 0 refers to the homopolymerizing system in which the monomer concentration is $[M_1]$, and the subscript i refers to the copolymerizing system in which the monomer concentrations are $[M_1]$ and $[M_2]$. Note that $[M_1]_0$ may be different from $[M_1]_i$. The values of the rate constants and parameters found were r_1=1.12, r_2=0.63, K_{11}=176 mol/L-sec, K_{22}=26 mol/L-sec, for polystyrene $K_p/K_t^{1/2}$=0.034 from which K_{t11}=2.7 x 10^7 mol/L-sec.

The molecular weight distribution of poly(α-methylstyrene) polymerized through anionic polymerization below T_c, using potassium as initiator, has been studied at length when different solvents are used in the polymerization. These solvents include tetrahydrofuran (THF) [Leonard and Malhotra (1976) and (1977)], p-dioxane [Malhotra and Leonard (1977)], and cyclohexane [Malhotra et.al.(1977)].

In tetrahydrofuran, the gel permeation chromatography (GPC) distributions of these polymers were found to be multimodal, yielding four components with a number average degree of polymerization, DP, of about 4, 16, 250, and 1000. The authors speculate around the idea that these multimodal distributions are a result of dead and temporarily dead (refer to as dormant) polymers formed by combination with polymers due to the formation of different, more stable, ion pairs. This idea is in opposition to the general belief that bimodal distributions are observed in this type of polymerization due to the existence of monofunctional and bifunctional living ends.

When p-dioxan was used as a solvent, bimodal and trimodal distributions were observed with peaks within the same range of those mentioned above. Polymerization of AMS in cyclohexane showed much slower rates than the former. Nevertheless, the GPC analyses of these polymers showed as well multimodal distributions which peaks could be split into similar components to those found when THF and p-dioxan were used as solvents, in spite of their different dielectric constants. These observations, indirectly corroborate their idea of a solvent-separated ion-pair termination mechanism.

Figure 2.10, below, shows the GPC chromatograms obtained for some of the aforementioned polymers. In this figure, the similar characteristics of the molecular weight distributions obtained at same conditions, regardless the solvent employed, can be seen.

Figure 2.10

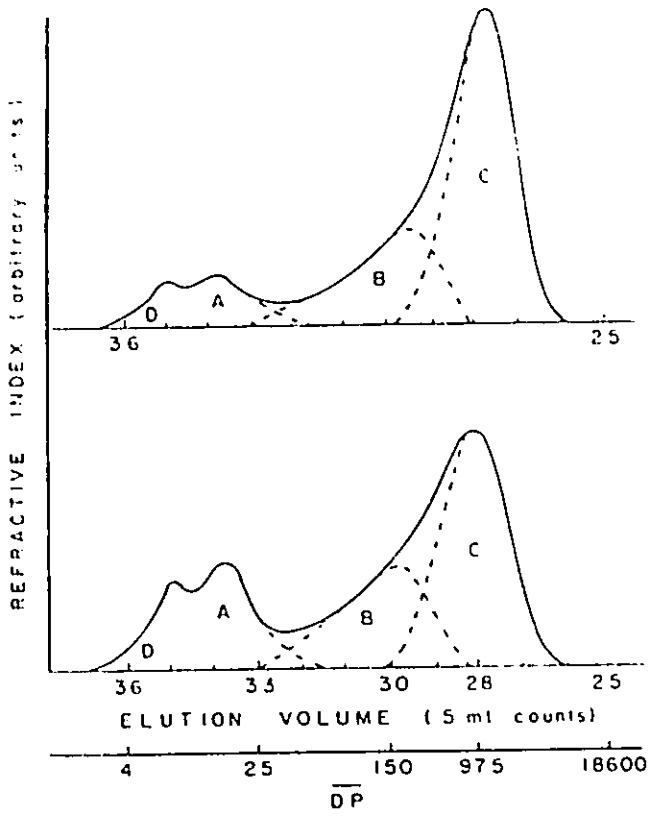

Figure 2.10. GPC molecular weight distributions of poly(α-methylstyrene) initiated with potassium at 25°C from a 4.5 M solution in (a) THF; and (b) p-dioxane. (From Leonard and Malhotra (1977)).

Malhotra (1978), characterized many of the poly(α-methylstyrene) products obtained under the conditions described above, via infrared spectroscopy (IR) and proton nuclear magnetic resonance (H-NMR). Some of his IR and H-NMR spectra can be seen below in figure 2.11, along with the H-NMR spectrum of the copolymer S/AMS reported by O'Driscoll and Gasparro

(1967). References to these spectra will be made in Chapters 5 to 8 of this thesis for the interpretation of the spectra obtained in the corresponding studies.

Figure 2.11

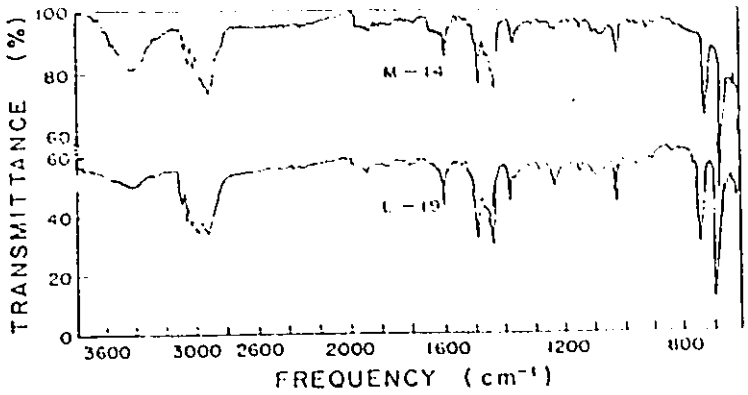

(a)

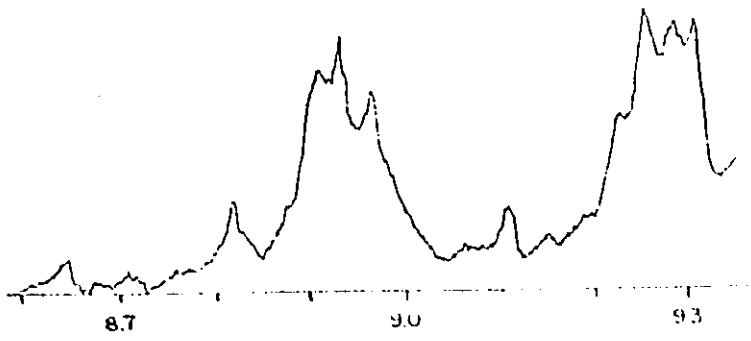

(b)

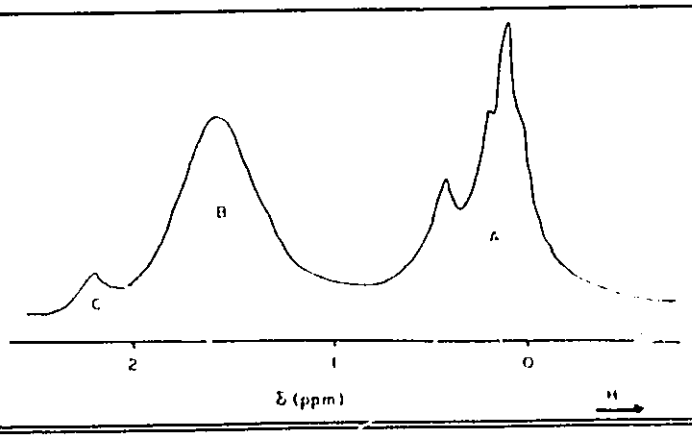

(c)

Figure 2.11. (a) IR spectra of two samples of poly-AMS; (b) H-NMR spectrum of low *MW* poly-AMS; and (c) H-NMR spectrum of S/AMS copolymer (F_2~70%). (a, b From Malhotra (1978), c from O'Driscoll and Gasparro (1967)).

Recently, Priddy et.al.(1990) have reported an experimental investigation on the synthesis of heat resistant S/AMS copolymers through anionic continuous polymerization at 100°C, using n-butyl lithium as initiator. They found that by keeping a high concentration of AMS relative to styrene in the continuous feed, higher amounts of AMS were bound in the copolymer than those obtained through batch copolymerization. The T_g of the copolymers obtained at different S/AMS ratios were established by DSC and the copolymer compositions were determined through gas chromatography (GC) of the residual comonomer mix.

The S/AMS copolymers thus synthesized showed T_g's that may be well approximated by Fox's model (see 2.1.4, above). Figure 2.12, below, shows the T_g vs copolymer composition plot, for this system.

Figure 2.12

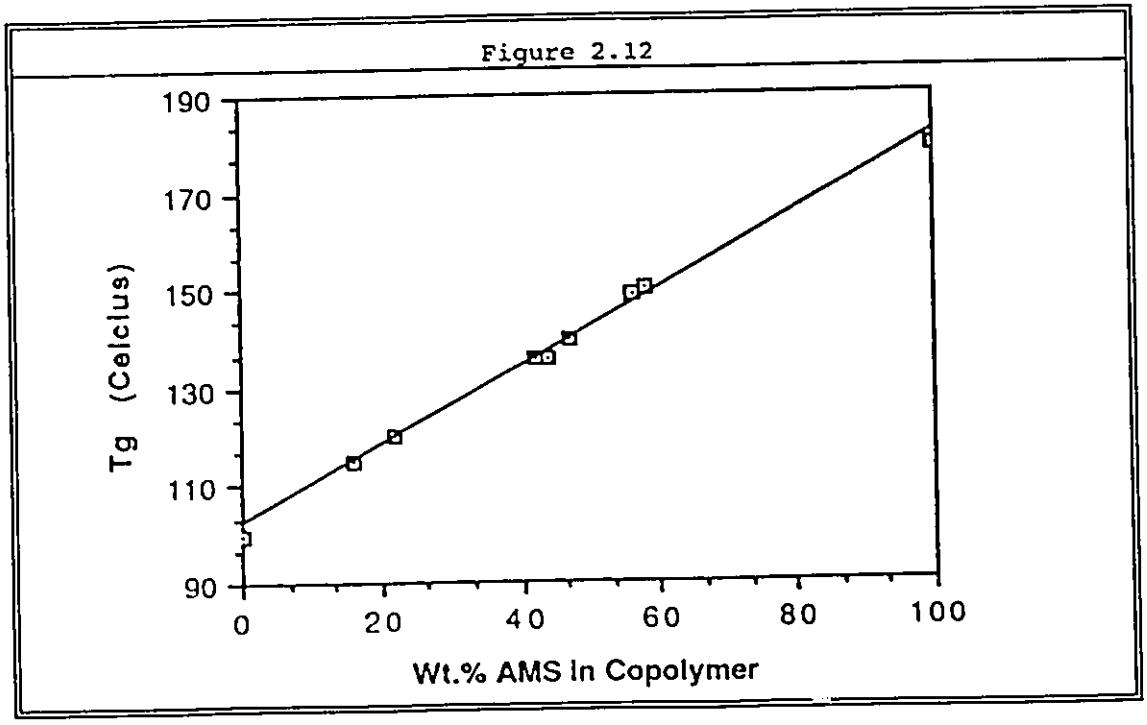

Figure 2.12. Glas transition temperature of S/AMS copolymers, made through anionic polymerization, vs wt % of AMS in copolymer. (From Priddy et.al.(1990)).

It is important to point out here that even with this technique, the maximum amount of AMS bound in the copolymer, could not exceed 66.7 mol% (69.04 wt%).

More important even is the finding that the main mechanism of thermal degradation of S/AMS copolymers is depolymerization rather than chain scission which is the dominant mechanism in PS degradation. This is evidenced through the fact that the relative rate of styrene monomer generation for free radical polystyrene (FRPS), anionic polystyrene (APS), and anionic styrene/α-methylstyrene (SAMS -50 wt% AMS-) followed the order SAMS > FRPS > APS, whereas the relative rate of loss of molecular weight for the three polymers was FRPS > APS > SAMS.

2.2.3 Donor-Acceptor Polymerization.

Since the late 1940's, several comonomer pairs, such as styrene (S) maleic anhydride(MA), were regarded as typical systems yielding alternating copolymers upon free radical copolymerization. Ever since, several propagation mechanisms incorporating the alternate tendency have been proposed.

Generally speaking these mechanisms may be classified into three types:

1) Complex mechanisms that imply the homopolymerization of molecular complexes (or charge transfer complexes, CTC) between electron donor and electron acceptor monomers [Bartlett and Nozaki (1946)].

2) Mechanisms in which electrostatic interactions between different polarized monomers and radicals decrease the activation energy for the alternating chain propagation [Price and Alfrey (1946)].

3) Mechanisms in which the resonance stabilization of the CTC between the radicals and monomers formed in the transition state promote the alternating copolymerization [Walling et.al. (1948)].

In spite of a great deal of experimental work in this field during the 1950's and 60's, it was not until the 1970's that the existence and propagation mechanism of the donor-acceptor complex (CTC), in alternating copolymerization were established.

Tsuchida and Tomono (1971), studied the copolymerization of styrene (donor) and maleic anhydride (acceptor) in different solvents. They detected the existence of a CTC and quantified its equilibrium constant by studying the ultra-violet and visible light (UV), and nuclear magnetic resonance (NMR) spectra, of the polymerizing system. Although they referred to them as initiation reactions with no distinction of the radical R•, they proposed the following four propagation reactions:

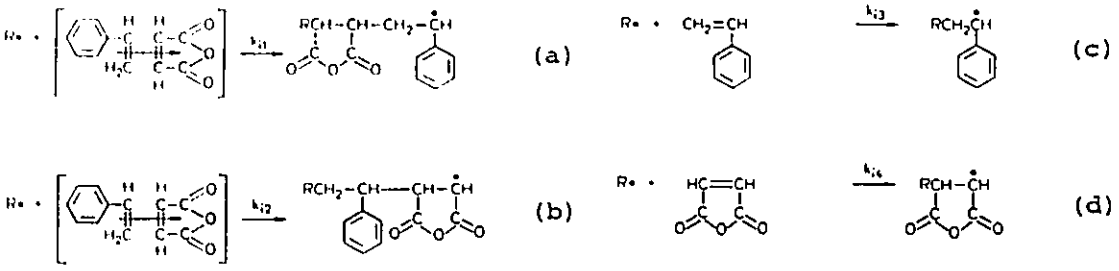

Considering the resonance stabilization of the radicals formed through reactions (b) and (d) they concluded that reactions (a) and (c) were more likely to occur than the former. Note that the four possible reactions represent a competitive mechanism between donor-acceptor and statistical copolymerization.

In a subsequent paper Tsuchida et.al.(1972) established the effect of the solvent in the donor-acceptor formation and copolymerization rate. They found that when a strong electron donor or acceptor was used as solvent two different types of complexes were formed; a monomer/monomer and a monomer/solvent complex. Generally speaking, the solvent interaction with one of the monomers caused a decrease in the copolymerization rate and a displacement of the equilibrium constant for the monomer/monomer complex formation.

It is important to point out here that with opposite behaviour to maleic anhydride which does not homopolymerize, NPMI, which is also a strong electron acceptor, is capable of both homo and copolymerization through free radical initiation.

Tanaka and Otsu (1977) proved this by carrying out donor-acceptor copolymerization of methyl-isopropenyl ketone cylodimer (MIPKD) with both MA and maleimide (MI), initiated with AIBN. They proved the existence of CTC complexes in both systems through UV and NMR characterization and found that a the MIPKD/MI copolymer was richer in MI, in contrast to the nearly 1:1 copolymer obtained in the MIPKD/MA at lower copolymerization rates. The difference was attributed to the formation of long MI sequences by homopropagation reactions.

The free radical homo and copolymerization of N-substituted maleimides is, then, a relatively new field of study. Barrales-Rienda et.al. (1977) studied the solid-state free radical Co-γrays induced homopolymerization of N-phenylmaleimide (NPMI) at different temperatures above and below the melting point of NPMI (T_m=84-86°C). The polymers thus synthesized bear decomposition temperatures varying within the range of 380 to 450°C depending on the polymerization temperature and degree of conversion.

These authors explained their results of high thermal stability of the products by assuming that the polymer has more ordered sequences of monomer units. Although it was proven that non-crystalline structures were obtained they found that long stereo-regular sequences of threo-di-syndiotactic conformation are formed.

This implies that short range order for packing in the solid state exists associated with the conformation described. Through IR spectroscopy they also demonstrated that poly-NPMI γ-ray and radical initiated have the same microstructure.

The radical copolymerization of MA with various nonconjugated cyclic dienes, CD, (electron donors) was studied by Gaylord and Deshpande (1977). They found that a transannular complex between the two monomers, which is able to propagate, was formed. The MA/CD copolymer composition varied between 1:1 to 1:1.5 for a very wide range of feed ratios. This was, again, attributed to the ability of CD to homopolymerize.

Zott and Heusinger (1978), disclosed the intermediate species formed during γ-ray and photolysis induced free radical polymerization of N-substituted maleimides, through the use of high resolution electron spin resonance (ESR) techniques. They pointed out that for N-alkyl maleimides the starting species of polymerization are formed by the abstraction of a hydrogen atom from the alkyl group in radiolysis as well as in photolysis. The structure of the propagating radical showed that polymerization proceeds via the vinylic double bond as in chemically initiated free radical polymerization. Moreover, they reported that radiolysis of maleimide and NPMI yields the same type of radicals and propagating species.

The initiation and propagation steps for γ-rays initiated homopolymerization of N-substituted maleimides, are schematically shown below:

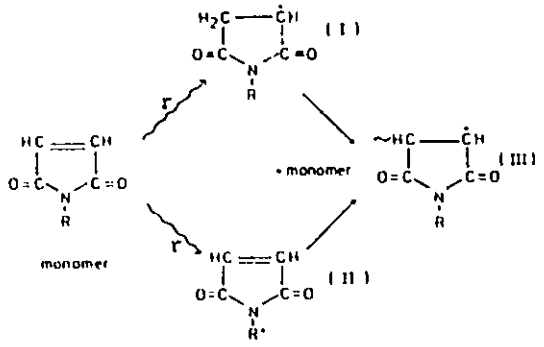

The ESR results showed, as previously suggested by O'Donnell and Sothman (1969), that polymerization occurs by addition of monomer to radicals I and II leading to radical III, which is the propagating species. However, the relative amounts of radicals I and II could not be established through ESR.

Georgiev and Zubov (1978) derived a kinetic method for the determination of the ratio for the addition of donor-acceptor and free monomer (statistical addition)) to the propagating centre. They emphasize that two general hypothesis are available for the mechanism of radical alternating copolymerization:

1. The "free monomer" mechanism supposes that the monomer molecules add only to unlike macroradicals. This hypothesis has its confirmation in the considerable stabilization of the transition state in donor-acceptor and electrostatic interaction between reacting molecules. This results in enhancement of cross propagation rate constants (K_{ij}).

2. The "complex" mechanism supposes that radical alternating copolymerization resembles homopolymerization of donor-acceptor complexes formed from the monomers. This hypothesis is consistent with the most typical features of alternating copolymerization, i.e. spontaneous initiation, polymerization rate dependent on the feed composition, and inhibition of chain transfer reactions. This consistency has resulted in some acceptance of this hypothesis.

In their model, they consider that monomers add to the propagating centre in both the free state and as donor-acceptor complexes. Accordingly, the following mechanism, for alternating copolymerization (M_1=acceptor, M_2=donor, C=complex) is proposed:

$$\sim M_1^{\bullet} + M_2 \rightarrow \sim M_2^{\bullet} \qquad (K_{12})$$

$$\sim M_2^{\bullet} + M_1 \rightarrow \sim M_1^{\bullet} \qquad (K_{21})$$

$$\sim M_1^{\bullet} + C \rightarrow \sim M_1^{\bullet} \qquad (K_{1c})$$

$$\sim M_2^{\bullet} + C \rightarrow \sim M_2^{\bullet} \qquad (K_{2c})$$

In this mechanism it is seen that at every propagation step, the donor-acceptor complex, C, and the free monomer M_1 or M_2 compete for adding to the radical centre.

The contribution of the donor-acceptor complex in propagation depends first on the ratios $\beta_1=K_{1c}/K_{12}$, and $\beta_2=K_{2c}/K_{21}$. These ratios can be calculated from the experimentally established relationship between copolymerization rate (R_i) and the monomer feed ratio ($[M_1]/[M_2]$) at constant total monomer concentration $[M]=[M_1]+[M_2]$.

According to this kinetic scheme, the rate of copolymerization may be calculated as:

(2.21)

$$R_p = K_{12} \frac{(R_i)^{1/2}}{(K_{t0})^{1/2}} \frac{[M_1]([M]-[M_1]+2\beta_1[C]) + ([M]-[M_1])([M_1]+2\beta_2[C])}{\alpha([M]-[M_1]) + [M_1]}$$

where R_i is the initiation rate, K_{t0} is the total rate constant for termination, and $\alpha=K_{12}/K_{21}$.

Equation (2.21) is the basis for calculating the ratios β_1 and β_2. This equation also describes the changes in R_p (i.e. changes in R_i and [C]) caused by variations of the monomer feed.

Two things are noteworthy from Georgiev and Zubov's scheme, the first is that implicitly, the addition of the complex to the radical centre is assumed to occur exclusively in cross fashion (i.e. radical M_i form the same radical M_i upon complex addition). The second is that homopropagation reactions have been completely neglected.

Although there is later experimental evidence for the validity of the first assumption, as shown below, the second assumption is only valid for some alternating systems, since in general, at least one of the free monomers is able to homopropagate.

Based on Georgiev and Zubov's mechanism, Kim et.al.(1978) studied the alternating copolymerization of indene (IN) and maleic anhydride. As shown in figure 2.13, below, they found that the copolymer composition was ~1:1 regardless of the feed composition. They also found that, in opposition to the expected equimolar feed composition, the maximum copolymerization rate was displaced toward an excess of IN in the feed when a strong donor (dioxane) was used as solvent. When acceptor solvents were used no effect in either the initial copolymerization rate or the position of the maximum rate were observed.

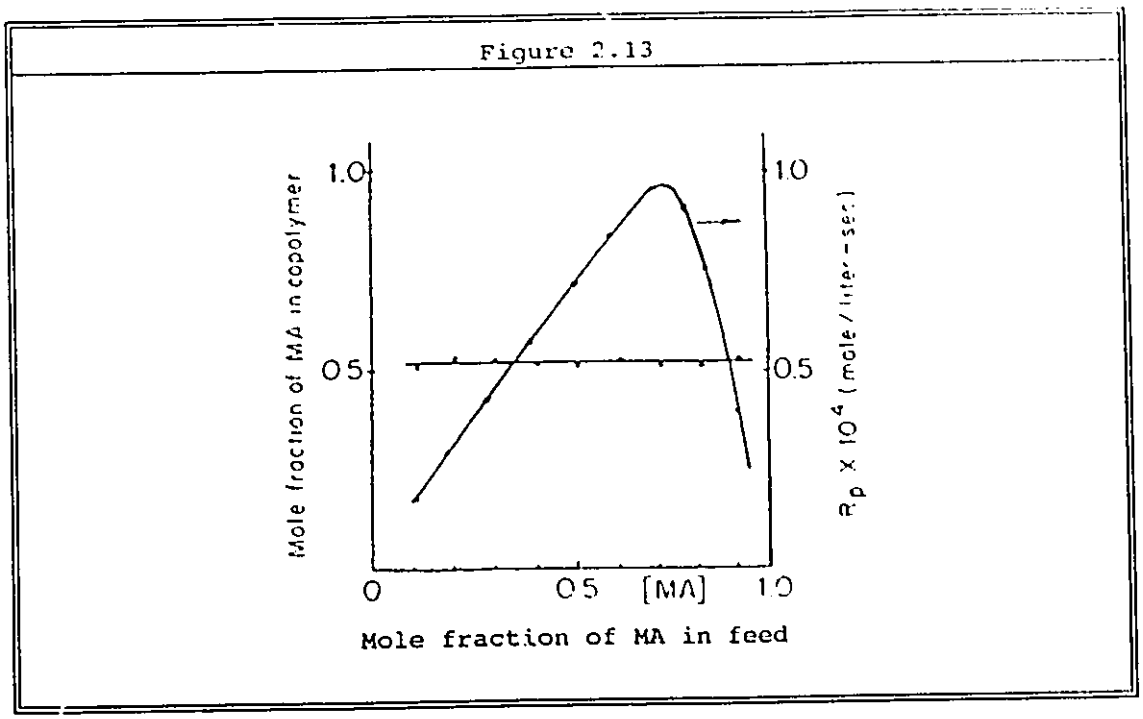

Figure 2.13. Dependence of copolymer composition and copolymerization rate on monomer feed composition, in free radical copolymerization of indene (IN) with maleic anhydride (MA), [M]=2 mol/L in dioxane, at 60°C and [BPO]=0.02 mol/L. (From Kim et.al. (1978)).

Caze and Loucheux (1978) proved the formation of donor-acceptor complexes for the system methylmethacrylate (MMA) and maleic anhydride. They found that the kinetic behaviour of the system was accurately explained by the terminal model with $r_{22}=0$ (no homopolymerization of MA), plus only one propagation reaction of the complex with radicals ending in MMA units (i.e. $\sim M_1^{\bullet} + C \rightarrow \sim M_1^{\bullet}$ (K_{1C})). Thus proving that the resonance stabilization of radicals ending in MA units averts the propagation of such specie. Gutmann (1979) gives support to this observation with his detailed description of structural changes in molecules due to donor-acceptor interactions.

At this point it is important to analyze whether the above considerations for exclusive cross addition of the complex to the radical centre is a fact or just a simplifying assumption:

Thorough characterization of S/MA copolymers (M_1/M_2) through H-NMR and C-NMR have showed the existence of the following triads $M_1M_2M_1$, $M_1M_1M_1$, $M_1M_1M_2$, and $M_2M_1M_1$ [Buchak and Ramey (1976)].

This would imply that at least styrene radicals can add to the complex in straight forward fashion (i.e. $-M_1^{\bullet} + C \rightarrow -M_1M_1M_2^{\bullet}$). However, triads with two or three M_1 units together may also be the product of free monomer addition to the radical centre and of termination by combination between radicals ending in M_1 units.

In addition, molecular weight distribution measurements of these polymers suggest that termination occurs exclusively by combination, with which the absence of M_2M_2 diads indicates both that termination between radicals ending in M_2 do not occur and that there is no straight addition of the complex to radicals ending in M_2. Which is in accordance with Caze and Loucheux's findings.

Barron et.al.(1984) give a great deal of insight for the solution of this problem. They characterized through C-NMR, (amongst others) a copolymer of S/MA synthesized from feed compositions bearing a great excess of MA. Since the equilibrium for the formation of complex is displaced toward complex in this way, no substantial amounts of free styrene monomer would be present in the mix, and since MA cannot homopolymerize at an appreciable rate, an almost perfect alternating copolymer should be obtained under these conditions. In this copolymer (styrene fraction = 0.52), they found that the triads $M_1M_1M_1$ were not present, and that the triads $M_1M_1M_2$ and $M_2M_1M_1$ were in a concentration close to 1 per copolymer chain, on average.

Since the bulk of the copolymer was comprised of $M_1M_2M_1$ triads, this demonstrates that the assumption of exclusive cross addition of the complex to the radical centre is adequate, and allows the formation of diads of the same unit solely as the result of free monomer addition and termination by combination between units able to homopropagate.

Figure 2.14, below, shows the evolution of the relative concentration of the aforementioned triads with copolymer composition. Note how the fraction of styrene diads increases dramatically at slightly higher concentrations of styrene in the copolymer. This observations were recently corroborated by Zeng and Shirota (1989) through fluorescence spectroscopy tests.

Figure 2.14

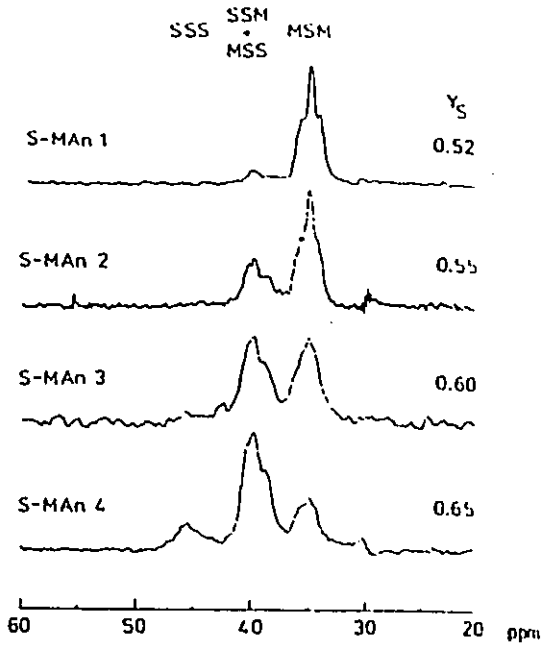

Figure 2.14. DEPT methylene C-NMR subspectra of S/MA copolymers showing the variation in triad sequence distribution with copolymer composition (Y_S=mole fraction of styrene in copolymer). (From Barron et.al.(1984)).

Regel and Canessa (1980) report equilibrium rate constants for the donor acceptor complex formation reaction ($M_1 + M_2 \leftrightarrow C$ (K_{eq})) of S/MA and AMS/MA. At 120°C they found K_{eq} = 0.33 and 0.23 for these systems, respectively.

Hill et.al.(1985) offered a complete analysis of the copolymerization mechanism of S/MA. They compare the predictions of copolymer composition from four different kinetic schemes, namely: terminal model, penultimate model, complex participation model plus terminal model, and complex dissociation model plus terminal model.

In their complex participation model they considered that cross and straight addition of the complex to the radical centre is possible, thus obtaining four propagation reactions in addition to the four of the terminal model, and defining six reactivity ratios.

The fourth model, introduced as complex-dissociation model, is similar to the third but considers that upon addition of the complex to the propagating centre the complex breaks down releasing one unit as free monomer. When styrene, maleic anhydride, and complex are represented as S, M, and SM or MS respectively, this mechanism may be written as:

$$-S^{\bullet} + MS \rightarrow -M^{\bullet} + S \qquad (K_{SMS})$$

$$-S^{\bullet} + SM \rightarrow -S^{\bullet} + M \qquad (K_{SSM})$$

$$-M^{\bullet} + MS \rightarrow -M^{\bullet} + S \qquad (K_{MMS})$$

$$-M^{\bullet} + SM \rightarrow -S^{\bullet} + M \qquad (K_{MSM})$$

From what has been explained before in this section, there is no support for the proposed breakage of the donor-acceptor complex upon addition to the radical centre, or the occurrence of the second and third reactions of this scheme.

The comparison of the best fit predictions from the copolymer composition equations derived with these schemes showed that the penultimate model yields slightly better agreement with experimental data. However, nothing is said with respect to predictions of copolymerization rate or other kinetic parameters.

Brown et.al.(1989), also compared the applicability of the terminal, penultimate, and complex plus terminal models, in the prediction of copolymer composition of S/MA and MA/vinyl acetate (VA) copolymers.

In this study, the penultimate model was found to best describe both systems, although in the case of MA/VA it offered only a marginal improvement over the terminal model. Although it was proven that significant monomer complexation occurs in both systems, they found that the complex model did not provide statistically significant improvement in the fit of the data compared to the terminal model.

Recently, Fles et.al.(1989) published the first study of the free radical solution copolymerization of AMS with NPMI, initiated by AIBN, at temperatures above the ceiling temperature of AMS. Their work, which is of most value for this project, can be summarized as follows.

In the copolymerization of AMS (donor) and NPMI (acceptor) the resulting copolymers, characterized by H-NMR, were found to have a high alternating structure regardless of the ratio of monomers in the feed, as can be seen in figure 2.15, below.

Figure 2.15

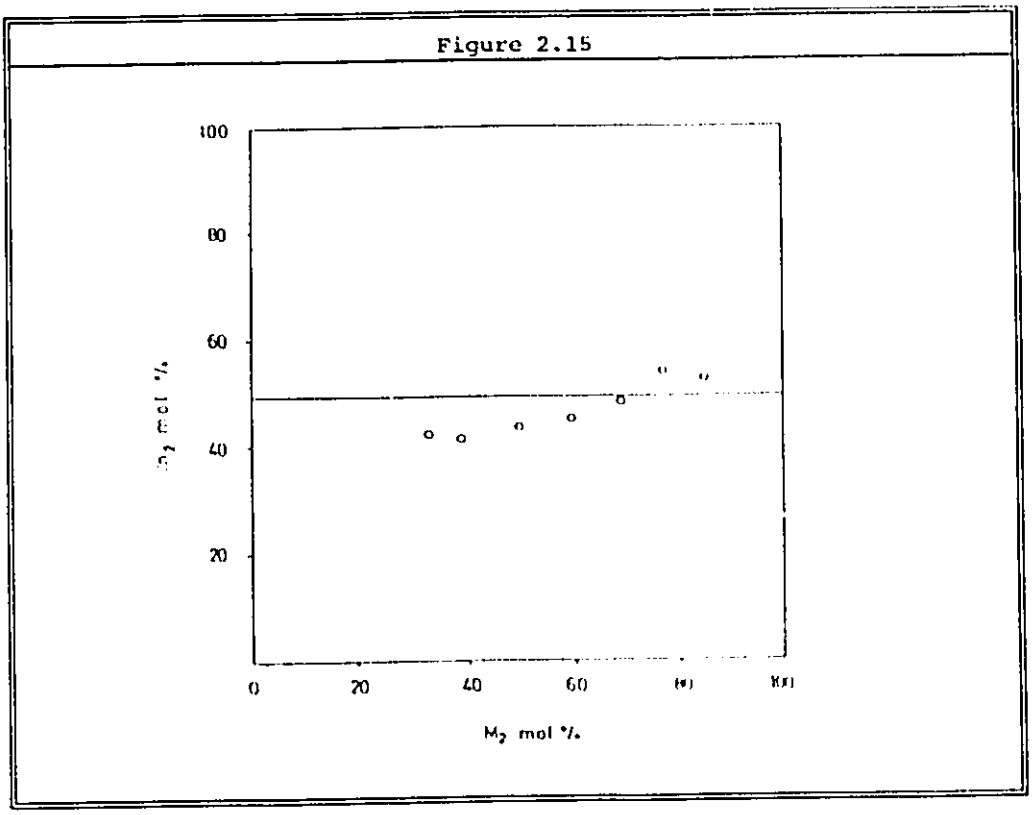

Figure 2.15. Instantaneous copolymer composition curve for NPMI/AMS (M_1/M_2) copolymerization, initiated with 0.3 wt % AIBN, at 70°C, in toluene ([M]=3 M/L). (From Fles et.al.(1989)).

From these data, the monomer reactivity ratios were evaluated as r_1=0.21 (NPMI) and r_2=0.03 (AMS) using the Kelen-Tudos method [Kelen and Tudos (1975)]. Note that the use of this method implies the validity of the terminal model, which the authors considered simultaneously with the complex model, thus introducing an error in the above determination of the reactivity ratios.

The initial rate of copolymerization was proportional to the square root of AIBN concentration, thus indicating bimolecular termination. The equilibrium constant for monomer complexation was determined by a modified Benesi-Hildebrand method [Benesi and Hildebrand (1949)], in deuterated chloroform at 35°C, from which the value of K=0.02 L/mol, was found. The time-conversion curves for the copolymerization of NPMI/AMS (1.0 mol/L in toluene, with 0.3 wt% AIBN), at different temperatures, are shown below in figure 2.16.

Figure 2.16

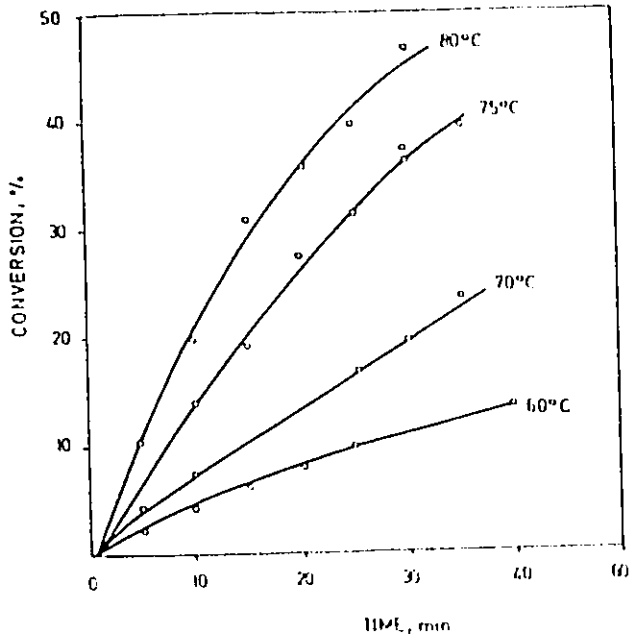

Figure 2.16. Time-conversion curves for free radical copolymerization of NPMI/AMS at different temperatures. [M]=3 mol/L in toluene, [AIBN]=0.3 wt %, f_{10}=0.5. (From Flee et.al. (1989)).

The total rate constants at 60, 70, 75, and 80°C were determined from the initial slopes of these curves as: K_{60}=0.0040, K_{70}=0.00716, K_{75}=0.0318, and K_{80}=0.02093 min^{-1}. Note from the units of K that, since the authors did not consider the radical concentration in the calculation, these K's are in fact $K_p(R_i/K_t)^{1/2}$.

A strong dependency of the initial copolymerization rate on the initial comonomer concentration was found. For a comonomer solution of 3 mol/L the total rate was found to be nearly twice the rate at 2 mol/L and 4 times the rate at 1 mol/L. This suggests that the more dilute systems favour the propagation through free monomer addition whereas higher concentrations favour the complex propagation reactions.

By assuming that the total copolymerization rate can be broken down in free monomer and complex contributions to propagation (i.e. $R_p = R_{p(f)} + R_{p(CT)}$), Shirota et.al. (1974) showed that a plot of $R_p/[M_1]$ against $[M_1]$ according to the equation:

$$R_p/[M_1] = A(X)\cdot K\cdot((K_{1c}/K_{12})+(K_{2c}/K_{21})X)[M_1] + A(X) \qquad (2.22)$$

gives a straight line for each ratio of monomer concentration $X = [M_2]/[M_1]$ (M_1=NPMI, M_2=AMS). Here K is the equilibrium constant for the comonomer complexation, and the intercept A(X) correlates the rate constants with X under the steady-state approximation:

$$A(X) = (2K_{21}K_{12}(R_i)^{1/2}X)/(K_{t11}K_{21}^2 + 2K_{t12}K_{21}K_{12}X + K_{t22}K_{12}^2X^2)^{1/2}$$

where R_i is the initiation rate, K_{ij} are the corresponding propagation rate constants (referred to erroneously as reactivity ratios by the authors), and K_{tij} are the termination rate constants.

Shirota et.al.(1974) showed that the corresponding products $A(X)[M_1]$ give the values of $R_{p(f)}$ as a function of comonomer composition. The difference, therefore, of R_p, from figure 2.16, and these values yield $R_{p(CT)}$.

Following this procedure, the relative participation of both mechanism competing for the propagation reactions were obtained.

Figure 2.17, below, shows this relative participation as a function of AMS concentration in the feed, at different comonomer initial concentrations.

Figure 2.17

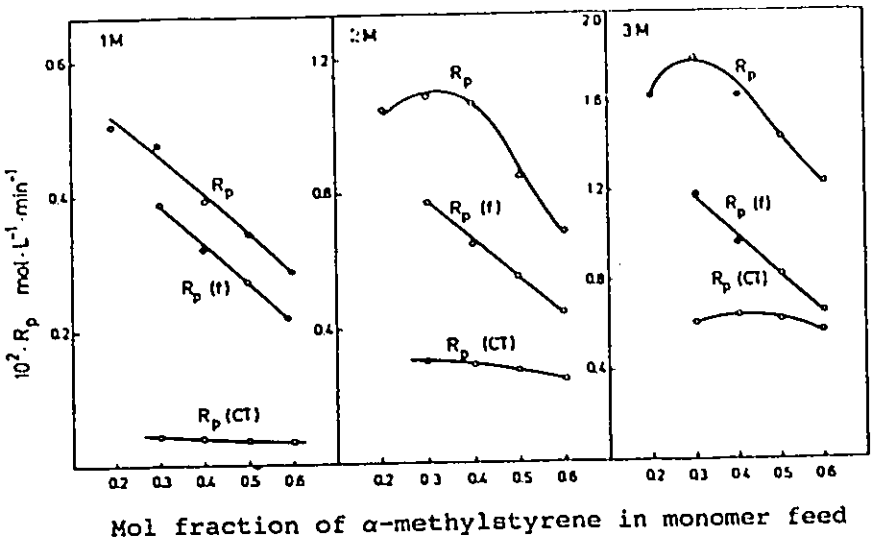

Figure 2.17. Relative participation of free monomer (f) and donor-acceptor complex (CT) in the copolymerization of NPMI/AMS at different monomer concentrations in toluene. T_p=70°, [AIBN]=0.3 wt %. (From Fles et.al.(1989)).

It is noteworthy how the complex participation in the propagation reactions of this NPMI/AMS system increases substantially with the increase in the comonomer concentration, becoming similar to the free monomer addition at 3 mol/L in toluene. Since for this system at equimolar monomer feed, the bulk comonomer concentration at 100°C is about 7.1 mol/L (see chapter 6 for physical data), it is expected that bulk or suspension polymerization under these conditions must proceed primarily by complex reactions at very high copolymerization rates.

In the same paper, Fles et.al.(1989) report the following numerical values of interest for this project:

$$K \cdot K_{1c}/K_{12} = 0.08; \quad K \cdot K_{2c}/K_{21} = 0.4; \quad \text{and} \quad K_{1c}K_{21}/(K_{2c}K_{12}) = 0.2$$

All these data at 80°C and [M]=1 M/L in toluene, independent of the comonomer feed ratio.

In addition, DSC and DTA characterization of the products showed that the T_g of the copolymer NPMI/AMS obtained at equimolar comonomer composition was T_g=266°C, and the copolymer was found to be stable up to 340°C where it abruptly decomposes with a loss of 100% of its mass at 440°C.

Finally, quite recently, Schmidt-Naake et.al. (1990,a,b) developed the model for terpolymerization in which one comonomer pair form a donor-acceptor complex.

Based exclusively on the terminal model for terpolymerization which takes into account 8 propagation reactions [Alfrey and Goldfinger (1946)], they showed that the terpolymer composition under these conditions can be calculated from their monomer feed when the values of the reactivity ratios for the three binary subsystems are known and the equation considers exclusively the propagation reactions that actually take place (i.e. some K_{ij}=0).

For the binary donor-acceptor systems of interest in the present research, Schmidt-Naake et.al.(1990,a,b) report the following values of reactivity ratios; S/NPMI: r_1=0.05 + 0.02, r_2=0.11 + 0.03; AMS/NPMI: r_1=0.06 + 0.03, r_2=0.

In addition, they demonstrated that the solution of the terpolymerization equation with these two sets of values for the reactivity ratios, along with the reactivity ratios for the third non complexing binary pair (S/AMS), does not reveal the existence of an azeotrope.

2.3 Copolymerization with Bifunctional Initiators

In spite of the great amount of work done on the synthesis, characterization and properties of bifunctional initiators (Simionescu et.al.(1986) in their complete review have more than 150 references on these topics), and their use in free radical homopolymerization (more than 80 references in the same review), very little comprehensive kinetic modelling work, considering the unique features of this type of free radical polymerization has been done to date [Choi and Lei (1987), Choi et.al.(1988), Villalobos (1989), Kim et.al.(1989), Villalobos et.al.(1991)].

With regard to free radical copolymerization with bifunctional initiators most of the work done to date has been developed with the intention of synthesizing block copolymers, by taking advantage of the sequential decomposition characteristics of these initiators.

By using asymmetrical bifunctional initiators with very different decomposition characteristics of the two peroxides, polymerization of monomer A can be carried out at a temperature favourable for the decomposition of the less stable peroxide group.

Upon consumption of monomer A, monomer B is introduced to the reaction mix and the temperature is raised to a point where the second peroxide decomposes, thus obtaining, in principle, block copolymers of the type AB [Waltz and Heitz (1978), Piirma and Chou (1979), Ivanechev (1979), Gunesin and Piirma (1981), Simionescu et.al.(1984), Yagci and Onen (1991)].

Following this procedure S/Bu, S/MMA, and S/AN block copolymers, among others, have been synthesized. However, none of the above works has succeeded in deriving quantitative kinetic expressions for copolymerization with bifunctional initiators or even in describing the reaction scheme for such two stage copolymerization.

Villalobos (1989) showed that different block structures are obtained through this type of polymerization. He established the reaction scheme of the proposed two stage copolymerization through bifunctional initiators as:

$$R\text{-}O\text{-}O\text{-}R\text{-}O\text{-}O\text{-}R \xrightarrow{} R^{\bullet} + R'^{\bullet} \qquad (K_{d1})$$

$$R^{\bullet} + A \xrightarrow{} A^{\bullet} \qquad \text{1st. stage initiation} \quad (K_1)$$

$$R'^{\bullet} + A \xrightarrow{} A'^{\bullet} \qquad (K_2)$$

$$A_n^{\bullet} + A \xrightarrow{} A_{n+1}^{\bullet} \qquad (K_{p1})$$

$$A_n'^{\bullet} + A \xrightarrow{} A_{n+1}'^{\bullet} \qquad \text{propagation} \quad (K_{p1})$$

$$A_n^{\bullet} + A_m^{\bullet} \xrightarrow{} A_{n+m} \qquad \text{termination by combination} \quad (K_{tc1})$$

$$A_n'^{\bullet} + A_m^{\bullet} \xrightarrow{} A_{n+m}' \qquad (K_{tc1})$$

$$A_n'^{\bullet} + A_m'^{\bullet} \xrightarrow{} A_{n+m}'' \qquad (K_{tc1})$$

$$A_n^{\bullet} + A_m^{\bullet} \xrightarrow{} A_n + A_m \qquad \text{termination by disproport.} \quad (K_{td1})$$

$$A_n'^{\bullet} + A_m^{\bullet} \xrightarrow{} A_n' + A_m \qquad (K_{td1})$$

$$A_n'^{\bullet} + A_m'^{\bullet} \xrightarrow{} A_n' + A_m' \qquad (K_{td1})$$

$$A_n' \xrightarrow{} R^{\bullet} + A_n^{\bullet} \qquad (K_{d2})$$

$$A_n'' \xrightarrow{} R^{\bullet} + A_n'^{\bullet} \qquad (2K_{d2})$$

$$A_n'B_m \xrightarrow{} R^{\bullet} + B_mA_n^{\bullet} \qquad (K_{d2})$$

$$A_n'B_mA_o' \xrightarrow{} R^{\bullet} + A_n'B_mA_o^{\bullet} \qquad \text{2nd stage initiation} \quad (2K_{d2})$$

$$R^{\bullet} + B \xrightarrow{} B^{\bullet} \qquad (K_3)$$

$$A_n^{\bullet} + B \xrightarrow{} A_nB^{\bullet} \qquad (K_4)$$

$$A_n'^{\bullet} + B \xrightarrow{} A_n'B^{\bullet} \qquad (K_5)$$

$$B_n^{\bullet} + B \xrightarrow{} B_{n+1}^{\bullet} \qquad (K_{p2})$$

$$A_nB_m^{\bullet} + B \xrightarrow{} A_nB_{m+1}^{\bullet} \qquad \text{propagation} \quad (K_{p2})$$

$$A_n'B_m^{\bullet} + B \xrightarrow{} A_n'B_{m+1}^{\bullet} \qquad (K_{p2})$$

$$B_n^{\bullet} + B_m^{\bullet} \xrightarrow{} B_{n+m} \qquad (K_{tc2})$$

$$B_n^{\bullet} + A_nB_m^{\bullet} \xrightarrow{} A_nB_{n+m} \qquad (K_{tc2})$$

$$B_n^{\bullet} + A_n'B_m^{\bullet} \xrightarrow{} A_n'B_{n+m} \qquad \text{termination by combination} \quad (K_{tc2})$$

$$A_nB_m^{\bullet} + A_oB_p^{\bullet} \xrightarrow{} A_nB_{m+p}A_o \qquad (K_{tc2})$$

$$A_nB_m^{\bullet} + A_o'B_p^{\bullet} \xrightarrow{} A_nB_{m+p}A_o' \qquad (K_{tc2})$$

$$A_n'B_m^{\bullet} + A_o'B_p^{\bullet} \xrightarrow{} A_n'B_{m+p}A_o' \qquad (K_{tc2})$$

$$B_n^{\bullet} + B_m^{\bullet} \xrightarrow{} B_n + B_m \qquad (K_{td2})$$

$$B_n^{\bullet} + A_nB_m^{\bullet} \xrightarrow{} B_n + A_nB_m \qquad (K_{td2})$$

$$B_n^{\bullet} + A_n'B_m^{\bullet} \xrightarrow{} B_n + A_n'B_m \qquad \text{termination by disproport.} \quad (K_{td2})$$

$$A_nB_m^{\bullet} + A_oB_p^{\bullet} \xrightarrow{} A_nB_m + A_oB_p \qquad (K_{td2})$$

$$A_nB_m^{\bullet} + A_o'B_p^{\bullet} \xrightarrow{} A_nB_m + A_o'B_p \qquad (K_{td2})$$

$$A_n'B_m^{\bullet} + A_o'B_p^{\bullet} \xrightarrow{} A_n'B_m + A_o'B_p \qquad (K_{tc2})$$

In the above reactions the dots (·) indicate radical species, the superscripts ' and " indicate one or two undecomposed terminal peroxide groups, respectively, and the subindexes the length of the growing chains and polymers. Note that species bearing undecomposed peroxide groups can further react through second stage initiation to form multi-block structures.

From the scheme proposed, it can be seen that regardless of the termination mechanism governing the copolymer production, formation of substantial amounts of homopolymer A and homopolymer B cannot be avoided. In addition to these homopolymers the following species will be formed depending on the termination mechanism governing each stage:

1. When termination by disproportionation dominates in both stages, only block copolymers AB are obtained.
2. When disproportionation dominates the first stage and combination the second stage a mixture of block copolymers AB, and ABA is obtained.
3. When combination dominates the first stage and disproportionation the second stage a mixture of block copolymers AB and BAB is obtained.
4. When combination dominates both stages, a mixture of block copolymers AB, ABA, BAB, and multi-block copolymers $(ABA)_n$ (n>1) is obtained.
5. When both mechanisms occur in the two stages, the same mixture as in (4) is obtained, however, the maximum number of multi-blocks (ABA) will be smaller, in average, than in the latter case.

It is evident that such complex mix of block copolymers and homopolymers, obtained through this kind of copolymerization with bifunctional initiators, compares very unfavourably with the nearly perfect and monodisperse tailored block formation obtained with anionic polymerization. Due to this fact, work in this direction has recently come to an almost complete halt.

In addition to this lack of work in two stage copolymerization with bifunctional initiators, a general kinetic model or reaction scheme has not been published for either statistical or donor-acceptor copolymerization with bifunctional initiators, as yet.

The problem of developing a general kinetic model for free radical statistical/donor-acceptor copolymerization with bifunctional initiators, as is contemplated in this thesis, seems to be most interesting and complex.

In statistical copolymerization with bifunctional initiators random copolymer chains with variable composition are formed at any time during the reaction. Since re-initiation of temporarily dead copolymer molecules is a unique feature of this type of copolymerization, a mixture of random copolymer blocks with different compositions is likely to be formed within most of the copolymer chains. The number of these random blocks within a given copolymer chain is also dependent upon conversion, initiator concentration, and reaction rate. In order to account for this phenomenon, the kinetic model must contemplate the actual birth conversion of the different copolymer species as well as the multiple re-initiation conversions of the same molecule, to accurately predict the instantaneous copolymer composition, as well as conversion, comonomer composition and molecular weight distribution development.

In addition, donor-acceptor copolymerization reactions increase the complexity of the model, since the alternating structures formed through these reactions must be adequately described, in order to predict the microstructure of the copolymer. An additional complexity is introduced by the fact that high T_g copolymers are expected to be synthesized at moderated temperatures, generally below such T_g's. This means that an early glassy effect must be expected for the systems contemplated in this research, and both diffusion controlled propagation and termination reactions must be considered.

Chapter 4, part of which has been published as a paper [Villalobos et.al. (1992)], contains, to the best knowledge of the author, the derivation of the first kinetic model for free radical copolymerization with bifunctional initiators.

This model as will be shown in chapters 5 to 8, has been successful in describing the main features of pure statistical (chapter 5), pure donor-acceptor (chapter 7), and simultaneous statistical/donor-acceptor copolymerization (chapter 6), for bulk and suspension batch copolymerization through bifunctional initiators.

CHAPTER 3

SUSPENSION POLYMERIZATION OF STYRENE IN THE PRESENCE OF N-PENTANE

In this chapter, the kinetics of styrene bulk and suspension polymerization is studied for cases when variable amounts of n-pentane are added to the reaction mix at different monomer conversions. The effects of n-pentane, on polymerization rate and molecular weight distribution development, are modeled using the free volume theory for both monofunctional and bifunctional initiation. Comprehensive comparison of the performance of each type of initiation mechanism for suspension polystyrene in the presence of n-pentane is made.

3.1 Introduction

Traditional manufacture of expandable polystyrene (EPS) in bead form involves two different processes:

First, free radical aqueous suspension polymerization of styrene is carried out at temperatures between 80 and 90°C with the aid of monofunctional initiators, such as azo-bis-isobutyronitrile (AIBN) or benzoyl peroxide (BPO) [Bishop (1971)].

The batch polymerization is carried out in a stirred reactor bearing a dispersed phase hold-up (ϕ=volume of disperse phase/total volume) in the range of 0.4 to 0.6, until the conversion where the beads become glassy owing to the fact that the T_g of the monomer/polymer mix increases reaching the polymerization temperature, T_p, [Horie et.al.(1968)].

During this process, the dispersed droplets reach a critical viscosity (μ_{cr1}~100 cp) at about 30% conversion, depending on the molecular weight and T, from which droplet coalescence rate overcomes the droplet breakup rate caused by the agitation system. As a result the mean particle size (MPS) starts to increase rapidly [Church (1966)]. The particle growth is controlled to the desired final size with the aid of suspending agents which may be insoluble inorganic powders, such as zinc oxide and tricalcium phosphate (TCP), or water-soluble polymers, such as polyvinyl alcohol (PVA), hydroxyethyl cellulose (HEC) or polyvinyl pyrrolidone (PVP).

Particle growth stops at a second critical viscosity (μ_{cr2}~10^5 cp), which is reached at about 70% conversion, due to the elastic nature of the particle collisions at this viscosity level which averts coalescence. This point is commonly referred to as the identity point and the growth stage as the "sticky stage". From the identity point on, the suspension is stable and the polymerization proceeds until the beads become glassy [Arai et.al.(1977)].

The second process, called the impregnation stage, consists of a high temperature-high pressure cycle ($T_i > T_g$) in which the blowing agent, commonly n-pentane, is loaded in the reactor and diffuses into the softened beads. In addition, exhaustion of the residual monomer is achieved simultaneously, with the aid of a finishing monofunctional initiator of higher half life than the one used during the polymerization process.

Depending on the impregnation temperature (T_i) and pressure (P_i) a minimum time must be allowed for the diffusion of the blowing agent to reach the core of the beads and for complete monomer exhaustion [Bishop (1971)]. At the end of the impregnation stage the suspension is cooled down to room temperature and the polymer is separated from the water in a centrifuge and then dried at low temperatures.

The main productivity limitation of these two processes consists of the long batch times necessary to carry them to completion.

Polymerization with monofunctional initiators at higher temperatures, as a means to increase productivity has not succeeded due to both lower molecular weights of the product (out of the processing range), and the enhanced particle coalescence observed at higher temperatures [Konno et.al.(1988)]. Moreover, addition of blowing agent before the glassy point, as another means to increase productivity in the commercial manufacture of EPS, has not been reported, in our knowledge, as yet.

Recently, suspension polymerization of styrene with bifunctional initiators, at temperatures above and below the glass transition temperature of polystyrene, has been studied at length [Villalobos (1989)]. In this study, it has been demonstrated that, due to the sequential decomposition characteristics of bifunctional initiators, the polymer molecules experience multiple re-initiation/propagation/ termination cycles. As a result, it is possible to achieve simultaneously high polymerization rates and high molecular weights.

In the same study, it was demonstrated that suspension polystyrene with the molecular weight characteristics of expandable polystyrene is obtained with bifunctional initiator 1,4-bis(tertbutyl peroxycarbo) cyclohexane (TBPCC), at 105°C, in a batch cycle 75% shorter than that obtained through the traditional monofunctional initiation system. Moreover, the enhanced particle coalescence observed at such polymerization temperature was completely overcome by the great real time reduction of the particle growth stage [Villalobos (1989)].

In the present study, the early presence of n-pentane in the polymerization mix, in both monofunctionally and bifunctionally initiated systems, is studied from two points of view: 1) Its effect on polymerization rate and molecular weight distribution development in bulk/solution polymerization of styrene; and 2) Its effect on suspension stability, mean particle size and particle size distribution in suspension polymerization of styrene.

The kinetic phenomena observed in this study are modeled, and simulated to compare with the experimental data obtained.

3.2 Reaction Schemes

It has been shown that both bulk and suspension free radical polymerization proceed through the same kinetic mechanism throughout the entire conversion range [Bamford et.al. (1958)]. The well known set of elementary reactions involved in monofunctionally initiated bulk or suspension polymerization of styrene, considered in this study, can be written as follows [Hamielec et.al.(1967), Friis and Hamielec (1975)].

Monofunctional System

Thermal initiation:

$$3M \xrightarrow{K_{th}} 2R_1^{\bullet} \qquad (3.1)$$

Chemical initiation:

$$I \xrightarrow{K_d} 2R_{in}^{\bullet} \qquad (3.2)$$

$$R_{in}^{\bullet} + M \xrightarrow{K_i} R_1^{\bullet} \qquad (3.3)$$

Propagation:

$$R_r^{\bullet} + M \xrightarrow{K_p} R_{r+1}^{\bullet} \qquad (r \geq 1) \quad (3.4)$$

Termination by combination:

$$R_r^{\bullet} + R_s^{\bullet} \xrightarrow{K_{tc}} P_{r+s} \qquad (r,s \geq 1) \quad (3.5)$$

Transfer to monomer:

$$R_r^{\bullet} + M \xrightarrow{K_{trm}} P_r + R_1^{\bullet} \qquad (r \geq 1) \quad (3.6)$$

In the above scheme I is a monofunctional initiator, $R_{in}^{\bullet}$ are the primary radicals, $R_i^{\bullet}$ are growing radicals of chain length i, M is styrene monomer, and P_i represents dead polymer molecules of chain length i.

A symmetrical bifunctional initiator molecule can be represented as:

$$R_1\text{-}O\text{-}O\text{-}R_2\text{-}O\text{-}O\text{-}R_1$$

The peroxide groups in such a diperoxide compound can undergo homolytic rupture of the O-O bonds by increasing the energy of the system. The primary homolysis of a diperoxide can be written as:

$$R_1\text{-}O\text{-}O\text{-}R_2\text{-}O\text{-}O\text{-}R_1 \rightarrow R_1\text{-}O^{\bullet} + R_1\text{-}O\text{-}O\text{-}R_2\text{-}O^{\bullet}$$

From this reaction two different radicals are formed, one similar to the radicals of monofunctional initiation, and one bearing an undecomposed peroxide. Upon polymerization, these two primary radicals will lead to the formation of two different populations of propagating radicals, with and without terminal undecomposed peroxide, respectively.

When termination by combination is the dominant bimolecular termination mechanism, such as for polystyrene, these two radical populations will yield three different polymer populations: i) dead polymer; ii) temporarily dead polymer with one terminal peroxide group; and iii) temporarily dead polymer with two undecomposed peroxide groups (one at each end). Since the terminal peroxide groups in these temporarily dead polymer populations can further undergo homolysis of the O-O bond, they will act as macro-initiators in subsequent stages of the polymerization, experiencing, as a result, a new initiation/propagation/termination cycle which may lead to the formation of either dead or temporarily dead polymer molecules, again [Villalobos et.al. (1991)].

This multiple re-initiation/propagation/termination phenomenon is responsible for the possibility of achieving high reaction rates and high molecular weights simultaneously in free radical polymerization with bifunctional initiators.

The set of elementary reactions involved in bifunctionally initiated free radical bulk or suspension polymerization of styrene, considered in this study, can be written as follows [Villalobos et.al.(1991)].

Bifunctional System

Thermal initiation:

$$3M \xrightarrow{K_{th}} 2R_1^{\bullet} \qquad (3.7)$$

Chemical initiation:

$$I_n \xrightarrow{2K_{d1}} R_{in}^{\bullet} + \widetilde{R}_{in}^{\bullet} \qquad (3.8)$$

$$R_{in}^{\bullet} + M \xrightarrow{K_1} R_1^{\bullet} \qquad (3.9)$$

$$\widetilde{R}_{in}^{\bullet} + M \xrightarrow{K_2} \widetilde{R}_1^{\bullet} \qquad (3.10)$$

$$\widetilde{P}_r \xrightarrow{K_{d2}} R_{in}^{\bullet} + R_r^{\bullet} \qquad (r \geq 2) \quad (3.11)$$

$$\widetilde{\widetilde{P}}_r \xrightarrow{2K_{d2}} R_{in}^{\bullet} + \widetilde{R}_r^{\bullet} \qquad (r \geq 2) \quad (3.12)$$

Propagation:

$$R_r^{\bullet} + M \xrightarrow{K_p} R_{r+1}^{\bullet} \qquad (r \geq 1) \quad (3.13)$$

$$\widetilde{R}_r^{\bullet} + M \xrightarrow{K_p} \widetilde{R}_{r+1}^{\bullet} \qquad (r \geq 1) \quad (3.14)$$

Termination by combination:

$$R_r^{\bullet} + R_s^{\bullet} \xrightarrow{K_{tc}} P_{r+s} \qquad (r,s \geq 1) \quad (3.15)$$

$$R_r^{\bullet} + \widetilde{R}_s^{\bullet} \xrightarrow{K_{tc}} \widetilde{P}_{r+s} \qquad (r,s \geq 1) \quad (3.16)$$

$$\widetilde{R}_r^{\bullet} + \widetilde{R}_s^{\bullet} \xrightarrow{K_{tc}} \widetilde{\widetilde{P}}_{r+s} \qquad (r,s \geq 1) \quad (3.17)$$

Transfer to monomer:

$$R_r^{\bullet} + M \xrightarrow{K_{Ftm}} P_r + R_1^{\bullet} \qquad (r \geq 1) \quad (3.18)$$

$$\widetilde{R}_r^{\bullet} + M \xrightarrow{K_{Ftm}} \widetilde{P}_r + R_1^{\bullet} \qquad (r \geq 1) \quad (3.19)$$

Here I_b is the bifunctional initiator, $\widetilde{R}_{1n}\bullet$ are primary radicals with one undecomposed peroxide, $\widetilde{R}_i\bullet$ are growing radicals of chain length i with one terminal peroxide group, and $\widetilde{P}_r$ and $\widetilde{\widetilde{P}}_r$ are temporarily dead polymer molecules with one and two terminal peroxide groups, respectively. The rest of the species are the same as in the monofunctional scheme.

From the above polymerization schemes note that n-pentane should not act as a chain transfer agent at the polymerization temperatures being used, since hydrogen abstraction from saturated hydrocarbons at this temperature level is very unlikely. Its role in the polymerization kinetics, therefore, may be limited to its plasticizing effect, as an inert solvent in the system. However, its influence over the extent of the transfer to monomer reactions will be addressed herein.

3.3 Kinetic Modelling

Considering the main underlying dissimilarities between monofunctionally and bifunctionally initiated polymerization, as shown by the distinct polymerization schemes, it is clear that different kinetic models must be developed for each type of initiation, in order to capture these basic differences. Detailed derivation of the corresponding kinetic models for polystyrene, taking into account the sets of elementary reactions considered above, have been reported elsewhere [Hui and Hamielec (1972), Villalobos et.al.(1991)].

The development of the kinetic models mentioned, are based on the application of the method of moments to the mass balances for each of the existing species in the polymerization mix.

Following this procedure, applying the steady state hypothesis for radical concentration, the long chain approximation for monomer consumption and simplifying by considering that $Y_2 > Y_1 > Y_0$, the following set of algebraic and ordinary differential equations are obtained for each mode of initiation.

Monofunctional Initiation	Bifunctional Initiation

Monomer Consumption:

$$\frac{1}{V}\frac{d([M]V)}{dt} = -K_p[M]Y_0$$

$$\frac{1}{V}\frac{d([M]V)}{dt} = -K_p[M]Y_{T0}$$

Initiator Consumption:

$$\frac{1}{V}\frac{d([I]V)}{dt} = -K_d[I]$$

$$\frac{1}{V}\frac{d([I_B]V)}{dt} = -2K_{d1}[I]$$

Initiation Rate:

$$R_I = 2fK_d[I] + 2K_{th}[M]^3$$

$$R_I = f(2K_{d1}[I_B] + K_{t2}(\tilde{Q}_0 + 2\tilde{\tilde{Q}}_0)) + 2K_{th}[M]^3$$

$$\tilde{R}_I = 2fK_{d1}[I_B]$$

Moments of the Live Polymer Concentration Distributions:

Zeroth

$$Y_0 = \frac{(R_I)^{1/2}}{(K_{tc})^{1/2}}$$

$$Y_0 = \frac{R_I + fK_{t2}\tilde{Q}_0 + K_{Tfm}[M]\tilde{Y}_0}{K_{tc}Y_{T0}}$$

$$\tilde{Y}_0 = \frac{\tilde{R}_I + 2fK_{t2}\tilde{\tilde{Q}}_0}{K_{Tfm}[M] + K_{tc}Y_{T0}}$$

First

$$Y_1 = \frac{R_I + K_p[M]Y_0}{K_{Tfm}[M] + K_{tc}Y_0}$$

$$Y_1 = \frac{R_I + fK_{t2}\tilde{Q}_1 + K_p[M]Y_0}{K_{Tfm}[M] + K_{tc}Y_{T0}}$$

$$\tilde{Y}_1 = \frac{\tilde{R}_I + 2fK_{t2}\tilde{\tilde{Q}}_1 + K_p[M]\tilde{Y}_0}{K_{Tfm}[M] + K_{tc}Y_{T0}}$$

Second

$$Y_2 = \frac{R_I + 2K_p[M]Y_1}{K_{Tfm}[M] + K_{tc}Y_0}$$

$$Y_2 = \frac{R_I + fK_{t2}\tilde{Q}_2 + 2K_p[M]Y_1}{K_{Tfm}[M] + K_{tc}Y_{T0}}$$

$$\tilde{Y}_2 = \frac{\tilde{R}_I + 2fK_{t2}\tilde{\tilde{Q}}_2 + 2K_p[M]\tilde{Y}_1}{K_{Tfm}[M] + K_{tc}Y_{T0}}$$

Monofunctional Initiation	Bifunctional Initiation

Moments of the Dead Polymer Concentration Distributions:

Zeroth

$$\frac{1}{V}\frac{d(Q_0V)}{dt} = \tfrac{1}{2}K_{tc}Y_0^2 + K_{Tfm}[M]Y_0$$

$$\frac{1}{V}\frac{d(Q_0V)}{dt} = \tfrac{1}{2}K_{tc}Y_0^2 + K_{Tfm}[M]Y_0$$

$$\frac{1}{V}\frac{d(\widetilde{Q}_0V)}{dt} = K_{tc}Y_0\widetilde{Y}_0 + K_{Tfm}[M]\widetilde{Y}_0 - K_{d2}\widetilde{Q}_0$$

$$\frac{1}{V}\frac{d(\widetilde{\widetilde{Q}}_0V)}{dt} = \tfrac{1}{2}K_{tc}\widetilde{Y}_0^2 - 2K_{d2}\widetilde{\widetilde{Q}}_0$$

First

$$\frac{1}{V}\frac{d(Q_1V)}{dt} = K_{tc}Y_1Y_0 + K_{Tfm}[M]Y_1$$

$$\frac{1}{V}\frac{d(Q_1V)}{dt} = K_{tc}Y_1Y_0 + K_{Tfm}[M]Y_1$$

$$\frac{1}{V}\frac{d(\widetilde{Q}_1V)}{dt} = K_{tc}(\widetilde{Y}_1Y_0+Y_1\widetilde{Y}_0) + K_{Tfm}[M]\widetilde{Y}_1 - K_{d2}\widetilde{Q}_1$$

$$\frac{1}{V}\frac{d(\widetilde{\widetilde{Q}}_1V)}{dt} = K_{tc}\widetilde{Y}_1\widetilde{Y}_0 - 2K_{d2}\widetilde{\widetilde{Q}}_1$$

Second

$$\frac{1}{V}\frac{d(Q_2V)}{dt} = K_{tc}(Y_1^2+Y_2Y_0)+K_{Tfm}[M]Y_2$$

$$\frac{1}{V}\frac{d(Q_2V)}{dt} = K_{tc}(Y_1^2+Y_2Y_0)+ K_{Tfm}[M]Y_2$$

$$\frac{1}{V}\frac{d(\widetilde{Q}_2V)}{dt} = K_{tc}(\widetilde{Y}_2Y_0+2Y_1\widetilde{Y}_1+Y_2\widetilde{Y}_0) + K_{Tfm}[M]\widetilde{Y}_2 - K_{d2}\widetilde{Q}_2$$

$$\frac{1}{V}\frac{d(\widetilde{\widetilde{Q}}_2V)}{dt} = K_{tc}(\widetilde{Y}_1^2+\widetilde{Y}_2\widetilde{Y}_0) - 2K_{d2}\widetilde{\widetilde{Q}}_2$$

In the above sets of equations V is the total volume of the reaction mix, f is the initiator and macroinitiator efficiencies, d/dt represents rate of change with time, and [] indicates concentration. The i-th moment (i=0,1,2) of the live (both with and without terminal peroxide), dead, and temporarily dead polymer concentration distributions, appearing in the above equations, are defined as:

$$Y_i = \sum_{r=1}^{\infty} r^i [R_r] \qquad \text{for live polymer}$$

$$\widetilde{Y}_i = \sum_{r=1}^{\infty} r^i [\widetilde{R}_r] \qquad \text{for live polymer with one terminal undecomposed peroxide group.}$$

$$Q_i = \sum_{r=1}^{\infty} r^i [P_r] \qquad \text{for dead polymer}$$

$$\widetilde{Q}_i = \sum_{r=1}^{\infty} r^i [\widetilde{P}_r] \qquad \text{for temporarily dead polymer with one terminal undecomposed peroxide.}$$

$$\widetilde{\widetilde{Q}}_i = \sum_{r=1}^{\infty} r^i [\widetilde{\widetilde{P}}_r] \qquad \text{for temporarily dead polymer with two terminal undecomposed peroxides.}$$

$$Y_{T0} = Y_0 + \widetilde{Y}_0 \qquad \text{total radical concentration } (Y_0 \text{ for monofunctional initiation})$$

The simultaneous numerical solution of the above equations through the use of a standard library subroutine (LSODE) has been the base for the development of the simulation programs MONOFUN and BIFUN, for bulk and suspension polymerization of styrene through monofunctional and bifunctional initiators, respectively [Villalobos (1989)].

From the integrated values of the variables involved in the kinetic models described, monomer conversion and molecular weight averages as a function of the polymerization time are calculated in both programs as:

$$X_t = \frac{N_{m0} - N_{mt}}{N_{m0}} \qquad (3.20)$$

$$M_{n(t)} = \frac{MW_M \ (\Sigma Q_{1(t)} + \Sigma Y_{1(t)})}{\Sigma Q_{0(t)} + \Sigma Y_{0(t)}} \qquad (3.21)$$

$$M_{w(t)} = \frac{MW_M \ (\Sigma Q_{2(t)} + \Sigma Y_{2(t)})}{\Sigma Q_{1(t)} + \Sigma Y_{1(t)}} \qquad (3.22)$$

Here X is the monomer conversion, N_m are the moles of monomer, MW_M is the molecular weight of monomer, M_n and M_w are the number-average and weight-average accumulated molecular weights of polymer, subindex 0 means initial value, subindex t means integrated value at time t, and the summations are over the different species present for the bifunctional system and over the only specie present for the monofunctional one. The details of the simulation program BIFUN may be found elsewhere [Villalobos et.al (1991)].

Since both simulation programs based their treatment of the diffusion controlled termination and propagation reactions at high monomer conversions, on the free volume theory, similar modifications have been introduced to both programs in order to account for the presence of n-pentane, fed into the reaction mix in batch fashion at some point in the reaction coordinate. The treatment may be described as follows.

At the beginning of the polymerization the value of the termination rate constant, K_{tc}, is given by:

$$K_{tc0} = A_{tc} \exp(-E_{tc}/RT) \qquad (3.23)$$

The monomer conversion at which the n-pentane is introduced to the reaction mix is denoted as $X_{ad}(C_5)$. Upon polymerization, the total volume of the system, temperature and conversion dependent, is calculated as:

$$V(X) = V_m(X) + V_p(X) \qquad \text{(for } X<X_{sol}\text{)} \quad (3.24)$$

or

$$V(X) = V_m(X) + V_p(X) + V_{C5} \qquad \text{(for } X\geq X_{sol}\text{)} \quad (3.25)$$

where the subindexes m, p and C5, denote monomer, polymer and n-pentane, respectively, and (X) denotes the value at conversion X. Note that since the mass of n-pentane does not change with conversion its volume is only temperature dependent.

The free volume of the species i in the reaction mix (monomer, polymer and n-pentane) is calculated as a function of conversion as [Williams et.al.(1955)]:

$$VF_i(X) = (0.025 + \alpha_i(T - T_{gi}))(V_i(X)/V(X)) \qquad (3.26)$$

where α_i is the thermal expansion coefficient of the specie i, T is the polymerization temperature, and T_{gi} is the glass transition temperature of the specie i. The free volume of the system at any monomer conversion is, then, given by:

$$VF(X) = VF_m(X) + VF_p(X) \qquad \text{(for } X<X_{sol}\text{)} \quad (3.27)$$

or

$$VF(X) = VF_m(X) + VF_p(X) + VF_{C5}(X) \qquad \text{(for } X\geq X_{sol}\text{)} \quad (3.28)$$

A critical value K_{cr} for the system, denoting the onset of the translational diffusion controlled termination reactions, is defined as a function of temperature only [Marten and Hamielec (1982)]. For every increment in conversion the parameter K is calculated as:

$$K(X) = M_w(X)^M \exp(A/VF(X)) \qquad (3.29)$$

where M and A are adjustable parameters.

When $K \leq K_{cr}$ the termination rate constant is considered to increase linearly with conversion, due to an increase in the segmental diffusion rate of the growing polymer chains as the concentration of polymer in the system increases and the coil sizes decrease [Mahabadi and O'Driscoll (1977)].

Accordingly:

$$K_{tcs}(X) = K_{tc0}(1 + \delta[P](X)) \qquad (3.30)$$

Here K_{tcs} is the segmental diffusion controlled termination rate constant, and δ is a parameter related to the rate of diffusion of the growing polymer chains and the quality of the solvent (monomer plus solvent if present). For homopolymerization of styrene this effect can be completely neglected in which case $K_{tcs} = K_{tc0}$ (i.e. $\delta=0$) [Bhattacharya and Hamielec (1986)].

At the conversion at which K becomes greater than K_{cr}, VF and M_w take their critical values (VF_{cr} and M_{wcr}) and from then on the termination rate constant is considered to decay exponentially according to:

$$K_{tc}(X) = K_{tcs}(M_{wcr}/M_w(X))^N \exp(-A(1/VF(X) - 1/VF_{cr})) \qquad (3.31)$$

where N is an adjustable parameter.

Whenever a free radical polymerization is carried out at temperatures below the glass transition temperature of the polymer being formed ($T<T_{gp}$), the glass transition temperature of the reaction mix (T_{gmix}), which depends on monomer conversion and polymer molecular weight, will equal the polymerization temperature at a critical conversion X_{cr} from which the reaction mix becomes glassy. In the vicinity of X_{cr} the propagation reaction becomes diffusion controlled since the diffusion of monomer to the reactive centre, through the glassy polymer matrix, is extremely slow.

This phenomenon, referred to as the glassy effect, is modeled after Marten and Hamielec (1984), by decreasing the propagation rate constant for $X > X_{cr}$, as:

$$K_p(X) = K_{p0}\exp(-B(1/VF(X) - 1/VF_{cr2})) \qquad (3.32)$$

Here VF_{cr2} is the free volume of the system at X_{cr}, and B is an adjustable parameter.

On the bases of this treatment the expected effect of n-pentane on the reaction rate can now be explained. Upon addition of n-pentane, the free volume of the system increases and so does the molecular mobility of the polymer chains. Since the small molecules of n-pentane diffuse across the polymer coils, the plasticizing effect thus induced facilitates the translational diffusion of the growing radicals, necessary to approach each other and terminate. As a result, the onset of the translational diffusion controlled termination reactions is delayed and a decrease in the polymerization rate must be expected according to the decrease of both [M] and R_I.

The decrease in the polymerization rate will proceed up to the conversion at which the free volume of the system is such that the termination reaction become translational diffusion controlled in spite of the plasticizing effect of n-pentane. However, if the concentration of n-pentane is high enough this point may never be reached, in which case a progressive decay of the polymerization rate must be observed.

With regard to the propagation reaction, the increase in free volume caused by the presence of n-pentane may be such that the critical free volume for the diffusion of monomer to the propagating centre may not be reached. That is, the T_{gmix} may never reach the polymerization temperature (i.e. the polymerization mix does not become glassy) due to the strong plasticizing effect caused by the high molecular mobility (low T_g) of n-pentane. In such cases K_p will not fall.

Since the onset of the diffusion controlled termination reaction occurs at a larger free volume than the onset of the diffusion control propagation reaction the following scenarios are possible depending on the amount of n-pentane in the reaction mix:

a) Delay of the onset of both diffusion controlled termination and propagation reactions. In this case, the gel effect and the glassy effect occur at higher conversion than in the absence of n-pentane with the consequent decrease in the polymerization rate during the delay until the system auto-accelerates.

b) Delay of the onset of diffusion controlled termination and absence of glassy effect. In this case, the gel effect will occur at higher conversions than in the absence of n-pentane with the consequent decrease in polymerization rate during the delay. However, once the gel effect occurs the auto-acceleration must lead to terminal conversions approaching 100 %.

c) Absence of both gel and glassy effects. In such case the polymerization rate will decrease progressively according to the decrease in [M] and $[I]^{1/2}$.

In all three cases lower molecular weights at terminal conversions should be expected inasmuch as the larger build-up of molecular weight occurs during the gel effect owing to the longer radical mean life times before termination caused by the lower translational diffusion of the growing radicals. In the limiting case, when the radicals remain alive due to immobility in the glassy medium, this phenomenon is referred to as radical trapping [Zhu et.al. (1990)].

3.4 Experimental

3.4.1 Materials

Styrene (Aldrich Chemical) was washed and distilled following standard procedures [Villalobos et.al.(1989)]. Monofunctional initiator benzoyl peroxide (Lucidol-BPO, Pennwalt-Lucidol Co.), and bifunctional

initiator 1,4-bis(tertbutyl peroxycarbo)cyclohexane (Initiator D 162, Akzo-Chemie) were used without any further purification. Chloroform, and methanol, both reactive grade, were used as polystyrene solvent and non-solvent, respectively. N-Pentane analytical grade (Aldrich Chemical) was employed in all studies.

3.4.2 Design of Experiments

First, in order to evaluate the effect of n-pentane concentration and monomer conversion at which is added, on polymerization rate and molecular weight distribution development, for monofunctional initiation, the following set of experiments were designed:

Experimental Design PS/C5-01

Monofunctional Bulk Polymerization of Styrene with N-Pentane

RUN (#)	[C5]o (wt%)	X_{AD} (%)	[BPO]o (M/L)	Tp (°C)	tp (hrs)
1	0.0	0 or 100	0.01	90	8.0
2	7.5	0	0.01	90	8.0
3	15.0	0	0.01	90	8.0
4	7.5	50	0.01	90	8.0

To evaluate the effect of the observed polymerization rate on MPS and PSD in monofunctionally initiated suspension polymerization of styrene with n-pentane, the following set of experiments were carried out.

Experimental Design PS/C5-02

Monofunctional Suspension Polymerization of Styrene with N-Pentane

RUN #	[C5] (wt%)	X_{AD} (%)	[BPO](M/L)	Tp (°C)	tp (hrs)
1	7.5	0	0.01	90	8.0
2	7.5	50	0.01	90	8.0
3	7.5	100	0.01	90	8.0
4	7.5	90	0.01	90	8.0

Similarly, to evaluate the effect of n-pentane concentration and monomer conversion when it is added, on polymerization rate and molecular weight distribution development, for bifunctionally initiated polystyrene, the following set of experiments were designed:

Experimental Design PS/C5-03

Bifunctional Bulk Polymerization of Styrene with N-Pentane

RUN (#)	[C5]o (wt%)	X_{AD} (%)	[TBPCC]o (M/L)	Tp (°C)	tp (hrs)
1	0.0	0 or 100	0.01	105	8.0
2	7.5	0	0.01	105	8.0
3	15.0	0	0.01	105	8.0
4	7.5	50	0.01	105	8.0

Finally, to evaluate the effect of the observed polymerization rate on MPS and PSD in bifunctionally initiated suspension polymerization of styrene with n-pentane, the following set of experiments were carried out.

Experimental Design PS/C5-04

bifunctional Suspension Polymerization of Styrene with N-Pentane

RUN #	[C5] (wt%)	X_{AD} (%)	[TBPCC](M)	Tp (°C)	tp (hrs)
1	7.5	0	0.01	105	6.0
2	7.5	50	0.01	105	6.0
3	7.5	90	0.01	105	6.0
4	7.5	100	0.01	105	6.0

3.4.3 Techniques

All isothermal bulk polymerizations of styrene with and without n-pentane were carried out in 5 mm (OD) glass ampoules to minimize local heat effects [Zhu (1991)]. The ampoule contents were degassed through the standard freeze-thaw cycles and sealed under a maximum pressure of 10^{-4} Torr.

The ampoules containing the reaction mix and n-pentane for the experiments at X_{nd} = 0, and the experiments without n-pentane (X_{nd}=1) were sealed in the standard way described, whereas the ampoules containing the reaction mix for the experiments at X_{nd}=0.5 were sealed with a microsyringe at the top, containing the required amount of n-pentane.

Polymerizations were carried out by immersing the ampoules in an oil bath at the required temperature. The ampoules were removed from the bath at the required times, and immediately quenched in liquid nitrogen. Based on the conversion data for the experiments without n-pentane the n-pentane was added to the ampoule mix, through the microsyringe, at a time when X=0.5. After addition, the new reaction mix was homogenized through agitation, to avoid possible phase separation.

Conversions in the ampoules were determined gravimetrically by dissolving the ampoule contents in chloroform, and precipitating the polymer with a ten fold excess of methanol. the slurry was vacuum filtered and washed thoroughly with methanol. The polymer was recovered and dried under vacuum at 100°C for 24 hours to eliminate all traces of solvent, non-solvent and n-pentane.

The molecular weight distributions of selected samples were determined by size exclusion chromatography (SEC) using tetrahydrofuran as carrier solvent in a Waters Scientific Model-150 GPC/ALC.

Model predictions for all the experiments carried out were performed with the modified versions of the MONOFUN and BIFUN simulation programs, described above, using the kinetic rate constants and model parameters values given in Table 3.1, below. The modified versions of these programs were named MONOPEN and BIPEN simulation programs.

Suspension polymerizations were carried out in a 1 gal. stainless steel pilot plant reactor vessel, scaled-down from plant data of two different commercial manufacturers of expandable polystyrene (Industrias Resistol, S.A., and PlastiFab LTD).

Table 3.1

Values of the Parameters Used in the Simulations

Parameter and Value Used	Units
Monofunctional System (BPO)	
$K_d = 2.2896 \times 10^{14} \exp(-27233/RT)$	min^{-1}
$f = 0.6$	
Bifunctional System (TBPCC)	
$K_{d1} = 2.117 \times 10^{14} \exp(-28064/RT)$	min^{-1}
$K_{d2} = 3.850 \times 10^{20} \exp(-40022/RT)$	min^{-1}
$f = 0.7$	
Both Systems	
$K_p = 6.128 \times 10^{8} \exp(-7068/RT)$	L/mol-min
$K_{tco} = 7.550 \times 10^{10} \exp(-1677/RT)$	L/mol-min
$K_{Tim} = 6.128 \times 10^{8} \exp(-13450/RT)$	L/mol-min
$K_{th} = 1.314 \times 10^{7} \exp(-27440/RT)$	min^{-1}
N-Pentane	
$T_g = 123$ °K; $\alpha = 0.00079$ (1/°K); $d = 0.649 - 0.00115(T°C)$ Kg/L	
Styrene	
$T_g = 185$ °K; $\alpha = 0.001$ (1/°K); $d = 0.924 - 0.000918(T°C)$ Kg/L	
Polystyrene	
$T_g = 370$ °K; $\alpha = 0.00048$ (1/°K); $d = 1.084 - 0.000605(T°C)$ Kg/L	
Gel and Glassy Effect Parameters	
$K = 9.44\exp(1929/T)$; $A = 0.348$; $M = 0.5$, $N = 1.75$; $B = 1.0$	
$\delta = 0$ $(X < X_{ad})$; $\delta = 1$ $(X \geq X_{ad})$; $VF_{cr2} = 0.0465$; $D = 1.75$	

The reactor internal arrangement and operating conditions can be seen in Table 3.2. Details of the scale-down procedure for EPS pilot plant reactors have been published elsewhere [Villalobos (1989)].

The MPS and PSD of the resulting beads were determined by sieving the samples through an adequate set of different mesh sizes. The terminal conversion of the PS beads was determined gravimetrically following the same procedure described above.

Table 3.2

Reactor Internal Arrangement and Operating Conditions

Recipe:	
Initial volume @ 25° C (deionized water + styrene)	V_0 = 3200 cc
Dispersed phase volume fraction (@ 25°C)	Φ = 0.4
Initiator concentration (BPO or TBPCC)	[I]o = 0.01 mol/L-sty
Suspending agent (TCP) concentration	[TCP]o = 7.5 g/L-sty
N-Pentane concentration	$[C_5]_{xad}$ = 0, 7.5, 15 wt % (wrt styrene)
Operating Conditions:	
Polymerization temperature	T_p = 90, 105°C
Polymerization pressure ($X < X_{ad}$)	P_0 = 275 KPa
Polymerization pressure ($X \geq X_{ad}$)	P = 825 KPa
Polymerization time (monofunctional,bifunctional)	t_m =8 hrs, t_b =6 hrs.
Agitation speed	N = 275 rpm
Geometrical Parameters	
Liquid height (Z) to tank diameter (T) ratio	Z/T = 1.2
Impeller diameter (D) to tank diameter (T) ratio	D/T = 0.6
Impeller type (turbine)	4-blade, 45°pitch
Number of impellers	No = 2
Position of bottom impeller (from reactor bottom)	H_1 = T/4
Position of top impeller (from reactor bottom)	H_2 = (2/3)Z
Blade width	W_i = 0.2 D
Number and position of baffles (offset T/44)	Bf = 4, every 90°
Baffle width	W_b = T/12

Impregnation efficiency was determined gravimetrically, quantifying the volatile contents of the beads (corrected for residual monomer), after expanding and melting the beads in vacuum at 180°C for 12 hours.

3.5 Results and Discussion

3.5.1 Monofunctionally Initiated Systems

According to the experimental design PS/C5-01, the effect of the concentration of n-pentane added from the beginning of the polymerization (X_{ad} = 0) on the styrene bulk polymerization rate and molecular weight distribution development, was studied first.

Figure 3.1, shows the experimental and model results of conversion history for bulk PS initiated with BPO (0.01 mol/L) at 90°C. In the absence of n-pentane ($[C_5]=0$) the curve shows the onset of the gel effect at about 50% conversion. When 7.5 wt% n-pentane is present, two main differences in the conversion history are observed. First an initial slight decrease in the polymerization rate and secondly no occurrence of gel effect.

The initial decrease in polymerization rate, in addition to the lower monomer and initiator concentrations due to the presence of n-pentane in the system, is due to an increase in the segmental diffusion controlled termination rate, caused by the decrease in growing polymer coil sizes in the pentane-plasticized system. This decrease in the coil sizes is brought about by the fact that the monomer/pentane mix is a poorer solvent for polystyrene than the pure monomer is (solubility parameters δ_s=9.3, δ_{c5}=7.08, δ_{PS}=8.72-9.11 $(cal/cc)^{1/2}$) [Sears and Darby (1982)]. In a poorer solvent, the coil sizes decrease and the segmental diffusion increases.

This behaviour was modelled by giving δ (in eq. 3.30) a value of δ = 1 to account for the increase in the segmental diffusion of the smaller coils. The reduction in magnitude of the gel effect is clear from the data (conversion/time) and was well simulated by the increase in the free volume of the system caused by the n-pentane.

The onset of translational diffusion controlled termination is not reached due to the plasticizing effect of the small pentane molecules which increases the translational diffusion of the growing polymer chains.

The limiting conversion observed is due to the decrease in the overall rate of reaction due to the low monomer concentration in the system and very low initiator concentration in the late stages of the reaction ($t_{1/2}$=1.5 hrs @ 90° for BPO).

The glassy effect does not occur in this system since the T_g of polystyrene with 7.5 wt% of n-pentane is well below 90°C ($T_{g_{MS}}$=97°C, $T_{g_{PS}}$=-150°C).

The curve for 15 wt% n-pentane in the initial polymerization mix shows a similar initial decrease in polymerization rate and absence of gel effect, with lower terminal conversion, as the former curve. The initial decrease in polymerization rate was explained and satisfactorily modelled as for the system with 7.5% pentane inasmuch as the coils sizes must decrease more in the poorer solvent at higher concentrations of n-pentane.

The absence of gel effect was also satisfactorily explained and simulated by the larger increase in the free volume of the system which averts the onset of the diffusion controlled termination. The lower terminal conversion is, then, due to the decrease in the polymerization rate as [M] and [I] decrease.

The evolution of the molecular weight averages with conversion for the three cases is shown in figure 3.2. In this figure it is remarkable how the molecular weight averages are similar throughout the entire conversion range, but especially at high conversions, in spite of the absence of gel effect for the systems with n-pentane.

Even though this behaviour can be partially explained by the low polymerization rates experienced by the systems with n-pentane at high conversions (X>50%) along with the low radical concentration in the system caused by the initiator depletion, which reduces the termination rate in chemically controlled termination, lower molecular weights than for the system without n-pentane, should be expected. Therefore, another phenomenon must also be responsible for the molecular weight build up in the systems with n-pentane.

The effect of solvents on the extent of chain transfer reactions have been reported elsewhere. For donor-acceptor systems it has been shown that the presence of non-polymerizing strong electron donor solvents inhibits chain transfer reactions by either solvation of free monomer or by secondary complex formation with the acceptor monomer [Carter et.al.(1965), Tsuchida et.al.(1972)].

For the case at hand since n-pentane is a stronger electron donor than styrene and even though styrene cannot be considered as an electron acceptor, pentane solvation of free monomer can obstruct the hydrogen abstraction necessary for chain transfer to monomer to occur. In such a case, the extent of chain transfer to monomer reactions will depend on the n-pentane concentration, and the extraordinary molecular weight build-up in the systems with n-pentane can be explained.

In order to account for this effect, the transfer to monomer rate constant was considered to decrease with n-pentane concentration in the system according to:

$$K_{Trm} = K_{Trm0} \exp(-D*VF_{C5}) \qquad (3.33)$$

Where K_{Trm0} is the transfer to monomer rate constant for the system without n-pentane, and D is an adjustable parameter.

This model was included in the simulation programs MONOPEN and BIPEN where the value of D was fit to 1.75 (see Table 3.1), with which the simulated molecular weight averages described the actual trend. All simulations reported herein were performed with the above treatment.

The effect of the conversion level for addition of n-pentane on styrene polymerization rate and molecular weight distribution development was studied. Figure 3.3, shows the experimental and model results for conversion history for the systems with 7.5 wt% n-pentane added at 0, 50 and 100% conversion. The curves for X_{ad}=0 and 100% conversion have been discussed above (curves for 7.5% and 0% pentane in figure 3.1).

When pentane is added at 50% conversion an immediate decrease in the polymerization rate is observed and the onset of the gel effect is delayed to conversions above 70% where a marginal increase in polymerization rate occurs. For this system the limiting terminal conversion (c.a. 90%) is higher than for the system where X_{nd}=0 but lower than for the system without n-pentane. This higher terminal conversion is obtained owing to the higher initial polymerization rate and the weak gel effect experienced.

Figure 3.4 shows the evolution of the molecular weight averages for the three cases considered. The M_n and M_w curves for X_{nd} = 0 and 100% have been discussed above (curves for 7.5% and 0% pentane in figure 3.2). As seen in this figure the initial fall in molecular weights following the addition of n-pentane at 50% conversion, and subsequent molecular weight build-up were properly described by the model. This behaviour is well explained by the delayed weak gel effect observed, along with limited transfer to monomer reactions from the point of addition on n-pentane.

Once the effect of n-pentane on polymerization rate (R_p) and molecular weight distribution development was established, suspension polymerizations with 7.5 wt% of n-pentane added at 0, 50 and 100% were carried out, under the same polymerization conditions (T=90°C, [BPO]=0.01 mol/L-styrene) according to the experimental design PS/C5-02, in order to evaluate the effect of pentane, R_p and MWD development on suspension stability, mean particle size (MPS), and particle size distribution (PSD).

The polymerization recipe and reactor operating conditions employed (see Table 3.2), correspond to the scaled-down system selected to obtain a MPS of 0.60 mm when monofunctional initiation with BPO (0.01 mol/L) at 90°C is used and no pentane is added during polymerization (see Villalobos (1989)).

Figure 3.5, shows the PSD obtained for the system with X_{nd}=100% (reference system with no pentane added). The MPS obtained was 0.598 mm with a PSD coefficient of variation CV=0.511. The coefficient of variation (CV) characterizes the spread of the distribution and is defined

as σ/MPS, where σ is the standard deviation of the distribution. The reference system, then, reproduced the MPS expected from to the scale-down procedure (target size 0.6 mm) [Villalobos (1989)].

The large spread of the distribution, and its bimodal character, are characteristics of suspension polymerizations carried out in small pilot reactors [Konno et.al.(1982)].

In large commercial reactors unimodal distributions with coefficients of variation ranging from 0.25 to 0.35 are obtained, when this MPS is produced [Villalobos (1989)].

The systems with X_{ad}=0, and 50%, both experienced suspension set-ups (massive particle agglomeration), after 6 and 6.5 hrs. of polymerization, respectively.

This behaviour can be explained in terms of the conversion curves shown in figure 3.3. For the system without n-pentane (X_{ad}=100%), the particle growth stage, occurring between 30 and 70% conversion, lasts for a total of three hours. When pentane is added from the beginning of the polymerization (X_{ad}=0) the critical viscosity for particle growth is reached after about 2 hrs. of polymerization. From then on particle coalescence is enhanced, even in the presence of suspending agent. Since the viscosity of the beads is lower in this system than for the system without n-pentane, owing to the plasticization of the matrix, the decrease in the polymerization rate prevents the system from reaching the identity point. As a result, coalescence continues indefinitely until suspension set-up (massive coagulation) occurs.

When n-pentane is added at 50% conversion (X_{ad}=50%), the beads are half way through the growth stage. In this case the plasticization of the beads, and the decrease in polymerization rate delay the attainment of the identity point. As a result the particle growth stage is extended for at least two more hours which is enough for total coalescence of the beads to occur.

In addition, the diffusion of n-pentane through the suspending agent-protected surface of the beads seems to increase the coalescence rate. This may be due to the diffusion mechanism of n-pentane in the monomer/polymer particles. It has been shown, that when n-pentane is added to the suspension at high conversions, it diffuses very rapidly into the periphery of the beads (diffusion coefficient D about 1.0×10^{-6} cm^2/s) where it concentrates. After almost complete n-pentane uptake in a few minutes, the pentane starts to diffuse more slowly towards the core of the beads (D from 2.0×10^{-7} to 1.0×10^{-10} cm^2/s, depending on the degree of conversion) [Villalobos (1992)].

As a consequence of this diffusion mechanism, after addition of n-pentane at 50% conversion, most of the n-pentane added will concentrate on the periphery of the beads plasticizing them to such a extent, that the surface viscosity of the particles decreases to levels at which particle coalescence is very effective. The net results being suspension instability and total coalescence.

In an attempt to stabilize these systems, the experiments were repeated after increasing the suspending agent concentration two fold. Although the initial suspensions seemed more stable, total coalescence occurred after 7 hrs. of polymerization. Moreover, an experiment with X_{ad}=90% was also attempted, under the same conditions, in which the resulting beads were extremely large (MPS > 2.5 mm) and completely deformed. This corroborated the effect of the diffusion mechanism of n-pentane on the coalescence rate.

It is obvious that the marginal increase in productivity achieved at X_{ad}=90% with respect to the current manufacturing processes in which n-pentane is added at the glassy point (about 96% conversion) does not compensate for the instability problems observed.

In light of these results, and since the systems with early addition of n-pentane cannot be taken to higher terminal conversions by increasing the initiator concentration without lowering the molecular weights of the product and in turn its processing characteristics and

mechanical properties, it is no wonder that early addition of n-pentane to the monofunctionally initiated suspension polymerization of PS has not found use in industry.

3.5.2 Bifunctionally Initiated Systems

As in the case of monofunctionally initiated systems and according to the experimental design PS/C5-03, the effect of the concentration of n-pentane, added from the beginning (X_{sd}=0) on styrene polymerization rate (R_p) and molecular weight distribution development (MWD) was studied first. Ampoule bulk polymerizations were carried at T=105°C, using TBPCC (0.01 mol/L) as bifunctional initiator.

Figure 3.6, shows the experimental and model results for conversion history for systems with 0, 7.5 and 15 wt% n-pentane. The first remarkable feature observed in these curves is that, in spite of the n-pentane concentration, all the systems reach terminal conversions close to 100%. For the system without n-pentane the onset of the gel effect occurs at about 50% conversion and since the polymerization temperature T is above the T_g of polystyrene no glassy effect occurs. Note that for this system 97% conversion is reached after only 2.5 hrs of polymerization.

The system with 7.5 wt% n-pentane shows a delay in the onset of the gel effect to conversions above 70%. The weak gel effect experienced by this system caused by the enhanced free volume and the plasticization of the polymer matrix, well represented by the kinetic model, was capable of carrying the polymerization to completion in about 6 hours.

For the system with 15 wt% n-pentane, an even more delayed and weaker gel effect occurs. The occurrence of this weak gel effect is only noticeable in that the reaction rate does not fall according to the decrease in [M] and $[I]^{1/2}$. For this system the moderated auto-acceleration experienced was capable of carrying the polymerization to completion in about 8 hours. In addition, for the two systems with n-pentane, the contribution of the thermal initiation of styrene to the total initiation

rate, at this temperature level, prevented lower terminal conversions caused by dead end polymerization after virtual initiator depletion at four hours ($t_{1/2}$=0.5 hrs.@ 105°C).

The experimental and model results for the effect of n-pentane concentration on MWD development for the above systems is shown in figure 3.7. Note that in spite of the high reaction rates reached (almost four times higher than for monofunctional initiation), the weight average molecular weight of the final products are only 15 to 20% lower than for the monofunctional case. The M_w obtained for all three cases are still within the range for adequate processing of EPS (M_w from 180,000 to 250,000) [Villalobos (1989)]. Moreover, the final M_n obtained is similar for both monofunctionally and bifunctionally initiated systems.

These results demonstrate the ability of bifunctional initiators to produce high molecular weight polymer at very high reaction rates. Note also in figure 3.7, that the model results closely follow the actual trend, which indicates that the model for enhanced free volume and limited chain transfer to monomer for polymerization in the presence of n-pentane applies as well for bifunctional initiation.

The effect of the conversion at which n-pentane is added, on R_i, and MWD development, in bulk polymerization of styrene initiated with bifunctional initiator TBPCC (0.01 mol/L) at 105°C was also studied, according to experimental design PS/C5-03. Figure 3.8 shows the conversion history for X_{ad} = 0, 50, and 100%. The curves for 0, and 100%, have been discussed above (curves for 7.5 and 0% n-pentane in figure 3.6).

For the system in which n-pentane is introduced at 50% conversion, the curve, as expected, shows an intermediate behaviour between the systems with X_{ad}=0% and X_{ad}=100% and the conversion approaches 100% at about 5 hours. In this curve, an immediate decrease in the polymerization rate is observed upon addition of n-pentane, followed by a delayed and weak gel effect which yields a reaction rate profile similar of that for the curve of X_{ad}=0%, but only at slightly higher conversions equal to the difference in conversions at the addition point.

In figure 3.9, the experimental and model results for the evolution of the molecular weight averages for this system, and the other two discussed before (see figure 3.7 for 0 and 7.5 wt% pentane), are shown. Note the similarity of the M_n curves for all three systems. The model M_w curve for the system with X_{ad}=50% crosses the curve for X_{ad}=0% at about 70% conversion due to the higher polymerization rate of the former at similar gel effect strength. In actuality, the experimental results show that this behaviour occurs at higher conversions.

The model predictions shown in figures 3.8 and 3.9 for the bifunctionally initiated system, closely follow the actual behaviour of the system, which indicates that the model for enhanced free volume and limited transfer to monomer applies also for additions of n-pentane at intermediate conversions.

After establishing the effect of the concentration and conversion at which n-pentane is added, on R_p and MWD development, according to the experimental design PS/C5-04, suspension polymerizations, at 105°C using bifunctional initiator TBPCC, under the same scaled-down conditions as for the monofunctional system, were carried out to evaluate the effect of these variables on suspension stability, MPS, and PSD.

Figure 3.10, shows the particle size distributions of the beads obtained for X_{ad}=0, 50, 90 and 100% conversion under the described conditions.

The similarity of the four distributions obtained is remarkable. The mean particle sizes calculated from the above distributions all were less than the 0.6 mm mean size of the monofunctional reference system (see figure 3.5). In addition, the spread of the PSD's obtained (CV) varied from 0.319 to 0.359 which means that both smaller MPS and narrower PSD are obtained at high polymerization rates, even at temperature above the T_g of polystyrene. Moreover, the final conversions reached were above 99% for all four products, and the impregnation efficiency (defined as the mass of n-pentane in the dry beads divided by the initial mass of n-pentane loaded to the reactor) was above 95% for all three products bearing n-pentane.

The explanation of the observed behaviour is as follows. In the bifunctionally initiated suspension polymerizations carried out, the MPS decreased very slightly from 0.551 mm to 0.542 mm when X_{ad} increased. This is expected inasmuch as the later the addition of n-pentane the shorter the duration of the particle growth stage.

Based on the results given in figure 8, it can be seen that the duration of the particle growth stage (30 to 70% conversion) is 1.2 hrs. for X_{ad}=100 and 90%, 1.4 hrs. for X_{ad}=50%, and 1.6 hrs for X_{ad}=0%. Moreover, it has been shown that the spread of the distribution increases with time during the particle growth stage [Konno et.al.(1982)]. Consequently, shorter growing periods must result in narrower PSD as observed herein.

From these results, it can be concluded that the enhanced particle coalescence caused by both the early presence of n-pentane in the suspension system and the higher polymerization temperatures is completely overcome if substantial reductions in the particle growth time are achieved.

Therefore, the main parameter controlling both MPS and PSD in suspension polymerization of styrene is the duration of the particle growth stage.

In the monofunctionally initiated system studied, the duration of the particle growth stage increases dramatically with the addition of n-pentane, due to a decrease in polymerization rate and limiting conversions which do not allow the system to reach the identity point. In addition, the plasticized polymer particle is more prone to coalescence than the particle without n-pentane. The sum of these effects yields suspension set-ups even at high suspending agent concentrations.

In the bifunctionally initiated systems, the decrease in the polymerization rate caused by the early presence of n-pentane does not limit the terminal conversion and as a result the systems reach the identity point after a particle growing period that is much shorter than that of the monofunctional system without n-pentane. Consequently, stable suspensions are observed, and smaller MPS and narrower PSD are achieved at

the end of the polymerization even with the enhanced particle coalescence caused by the particle plasticization.

Table 3.3, below, summarizes all the experimental results for these systems.

Table 3.3

Suspension Polymerization Experimental Results

Initiator Type	[TCP]o (g/Lst)	X_{ad} (%)	MPS (mm)	σ (mm)	CV (σ/MPS)	CONV (%)	Imp.ef (%)
BPO	7.5	100	0.598	0.306	0.511	96.8	**
TBPCC	7.5	0	0.551	0.176	0.319	>99	95.4
TBPCC	7.5	50	0.550	0.178	0.324	>99	95.9
TBPCC	7.5	90	0.543	0.195	0.359	>99	96.1
TBPCC	7.5	100	0.542	0.196	0.361	>99	**
TBPCC	5.0	50	0.695	0.191	0.275	>99	95.0
TBPCC	3.5	50	0.954	0.266	0.278	>99	97.3

** No n-pentane added.

From the PSD results, it may be suggested that the minimum effect on MPS and PSD observed in the bifunctionally initiated suspension polymerizations of styrene in the presence of n-pentane can be caused by over-stabilization of the system. In spite of the results for the monofunctional system showing that the suspension is not over-stabilized, two additional experiments at X_{ad}=50% with lower suspending agent concentration, were carried out to show the response of the system to changes in stabilizer concentration.

Figure 3.11, below, shows the suspension particle size distributions obtained at different stabilizer concentrations, for the bifunctionally initiated systems (TBPCC=0.01 mol/l, T=105°C), with 7.5 wt% n-pentane added at X_{ad}=50%. The results for MPS, PSD, terminal conversion and impregnation efficiency of these systems are also shown in Table 3.3.

From the results shown in figure 3.11, it is obvious that the system is very sensitive to changes in stabilizer concentration and, therefore, is not over-stabilized.

As expected, the MPS increases as the suspending agent concentration decreases but not so the terminal conversion nor the impregnation efficiency (see Table 3.3).

Note how the distributions become unimodal at larger MPS. The shape of the PSD depending on the MPS in pilot plant reactors has been explained elsewhere [Villalobos (1989)].

Additionally, it has also been proven that all the different commercial EPS bead sizes (0.45 to 2.0 mm) can be obtained in a single stage process, through bifunctionally initiated suspension polymerization of styrene with early addition of n-pentane.

3.6 Conclusions

In this study is reported the modification of previously published kinetic models to account for the unique features of styrene free radical polymerization in the presence of n-pentane, for both monofunctional and bifunctional initiation. The modifications proposed, based on enhanced free volume and limited transfer to monomer reactions caused by the early presence of n-pentane in the polymerizing system, fully describe and closely follow the behaviour of the systems studied.

As a result of the modifications introduced, two simulation programs that forecast monomer conversion and molecular weight distribution development for each type of initiation, have been developed.

The feasibility of carrying out suspension polymerizations of styrene in the presence of n-pentane under different addition conditions, to obtain EPS type beads in a single stage process, has been fully demonstrated for bifunctionally initiated systems.

The high suspension stability exhibited by these systems, corroborates previous findings in that the duration of the particle growth stage is the main parameter determining the stability of the suspension.

For monofunctionally initiated systems, enhanced particle coalescence leading to suspension set-up, caused by the early presence of n-pentane with the consequent inability of the system to reach the identity point, could not be overcome in any of the systems studied.

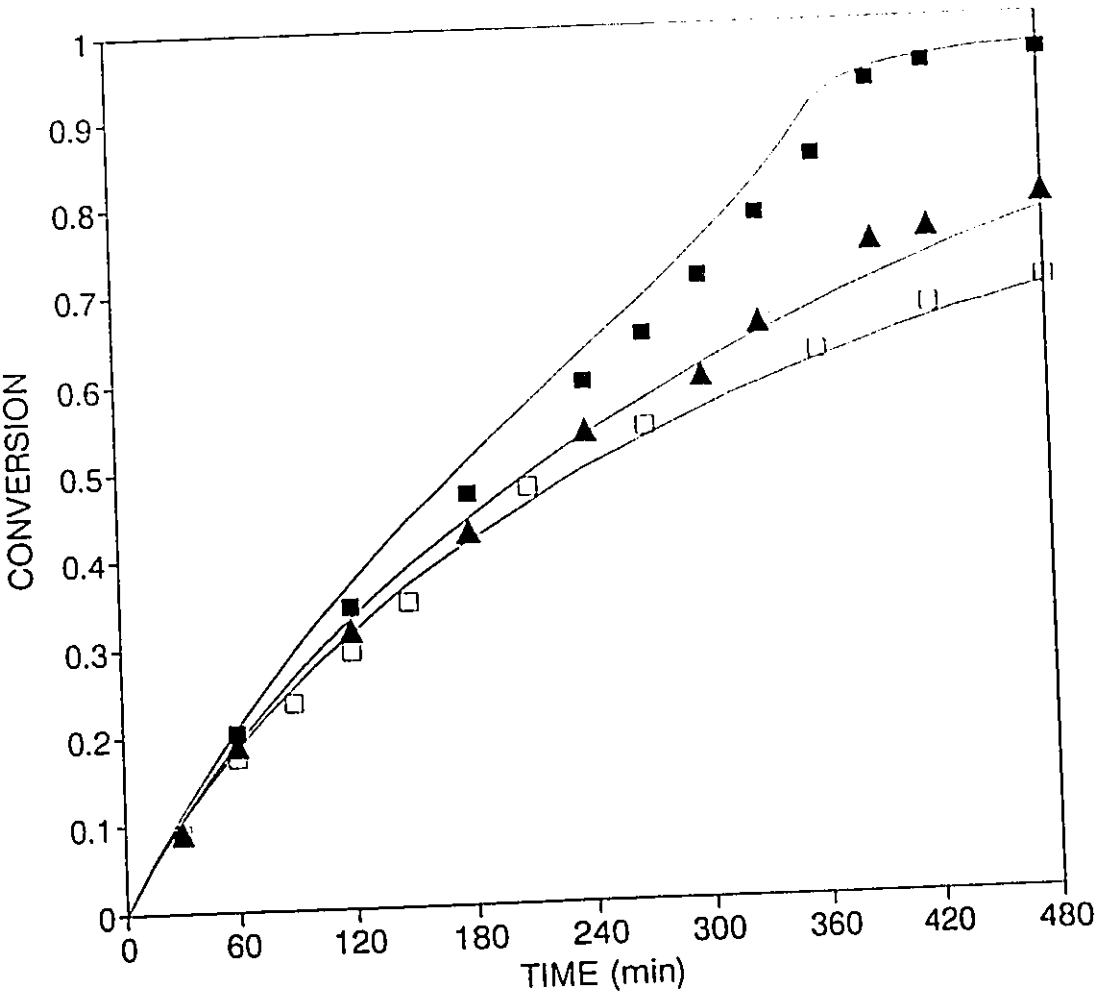

Fig. 3.1. Effect of n-pentane concentration, X_{Ad}=0%, on polymerization rate of styrene initiated with [BPO]=0.01 mol/L, at 90°C. Experimental monomer conversion for 0 (■), 7.5 (▲) and 15.0 (□) wt% n-pentane. Model predictions (——).

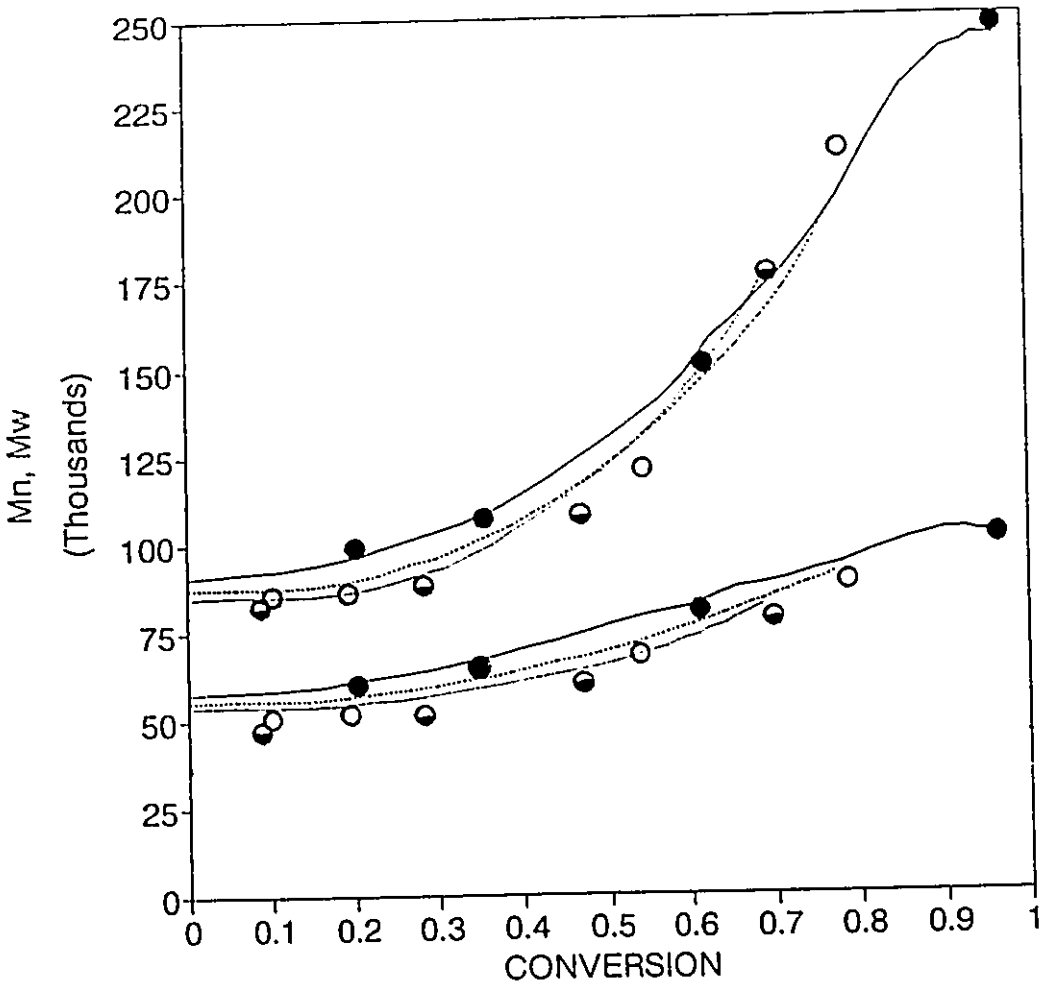

Fig. 3.2. Effect of n-pentane concentration, X_{add}=0%, on molecular weight distribution development of polystyrene initiated with [BPO]=0.01 mol/L, at 90°C. Experimental M_n and M_w for 0 (●), 7.5 (○), and 15.0 (◒) wt% n-pentane. Model predictions for 0 (——), 7.5 (---), and 15.0 (···) wt% n-pentane.

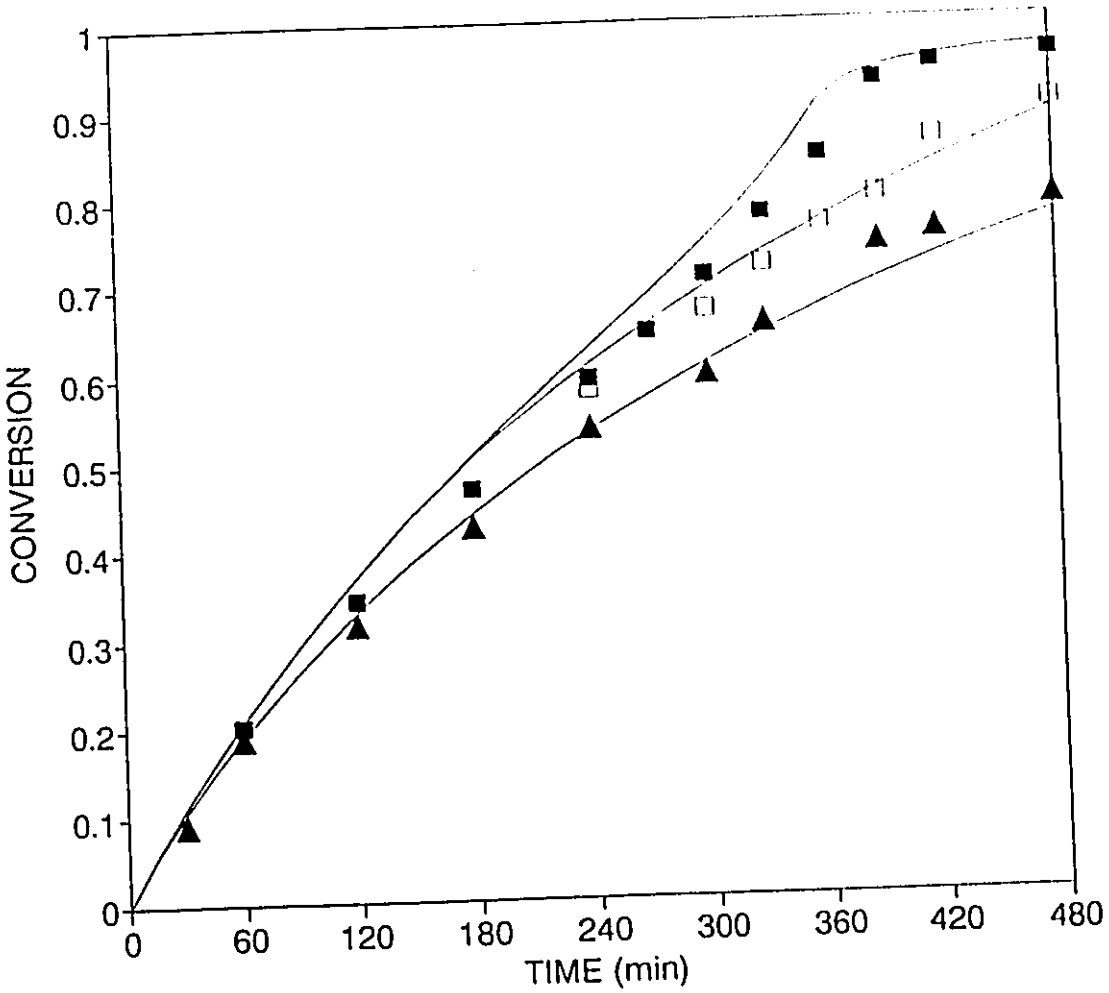

Fig. 3.3. Effect of conversion of addition of n-pentane, [C_5]=7.5 wt%, on polymerization rate of styrene initiated with [BPO]=0.01 mol/L, at 90°C. Experimental monomer conversion for X_{ad} = 0% (▲), 50% (□), and 100% (■). Model predictions (——).

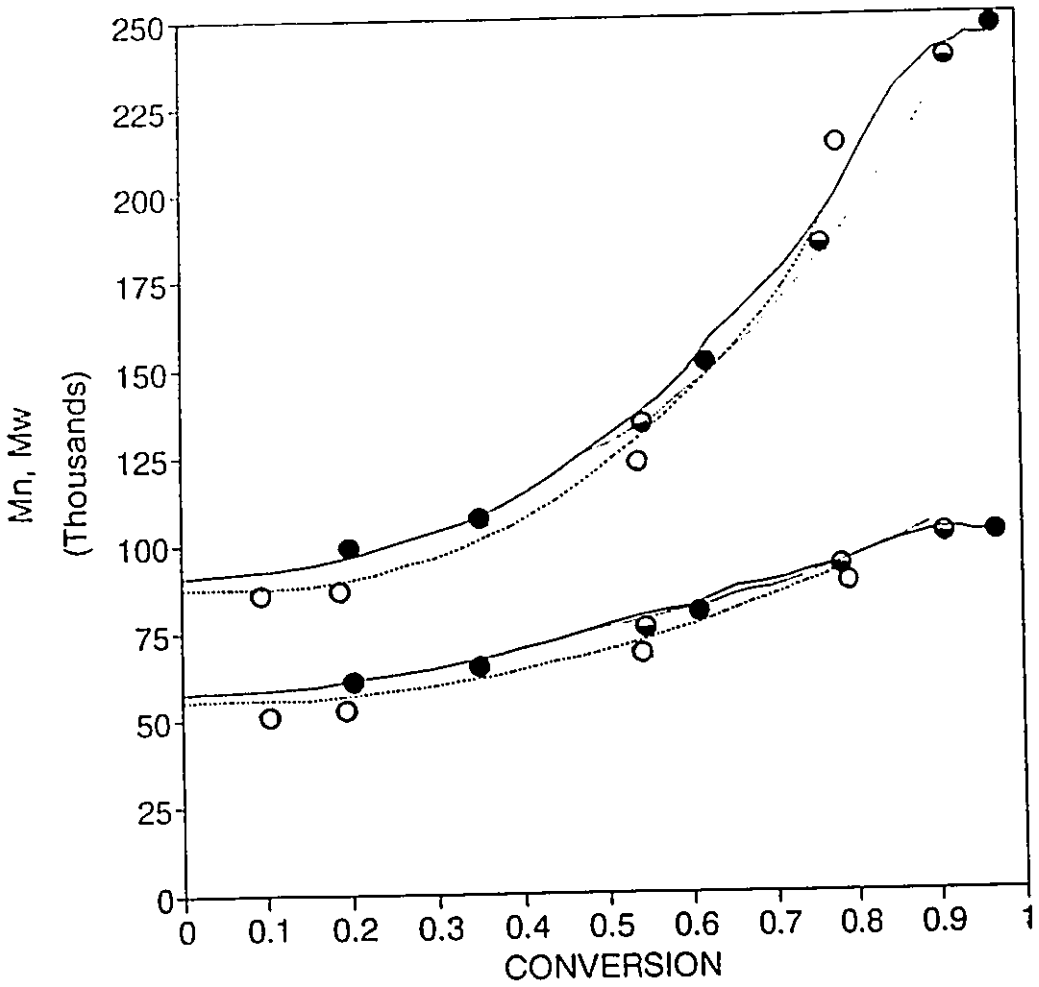

Fig. 3.4. Effect of conversion of addition of n-pentane, [C_5]=7.5 wt%, on molecular weight distribution development of polystyrene initiated with [BPO]=0.01 mol/L, at 90°C. Experimental M_n and M_w for X_{ad}= 0% (O), 50% (◒), and 100% (●). Model predictions for X_{ad} = 0% (---), 50% (···), and 100% (——).

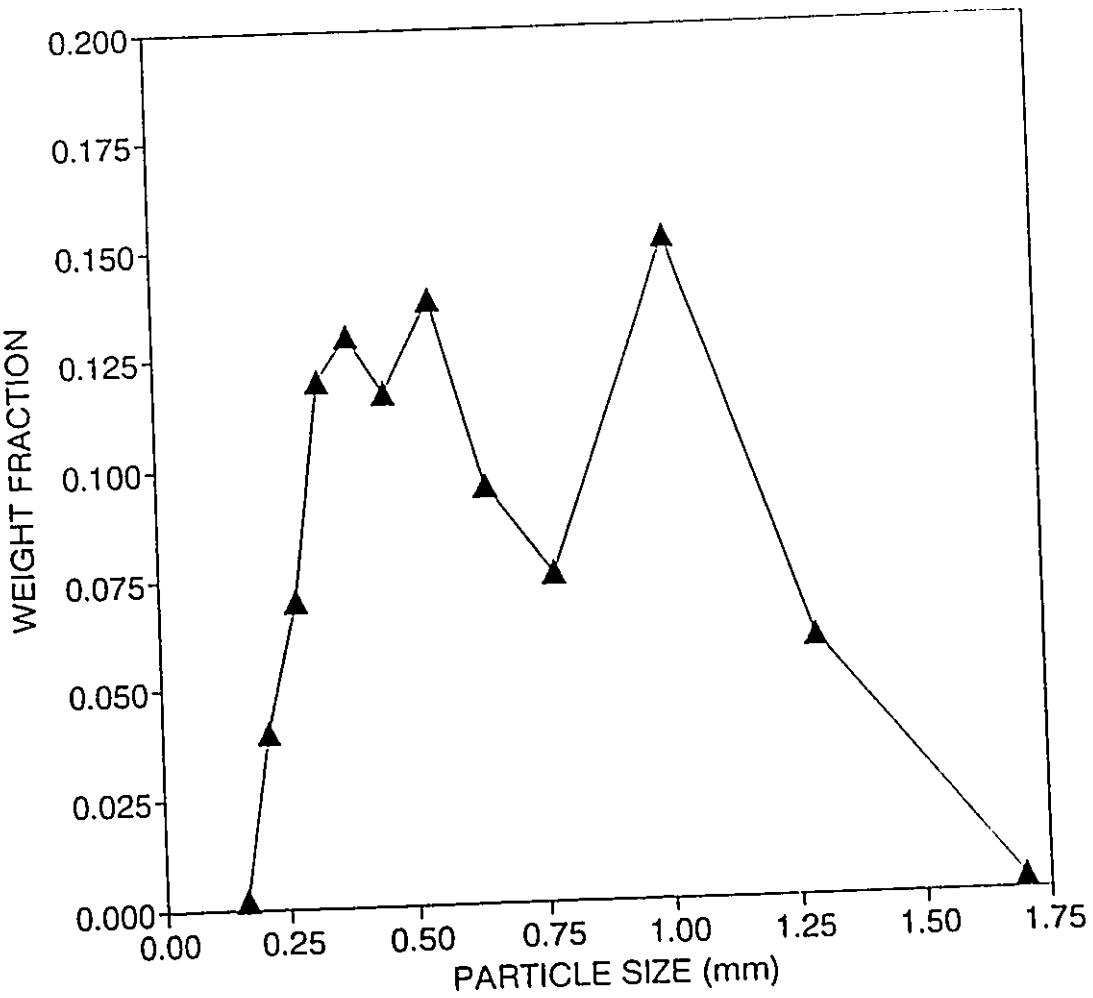

Fig. 3.5. Particle size distribution for suspension polystyrene beads initiated with [BPO]=0.01 mol/L, at 90°C, without n-pentane. Reference system (see Table 2 for reactor operating conditions).

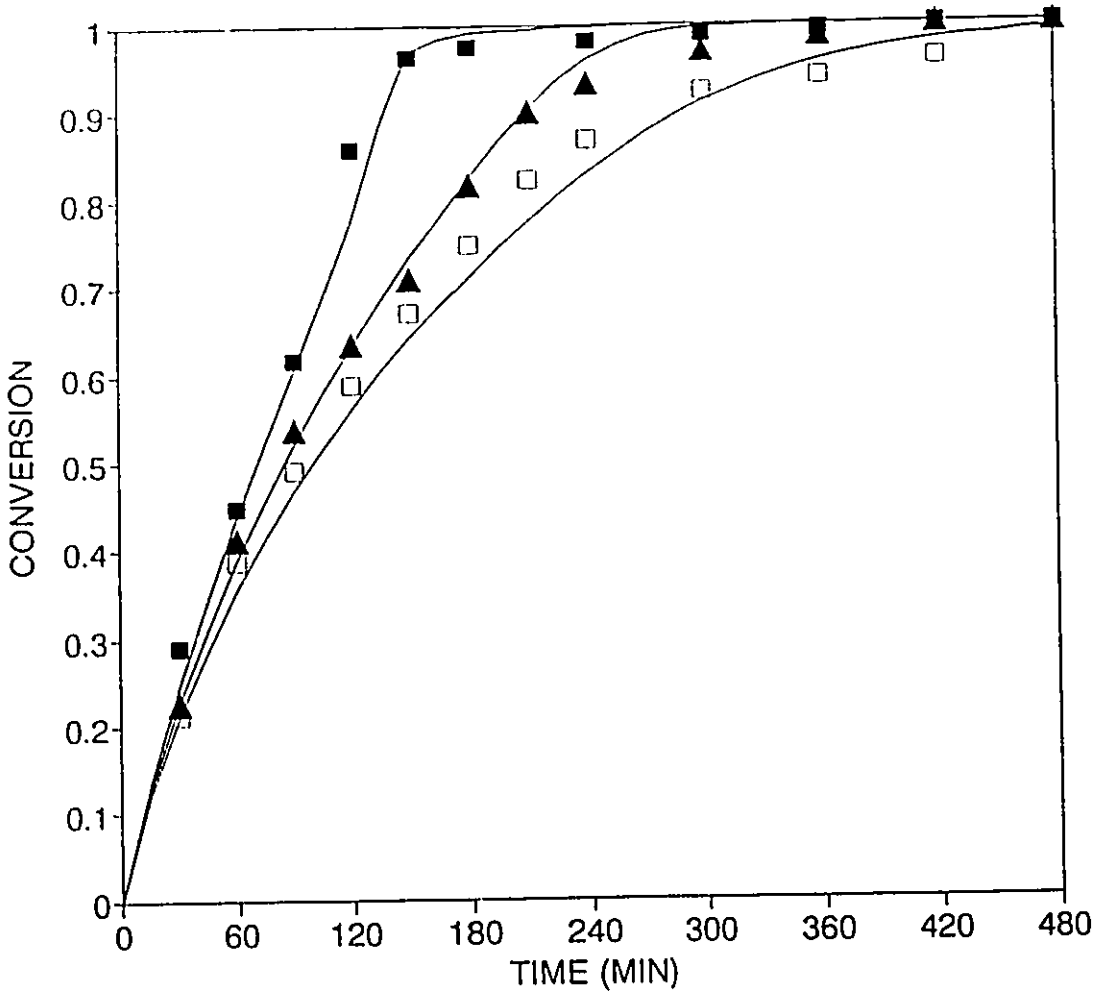

Fig. 3.6. Effect of n-pentane concentration, X_{ad}=0%, on polymerization rate of styrene initiated with [TBPCC]=0.01 mol/L, at 105°C. Experimental monomer conversion for 0 (■), 7.5 (▲) and 15.0 (□) wt% n-pentane. Model predictions (——).

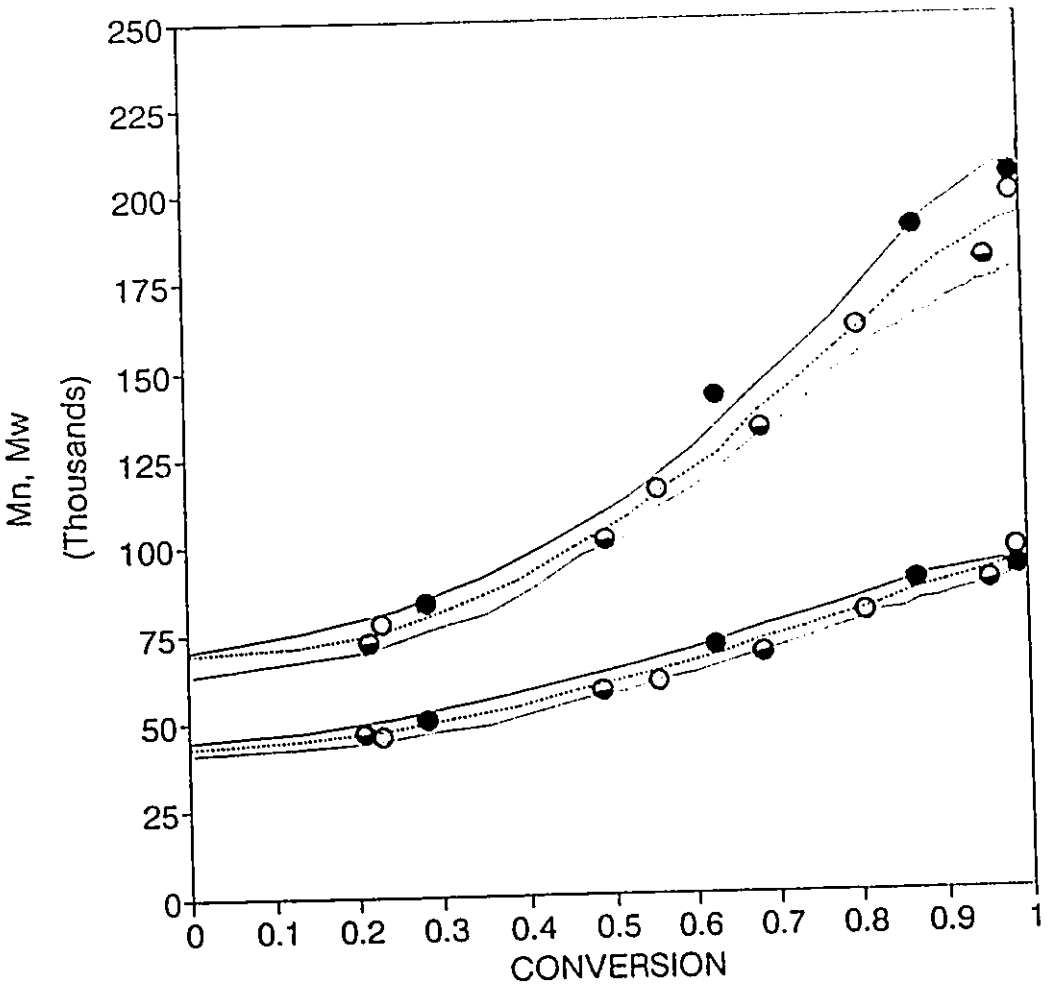

Fig. 3.7. Effect of n-pentane concentration, X_{nd}=0%, on molecular weight distribution development of polystyrene initiated with [TBPCC]= 0.01 mol/L, at 105°C. Experimental M_n and M_w for 0 (●), 7.5 (○), and 15.0 (◒) wt% n-pentane. Model predictions for 0 (——), 7.5 (---), and 15.0 (···) wt% n-pentane.

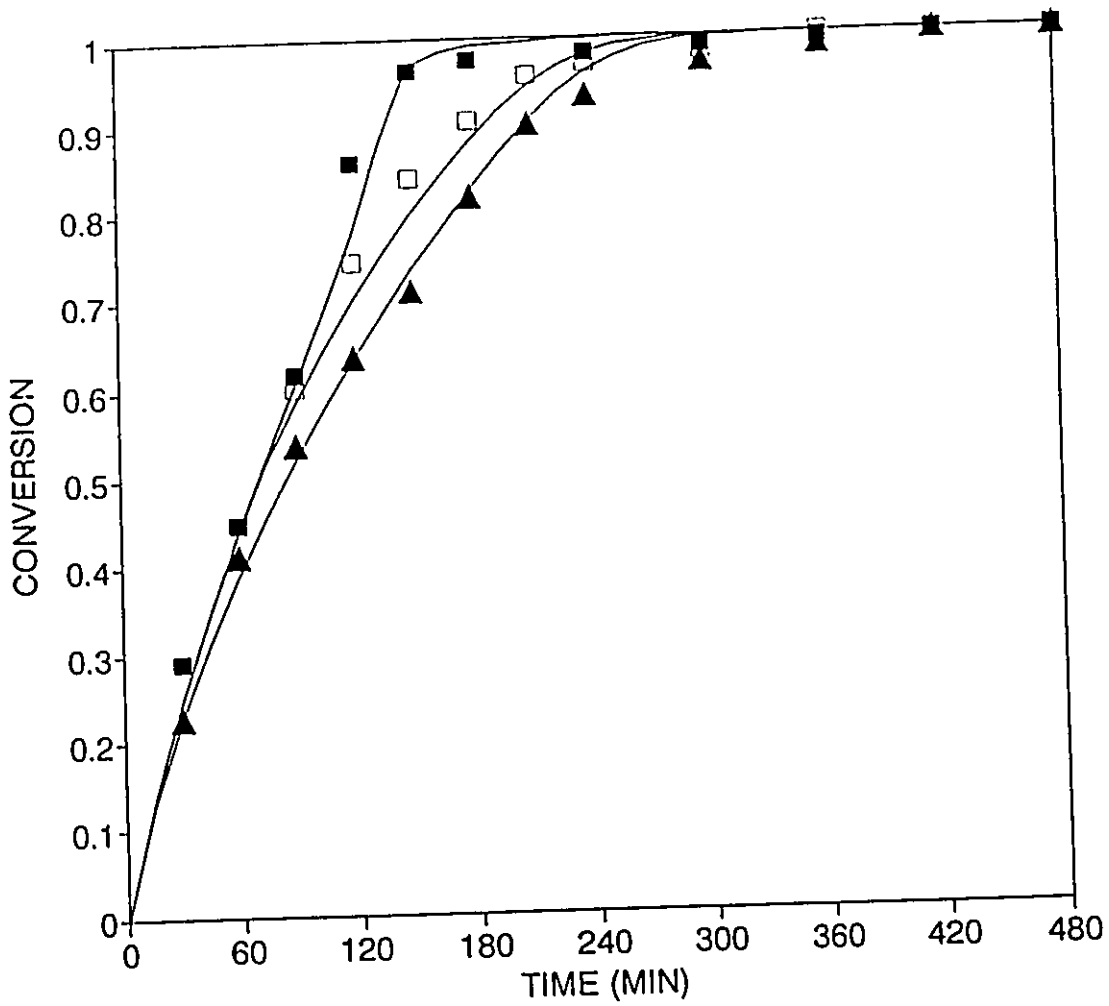

Fig. 3.8. Effect of conversion of addition of n-pentane, $[C_5]$=7.5 wt%, on polymerization rate of styrene initiated with [TBPCC]=0.01 mol/L at 105°C. Experimental monomer conversion for X_{ad} = 0% (▲), 50% (□), and 100% (■). Model predictions (——).

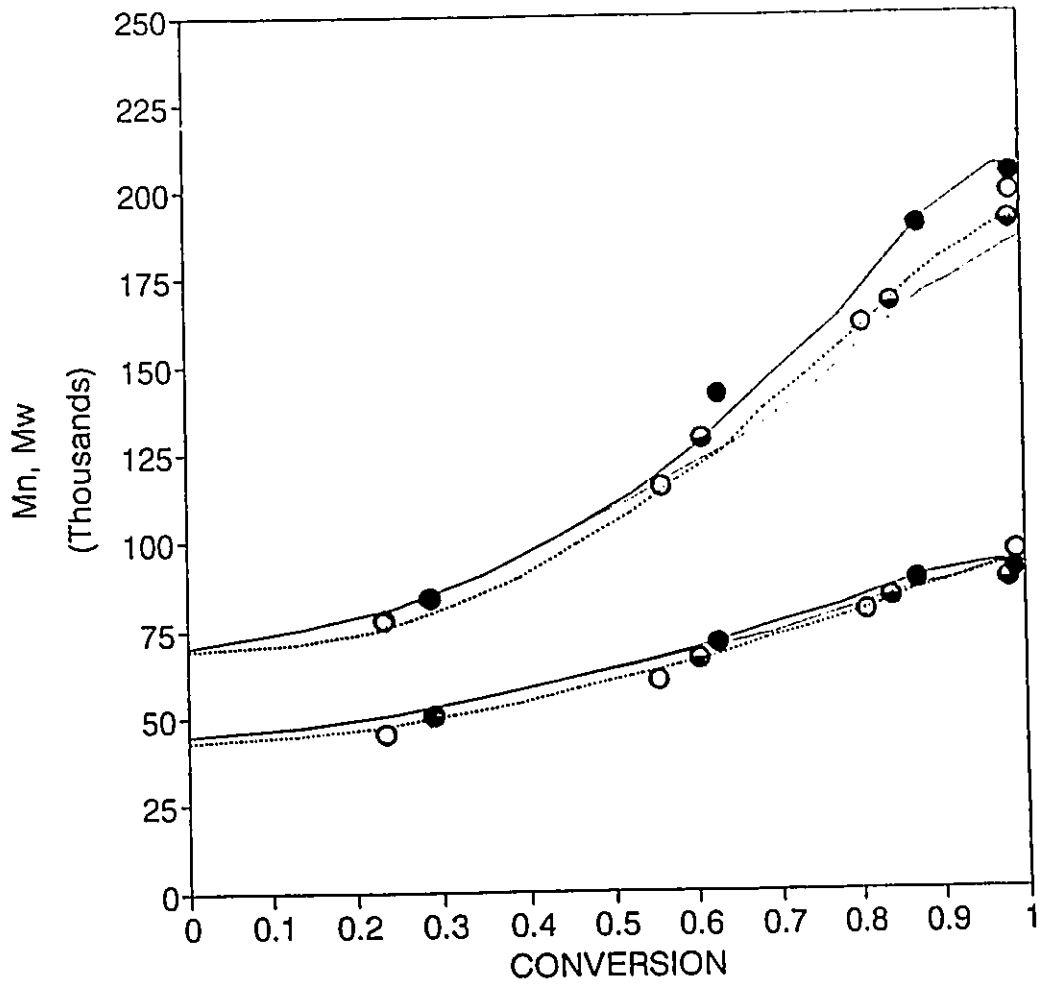

Fig. 3.9. Effect of conversion of addition of n-pentane, [C_5]=7.5 wt%, on molecular weight distribution development of polystyrene initiated with [TBPCC]=0.01 mol/L, at 105°C. Experimental M_n and M_w for X_{ad}= 0% (O), 50% (Θ), and 100% (●). Model predictions for X_{ad}=0% (---), 50% (···), and 100% (——).

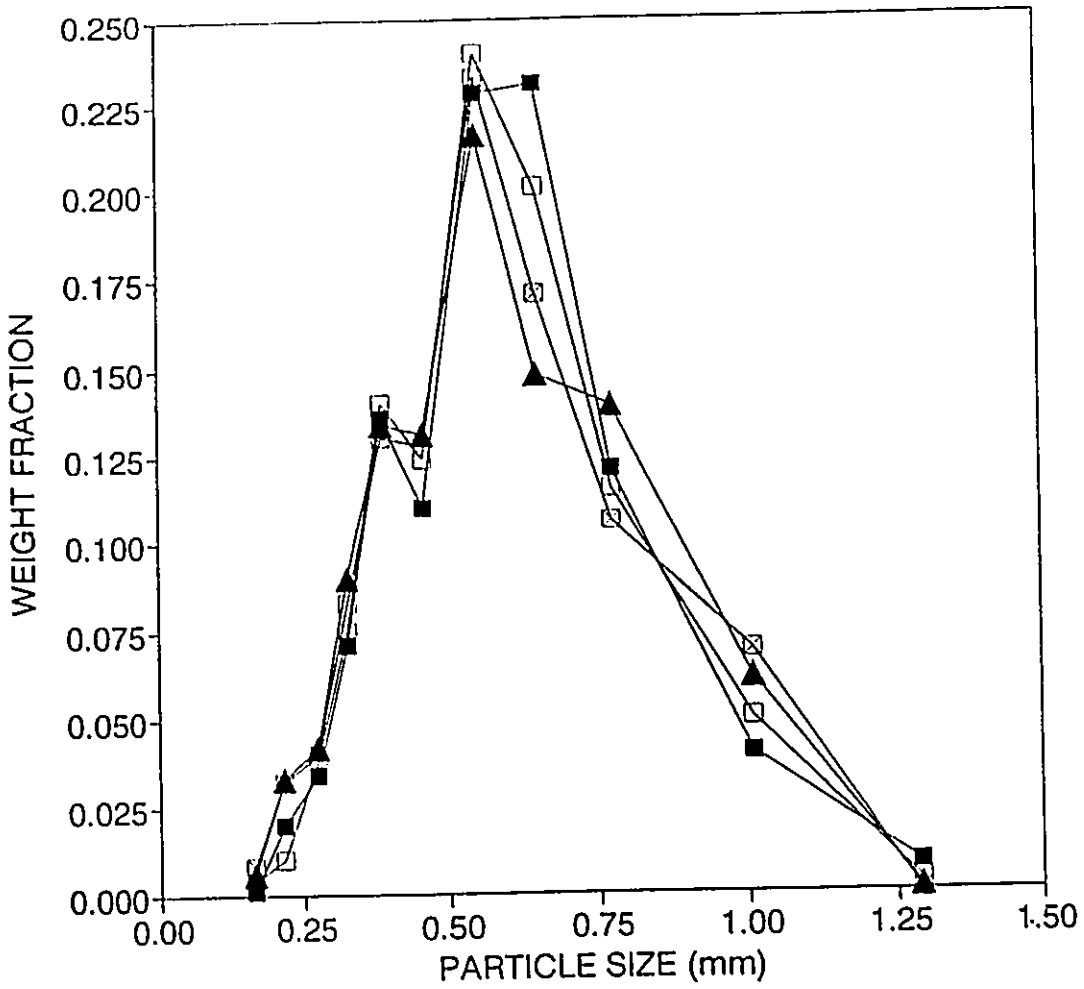

Fig. 10. Effect of conversion of addition of n-pentane, $[C_5]$=7.5 wt%, on particle size distribution for suspension polystyrene beads initiated with [TBPCC]=0.01 mol/L, at 105°C. Experimental results for X_{ad} = 0% (■), 50% (□), 90% (⊠), and 100% (▲) (see Table 2 for reactor operating conditions).

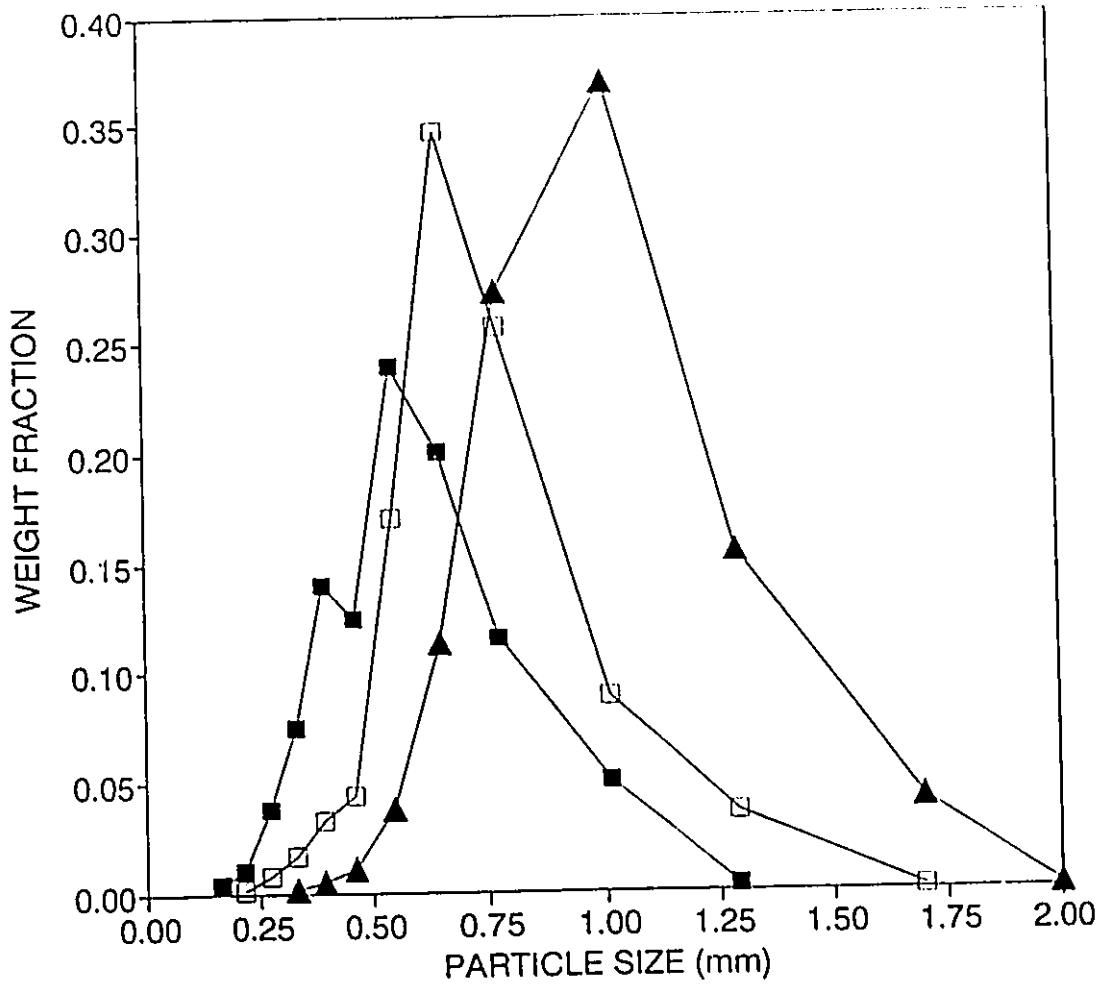

Fig. 3.11. Effect of suspending agent concentration on particle size distribution for suspension polystyrene with early addition of n-pentane, X_{ad}=50%, initiated with [TBPCC]=0.01 mol/L, at 105°C. Experimental results for [TCP] = 7.5 (■), 5.0 (□) and 3.5 (▲) g/L(styrene) (see Table 2 for reactor operating conditions).

CHAPTER 4

FREE RADICAL COPOLYMERIZATION KINETICS WITH BIFUNCTIONAL INITIATORS

In this chapter, the development of the kinetic model for simultaneous statistical/donor-acceptor copolymerization with bifunctional initiators, is explained in detail. A general copolymerization scheme, on which elementary reactions the kinetic model is based, is proposed. Theoretical support for the different stages of the modelling, is given throughout. In addition, a statistical model describing the development of the copolymer micro-structure in bifunctionally initiated free radical copolymerization, is introduced, along with the concepts of effective instantaneous copolymer composition, and distribution of number of segments per copolymer chain.

4.1 Introduction

As mentioned in Chapter 2, bifunctional initiators are diperoxide or di-azo compounds which may be symmetrical or asymmetrical. Their main characteristic is their sequential decomposition kinetics which upon polymerization leads to the formation of temporarily dead polymer chains with terminal undecomposed peroxide groups [Prisyazhnyuk and Ivanechev (1970)].

Around this unique feature, in the late 70's, the idea of synthesizing block copolymers via free radical copolymerization with bifunctional initiators, was developed.

The polymerization of one monomer (A) to form polymer with undecomposed peroxide groups at one or both ends followed by the addition of a comonomer (B), at a more suitable decomposition temperature for the

decomposition of such peroxide group, should lead, in principle, to the formation of free radical block copolymers (AB) [Waltz and Heitz (1978), Piirma and Chou (1979), Ivanechev (1979), Gunesin and Piirma (1981)].

Unfortunately, the formation of considerable amounts of homopolymer (A and B) in their respective polymerization stages, with the consequent phase separation problems, was inevitable. This discouraged further research in this field for quite some time.

In the late 80's, the disclosure of the set of elementary reactions involved in this two stage copolymerization with bifunctional initiators showed that not only were both homopolymers formed, but also a complex mix of block copolymers, with variable number of AB blocks [Villalobos (1989)]. In addition, the length of such blocks, and the very number of them, was of random nature.

These undesirable features, made the free radical block copolymerization with bifunctional initiators much less attractive than using anionic block copolymerization which, due to its live polymer nature, leads to almost perfect block formation and nearly monodisperse block length distribution.

Recently, the use of bifunctional initiators as a means to increase the productivity of free radical polymerization processes has been investigated. The possibility of simultaneously obtaining high polymerization rates and high molecular weights with these initiators has been proven, and at least two similar kinetic models for homopolymerization with bifunctional initiators have been published [Choi and Lei (1987), Villalobos et.al.(1991)]. However, no kinetic model describing the complex features of free radical copolymerization with bifunctional initiators exists as yet.

This chapter, presents the elementary reaction scheme for binary copolymerization with bifunctional initiators and a detailed description of the kinetic model developed from it. Both the reaction scheme and kinetic treatment are general inasmuch as they consider all reactions involved in statistical and donor-acceptor alternating copolymerization as

well as the possibility of their simultaneous and competitive occurrence.

The kinetic model developed with the use of the pseudo-kinetic rate constant method is solved using the method of moments to obtain the system of equations describing monomer and initiator conversion, molecular weight distribution development, and copolymer composition.

4.2 Reaction Scheme

Bifunctional initiators in general may be represented as

$$R_1\text{-O-O-}R_2\text{-O-O-}R_3$$

Here, R_{1-3} represent, most commonly, hydrocarbon ligands, and O-O peroxide (or azo) groups. If R_1 and R_3 are identical the diperoxide is symmetric otherwise is asymmetric.

The peroxide groups in the above molecule can undergo a primary homolytic rupture of the most labile O-O bond by increasing the energy of the system via temperature, radiation or otherwise

$$R_1\text{-O-O-}R_2\text{-O-O-}R_3 \xrightarrow{K_d} R_1\text{-O}^{\bullet} + R_3\text{-O-O-}R_2\text{-O}^{\bullet}$$

or in initiation notation

$$I \xrightarrow{K_d} R_{in}^{\bullet} + \widetilde{R}_{in}^{\bullet}$$

Regardless of the symmetry, it has been proven that the reactivity of the second peroxide group decreases once the first one has reacted. This prevents the formation of a significant number of di-radical species and makes the kinetic treatment equal for both kinds of bifunctional initiators [Villalobos et.al (1991)].

The proposed copolymerization scheme is given by the following set of elementary reactions:

Donor-Acceptor Complex Formation:

$$M_1 + M_2 \underset{K_c'}{\overset{K_c}{\rightleftharpoons}} C \qquad (4.1)$$

Initiation:

$$I \xrightarrow{2K_{di}} R_{in}^{\bullet} + \widetilde{R}_{in}^{\bullet} \qquad (4.2)$$

$$R_{in}^{\bullet} + M_1 \xrightarrow{K_1} R_{1,1}^{\bullet} \qquad (4.3)$$

$$R_{in}^{\bullet} + M_2 \xrightarrow{K_2} R_{1,2}^{\bullet} \qquad (4.4)$$

$$R_{in}^{\bullet} + C \xrightarrow{K_3} R_{2,1}^{\bullet} \qquad (4.5)$$

$$R_{in}^{\bullet} + C \xrightarrow{K_4} R_{2,2}^{\bullet} \qquad (4.6)$$

$$\widetilde{R}_{in}^{\bullet} + M_1 \xrightarrow{\widetilde{K}_1} \widetilde{R}_{1,1}^{\bullet} \qquad (4.7)$$

$$\widetilde{R}_{in}^{\bullet} + M_2 \xrightarrow{\widetilde{K}_2} \widetilde{R}_{1,2}^{\bullet} \qquad (4.8)$$

$$\widetilde{R}_{in}^{\bullet} + C \xrightarrow{\widetilde{K}_3} \widetilde{R}_{2,1}^{\bullet} \qquad (4.9)$$

$$\widetilde{R}_{in}^{\bullet} + C \xrightarrow{\widetilde{K}_4} \widetilde{R}_{2,2}^{\bullet} \qquad (4.10)$$

$$\widetilde{P}_r \xrightarrow{K_{di2}} R_{in}^{\bullet} + R_r^{\bullet} \qquad (4.11)$$

$$\widetilde{\widetilde{P}}_r \xrightarrow{2K_{di2}} R_{in}^{\bullet} + \widetilde{R}_r^{\bullet} \qquad (4.12)$$

Propagation ($r \geq 1$):

$$R_{r,1}^{\bullet} + M_1 \xrightarrow{K_{11}} R_{r+1,1}^{\bullet} \qquad (4.13)$$

$$R_{r,1}^{\bullet} + M_2 \xrightarrow{K_{12}} R_{r+1,2}^{\bullet} \qquad (4.14)$$

$$R_{r,1}^{\bullet} + C \xrightarrow{K_{1C}} R_{r+2,1}^{\bullet} \qquad (4.15)$$

$$R_{r,2}^{\bullet} + M_1 \xrightarrow{K_{21}} R_{r+1,1}^{\bullet} \qquad (4.16)$$

$$R_{r,2}^{\bullet} + M_2 \xrightarrow{K_{22}} R_{r+1,2}^{\bullet} \qquad (4.17)$$

$$R_{r,2}^{\bullet} + C \xrightarrow{K_{2C}} R_{r+2,2}^{\bullet} \qquad (4.18)$$

$$\widetilde{R}_{r,1}^{\bullet} + M_1 \xrightarrow{\widetilde{K}_{11}} \widetilde{R}_{r+1,1}^{\bullet} \qquad (4.19)$$

$$\widetilde{R}_{r,1}^{\bullet} + M_2 \xrightarrow{\widetilde{K}_{12}} \widetilde{R}_{r+1,2}^{\bullet} \qquad (4.20)$$

$$\widetilde{R}_{r,1}^{\bullet} + C \xrightarrow{\widetilde{K}_{1C}} \widetilde{R}_{r+2,1}^{\bullet} \qquad (4.21)$$

$$\widetilde{R}_{r,2}^{\bullet} + M_1 \xrightarrow{\widetilde{K}_{21}} \widetilde{R}_{r+1,1}^{\bullet} \qquad (4.22)$$

$$\widetilde{R}_{r,2}^{\bullet} + M_2 \xrightarrow{\widetilde{K}_{22}} \widetilde{R}_{r+1,2}^{\bullet} \qquad (4.23)$$

$$\widetilde{R}_{r,2}^{\bullet} + C \xrightarrow{\widetilde{K}_{2C}} \widetilde{R}_{r+2,2}^{\bullet} \qquad (4.24)$$

Termination by Combination (r,s≥1):

$$R^{\bullet}_{r,1} + R^{\bullet}_{s,1} \xrightarrow{K_{tc11}} P_{r+s} \quad (4.25)$$

$$R^{\bullet}_{r,1} + R^{\bullet}_{s,2} \xrightarrow{K_{tc12}} P_{r+s} \quad (4.26)$$

$$R^{\bullet}_{r,2} + R^{\bullet}_{s,2} \xrightarrow{K_{tc22}} P_{r+s} \quad (4.27)$$

$$R^{\bullet}_{r,1} + \widetilde{R}^{\bullet}_{s,1} \xrightarrow{\widetilde{K}_{tc11}} \widetilde{P}_{r+s} \quad (4.28)$$

$$R^{\bullet}_{r,1} + \widetilde{R}^{\bullet}_{s,2} \xrightarrow{\widetilde{K}_{tc12}} \widetilde{P}_{r+s} \quad (4.29)$$

$$R^{\bullet}_{r,2} + \widetilde{R}^{\bullet}_{s,1} \xrightarrow{\widetilde{K}_{tc21}} \widetilde{P}_{r+s} \quad (4.30)$$

$$R^{\bullet}_{r,2} + \widetilde{R}^{\bullet}_{s,2} \xrightarrow{\widetilde{K}_{tc22}} \widetilde{P}_{r+s} \quad (4.31)$$

$$\widetilde{R}^{\bullet}_{r,1} + \widetilde{R}^{\bullet}_{s,1} \xrightarrow{\widetilde{\widetilde{K}}_{tc11}} \widetilde{\widetilde{P}}_{r+s} \quad (4.32)$$

$$\widetilde{R}^{\bullet}_{r,1} + \widetilde{R}^{\bullet}_{s,2} \xrightarrow{\widetilde{\widetilde{K}}_{tc12}} \widetilde{\widetilde{P}}_{r+s} \quad (4.33)$$

$$\widetilde{R}^{\bullet}_{r,2} + \widetilde{R}^{\bullet}_{s,2} \xrightarrow{\widetilde{\widetilde{K}}_{tc22}} \widetilde{\widetilde{P}}_{r+s} \quad (4.34)$$

Termination by Disproportionation (r,s≥1):

$$R^{\bullet}_{r,1} + R^{\bullet}_{s,1} \xrightarrow{K_{td11}} P_r + P_s \quad (4.35)$$

$$R^{\bullet}_{r,1} + R^{\bullet}_{s,2} \xrightarrow{K_{td12}} P_r + P_s \quad (4.36)$$

$$R^{\bullet}_{r,2} + R^{\bullet}_{s,2} \xrightarrow{K_{td22}} P_r + P_s \quad (4.37)$$

$$R^{\bullet}_{r,1} + \widetilde{R}^{\bullet}_{s,1} \xrightarrow{\widetilde{K}_{td11}} P_r + \widetilde{P}_s \quad (4.38)$$

$$R^{\bullet}_{r,1} + \widetilde{R}^{\bullet}_{s,2} \xrightarrow{\widetilde{K}_{td12}} P_r + \widetilde{P}_s \quad (4.39)$$

$$R^{\bullet}_{r,2} + \widetilde{R}^{\bullet}_{s,1} \xrightarrow{\widetilde{K}_{td21}} P_r + \widetilde{P}_s \quad (4.40)$$

$$R^{\bullet}_{r,2} + \widetilde{R}^{\bullet}_{s,2} \xrightarrow{\widetilde{K}_{td22}} P_r + \widetilde{P}_s \quad (4.41)$$

$$\widetilde{R}^{\bullet}_{r,1} + \widetilde{R}^{\bullet}_{s,1} \xrightarrow{\widetilde{\widetilde{K}}_{td11}} \widetilde{P}_r + \widetilde{P}_s \quad (4.42)$$

$$\widetilde{R}^{\bullet}_{r,1} + \widetilde{R}^{\bullet}_{s,2} \xrightarrow{\widetilde{\widetilde{K}}_{td12}} \widetilde{P}_r + \widetilde{P}_s \quad (4.43)$$

$$\widetilde{R}^{\bullet}_{r,2} + \widetilde{R}^{\bullet}_{s,2} \xrightarrow{\widetilde{\widetilde{K}}_{td22}} \widetilde{P}_r + \widetilde{P}_s \quad (4.44)$$

Transfer to Small Molecule (r≥1):

$$R^{\bullet}_{r,1} + T \xrightarrow{K_{ft1}} P_r + T^{\bullet} \quad (4.45)$$

$$R^{\bullet}_{r,2} + T \xrightarrow{K_{ft2}} P_r + T^{\bullet} \quad (4.46)$$

$$\widetilde{R}^{\bullet}_{r,1} + T \xrightarrow{\widetilde{K}_{ft1}} \widetilde{P}_r + T^{\bullet} \quad (4.47)$$

$$\widetilde{R}^{\bullet}_{r,2} + T \xrightarrow{\widetilde{K}_{ft2}} \widetilde{P}_r + T^{\bullet} \quad (4.48)$$

Transfer to Monomer ($r \geq 1$):

$$R^{\bullet}_{r,1} + M_1 \xrightarrow{K_{111}} P_r + R^{\bullet}_{1,1} \quad (4.49)$$

$$R^{\bullet}_{r,1} + M_2 \xrightarrow{K_{112}} P_r + R^{\bullet}_{1,2} \quad (4.50)$$

$$R^{\bullet}_{r,2} + M_1 \xrightarrow{K_{121}} P_r + R^{\bullet}_{1,1} \quad (4.51)$$

$$R^{\bullet}_{r,2} + M_2 \xrightarrow{K_{122}} P_r + R^{\bullet}_{1,2} \quad (4.52)$$

$$\widetilde{R}^{\bullet}_{r,1} + M_1 \xrightarrow{\widetilde{K}_{111}} \widetilde{P}_r + R^{\bullet}_{1,1} \quad (4.53)$$

$$\widetilde{R}^{\bullet}_{r,1} + M_2 \xrightarrow{\widetilde{K}_{112}} \widetilde{P}_r + R^{\bullet}_{1,2} \quad (4.54)$$

$$\widetilde{R}^{\bullet}_{r,2} + M_1 \xrightarrow{\widetilde{K}_{121}} \widetilde{P}_r + R^{\bullet}_{1,1} \quad (4.55)$$

$$\widetilde{R}^{\bullet}_{r,2} + M_2 \xrightarrow{\widetilde{K}_{122}} \widetilde{P}_r + R^{\bullet}_{1,2} \quad (4.56)$$

Based on this scheme, the following species may be present at any time during a bifunctionally initiated binary copolymerization:

M_{1-2}	Monomer (1 or 2),
I	Bifunctional Initiator,
C	Donor-Acceptor Complex,
T	Chain Transfer Agent,
$R^{\bullet}_{in}$	Initiator Radical,
$\widetilde{R}^{\bullet}_{in}$	Initiator Radical with one undecomposed peroxide,
$R^{\bullet}_{r,1-2}$ $(r \geq 1)$	Macroradical of chain length r, with active centre in monomer unit 1 or 2,
$\widetilde{R}^{\bullet}_{r,1-2}$ $(r \geq 1)$	Macroradical of chain length r, with active centre in monomer unit 1 or 2 and one undecomposed peroxide,
P_r $(r \geq 1)$	(R----R) Dead Copolymer molecule,
$\widetilde{P}_r$ $(r \geq 1)$	($\widetilde{R}$----R) Temporarily Dead Copolymer (or macro-initiator) molecule of chain length r, with one undecomposed peroxide,
$\widetilde{\widetilde{P}}_r$ $(r \geq 2)$	($\widetilde{R}$----$\widetilde{R}$) Temporarily Dead Copolymer (or macro-initiator) molecule of chain length r, with two undecomposed peroxides.

(~ undecomposed peroxide groups, ---- polymer chain).

It is easy to see that the above mechanism is based on the terminal model for binary copolymerization [Alfrey and Glodfinger (1944), Mayo and Lewis (1944)].

The extension of this model to take into account simultaneous donor-acceptor copolymerization reactions might have followed two different approaches:

In the first one the addition of the donor ($-M_1^{\bullet}$) or acceptor ($-M_2^{\bullet}$) radical to the complex (M_1M_2) can only occur in cross fashion (i.e $-M_1^{\bullet} + M_1M_2 = -M_1M_2M_1^{\bullet}$ and $-M_2^{\bullet} + M_1M_2 = -M_2M_1M_2^{\bullet}$), which leads to the formation of alternating triads [Georgiev and Zubov (1978)].

In the second approach, the straight reactions are also allowed (i.e $-M_1^{\bullet} + M_1M_2 = -M_1M_1M_2^{\bullet}$ and $-M_2^{\bullet} + M_1M_2 = -M_2M_2M_1^{\bullet}$), which leads to the formation of alternating and homo-diads distributed randomly [Hill et.al.(1985), Brown et.al.(1989)].

Characterization of the microstructure of purely donor-acceptor copolymers showed the presence of all the triads shown above with a predominance of the alternating ones [Buchak and Ramey (1976), Barron et.al.(1984), Zeng and Shirota (1989)]. This indicates that the second approach, or a combination of the first one with statistical copolymerization will lead to the actual sequence distribution in donor-acceptor systems.

In this thesis, the combination of the first approach with statistical copolymerization was preferred for being more general in the sense that it reduces to statistical copolymerization in the absence of donor-acceptor complex formation.

The extraordinary number of elementary reactions already involved in the proposed mechanism along with the fact that most copolymer systems can be satisfactorily described by either the terminal model or the donor-acceptor model, or by a combination of both, make the consideration of penultimate or longer range effects impractical.

Let us now examine the copolymerization scheme. The first remarkable feature is the formation of two different radical populations ($R_{r\cdot}$ and $\widetilde{R}_{r\cdot}$) from the decomposition of the bifunctional initiator. These different radicals upon propagation lead to the two macroradical populations that will define the type of copolymeric species that will form upon termination and/or transfer reactions.

When termination by disproportionation and/or transfer reactions control the chain growth, two different copolymer populations are formed (P_r and $\widetilde{P}_r$). Reactions (4.11) and (4.35 to 4.56) show that the temporarily dead copolymer population ($\widetilde{P}_r$) will only be subjected to a single re-initiation/propagation/termination cycle before decaying to the dead copolymer population (P_r). As a result, the bifunctional initiation characteristic of simultaneously achieving high polymerization rates and high molecular weights is thwarted, and only marginal increases in Mw would be observed at a given polymerization rate as compared to monofunctional initiation.

When termination by combination controls the chain growth three different copolymer populations are formed (P_r, $\widetilde{P}_r$, and $\widetilde{\widetilde{P}}_r$). Reactions (4.11-4.12) and (4.25 to 4.34) show that a temporarily dead copolymer population ($\widetilde{\widetilde{P}}_r$) will undergo a statistical distribution of re-initiation/propagation/termination cycles before decaying to the also temporarily dead copolymer population ($\widetilde{P}_r$). In turn, this population will undergo a different statistical distribution of re-initiation/propagation/termination cycles before decaying to the dead copolymer population (P_r).

It is this multiple initiation/propagation termination phenomenon which allows for the simultaneous achievement of high polymerization rates and high molecular weights, which cannot be accomplished with monofunctional initiation.

When both bimolecular termination mechanisms, and transfer reactions are important, the relative magnitude of them will define the average number of initiation/propagation/termination cycles that $\widetilde{\widetilde{P}}_r$ must undergo before decaying to $\widetilde{P}_r$, and the average number of cycles that $\widetilde{P}_r$ must

undergo before decaying to P_r. The effect of the bifunctional initiator on the molecular weight and distribution will depend on these average number of cycles at different polymerization rates [Villalobos et.al. (1991)].

The most remarkable feature of these successive initiation/ propagation/termination cycles in bifunctionally initiated copolymerization is given by the fact that a temporarily dead copolymer molecule formed at a given conversion and with a given composition, may remain dead for quite some time during the reaction before undergo re-initiation. When this phenomenon takes place the new copolymer segment added to the chain (random block) may have a very different copolymer composition than the original chain if compositional drift is important. As a result, otherwise incompatible copolymers may be linked together in the same copolymer molecule combining the properties of the different segments added. In addition, the copolymer chains thus formed, may act as compatibilizer of single-segment copolymer chains with different compositions.

When this process takes place, on average, several times per copolymer molecule, the actual compositional drift is reduced and higher copolymer compatibility is achieved, as demonstrated below. However, as was stated above, the formation of considerable amounts of single-segment dead copolymer molecules, with compositions varying according to the drift during the course of the reaction, is unavoidable.

Figure 4.1, below, shows schematically the multiple re-initiation phenomenon and its implications in binary copolymerization with compositional drift.

4.3 Kinetic Model Development

First, let us analyze the kinetic constants involved in the proposed copolymerization scheme.

It is evident that a model containing such a great number of rate constants would be impractical. Moreover, an attempt to evaluate the rate constants for the reactions involving radicals with one undecomposed peroxide group (i.e. all $\widetilde{K}_{ij}$ and $\widetilde{\widetilde{K}}_{ij}$) would be, in the best case, extremely complicated for it would involve the isolation of $\widetilde{R}^{\bullet}_{in}$ radicals from $R^{\bullet}_{in}$ after the bifunctional initiator decomposition.

From the proposed scheme, it is much easier to realize that the effect that different chain ends may have on propagation, termination, and transfer reaction rates is only important for the first few monomer units added to the radical centre (c.a. r≤10). For high polymers, the chemical nature of the chain end will be of no importance in the overall value of the rate constants because the contribution of polymer radicals with chain length smaller than ten will be negligible [Ham (1960), Guyot and Guillot (1967)].

Accordingly, the set of kinetic rate constants needed to evaluate the binary copolymerization reaction rates with bifunctional initiators reduces to that of the terminal model plus those present in the donor-acceptor reactions considered. Therefore:

$$\widetilde{K}_{ij} = K_{ij} \qquad (i,j=1,2,C)$$

$$\widetilde{\widetilde{K}}_{tcij} = \widetilde{K}_{tcij} = K_{tcij} \qquad (i,j=1,2)$$

$$\widetilde{\widetilde{K}}_{tdij} = \widetilde{K}_{tdij} = K_{tdij} \qquad (i,j=1,2) \quad (4.57)$$

$$\widetilde{K}_{fij} = K_{fij} \qquad (i,j=1,2)$$

$$\widetilde{K}_{fTj} = K_{fTj} \qquad (j=1,2)$$

Let us now examine the consistency of what was stated above with the applicability of the pseudo-kinetic rate constant method that will be employed to develop the kinetic model.

In Appendix A it is shown that the necessary condition for the applicability of the pseudo-kinetic rate constants is that the mole fraction of any radical type does not change with chain length (i.e. $\Phi_i=\Phi_{1,i}=\Phi_{2,i}=\ldots=\Phi_{r,i}$). It has been proved elsewhere that this condition is fully satisfied when the number-average chain length is greater than a few hundred [Hamielec et.al.(1987), Tobita (1990)].

Consistent with the above is also the fact that for long chains, the fraction of polymer radicals of type i without undecomposed peroxide, Φ_i, is equal to the fraction of polymer radicals of the same type with one undecomposed peroxide, $\widetilde{\Phi}_i$, or:

$$\Phi_1 = \widetilde{\Phi}_1 = \frac{K_{21}f_1}{K_{21}f_1 + K_{12}f_2} \qquad (4.58)$$

and

$$\Phi_2 = \widetilde{\Phi}_2 = (1 - \Phi_1) \qquad (4.58')$$

A demonstration is also offered in Appendix A.

Let us now introduce the following definitions:

$f_1=[M_1]/[M]$	fraction of monomer 1.
$f_2=[M_2]/[M]$	fraction of monomer 2.
$f_c=[C]/[M]$	fraction of donor-acceptor complex.
$[M]=[M_1]+[M_2]+[C]$	total monomer concentration.
$\Phi_i=[R_i^\bullet]/[R^\bullet]=\widetilde{\Phi}_i=[\widetilde{R}_i^\bullet]/[\widetilde{R}^\bullet]$	fraction of radicals with active centre on monomer unit i (i=1,2).
$\Phi_{r,i}=[R_{r,i}^\bullet]/[R_{r,\cdot}^\bullet]=\widetilde{\Phi}_{r,i}=[\widetilde{R}_{r,i}^\bullet]/[\widetilde{R}_{r,\cdot}^\bullet]$	fraction of radicals of chain length r with active centre on monomer unit i (i=1,2).
$[R_1^\bullet]=\sum_{r=1}^{\infty}[R_{r,1}^\bullet]$	concentration of radicals with active centre on monomer unit 1.
$[\widetilde{R}_1^\bullet]=\sum_{r=1}^{\infty}[\widetilde{R}_{r,1}^\bullet]$	concentration of radicals with one peroxide and active centre on monomer unit 1.
$[R_2^\bullet]=\sum_{r=1}^{\infty}[R_{r,2}^\bullet]$	concentration of radicals with active centre on monomer unit 2.
$[\widetilde{R}_2^\bullet]=\sum_{r=1}^{\infty}[\widetilde{R}_{r,2}^\bullet]$	concentration of radicals with one peroxide and active centre on monomer unit 2.

$[R^{\cdot}] = [R_1^{\cdot}] + [R_2^{\cdot}] = Y_0$ — total concentration of radicals without undecomposed peroxide (zeroth moment of the radical, R , distribution).

$[\widetilde{R}^{\cdot}] = [\widetilde{R}_1^{\cdot}] + [\widetilde{R}_2^{\cdot}] = \widetilde{Y}_0$ — total concentration of radicals with one undecomposed peroxide (zeroth moment of the radical, R , distribution).

$Y_{T0} = Y_0 + \widetilde{Y}_0 = [R^{\cdot}] + [\widetilde{R}^{\cdot}]$ — Total radical concentration.

In the above definitions note, from the reaction scheme, that even though $\Phi_1 = \widetilde{\Phi}_1$, in general $[R_1^{\cdot}] \neq [\widetilde{R}_1^{\cdot}]$.

When (4.57) and (4.58) are valid, a unique set of pseudo-kinetic rate constants may be defined for statistical/donor-acceptor copolymerization through bifunctional initiators as:

Propagation: (4.59)

$$K_p = (K_{11}f_1 + K_{12}f_2 + K_{1c}f_c)\Phi_1 + (K_{21}f_1 + K_{22}f_2 + K_{2c}f_c)\Phi_2$$

Termination by Combination: (4.60)

$$K_{tc} = K_{tc11}\Phi_1\Phi_1 + 2K_{tc12}\Phi_1\Phi_2 + K_{tc22}\Phi_2\Phi_2$$

Termination by Disproportionation: (4.61)

$$K_{td} = K_{td11}\Phi_1\Phi_1 + 2K_{td12}\Phi_1\Phi_2 + K_{td22}\Phi_2\Phi_2$$

Transfer to Small Molecule: (4.62)

$$K_{ft} = K_{ft1}\Phi_1 + K_{ft2}\Phi_2$$

Transfer to Monomer: (4.63)

$$K_{fm} = (K_{f11}f_1 + K_{f12}f_2)\Phi_1 + (K_{f21}f_1 + K_{f22}f_2)\Phi_2$$

Details on the derivation of the above pseudo-kinetic rate constants are given in Appendix A.

Note that each of the pseudo-kinetic rate constants are monomer and/or radical mole fraction dependent [Hamielec et.al.(1987)]. This means that they will vary, during the course of the reaction, within the

limits given by the largest and smaller of the rate constants involved. The concept, though, facilitates the kinetic treatment greatly as these constants can be computed coupled with the main system of kinetic equations as shown below.

It is important to point out here that the pseudo-kinetic rate constants for both types of bimolecular termination (K_{tc} and K_{td}) as defined here are chain length independent and therefore they represent number-average termination rate constants. These number-average termination pseudo-rate constants will allow the correct calculation of conversion and number average molecular weight (Mn). However, the weight-average molecular weight (Mw) will be slightly underestimated [Zhu and Hamielec (1989)]. In actual simulations this problem is partially overcome by adequate modelling of the diffusion controlled termination phenomenon, as will be shown below.

Modelling of chain length dependent termination rate constants has been reported elsewhere [Zhu and Hamielec (1989)].

The ith moment of the concentration distribution of copolymer species (dead and temporarily dead), and radicals (live copolymer) are defined as:

$$Q_i = \sum_{r=1}^{\infty} r^i [P_r]$$ dead copolymer

$$\widetilde{Q}_i = \sum_{r=1}^{\infty} r^i [\widetilde{P}_r]$$

temporarily dead copolymer

$$\widetilde{\widetilde{Q}}_i = \sum_{r=1}^{\infty} r^i [\widetilde{\widetilde{P}}_r]$$

$$Y_i = \sum_{r=1}^{\infty} r^i [R^{\bullet}_{r,\bullet}]$$

live copolymer

$$\widetilde{Y}_i = \sum_{r=1}^{\infty} r^i [\widetilde{R}^{\bullet}_{r,\bullet}]$$

The radical mass balances for a batch reactor are developed from the reaction mechanism and the above definitions.

For primary radicals:

$R_{in}^{\cdot}$:

$$\frac{1}{V}\frac{d([R_{in}^{\cdot}]V)}{dt} = 2f_1K_{d1}[I] + f_2K_{t2}\widetilde{Q}_0 + 2f_2K_{t2}\widetilde{\widetilde{Q}}_0 - (K_1[M_1] + K_2[M_2] + (K_3 + K_4)[C] + K_{tc}Y_{T0})[R_{in}^{\cdot}] \quad (4.64)$$

$\widetilde{R}_{in}^{\cdot}$:

$$\frac{1}{V}\frac{d([\widetilde{R}_{in}^{\cdot}]V)}{dt} = 2f_1K_{d1}[I] - (\widetilde{K}_1[M_1] + \widetilde{K}_2[M_2] + (\widetilde{K}_3 + \widetilde{K}_4)[C] + K_{tc}Y_{T0})[\widetilde{R}_{in}^{\cdot}] \quad (4.65)$$

Here f_1 is the bifunctional initiator efficiency and f_2 is the macroinitiator efficiency (distinct from the comonomer composition fractions f_1 and f_2) which may be considered different. Order of magnitude estimates show that the bimolecular termination terms in eqs. (4.64) and (4.65) are negligible.

Applying the steady state hypothesis (SSH) for radical concentrations on eqs. (4.64) and (4.65) we get:

$$[R_{in}^{\cdot}] = \frac{2f_1K_{d1}[I] + f_2K_{t2}\widetilde{Q}_0 + 2f_2K_{t2}\widetilde{\widetilde{Q}}_0}{K_1[M_1] + K_2[M_2] + (K_3+K_4)[C]} \quad (4.66)$$

and

$$[\widetilde{R}_{in}^{\cdot}] = \frac{2f_1K_{d1}[I]}{\widetilde{K}_1[M_1] + \widetilde{K}_2[M_2] + (\widetilde{K}_3+\widetilde{K}_4)[C]} \quad (4.67)$$

From these equations the initiation rates for radicals with and without peroxide groups are obtained as:

$$R_i^{\bullet} = K_1[M_1] + K_2[M_2] + (K_3+K_4)[C] = 2f_1K_{d1}[I] + f_2K_{d2}(\widetilde{Q}_0 + 2\widetilde{\widetilde{Q}}_0) \quad (4.68)$$

and

$$\widetilde{R}_i^{\bullet} = \widetilde{K}_1[M_1] + \widetilde{K}_2[M_2] + (\widetilde{K}_3 + \widetilde{K}_4)[C] = 2f_1\widetilde{K}_{d1}[I] \quad (4.69)$$

For growing radicals without undecomposed peroxide:

$R_{1,\bullet}^{\bullet}$: (4.70)

$$\frac{1}{V}\frac{d([R_{1,\bullet}^{\bullet}]V)}{dt} = R_i^{\bullet} + f_2K_{d2}[\widetilde{P}_1] + (K_{tc}[T] + K_{tm}[M])Y_{T0} - (K_p[M] + (K_{tc} + K_{td})Y_{T0} + K_{tc}[T] + K_{tm}[M])[R_{1,\bullet}^{\bullet}] - (K_3 + K_4)[C][R_{in}^{\bullet}]$$

$R_{2,\bullet}^{\bullet}$: (4.71)

$$\frac{1}{V}\frac{d([R_{2,\bullet}^{\bullet}]V)}{dt} = (K_3 + K_4)[C][R_{in}^{\bullet}] + f_2K_{d2}[\widetilde{P}_2] + K_p[M][R_{1,\bullet}^{\bullet}] - (K_p[M] + (K_{tc} + K_{td})Y_{T0} + K_{tc}[T] + K_{tm}[M])[R_{2,\bullet}^{\bullet}] - (K_{1c}\Phi_1 + K_{2c}\Phi_2)f_c[M][R_{1,\bullet}^{\bullet}]$$

$R_{r,\bullet}^{\bullet}$ $(r\geq 3)$: (4.72)

$$\frac{1}{V}\frac{d([R_{r,\bullet}^{\bullet}]V)}{dt} = f_2K_{d2}[\widetilde{P}_r] + K_p[M][R_{r-1,\bullet}^{\bullet}] + (K_{1c}\Phi_1 + K_{2c}\Phi_2)f_c[M][R_{1,\bullet}^{\bullet}] - (K_p[M] + (K_{tc} + K_{td})Y_{T0} + K_{tc}[T] + K_{tm}[M])[R_{r,\bullet}^{\bullet}]$$

Adding up eqs. (4.70) to (4.72) we get

$R_{1,\bullet}^{\bullet}$ $(r\geq 1)$: (4.73)

$$\frac{1}{V}\frac{d([R_{1,\bullet}^{\bullet}]V)}{dt} = R_i^{\bullet} + f_2K_{d2}[\widetilde{P}_r] + K_p[M]([R_{r-1,\bullet}^{\bullet}] - [R_{r,\bullet}^{\bullet}]) + (K_{tc}[T] + K_{tm}[M])Y_{T0} - ((K_{tc} + K_{td})Y_{T0} + K_{tc}[T] + K_{tm}[M])[R_{r,\bullet}^{\bullet}]$$

For growing radicals with undecomposed peroxide

$\widetilde{R}^{\bullet}_{1,\bullet}$: (4.74)

$$\frac{1}{V}\frac{d([\widetilde{R}_{1,\bullet}]V)}{dt} = \widetilde{R}^{\bullet}_{i} - (\widetilde{K}_3 + \widetilde{K}_4)[C][\widetilde{R}^{\bullet}_{in}] - (K_p[M] + (K_{tc} + K_{td})Y_{T0} + K_{ft}[T] + K_{fm}[M])[\widetilde{R}^{\bullet}_{1,\bullet}]$$

$\widetilde{R}^{\bullet}_{2,\bullet}$: (4.75)

$$\frac{1}{V}\frac{d([\widetilde{R}^{\bullet}_{2,\bullet}]V)}{dt} = (\widetilde{K}_3 + \widetilde{K}_4)[C][\widetilde{R}^{\bullet}_{in}] + 2f_2K_{d2}[\widetilde{\widetilde{P}}_2] + K_p[M][\widetilde{R}^{\bullet}_{1,\bullet}] - (K_p[M] + (K_{tc} + K_{td})Y_{T0} + K_{ft}[T] + K_{fm}[M])[\widetilde{R}^{\bullet}_{2,\bullet}] - (K_{1c}\Phi_1 + K_{2c}\Phi_2)f_c[M][\widetilde{R}^{\bullet}_{1,\bullet}]$$

$\widetilde{R}^{\bullet}_{r,\bullet}$ $(r\geq 3)$: (4.76)

$$\frac{1}{V}\frac{d([\widetilde{R}^{\bullet}_{r,\bullet}]V)}{dt} = 2f_2K_{d2}[\widetilde{\widetilde{P}}_r] + K_p[M][\widetilde{R}^{\bullet}_{r-1,\bullet}] + (K_{1c}\Phi_1 + K_{2c}\Phi_2)f_c[M][\widetilde{R}^{\bullet}_{1,\bullet}] - (K_p[M] + (K_{tc} + K_{td})Y_{T0} + K_{ft}[T] + K_{fm}[M])[\widetilde{R}^{\bullet}_{r,\bullet}]$$

Adding up eqs. (4.74) to (4.76) we get

$\widetilde{R}^{\bullet}_{r,\bullet}$ $(r\geq 1)$: (4.77)

$$\frac{1}{V}\frac{d([\widetilde{R}^{\bullet}_{r,\bullet}]V)}{dt} = \widetilde{R}^{\bullet}_{i} + 2f_2K_{d2}[\widetilde{\widetilde{P}}_r] + K_p[M]([\widetilde{R}^{\bullet}_{r-1,\bullet}] - [\widetilde{R}^{\bullet}_{r,\bullet}]) - ((K_{tc} + K_{td})Y_{T0} + K_{ft}[T] + K_{fm}[M])[\widetilde{R}^{\bullet}_{r,\bullet}]$$

The polymer mass balances, developed from the reaction scheme, may be expressed for a batch reactor as:

For dead copolymer:

P_r $(r\geq 1)$: (4.78)

$$\frac{1}{V}\frac{d([P_r]V)}{dt} = 1/2\ K_{tc}\sum_{n=1}^{r-1}[R^{\bullet}_{n,\bullet}][R^{\bullet}_{r-n,\bullet}] + (K_{td}Y_{T0} + K_{ft}[T] + K_{fm}[M])[R^{\bullet}_{r,\bullet}]$$

For temporarily dead copolymer:

$\widetilde{P}_r$ (r≥1):

$$\frac{1}{V}\frac{d([\widetilde{P}_r]V)}{dt} = K_{tc}\sum_{s=1}^{r-1}[\widetilde{R}^{\bullet}_{s}][\widetilde{R}^{\bullet}_{r-s}] + (K_{td}Y_{T0} + K_{fc}[T] + K_{fm}[M])[\widetilde{R}^{\bullet}_{r}] - K_{d2}[\widetilde{P}_r] \tag{4.79}$$

$\widetilde{\widetilde{P}}_r$ (r≥2):

$$\frac{1}{V}\frac{d([\widetilde{\widetilde{P}}_r]V)}{dt} = 1/2\ K_{tc}\sum_{s=1}^{r-1}[\widetilde{R}^{\bullet}_{s}][\widetilde{R}^{\bullet}_{r-s}] - 2K_{d2}[\widetilde{\widetilde{P}}_r] \tag{4.80}$$

The batch reactor mass balances for the remainder of the species involved in the copolymerization scheme are given below.

Monomer consumption:

The long chain approximation (LCA) is assumed to be valid for monomer consumption. This implies that monomer consumption through initiation and transfer reactions is negligible as compared to the monomer consumed through propagation.

$$\frac{1}{V}\frac{d([M]V)}{dt} = -K_p[M]Y_{T0} \tag{4.81}$$

or for each monomer species

$$\frac{1}{V}\frac{d([M_1]V)}{dt} = [M](K_c(f_c/K_{EC} - f_1f_2[M]) - (K_{11}\Phi_1 + K_{21}\Phi_2)f_1Y_{T0}) \tag{4.82}$$

$$\frac{1}{V}\frac{d([M_2]V)}{dt} = [M](K_c(f_c/K_{EC} - f_1f_2[M]) - (K_{12}\Phi_1 + K_{22}\Phi_2)f_2Y_{T0}) \tag{4.83}$$

$$\frac{1}{V}\frac{d([C]V)}{dt} = [M](2K_c(f_1f_2[M] - f_c/K_{EC}) - (K_{1c}\Phi_1 + K_{2c}\Phi_2)f_cY_{T0}) \tag{4.84}$$

In the above equations K_{fc} represents the equilibrium constant for the formation of donor-acceptor complex ($K_{fc} = K_c/K_c'$). Note that the sum of eqs. (4.82) to (4.84) equals eq. (4.81), as expected.

Initiator consumption:

$$\frac{1}{V}\frac{d([I]V)}{dt} = -2K_{di}[I] \qquad (4.85)$$

Chain transfer agent consumption:

$$\frac{1}{V}\frac{d([T]V)}{dt} = -K_{ft}[T]Y_{T0} \qquad (4.86)$$

4.4 Kinetic Model Solution

Eqs. (4.73) and (4.77), and (4.78) to (4.80), above, are in fact an infinite number of equations representing the variation of the entire radical and copolymer concentration distributions with polymerization time.

Such sets of equations should, in principle, be solved simultaneously with eqs. (4.58) to (4.63), (4.68), (4.69), and (4.81) to (4.86) for finite increments in time, to obtain monomer conversion history, comonomer composition development and molecular weight distribution development. However, the computational effort involved to obtain such a solution, even within practical limits of chain lengths to get a finite number of equations, would be formidable.

Instead, the application of the method of moments integrates each of such infinite sets of equations into a set of a small number of moment equations, which may be solved simultaneously with the remaining equations mentioned, with small computational effort for each time interval.

The penalty introduced by doing this is that only specific points (moments) of the radical and copolymer concentration distributions are obtained instead of the whole distribution. Ratios of such moments define the molecular weight averages. The calculation of the monomer conversion history and comonomer composition development is not affected by the use of the moment equations.

4.4.1 Moment Equations for Live Copolymer

Starting from eqs. (4.73) and (4.77) the equations describing the variation with time of the zeroth, first, and second moments of the concentration distribution of radicals, with and without peroxide groups, are derived below through the use of the i-th moment definitions given above. These moments are commonly used for they lead to the further calculation of M_n and M_w as it will be shown. Higher order moments may be calculated to establish higher order molecular weight averages.

Zeroth moment:

$$\frac{1}{V}\frac{d(Y_0V)}{dt} = R_i^{\bullet} + f_2K_{d2}\widetilde{Q}_0 + (K_{fc}[T] + K_{fm}[M])\widetilde{Y}_0 - (K_{tc} + K_{td})Y_{T0}Y_0 \tag{4.87}$$

$$\frac{1}{V}\frac{d(\widetilde{Y}_0V)}{dt} = \widetilde{R}_i^{\bullet} + 2f_2K_{d2}\widetilde{\widetilde{Q}}_0 - ((K_{tc} + K_{td})Y_{T0} + K_{fc}[T] + K_{fm}[M])\widetilde{Y}_0 \tag{4.88}$$

First moment:

$$\frac{1}{V}\frac{d(Y_1V)}{dt} = R_i^{\bullet} + f_2K_{d2}\widetilde{Q}_1 + K_p[M]Y_0 - (K_{tc} + K_{td})Y_{T0}Y_1 - (K_{fc}[T] + K_{fm}[M])(Y_1 - Y_{T0}) \tag{4.89}$$

$$\frac{1}{V}\frac{d(\widetilde{Y}_1V)}{dt} = \widetilde{R}_i^{\bullet} + 2f_2K_{d2}\widetilde{\widetilde{Q}}_1 + K_p[M]\widetilde{Y}_0 - ((K_{tc} + K_{td})Y_{T0} + K_{fc}[T] + K_{fm}[M])\widetilde{Y}_1 \tag{4.90}$$

Second moment:

$$\frac{1}{V}\quad\frac{d(Y_2V)}{dt} = R_i^{\bullet} + f_2K_{d2}\widetilde{Q}_2 + K_p[M](2Y_1 + Y_0) - (K_{tc} + K_{td})Y_{T0}Y_2 - (K_{ft}[T] + K_{fm}[M])(Y_2 - Y_{T0}) \tag{4.91}$$

$$\frac{1}{V}\quad\frac{d(\widetilde{Y}_2V)}{dt} = R_i^{\bullet} + 2f_2K_{d2}\widetilde{\widetilde{Q}}_2 + K_p[M](2Y_1 + \widetilde{Y}_0) - ((K_{tc} + K_{td})Y_{T0} + K_{ft}[T] + K_{fm}[M])\widetilde{Y}_2 \tag{4.92}$$

The above ordinary differential equations are simplified to a set of algebraic equations by applying the steady state hypothesis for radical concentration. Note that a further simplification is introduced since $Y_2>Y_1>Y_0$ for both types of radicals by considering that $(2Y_1 + Y_0) \approx 2Y_1$, $(2\widetilde{Y}_1 + \widetilde{Y}_0) \approx 2\widetilde{Y}_1$, $(Y_1 - Y_{T0}) \approx Y_1$, and $(Y_2 - Y_{T0}) \approx Y_2$.

$$Y_0 = \frac{R_i^{\bullet} + f_2K_{d2}\widetilde{Q}_0 + (K_{ft}[T] + K_{fm}[M])\widetilde{Y}_0}{(K_{tc} + K_{td})Y_{T0}} \tag{4.93}$$

$$\widetilde{Y}_0 = \frac{\widetilde{R}_i^{\bullet} + 2f_2K_{d2}\widetilde{\widetilde{Q}}_0}{(K_{tc} + K_{td})Y_{T0} + K_{ft}[T] + K_{fm}[M]} \tag{4.94}$$

$$Y_1 = \frac{R_i^{\bullet} + f_2K_{d2}\widetilde{Q}_1 + K_p[M]Y_0}{(K_{tc} + K_{td})Y_{T0} + K_{ft}[T] + K_{fm}[M]} \tag{4.95}$$

$$\widetilde{Y}_1 = \frac{\widetilde{R}_i^{\bullet} + 2f_2K_{d2}\widetilde{\widetilde{Q}}_1 + K_p[M]\widetilde{Y}_0}{(K_{tc} + K_{td})Y_{T0} + K_{ft}[T] + K_{fm}[M]} \tag{4.96}$$

$$Y_2 = \frac{R_i^{\bullet} + f_2K_{d2}\widetilde{Q}_2 + 2K_p[M]Y_1}{(K_{tc} + K_{td})Y_{T0} + K_{ft}[T] + K_{fm}[M]} \tag{4.97}$$

$$\widetilde{Y}_2 = \frac{\widetilde{R}_i^{\bullet} + 2f_2K_{d2}\widetilde{\widetilde{Q}}_2 + 2K_p[M]\widetilde{Y}_1}{(K_{tc} + K_{td})Y_{T0} + K_{ft}[T] + K_{fm}[M]} \tag{4.98}$$

4.4.2 Moment Equations for Dead Copolymer

The set of ordinary differential equations describing the variation with time of the moments of the dead and temporarily dead copolymer distributions are derived below by applying the ith moment definitions on the polymer balances [eqs. (4.78) to (4.80)], tc integrate over the whole range of chain lengths.

Zeroth moment:

$$\frac{1}{V}\frac{d(Q_0V)}{dt} = (1/2\ K_{tc}Y_0 + K_{td}Y_{T0} + K_{fc}[T] + K_{fm}[M])Y_0 \qquad (4.99)$$

$$\frac{1}{V}\frac{d(\widetilde{Q}_0V)}{dt} = (K_{tc}Y_0 + K_{td}Y_{T0} + K_{fc}[T] + K_{fm}[M])\widetilde{Y}_0 - K_{d2}\widetilde{Q}_0 \qquad (4.100)$$

$$\frac{1}{V}\frac{d(\widetilde{\widetilde{Q}}_0V)}{dt} = 1/2\ K_{tc}\widetilde{Y}_0^2 - 2K_{d2}\widetilde{\widetilde{Q}}_0 \qquad (4.101)$$

First moment:

$$\frac{1}{V}\frac{d(Q_1V)}{dt} = (K_{tc}Y_0 + K_{td}Y_{T0} + K_{fc}[T] + K_{fm}[M])Y_1 \qquad (4.102)$$

$$\frac{1}{V}\frac{d(\widetilde{Q}_1V)}{dt} = K_{tc}(Y_0\widetilde{Y}_1 + Y_1\widetilde{Y}_0) + (K_{td}Y_{T0} + K_{fc}[T] + K_{fm}[M])\widetilde{Y}_1 - K_{d2}\widetilde{Q}_1 \qquad (4.103)$$

$$\frac{1}{V}\frac{d(\widetilde{\widetilde{Q}}_1V)}{dt} = K_{tc}\widetilde{Y}_0\widetilde{Y}_1 - 2K_{d2}\widetilde{\widetilde{Q}}_1 \qquad (4.104)$$

Second moment:

$$\frac{1}{V}\frac{d(Q_2V)}{dt} = K_{tc}(Y_1^2 + Y_0Y_2) + (K_{td}Y_{T0} + K_{fc}[T] + K_{fm}[M])Y_2 \qquad (4.105)$$

$$\frac{1}{V}\frac{d(\widetilde{Q}_2V)}{dt} = K_{tc}(Y_0\widetilde{Y}_2+2Y_1\widetilde{Y}_1+Y_0\widetilde{Y}_2) + (K_{td}Y_{T0} + K_{fc}[T] + K_{fm}[M])\widetilde{Y}_2 - K_{d2}\widetilde{Q}_2 \qquad (4.106)$$

$$\frac{1}{V}\frac{d(\widetilde{\widetilde{Q}}_2V)}{dt} = K_{tc}(\widetilde{Y}_1^2 + \widetilde{Y}_0\widetilde{Y}_2) - 2K_{d2}\widetilde{\widetilde{Q}}_2 \qquad (4.107)$$

Note that the above moment equations for both live and dead copolymer are the same as those developed by Villalobos et.al.(1991) for homopolymerization through bifunctional initiators. Moreover, in this case the previous model has been expanded to a more general one which takes into account termination by disproportionation and transfer to small molecule reactions.

This has two main implications, the first one is that it has been proven that an appropriate definition of the pseudo-kinetic rate constants does reduce the kinetic treatment of copolymerization to that of homopolymerization, even for a complex copolymerization scheme as the one presented herein.

The second one is that the solution of the model for homopolymerization through bifunctional initiators has been already obtained and proved efficient to forecast conversion history and molecular weight distribution development [Villalobos et.al. (1991)]. Therefore, its generalization may be solved numerically in the same way regardless whether it represents a homo or copolymerization system.

Accordingly, the simultaneous solution of the system of algebraic equations [eqs. (4.58)-(4.63), (4.68)-(4.69), and (4.93)-(4.98)], and differential equations [eqs. (4.81)-(4.86), and (4.99)-(4.107)], necessary to simulate the monomer and initiator conversion history, comonomer composition, and molecular weight distribution development can be obtained numerically by using a standard library integration subroutine.

The solution will allow the evaluation of the moments of the radical and copolymer concentration distributions along with the monomers, transfer agent and initiator concentrations for each finite increment in polymerization time.

From these values the accumulated conversion, comonomer composition, and molecular weight averages are calculated as:

$$X(t) = \frac{[M]_0 - [M](t)}{[M]_0} \qquad (4.108)$$

$$X_i(t) = \frac{[M_i]_0 - [M_i](t)}{[M_i]_0} \tag{4.109}$$

$$f_i(t) = \frac{[M_i](t)}{[M](t)} \tag{4.110}$$

$$M_n(t) = \frac{M_m(Q_1(t) + \widetilde{Q}_1(t) + \widetilde{\widetilde{Q}}_1(t) + Y_1(t) + \widetilde{Y}_1(t))}{Q_0(t) + \widetilde{Q}_0(t) + \widetilde{\widetilde{Q}}_0(t) + Y_0(t) + \widetilde{Y}_0(t)} \tag{4.111}$$

$$M_w(t) = \frac{M_m(Q_2(t) + \widetilde{Q}_2(t) + \widetilde{\widetilde{Q}}_2(t) + Y_2(t) + \widetilde{Y}_2(t))}{Q_1(t) + \widetilde{Q}_1(t) + \widetilde{\widetilde{Q}}_1(t) + Y_1(t) + \widetilde{Y}_1(t)} \tag{4.112}$$

Where M_m is the monomer molecular weight, (t) means the integrated value of the variable at time t, and the subindex (0) for the monomer concentration means initial value. Note that $f_{i0} = [M_i]_0/[M]_0$.

In copolymerization, a problem arises from the definition of M_m in the above equations, due to the different molecular weights of the comonomers. For the general case at hand, following the approach of Tacx et.al.(1988), the following definition may be used:

$$M_{m(cop)} = (M_{w1}F_1 + M_{w2}F_2 + M_{wc}F_c)\lambda \tag{4.113}$$

where M_{wi} is the molecular weight of monomer i, M_{wc} is the molecular weight of the donor-acceptor complex (i.e. $M_{wc}=M_{w1}+M_{w2}$), F_i is the instantaneous fraction of monomer i (or complex C) bound in the copolymer (as defined below), and λ is a correction factor.

The correction factor λ is introduced to account for the difference between the instantaneous average molecular weight of the comonomer units bound in the individual copolymer chains, and the accumulated average molecular weight of the comonomer units in all chains. This has to be considered since the average copolymer molecular weights calculated through eqs. (4.111) and (4.112) are accumulated averages.

According to Tacx (1988) the correction factor, adapted for the general case at hand, may be defined as:

$$\lambda = (M_{w1}F_1 + M_{w2}F_2 + M_{wc}F_c) / (M_{w1}F_{1acc} + M_{w2}F_{2acc} + M_{wc}F_{cacc}) \qquad (4.114)$$

where the subindex (acc) indicates accumulated value.

4.4.3 Diffusion Controlled Reactions

In this discussion, the free volume theory approach to model diffusion controlled termination and propagation reactions, given by Hamielec et.al.(1987), has been closely followed and integrated into the kinetic model proposed herein. This approach may be summarized as follows.

In the early stages of a batch copolymerization the termination reactions are chemically controlled and the compositional drift is usually small. Then, a single termination pseudo-kinetic rate constant $K_t = K_{tc}+K_{td}$ (eqs. 4.60 and 4.61) may be used to model copolymerization rate and molecular weight development up to conversions where these reactions become diffusion controlled. Nevertheless, if high molecular weight copolymer is being produced at low conversions, the termination rate may be controlled by segmental diffusion. Mahabadi and O'Driscoll (1977) have proposed the following model for segmental diffusion controlled termination:

$$K_{t_{seg}}/K_t = 1 + \delta[P] \qquad (4.115)$$

where $K_{t_{seg}}$ is the segmental diffusion-controlled termination rate constant, [P] is the total polymer concentration, and δ is a parameter which depends on the polymer molecular weight and quality of the solvent (monomers plus solvent if present).

Since monomers are commonly good solvents for the copolymer formed, the coil size of the polymer chains decreases increasing g the gradient concentration of radicals across the coil and thus the diffusion rate of the radicals. As a result the termination rate constant increases with monomer conversion until the translational diffusion of the macro-radicals controls the termination rate and then K_t starts to fall rapidly. In most cases, the contribution of the term $\delta[P]$ is small and can be neglected in the calculations [Battacharya and Hamielec (1986)].

From the beginning of the copolymerization, the free volume of the system may be calculated, as a function of conversion, as:

$$V_F(X) = \Sigma(0.025 + \alpha_i(T - T_{gi}))V_i(X)/V_T \qquad (4.116)$$

where $V_F(X)$ is the free volume of the system at conversion X, V_i is the volume of the species i in the reaction mix, V_T is the total volume of the polymerizing system, T is the polymerization temperature, T_{gi} is the glass transition temperature of the species i, and α_i is the thermal expansion coefficient of the species i. The summation is over all the species present in the reaction mix (monomers, polymer, and solvent if present).

The parameter K is defined as a function of conversion as:

$$K(X) = M_w(X)^M \exp(A/V_F) \qquad (4.117)$$

where M and A are adjustable parameters.

The adjustable parameter K_j, which follows an Arrhenius dependence on temperature, marking the onset point for the change from segmental to translational diffusion-controlled termination has been defined by Marten and Hamielec (1982), as:

$$K_j = (M_{wcrl})^M \exp(A/V_{Fcrl}) \qquad (4.118)$$

where M_{wcrl} and V_{Fcrl} are the accumulated weight average molecular weight and free volume at the conversion where $K = K_j$.

While $K \leq K_1$ the termination rate constant for the system is given by eq. (4.115) in which K_t is the pseudo kinetic rate constant defined by eqs. (4.60) and (4.61).

At the conversion at which K becomes greater than K_1, V_f and M_w become V_{fcr1} and M_{wcr1}, respectively, and from then on the value of the pseudo kinetic rate constant K_t takes a single value K_{t0}. Without further calculation of pseudo kinetic rate constat the termination rate constant decays exponentially according to:

$$K_t = K_{t0}(M_{wcr1}/M_w(X))^N \exp(-A(1/V_f(X) - 1/V_{fcr1})) \qquad (4.119)$$

where N is an adjustable parameter.

When a polymerization is carried out at temperatures below the glass transition temperature of the polymer being synthesized, the T_g of the monomer/polymer mix (T_{gmix}), which is function of conversion, X, will reach the polymerization temperature, T, at a critical conversion X_{cr}. For $X > X_{cr}$, $T_{gmix} > T$ and the reaction mix becomes glassy. Within this glassy polymer matrix the diffusion rate of monomer toward the active chain end decreases, limiting the final conversion.

In copolymerization, this phenomenon can be modeled by decreasing the individual propagation rate constants, for $X > X_{cr}$, according to:

$$K_{ij}(X) = (K_{ij})_0 \exp(-B_j(1/V_f(X) - 1/V_{fcrj})) \qquad (4.120)$$

and then calculate the pseudo kinetic rate constant K_{p_i} according to eq. (4.59). In the above equation: V_{fcrj} is the free volume of monomer j at $X=X_{cr}$, $(K_{ij})_0$ is the chemically controlled propagation rate constant for the reaction between radical i and monomer j, and B_j's is an adjustable parameter for monomer J.

Since the initiator and macro-initiator efficiencies also fall dramatically at X_{cr}, due to an enhancement of the cage effect, caused by the impossibility of the primary radicals formed to diffuse away from the

initiator and macro-initiator molecules, eq. (4.120) may in fact correlate $K_i f^{1/2}$ vs V_f to account for this phenomenon.

4.5 Copolymer Composition

The instantaneous copolymer composition is defined as:

$$F_i = \frac{d[M_i]}{d[M]} \tag{4.121}$$

Whenever monomer consumption by donor-acceptor complex formation and propagation through this complex is not negligible (i.e. K_c, and K_{ic} are comparable to K_{ij}), the knowledge of the reactivity ratios r_1 and r_2, which are defined with respect to monomer units, is insufficient to calculate the change in copolymer composition during copolymerization. In this case, the application of the Mayo-Lewis equation:

$$F_1 = \frac{r_1 f_1^2 + f_1 f_2}{r_1 f_1^2 + 2 f_1 f_2 + r_2 f_2^2} \tag{4.122}$$

or its integrated form, the Meyer-Lowry equation:

$$1 - X = (f_1/f_{10})^{\alpha} \, (f_2/f_{20})^{\beta} \, [(f_{10} - \delta)/(f_1 - \delta)]^{\gamma} \tag{4.123}$$

where: $\alpha = r_2/(1-r_2)$; $\beta = r_1/(1-r_1)$; $\gamma = (1-r_1 r_2)/[(1-r_1)(1-r_2)]$; $\delta = (1r_2)/(2-r_1-r_2)$; and $f_{i0} = f_i$ @ $t=0$.

is, of course, not exact.

Note that very often the copolymerization reactivity ratios r_1 and r_2 are obtained by adjusting experimental conversion and composition data to the Meyer-Lowry equation. If donor-acceptor reactions are important the reactivity ratios estimated in this form will be incorrect.

For the general case at hand, the following reactivity ratios can be defined:

$$r_1 = K_{11}/K_{12} \; ; \quad r_2 = K_{22}/K_{21} \; ; \quad \beta_1 = K_{1c}/K_{12} \; ; \quad \beta_2 = K_{2c}/K_{21}$$

Now the copolymer composition equations can be obtained by applying the definition given by eq. (4.121). This is achieved by dividing each one of eqs. (4.82) to (4.84) by eq. (4.81).

$$F_1 = \frac{d[M_1]}{d[M]} = \frac{K_c(f_c/K_{EQ} - f_1 f_2[M]) - (K_{11}\Phi_1 + K_{21}\Phi_2) f_1 Y_{T0}}{- K_p Y_{T0}} \qquad (4.124)$$

Rearranging eq. (4.124), and expanding K_p we obtain:

(4.125)

$$F_1 = \frac{K_c(f_1 f_2[M] - f_c/K_{EQ})}{K_p Y_{T0}} + \frac{(K_{11}\Phi_1 + K_{21}\Phi_2) f_1}{(K_{11}f_1 + K_{12}f_2 + K_{1c}f_c)\Phi_1 + (K_{21}f_1 + K_{22}f_2 + K_{2c}f_c)\Phi_2}$$

Considering that $K_{12}f_2\Phi_1 = K_{21}f_1\Phi_2$ we finally get:

(4.126)

$$F_1 = \frac{K_c(f_1 f_2[M] - f_c/K_{EQ})}{K_p Y_{T0}} + \frac{r_1 f_1^2 + f_1 f_2}{(r_1 f_1^2 + 2f_1 f_2 + r_2 f_2^2) + (\beta_1 f_1 + \beta_2 f_2) f_c}$$

Equation (4.126) is a general equation for copolymer composition applicable when donor-acceptor and statistical copolymerization occur simultaneously and competitively in both monofunctionally and bifunctionally initiated free radical copolymerization. This equation is a general form of the Mayo-Lewis equation inasmuch as it reduces to equation (4.122) when there is no formation of donor-acceptor complex (i.e. $K_c, f_c = 0$).

Similarly:

$$F_2 = \frac{K_c(f_1 f_2[M] - f_c/K_{tO})}{K_t Y_{T0}} + \frac{r_2 f_2^2 + f_1 f_2}{(r_1 f_1^2 + 2f_1 f_2 + r_2 f_2^2) + (\beta_1 f_1 + \beta_2 f_2) f_c}$$

and

$$F_c = \frac{2K_c(f_c/K_{tO} - f_1 f_2[M])}{K_t Y_{T0}} + \frac{(\beta_1 f_1 + \beta_2 f_2) f_c}{(r_1 f_1^2 + 2f_1 f_2 + r_2 f_2^2) + (\beta_1 f_1 + \beta_2 f_2) f_c}$$

Here F_1 and F_2 both have their traditional meaning of being the fraction of monomer units 1 and 2 bound to the copolymer through free monomer addition reactions. F_c, however, is the fraction of diads M_1M_2 bound to the copolymer by the donor-acceptor complex propagation reactions (note that the condition $F_1 + F_2 + F_c = 1$ is met). Therefore, caution has to be exercised when talking about global composition of monomers 1 and 2 in the copolymer, in which case $F_1' = F_1 + F_c/2$, and $F_2' = 1 - F_1'$.

Accordingly, the accumulated copolymer composition is established by a mere mass balance as:

$$F_1' = [f_{10} - (f_1+f_c)(1 - X)]/X$$

and

$$F_2' = [f_{20} - (f_2+f_c)(1 - X)]/X$$

Here X is the fractional conversion on a mol basis. Note that the above definition of the accumulated copolymer composition (F'), contains the contribution of the alternating donor-acceptor sequences.

This definition was preferred to a different one separating the accumulation of diads in the copolymer (i.e. $F_i=[f_{i0} - f_i(1-X)]/X$), since H-NMR characterization of copolymer composition cannot quantify the accumulated composition of diads M_1M_2 in copolymers, and the model defines the initial concentration of donor-acceptor complex $[C]_0$ as zero (i.e. $f_{c0}=0$).

Note that all these parameters needed for the evaluation of the instantaneous and accumulated copolymer composition are also obtained with the proposed solution of the kinetic model.

4.6 Effective Instantaneous Copolymer Composition

Let us analyze here the development of the copolymer chain microstructure, with regard to the random formation of blocks that occurs whenever combination is the dominant bimolecular termination mechanism.

In free radical copolymerization with bifunctional initiators, the instantaneous copolymer composition, as derived above, accounts only for the composition of the growing chains at a given time in the reaction coordinate. However, as it is depicted in figure 4.1, some of those chains are actually "segments" growing from chains, previously formed, which bear a different composition.

Since successive re-growth occurs at different stages in the reaction, dead and temporarily dead copolymer molecules bearing from one up to several segments of different composition, may be found in the reaction mix.

Owing to this, the actual instantaneous copolymer composition of chains with two or more segments will be different to that defined by equation (4.126).

Therefore, the concept of instantaneous composition, in this case, applies only to the composition of both the last growing segment attached to the three copolymer species, and the single-segment P_1 molecules formed instantaneously.

In order to properly quantify the actual instantaneous copolymer composition of the individual species, and the copolymer as a whole, the concept of Effective Instantaneous Copolymer Composition (EICC) is introduced here.

To understand this concept, let us go back to figure 4.1. At monomer conversion $\Psi = \Psi_1$, the instantaneous fraction of monomer i bound to the P_t molecule formed is F_{i1}. Assume that this chain remains "dead" until conversion Ψ_2 is reached. At Ψ_2 one of the terminal peroxide groups decomposes, from which a new segment of the chain, with composition F_{i2} is formed upon termination. From the point of view of the newly formed Pr molecule, its instantaneous copolymer composition would be given by F_{i2} (i=1,2). However, as a whole the new P_r molecule bears a different instantaneous composition, which depends on both the birth and re-growth conversions. Such composition may be expressed as:

$$F_{ei}(\Psi_2) = \frac{F_i(\Psi_1)*\Gamma_n(\Psi_1) + F_i(\Psi_2)*\Gamma_n(\Psi_2)}{\Gamma_n(\Psi_{1,2})}$$

where: $F_{ei}(\Psi_2)$ is the effective instantaneous composition of the P_r molecule given, with its last segment born at conversion Ψ_2; $F_i(\Psi_1)$, $F_i(\Psi_2)$ are the instantaneous compositions of the segments born at Ψ_1 and Ψ_2, respectively; $\Gamma_n(\Psi_1)$, $\Gamma_n(\Psi_2)$ are the instantaneous number-average chain lengths of the segments born at conversions Ψ_1 and Ψ_2, respectively; and $\Gamma_n(\Psi_{1,2})$ is number-average chain length, of the Pr molecule given, accumulated between conversions Ψ_2 and Ψ_1.

Generalizing for S segments and weighing the contribution of all molecules with different number of segments, in each copolymer specie, with their individual frequency of occurrence ($\nu_{s,}$) which are defined below, we get the expression defining the effective instantaneous copolymer composition (EICC), at the birth conversion of the last segment added, as:

$$F_{ei}(\Psi_s) = \sum_{j=1}^{\infty} \nu_j/\Gamma_n(\Psi_{1,j}) * \sum_{s=1}^{j} F_i(\Psi_s)\Gamma_n(\Psi_s) + \sum_{j=1}^{\infty} \widetilde{\nu}_j/\widetilde{\Gamma}_n(\Psi_{1,j}) * \sum_{s=1}^{j} F_i(\Psi_s)\Gamma_n(\Psi_s)$$

$$+ \sum_{j=1}^{\infty} \widetilde{\widetilde{\nu}}_j/\widetilde{\widetilde{\Gamma}}_n(\Psi_{1,j}) * \sum_{s=1}^{j} F_i(\Psi_s)\Gamma_n(\Psi_s) \qquad (4.127)$$

It may not be obvious at first the extreme complexity of the solution of eq. (4.127). On the one hand all the number of segments frequency distribution, the segment chain lengths, and the instantaneous compositions of the segments, are conversion dependant. On the other hand, and most importantly, the reference birth conversion Ψ_1 moves along with the reaction coordinate and must be kept track of.

This means that eq. (4.127) is in reality a set of an infinite number of equations which must be solved for differential changes in birth conversion. Therefore, its solution requires, for any differential change in conversion, one to quantify the amount of copolymer molecules being born at such interval, and keep track on the distribution of the number of segments that molecules, born in different intervals but re-growing at the given interval, have.

Presumably, the problem represented by the effective instantaneous copolymer composition equation, is mathematically similar to that of the instantaneous molecular weight distribution calculation, during the pre-gelation stage, of vinyl-divinyl free radical copolymerization with monofunctional initiators. Resent approaches describing the model solution for such problem may be found in Tobita (1990).

The task of adapting such a model solution to the problem at hand is of enormous proportions and well beyond the objectives of this thesis. Therefore, it will not be attempted here.

Instead the concept of Average Number of Segments (ANS) which defines the parameters in the effective instantaneous copolymer composition equation (EICC eq. 4.127), and gives a practical approach for its solution, is introduced in the next section.

It is worth noting that in the limiting case where the number of segments of the P_i species, goes to infinity, and the frequency for such specie (ν_i) approaches unity, the EICC equation becomes the mass balance which defines the accumulated copolymer composition.

This limiting case may be pictured as a single molecule with infinite number of segments bearing all the different compositions from F_{i0} to $F_i(\Psi)$. For such case the effective copolymer composition will be equal to the accumulated copolymer composition at any conversion.

Thus, the average number of segments that the copolymer accumulates at any conversion will be directly related to the extent of the compositional drift. The larger the average number of segments, the lesser the effective compositional drift.

It is important, then, to define a frequency distribution for the number of segments in the copolymer molecules, as a function of conversion, to determine such average number of segments.

4.7 Average Number of Segments per Copolymer Chain

In this discussion the work by Wittmer (1989) regarding the statistics of polyrecombinations in polymerization with symmetrical bifunctional initiators, will be closely followed. His concepts and nomenclature, have been adapted to be consistent with the present model. The analysis is valid for both homo and copolymerization with symmetrical bifunctional initiators and can be extended to consider asymmetrical bifunctional initiators, easily.

Let us write the bifunctional initiator molecule as:

R-O-O-Q-O-O-R

Upon polymerization, and in accordance with the reaction scheme described earlier, individual segments of coupled Shultz-Flory distributions will form between the individual R and Q, or Q and Q groups, which leads to the formation of the three copolymer species, defined here as:

a) P_i : $R-(Q)_i-R$ $(i=0,1,2,3,\ldots)$

Number of segments : $S = i + 1$

b) $\widetilde{P}_i$: $R-O-O-(Q)_i-R$ $(i=1,2,3,\ldots)$

Number of segments : $S = i$

c) $\widetilde{\widetilde{P}}_i$: $R-O-O-(Q)_i-O-O-R$ $(i=2,3,4,\ldots)$

Number of segments : $S = i - 1$

Let the number of polymer molecules with a number i of Q units be N_i, $\widetilde{N}_i$, and $\widetilde{\widetilde{N}}_i$, for the three copolymeric species, respectively.

At any time in the reaction, the number of undecomposed peroxide groups N_t, is given by:

$$N_t = 2\sum_{i=1}^{\infty}\widetilde{\widetilde{N}}_i + \sum_{i=1}^{\infty}\widetilde{N}_i$$

Note that $\widetilde{\widetilde{N}}_i$ is the number of bifunctional initiator molecules present at any time in the reaction, and $N_t - \widetilde{\widetilde{N}}_i$ is the number of macroinitiator molecules present at the same instant.

It has been shown by Wittmer (1989), that when combination is the only termination mechanism, probability calculations similar to those employed for the molecular weight distribution in polyrecombinations lead to:

$$N_i = \frac{1}{4} * \frac{A^{i+1}}{(4N_0)^i} \qquad (4.128)$$

$$\widetilde{N}_i = (2N_0 - A) * \frac{A^i}{(4N_0)^i} \qquad (4.129)$$

$$\widetilde{\widetilde{N}}_i = (2N_0 - A)^2 * \frac{A^{i-1}}{(4N_0)^{i-1}} \qquad (4.130)$$

In the above equations: A is the number of decomposed peroxide groups at a given time, and N_0 is the number of initiator molecules at the beginning of the reaction that will produce polymer chains (strictly fN_{i0}, where N_{i0} is the total initial number of initiator molecules and f is the initiator efficiency). The complete derivation of equations (4.128) to (4.130) is given in Appendix B.

The total number of molecules always remains equal to N_0, since each molecule contains a terminal R group on each side. Therefore, a summation over all values of i in eqs. (4.128) - (4.130) gives N_0 independently of the conversion.

The conversion of the peroxide groups (q), in the bifunctional initiator and macroinitiators, is defined as:

$$q = A/2N_0 \tag{4.131}$$

Substituting eq. (4.131) into eqs. (4.128) - (4.130), dividing each equation by N_0, and normalizing with respect to polymer molecules with at least one segment, to avoid taking into account the molecules of the bifunctional initiator ($\approx\!\!\approx N_1$), we get the number fraction (ν_s) of each individual species bearing different number of segments (S), in the copolymer mix, as a function of the conversion of peroxide groups, as:

$$\nu_s = \frac{(q/2)^s}{[1 - (1 - q)^2]} \tag{4.132}$$

$$\tilde{\nu}_s = \frac{2(1 - q)(q/2)^s}{[1 - (1 - q)^2]} \tag{4.133}$$

$$\approx\!\!\approx\nu_s = \frac{(1 - q)^2(q/2)^s}{[1 - (1 - q)^2]} \tag{4.134}$$

(S=1,2,3,..)

The summation over all values of S in eqs. (4.132) - (4.134) yields the distribution of copolymeric species as a function of the peroxide conversion, as:

$$Y(q) = \sum_{S=1}^{\infty} \nu_S \qquad (4.135)$$

$$\widetilde{Y}(q) = \sum_{S=1}^{\infty} \widetilde{\nu}_S \qquad (4.136)$$

$$\widetilde{\widetilde{Y}}(q) = \sum_{S=1}^{\infty} \widetilde{\widetilde{\nu}}_S \qquad (4.137)$$

where: Y is the number fraction of each of the three existent copolymer species in the copolymer mix. The individual number of segments frequency distribution, for each copolymer species, will be given by

$$Fr_S(q) = \nu_S/Y \qquad (4.138)$$

$$\widetilde{Fr}_S(q) = \widetilde{\nu}_S/\widetilde{Y} \qquad (S=1,2,3\ldots) \qquad (4.139)$$

$$\widetilde{\widetilde{Fr}}_S(q) = \widetilde{\widetilde{\nu}}_S/\widetilde{\widetilde{Y}} \qquad (4.140)$$

where: Fr_S is the frequency (number fraction) of the molecules with S segments within its own polymer specie (P_r, $\widetilde{P}_r$, and $\widetilde{\widetilde{P}}_r$, respectively).

Figure 4.2, shows the number of segments frequency distribution for the dead copolymer molecules P_r, at different peroxide conversions.

In this plot, Only the molecules with number fraction higher than 0.1% have been taken into consideration. Since at q=1 all the species have become dead copolymer molecules, P_r, no more polymerization will take place at this point. The curve at q=1 shows, then, the final number of segments distribution for a given polymer.

It is noticeable that one half of all the molecules formed will consist of a single segment. This means that, on average, half of the copolymer formed is similar to that formed in monofunctionally initiated copolymerization. Obviously the copolymer thus formed will follow the normal compositional drift.

It is also important to point out, from the plot, the fact that the frequency of the copolymer molecules bearing higher number of segments increases with peroxide conversion. This is in accordance with what is expected, since at the beginning of the polymerization the first molecules formed will have, evidently, only one segment.

Knowing the number of segments frequency distribution for each copolymer specie, we can now define the following averages:

$$S_n(q) = \sum_{S=1}^{\bar{S}} S\nu_S + \sum_{S=1}^{\bar{S}} S\tilde{\nu}_S + \sum_{S=1}^{\bar{S}} S\tilde{\tilde{\nu}}_S \qquad (4.141)$$

$$S_w(q) = \frac{\sum_{S=1}^{\bar{S}} S^2\nu_S + \sum_{S=1}^{\bar{S}} S^2\tilde{\nu}_S + \sum_{S=1}^{\bar{S}} S^2\tilde{\tilde{\nu}}_S}{S_n} \qquad (4.142)$$

where: S_n is the number-average number of segments; and S_w is the weight-average number of segments, at peroxide conversion q.

Figure 4.3, shows both number and weight-average number of segments as a function of the peroxide conversion q. In this plot it is important to note how the number, and weight averages approach their limiting value of 2, and 3 , respectively, at q=1. This describes very graphically, the accumulation of segments that some copolymer chains undergo during the course of the reaction, since the dispersity of this distribution (S_w/S_n) goes from 1 at q=0 to 1.5 at q=1.

4.8 Sample Simulation

In order to test the kinetic model proposed, and the stability of the numerical solution, a simulation was carried out. For this purpose,

a hypothetical copolymerization pair, undergoing exclusively statistical isothermal batch copolymerization, without compositional drift (azeotrope composition), was tested. Termination by combination was the only mechanism considered. This case was chosen for being the simplest. The application of the model to more complicated cases, given by the copolymer systems studied in this thesis, will be seen in chapters 5 to 8.

The simulation program BIFUN for homopolymerization with bifunctional initiators, was extended to simultaneous and competitive statistical/donor-acceptor copolymerization according to the models presented herein, with which the program BICOP was obtained. The treatment of the diffusion controlled rate constants followed the semi-empirical approach based on the free volume theory for polymer solutions, using for this sample simulation, the parameters for polystyrene. Very wide descriptions of the numerical solution strategy, and the information flow chart of the simulation program BIFUN, can be found elsewhere [Villalobos (1989)].

The kinetic parameters used for this simulation are reported in Table 4.1, below. Simulation results for copolymerization rate, molecular weight distribution development, copolymer species distribution, dead polymer segment distribution, and average number of segments, as a function of monomer conversion, were obtained, and can be explained as follows.

Figure 4.4, shows the comparison of the simulation results for conversion history of monofunctionally and bifunctionally initiated copolymerizations. The same concentration of peroxide groups (double initiator concentration) with the same decomposition constant, was employed for the monofunctional system (see Table 4.1). The peroxide conversion (q) is plotted as well to establish its correspondence with the monomer conversion.

The acceleration observed in the bifunctionally initiated copolymerization is expected, mainly due to the earlier onset of the gel effect, triggered by the higher molecular weight of the multi segment

copolymer chains present in the reaction mix. The higher the molecular weight, the faster the decay in the termination rate and the stronger the gel effect.

Figure 4.5, shows a comparison of the simulation results for molecular weight averages of monofunctional and bifunctionally initiated copolymerization as a function of monomer conversion. The expected higher molecular weight build up, for the bifunctional system is clear, and explains, again, the higher copolymerization rate observed in fig. 4.4. In these two figures becomes clear the main feature of bifunctionally initiated polymerization, which is the simultaneous obtention of higher molecular weights at higher reaction rates than with monofunctional initiation.

Figure 4.6, shows the comparison of the copolymer species distribution as a function of monomer conversion. The solid lines are the solution of eqs.(4.135) - (4.137), and the dashed lines are obtained from the solution of the kinetic model at each integration step as $Y=Q_0/Q_t$ ($Q_t = Q_0 + Q_0 + Q_0$), for each copolymer specie. It is remarkable how close both solutions are, considering that the first is based exclusively on a statistical scheme and the other on a kinetic model. The results in this regard prove that both the statistical and kinetic approaches used to compute the distribution of polymer species as a function of monomer conversion in free radical polymerization with bifunctional initiators, are essentially equivalent. The slight disagreement observed in the curves is likely due to the variation in initiator efficiency considered by the model, within the decay of the termination rate constant [Villalobos et.al.(1991)]. Such variations lead to a different number of total peroxide groups in each scheme.

Figure 4.7, shows the frequency distribution of number of segments in the dead copolymer molecules P_r, as calculated through eq. (4.138). The solution of this equation was linked to the simulation program to obtain the distribution as a function of monomer conversion.

In this plot it is clearly seen how the concentration of multi-segment copolymer chains increases with monomer conversion. The change of slope observed at the end of each curve, is due to the continuous increase in peroxide conversion even at the point where the propagation has nearly stopped due to the decay in K_p. This may be interpreted as copolymer chain recombination of the species P_r, and P_t still present in the system, accompanied by negligible conversion, which happens through termination by propagation at very high monomer conversions, when the glassy effect is present [Hamielec et.al.(1987)].

Same as with eq. (4.138), eqs. (4.141) and (4.142) were integrated to the kinetic simulation program to link the peroxide conversion to the monomer conversion, calculated at every integration step. For the simulation at hand, figure 4.8, shows the number and weight average number of segments of the copolymer chains as a function of monomer conversion. The expected values according to the relation between monomer to peroxide conversion given in fig. 4.2, were obtained. The continuous increase in the average number of segments proves, once more, the multiple initiation/propagation/termination cycles, experienced by some copolymer molecules in this type of copolymerization.

Both the kinetic model, and the stability of the numerical solution employed have proved adequate. The simulation results given, show all the correct behaviour, expected in free radical copolymerization with bifunctional initiators, for all the variables tested, which gives confidence for its employment with the copolymers studied in this thesis.

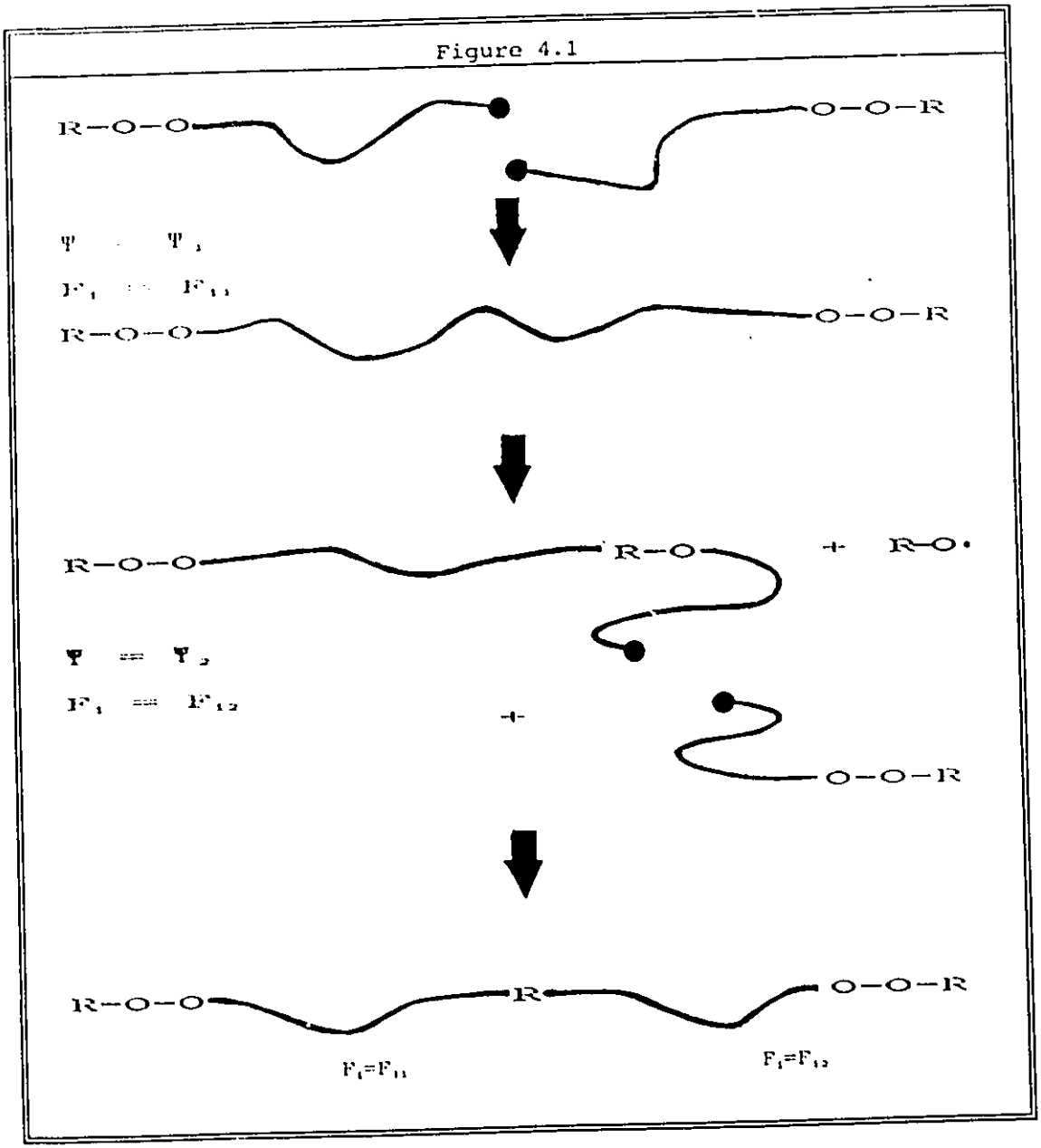

Figure 4.1. Schematic representation of a single re-initiation/ propagation/termination cycle in free radical copolymerization with bifunctional initiators (Ψ=birth conversion, F_i=fraction of monomer i bound in copolymer).

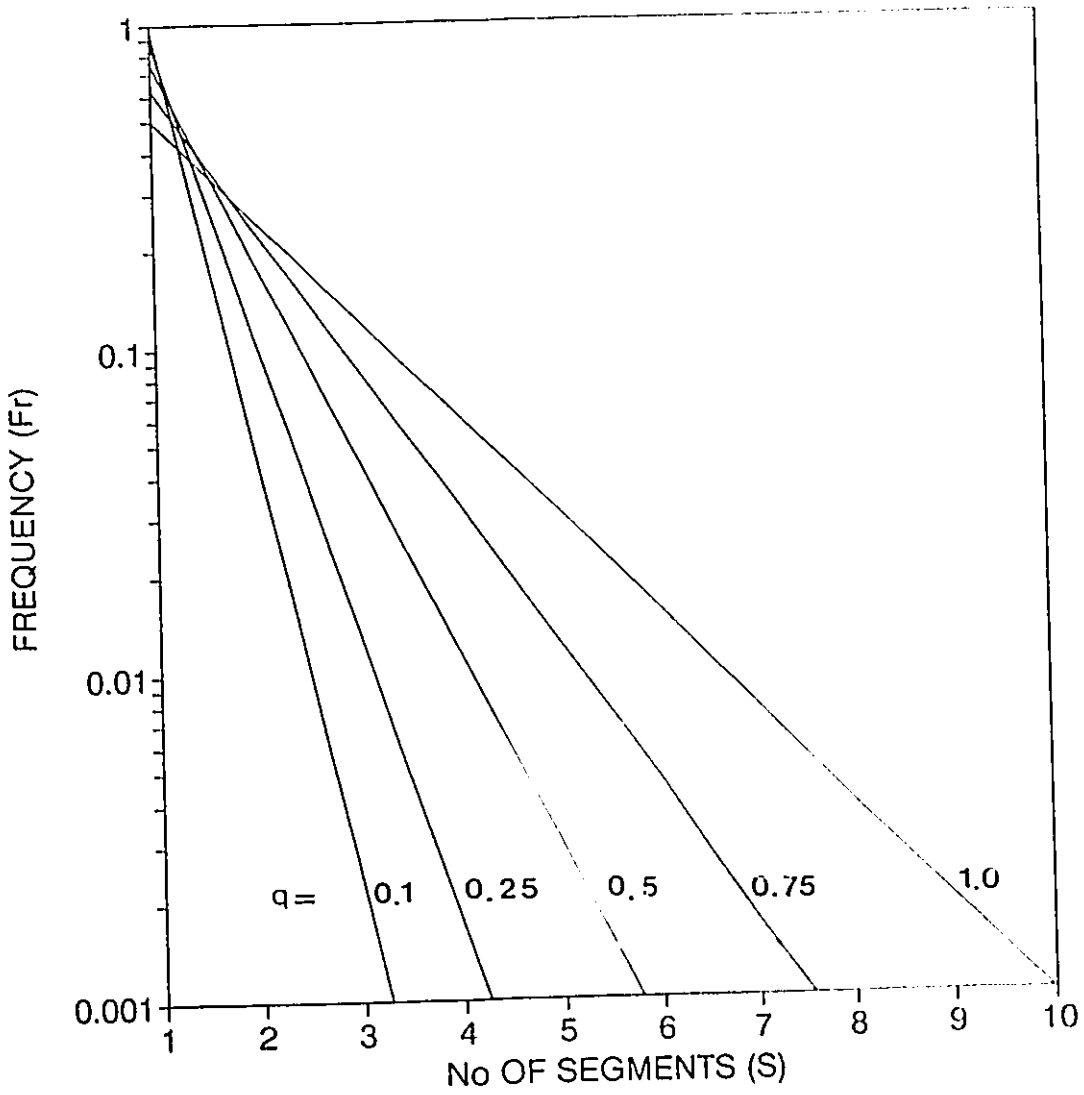

Figur : 4.2. Frequency distribution (number fraction) of segments in the dead copolymer molecules (P_r), at different peroxide conversions (q).

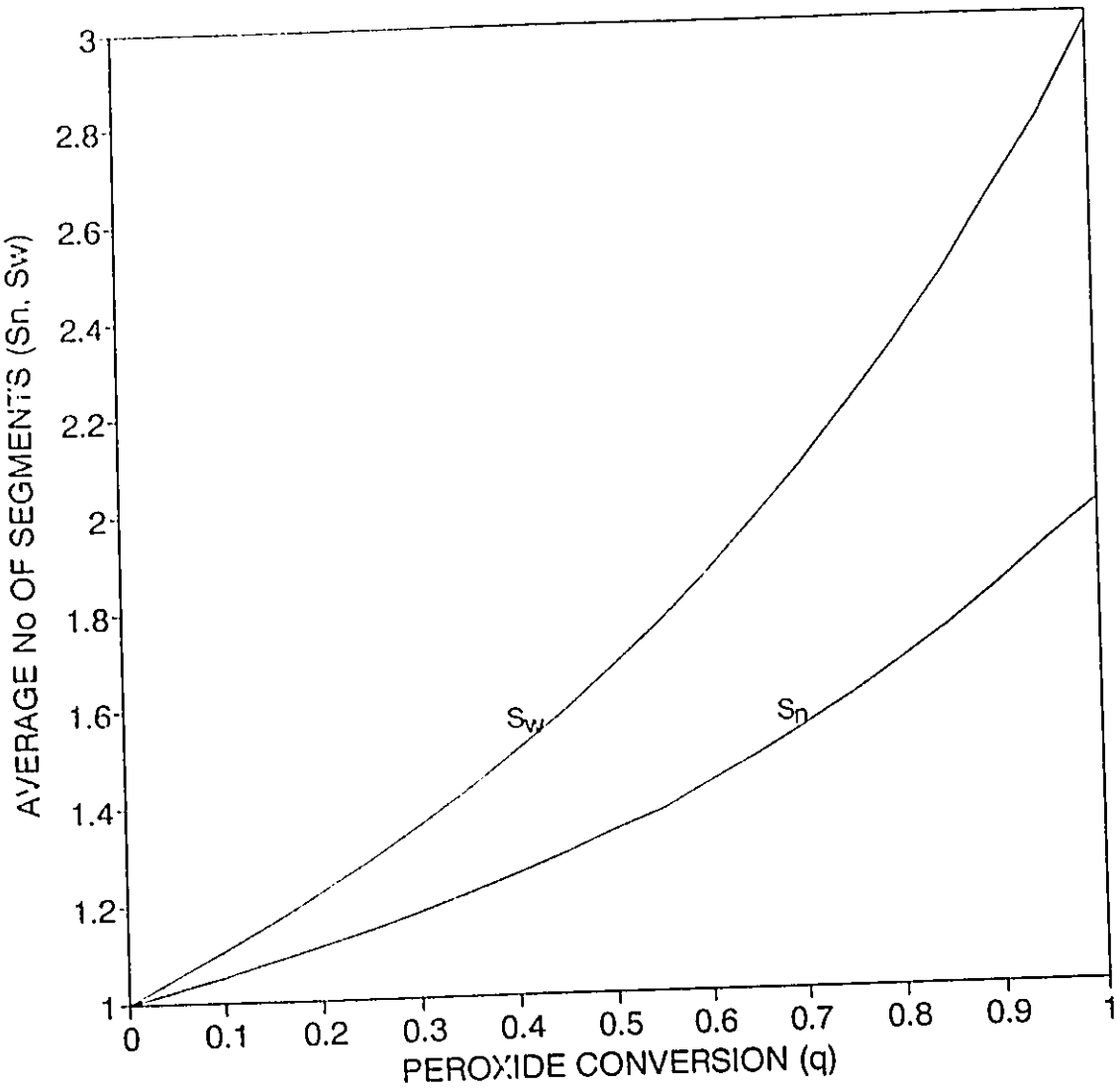

Figure 4.3. Number-average (S_n), and weight-average number of segments (S_w) per copolymer chain, as a function of peroxide conversion (q).

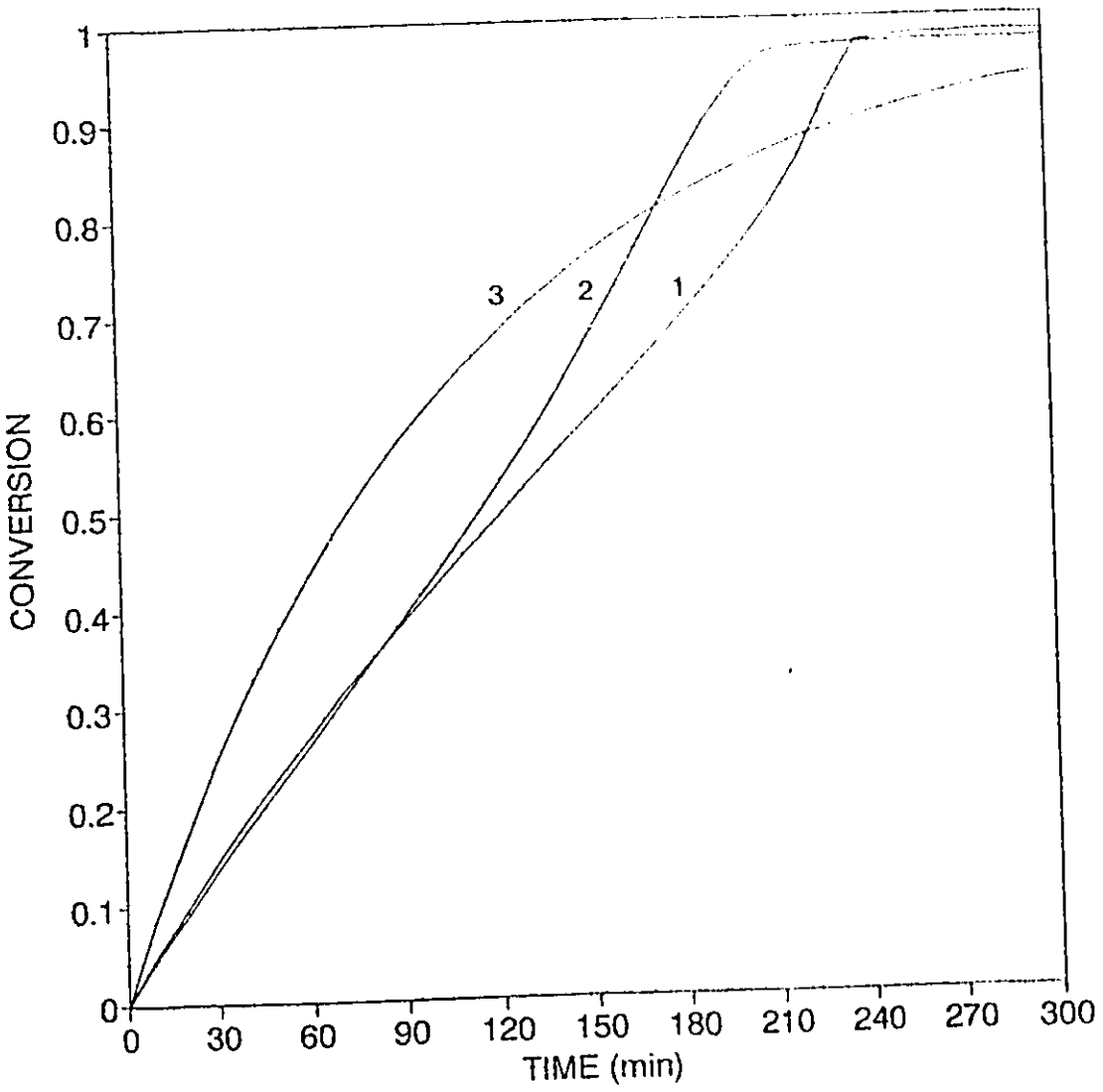

Figure 4.4. Comparison of model solutions for monomer conversion history of: (1) Monofunctionally, and (2) bifunctionally initiated isothermal batch copolymerization, without compositional drift. (3) Peroxide conversion (q).

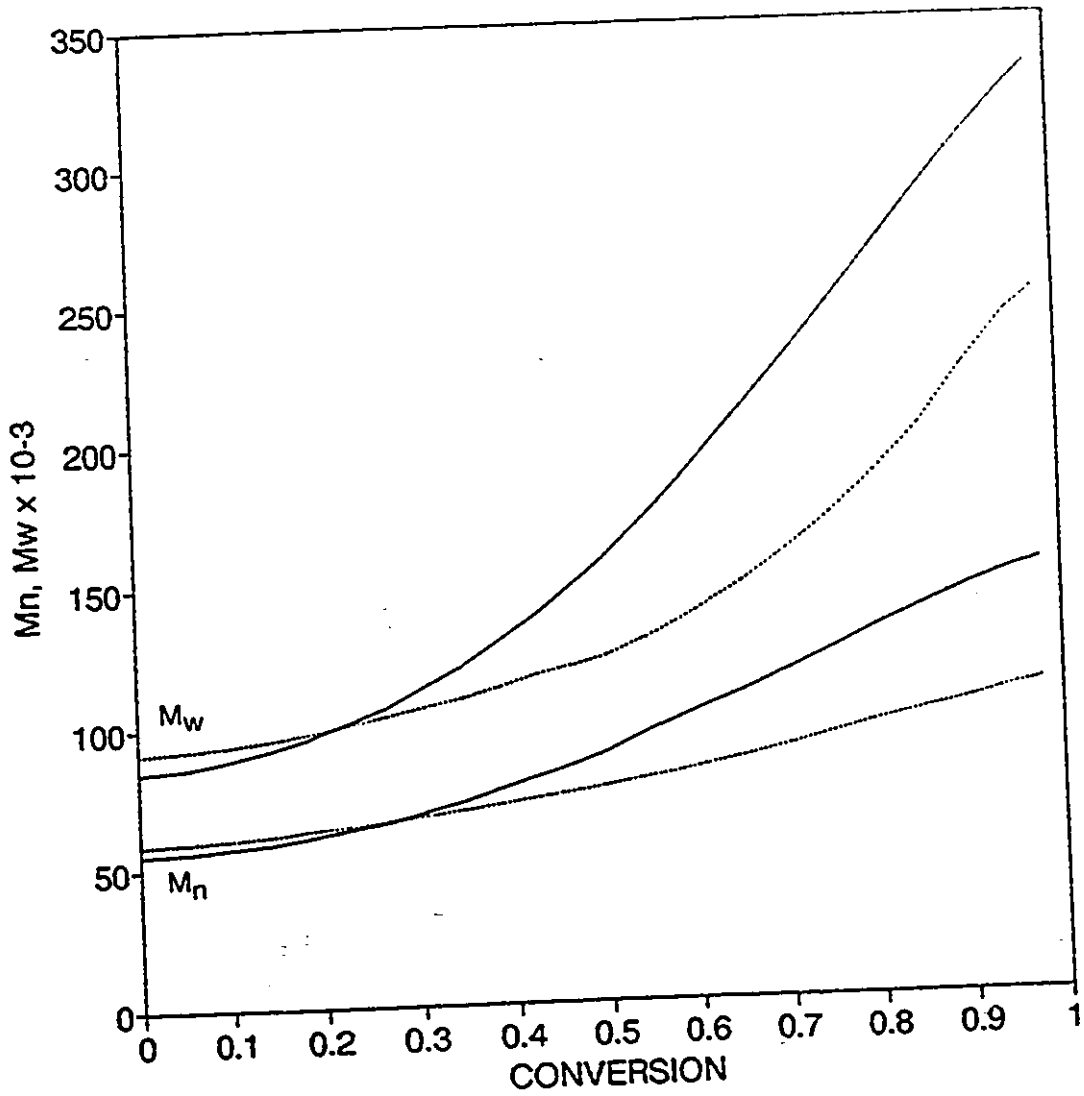

Figure 4.5. Comparison of model solutions for molecular weigh distribution development for:(---) monofunctionally, and (——) bifunctionally initiated isothermal batch copolymerization, without compositional drift.

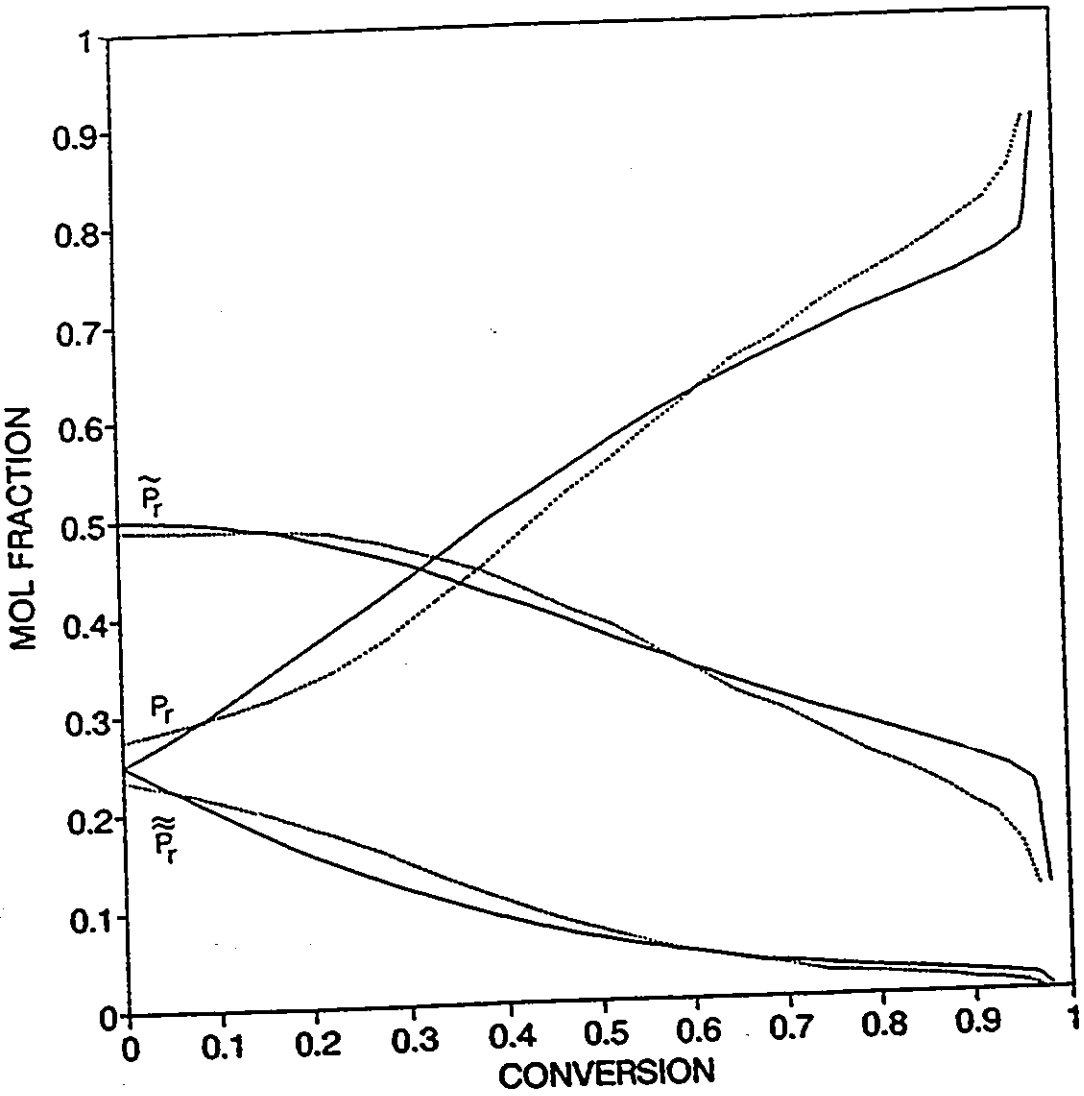

Figure 4.6. Distribution of copolymer species as a function of monomer conversion, from: (——) eqs.(4.135) to (4.137); and (– – –) Kinetic model prediction Q_0/Q_1.

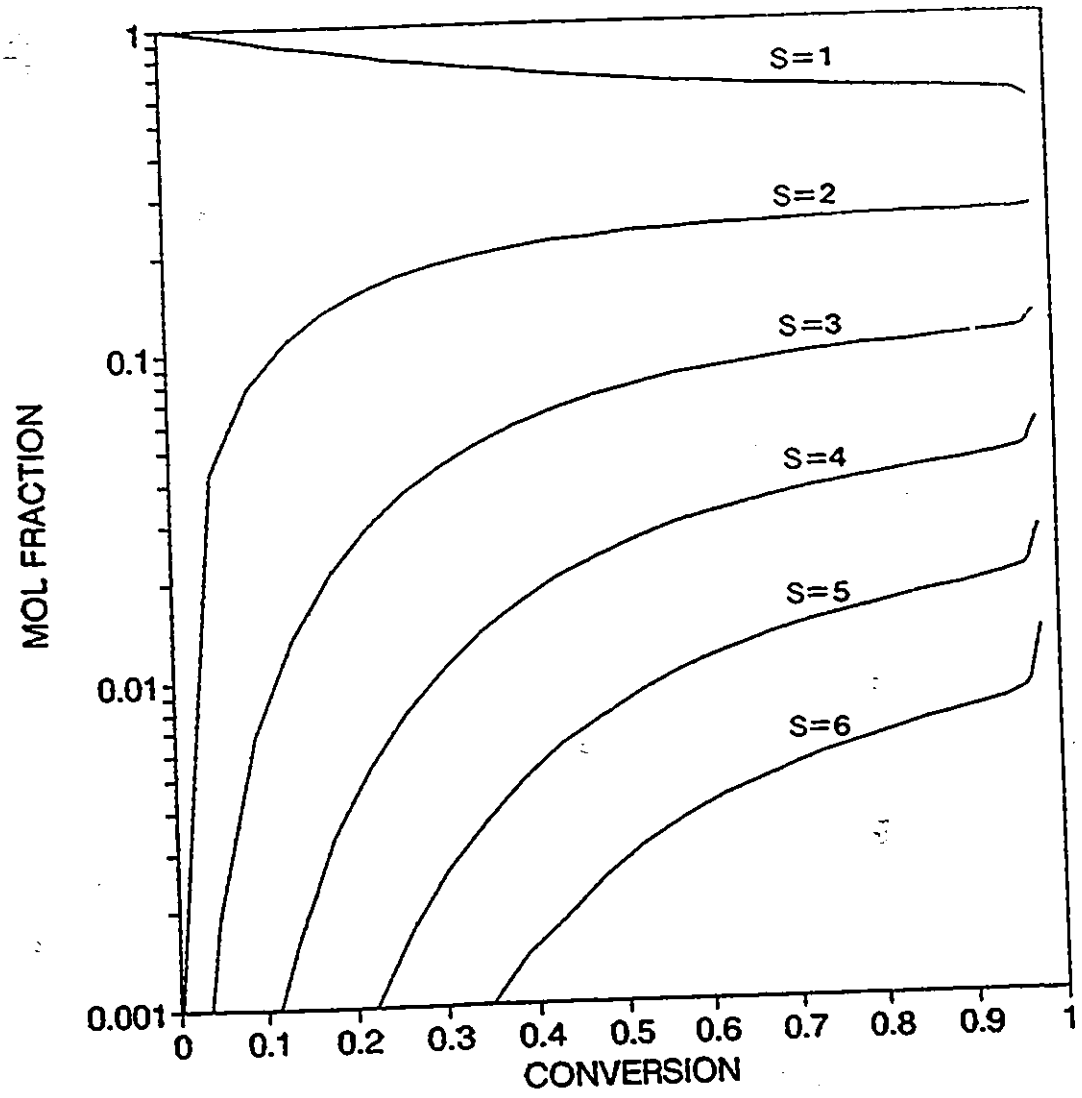

Figure 4.7. Frequency distribution of the number of segments for dead copolymer molecules (P_r), as a function of monomer conversion.

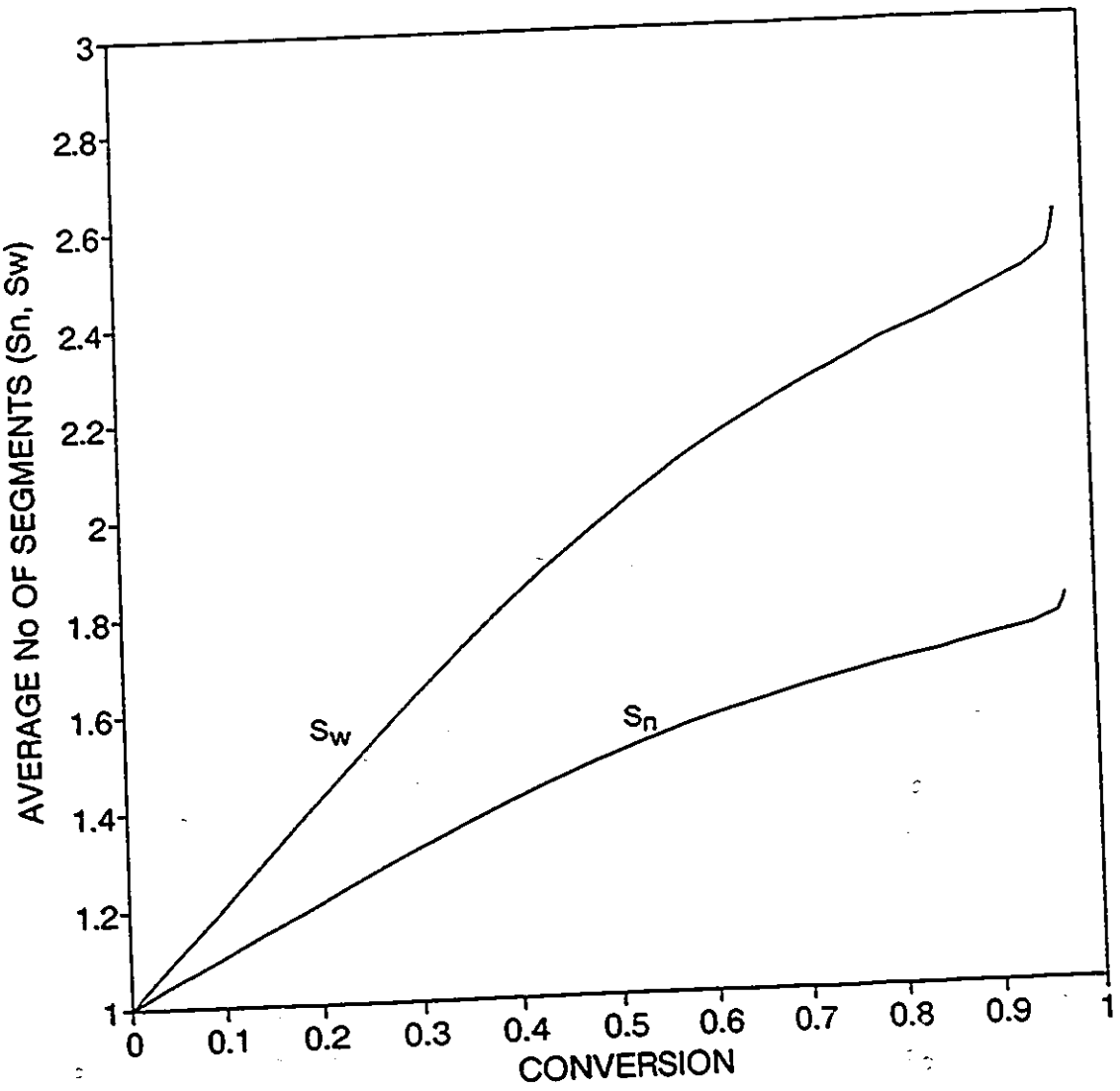

Figure 4.8. Number-average (S_n) and weight-average (S_w) number of segments per dead copolymer chain, as a function of monomer conversion.

CHAPTER 5

STYRENE/α-METHYLSTYRENE COPOLYMERS

In this chapter, the synthesis and characterization of high T_c Styrene/α-Methylstyrene (SAMS) engineering copolymers, through bulk copolymerization with bifunctional initiator, is described. From the experimental results obtained, the rate constants and other parameters necessary for the simulation of the copolymerization kinetics for this system are estimated. Literature data for these parameters are also employed whenever available. The experimental results for conversion history, and the development of molecular weight averages, comonomer and copolymer composition, copolymer glass transition temperature, and copolymer micro-structure, are compared with the simulation results obtained with the simulation program BICOP, described in Chapter 4. Under optimized conditions, suspension copolymerizations are carried out to obtain copolymers with the desired characteristics of residual monomer levels, molecular weight distribution, and glass transition temperature.

5.1 Introduction

As described in detail in Chapter 2, the main problems regarding the synthesis of SAMS copolymers are brought about by the low ceiling temperature of α-methylstyrene (T_c = 61°C) [Dainton and Ivin (1948)]. In copolymerization above this temperature the reversible nature of the propagation reactions involving the formation of α-methylstyrene diads accounts for the low polymerization rates and low molecular weights observed [O'Driscoll and Gasparro (1967), O'Driscoll and Dickson (1968)].

The possibility of increasing the copolymerization rate while producing high molecular weight copolymers, through the use of bifunctional initiators, is contemplated in this study as the best means to synthesize high T_g SAMS copolymers at a commercially competitive rate [Villalobos et.al. (1991)].

Several alternatives for kinetic modelling arise when dealing with reversible propagation steps. The use of antepenultimate effect [Ham (1960,b)], penultimate effect with reversibility [O'Driscoll and Dickson (1968)], and terminal model with reversibility [Fischer (1972)] have shown, if any, only marginal improvements over the results obtained when the terminal model is employed without taking into account reversible propagation steps [Johnston and Rudin (1971)]. In addition, the complexities involved in the estimation of the rate constants considered when reversibility and/or penultimate effects are taking into account, make the solution of such schemes more a numerical problem than a close representation of the system.

Consequently, in this study, the terminal model without reversibility of the α-methylstyrene propagation reactions, proposed in Chapter 4, has been considered as the basis for the simulation of this copolymerization system.

In this system both styrene and α-methylstyrene are electron donors, thus, no possibility of donor-acceptor complex formation exists. Owing to this fact, the treatment for this system is that of a purely statistical copolymerization. Since the simulation program BICOP allows for the simultaneous and competitive statistical/donor-acceptor copolymerization the model proposed reduces to a consideration of exclusively statistical copolymerization when the rate constant for the donor-acceptor complex formation (K_c) is set to zero (see reaction scheme in Chapter 4). Note that a dummy value for the equilibrium constant for donor-acceptor complex formation (K_{eq}) must be introduced to the simulation in order to prevent run time errors due to division by zero in the individual monomer consumption equations.

In addition, in the simulation program, the total monomer conversion was defined on a mass basis to directly compare with the experimental results for conversion which are established on the same mass basis, as explained below.

5.2 Design of Experiments

According to the detailed structure of this project stage (see Chapter 1), the experimental program was divided in three phases. The first one comprises exploratory research to evaluate the effect of comonomer feed composition (f), on copolymerization rate (R_p), molecular weight distribution (MWD), copolymer composition (F), and copolymer glass transition temperature (T_g), at terminal conversion, through isothermal bulk copolymerization in DSC cells and ampoules. The copolymerizations were carried out under optimal polymerization conditions for suspension polystyrene synthesis (i.e. T_p = 105°C, [TBPCC] = 0.01 M/L) [Villalobos et.al.(1991)]. The experimental design SAMS-01 for this exploratory phase is shown in Table 5.1, below.

Table 5.1

Experimental Design SAMS-01 for the Exploratory Research

RUN SAMS-01	f_{1o} (mol)	T_p (°C)	[TBPCC]o (Mol/L)	POLYM. TIME (hrs)
1	1.00	105	0.01	8.0
2	0.90	105	0.01	8.0
3	0.80	105	0.01	8.0
4	0.75	105	0.01	8.0
5	0.70	105	0.01	8.0
6	0.60	105	0.01	8.0
7	0.50	105	0.01	8.0

From the results obtained in the exploratory phase, discussed below in section 5.4, an optimization experimental phase was designed in order to evaluate the effect of polymerization temperature (T_p), and bifunctional initiator concentration ([TBPCC]), on R_p, MWD, F, and T_g development with conversion. In this phase isothermal bulk copolymerizations with bifunctional initiator TBPCC, were carried out in ampoules, under the optimal monomer feed composition selected from phase one. The experimental design selected for this optimization phase, was a complete factorial 2^2 plus the experimental centre. This design (SAMS-02) is given below in Table 5.2.

Table 5.2

Experimental Design SAMS-02 for the Optimization Research

Run SAMS-02	f_{10} (mol)	T_p (°C)	[TBPCC]o (Mol/L)	POLYM. TIME (hrs)
1	0.85	120	0.0100	24
2	0.85	120	0.0050	24
3	0.85	90	0.0100	24
4	0.85	90	0.0050	24
5	0.85	105	0.0075	24

The sum of the experimental results of phases one and two, allowed for the complete parameter estimation of the simulation program BICOP. Simulation of all the experimental runs of both stages were performed to evaluate the goodness of the fit and the ability of the simulation program to forecast all the variables mentioned plus some micro-structural features of the copolymer, according to the model proposed in Chapter 4.

In the third experimental stage, suspension copolymerizations were carried out, at the simulation assisted optimal conditions selected, to evaluate the effect of R_p on suspension stability, mean particle size (MPS) and particle size distribution (PSD), under reactor scaled-down conditions for pure polystyrene suspension polymerization [Villalobos (1989)].

The suspension copolymers obtained were also characterized to compare measured values against model predictions, and processed through extrusion in order to evaluate their feasibility for commercial production and processability. The experimental design of this phase is given in table 5.3, below.

Table 5.3

Experimental Design SAMS-03, Suspension Copolymerization Scaled Reactor Arrangement, Recipes and Operating Conditions

RUN SAMS-03	f_{10} (mol)	[TBPCC]o (Mol/L) (org. phase)	T_p (°C)	TIME @ T_p (hrs)
REFERENCE	1.00	0.0100	105	4
1	0.85	0.0075	105 120	13 3
2	0.85	0.0090 2.5 wt% TOLUENE	105	16

Recipe	
Initial volume @ 25°C (water + organic phase)	V_0 = 3200 cc
Dispersed phase volume fraction (@ 25°C)	Φ = 0.4
Suspending agent (TCP) concentration	[TCP]o = 7.5 g/L_{org}
Reactor Operating Conditions	
Copolymerization temperature (T_p)	As in design
Copolymerization time (t)	As in design
Copolymerization pressure	P_0 = 275 KPa
Agitation speed	N = 275 rpm
Reactor Geometrical Parameters	
Liquid height (Z) to tank diameter (T) ratio	Z/T = 1.2
Impeller diameter (D) to tank diameter ratio	D/T = 0.6
Impeller type (turbine)	4-blade, 45°pitch
Number of impellers (pumping downward)	No = 2
Bottom imp. position (from reactor bottom)	H_1 = T/4
Top impeller position (from reactor bottom)	H_2 = (2/3)Z
Blade width	W_1 = 0.2 D
Number and position of baffles	B_f = 4, spaced 90°
Baffle width (offset from the wall T/44)	W_B = T/12

All the synthesis and characterization techniques employed in these experimental stages are described below.

5.3 Experimental

5.3.1 Materials

Styrene, and α-methylstyrene (Aldrich Chemical) were washed with NaOH solution (10%) to remove inhibitor (12 ppm p-tertbutylcatechol) and then distilled under vacuum at room temperature, following standard procedures [Villalobos (1989)].

The bifunctional initiator selected for this study: 1,4-bis(tertbutyl peroxycarbo)cyclohexane (TBPCC), supplied by Akzo-Chemie as initiator D-162, was used without any further purification. Chloroform, and methanol, both reactive grade, were used as copolymer solvent and non-solvent, respectively. Toluene, analytical grade, was used as solvent in a suspension copolymerization run according to the experimental plan described.

5.3.2 Techniques

For the exploratory research phase, isothermal bulk copolymerizations of styrene/α-methylstyrene with bifunctional initiator TBPCC, were carried out in DSC cells, in a Du-Pont 910 Differential Scanning Calorimeter, from master batch reaction mixtures previously prepared. The reactions were allowed to proceed for 8 hours at the temperature selected (see Table 5.1 for experimental design).

Simultaneously, bulk polymerization in ampoules were carried out, at the same conditions and from the same master batch reaction mixtures. For each experiment two (ampoule) samples were taken at 0.25 and 8 hrs to characterize initial copolymerization rate, and terminal conversion, respectively. Ampoule polymerization has been described in detail elsewhere [Villalobos (1989)].

The time-integrated heat of copolymerization obtained from the DSC results, translates directly into monomer conversion when normalized with respect to the observed terminal conversion, if both compositional drift is negligible (or heats of polymerization are similar for both monomers), and no other thermal events occur during the polymerization. Since, as it will be shown below, very slight compositional drift occurs at the selected conditions, and no other thermal events were observed during the allotted polymerization time, monomer conversion curves for all these experiments were obtained through the method described.

The contents of the ampoules were dissolved in chloroform at room temperature (chloroform and methanol-soluble p-tertbutylcatechol was added as inhibitor) and the copolymer was precipitated with a ten fold excess of methanol. The slurry was vacuum filtered and washed thoroughly with methanol. The copolymer was recovered and dried under vacuum at 70°C for 12 hours to eliminate all traces of solvent and non-solvent. Total monomer conversion both initial and terminal, on a mass basis, was established gravimetrically.

The copolymer composition of the purified copolymers thus obtained, were characterized through Proton Nuclear Magnetic Resonance (H-NMR), from solutions in deuterated chloroform in a Bruker-1.6 MHz NMR Spectrometer. The interpretation of the spectra was performed following the procedure reported by O'Driscoll and Gasparro (1967).

Molecular weight distribution of the terminal conversion copolymers were obtained through Size Exclusion Chromatography (SEC) in a Waters 150-C GPC/ALC, using polystyrene standards and THF as carrier solvent, with a suitable column arrangement.

Glass transition temperature of the copolymers obtained at terminal conversion were determined by DSC in a Du-Pont 910 Differential Scanning Calorimeter, using a constant temperature raise at 10°C/min, from room temperature to 200°C.

For the optimization experimental stage, isothermal bulk copolymerizations in ampoules at the designed conditions were carried out (see Table 5.2). Ampoules of 0.5 mm (OD) were selected in order to minimize heat effects according to the recommendations reported by Zhu and Hamielec (1990). The total polymerization time allotted was 24 hours. Samples were removed from the constant temperature oil bath and quenched in liquid nitrogen, at previously selected sampling times. The contents of all the samples thus obtained, were dissolved in chloroform, precipitated with methanol, washed, and dried, following the procedure described above.

Monomer conversion of each sample (mass basis) were established gravimetrically. Characterization of the molecular weight distribution by SEC, copolymer composition by H-NMR, and copolymer glass transition temperature by DSC, were performed through the same procedures described above.

For the third experimental phase, suspension copolymerizations at the designed conditions, were carried out in a 1 gallon stainless steel stirred pilot plant reactor vessel.

The reactor internal arrangement and operating conditions correspond, as mentioned before, to the scaled-down system for optimized suspension polystyrene (T_p=105°C, [TBPCC]=0.01 M/L, [TCP]=7.5 g/L-monomer), and are given in Table 5.3 along with the experimental design. The reference system was used to compare suspension stability, MPS and PSD, of the suspension copolymers obtained (see Chapter 3, Table 3.3 for reference values of these parameters).

The characterization of the MPS and PSD of the suspension copolymer beads obtained was performed following the procedure described in the experimental section of Chapter 3. Terminal conversion, molecular weight distribution, copolymer composition, and copolymer glass transition temperature, of the suspension copolymers obtained were also established by the same procedures described above.

To asses the feasibility of product processing, the copolymer beads were extruded in a single screw (0.25", L/D=24) RandleCastle Minitruder, at 225°C and 50 RPM. The T_g of the extrudate, and percent of mass loss and MWD after 5 and 10 hrs at 225°C of extrudate samples, were determined by DSC and SEC, respectively, following the procedures described, to evaluate annealing effects on T_g and copolymer degradation, respectively.

In what follows, all the experimental and model results are explained and discussed in detail.

5.4 Results and Discussion

5.4.1 Exploratory Research

According to the experimental design SAMS-01 and objectives of this experimental phase (see Table 5.1), the effect of the comonomer feed composition on R_p was studied first. Figure 5.1, shows the DSC (translated) experimental results for monomer conversion history as a function of the styrene/α-methylstyrene feed composition (mol %). The curve for 100/0 feed composition corresponds to the homopolymerization of styrene at the conditions given (T_p=105°C, [TBPCC]=0.01 M/L). This curve perfectly superimposes on the experimental conversion curve for this reference system, shown in figure 3.6 (Chapter 3). This implies high reliability of the DSC experiments.

The most remarkable feature observed in figure 5.1, is the strong effect of the amount of α-methylstyrene (AMS) in the comonomer feed on the copolymerization rate. A mere 10 mol% of AMS prevents the system from reaching total monomer conversion in the allotted time. While pure PS approaches 100% conversion in about 3 hours, less than 90 % conversion is reached in 8 hours for this system. The progressive decay in the copolymerization rate is evident as the amount of AMS in the comonomer feed increases. As shown, the system with 50 mol% of AMS in the feed reaches only 27 % conversion after 8 hours.

Another remarkable feature in the conversion curves for the systems with AMS, only noticeable in the curves with 10, 20 and 30 % AMS, is the change in concavity, from downward to upward, characteristic of the onset of the gel effect, occurring at about 30% conversion. This value is slightly lower than that of pure PS at the conditions and MWD given which is estimated to occur at about 35 % conversion as shown in the corresponding curve [Marten and Hamielec (1982)].

In addition, the curve for 10 % AMS seems to indicate that the strength of the gel effect is lower for the copolymer than for polystyrene. This is in part due to the lower copolymer molecular weights achieved (see below) which allow higher molecular mobility at similar conversions, however this fact by itself does not explain the moderate auto-acceleration observed since polystyrene at this molecular weight level experiences a stronger gel effect (see Villalobos et.al. 1991).

An explanation for the weaker gel effect observed may be given in terms of the strong plasticizing effect caused by the low molecular weight chains (oligomers) formed when AMS is polymerized above its T_c [O'Driscoll and Dickson (1968)].

The model predictions for conversion history at the given conditions, almost perfectly superimpose on the curves shown in figure 5.1, and as a result, are not show in the plot.

For clarity, an explanatory note is needed here. Once the experimental phases one and two were completed, model parameter estimation was performed (see parameter estimation section below), and then all the simulations of the experiments performed in these two phases were carried out. Therefore, all the model results presented in this and the following section refer to the completely adjusted model, whose parameters and estimation procedure are reported below.

In figure 5.2, the experimental and model terminal conversions reached after 8 hours of polymerization are shown as a function of the mol fraction of AMS in the monomer feed. Since all the experimental curves were perfectly copied by the simulation, throughout the entire conversion

range, it is no wonder than the terminal conversions predicted also agree with the experimental results.

More significant is the effect of AMS concentration on the copolymerization rate. Figure 5.3, shows the experimental and model results for the initial copolymerization rate, relative to the styrene homopolymerization rate at the conditions given. A clear exponential decay in copolymerization rate is observed as the content of AMS in the monomer feed increases. These results follow the same trend observed in earlier works with this system, when monofunctional initiator (BPO) was used at 60°C [O'Driscoll and Dickson (1968), Rudin and Chiang (1974)].

This trend shows that the initial copolymerization rate observed in S-AMS copolymerization at given T_p and [I], is highly dependent upon comonomer composition and independent of the functionality of the initiator. Nevertheless, the larger molecular weight build-up in bifunctionally initiated than in monofunctionally initiated copolymerization may account for earlier onset of the gel effect and higher copolymerization rates during the auto-acceleration period, as shown before in figures 4.4 and 4.5 (Chapter 4).

The effect of the feed concentration of AMS on number and weight average molecular weights of the copolymers obtained at terminal conversion is shown in figure 5.4. Again, the exponential decay in the copolymerization rate, brought about by the low propagation rate and high termination rates characteristic of AMS polymerization (see below), along with the low terminal conversions and weakness of the gel effect, when present, cause the nearly exponential decay observed in both the number and weight average molecular weights, as the concentration of AMS in the feed increases.

Note in the model results for molecular weigh averages that the terminal M_w observed for all feed compositions has been properly predicted, whereas M_n is consistently over-estimated (by about 6000 Dalton, in average).

As mentioned in Chapter 4, the pseudo-kinetic termination rate constants employed in the model are number average rate constants [Zhu and Hamielec (1989)]. As a result, fitting of M_n for the system causes under-estimation of M_w, and fitting of M_w causes over-estimation of M_n. Since M_w is more closely related to the mechanical properties of the product than M_n, in this work it was preferred to use the latter approach for model fitting.

It is important to point out here the semi-quantitative nature of the molecular weight distribution results, obtained through SEC, for these and other copolymers. With Size Exclusion Chromatography, the fractionation of the polymer is carried out in packed columns according to the hydrodynamic radii of the chains in a suitable solvent. The time dependent concentration of polymer in the solution leaving the column is determined by a suitable detector, UV or otherwise. The elution volumes as a function of time are then compared against those for monodisperse standards which molecular weight has been previously characterized by an absolute method, such as light scattering. When standard and sample have the same chemical structure (i.e. same polymer), the molecular weight distribution results obtained are quantitave, inasmuch as sample and standard of same molecular weight will show equal elution times.

When sample and standard have different chemical composition, as it is the case here where polystyrene standards have been employed, the molecular weight distribution obtained is only semi-quantitative, since the hydrodynamic radii of the copolymer chains in the carrier solvent are strongly affected by the chain composition. As a result, similar hydrodynamic radii between sample and standard (i.e. similar elution times) will only represent equal molecular weights when the effect of the solvent on the conformation of the coils in solution is either equal or negligible, otherwise an error in the determination is introduced. Corrections may be introduced in the computed MWD if the sample-solvent interactions are quantified.

Owing to this, when characterizing MWD of copolymers for which no standards are available, the SEC results are commonly reported either as MWD relative to the standards employed, or as elution volume curves as a function of time. In this study, all copolymer molecular weight averages reported are relative to polystyrene.

The effect of the feed monomer composition on the initial copolymer composition (instantaneous), and copolymer composition at terminal conversion (accumulated) are shown in figure 5.5. The lower curve in this figure represents the instantaneous copolymer composition as a function of AMS in the monomer feed. Results reported by fischer (1972), for monofunctionally initiated S-AMS copolymerization at similar conditions, are also shown in this figure for comparison. Note that the instantaneous copolymer composition, and therefore the reactivity ratios, are independent of the functionality of the initiator.

The upper curve in figure 5.5, is the accumulated copolymer composition observed at terminal conversion. The gap between the two curves characterizes the compositional drift between the zero and terminal conversions. The compositional drift, as shown, is almost negligible in the experimental range, since at low AMS feed compositions the instantaneous copolymer composition deviates little from the feed composition, and at high AMS feed compositions, where higher deviations are observed, the terminal conversions are low, thus preventing the system from larger compositional drift.

Note that the compositional drifts referred to here are those defined through the Meyer-Lowry equation. The actual compositional drift of the system, given by the EICC equation (4.127), must be even smaller, according to the multi-combination of chains with different composition characteristic of bifunctional initiation. As a result, the translation of the DSC results to conversion curves as performed above (see figure 5.1) is valid.

The model predictions for both, instantaneous and accumulated copolymer compositions were accurate in the experimental range. In the model, values of the reactivity ratios reported by Fischer (1972), were employed (see below).

Figure 5.6, shows the H-NMR spectra for different SAMS terminal copolymer compositions. Note in this figure, the increase in the characteristic peak of the CH_3 protons of AMS at 0.5 ppm as its concentration in the feed increases.

The effect of copolymer composition on the glass transition temperature of the copolymer, observed at terminal conversion, is shown in figure 5.7. The experimental results reasonably follow the fox model:

$$1/T_g = W_s/T_{gs} + W_{AMS}/T_{gAMS}$$

when $T_{gs} = 370 - 1.7x10^5/M_n$, (°K), $T_{gAMS} = 453 - 3.1x10^5/M_n$, (°K), [Malhotra et.al.(1978)], and W_i is the accumulated weight fraction of monomer i in the copolymer.

This model for T_g was introduced in the simulation program BICOP. The model predictions, shown in figure 5.7, however, over-estimated T_g throughout the entire feed composition range tested, by an average of two degrees. This was entirely due to the over-estimation of M_n in the simulation, explained before.

To take into account the over-estimation in M_n by the kinetic model in subsequent simulations, the equation reported by Cowie and Toporowski (1968) for glass transition temperature of AMS polymers was introduced to the above model as: $T_{gAMS} = 446 - 3.6 \times 10^5/M_n$, with which the model predictions fit the experimental results, as shown below.

All the different copolymers synthesized were shown to melt over a wide range between 207 and 231°C. The onset of this transition, identified here as the melting point (T_m) was shown to vary little around 210°C.

The summary of experimental and model results for this exploratory research phase is given in Table 5.4, below.

Table 5.4

Summary of Experimental and Model Results for the Exploratory Research Phase SAMS-01

RUN SAMS-01	f_{20} (mol)	EXP Xt @8 hrs	MODEL Xt @8 hrs	EXP Rpo/Rp @ X=0	MODEL Rpo/Rp @ X=0	EXP Mn @ Xt	MODEL Mn @ Xt
1	0.00	0.9999	0.9998	1.0000	1.0000	83870	84998
2	0.10	0.8980	0.9005	0.6123	0.6154	57152	67318
3	0.20	0.5515	0.5485	0.4214	0.4204	34121	39672
4	0.25	0.4890	0.4756	0.3611	0.3599	25678	32898
5	0.30	0.4102	0.4088	0.3141	0.3131	19871	27901
6	0.40	0.3298	0.3267	0.2471	0.2469	15268	21367
7	0.50	0.2707	0.2666	0.2012	0.2003	9096	14820

RUN SAMS-01	f_{20} (mol)	EXP Mw @ Xt	MODEL Mw @ Xt	EXP F2 @ Xt	MODEL F2 @ Xt	EXP Tg(°C) @ Xt	MODEL Tg(°C) @ Xt
1	0.00	203011	212415	0.0000	0.0000	98.60	97.06
2	0.10	155668	149932	0.0960	0.0954	105.39	107.01
3	0.20	83224	81102	0.1811	0.1765	108.94	110.95
4	0.25	66209	66511	0.2231	0.2159	110.25	112.23
5	0.30	55362	55274	0.2603	0.2548	111.33	113.45
6	0.40	39618	42188	0.3367	0.3315	113.47	115.95
7	0.50	29071	33230	0.3922	0.3999	115.66	117.35

5.4.2 Optimization Research

Since the main objective of this research project is to synthesize high molecular weight copolymers, with high T_g, at commercially competitive rates (compared to suspension polystyrene), the results of the exploratory phase clearly indicate that for this copolymer system this can only be achieved if the concentration of AMS in the feed is kept below 20 mol%,

and the molecular weight of the product is increased to levels of M_n above 50,000 Dalton. In this way, if high conversions are reached in a "reasonable" batch time, high SAMS copolymers bearing T_g's about 115 °C, which may be attractive for commercial production, can be synthesized.

Undoubtedly, higher T_g copolymers can be obtained at higher AMS concentrations, if very low copolymerization rates are achieved, in order to produce high molecular weight copolymers. This option, however, is not feasible for suspension copolymers, since long batch times lead to suspension instability, as explained before.

Simulations performed with 30 mol% AMS in the feed, and lower bifunctional initiator concentrations, at this temperature level, showed that more than 35 hours of polymerization are needed in order to obtain SAMS copolymers with a reasonably good balance of conversion-molecular weight-T_g ($X > 0.8$, $M_n > 50,000$, $T_g > 115$ °C). This, of course, is absolutely not attractive for commercial suspension production.

Accordingly, for this optimization research phase, the AMS feed composition was set to 0.15 mol%, and the experiments were designed in order to evaluate the effect of the copolymerization temperature (T_p), and bifunctional initiator concentration ([TBPCC]), on copolymerization rate, and the development of molecular weight distribution, copolymer composition, copolymer glass transition temperature, and copolymer microstructure (see design SAMS-02 in Table 5.2).

Figure 5.8, shows the effect of T_p and [TBPCC] on monomer conversion history (mass basis). In this plot, three different kinds of curves are observed. For the copolymerizations at 90°C the initiator decomposition is slow ($t_{1/2}$~4.5 hrs) and, as a result, low initial copolymerization rates are observed. At about 30% conversion, the onset of a weak gel effect is noticeable in both curves, after which the reactions proceed at a nearly constant rate for some 10 hours. From then on, the auto-acceleration is more evident.

After 24 hours of polymerization, the system with [TBPCC]=0.01 Mol/L reaches what seems to be a nearly limiting conversion close to 90%, whereas the system with [TBPCC]=0.005 Mol/L approaches 75% conversion. With such low polymerization rates (i.e. long batch cycles) both systems are very unlikely to be stable in suspension polymerization.

The copolymerizations at 120°C with the two levels of bifunctional initiator, show the typical behaviour of nearly dead end polymerization of systems with thermal initiation. At this temperature level the initiator decomposition is very fast ($t_{1/2}$=0.1 hrs). As a result, high initial copolymerization rates are observed for the first 2 hours of polymerization, after which virtual initiator depletion is observed. From then on, both reactions proceed solely through thermal initiation, helped by the weak gel effect described.

After 24 hours, the system with higher initial TBPCC concentration reaches a conversion about 84%, whereas the system with lower TBPCC approaches only 80% conversion. Again, the very long times necessary to reach high conversions make these systems not adequate for suspension polymerization.

The copolymerization carried out at 105°C and [TBPCC]=0.0075 Mol/L, appeared to be the most effective to obtain an adequate balance of copolymerization rate and terminal conversion. As shown in figure 5.8, the system at these conditions reaches a limiting conversion of about 93% after 13 hours of polymerization. The limiting conversion is a result of the glassy effect experienced by the system at this conversion level due to the fact that the T_g of the copolymer is higher than T_p (see below).

As for pure polystyrene, this temperature level was the most effective for an efficient initiator decomposition ($t_{1/2}$=1 hr), causing high initial copolymerization rates followed by nearly constant polymerization rate after the onset of the weak gel effect, described earlier.

In comparing this conversion curve with the one for pure polystyrene at the same conditions (see Villalobos 1989) it is remarkable that 15 mol% of AMS in the feed reduces the overall polymerization rate by

a factor of three. This, evidently is the sum of the low propagation rates, high termination rates and reversibility of reactions involving AMS units.

As shown in figure 5.8, the model predictions for conversion history are in very good agreement with the experimental data throughout the entire conversion range, in all the experimental areas studied.

It seems clear that a minimum of 13 hours per batch for this system is not at all competitive with the 3 hours needed for pure suspension polystyrene, however, the high T_g characteristics of this copolymer, as shown below, may still make it attractive even at this low productivity. Let us examine the copolymer characteristics.

In figure 5.9, the experimental and model results for the effect of T_p and [TBPCC] on the development of M_n are shown. As expected, the two systems at 90°C show higher initial M_n than the systems at 120°C due to the lower copolymerization rates observed. At T_p=90°C, the slow initial increase in M_n followed by larger build-up after the onset of the gel effect is typical of systems experiencing the conversion history described. Also expected is the result that lower initiator concentrations lead to larger M_n at similar conversion levels, especially in bifunctionally initiated systems [Villalobos et.al. (1991)].

At T_p=120°C, the shape of the curves is totally different. Very low initial M_n are observed in both curves due to the high initial copolymerization rates. After initiator depletion at about 40% conversion, M_n builds-up more slowly due to the weaker gel effect experienced owing to the formation of oligomers at low conversions. In addition the overall rate of reaction decreases since the thermal initiation rate decreases as the monomer is consumed while high termination rates remain.

Note in figure 5.9, that all the model predictions slightly over-estimate the M_n, especially at conversions above 30%, owing to the use of number-average termination rate constant employed to calculate M_n, as explained above.

In figure 5.10, the experimental and model results for the effect of T_p and [TBPCC] on the development of M_w, are shown. The behaviour, and therefore the explanation, for the four experiments is the same as for the M_n curves. The only difference being the larger build-up observed in M_w, as expected, after the onset of the gel effect, due to the longer chains formed during the decay of the termination rate. This, of course, is responsible for the broadening of the MWD with conversion. Note in this figure how the model predictions for the evolution of M_w closely follow the actual behaviour of the system.

Figure 5.11, shows the development of M_n and M_w with conversion, for the most efficient system, rate and conversion-wise, found (T_p=105°C, [TBPCC]=0.0075 Mol/L). Even though the initial molecular weights are lower for this system than for the polystyrene reference system (see figure 3.6 and 3.7 in Chapter 3 for comparison), the average molecular weights reached at terminal conversion are virtually the same (M_n=80,000; M_w=205,000). This, again, makes this system the only one attractive for suspension polymerization, of the five tested. Note in this figure, the accurate model prediction for the evolution of M_w throughout the entire conversion range, as well as the slight over-estimation of the M_n predicted.

The evolution with conversion of the full MWD obtained through SEC for this system (T_p=105°C, [TBPCC]=0.0075 Mol/L), is shown below in figure 5.12. It is worth noting in this figure the substantial amount, at low conversions, of copolymer chains with molecular weights between 1000 and 10,000. This corresponds to chain lengths from 9 to 90 units, which corroborates the existence of oligomers and low molecular weight copolymer chains in the system, responsible for plasticization of the polymer matrix, and consequently, for the weak gel effect observed. Moreover, the number average chain length for this system at extrapolated at zero conversion, is about 200, which is barely within the limit of applicability of the pseudo-kinetic rate constant method.

As a result, some deviations between model predictions and actual behaviour could be observed at very low conversions. In this study, such deviations were not observed, inasmuch as the search was aimed at the whole conversion range and not to very low conversions, exclusively. The overall behaviour, nevertheless, seems to be predicted quite satisfactorily by the model, even within the lower limits of molecular weights observed.

The concentration of these low molecular weight copolymer chains becomes negligible at high conversions, however, their plasticizing effect may still be important.

The experimental and model results for the evolution of the accumulated copolymer composition with monomer conversion, are shown in figure 5.13. Note that the initial copolymer composition is very similar for f_{10}=0.85, and the total compositional drift is almost negligible at the three different temperatures, in spite of the difference in reactivity ratios. Owing to this, the model curves for the three different polymerization temperatures tested follow very close paths. As expected, the model curves for the runs carried out at the same temperature are identical in their respective conversion ranges.

The experimental results, although somewhat scattered, follow the same trend predicted by the model. Note from the scale of the plot that the largest deviations between experimental and model results throughout the entire conversion range are less than 2%. This is well within the experimental error of the H-NMR determinations.

Figure 5.14, shows the experimental and model results for the effect of T_p and [TBPCC] on the development of the copolymer glass transition temperature. The experiments shown in this plot correspond to those with the largest differences in MWD development. For the only system of interest for suspension polymerization (T_p=105°C, [TBPCC] = 0.0075 Mol/L), a T_g = 115.43°C was obtained.

At this monomer feed composition, the maximum T_g expected for this copolymer, at high conversion and molecular weights, is about 116°C. Therefore, the value obtained for the best system of the five tested, may be considered as very close this limit. Note also that this copolymer has a T_g within the range of engineering polymers, which is what is being aimed for.

The most relevant microstructural feature of the statistical SAMS copolymers synthesized is, undoubtedly, the average number of segments per copolymer chain (S_n), due to its relation with the effective compositional drift and copolymer homogeneity. Figure 5.15 shows the model predictions for the development of the number average number of segments per copolymer chain. In this figure, it is noticeable that the copolymers synthesized at 120°C approach the limiting value of 2 segments per copolymer chain at the conversion of initiator depletion (see Chapter 4).

Before this point the number of copolymer chains initiated thermally is negligible when compared with the number of chemically initiated chains. After the initiator has been consumed, the average number of segments per chain decreases linearly inasmuch as all the new copolymer chains formed thermally will be monosegmental. This is undesirable since the degree of coupling between copolymer chains formed with different compositions decreases, increasing the effective compositional drift.

As shown in this figure suitable modifications were introduced to the microstructure model in order to take into account the copolymer chains formed after bifunctional initiator depletion.

For the copolymers synthesized at 90°C the slower initiator and macro-initiator decomposition prevents the system from reaching a higher average number of segments per chain. Since the compositional drift is reduced in direct proportion to this average, this situation is not optimal.

For the most efficient copolymer synthesized at 105°C and intermediate initiator concentration, the optimal initiator decomposition rate observed also leads to the highest number average number of segments per copolymer chain. Consequently, this copolymer is also the most homogeneous one, showing the minimum effective compositional drift. Note, in the curve for this system, the rapid increase in S_n during the glassy effect. During this period, the propagation rate falls dramatically, nevertheless, recombination of previously formed temporarily dead copolymer molecules is possible. As a result S_n increases rapidly while the conversion remains nearly constant.

Experimental verification of these microstructures predicted by the model is, at best, extremely complex and was not attempted in this study. However, as shown in the test simulation of Chapter 4, the fact that both the kinetic and microstructure models predict the same evolution of the copolymer populations with conversion, gives certain confidence that the predictions of the model may reflect the actual copolymer microstructure as well.

5.4.3 Model Parameter Estimation

The procedure and criteria followed for the estimation of all the parameters appearing in the kinetic model may be summarized as follows (S=monomer 1, AMS=monomer 2):

For homo-polystyrene reactions all the literature parameters for K_{p11}, K_{tc11}, K_{td11}, and K_{trM11}, employed and reported in Chapter 3, were used in the model. The decomposition rate constants used for TBPCC (K_{d1}), and macro-initiator (K_{d2}), were those previously found by Villalobos (1989), and reported in Chapter 3. The initiator efficiency (f_1) and macro-initiator efficiency (f_2) were set to 0.7 and 0.8, respectively, after theoretical considerations given in Chapters 2 and 4.

For homo-α-methylstyrene and cross reactions the following parameters were fixed according to the literature data available.

Styrene and AMS being both electron donors do not form a donor-acceptor complex, therefore K_c was set to zero in the model.

O'Driscoll and Dickson (1968), Fischer (1972), and Rudin and Chiang (1974), using different kinetic models, as explained before, all found that for SAMS copolymers MWD information suggests that bimolecular termination occurs exclusively by combination. Since the MWD results of this work are in agreement with these observations, all K_{tdij} (i,j=1,2) were set to zero in the model.

O'Driscoll and Dickson (1968) found in their study at low temperatures (60°C) that K_{tc22} must be 3 orders of magnitude larger than K_{tc11}. However, Fischer in his work at higher temperatures considers this constant to be only 2 orders of magnitude larger than K_{tc11}, and fixes the value of the cross termination constant K_{tc12} to ten times the value for polystyrene. Almost in agreement with this latter observation, Ruding and Chiang (1974) found K_{tc22} to be nearly 50 times larger than K_{tc11} at 60°C.

Since the only complete study performed at temperature levels similar to those of this work is that by Fischer, K_{tc22} was set to 10^2*K_{tc11} and K_{tc12} to $10*K_{tc11}$ in the model, for the present simulations.

For to the same reasons the reactivity ratios (r_1 and r_2) at the temperatures tested were obtained from Fischer's relationships for these parameters, applicable between 60 and 150°C.

As mentioned in Chapter 2, it has been shown that AMS polymerizes thermally, yet no kinetic expression for the rate of thermal initiation was found in the literature reviewed. Therefore, the thermal initiation rate for AMS was assumed equal to that of polystyrene.

The temperature dependent onset of the gel effect (K), extracted from the exploratory and optimization conversion vs time curves, was found to follow the Arhenius form: $K = 6.5 \exp(1929/T)$. The exponents M and N for the effect of M_w on the parameter K and the rate of decay of the termination rate were, set to 0.5 and 1.75 after Marten and Hamielec (1982) and Hamielec et.al.(1987). The rate of increase of K_t for segmental diffusion was neglected for this system (i.e. $\delta=0$) [Hamielec et.al.(1987)].

The rate of decay of the individual K_{pij} during the glassy effect (B_j) were both set to 1.0 [Hamielec et.al. (1987)]. The critical free volume for the onset of the glassy effect was estimated in Chapter 3 for polystyrene as: $VF_{crs} = 0.0465$. Considering that diffusivity of AMS in the reaction mix must be smaller than that of styrene a value of $VF_{crAMS} = 0.0475$ was used in the model.

With all these parameters fixed in the model, the remaining kinetic parameters (K_{22}, K_{fm22}, K_{fm12}, and K_{fm21}) were estimated with the aid of the nonlinear parameter estimation routine UWHAUS, as follows. First, it was assumed that the rate of transfer to monomer reactions is only dependent on the type of monomer and not on the type of radical (i.e. $K_{fm11} = K_{fm21}$). This, presumably, is a satisfactory assumption inasmuch as the controlling step for this reaction is the hydrogen abstraction from the monomer. With this, the value of K_{fm21} was set equal to K_{fm11}, which is known. Then, the overall rate of polymerization equation, along with the pseudo kinetic rate constants and fraction of radicals definitions, and the computed initiation rates, were fit through UWHAUS to the experimental results for initial copolymerization rates and extrapolated initial molecular weights, for all the different temperatures tested. The only parameters in these nonlinear regressions thus being K_{22} and K_{fm22}. The values reported by Fischer (1972) for K_{22}, at the corresponding temperatures, along with the value $K_{fm22}=K_{fm11}$ were used as initial guesses.

The temperature dependent Arhenius expression found for K_{22} is given by: $K_{22} = 1.588 \times 10^{10}\exp(-9992/RT)$, which yields values within 10% difference, of those reported by Fischer in the same temperature range. The estimated value for K_{fm22} was, consistently, one order of magnitude larger than K_{fm11} (±5%), in the temperature range of interest. Then K_{fm22} was used in the model as $10*K_{fm11}$.

With all the above parameters in the model, the remaining parameter, A, related to both the onset and strength of the gel effect, was estimated from the experimental results for overall rate of reaction after the onset of the gel effect, as A=0.25. This value, reflects the

weak nature of the gel effect experienced by this copolymer system.

Table 5.5 summarizes all these parameters used in the BICOP simulation program for SAMS copolymerization with bifunctional initiator TBPCC.

Table 5.5

Values of the Parameters Used in the Simulations

Initiation Chemical (TBPCC) and Thermal	
$K_{d1} = 2.117 \times 10^{14} \exp(-28064/RT)$; $f_1 = 0.8$	Min^{-1}
$K_{d2} = 3.850 \times 10^{20} \exp(-40022/RT)$; $f_2 = 0.7$	Min^{-1}
$K_{ths} = K_{thAMS} = 1.314 \times 10^{7} \exp(-27440/RT)$	Min^{-1}
Propagation	
$K_{11} = 6.128 \times 10^{8} \exp(-7068/RT)$	L/mol-min
$K_{22} = 1.588 \times 10^{10} \exp(-9992/RT)$	L/mol-min
$r_1 = K_{11}/K_{12} = 2.146 \exp(-246/T)$	60 to 150°C
$r_2 = K_{22}/K_{21} = 228.2 \exp(-2410.6/T)$	60 to 150°C
$K_c = K_{1c} = K_{2c} = 0$ (no donor-acceptor complex)	
Termination	
$K_{tdij} = 0$ (i,j=1,2)	
$K_{tc11} = 7.55 \times 10^{10} \exp(-1677/RT)$	L/mol-min
$K_{tc12} = 7.55 \times 10^{11} \exp(-1677/RT)$	L/mol-min
$K_{tc22} = 7.55 \times 10^{12} \exp(-1677/RT)$	L/mol-min
Transfer to Monomer	
$K_{fm11} = K_{fm21} = 6.128 \times 10^{8} \exp(-13450/RT)$	L/mol-min
$K_{fm22} = K_{fm12} = 6.128 \times 10^{9} \exp(-13450/RT)$	L/mol-min
Free Volume Variables (T_g in °K, α in 1/°K, d in Kg/L)	
$T_g = 184.95$; $\alpha = 0.001$; $d = 0.924 - 0.000918*T(°C)$	Styrene
$T_g = 192.15$; $\alpha = 0.001$; $d = 0.925 - 0.0009*T(°C)$	AMS
$T_g = 113.30$; $\alpha = 0.001$; $d = 0.879 - 0.0005*T(°C)$	Toluene
T_g (see text); $\alpha = 0.00048$; $d = 1.084 - 0.000605*T(°C)$	Copolymer
Gel and Glassy Effect Parameters	
$K = 6.5 \exp(1929/T)$; $\delta = 0$; $A = 0.25$; $M = 0.5$; $N = 1.75$ (gel effect)	
$VF_{crs} = 0.0465$; $VF_{crAMS} = 0.0475$; $B_i = 1.0$ (i = 1,2) (glassy effect)	

5.4.4 S-AMS Suspension Copolymerization

Using the best synthesis conditions found during the optimization research phase as centre point (i.e. T_p = 105°C, [TBPCC] = 0.0075 Mol/L, f_{i0} = 0.85), simulations scanning the initiator concentration range from 0.005 to 0.001 Mol/L, at 0.0005 intervals, were performed in order to find the optimal system for suspension copolymerization. The optimality criteria is given, as explained above, by the best balance between copolymerization rate, and molecular weight distribution, which in turn yields a high copolymer glass transition temperature and maximum average number of segments per copolymer chain.

Not surprisingly, the system used as centre point was found to be optimal. Higher initiator concentrations led to weight averages molecular weights below the target value of 200,000, with marginal increases in polymerization rate. Lower initiator concentrations led to unsatisfactorily large copolymerization times to reach limiting conversion. As a result, this system was chosen as the best for SAMS suspension copolymerization with bifunctional initiator TBPCC.

A limitation for this system, however, is imposed by the limiting conversion attained at about 94%, as a consequence of the glass transition experienced by the reaction mix. Alternatives to obtain monomer-free suspension products are: 1) Devolatilization of the product obtained at limiting conversion to eliminate residual monomer. 2) Addition of a high temperature monomer exhaustion stage, after limiting conversion has been reached. Such stage must be carried out at temperature above the T_g of the copolymer (i.e. T > 116°C). 3) Addition of low T_g solvent in such amount as to lower the T_g of the reaction mix, at 100% monomer conversion, below T_p. This must be followed by devolatilization of the product to eliminate the solvent added.

From the commercial point of view, alternatives 2 and 3 are more plausible than the first inasmuch as this one requires further separation of the monomer mix extracted.

In this study, both of these alternatives (2 and 3) were employed to synthesize the final suspension SAMS copolymers.

As shown in the experimental design given in Table 5.3, run SAMS-03-1 (T_p=105°C, [I]=0.0075 Mol/L, f_{10}=0.85) was completed by adding 3 hours at 120°C for monomer exhaustion, after 13 hours of reaction. Simulation for this system with the temperature program described, predicts terminal conversions above 99%, as shown in figure 5.16.

In run SAMS-03-2, toluene was used as solvent for matrix plasticization. The required amount, 2.5 wt%, was calculated from the Fox model to get a final T_g of the polymer/solvent mix, at 100% monomer conversion, of 100°C. With this amount of solvent, neglecting transfer to solvent reactions, simulations were carried out to find the initiator concentration needed to get the same conversion vs time curve as SAMS-03-1, by polymerizing isothermally at 105°C, provided the weight average molecular weight were also within target value. An initiator concentration of 0.009 Mol/L_{mix} was found to be the best for this effect. However, a small decrease in M_w was expected, due to the weaker gel effect experienced in the plasticized copolymer matrix.

Figures 5.16 and 5.17, show the simulated monomer conversion history and molecular weight distribution development, respectively, for the suspension runs carried out in this study, according to the design and reactor operating conditions given in Table 5.3.

Both suspension runs of the design were successfully completed inasmuch as spherical/non-aggregated beads were obtained as final product in both cases.

Figure 5.18 shows the results for the effect of the imposed copolymerization rate on the particle size distribution (PSD). The distribution obtained for the reference polystyrene system is also shown for comparison (see Chapter 3 for conditions). It is evident, from this figure, that larger mean particle sizes (MPS) and broader PSD were obtained for both SAMS copolymers than those of the reference polystyrene.

The MPS computed from these distributions, yielded values of 0.753 and 0.837 mm, for runs 1 and 2, respectively, compared with 0.542 mm of the reference system. The spread of the PSD, characterized by the coefficient of variation (CV=standard deviation/MPS) were 0.451 and 0.467, for runs 1 and 2, against 0.361 of the reference system.

Considering that the particle growth stage, occurring between 30 and 65% conversion (see Chapter 3), is ten times longer for the copolymer systems than for the reference system (5 hrs vs 0.5 hrs as shown in figure 5.16), large MPS and broad PSD were expected, according to the particle growth mechanism and PSD development in suspension polymerization described by Villalobos (1989).

The fact that neither ill shaped beads nor particle aggregates were observed at these extremely long growing periods, characterizes these suspension copolymerizations as very stable.

The appearance of the beads was transparent for run 1, similar to crystal polystyrene beads, and opaque for run 2. The former implying high monomer conversion and copolymer homogeneity, and the latter due to the difference in refractive index between the copolymer and toluene.

The differences in MPS and PSD for the SAMS copolymers observed in runs 1 and 2, were brought about by the extended particle growth period experienced by the toluene-plasticized system (run-2).

Samples of the beads obtained in both experiments were dissolved in chloroform and precipitated in methanol, according to the procedures described above. The purified copolymer terminal conversion, MWD, and T_g, were characterized following the techniques described before. Terminal monomer conversion close to 100%, M_w about 200,000, and T_g's about 115.5°C were obtained in both cases, following closely the model predictions.

Table 5.6, below, summarizes the experimental and model results for MPS, PSD, terminal conversion, MWD, and T_g of the suspension copolymers synthesized.

Table 5.6

Summary of Suspension Copolymerization Results

RUN → VARIABLE	EXP REF. PS(*)	MODEL REF PS(*)	EXP SAMS-03-01	MODEL SAMS-03-01	EXP SAMS-03-02	MODEL SAMS-03-02
MPS (mm)	0.542	**	0.753	**	0.837	**
σ (mm)	0.196	**	0.340	**	0.391	**
CV=σ/MPS	0.361	**	0.451	**	0.467	**
CONV	0.9999	0.9998	0.9856	0.9976	0.9872	0.9913
Mn	83870	84998	76208	86203	72111	81053
Mw	203011	212415	206770	203416	188754	185894
T_g (°C)	98.60	97.06	115.73	115.55	115.34	114.95

* See Chapter 3 for reference system results.
** Model does not predict PSD.

Samples of the beads obtained in both runs were extruded, following the procedures described in the experimental section. Opaque continuous extrudates were obtained in both cases mainly due to residual monomer and solvent bubbling during extrusion.

The mean residence time of the copolymer within the extruder was calculated as 1.33 minutes at the extrusion conditions given.

The T_g of the extrudates showed variations within 5% with respect to the purified copolymers, which shows not sensitive annealing effects or degradation during extrusion.

Samples of the extrudates were exposed in open DSC cells, N_2 atmosphere, to thermolysis at temperatures of 225°C for 5 and 10 hours. Gravimetric determinations showed that both copolymers lost about 0.7 and 1.7 % of their initial mass, at the give times, respectively. These values are twice as large as those reported by Priddy et.al.(1990), for anionic SAMS copolymers of similar molecular weight (equimolar copolymer composition), at the same conditions.

The observed difference is likely due to a larger number of depolymerizable diads of AMS units present in the statistical copolymers synthesized in this study, in comparison with the anionic continuous copolymerization SAMS synthesized by Priddy et.al. with a feed policy aimed to prevent formation of AMS sequences.

MWD determinations of the exposed samples showed virtually no change in M_w, under the prescribed conditions. This corroborates the findings by Priddy et.al.(1990), in the sense that SAMS degradation occurs mostly by depolymerization, rather than chain scission, with which relatively large mass losses are accompanied by small M_w decrements. This also demonstrates that the SAMS copolymers synthesized are thermally stable under the processing conditions tested.

Table 5.7 summarizes the copolymer bead extrusion results for T_g and degradation.

Table 5.7

Copolymer Extrusion and Degradation Results

SAMPLE SAMS-03-	BEADS T_g (°C)	EXTRUD T_g (°C)	MASS LOSS* 5 hrs @225°C	MASS LOSS* 10 hrs @225°C	BEADS Mw	EXTRUD Mw* 5 hrs @225°C	EXTRUD Mw* 10 hrs @225°C
1	115.73	115.44	0.659	1.819	206770	199308	201906
2	115.34	115.41	0.733	1.614	188754	185444	183011

* Results of sample characterization after exposure to the prescribed conditions.

5.5 Conclusions

Styrene/α-methylstyrene engineering copolymers bearing glass transitions temperatures about 115°C, can be synthesized up to high conversions and high molecular weights through bifunctionally initiated suspension copolymerization.

Two optimal synthesis routes yielding the best balance of copolymer properties, terminal conversion, and copolymerization rate, when using 1,4,-bis(tertbutyl peroxycarbo)cyclohexane as bifunctional initiator, and an initial comonomer composition of 85/15 (S/AMS mol) where found. The first one involves a temperature program of 13 hours at T_p = 105°C, followed by 3 hours at 120°C and initiator concentration of 0.0075 Mol/L. The second one involves the initial addition of 2.5 wt% of toluene, as reacting mix glass transition depressor, and 16 hour of polymerization at 105°C with [TBPCC] = 0.009 Mol/L_{mix}.

The suspensions in both synthesis were stable, even through the extremely large particle growth period stage, however larger particles and broader distributions were obtained compared to suspension polystyrene at similar conditions. This translates into larger amounts of stabiliser needed for commercial production compared to suspension polystyrene. Due to the suspension stability exhibited by these systems process scale-up is certainly technically feasible.

The copolymers showed to be processable through extrusion, and thermally stable at the processing conditions tested.

The batch times necessary for these syntheses are four times larger than those for styrene homopolymer (16 vs 4 hours), which is hardly competitive on a productivity basis. Nevertheless, the fact that engineering copolymers with this level of T_g are currently consumed in much smaller volumes than polymer commodities (see Chapter 1), may still make this copolymer attractive for commercial production.

Larger concentrations than 15 mol% of AMS in the monomer feed seem to be clearly uneconomical for the synthesis of high molecular weight copolymers, even using bifunctional initiators. Although there are some possibilities to produce high SAMS copolymers with larger concentrations of AMS by promoting slight crosslinking of the chains, the copolymer thermal stability is known to decrease in direct prcportion to the concentration of AMS diads in the copolymer as well as the copolymerization rate.

As a result, a practical limit for the batch free radical synthesis of this type of copolymers seems to be given at $f_{20} < 0.2$.

In addition to the suspension copolymers synthesized, the experimental studies presented herein give also the bases for free radical bulk and solution synthesis of high T_g SAMS copolymers through bifunctional initiators, in wide ranges of temperature and initiator concentration.

Finally, the kinetic and microstructural models proposed in Chapter 4, integrated into the simulation program BICOP, were able to predict with adequate degree of accuracy all the most important features of commercial interest for this type of copolymerization, using almost exclusively literature values for the parameters needed. This, undoubtedly, makes it a very valuable tool for optimization and scale up of this and other copolymer systems.

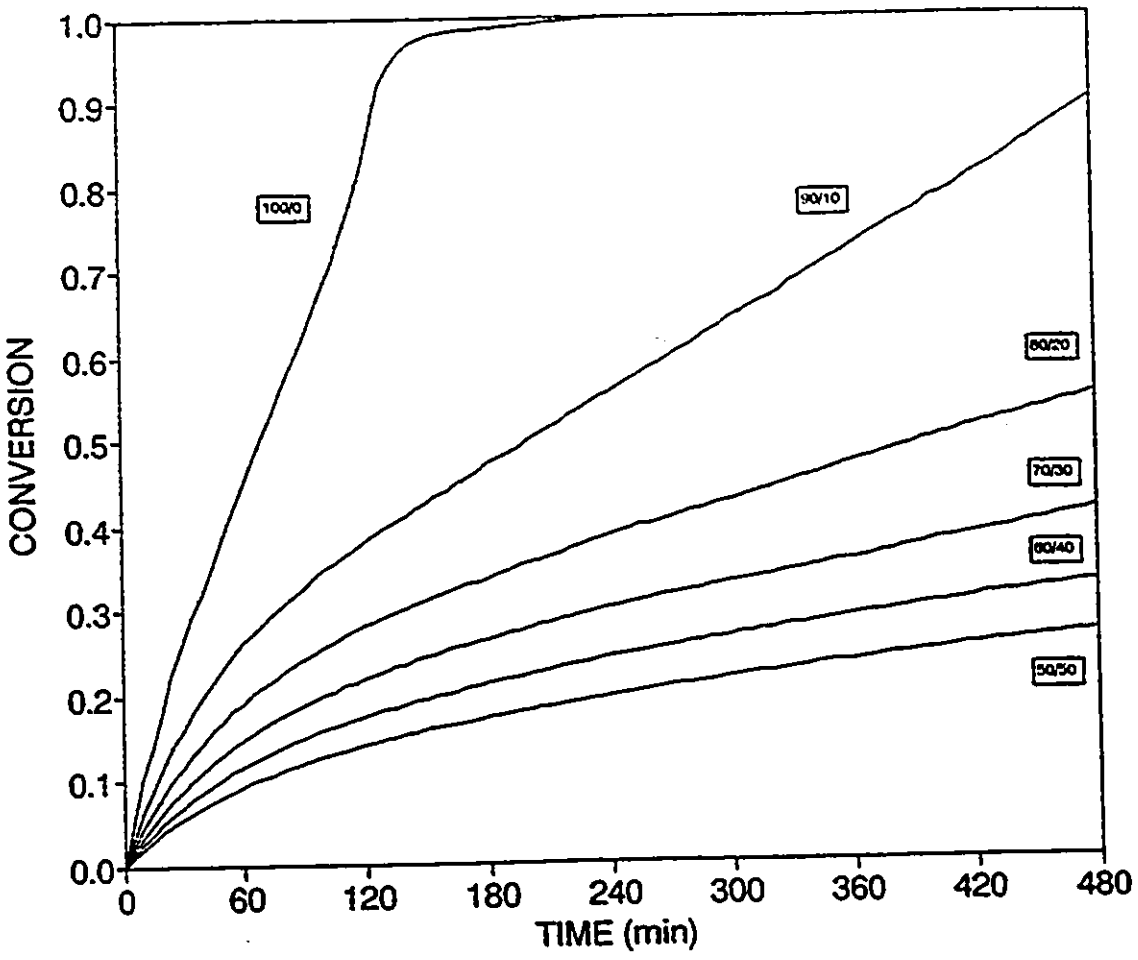

Fig. 5.1 Effect of comonomer feed composition on monomer conversion history for SAMS bulk copolymerization with bifunctional initiator [TBPCC]=0.01 M/L, at 105°C. Parameter monomer feed composition mol% S/AMS.

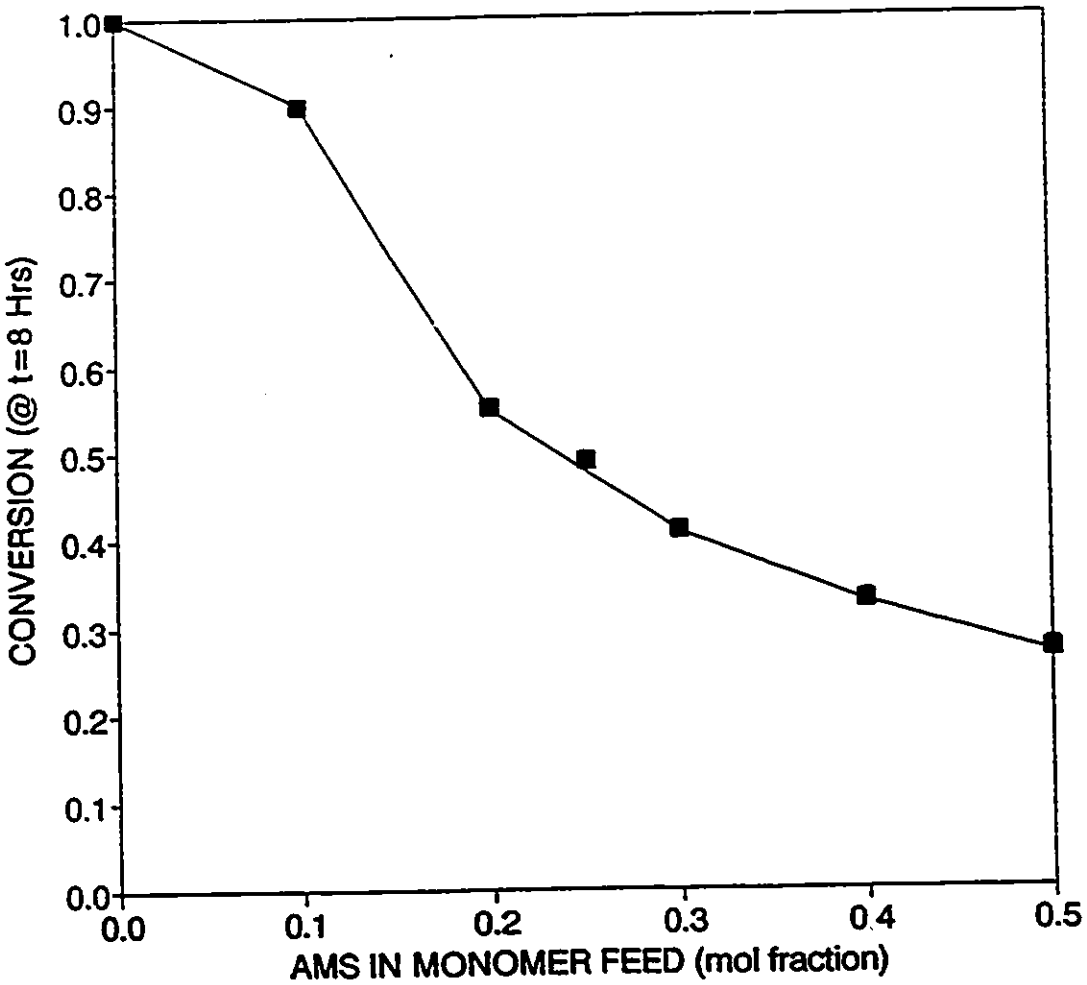

Fig. 5.2. Effect of comonomer feed composition on terminal conversion reached after 8 hours of SAMS bulk copolymerization with bifunctional initiator [TBPCC]=0.01 M/L, at 105 °C. Experimental results (■). Model predictions (——).

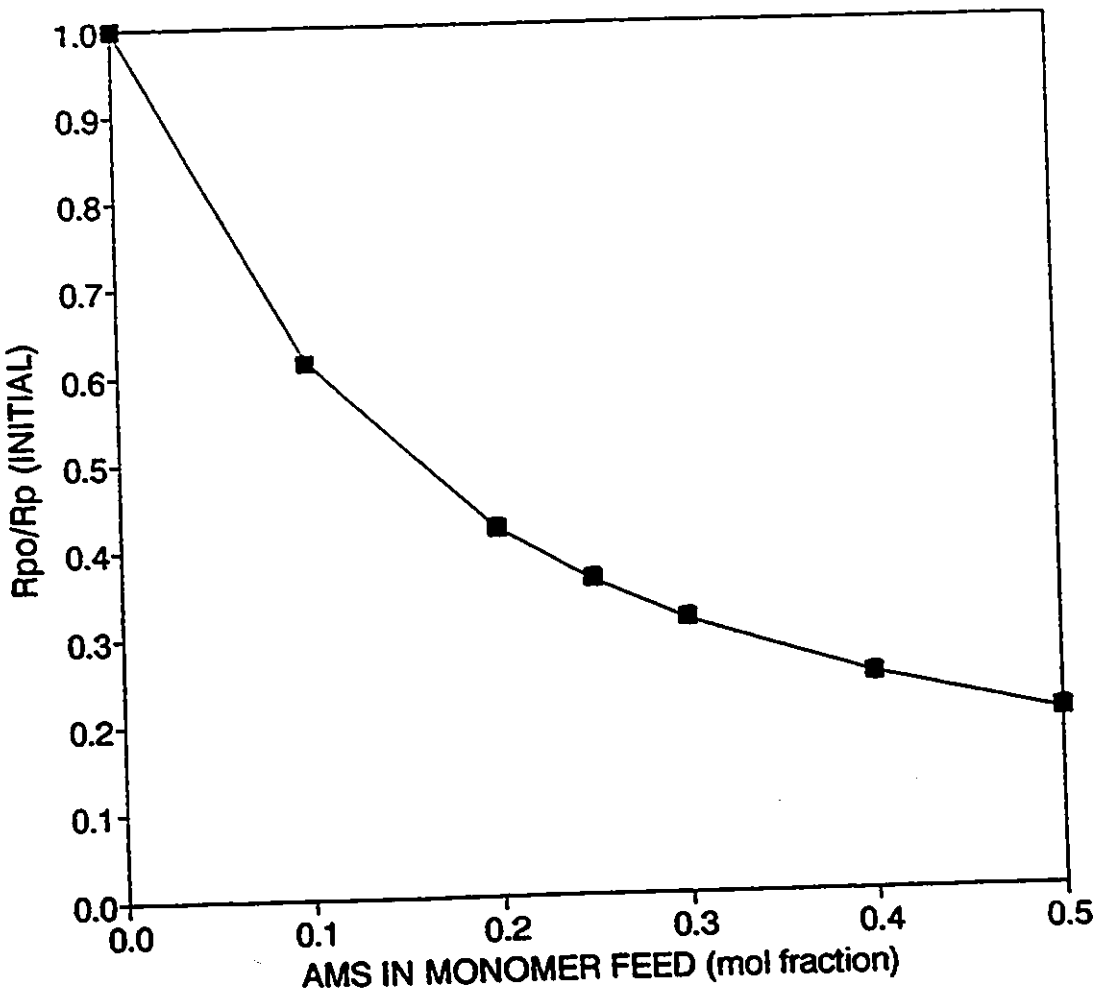

Fig. 5.3. Effect of comonomer feed composition on copolymerization rate (relative to styrene polymerization rate) for SAMS bulk copolymerization with bifunctional initiator [TBPCC]=0.01 M/L, at 105°C. Experimental results (▪). Model predictions (——).

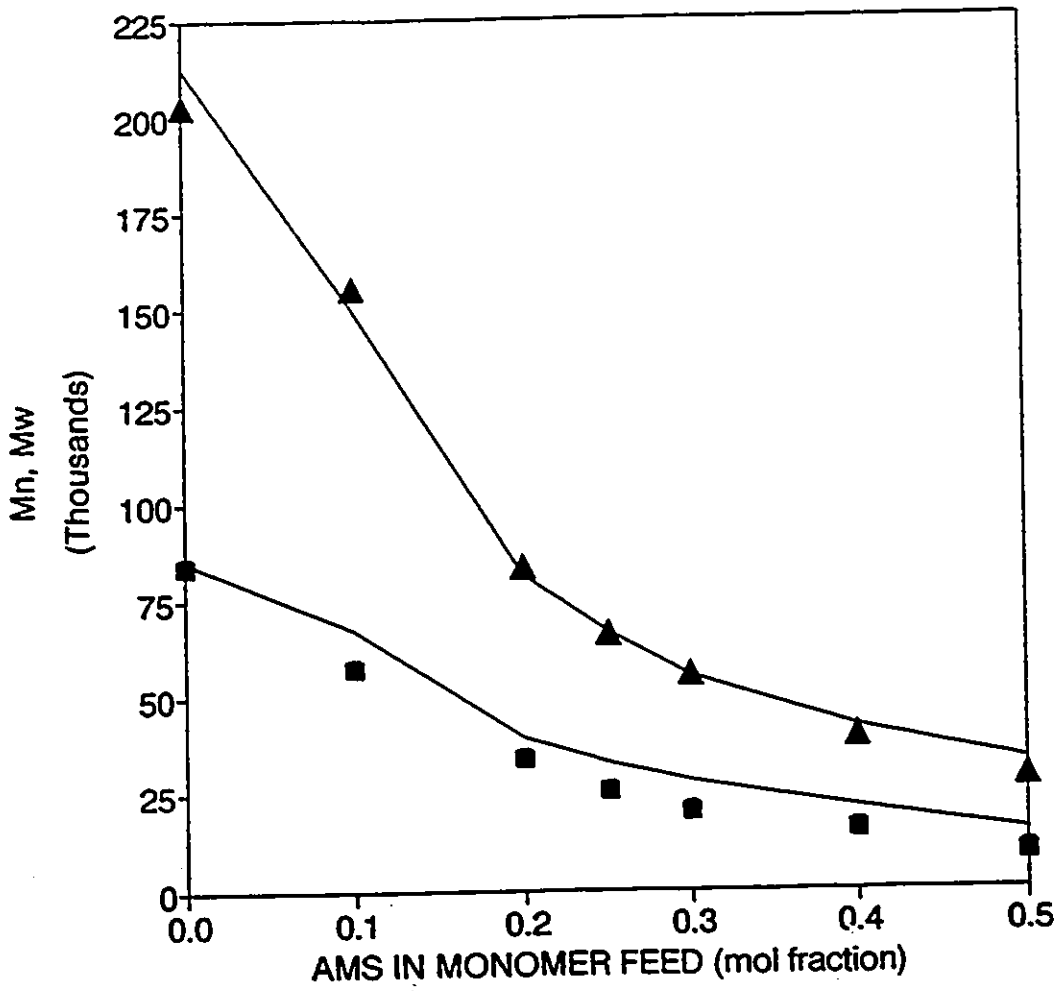

Fig. 5.4. Effect of comonomer feed composition on MWD of SAMS copolymer at terminal conversion. Bulk copolymerization with bifunctional initiator [TBPCC]=0.001 M/L, at 105°C. Experimental M_n (■), and M_w (▲). Model predictions (——).

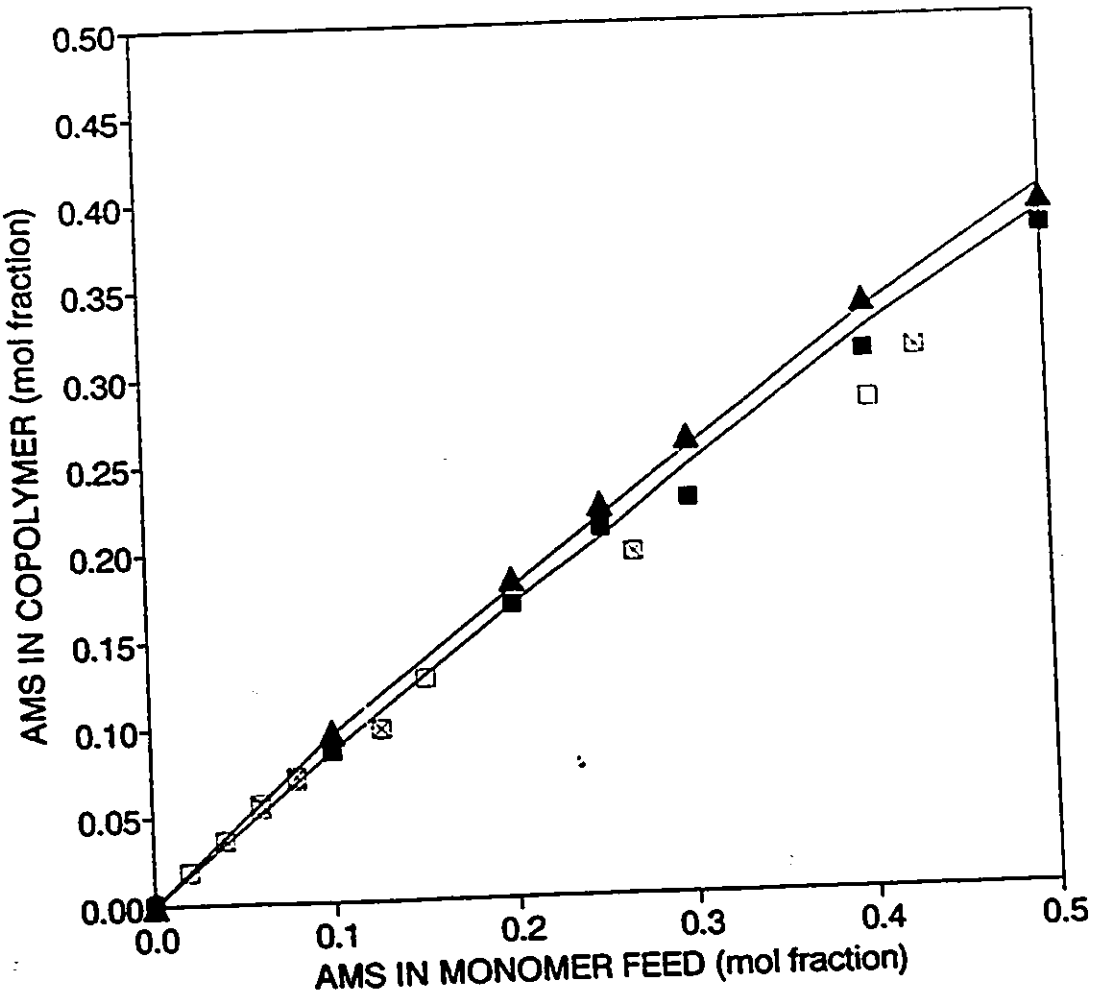

Fig. 5.5. Effect of comonomer feed composition on observed compositional drift of SAMS copolymers. Bulk copolymerization with bifunctional initiator [TBPCC]=0.01 M/L, at 105°C. Experimental instantaneous (X=0) copolymer composition (■) [this work], (□,⊠) [data from Fischer (1972) for SAMS initiated with AIBN at 90 and 110°C, respectively], and accumulated (X=Xt) copolymer composition (▲). Model predictions (——).

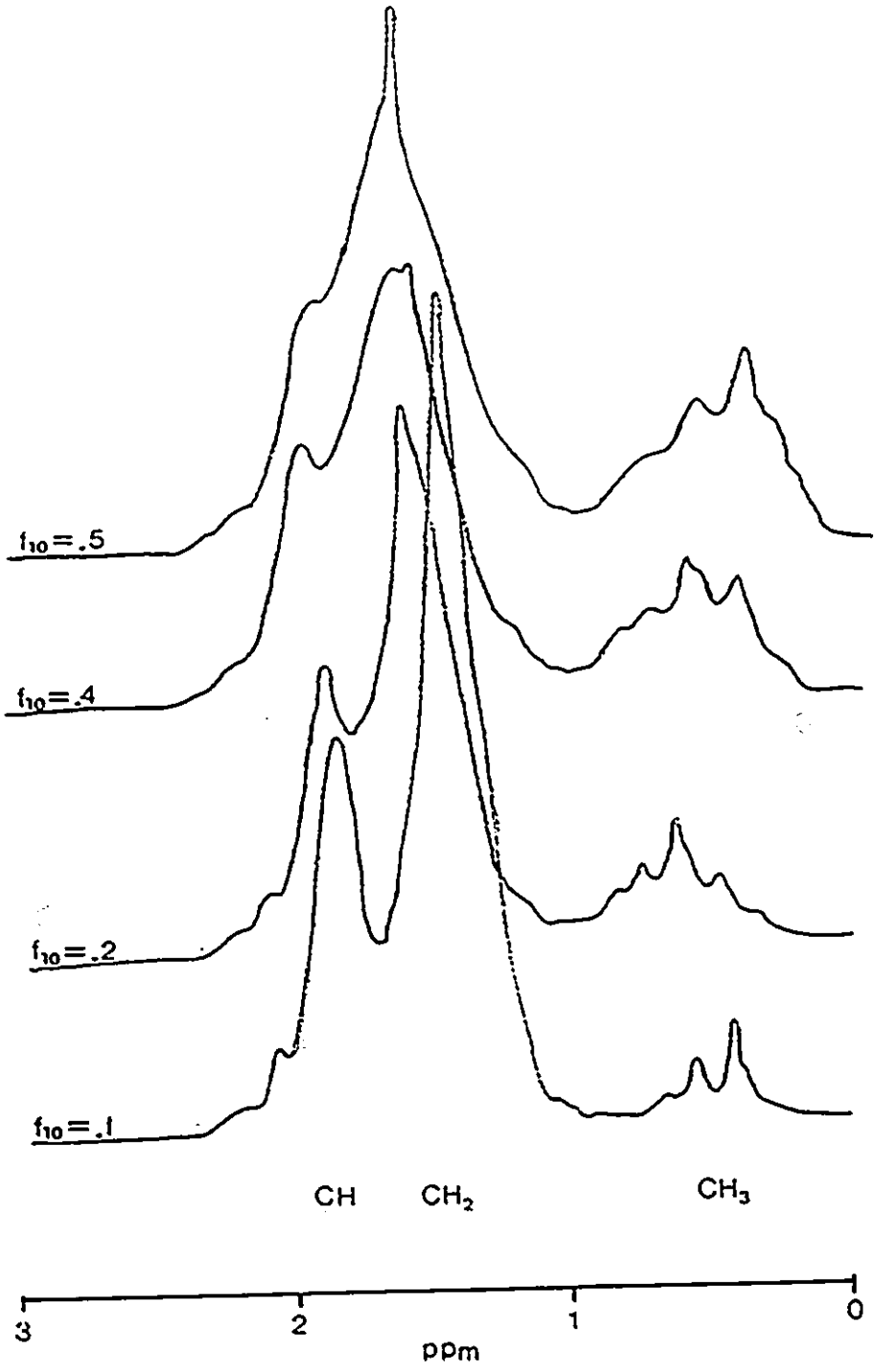

Fig. 5.6. Evolution of the H-NMR spectrum (portion between 0 and 3 ppm) with monomer fed composition for SAMS copolymers at terminal conversion. Bulk copolymerization with bifunctional initiator [TBPCC]=0.01 M/L, at 105°C.

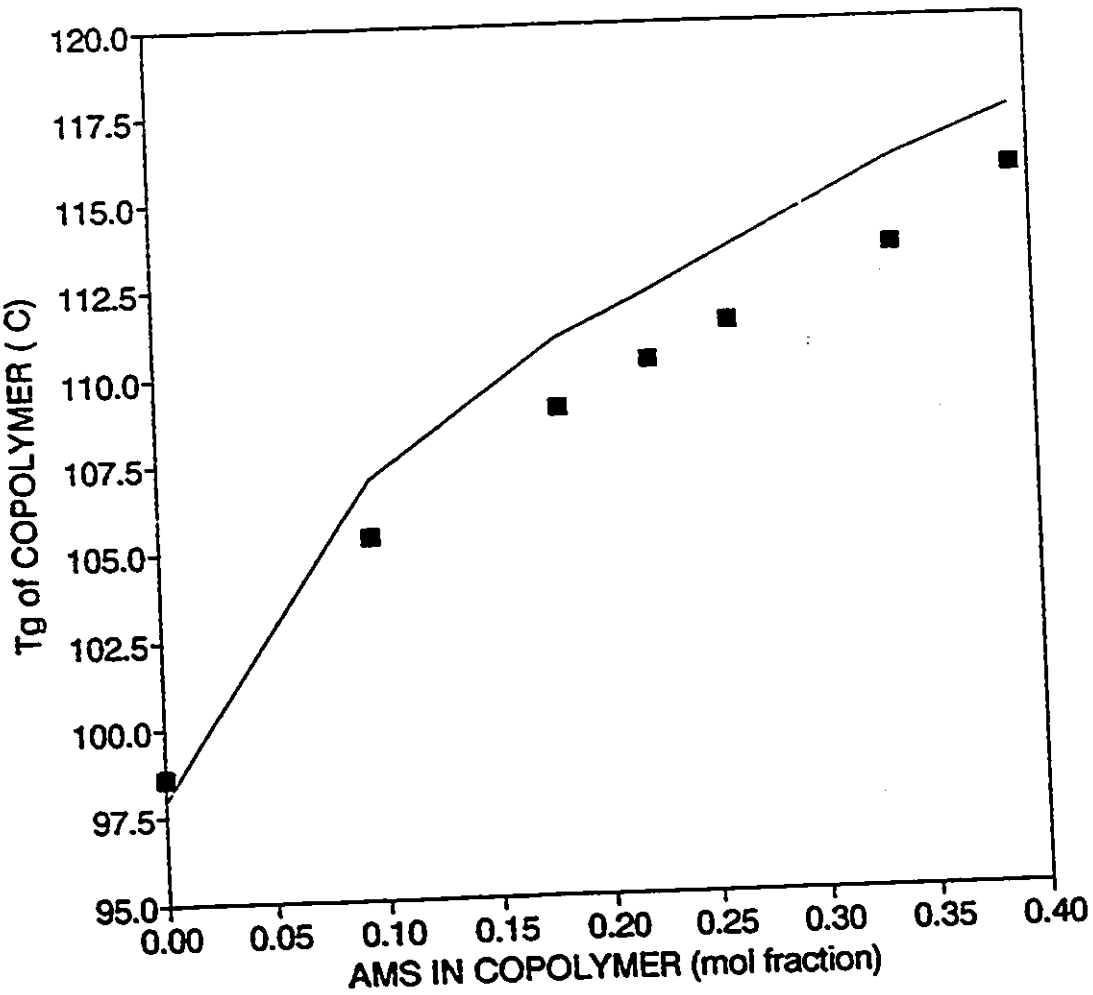

Fig. 5.7. Effect of SAMS copolymer composition at Xt, on glass transition temperature. Bulk copolymerization with bifunctional initiator [TBPCC]=0.01 M/L, at 105°C. Experimental results (■). Model prediction (——).

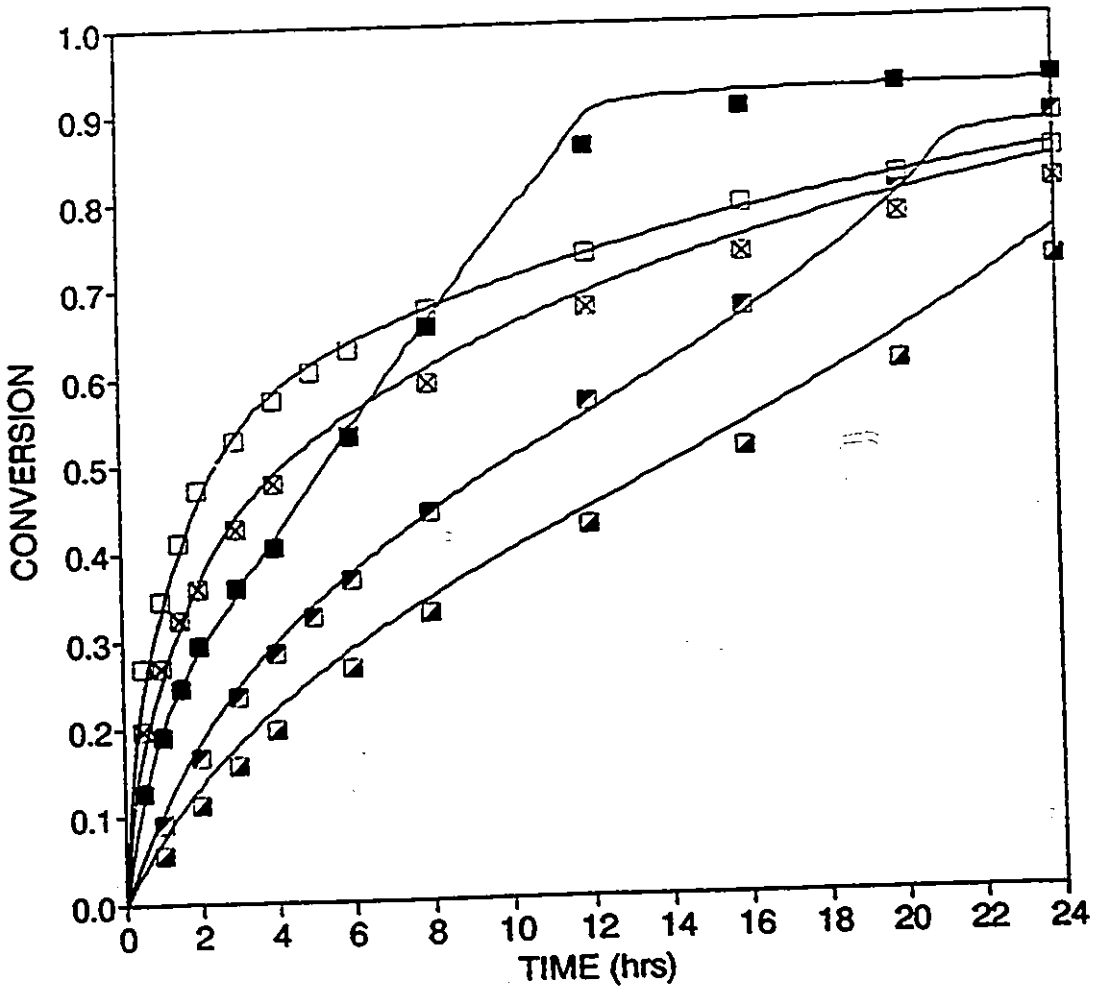

Fig. 5.8. Effect of T_p and [TBPCC] on monomer conversion history in SAMS bulk copolymerization (f_{10}=0.85). Experimental results for: T_p=90°C, [I]=0.005 M/L (◪); T_p=90°C, [I]=0.01 M/L (◪); T_p=105°C, [I]=0.0075 M/L (■); T_p=120°C, [I]=0.005 M/L (□); T_p=120°C, [I]=0.01 M/L (□). Model predictions (——).

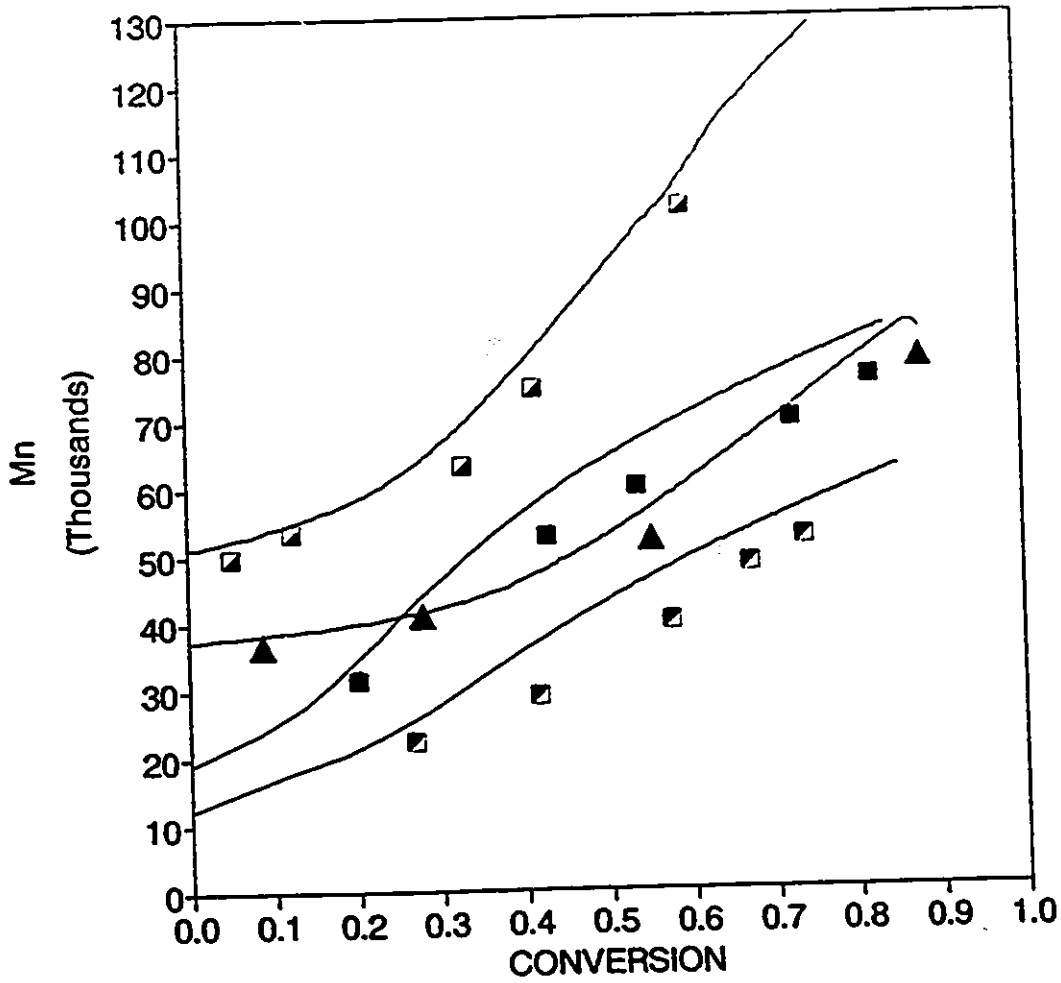

Fig. 5.9. Effect of T_p and [TBPCC] on the development of M_n with conversion in SAMS bulk copolymerization (f_{10}=0.85). Experimental results for: T_p=90°C, [I]=0.005 M/L (◪); T_p=90°C, [I]=0.01 M/L (▲); T_p=120°C, [I]=0.005 M/L (■); T_p=120°C, [I]=0.01 M/L (◪). Model predictions (——).

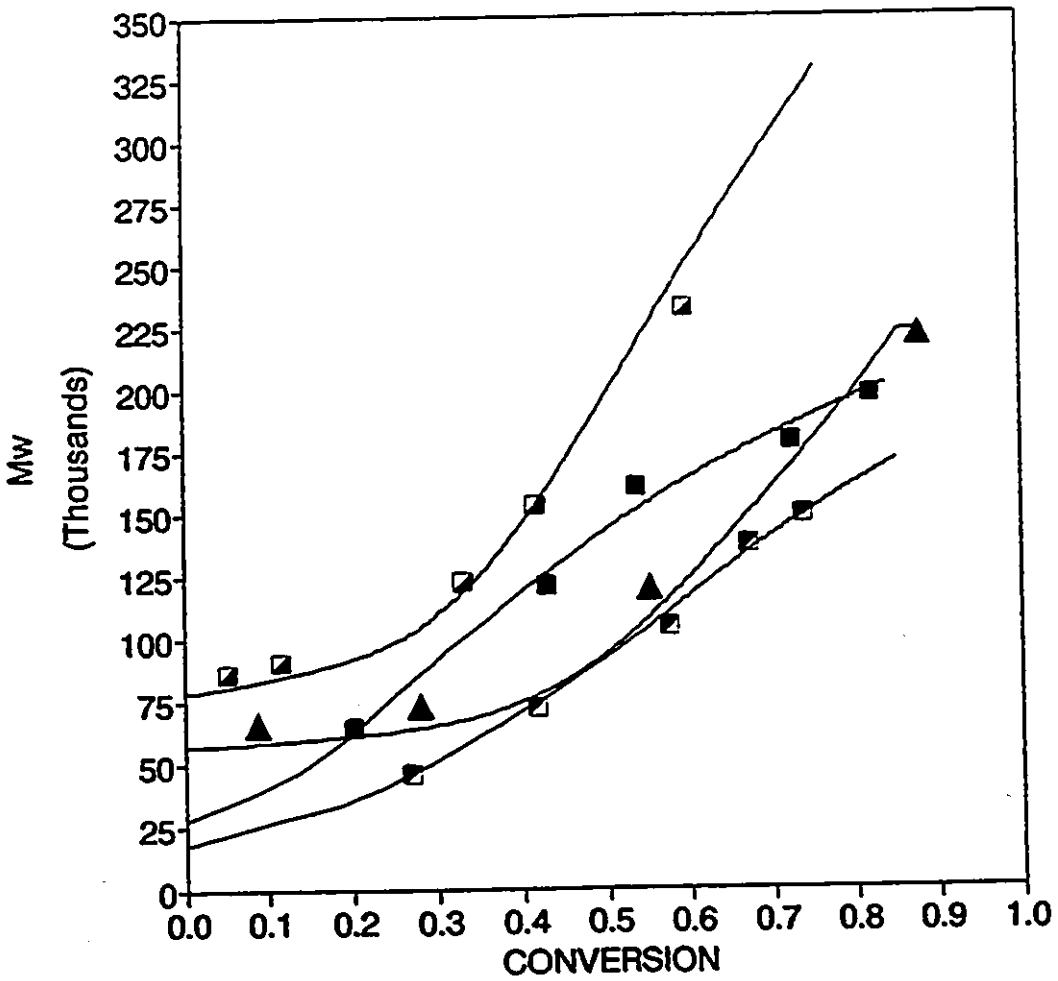

Fig. 5.10. Effect of T_p and [TBPCC] on the development of M_w with conversion in SAMS bulk copolymerization (f_{10}=0.85). Experimental results for: T_p=90°C, [I]=0.005 M/L (◪); T_p=90°C, [I]=0.01 M/L (▲); T_p=120°C, [I]=0.005 M/L (■); T_p=120°C, [I]=0.01 M/L (◪). Model predictions (——).

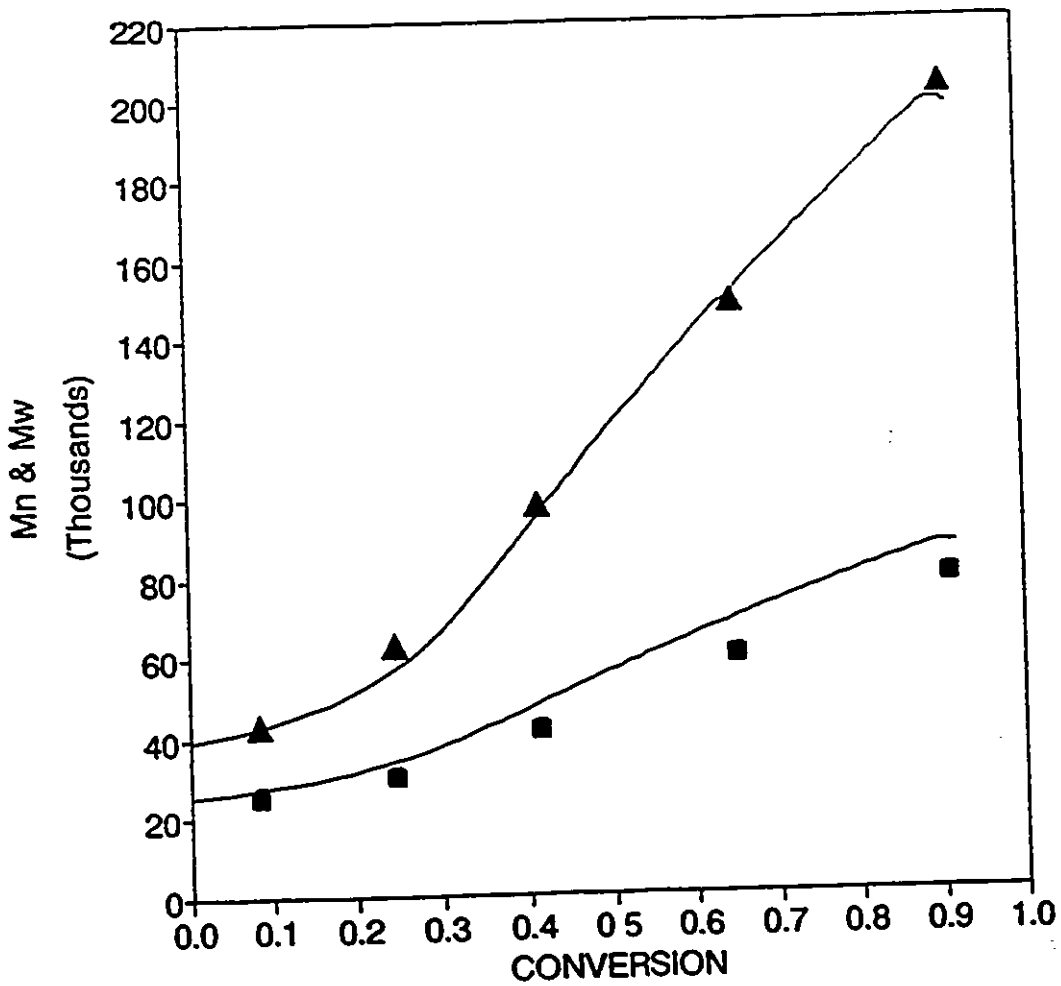

Fig. 5.11. Molecular weight distribution development with conversion in SAMS bulk copolymerization (f_{10}=0.85) with bifunctional initiator [TBPCC]=0.0075 M/L, at 105°C. Experimental M_n (■) and M_w (▲). Model predictions.

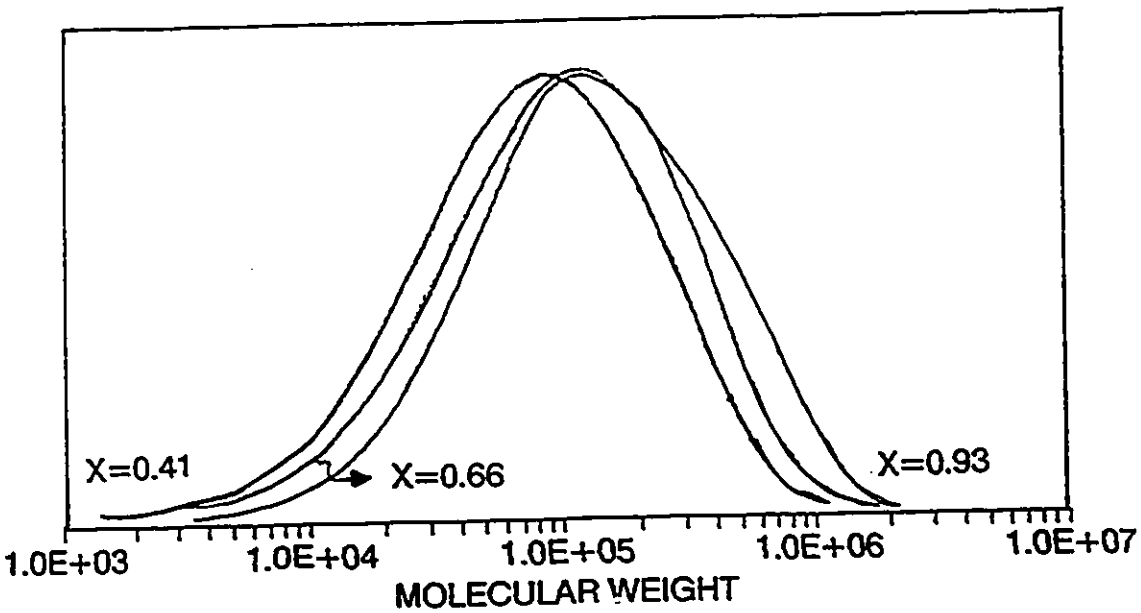

Fig. 5.12. Evolution of the MWD with conversion in SAMS bulk copolymerization (f_{10}=0.85) with bifunctional initiator [TBPCC]=0.0075 M/L, at 105°C. Curves show the experimental SEC results.

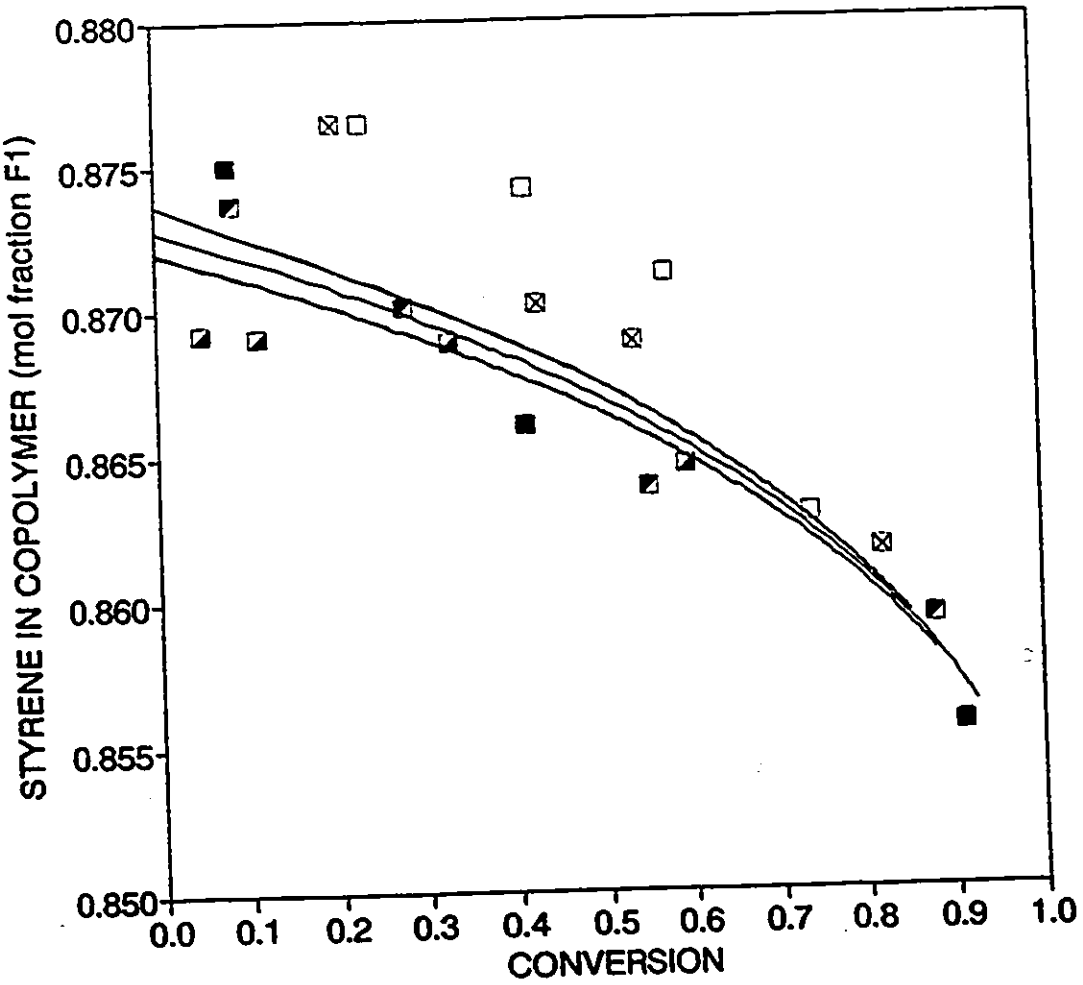

Fig. 5.13. Effect of T_p and [TBPCC] on copolymer composition development with conversion in SAMS bulk copolymerization (f_{1_0}=0.85). Experimental (H-NMR) results for: T_p=90°C, [I]=0.005 M/L (◪); T_p=90°C, [I]=0.01 M/L (▣); T_p=105°C, [I]=0.0075 M/L (■); T_p=120°C, [I]=0.005 M/L (▨); T_p=120°C, [I]=0.01 M/L (□). Model predictions (——).

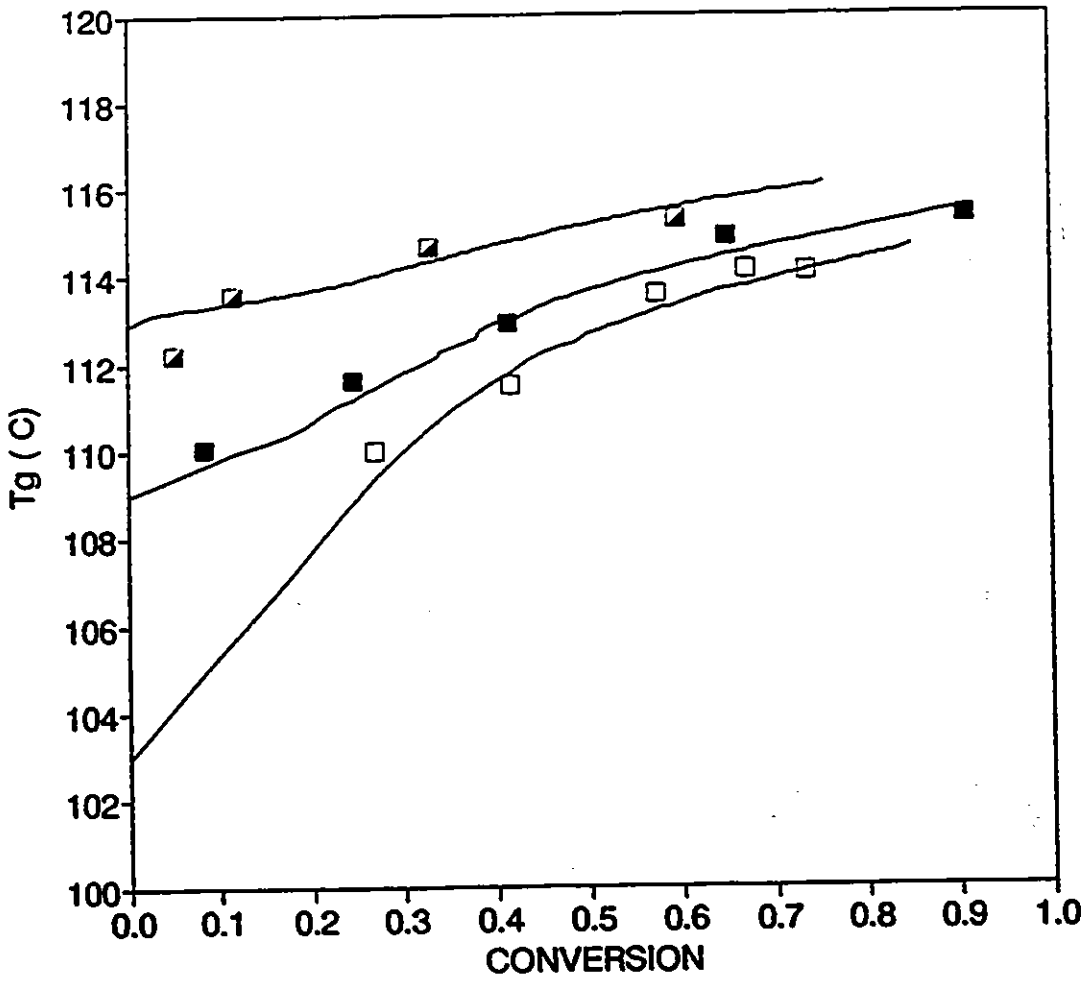

Fig. 5.14. Effect of T_p and [TBPCC] on copolymer T_g development with conversion in SAMS bulk copolymerization (f_{10}=0.85). Experimental (DSC) results for: T_p=90°C, [I]=0.005 M/L (◪); T_p=105°C, [I]=0.0075 M/L (■); T_p=120°C, [I]=0.01 M/L (□). Model predictions (——).

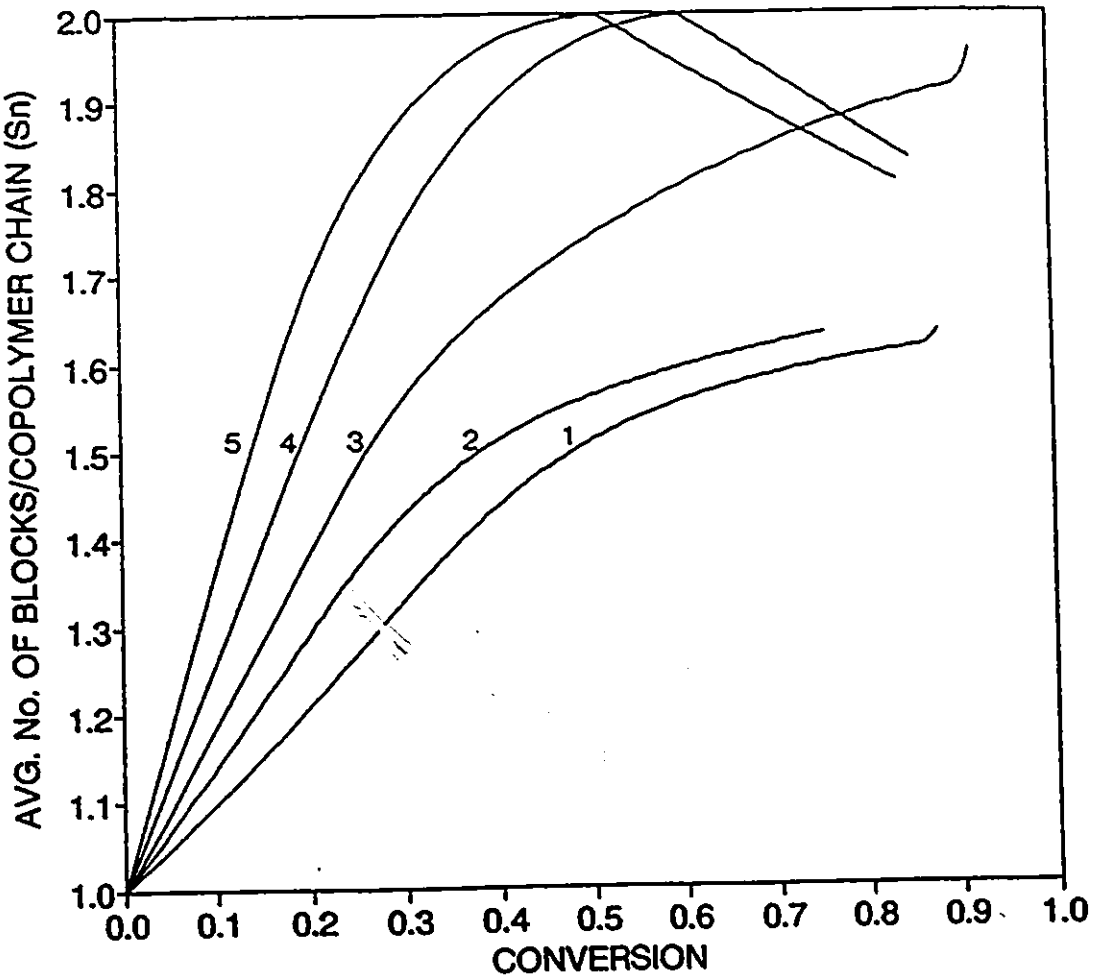

Fig. 5.15. Effect of T_p and [TBPCC] on the development of number of segments per copolymer chain, in SAMS bulk copolymerization (f_{10}=0.85). Model results for: T_p=90°C, [I]=0.005 M/L (1); T_p=90°C, [I]=0.01 M/L (2); T_p=105°C, [I]=0.0075 M/L (3); T_p=120°C, [I]=0.005 M/L (4); T_p=120°C, [I]=0.01 M/L (5).

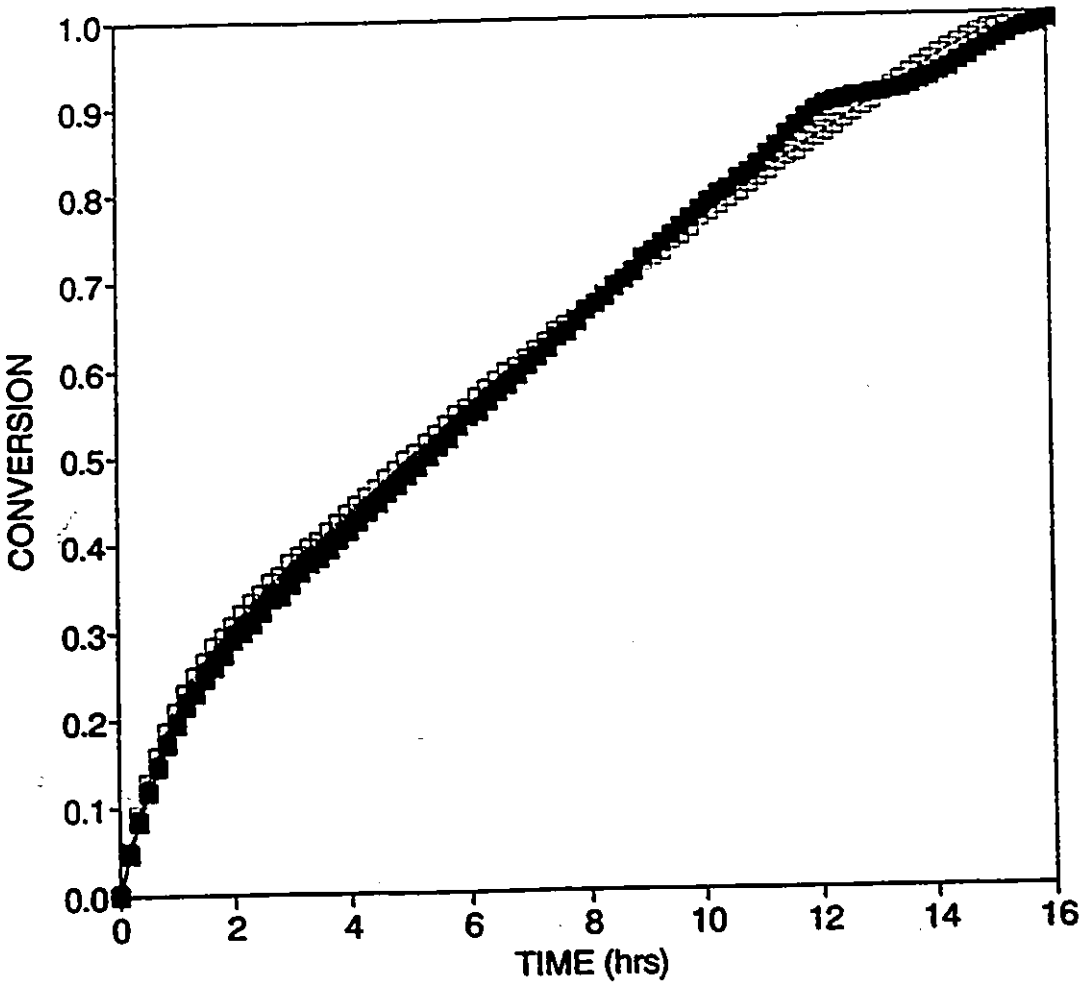

Fig. 5.16. Simulation of conversion history for optimal SAMS suspension copolymerization (f_{10}=0.85) with bifunctional initiator TBPCC. Experiment SAMS-03-01 (■); experiment SAMS-03-02 (□) (see table 5.3 for operating conditions).

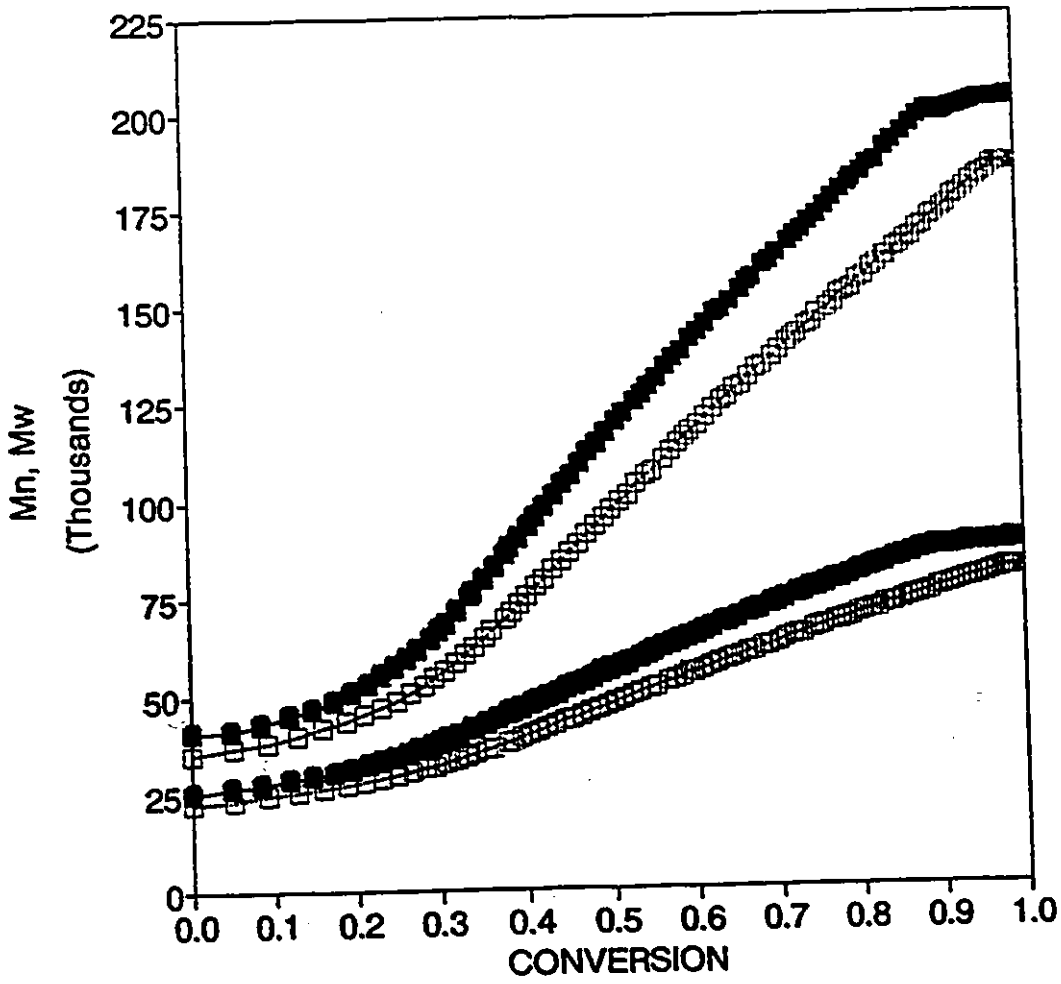

Fig. 5.17. Simulation of the molecular weight distribution development with conversion, for optimal SAMS suspension copolymerization (f_{I_0}=0.85) with bifunctional initiator TBPCC. M_n and M_w for experiments SAMS-03-01 (■), and experiment SAMS-03-02 (□) (see table 5.3 for operating conditions).

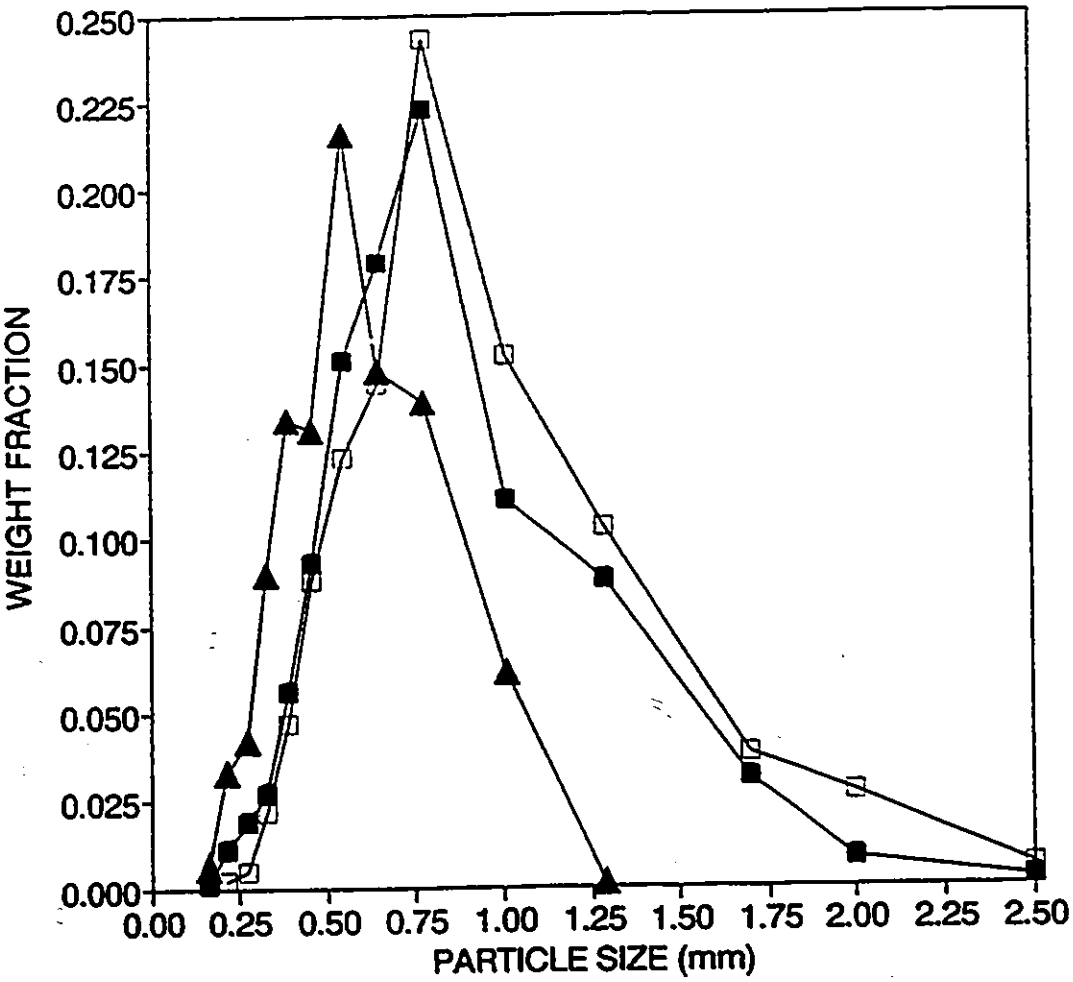

Fig. 5.18. Particle size distribution for optimal SAMS suspension copolymerization (f_{10}=0.85) with bifunctional initiator TBPCC. Discrete measurements of bead particle size vs weight fraction for: reference polystyrene system (▲), and experiments SAMS-03-01 (■) and SAMS-03-02 (□) (see table 5.3 for operating conditions).

CHAPTER 6

STYRENE/N-PHENYLMALEIMIDE COPOLYMERS

In this chapter, the synthesis and characterization of styrene-n-phenylmaleimide (S-NPMI) engineering copolymers, through free radical bulk and suspension copolymerization with bifunctional initiators, is described in detail. Experimental and model results are explained and compared throughout, to assess the adequacy of the kinetic and microstructure models proposed. The bases for the design of high T_g-high molecular weight S-NPMI copolymers are established, and the feasibility for scaling-up this copolymerization process to commercial production is evaluated.

6.1 Introduction

From the point of view of its copolymerization kinetics, S-NPMI copolymerization to high conversions may be considered as a very complex process, especially when non-equimolar concentrations are employed.

First, the electron donor-acceptor characteristics of this comonomer pair causes the rapid formation of large amounts of charge-transfer complex (CTC) in the reaction mix, thus reducing the amount of free monomer in the system [Shmidth-Naake et.al.(1990,a,b)].

Secondly, the extraordinarily high propagation rate exhibited by these complexes readily consumes the complexed monomer, thus displacing the equilibrium between complex and free monomers towards complex production, nearly depleting the free monomer, or the comonomer present in lesser concentration, from the polymerizing system [Shirota et.al.(1974), Georgiev and Zobov (1978), Barron et.al.(1984)].

As a consequence, very high initial copolymerization rates are reached, up to the point were the concentration of CTC in the system is

low enough to reduce the copolymerization rate to levels similar to the statistical copolymerization rate of the free monomer, occurring simultaneously when both free monomers are able to both homo and copolymerize, as it is the case for the S-NPMI pair [Barrales-Rienda et.al.(1977), Zott and Heusinger (1978)].

Owing to the simultaneous and competitive nature of both mechanisms, and since the propagation of donor-acceptor complexes leads to the formation of perfectly alternating sequences, whereas the propagation of free monomer leads to statistical sequences within the same copolymer chain, both microstructure and copolymer composition change drastically during the copolymerization [Kim et.al.(1978), Barron et.al(1984), Zeng and Shirota (1989)].

At low conversions, high concentration of CTC in the system leads to the formation of nearly alternating copolymer. The alternating sequences being disrupted only by free monomer addition through statistical copolymerization. At intermediate conversions, low CTC concentration causes the formation of a random combination of both alternating and statistical sequences within each copolymer chain. At high conversions, if non-equimolar initial concentration of monomers are employed, the nearly complete depletion of the monomer present in lesser concentration prevents the formation of significant amounts of CTC and, as a result, statistical copolymerization with one of the monomers in great excess (nearly homopolymerization) takes place.

The copolymer chains thus formed at high conversions, are completely different in microstructure, composition, and very likely in molecular weight, to those formed at low conversions. As a consequence copolymer heterogeneity and dissimilar thermal and mechanical properties of the copolymer may be observed, when monofunctional initiators are used.

The use of bifunctional initiators may alleviate this problem to a great extent inasmuch as successive chemical combination of copolymer chains formed at different stages in the reaction, occurring in a random fashion, produces multi-block structures, reducing the effective

compositional drift. As a result, copolymer chains bearing blocks (segments) with compositions ranging from alternating copolymer to nearly homopolymer will conform the final product. The formation of a substantial amount of mono-segmental copolymer chains bearing different composition according to the specific drift, however, cannot be avoided [Villalobos et.al. (1992,a), see also Chapter 4].

Since NPMI is introduced as a comonomer for styrene in order to provide the necessary chain stiffness to promote the formation of high T_g copolymers (see Chapter 2), segments bearing high concentrations of NPMI will exhibit very high T_g (hard segments), whereas segments bearing high concentration of styrene units will show lower T_g (soft segments), within the same copolymer chain.

The overall performance of the product may be enhanced by this combination of hard and soft segments in the copolymer chains inasmuch as a better balance of mechanical, thermal and processing properties may be conferred to the copolymer. Thermoplastic elastomers are good examples of hard-soft block copolymers with excellent balance of the above properties [Estes et.al.(1970)].

Several problems arise in the kinetic modelling of S-NPMI copolymerization, as well as for the interpretation of the scarce experimental data available in the literature for this system. At least four different schemes have been traditionally followed to describe donor-acceptor copolymerization, namely, terminal model, penultimate model, terminal model plus complex dissociation, and terminal model plus complex participation [Shirota et.al.(1974), Georgiev and Zubov (1978), Hill et.al.(1985), Shmidt-Naake et.al.(1990,a,b)].

Schmidt-Naake et.al.(1990,b) employed the terminal model for the simulation of S-NPMI copolymerization. Values for the reactivity ratios of this system, calculated from the Mayo-Lewis equation neglecting complex participation were r_1=0.05, and r_2=0.11. These values reflect the high tendency toward alternation exhibited by this system, and adequately predict overall reaction rate, copolymer composition and microstructure.

In spite of this, the validity of the model as a comprehensive description of the events involved, can be questioned inasmuch as complex formation and participation in propagation reactions has been fully demonstrated [Tsuchida and Tomono (1971), Tsuchida et.al.(1972), Caze and Loucheux (1978)].

When using the penultimate model for the description of this system, additional questions arise in relation to the physical significance of the four reactivity ratios involved, when the complex participation is ignored. Moreover, the effect of the donor or acceptor character of the solvent on the reaction rate cannot be explained by either the terminal or the penultimate models, without changing the reactivity ratios. When complex formation is considered, this phenomenon is explained, and fully captured, by assessing the effect of the solvent in the equilibrium of donor-acceptor formation [Kim et.al.(1978)].

The above considerations are surely sufficient for one to prefer models which take into account complex participation over terminal and penultimate models.

The third type of model, employed when dealing with donor-acceptor copolymerization, proposed by Hill et.al. (1985), does consider complex formation and propagation, however, it considers dissociation of complex after propagating (see Chapter 2). Since there is neither theoretical nor experimental evidence for the occurrence of such dissociation, this type of model is likely not valid.

As mentioned in Chapter 4, the use of the terminal plus complex participation model gives clear physical meaning to the reactivity ratios involved (i.e. r_1, r_2, β_1, and β_2), and fully describes the behaviour of the system throughout the entire conversion range [Georgiev and Zobov (1978)]. This model, then, must be considered as the most comprehensive one when dealing with donor-acceptor copolymerization.

Whenever complex participation is taken into account the values of r_1 and r_2 calculated from the terminal model, as those reported above for this system, may not be valid. Instead, these ratios must be computed

from a consistent model when considering such complex participation.

It is worth noting that since the alternating sequences formed in the copolymer are well described by the donor-acceptor propagation reactions, it is unlikely that the statistical copolymerization, taking place simultaneously, be highly alternating as well. The evolution of the microstructure of styrene/maleic anhydride copolymers, when one of the complexing comonomers is used in excess, seems to corroborate this hypothesis [Barron et.al.(1984)].

Accordingly, the kinetic and microstructure models proposed in this thesis, are based on terminal plus complex participation mechanisms to represent simultaneous and competitive statistical/donor-acceptor copolymerization, along with the unique features of multiple re-initiation/propagation/termination of bifunctionally initiated free radical polymerization (see Chapter 4). This model, as it will be shown, fully describes all the aforementioned phenomena observed in this type of copolymerization.

6.2 Design of Experiments

Similarly to the study of S-AMS shown in Chapter 5, and according to the main objectives of this thesis and general experimental plan described in Chapter 1, the experimental work of this study was divided in three different phases: 1) exploratory; 2) optimization; and 3) optimal suspension copolymerization.

Previous to the exploratory phase, however, characterization of the properties of molten NPMI, and a study on the homopolymerization of NPMI, in the temperature range of interest, were carried out to generate all the information required in the model for reactions involving two NPMI units. This was necessary due to the almost complete lack of physical properties, and kinetic information for this system, in the open literature.

For the NPMI bulk homopolymerization with bifunctional initiator study, two runs with [TBPCC]= 2.0 wt%, at 105 and 130°C, respectively, were designed.

With the homopolymerization information compiled, the exploratory phase, designed with wide ranges in process variables, was done to establish the effect of initial comonomer feed composition (f), and polymerization temperature (T_p) on copolymerization rate (R_p), terminal conversion (X_t), copolymer molecular weight distribution (MWD), copolymer composition (F), and copolymer glass transition temperature (T_g), in bulk batch free radical copolymerization with bifunctional initiator 1,4-bis(tertbutyl peroxycarbo)cyclohexane (TBPCC).

Different from the exploratory phase for S-AMS copolymers given in Chapter 5, two different temperatures (105 and 130°C) were employed in this phase in order to generate enough data for the subsequent model parameter estimation. This was really necessary because of the almost complete lack of literature data available for S-NPMI free radical copolymerization. The experimental design S/NPMI-01, for this exploratory phase is given below in Table 6.1.

Table 6.1

Experimental Design S/NPMI-01 for the Exploratory Research

RUN S/NPMI-01	f_{10} (mol)	T_p (°C)	[TBPCC]o (Mol/L)	POLYM. TIME (hrs)
1, 7	1.00	105, 130	0.01	4.0
2, 8	0.90	105, 130	0.01	4.0
3, 9	0.80	105, 130	0.01	4.0
4, 10	0.70	105, 130	0.01	4.0
5, 11	0.60	105, 130	0.01	4.0
6, 12	0.50	105, 130	0.01	4.0

From the results of the exploratory phase, the conditions yielding the best balance of copolymerization rate and copolymer characteristics were selected. The criteria followed in this selection, were both comparison with the reference PS system (see Chapters 3 and 5), and the constraints in the design of suspension polymers (see Chapter 1).

Accordingly, the experiments S-NPMI-02 were designed to evaluate, in a narrower experimental range, the effects of f, T_p and [TBPCC], on R_p, and the development of MWD, f, F, and T_g with conversion, in bulk batch free radical copolymerization with bifunctional initiator TBPCC. The experimental design S/NPMI-02 of this experimental optimization phase is shown below in Table 6.2.

Table 6.2

Experimental Design S/NPMI-02 for the Optimization Research

Run S/NPMI-02	f_{10} (mol)	T_p (°C)	[TBPCC]o (Mol/L)	POLYM. TIME (hrs)
1	0.90	130	0.010	2.0
2	0.90	105	0.010	2.0
3	0.80	130	0.010	2.0
4	0.80	105	0.010	2.0
5	0.70	130	0.010	2.0
6	0.70	130	0.005	2.0

After the optimization phase was performed, the model parameter estimation was completed, and BICOP simulations for the runs of the three experimental phases were performed.

From the results of the optimization phase, the simulation assisted suspension copolymerization runs S-NPMI-03 were established as the optimal routes for high T_g S-NPMI bifunctionally initiated suspension copolymer syntheses.

The optimality criteria followed was the same as for the optimization phase plus some considerations of heat generation rate. The experimental design S-NPMI-03 is given below in Table 6.3.

Table 6.3

Experimental Design S/NPMI-03, Suspension Copolymerization Scaled Reactor Arrangement, Recipes, and Operating Conditions

RUN S/NPMI-03	f_{io} (mol)	[TBPCC]o (Mol/L) (org. phase)	T_p (°C)	TIME @ T_p (min)
REFERENCE	1.00	0.010	105	240
1	0.80	0.010	105 140	60 30
2	0.80	0.012 5.0 wt% TOLUENE	105	90

Recipe	
Initial volume @ 25°C (water + organic phase)	V_o = 3200 cc
Dispersed phase volume fraction (@ 25°C)	Φ = 0.4
Suspending agent (TCP) concentration	[TCP]o = 7.5 g/L_{org}
Reactor Operating Conditions	
Copolymerization temperature (T_p)	As in design
Copolymerization time (t)	As in design
Copolymerization pressure	P_o = 275 KPa
Agitation speed	N = 275 rpm
Reactor Geometrical Parameters	
Liquid height (Z) to tank diameter (T) ratio	Z/T = 1.2
Impeller diameter (D) to tank diameter ratio	D/T = 0.6
Impeller type (turbine)	4-blade, 45°pitch
Number of impellers (pumping downward)	No = 2
Bottom imp. position (from reactor bottom)	H_1 = T/4
Top impeller position (from reactor bottom)	H_2 = (2/3)Z
Blade width	W_1 = 0.2 D
Number and position of baffles	B_f = 4, spaced 90°
Baffle width (offset from the wall T/44)	W_B = T/12

In what follows, the experimental techniques employed in each experimental phase are described. Since most of these techniques are the same as those described in Chapters 3 and 5, constant reference to these Chapters is made in order to avoid repetition. However, differences in conditions from the experiments of this study and the previous two are specified.

6.3 Experimental

6.3.1 Materials

Styrene (Aldrich Chemical), TBPCC (Akzo-Chemie), chloroform (copolymer solvent), methanol (copolymer non-solvent), and toluene (T_g depressor), were treated and used as in Chapter 5. N-Phenylmaleimide (Aldrich) 99.6 % pure, was re-crystallized from methanol at room temperature in vacuo, dried in vacuo for 24 hours at 50°C, pulverized manually in a mortar, sieved through 100 mesh USS (MPS < 150 μm), and stored at room temperature.

6.3.2 Techniques

Previous to the exploratory research phase, and since no information regarding properties of NPMI in the molten state, needed for free volume determinations in the model, were found in the open literature, the following techniques were employed to generate such information.

Characterization of the density of NPMI in the molten state was carried out by dilatometry in sealed micro-pipets of 1 cc and minimum scale of 0.01 cc. Five micro-pipets containing 1.0±.05 g of purified NPMI were immersed in a constant temperature oil bath set initially at 100°C. The volume of the micro-pipet contents were read from 100°C to 130°C at 5°C intervals, after allowing the system to reach equilibrium temperature for 30 min.

Glass transition temperature of NPMI (T_{g2}), melting point (M_p), and ability of NPMI to initiate thermal polymerization were determined in triplicate, through DSC, in a DuPont 910 Calorimeter at 10°C/min heating rate ramp, from -50 to 200°C, followed by 2 hours at 200°C.

To complement the scarce published data on poly-NPMI, heat of homopolymerization, and heat generation rate were measured, in DSC closed cells, N_2 atmosphere, at 105°C and 130°C, for 1 hour, using TBPCC (2 wt%) as initiator. The NPMI/TBPCC reaction mixtures were prepared in a master batch solution of 98/2 (NPMI/TBPCC g) in 150 ml of methanol. Methanol was evaporated from the system at room temperature in vacuo for 12 hrs. The powder mix thus obtained was homogenized and stored at 0°C, until used.

In order to translate total heat evolved and heat generation rate data from the above DSC experiments, into conversion history and molar heat of NPMI polymerization, ampoule polymerization of the same master batch mixtures, at the same conditions, were carried out simultaneously. The ampoule contents after 5 and 60 minutes of polymerization were dissolved, precipitated, washed, and dried, following the techniques described in Chapter 5.

Gravimetric determinations of conversion (mass basis) and SEC determinations of MWD (relative to PS standards) were performed for the four NPMI homopolymers obtained, following the techniques described in Chapter 5.

Determinations of the glass transition temperature of poly-NPMI (T_{gp2}), and onset of melting (T_M), were made for the two purified samples obtained at 60 minutes of polymerization, through DSC at 10°C/min, from 25 to 400°C.

For the exploratory research phase, bulk copolymerizations in DSC cells were carried out at the conditions given in the experimental design S-NPMI-01 (Table 6.1), according to the procedures described in Chapter 5. The preparation of the master batch copolymerization mixtures, however, was extremely complicated due to the limited solubility of NPMI in styrene (Sol < 0.04 g/ml or 4.5 wt% @ 25°C -estimated-).

First, the insoluble S/NPMI mixtures, without initiator, were placed in a 25 cc test tube. Then, 10 ppm of p-tertbutylcatechol were added to the mix as inhibitor of thermal polymerization. The mixtures were immersed in a 70°C oil bath and agitated until a homogeneous solution was observed (less than 1 minute). Simultaneously, a 10 cc glass syringe containing the required amount of TBPCC were kept at 70°C in the oil bath. Once a homogeneous S-NPMI solution was observed, 10 cc of this solution were sucked into the syringe, quickly agitated, and added to the DSC cells.

The corresponding ampoule S-NPMI bulk copolymerizations were carried out at the same conditions given by the design S/NPMI-01. For each run samples were taken after 1 and 240 minutes of polymerization. Each ampoule was prepared by loading them with 1.0±0.1 g of NPMI purified powder first, and then adding the required amount of the styrene/TBPCC mixture, previously prepared as a master batch solution, according to the conditions given by the experimental design. Ampoule preparation and polymerization has been described in detail in Chapter 3.

From the ampoule contents, after the allotted copolymerization times, initial and terminal conversion (X_i and X_t), MWD at X_t, initial (instantaneous) copolymer composition (at X_i), and terminal (accumulated) copolymer composition (at X_t), were determined through the procedures described in chapter 5.

Conversion history for the DSC copolymerization runs, was established by normalizing each of the integrated heats of reaction with respect to the corresponding terminal conversions obtained from the ampoule runs. According to the procedure described in Chapter 5, direct translation from accumulated heat of reaction to conversion was possible since similar heats of polymerization for NPMI and styrene were determined, and no other thermal events occurred during the polymerization time allotted (see results below).

Glass transition temperature (T_g) and onset of melting (T_M) of the purified copolymers, obtained at terminal conversion in the ampoule

experiments, were determined by DSC, at 10°C/min heating rate, from 25 to 400°C. In samples displaying two different glass transition temperatures ($T_{ghard} > T_{gsoft}$), the fraction (mol) of soft chains in the copolymer (Fsoft), was established by dividing the heat consumed during the transition at lower temperature (T_{gsoft}) by the sum of the heat consumed in both the low and high temperature transitions. Calculation, in this way assumes that the molar enthalpy change during each glass transition is independent of the copolymer composition.

For the optimization research phase, ampoule bulk copolymerization of S-NPMI, using TBPCC as bifunctional initiator, were carried out at the conditions established in the experimental design S-NPMI-02 (Table 6.2), following the procedures described above as well as in Chapter 5.

From the ampoule contents after the previously selected polymerization times, total monomer conversion (gravimetry), and the development of MWD (SEC), copolymer composition (H-NMR), copolymer T_{gsoft} and T_{ghard} (DSC), and fraction of soft copolymer (DSC), were established by following the procedures described above as well as in Chapters 3 and 5.

For the optimal S-NPMI suspension copolymerization runs, initiated with bifunctional initiator TBPCC, at the conditions given by the simulation assisted design S-NPMI-03 (Table 6.3), the reactor geometry and operating conditions, internal arrangement, and recipes used were the same as those previously employed for styrene/n-pentane and S-AMS suspension copolymerization (see Table 5.3, Chapter 5).

Determination of MPS and PSD from the copolymer beads obtained, as well as conversion, MWD, and T_g, of the purified copolymer recovered from the beads were performed following the procedures described in Chapter 5.

Extrusion of the beads was carried out at 275°C in a Randelcastle Minitruder (50 rpm) following the procedures described in Chapter 5. Annealing effects on the T_g of the extrudate, as well as mass losses and Chain degradation after 5 and 10 hours at 300°C, were determined through the same procedures described in Chapter 5.

6.4 Results and Discussion

6.4.1 N-Phenylmaleimide Homopolymerization

Dilatometry experiments on molten NPMI samples showed that the density of this monomer follows a linear temperature dependency, valid in the 100-130°C range, given by:

$$d_{NPMI} = (1.31 - 0.0011*T(°C)) \pm 0.036 \quad (g/ml, Kg/L) \qquad (6.1)$$

DSC results for pure NPMI monomer showed: i) NPMI does not homopolymerize thermally at a measurable rate at temperatures up to 200°C; ii) reproducible values for melting point of M_p = 86.04 ± 0.11°C were found in agreement with the manufacturer information; and iii) No second order transition was observed in the experimental range in any of the three runs performed. This suggests that the glass transition temperature of NPMI monomer, if existent, is below -50.0°C.

Figure 6.1 shows the conversion history, translated from heat generation DSC results, for NPMI bulk copolymerization initiated with TBPCC (2.0 wt%) at 105 and 130°C. In this figure, note that limiting conversions X_t = 0.68 and X_t = 0.79, are reached before 1 hour of polymerization at 105 and 130°C, respectively. The slow decay in the polymerization rate observed after the gel effect in the curve at 105°C, suggests that the decay of the propagation rate, due to monomer diffusion controlled in the vicinity of the glass transition, is not as large as for other vinyl monomers. This observation seems to be corroborated that the fact that NPMI in the solid state is able to polymerize at a noticeable rate through γ-rays induced radical polymerization [Barrales-Rienda et.al.(1977), Zott and Heusinger (1978)].

From the total heat evolved during the reaction, and the terminal conversions observed, the heat of NPMI polymerization was computed as: $(-\Delta H_p)$ = 15.77 ± 0.35 Kcal/mol. Note that this value is very close to that of polystyrene ($-\Delta H_p$= 15.9 - 16.2 Kcal/mol).

From the slope of these curves at X=0, initial polymerization rates of 0.059 and 0.202 Mol/L-min were calculated at 105 and 130°C, respectively. Computing the initiation rate R_i at both temperatures from Kd and initial bifunctional initiator concentration data (see Table 5.5 Chapter 5), the ratios $K_p/K_t^{1/2}$ were calculated as 0.227 and 0.256, at 105 and 130°C, respectively.

The value at 105°C is in good agreement with that calculated from data reported by Barrales-Rienda et.al.(1977), for bulk NPMI polymerization, initiated with 0.2 wt% AIBN, at this temperature ($K_p/K_t^{1/2}$ = 0.2182). For the latter calculation, the value of K_d for AIBN at 105°C used was 0.1112 min^{-1}, estimated from half life data.

The weight average molecular weight (M_w), obtained through SEC with PS standards, evolved from an initial value about 20,000 (X=0.056) to nearly 60,000 at X_c, for the polymerization at 105°C, and from about 11,000 (X=0.14) to 55,000 at X_c, during the polymerization at 130°C.

Calculation, from the experimental data at 105°C, of the initial weight average molecular weight as:

$$M_w = MW_m(2\tau+3\beta)/(\tau+\beta)^2$$

Where MW_m is the monomer molecular weight (173.17 for NPMI); $\tau=(R_i*K_{td})^{1/2}/K_p[M]$; and $\beta=(R_i*K_{tc})^{1/2}/K_p[M]$, yields the value of M_w = 21,858 when τ=0, and M_w = 14,572 when β=0. Note that the first value compares better with the experimental result, which demonstrates that combination is the dominant bimolecular termination mechanism in NPMI homopolymerization. The differences in the observed and theoretical values may be due to limited chain transfer to monomer.

The glass transition temperature, at terminal conversion, of the two poly-NPMI synthesized was T_g = 348.12 ± 0.65°C. This value shows that the selection of this monomer (NPMI) to enhance the chain stiffness of polystyrene, is adequate. The observed T_g is within the range of T_g's for the family of step-polymerization polyimides, reported by Lee (1989).

6.4.2 Exploratory Research

According to the experimental design S-NPMI-01, the effect of the comonomer feed composition (f), and copolymerization temperature (T_p), on reaction rate (R_p), terminal conversion (X_t), molecular weight distribution (MWD), copolymer composition (F), and copolymer glass transition (T_g), was studied for bulk S-NPMI copolymerization at 105 and 130°C, using [TBPCC]=0.01 Mol/L, as bifunctional initiator.

Figures 6.2 and 6.3 show the translated DSC results for conversion history as a function of comonomer feed composition, for bulk S-NPMI copolymerization at 105 and 130°C, respectively. Direct translation from the integrated heat of copolymerization, normalized to the terminal conversions, was possible without corrections for copolymer composition due to the similarities of heat of polymerization of the two monomers (see above). The enlarged areas in the above two figures, show the first 20 minutes of copolymerization in which most of the changes occur. The curves for 100/0 composition, correspond to the reference polystyrene systems at the same conditions.

In the conversion curves at both temperatures, it is quite evident the existence of two competing propagation mechanisms. As the concentration of NPMI in the feed increases, the initial copolymerization rate increases dramatically, up to certain conversion, at which it rapidly decreases to values similar of polystyrene (see curves at 90/10 and 80/20 composition). This demonstrates that the very rapid complex propagation dominates at the beginning of the polymerization up to the point where the concentration of NPMI is low enough as to prevent extensive formation of donor-acceptor complex. From then on, the copolymerization proceeds primarily through the statistical addition of free monomer (mostly styrene) to the radical centres. As a result, highly alternating copolymer chains are formed in the first stages of the reaction (hard segments), whereas statistical styrene reach copolymer chains are formed at high conversions.

As the feed concentration of NPMI approaches the equimolar composition, limiting conversions are nearly reached in less than 5 minutes, at 105°C, and less than 3 minutes, at 130°C. The extraordinarily high copolymerization rates observed for the systems with more than 30 mol% NPMI in the feed, make these recipes technically infeasible for large scale production, through batch suspension polymerization, due to the equally high heat generation rate. Nevertheless, bulk (casting), solution, or even reaction injection molding (RIM), may be viable and very attractive alternatives for these systems.

The curves for 20 and 30 mol% NPMI in the feed (at 105°C), show at high conversions typical auto-acceleration behaviour, due to gel effect, after a short period of low polymerization rate following the depletion of donor-acceptor complex. Although, the initial copolymerization rate is very high for these systems, suspension copolymerization within this initial monomer composition range, may be possible (see below).

The experimental and model results for terminal (limiting) conversions observed for all these systems, after 4 hours of polymerization, are plotted in figure 6.4 against the monomer feed composition. In the same figure the expected limiting conversions, calculated from the Fox model [Fox (1956)] considering the non-converted fraction as styrene monomer and using the experimental copolymer T_g values reported below, are also shown for comparison.

It is very noticeable in this figure that the observed limiting conversions, all above 90%, are much higher than those expected for such high T_g copolymers (T_g>210°C see below) synthesized at relatively low temperatures (i.e. earlier onset of the glassy effect expected). Possible explanations for this behaviour include either or a combination of:

a) Local temperature increase, within the unstirred ampoule, due to nearly adiabatic polymerization brought about by the extremely high initial polymerization rates [Zhu and Hamielec (1990)].

b) A combination of both high residual monomer-induced copolymer plasticization, due to low comonomer T_g, and slow decay in the propagation rate during the glass transition.

c) Continued propagation occurring in the soft (low T_g) fraction of the copolymer matrix.

While the first possibility is plausible for the systems with 40 and 50 mol% NPMI in the feed (see figures 6.2 and 6.3), ampoule heat effects do not seem important at lower NPMI fractions in the feed since these systems undergo at high conversions, as explained above, reaction rates similar to polystyrene, for which level it has been demonstrated that no appreciable heating occurs within ampoule of the selected diameter [Zhu and Hamielec (1990)].

The other two possible explanations of the observed behaviour are addressed at the end of this section.

Figure 6.5 shows the experimental and model results for the initial polymerization rate as a function of the monomer feed composition, at both temperatures tested. The model shows good agreement with the experimental results in all the range studied, except at f_{20}=0.1 and T_p=105°C where a large overestimation of the initial rate is obtained.

In this figure it can be observed how the initial polymerization rate increases dramatically between 0 and 20 mol% of NPMI, approaching a limiting value as the concentration of NPMI in the feed increases further. This represent more evidence that the very high donor-acceptor complex propagation dominates the early stages of the reaction since the observed polymerization rate increases up to nearly one order of magnitude at 130°C and 25 times at 105°C, with respect to the styrene initial polymerization rate. These extremely high propagation rates are rarely exhibited in purely statistical copolymerization [Georgiev and Zobov (1978)].

Opposite to the behaviour at 130°C which shows that the system is close to its maximum rate, at 105°C the curve indicates that further increases in NPMI feed concentration would yield higher initial copolymerization rates.

This is in complete agreement with earlier observations that the equilibrium constant for donor-acceptor complex formation decreases (i.e. is displaced towards free monomer) as the temperature increases [Tsuchida et.al.(1972)]. If the equilibrium constant reaches a point where the complex dissociates to free monomer at similar rates as it is consumed through propagation reactions the system will reach its maximum copolymerization rate at this point. Lower equilibrium constants, brought about by higher temperatures, will further displace the equilibrium towards free monomer, thus increasing the participation of statistical addition, and decreasing the overall copolymerization rate.

The whole evolution of the copolymerization mechanism may, then, be pictured as follows. At a given temperature, at low conversions the net rate of complex formation must be larger than the very high observed complex propagation rate. As a result, complex accumulation in the system occurs and little participation of free monomer addition takes place. As conversion increases (i.e. monomer concentration decreases) the rate of complex formation decreases to levels below the complex propagation rate, thus consuming the accumulated complex and increasing statistical monomer addition. As conversion increases further, the accumulated complex has been consumed and the rate of complex production will create a starving feed of complex to the reaction mix, with the consequent increase in the amount of free monomer participating in statistical copolymerization. Finally, at very high conversions the rate of complex formation falls below the rate of statistical copolymerization, thus creating exclusively statistical copolymer chains.

In figure 6.6 the experimental and model results for M_n and M_w of the copolymers obtained at terminal conversion are shown as a function of the monomer feed composition. At both temperatures tested the trends clearly show a very moderated increase in M_w as the concentration of NPMI in the feed increases, especially at $f_{20} > 0.20$ where it remains nearly constant about 250,000 for copolymerization at 105°C and about 175000 at 130°C.

Differently, the M_n shows a rapid decrease for f_{20} between 0 and 0.3, followed by nearly constant values about 40,000, at both temperatures, at higher initial concentrations of NPMI.

Note that the model predictions for M_w although following the adequate trend, overestimate the final value by about 10% throughout the entire range of feed compositions studied. Moreover, model predictions of M_n only follow the observed trend at $f_{20} < 0.2$, where overestimation of the final values ranges between 5 and 20% at both temperatures. At higher initial concentrations the model disagreement is larger and no clear trends are observed. Explanation of the sources of model-experimental results disagreement are given next.

While the M_w behaviour could be explained in terms of the rapid increase in R_{p0} between 0 and 20 mol% of NPMI in the feed, followed by the slow increase at higher f_{20}, as explained above, the M_n trend cannot be explained in this manner inasmuch as a similar increasing trend would be observed if the initial increase in R_p were the main variable shaping the molecular weight distribution.

The complete MWD obtained using SEC for the terminal conversion copolymers, shown in figure 6.7, give an answer to the observed molecular weight behaviour. In this figure, the MWD of the copolymer obtained at 20 mol% of NPMI in the feed shows an unimodal character, however, a tail of low molecular weight copolymer is observed. For the copolymer synthesized from f_{20} = 40 mol% the MWD broadens considerably, and a second peak at low molecular weights develops. The copolymer synthesized at equimolar monomer feed composition, shows a bimodal MWD with a narrow peak at low molecular weights, and a broad peak at high molecular weights.

Considering the high initial copolymerization rates observed, and the relative amounts of low and high molecular weight copolymer in the two peaks, it follows that high molecular weight chains are formed in the early stages of the reaction, mainly due to fast complex propagation, and low molecular weight chains are formed at high conversions owing to the slower statistical monomer addition to the radical chains.

As a result the molecular weights decrease with monomer conversion up to a point were the M_w does not change sensibly yet the M_n decreases further, owing to the broadening of the distribution towards low molecular weights.

From the model results, as shown below, the correct decreasing molecular weight trend with conversion is followed. However, the calculation of only three moments of the MWD distribution is not enough to capture the substantial broadening of the distribution and the development of a bimodal MWD, especially at high concentrations of NPMI in the feed. In order to capture this very complex molecular weight behaviour, the complete molecular weight distribution, or at least six moments of the distribution, should be calculated at each integration step.

The extreme complexity and computational effort required to solve such a model are well beyond the scope of this study, and will not be attempted here. As a result, the model predictions for M_w must be taken only as an approximation of the actual system behaviour, whereas the model predictions for M_n only as a trend with substantial overestimation at high conversions, especially at high NPMI concentrations in the feed.

Figure 6.8 shows the experimental and model results for the instantaneous (X=0) copolymer composition as a function of the monomer feed composition, at both temperatures tested. As expected, the initial composition approaches rapidly the perfect alternation as the concentration of NPMI in the feed increases. Note that even for the system with only 10 mol% NPMI in the feed, the copolymer composition approaches 40 mol% of NPMI units. For this system at 105°C, the slight model overestimation predicted by the model is entirely due to the overestimation in initial rate, mentioned above.

In the same figure the model predictions for initial donor-acceptor complex concentration in the copolymerization mix, shows that larger accumulation of complex in the mix occurs at higher NPMI concentrations, as expected from the increased net complex production rate.

Consequently, most of the initial copolymerization takes place through complex propagation (i.e. low concentrations of free monomer), thus producing the nearly equimolar concentrations observed, and highly alternating copolymers. This is in agreement with the mechanism explained above. Note that the initial value of f_c refers to the concentration an instant after the copolymerization starts, since f_{c0} is defined in the model as zero.

The observed compositional drift between zero and terminal conversion is shown in figure 6.9 for these copolymerization systems as a function of the monomer feed composition, at both temperatures tested. The compositional drift follows the direction of the arrow. The composition at terminal conversion approaches the feed composition owing to the high terminal conversions obtained. This figure corroborates the dramatic changes expected in copolymer composition, from nearly alternating to nearly homo-polystyrene, as the copolymerization progresses, especially at low NPMI concentrations in the feed. As the system approaches the equimolar feed composition, the compositional drift becomes negligible.

The consequence of such a large compositional drift in monofunctionally initiated batch S-NPMI copolymerization would be the production of a heterogeneous copolymer mix of multiple copolymer compositions, with heterogeneous properties that may lead to phase separation. If, in addition, the early formed alternating copolymer chains bear high molecular weights and the later formed statistical ones bear low molecular weights, as explained above, the heterogeneity will be more pronounced.

The ability of bifunctional initiators to chemically bind together copolymer chains formed at different stages in the reaction, thus reducing the compositional drift according to the effective compositional drift theory developed in Chapter 4, is fully corroborated through the outstanding thermal behaviour exhibited by these copolymers, which is shown below in figures 6.10 and 6.11.

For the bulk S-NPMI copolymers synthesized with f_{20}=0.1, at 105 and 130°C, figures 6.10 and 6.11, respectively, show a single T_g about 110°C when the copolymer composition bears about 10 mol% of NPMI units. For this system, it is proposed that the fraction of copolymer chains formed in the early stages of the reaction, which should show a higher glass transition temperature (T_{ghard}), get bonded to the chains formed later on in the reaction which bear the glass transition temperature observed (T_{gsoft}). As a result of the larger molecular mobility of the latter, the whole copolymer mix behaves as a soft copolymer with the T_g observed.

For the copolymers synthesized with f_{20}=0.2, these figures show that the copolymers (bearing compositions close to 20 mol% NPMI) exhibit two different glass transition temperatures. The soft copolymer fractions comprising about 27 and 16 mol% of the total copolymer mix, for syntheses at 105 and 130°C respectively, show a T_{gsoft} about 112°C, while the remainder of the copolymer shows a very high T_{ghard} about 212°C.

Considering that these copolymers synthesized at the same conditions with monofunctional initiators should bear soft fractions around 60 mol% (i.e. about 40 mol% of hard copolymer would be produced) the much lower soft fractions observed offer irrefutable prove that multiple chain recombination occurs in free radical copolymerization with bifunctional initiators.

For the copolymers synthesized with f_{20}=0.3 at 105°C, two glass transition temperatures were also observed, T_{gsoft} about 113°C, and T_{ghard} about 215°C. In this case, the fraction of soft copolymer chains was less than 5 mol%. Consequently, the overall thermal characteristics of the copolymer mix follow the behaviour of the T_{ghard} copolymer. For the copolymer synthesized at 130°C, only a single T_{ghard} about 216°C, was observed.

Similarly, for the copolymers synthesized at $f_{20} > 0.3$, at both temperatures, a single T_{ghard} ranging from 216 to 221°C, was observed.

All the copolymer samples taken at the beginning of each of the eight polymerizations carried out, show a single T_{ghard} from 212 to 221°C. This, once again, demonstrates that complex propagation leading to the formation of alternating copolymer chains dominates the early stages of the copolymerization. The T_{ghard} value extrapolated at zero conversion yields the glass transition temperature for the perfectly alternating copolymer T_{galt} = 222.07°C.

Due to the complex thermal behaviour observed in these copolymers, and since no published model representing the evolution of a double T_g with the accumulated copolymer composition was found in the literature surveyed, empirical models for T_{ghard} and T_{gsoft}, obtained through non-linear multiple variable regression from the experimental data of T_g, F_1, and M_n, were introduced in the simulation program BICOP as:

$$T_{ghard} = 525.54 \exp(-0.1101*F_{1acc}) - (1.7 \times 10^5/M_n) \qquad (6.2)$$

and

$$T_{gsoft} = 450.53 \exp(-0.1848*F_{1acc}) - (1.7 \times 10^5/M_n) \qquad (6.3)$$

where T_g's are in degrees Kelvin, F_{1acc} is the accumulated mol fraction of styrene in the copolymer, and M_n is the number average molecular weight of the accumulated molecular weight distribution.

For free volume calculation purposes, the following weighed average was used in the simulation program BICOP as a representative copolymer glass transition temperature (T_{gp}):

$$T_{gp} = f_{soft}*T_{gsoft} + f_{hard}*T_{ghard} \qquad (6.4)$$

Here f_{soft} is the observed mol fraction of soft copolymer, and $f_{hard}=(1-f_{soft})$ is the mol fraction of hard copolymer, in the copolymer mix.

To copy the S shape of this functions, with respect to styrene composition in the copolymer, the experimental curves for f_{soft} at 105 and 130°C were introduced in the simulation program as fourth order

polynomials of F_{iacc} at each temperature. As a result of this empirical modelling, the simulation predictions for T_{ghard}, T_{gsoft} and f_{soft}, shown in figures 6.10 and 6.11, are in close agreement with the experimental results throughout the entire experimental range.

From the thermal behaviour of the different copolymers, the observed high terminal conversions for these systems, can now be explained as follows (see discussion of figure 6.4,above).

The existence of a mixture of monosegmental soft and hard copolymer chains, as well as soft and hard segments within most of the multi-segmental copolymer chains in the copolymer matrix, may provide the conditions for soft and hard micro-domain separation, as it has been observed through scanning electron microscopy (SEM) in several others soft-hard block copolymers [Estes et.al.(1970)].

When such micro-domain formation occurs, propagation reactions within the multiple soft micro-domains may proceed at a considerable rate, even when the copolymer matrix, as a whole, becomes glassy. If, in addition, one of the comonomers is able to propagate in the glassy state at a measurable rate, as it is the case of NPMI, the combined effect must result in higher terminal conversions than those limited by the glass transition of the polymer/monomer mix at a given polymerization temperature.

6.4.3 Optimization Research

From the results obtained in the exploratory research phase, and according to the objectives of this study, selection of the conditions of the optimization research were made by following these criteria:

Concentrations of NPMI in the feed exceeding 30 mol%, produce such a high copolymerization rate that they are considered impractical for suspension polymerization. Therefore, concentrations between 10 and 30% were selected.

In addition, the range of temperatures and initiator concentrations tested in the exploratory phase, led to the formation of copolymers with M_w close to the target value of 200,000 of the reference polystyrene system (i.e. M_w about 175,000 and 250,000 at 130 and 105°C, respectively). Then, it was decided to perform the detailed experimentation in the same temperature range and with the same initiator concentrations. As a result, the experimental design S/NPMI-02, shown above in Table 6.2, was established.

Note that five of the six runs of this design, correspond to S/NPMI-01 experiments. The sixth run was designed to evaluate the effect of initiator concentration on the copolymer and copolymerization characteristics. The results obtained in this optimization research phase are summarized in what follows.

The effect of copolymerization temperature on monomer conversion history, at two different initial feed compositions (f_{10}=0.9 and 0.8), in bulk S-NPMI copolymerization with bifunctional initiator [TBPCC]=0.01 M/L, is shown in figure 6.12. In this figure note that both the experimental and model results follow closely the curves obtained through DSC in the exploratory phase, at the same conditions. the enlarged area in this figure shows the first hour of polymerization to observe in detail the rapid early changes in conversion, and the goodness of the model fits.

In this figure the curves at 130°C, show a nearly dead end behaviour at high conversions due to rapid initiator consumption ($t_{1/2}$=0.5 hours), followed mostly by styrene thermal initiation. At 105°C the curves at both initial comonomer compositions show high initial copolymerization rates followed by a rapid decay at intermediate conversions due to donor-acceptor complex depletion, and then followed by auto-acceleration caused by the gel effect. For these systems, limiting conversions above 90% are reached after 90 and 60 minutes, at f_{10}=0.9 and 0.8, respectively. The observed copolymerization rates make these system feasible for suspension polymerization.

In figure 6.13, the effect of comonomer composition on copolymerization rate, in bulk S-NPMI at 130°C, is shown. The enlarged area in this figure, shows the first hour of polymerization, to permit observation of the conversion changes in detail and the close agreement of model and experimental results throughout the conversion range.

In this figure, it is evident that the initial copolymerization rate increases dramatically as the concentration of NPMI in the feed increases. At this temperature, the system with f_{10}=0.7 reaches its limiting conversion after 20 minutes of polymerization, whereas the system with f_{10}=0.8 does it after 60 minutes. The extremely high initial copolymerization rate of these systems may make them unsuitable for suspension polymerization. For the system with f_{10}=0.9, dead end copolymerization is observed after 90 minutes, with the consequent lower terminal conversion reached.

The effect of bifunctional initiator concentration, in bulk S-NPMI copolymerization at 130°C, is shown in figure 6.14. The curve for [TBPCC]=0.01 M/L has been described above. The curve for [TBPCC]=0.005 M/L, shows the expected lower initial copolymerization rates, with the system needing 30 minutes to reach its limiting conversion at about 93%. Model predictions are in good agreement with the experimental results throughout the conversion range, with the exception of a more pronounced shoulder exhibited by the low initiator concentration system at intermediate conversions.

The effect of polymerization temperature on the molecular weight averages development, in bulk S-NPMI copolymerization with TBPCC, at f_{10}=0.8, is shown in figure 6.15. Note in this figure how the decreasing trend with conversion observed for both averages, is followed by the model, with the M_w curve giving good ball park estimates of the actual behaviour throughout the entire conversion range, and the M_n curve showing only trends with over-estimation, especially at high conversions.

The observed behaviour can be explained as follows: At low conversions high molecular weight alternating copolymer is formed with progressive decrease of complex accumulated in the system. Therefore, slow decay in molecular weight is experienced, in direct proportion to the increase of statistical free monomer addition into the alternating sequences.

At intermediate conversion the change in the dominant propagation mechanism, from alternating to statistical, produces much shorter chains as a consequence of the rapid decrease in the observed propagation rate. As a result, the MWD broadens towards low molecular weights, decreasing the average values.

Finally, at high conversions the molecular weights of the chains formed start to increase again due to both the gel effect experienced by the system, and recombination of previously formed copolymer chains, due to the re-initiation/propagation/termination reactions of the macro-radicals (see Chapter 4). Consequently, the distribution now broadens slowly towards high molecular weights, and the averages remain nearly constant or increase slowly, depending on the conversions at which the gel effect starts and ends.

Corroboration of this picture, is given by the evolution of the entire molecular weight distribution (obtained by SEC), that is given for the system with f_{10}=0.8, at 105°C, in figure 6.16.

Figure 6.17, shows the effect of f_{10} on the development of M_w, for bulk S-NPMI copolymerization with bifunctional initiator [TBPCC]=0.01 M/L, at 130°C. In this figure the curves for f_{10}=0.8 and 0.7, showed the described behaviour and the expected initial higher M_w for higher NPMI concentration in the feed, followed by progressive decrease in M_w, owing to the fact that the expected increase in molecular weights during the gel effect is completely overcome by the larger molecular weights produced through donor-acceptor complex propagation, which dominates up to very high conversions.

The curve for the system with $f_{..}$=0.9 shows much lower initial molecular weights than the former, due to the lesser initial participation of complex propagation at this level of NPMI in the feed (see figure 6.8). The great increase in M_w at high conversions, after a slow decrease at low conversions, is brought about by the long nearly dead end thermal polymerization period experienced by this system (see figure 6.12), which under diffusion controlled termination conditions, produces high molecular weight copolymer which broadens the distribution towards high molecular weights.

The effect of bifunctional initiator concentration on the development of M_w with conversion, in bulk S-NPMI copolymerization at 130°C, is shown in figure 6.18. The observed behaviour at high initiator concentration has been explained above. Lower initiator concentrations produce higher initial molecular weights followed by a steeper decrease at intermediate conversions (with respect to the system with high [TBPCC]) caused by the faster decay in copolymerization rate (i.e. more free monomer participation). At high conversions, however, this system experiences auto-acceleration, thus broadening the distribution towards high molecular weights with the consequent slight increase in M_w observed.

The experimental and model results for the development of the copolymer composition with conversion (compositional drift path), in bulk S-NPMI copolymerization with [TBPCC]=0.01 M/L, at 130°C, is shown in figure 6.19, for the three different initial comonomer compositions studied. The model predictions shown are in good agreement with the experimental results throughout the entire conversion range. The observed behaviour is explained as follows.

At low conversions nearly alternating copolymer is formed through the dominating complex propagation during a conversion period roughly proportional to the double of the NPMI composition in the feed. As complex participation decreases, at intermediate conversions, the slope of the compositional drift path increases according to the extent and characteristics of the increasing statistical copolymerization

participation. At high conversions the compositional drift path approaches rapidly the initial feed composition according to the formation of styrene reach copolymer chains.

It is important to point out here that the observed compositional drift paths give further evidence of the adequacy of the proposed copolymerization scheme.

Figure 6.20 shows the evolution of the H-NMR spectrum with conversion, during S-NPMI bulk-copolymerization (f_{10}=0.8) with bifunctional initiator [TBPCC]=0.01 M/L, at 105°C. From the chemical structures of styrene and NPMI monomers, shown in Chapter 2, note that NPMI copolymer units bear two aliphatic protons (CH) and five aromatic protons (CH), whereas styrene units bear one aliphatic proton (CH), one aliphatic proton (CH_2) and five aromatic protons (CH). Accordingly in this figure it can be seen:

a) The similarity of the spectra at low and intermediate conversions shows that little compositional changes occur within this conversion range.

b) The increase in the area of the aliphatic CH_2 protons (peak about 1.85 ppm), along with the decrease in the area of aliphatic protons CH (peak about 2.25 ppm), at high conversions, shows that most of the compositional changes take place within this conversion range owing to an increase in the styrene concentration in the copolymer.

Since no reported spectra interpretation for this copolymer was found in the literature surveyed, according to the guidelines given by Dr. Harold Stover (Chemistry Department McMaster University), the interpretation of the H-NMR spectra in this study, was performed by quantifying the ratio of all aromatic (peak about 7.0 pmm) to aliphatic protons observed (ratio = 1.67 for styrene units and 2.5 for NPMI units), thus establishing the copolymer composition by a mol balance from this ratio.

These values were then double-checked by calculating the composition from the ratio of CH to CH_2 proton areas of the spectra, corrected for molar participation of each unit. Although both methods yielded very similar results (largest difference of F_1 calculated < 2%), the compositions computed from the first method were considered more reliable owing to the large overlapping of the aliphatic CH and CH_2 protons areas. Therefore, all the experimental copolymer compositions reported in this study were calculated using this procedure.

The experimental and model results for the development of T_g with conversion in bulk S-NPMI copolymerization with [TBPCC]=0.01 M/L, at 130°C, for the three different initial feed compositions studied, are shown in figure 6.21.

For the system with f_{10}=0.9, note how the model predicts the formation of high T_g copolymer up to 75% conversion, and formation of low T_g copolymer from 45% to terminal conversion. While the development of the low T_g fraction of the copolymer was well represented by the model, the small fraction of high T_g copolymer expected to be formed at high conversions, was not observed at conversions above 50%. This may be interpreted as the hard fraction of the chains becoming more mobile due to their progressive chemical binding to highly mobile low T_g segments, formed later on in the reaction, with the consequent over-all thermal behaviour of the low T_g larger fraction of copolymer.

For the system with f_{10}=0.8, the model overestimates the observed high T_g of the hard fraction of copolymer by 4 to 5 degrees in most of the conversion range.

This, however, may be considered as reasonable agreement given the high T_g's observed (largest difference < 2.5 %). For this system the model predicts the formation of a small fraction (< 7 mol%) of soft copolymer at conversions above 84%, however, such small fraction was not observed in the experimental determinations.

The system with f_{10}=0.7, showed very good agreement between model and experimental results throughout the entire conversion range. In this system the single high T_g expected was observed to decrease from the estimated value for perfectly alternating copolymer (T_{galt} = 222.07°C) at low conversions, to a value of T_{ghard}=215.67°C at terminal conversion.

The onset of the melt transition for all these copolymers was found to vary little about 265°C (T_m=266.7±4.76°C). This allowed the temperature for the extrusion experiments in the third experimental phase, to be set to 275°C, which is well within the limits of this processing operation. Note that the onset of the melting is quite close to the glass transition temperature of the hard copolymers (less than 50°C difference).

These results show that S-NPMI copolymers of very high glass transition temperature (T_g > 212°C) can be synthesized in bulk from initial feed compositions between 20 and 30 mol% of NPMI. Note that the addition of only 20 mol% of NPMI to the styrene system raises the T_g of the product by more than 110°C.

To conclude the optimization research phase discussion, the model results for the evolution of the multi-segment copolymer structure with conversion, characterized by the number average number of segments per copolymer chain, at all six experimental conditions, are shown in figure 6.22.

Note in this figure the increase in number of segments per copolymer chain as the polymerization temperature increases. This is due to the larger macro-initiator decomposition and, therefore recombination, promoted at higher temperatures, at similar conversion levels. Note also that the system at f_{10}=0.8 and T_p=105°C, which may be the most attractive for suspension copolymerization reaches at value of S_n=1.62 at terminal conversion.

In what follows the model parameter estimation procedure followed, is described.

6.4.4 Model Parameter Estimation

With the exploratory phase completed, the model parameter estimation was carried out as follows.

First, all bifunctional initiator (TBPCC) parameters as well as those involving two styrene units (monomer and radicals) were taken as in Chapter 5 (see Table 5.5).

Then, from the NPMI homopolymerization results the values of $K_p/K_{tc}^{1/2}$ measured, were separated into K_{22} and K_{tc22} by setting $K_{tc22}=K_{tc11}$, and running an exponential regression with the two values of K_{22} obtained at 105 and 130°C, respectively, yielding the following temperature dependence of K_{22}:

$$K_{22} = 4.301 \times 10^5 \exp(-2290/RT) \qquad \text{(L/Mol-min)}$$

The self transfer to monomer rate constant K_{fm22}, was established from the experimental data by non-linear regression of the observed M_n and M_w, at X=0, with the τ, β theoretical values of these averages, neglecting termination by disproportionation and any other transfer reaction. The computed value showed to be consistently about 20 times larger than that for polystyrene at the same temperatures, with which the following expression was obtained:

$$K_{fm22} = 1.225 \times 10^{10} \exp(-13450/RT) \qquad \text{(L/Mol-min)}$$

From the limiting conversions exhibited by the NPMI homopolymerization at both temperatures, and the polymer glass transition temperature observed (603.15°K), an operative T_{g2} for this monomer was calculated through a Fox relationship as: T_{g2} = 201.15°K.

All these values, along with the temperature dependent density functions for NPMI monomer and polymer established experimentally, were set into the homopolymerization through bifunctional initiators simulation program BIFUN [Villalobos et.al.(1991)], which was run interactively with

the non-linear parameter estimation subroutine UWHAUS, to find the free volume parameters that best fit both the experimental conversion histories and limiting average molecular weights.

To minimize the number of simulation runs, the values of the parameters δ, M and N (see equations 4.117 to 4.119 in Chapter 4) were set as in the previous studies to 0.5 and 1.75, and the values of polystyrene for K_3, A, B and V_{fcr2} were taken as initial guesses [Hamielec et.al.(1987), Marten and Hamielec (1982)]. Through this procedure, the optimal values for these parameters found were:

$$K_3=6.55\ \exp(1929/T);\ A=0.265;\ VF_{crNPMI}=0.0453;\ \text{and}\ B_2=0.6.$$

Note that the gel effect parameters are very similar to those of SAMS copolymerization, and that the glassy effect parameter B_2 reflects the slow decay in propagation rate in the vicinity of the glass transition of the polymer/monomer mix, exhibited by poly-NPMI.

Next, the four reactivity ratios (r_1, r_2, β_1, and β_2) and the ratio K_c/K_{eq}, were estimated first at 105°C, from the experimental data of the evolution of the accumulated copolymer composition and evolution of the observed $K_p[R]$ with conversion, by solving the differential form of the general copolymer composition equation, developed in Chapter 4, for simultaneous statistical/donor-acceptor copolymerization (eq. 4.126), within the non-linear parameter estimation subroutine UWHAUS.

This proved to be an extremely complex process, inasmuch as a one dimensional grid solution for initial values of the K_c/K_{eq} had to be run for each determination, after setting the initial production rate of donor-acceptor complex R_{co} to be 2 times the largest R_p observed at zero conversion, in order to estimate the fraction of donor-acceptor complex in the mix for each K_c/K_{eq} value tested. The values estimated for R_{co} are of the same order of magnitude as those calculated from the experimental data for the system styrene-maleic anhydride [Tsuchida and Tomono (1971)].

The minimum variance results yielded values of K_c=0.1 L/Mol-min K_{eq}=0.33; $r_1=K_{11}/K_{12}$=0.225, $r_2=K_{22}/K_{21}$=0.200, $\beta_1=K_{1c}/K_{12}$=17.0, and $\beta_2=K_{2c}/K_{21}$=20.0.

Owing to the high correlation between parameters found, especially between the four reactivity ratios, the estimation of these model parameters at 130°C was performed following the same procedure after fixing the values of β_1 and β_2 to 17.0 and 20.0, respectively. At this temperature, the best fit parameters found were: K_c=0.5 L/Mol-min, K_{eq}=0.25, r_1=0.155, and r_2=0.097.

From these values the expressions for temperature dependence for each parameter, introduced in the simulation program BICOP, were found by exponential regression, as:

$$K_c = 1.869 \times 10^{10} \exp(-19501/RT) \quad \text{(L/Mol-min)}$$

$$K_{eq} = 3.75 \times 10^{-3} \exp(1693/T)$$

$$r_1 = 5.523 \times 10^{-4} \exp(2273/T)$$

$$r_2 = 1.711 \times 10^{-6} \exp(4413/T)$$

$$\beta_1=17.0 \; ; \quad \beta_2=20.0$$

All these relations are valid only in the 105 to 130°C range.

Finally, all the above parameters, along with the physical properties of monomers and polymer, and the empirical copolymer glass transition model, required by the kinetic and microstructure models, were introduced into the simulation program BICOP. The program was run interactively with the non-linear parameter estimation subroutine to find the copolymerization gel effect parameters and cross termination by combination rate constant (K_{tc12}) that best fit the experimental monomer conversion histories and molecular weight distribution development.

Through this procedure, the following values for these parameters were found:

$$K_{tc12} = 1.00 \times 10^{12} \exp(-1677/RT) \quad \text{(L/Mol-min)}$$

$$K_j = 7.5 \exp(1929/T) \; ; \quad A = 0.275$$

The summary of all the model parameter values, is shown in Table 6.4, below. With all the model parameters adjusted, all the simulation (model) results shown in the three experimental phases of this study were performed.

Table 6.4

Values of the Parameters Used in the Simulations

Initiation Chemical (TBPCC) and Thermal	
$K_{d1} = 2.117 \times 10^{14} \exp(-28064/RT)$; $f_1 = 0.8$	Min^{-1}
$K_{d2} = 3.850 \times 10^{20} \exp(-40022/RT)$; $f_2 = 0.7$	Min^{-1}
$K_{ths} = 1.314 \times 10^{7} \exp(-27440/RT)$	Min^{-1}
Propagation	
$K_{11} = 6.128 \times 10^{8} \exp(-7068/RT)$	L/mol-min
$K_{22} = 4.301 \times 10^{5} \exp(-2290/RT)$	L/mol-min
$r_1 = K_{11}/K_{12} = 5.523 \times 10^{-4} \exp(2273/T)$	105 -130°C
$r_2 = K_{22}/K_{21} = 1.711 \times 10^{-6} \exp(4413/T)$	105 - 130°C
$\beta_1 = 17.0$; $\beta_2 = 20.0$; $K_{eq} = 1.869 \times 10^{-3} \exp(1693/T)$	105 - 130°C
$K_c = 1.869 \times 10^{10} \exp(-19501/RT)$	L/mol-min
Termination	
$K_{tc11} = 7.55 \times 10^{10} \exp(-1677/RT)$	L/mol-min
$K_{tc12} = 1.00 \times 10^{12} \exp(-1677/RT)$	L/mol-min
$K_{tc22} = 7.55 \times 10^{10} \exp(-1677/RT)$	L/mol-min
Transfer to Monomer	
$K_{fm11} = K_{fm21} = 6.128 \times 10^{8} \exp(-13450/RT)$	L/mol-min
$K_{fm22} = K_{fm12} = 1.225 \times 10^{10} \exp(-13450/RT)$	L/mol-min
Free Volume Variables (T_g in °K, α in 1/°K, d in Kg/L)	
$T_g = 184.95$; $\alpha = 0.001$; $d = 0.924 - 0.000918*T(°C)$	Styrene
$T_g = 201.15$; $\alpha = 0.001$; $d = 1.310 - 0.0011*T(°C)$	NPMI
$T_g = 113.30$; $\alpha = 0.001$; $d = 0.879 - 0.0005*T(°C)$	Toluene
T_g (see text); $\alpha = 0.00048$; $d = 1.145 - 0.000905*T(°C)$	Copolymer
Gel and Glassy Effect Parameters	
$K = 7.5\exp(1929/T)$; $\delta = 0$; $A = 0.275$; $M = 0.5$; $N = 1.75$ (gel effect)	
$VF_{crs} = 0.0465$; $VF_{crNPMI} = 0.0453$; $B_1 = 1.0$, $B_2 = 0.6$ (glassy effect)	

6.4.5 S-NPMI Suspension Copolymerization

From the optimization study, it is clear that the best balance of reaction rate-copolymer properties, within the constraints of suspension polymer syntheses explained in Chapter 1, is achieved at f_{10}=0.8, T_p=105°C, and bifunctional initiator [TBPCC]=0.01 M/L.

While higher initial concentrations of NPMI in the feed lead to only marginal increases in glass transition temperature, and produce polymerization rates which may be very difficult to control in large reactors, lower concentrations of NPMI lead to the formation of large amounts of lower T_g (112°C) copolymer, which is undesirable once proven that copolymers with 100°C higher glass transition may be synthesized at f_{10}=0.8. Moreover, the marginal increases in copolymer T_g and high polymerization rates observed at T_p=130°C, do not justify the use of higher temperatures.

To increase the limiting conversion of this selected system from 93%, to levels above 99%, the same two approaches as for the optimal S-AMS suspension copolymers were followed. These are, increasing the temperature after the initial limiting conversion has been reached, and using small amounts of solvent, as depressor of the glass transition temperature of the copolymerization mix.

With the aid of the simulation program BICOP, different temperature profiles were tested after one hour of polymerization at 105°C. Simulation results showed that 30 minutes at 140°C were sufficient to increase the terminal conversions above 99%. Therefore, this temperature profile and conditions were established as optimal suspension run S-NPMI-03-01.

Simulations of the selected system with variable amounts of toluene, introduced as solvent, were performed in order to reproduce the conversion history established for the first run, without changing sensibly the molecular weight distribution.

Conditions of 5 wt% toluene in the mix, and [TBPCC]=0.012 M/L were found to carry the copolymerization to conversions above 99%, and produce copolymer with M_w around the 200,000 target, after 90 minutes of polymerization at 105°C, with f_{10}=0.8. These conditions were set as optimal suspension run S-NPMI-03-01.

The reactor internal arrangement, operating conditions, and recipes used, were the same scaled-down conditions used in the studies of S/N-pentane and S-AMS copolymers. The same optimal suspension polystyrene system ([TBPCC]=0.01 M/L, T_p=105°C, [TCP]=7.5 g/L) was used like a reference, as before (see design and conditions in Table 6.3).

Figure 6.23 and 6.24, show the simulated monomer conversion history and molecular weight distribution development, respectively, for the optimal suspension runs of this study. Note from the conversion histories that the particle growth period ("sticky stage"), assumed for this copolymer system to occur at conversions roughly between 30 and 70%, lasts less than 15 minutes, which is half the time as that for the reference polystyrene system.

Based on the mechanism of particle formation and growth in suspension polymerization, it is known that shorter particle growth periods lead to the formation of smaller particles with narrower distributions. However, very high reaction rates, at a given polymerization temperature, enhance particle coalescence leading to rapid particle growth. The relative importance and balance of these two opposite effects, limits the mean particle size (MPS), and particle size distribution (PSD) of the beads formed [Villalobos (1989)]. For the suspension copolymer systems of this study both effects may be equally important in defining the final PSD of the product.

Following the conditions of the experimental design, both suspension copolymerization runs were successfully carried out. Spherical non aggregated beads, with a slight beige coloration, were obtained in both cases.

Figure 6.25 shows the experimental results for the effect of the imposed copolymerization rate on the particle size distribution (PSD) for these S-NPMI optimal suspension copolymerization runs. In this figure the distribution of the reference polystyrene system is also shown for comparison.

For the S/NPMI-03-01 suspension copolymerization system a mean particle size MPS=0.528 mm, with a coefficient of variation CV=0.327 were calculated from the observed final bead size distribution. Note that this values show smaller MPS and narrower PSD than the polystyrene reference system (MPS=.542 mm, CV=.361).

This means that the suspension stabilizing effect brought about by the reduction of the particle growth period, completely overcomes the adverse effects of enhanced particle coalescence caused by the extremely high initial copolymerization rates.

For the S/NPMI-03-02 suspension copolymerization system, bead sizes distributed with a MPS=.616 mm, and CV=0.353, were produced. This values indicate that the toluene-induced plasticization of the copolymer matrix both enhances slightly particle coalescence, and extends the particle growth period. These adverse effects, however, are minimal (the MPS increased less than 15% with respect to system 01) and easily controllable through the an increase in the suspension stabiliser (TCP) concentration.

Characterization of the beads, through the procedures described in the experimental section, showed terminal conversions above 98% for both products (slight model design over-estimation), M_w about 260,000 and 225,000 for products 1 and 2, respectively, and a single T_g about 212°C, for both suspension copolymers.

Table 6.5, summarizes the model designed and experimental results for MPS, PSD, terminal conversion, MWD, and T_g of the S-NPMI suspension copolymers synthesized.

Table 6.5

Summary of Suspension Copolymerization Results

RUN → VARIABLE	EXP REF. PS(*)	MODEL REF PS(*)	EXP SNPMI-03-01	MODEL SNPMI-03-01	EXP SNPMI-03-02	MODEL SNPMI-03-02
MPS (mm)	0.542	**	0.528	**	0.616	**
σ (mm)	0.196	**	0.173	**	0.217	**
CV=σ/MPS	0.361	**	0.327	**	0.353	**
CONV	0.9999	0.9998	0.9828	0.9903	0.9815	0.9916
Mn	83870	84998	67915	98777	56484	73569
Mw	203011	212415	258144	233676	226663	199319
T_g (°C)	98.60	97.06	211.75	207.36	211.18	206.77

* See Chapter 3 for reference system results.
** Model does not predict PSD.

Extrusion of the beads was carried out following the procedures described above. Opaque continuous extrudates with appreciable swelling ratio (die diameter/extrudate diameter) about 2.11, at the described conditions with a mean residence time in the extruder of 1.47 minutes, were obtained for both products. Toluene bubbling in the extrudate was observed at the die outlet, for the second product. This, however, does not represent a problem for large production of this copolymer since toluene should be eliminated before extrusion by devolatilization of the product.

The single T_g determined for both extrudates showed an increase of 0.81 and 1.49°C, for products 1 and 2, respectively, in comparison to the purified copolymer before extrusion (see Table 6.5). This may be due to further monomer exhaustion and chain recombination during extrusion, although the slight relative increases observed of less than 1%, may well be within the experimental error in DSC determinations.

Samples of the extrudates exposed to N_2 at 300°C for 5 and 10 hours, according to the procedures described above, were completely thermally stable at this temperature, since no mass losses were observed after the prescribed high temperature exposure times.

The T_g of the extrudates, after the high temperature exposure showed no sensible variation. This proves that no measurable chain degradation occurred during the high temperature exposure period. As a result the MWD distribution of the exposed extrudates was not re-determined.

Table 6.6 summarizes the copolymer bead extrusion and degradation results.

Table 6.6

Copolymer Extrusion and Degradation Results

SAMPLE S/NPMI-03-	BEADS T_g (°C)	EXTRUD T_g (°C)	MASS LOSS(%)* 5 hrs @300°C	MASS LOSS(%)* 10 hrs @300°C	BEADS Mw
1	211.75	212.56	0.000	0.000	258414
2	211.18	212.67	0.000	0.000	226663

* Results of sample characterization after exposure to the prescribed conditions (variations observed where only within the limit of precision of the analytical balance used).

6.5 Conclusions

Styrene/N-phenylmaleimide engineering copolymers having glass transition temperatures above 210°C, can be synthesized up to high conversions and high molecular weights through bifunctionally initiated suspension copolymerization.

Two optimal synthesis routes yielding the best balance of copolymer properties, copolymerization rate, and terminal conversions, when using 1,4-bis(tertbutyl peroxycarbo)cyclohexane as bifunctional initiator, and a monomer feed composition of 80/20 (S/NPMI mol%) were found.

The first synthesis route comprises a temperature program of 60 minutes at 105°C followed by 30 minutes at 140°C, and a bifunctional initiator concentration [TBPCC]=0.01 M/L.

The second synthesis route involves the initial addition of 5.0 wt% toluene, as depressor of the glass transition temperature of the copolymerization mix, and 90 minutes of polymerization at 105°C with [TBPCC]=0.012 M/L.

Both suspension copolymerization systems were completely stable, even at the extremely high initial copolymerization rates. The copolymer beads obtained through the first synthesis route showed smaller mean particle size and narrower distribution than the reference polystyrene system. The copolymer beads obtained through the second synthesis route showed slightly higher mean particle size yet narrower distribution, than the reference.

Taking into account that the reference suspension polystyrene system has been successfully synthesized in large reactors, it follows that these similarly (or more) stable suspension copolymer systems can also be produced at such volumes (see Chapter 3). Therefore the scale-up to commercial production is entirely feasible.

In addition, possible limitations in the maximum dispersed phase hold-up manageable for these syntheses in large reactors, due to heat removal rate constraints, are "affordable" provided the extraordinarily short batch times necessary for these syntheses (i.e. 90 minutes versus more than 3 hours for the reference polystyrene system). Moreover, the outstanding thermal characteristics of these S-NPMI copolymers, may justify low (and highly controllable) disperse phase hold-ups, for low volume commercial production.

The suspension copolymers synthesized, bearing T_g about 212°C, and T_M about 265°C, were processable through extrusion at moderate temperatures (275°C), and thermally stable at 300°C. Therefore, it is realistic to state that these copolymers may be employed in extrusion (and very likely injection molding) engineering applications to temperatures up to 200°C.

The fact than only 20 mol% NPMI in the feed is necessary to so outstandingly enhance the polystyrene thermal characteristics, going from a polymer commodity to an engineering copolymer approaching the thermal behaviour of high performance polymers, makes this copolymer extremely attractive for commercial production.

The kinetic and microstructural models integrated into the simulation program BICOP, could reasonably accurately explain the behaviour observed for monomer conversion history, copolymer composition and glass transition temperature development, throughout the entire very wide experimental range studied.

With respect to the extremely complex evolution of the molecular weight distribution with conversion in this type of copolymerization, the simulation program follows the experimental trends and gives ball park estimates (within 20% difference) exclusively for M_w.

Finally, in addition to the suspension copolymers synthesized, this study gives the theoretical and experimental bases for the synthesis of high T_g S-NPMI engineering copolymers, through bulk and solution free radical copolymerization with bifunctional initiators, in a wide composition and temperature ranges.

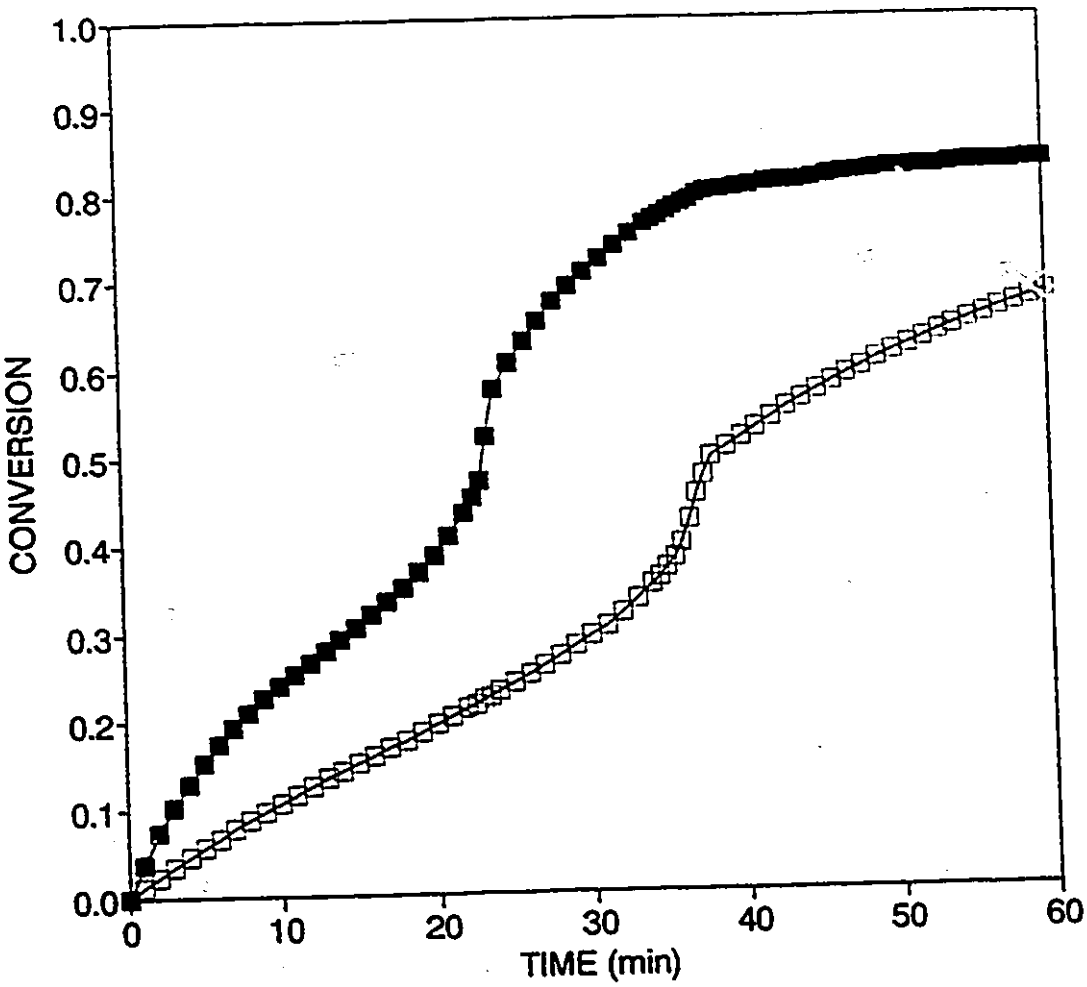

Fig. 6.1. Experimental (DSC) results for monomer conversion history in Bulk poly-NPMI, bifunctionally initiated with 2 wt% TBPCC, at 105°C (□); and 130°C (■).

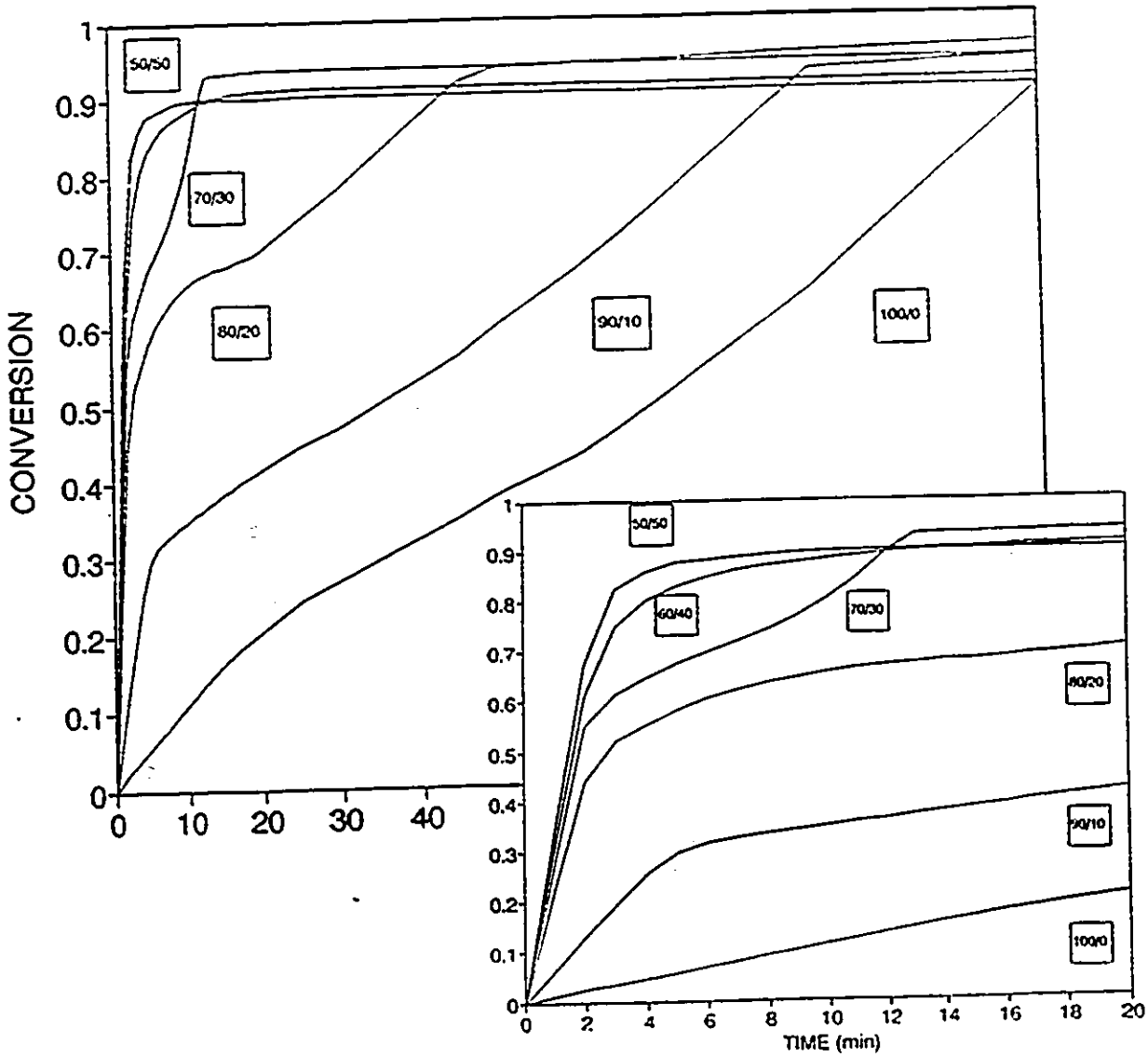

Fig. 6.2. Effect of comonomer feed composition on monomer conversion history for S/NPMI bulk copolymerization with bifunctional initiator [TBPCC]=0.01 M/L, at 105°C. Parameter monomer feed composition (mol% S/NPMI).

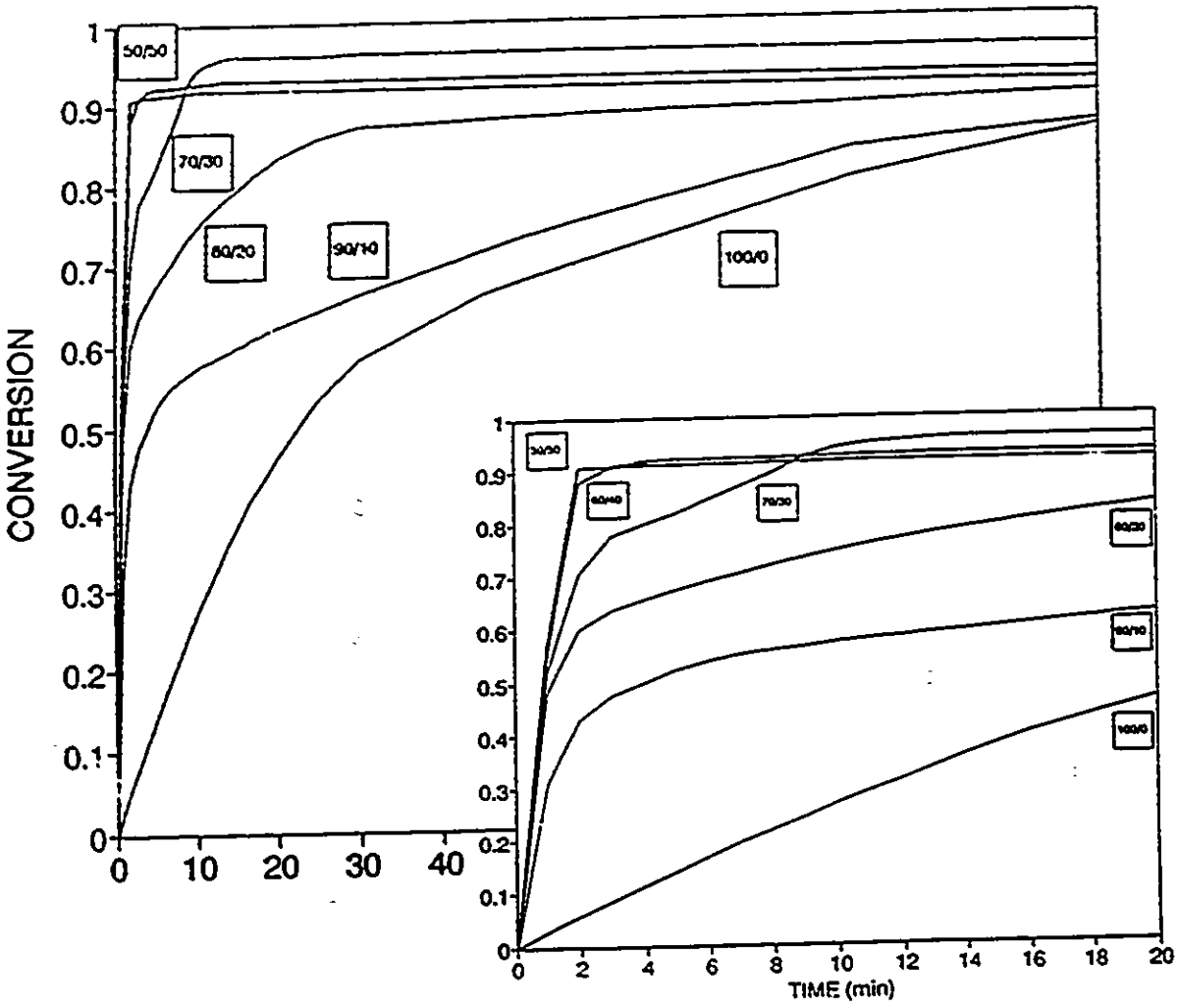

Fig. 6.3. Effect of comonomer feed composition on monomer conversion history for S/NPMI bulk copolymerization with bifunctional initiator [TBPCC]=0.01 M/L, at 130°C. Parameter monomer feed composition (mol% S/NPMI).

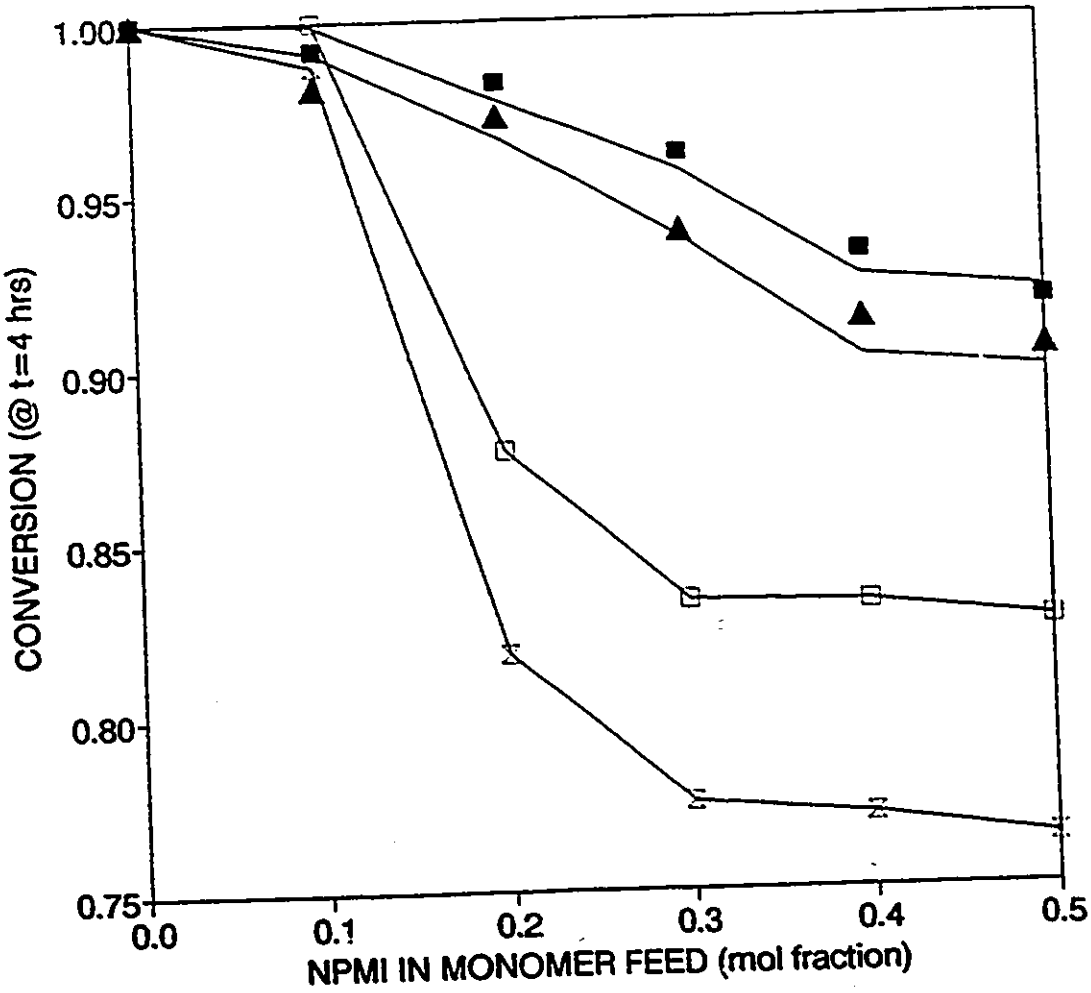

Fig. 6.4 Effect of comonomer feed composition on terminal conversion reached after 4 hours of S/NPMI bulk copolymerization with bifunctional initiator [TBPCC]=0.01 M/L. Experimental results at 130 °C (■), and 105°C (▲). BICOP model predictions (——). Expected terminal conversions (Fox model) at 130°C (■) and 105°C (X)

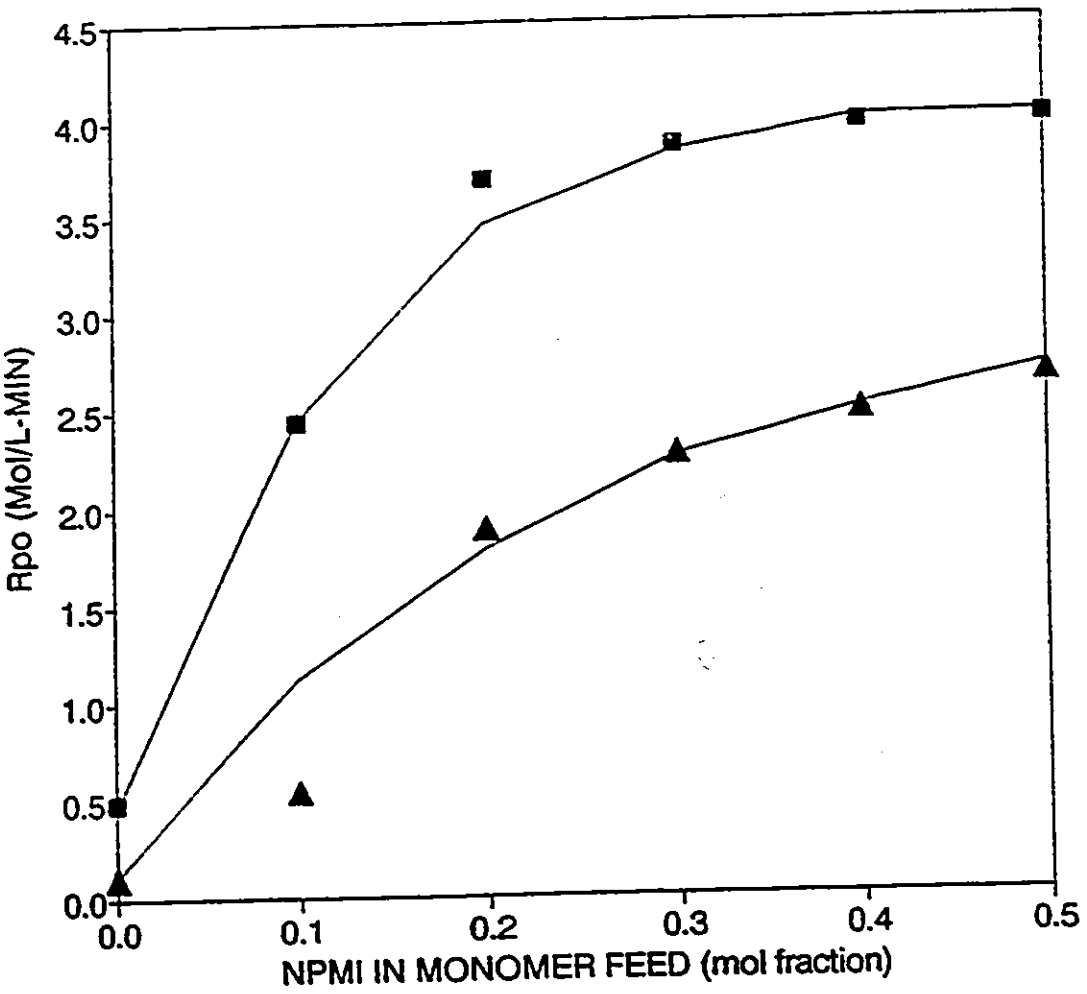

Fig. 6.5. Effect of comonomer feed composition on initial copolymerization rate for S/NPMI bulk copolymerization with bifunctional initiator [TBPCC]=0.01 M/L. Experimental results at 130°C(■) and 105°C (▲). Model predictions (——).

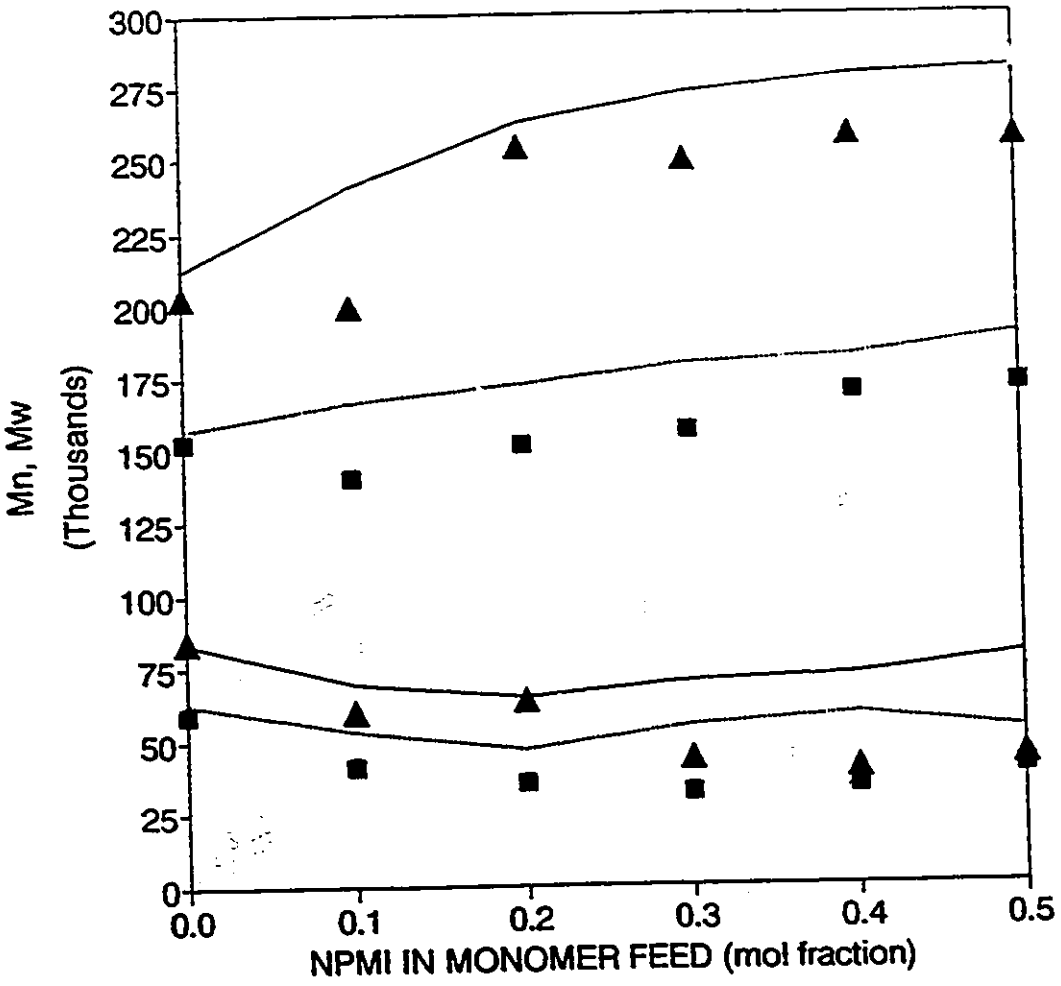

Fig. 6.6. Effect of comonomer feed composition on MWD of S/NPMI copolymers at terminal conversion. Bulk copolymerization with bifunctional initiator [TBPCC]=0.001 M/L. Experimental M_n and M_w at 130°C (■), and 105°C(▲). Model predictions at 130°C(---), and 105°C (——).

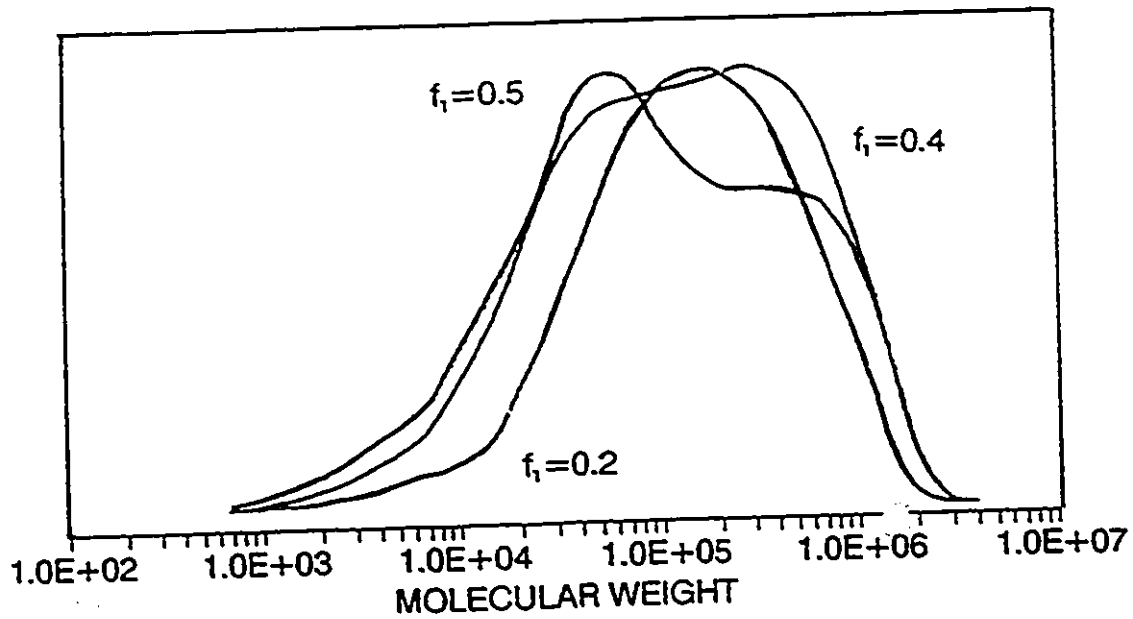

Fig. 6.7. Shape of the MWD distribution of S/NPMI copolymers at terminal conversion for different feed compositions. Bulk copolymerization with [TBPCC]=0.01 M/L, at 105°C. parameter f_{10}.

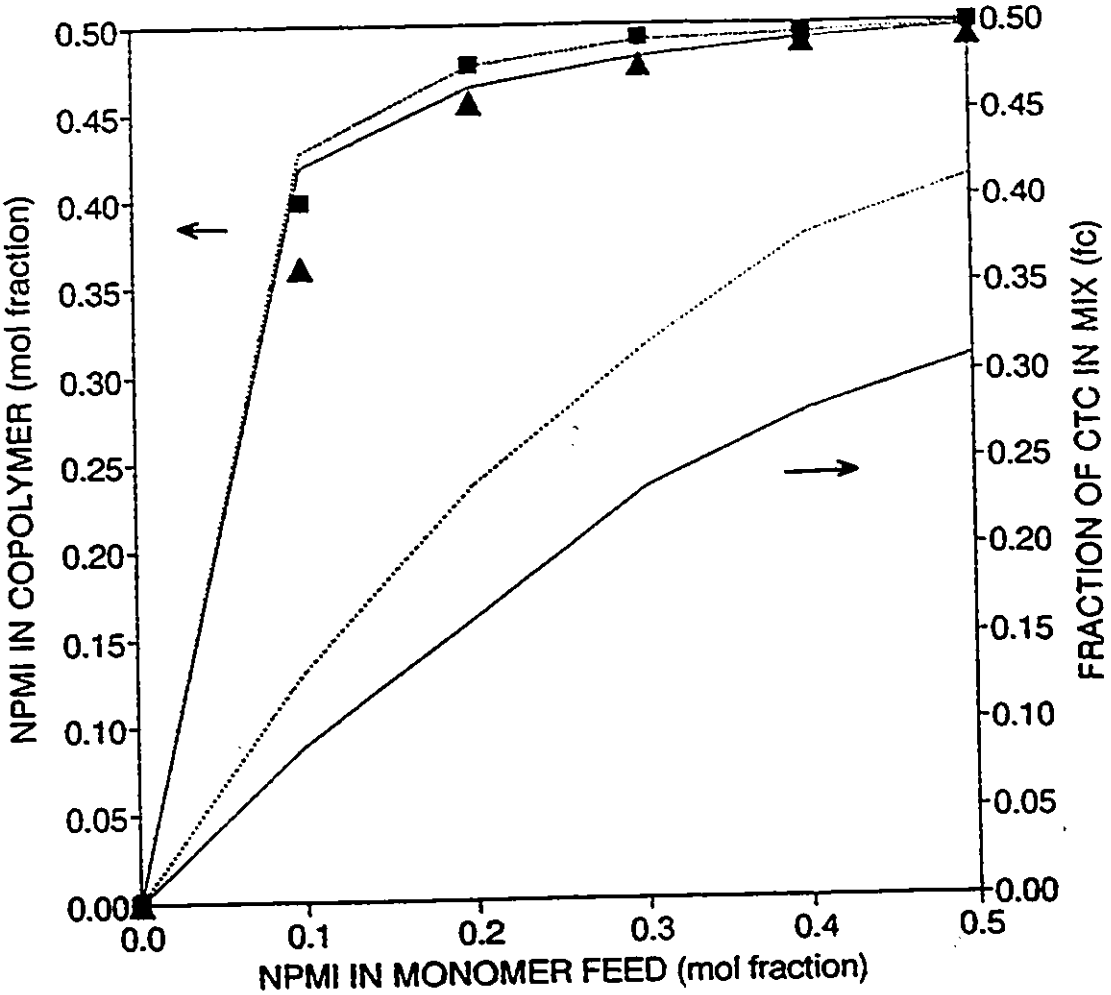

Fig. 6.8. Effect of the monomer feed composition on the instantaneous copolymer composition in S/NPMI bulk copolymerization with [TBPCC]=0.01 M/L. Experimental results at 130°C (■) and 105°C (▲). Model results at 130°C (---) and 105°C (——).

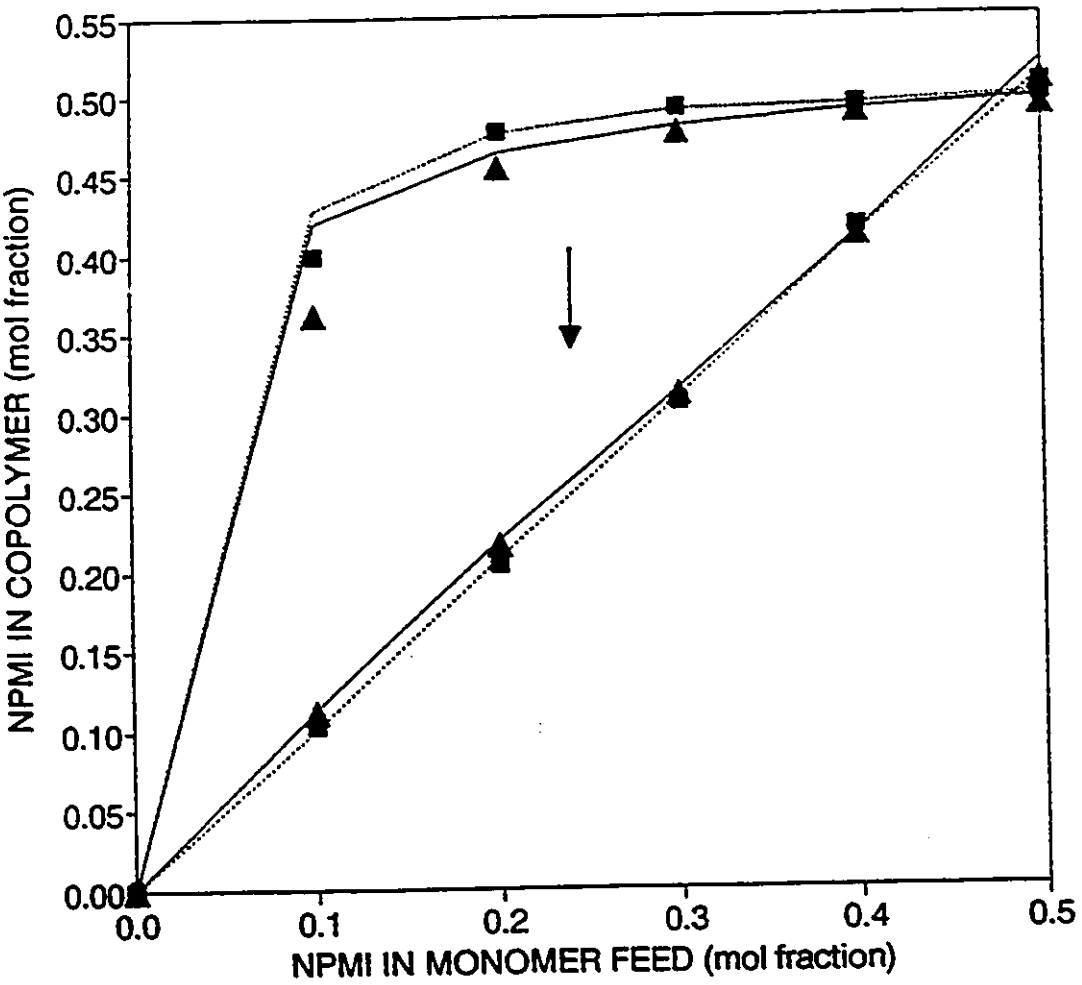

Fig. 6.9. Effect of comonomer feed composition on observed compositional drift of S/NPMI copolymers. Bulk copolymerization with bifunctional initiator [TBPCC]=0.01 M/L. Experimental initial (X=0) and accumulated (X=Xt) copolymer composition at 130°C (■) and 105°C (▲). Model predictions at 130°C(---), and 105°C (——).

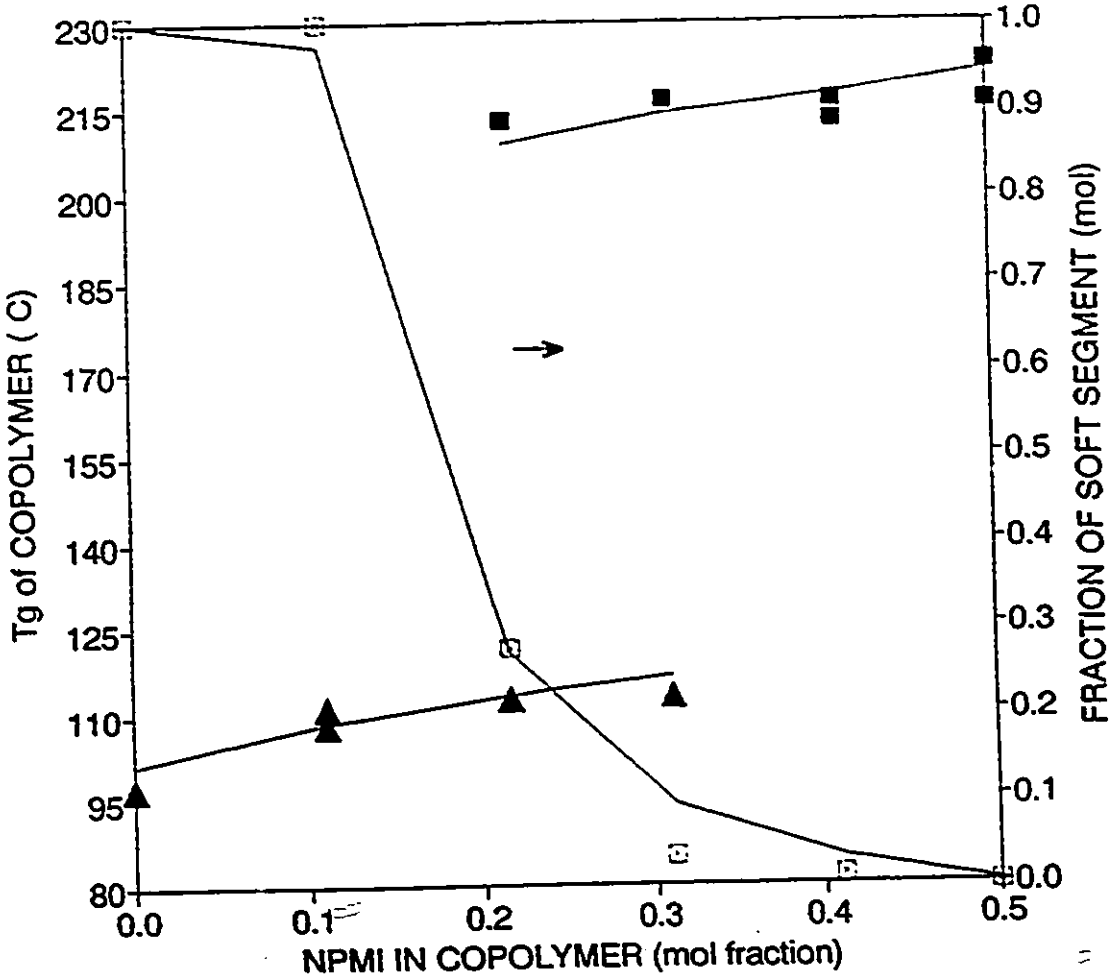

Fig. 6.10. Effect of S/NPMI copolymer composition at Xt, on glass transition temperature and fraction of soft copolymer. Bulk copolymerization with bifunctional initiator [TBPCC]=0.01 M/L, at 105°C. Experimental results for T_{ghard} (■), T_{gsoft} (▲), and f_{soft} (⊡). Model predictions (——).

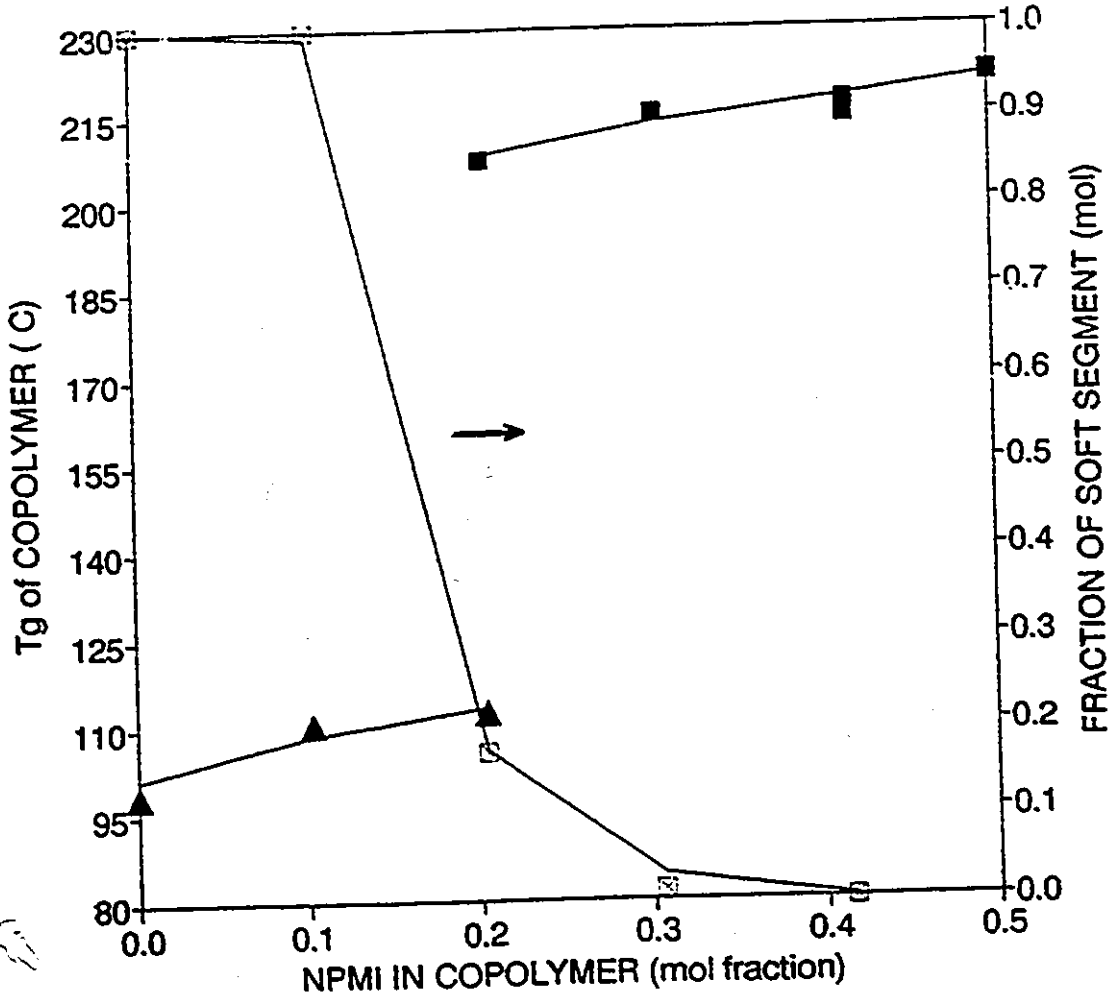

Fig. 6.11. Effect of S/NPMI copolymer composition at Xt, on glass transition temperature and fraction of soft copolymer. Bulk copolymerization with bifunctional initiator [TBPCC]=0.01 M/L, at 130°C. Experimental results for T_{ghard} (■), T_{gsoft} (▲), and f_{soft} (⊠). Model predictions (——).

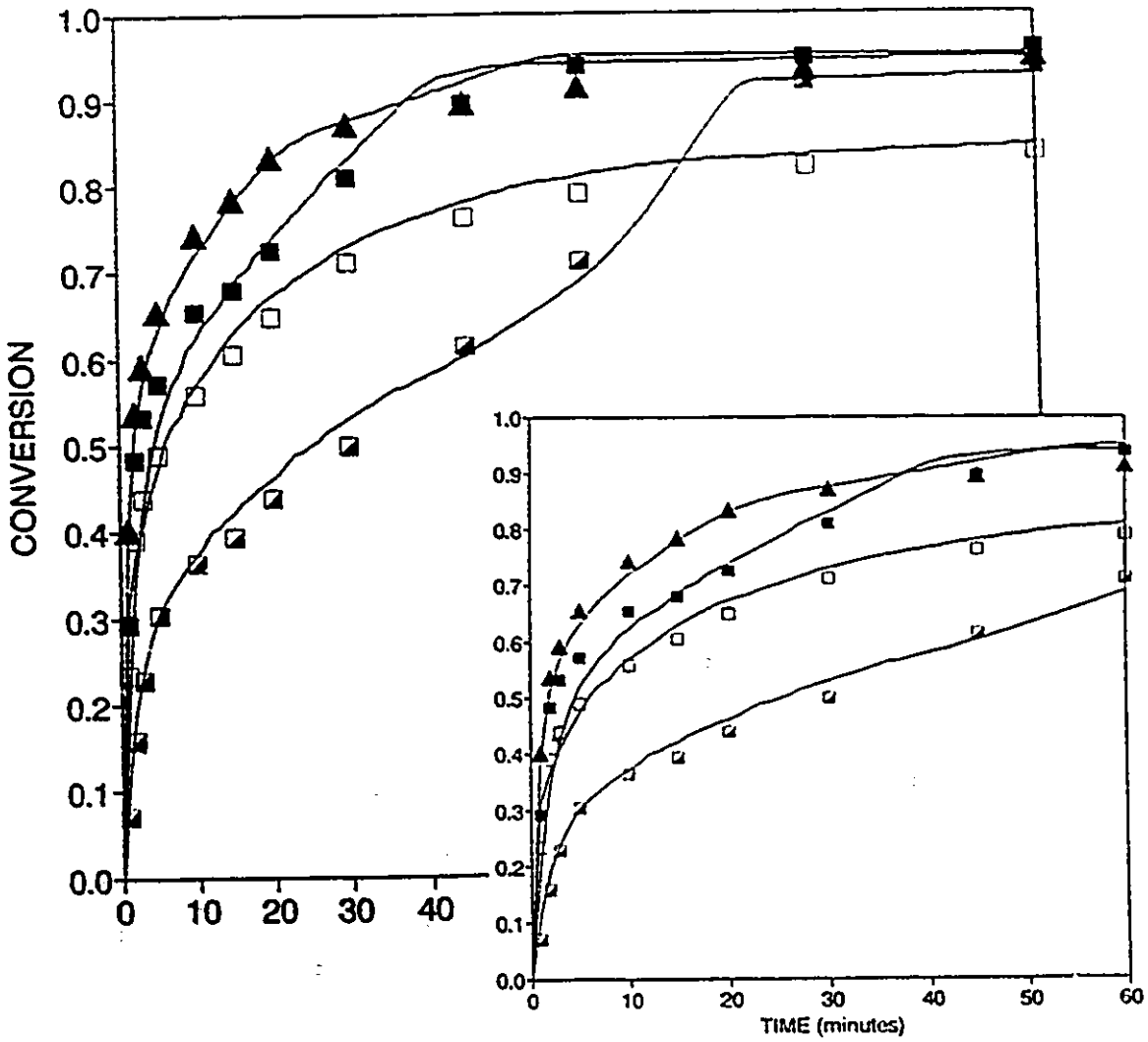

Fig. 6.12. Effect of polymerization temperature on monomer conversion history in S/NPMI bulk copolymerization with [TBPCC]=0.01 Mol/L. Experimental results for: T_p=105°C, f_{10}=0.9 (◪); T_p=130°C, f_{10}=0.9 (□); T_p=105°C, f_{10}=0.8 (■); T_p=130°C, f_{10}=0.8 (▲). Model predictions (——).

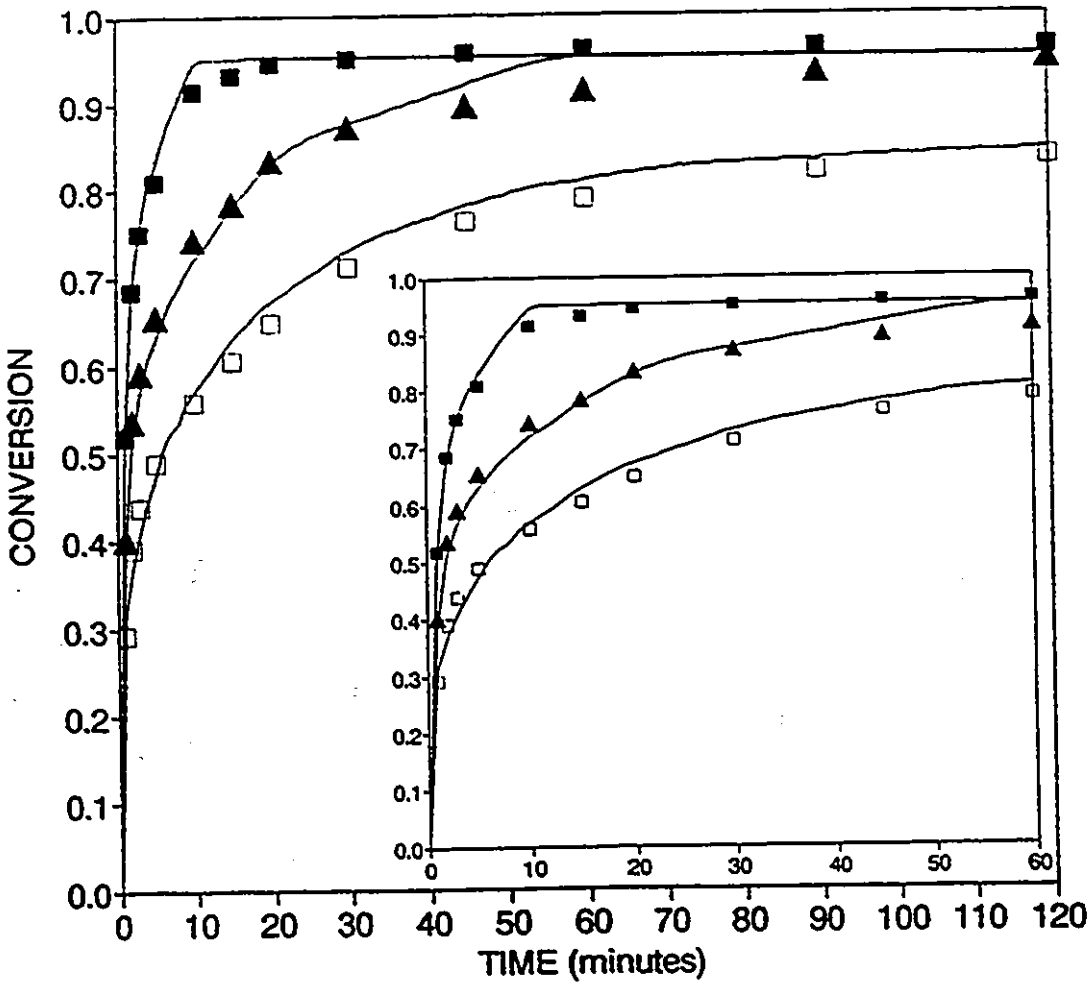

Fig. 6.13. Effect of monomer feed composition on monomer conversion history in S/NPMI bulk copolymerization with [TBPCC]=0.01 Mol/L, at 130°C. Experimental results for: f_{10}=0.9 (□); f_{10}=0.8 (▲); and f_{10}=0.7 (■). Model predictions (——).

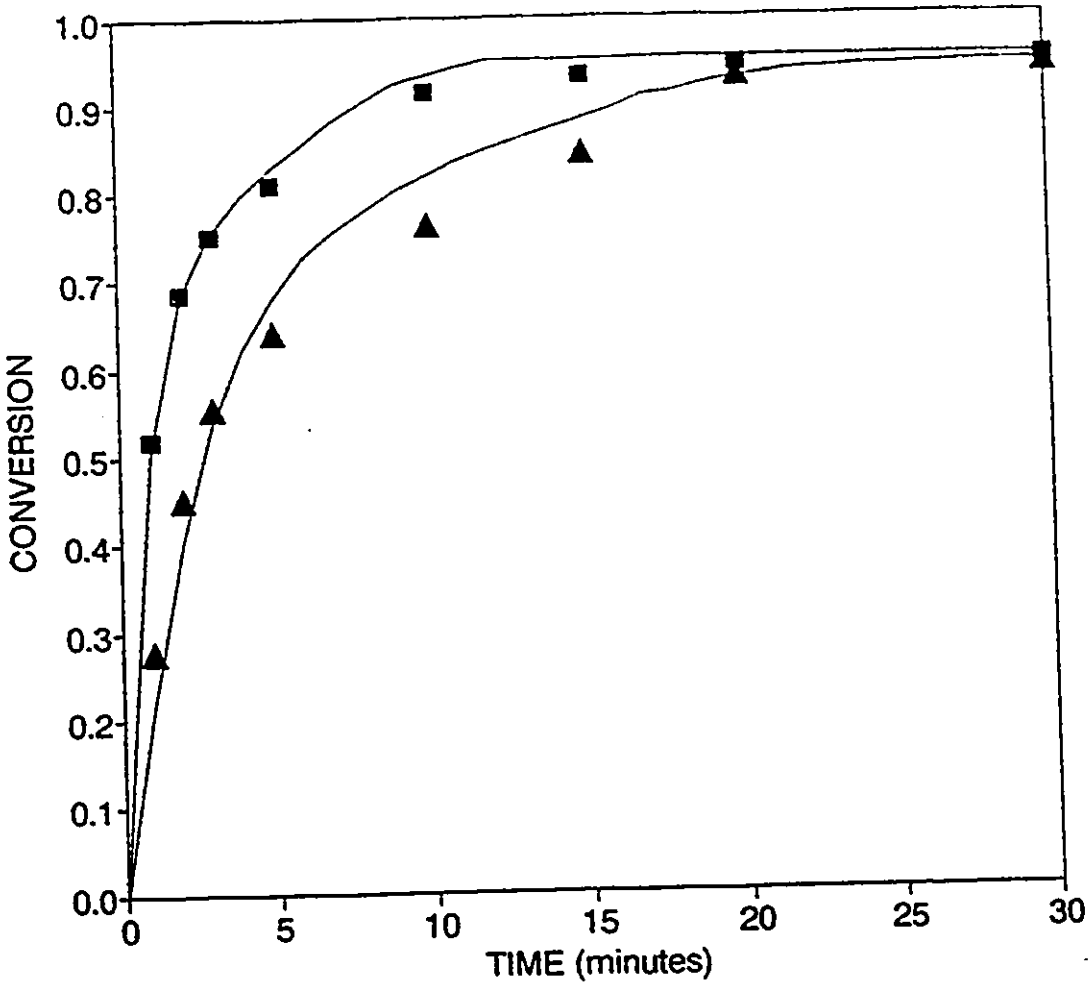

Fig. 6.14. Effect of bifunctional initiator concentration on monomer conversion history in S/NPMI bulk copolymerization with f_{10}=0.7, at 130°C. Experimental results for: [TBPCC]=0.01 M/L (□); and [TBPCC]=0.005 M/L (▲). Model predictions (——).

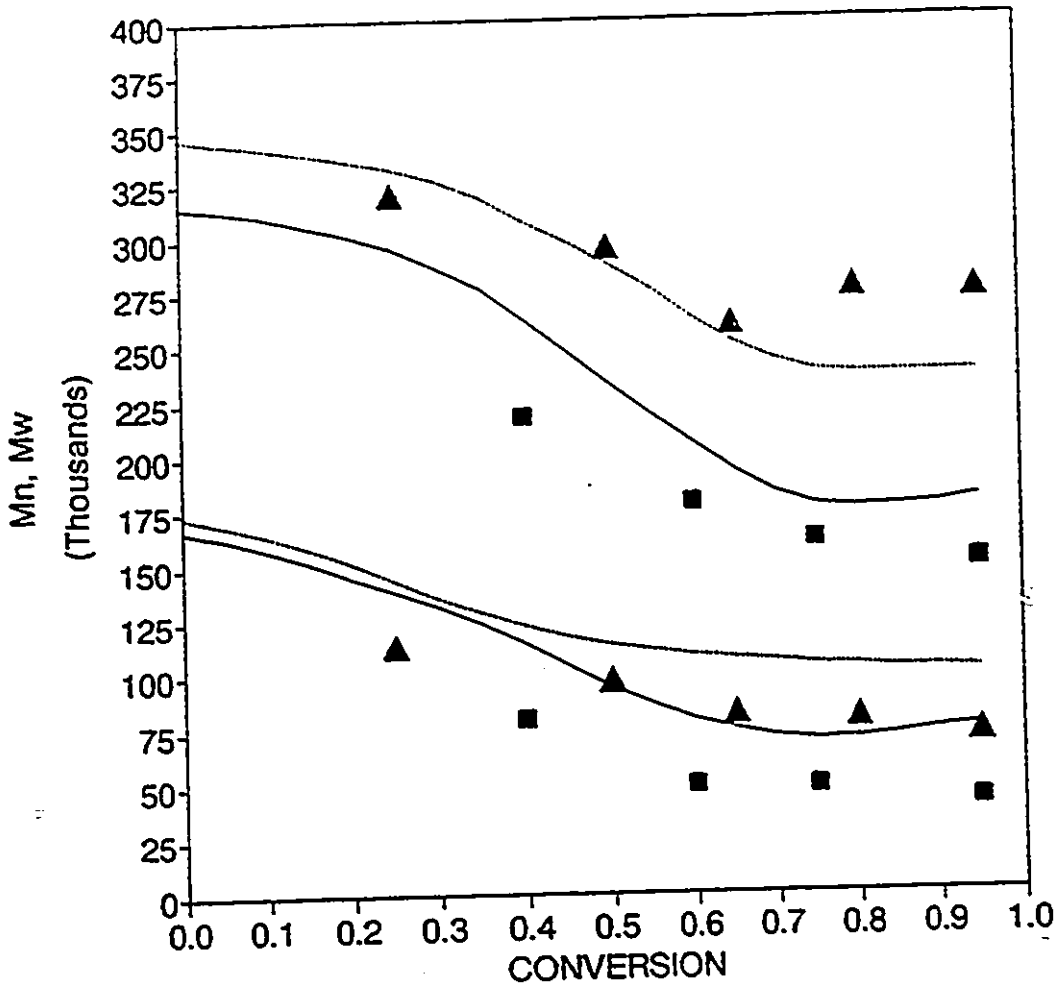

Fig. 6.15. Effect of polymerization temperature on MWD development, in bulk S/NPMI copolymerization at f_{10}=0.8, [TBPCC]=0.01 M/L. Experimental results for M_n and M_w at 130°C (■); and 105°C (▲). Model predictions at 130°C (——); and 105°C (---)

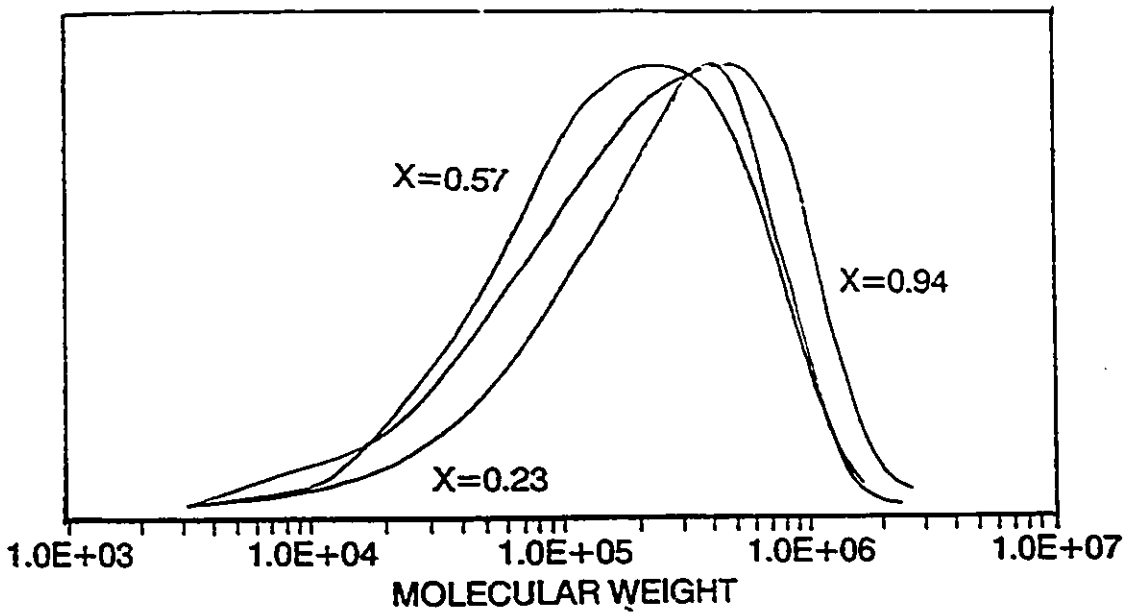

Fig. 6.16. Evolution of the molecular weight distribution with conversion in S/NPMI bulk copolymerization at f_{10}=0.8, [TBPCC]=0.01 M/L. and 105°C. Experimental SEC curves.

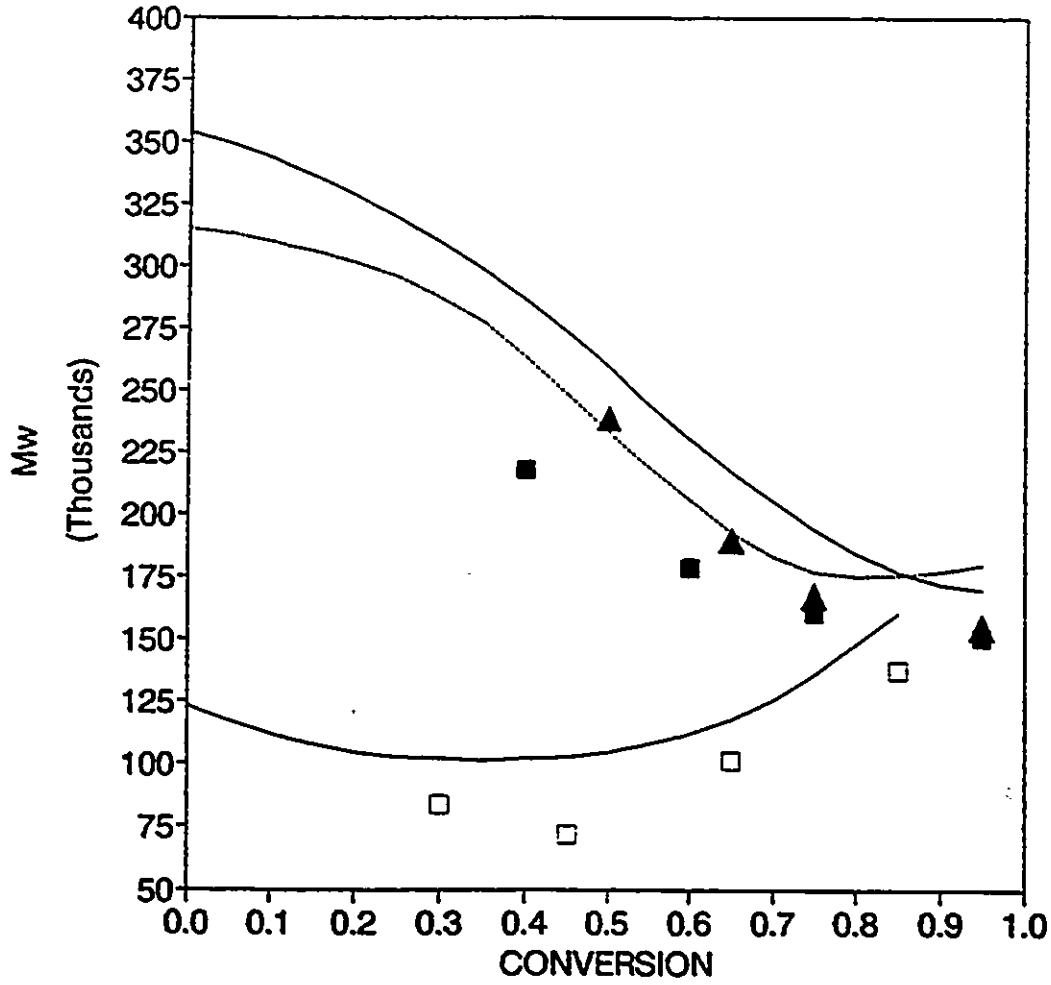

Fig. 6.17. Effect of monomer feed composition on the development of weight average molecular weight, in S/NPMI bulk copolymerization with [TBPCC]=0.01 Mol/L, at 130°C. Experimental results for M_w at: f_{10}=0.9 (□); f_{10}=0.8 (■); and f_{10}=0.7 (▲). Model predictions at; f_{10}=0.9, 0.7 (——); and f_{10}=0.8 (---).

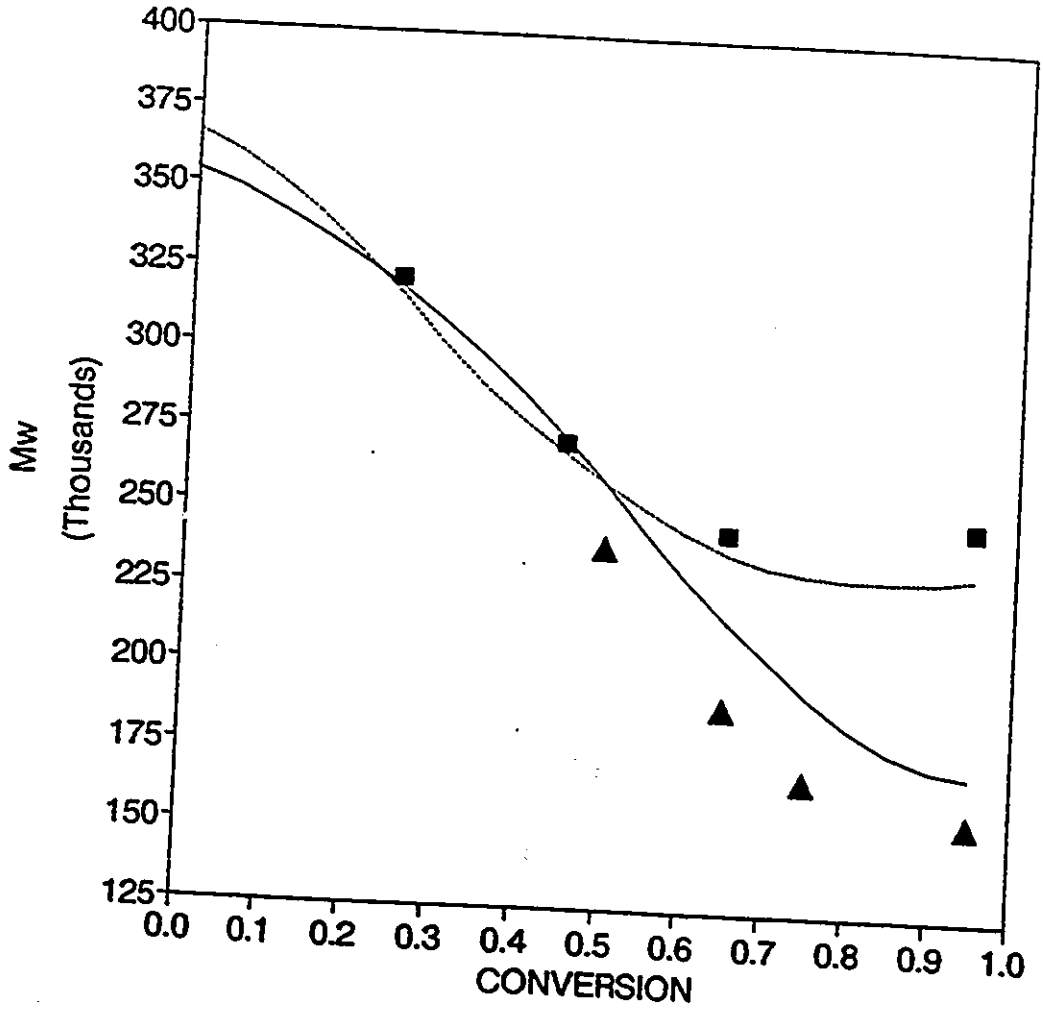

Fig. 6.18. Effect of bifunctional initiator concentration on the development of weight average molecular weight, in S/NPMI bulk copolymerization with f_{10}=0.7, at 130°C. Experimental results for [TBPCC]=0.01 (▲); and [TBPCC]=0.005 M/L (■). Model predictions at [TBPCC]=0.01 (——) and [TBPCC]=0.005 M/L (---).

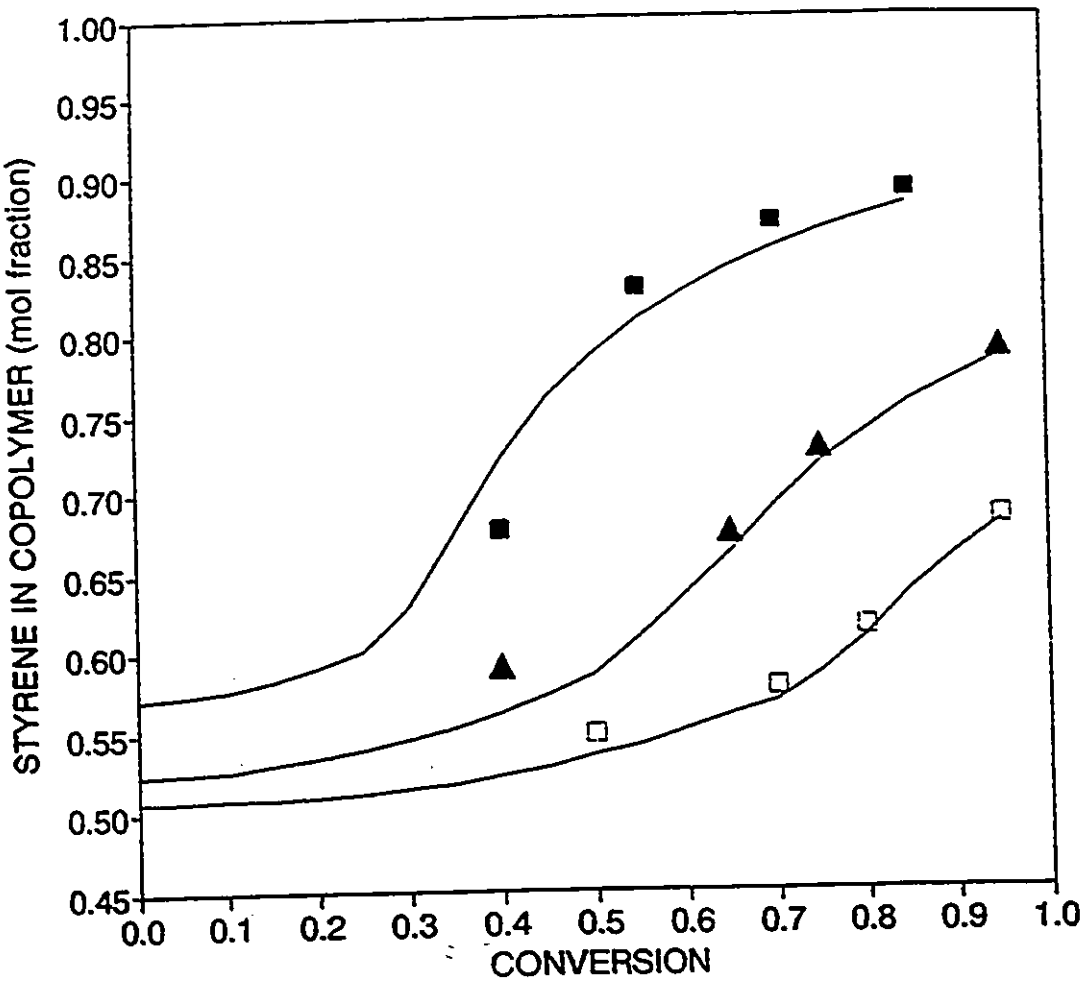

Fig. 6.19. Effect of monomer feed composition on the development of copolymer composition, in Bulk S/NPMI copolymerization with [TBPCC]=0.01 M/L, at 130°C. Experimental results of F_1 vs X at: f_{10}=0.9 (■); f_{10}=0.8 (▲); and f_{10}=0.7 (□). Model predictions (——).

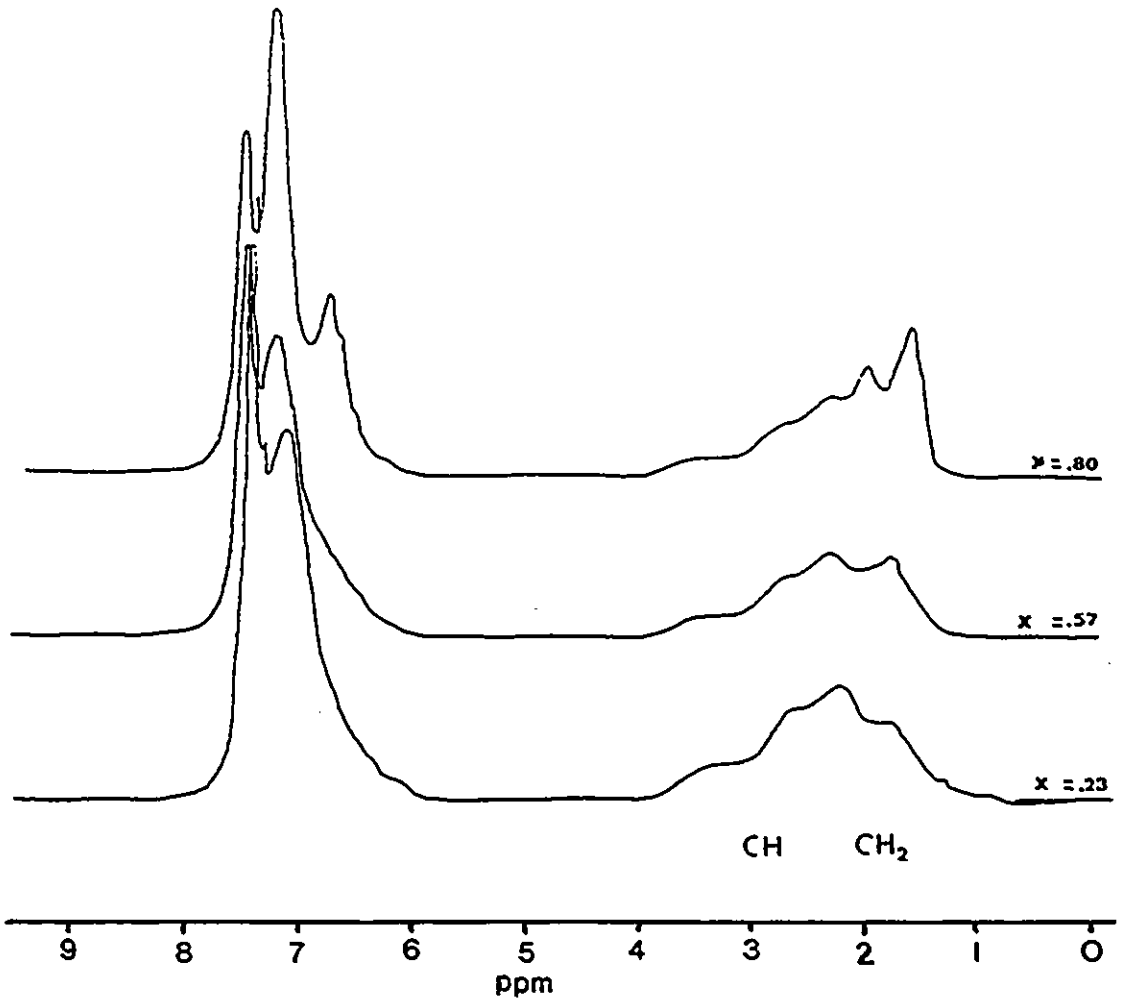

Fig. 6.20. Evolution of the H-NMR spectra with conversion, during bulk S/NPMI copolymerization with [TBPCC]=0.01 M/L, f_{10}=0.8, at 105°C.

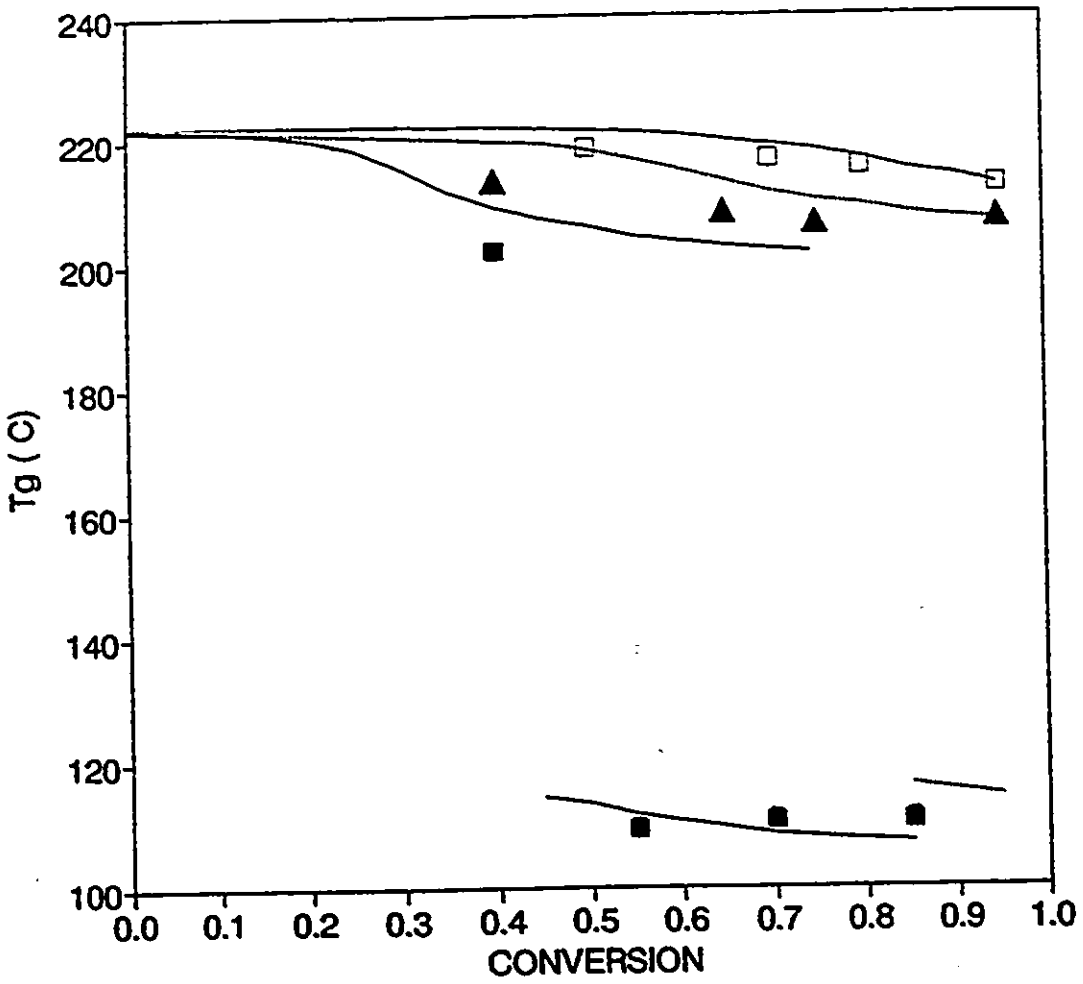

Fig. 6.21. Effect of the monomer feed composition on the development of the copolymer glass transition temperature with conversion, in bulk S/NPMI copolymerization with [TBPCC]=0.01 M/L, at 130°C. Experimental T_g results at: f_{10}=0.9 (■); f_{10}=0.8 (▲); and f_{10}=0.7 (□). Model results for f_{10}=0.9 (——), 0.8 (---) and 0.7 (···).

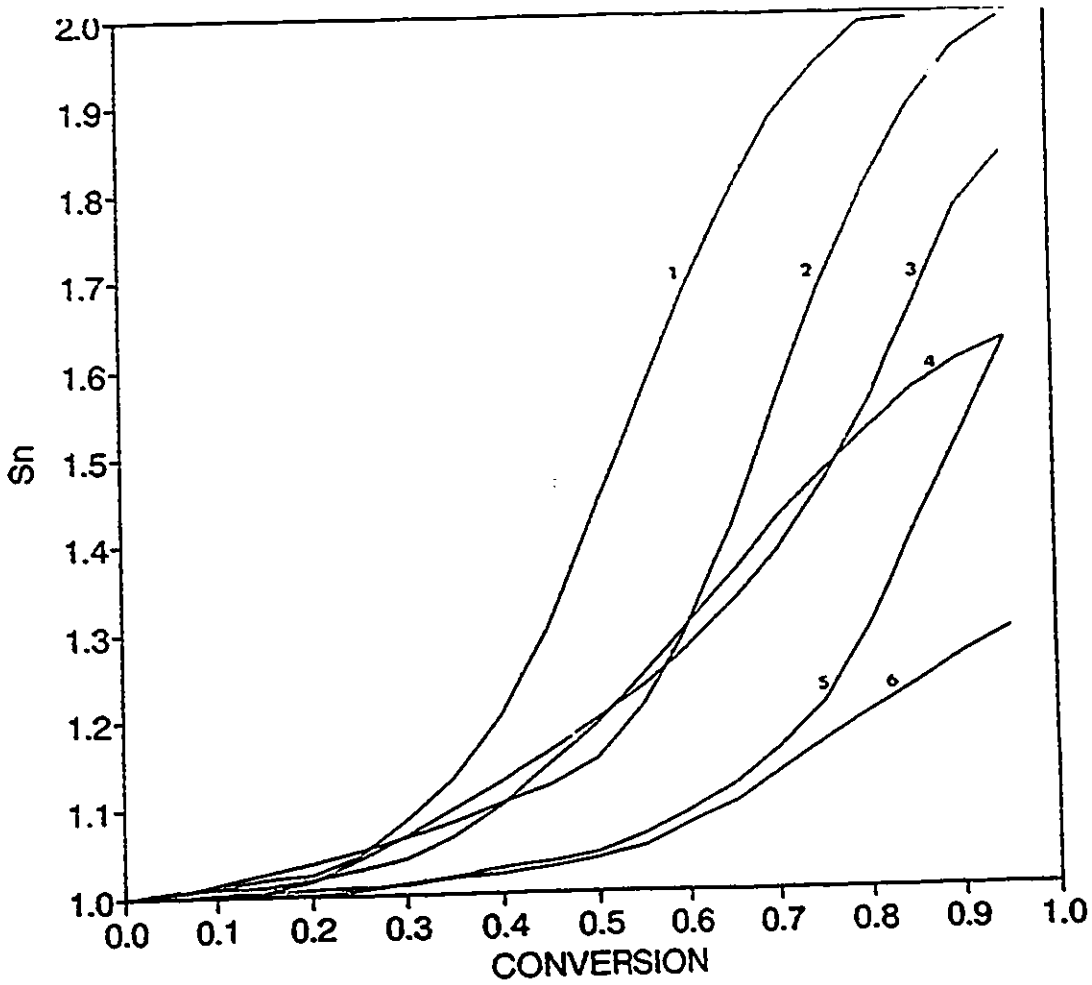

Fig. 6.22. Effect of T_p and f_{10} on the development of number of segments per copolymer chain, in S/NPMI bulk copolymerization with [TBPCC]=0.01 M/L. Model results for: f_{10}=0.9, T_p=130°C (1); f_{10}=0.8, T_p=130°C (2); f_{10}=0.7, T_p=130°C (3); f_{10}=0.9, T_p=105°C (4); f_{10}=0.7, T_p=130°C, [I]=0.005 (5); f_{10}=0.8, T_p=105°C (6).

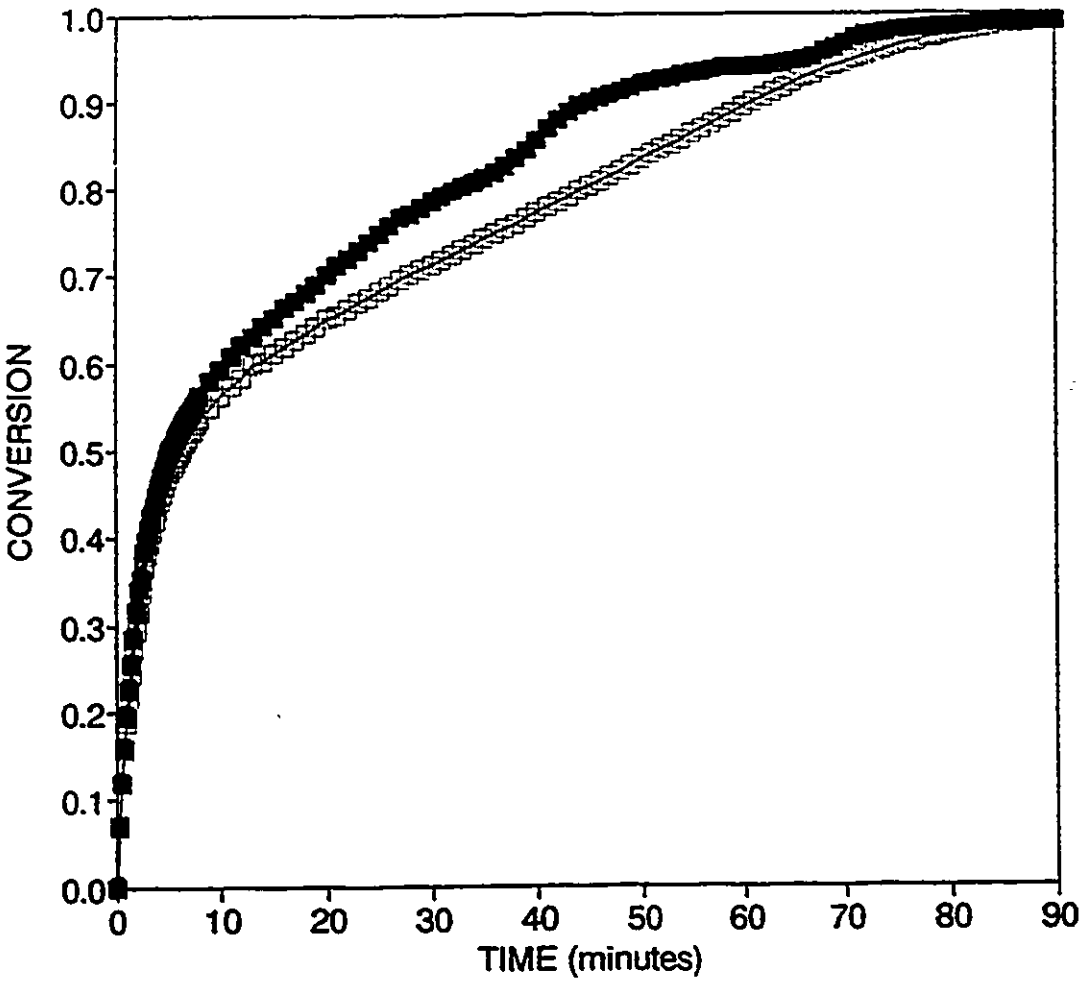

Fig. 6.23. Simulation of conversion history for optimal S/NPMI suspension copolymerization (f_{10}=0.8) with bifunctional initiator TBPCC. Experiment S/NPMI-03-01 (■); experiment S/NPMI-03-02 (□) (see table 6.3 for operating conditions).

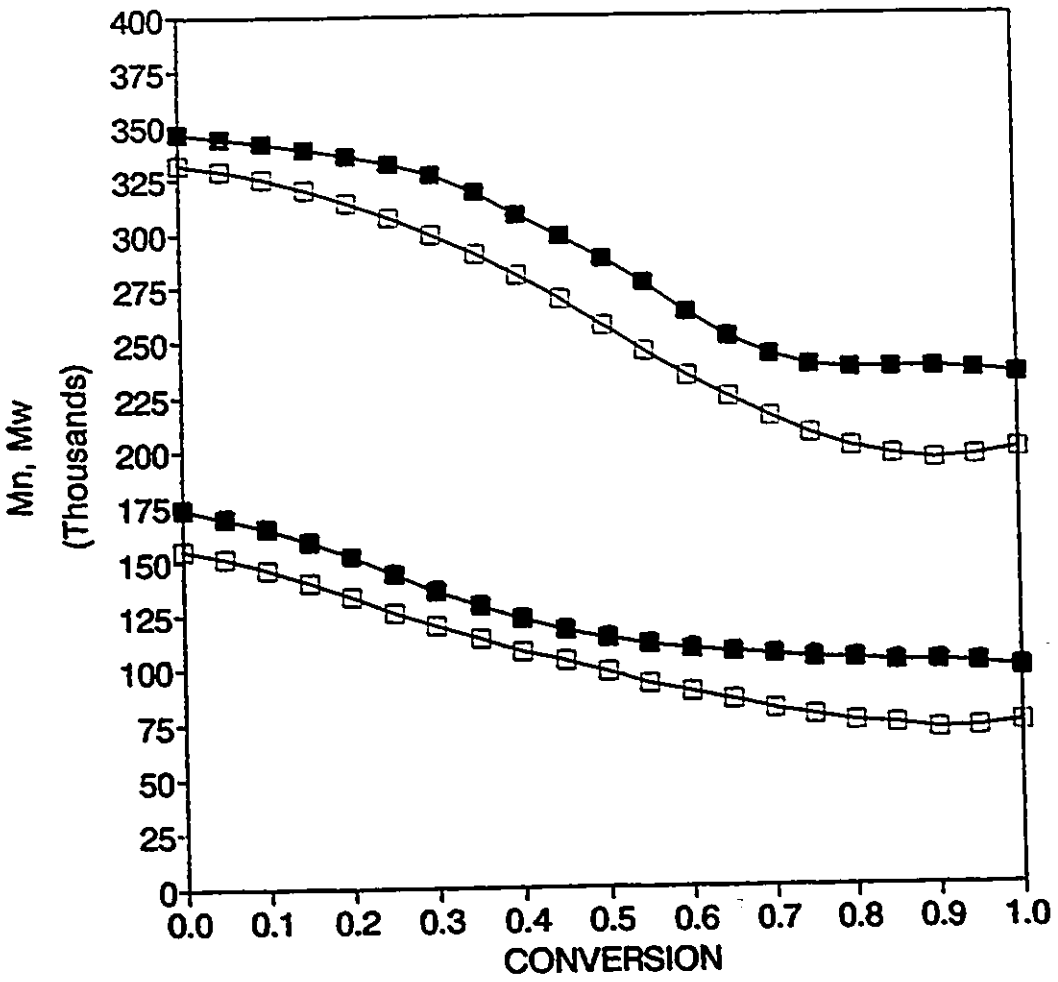

Fig. 6.24. Simulation of the molecular weight distribution development with conversion, for optimal S/NPMI suspension copolymerization (f_{10}=0.8) with bifunctional initiator TBPCC. M_n and M_w for experiments S/NPMI-03-01 (■), and experiment S/NPMI-03-02 (□) (see table 6.3 for operating conditions).

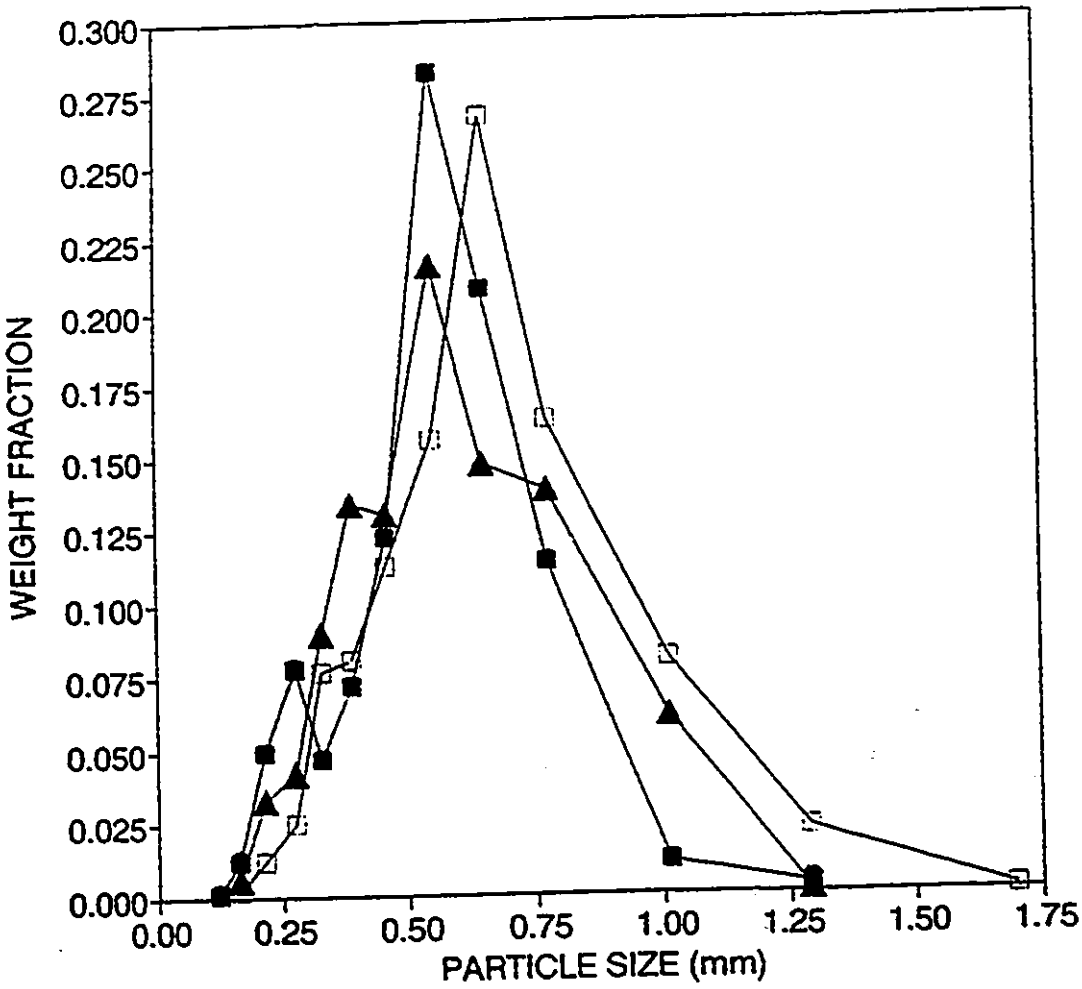

Fig. 6.25. Particle size distribution for optimal S/NPMI suspension copolymerization (f_{10}=0.8) with bifunctional initiator TBPCC. Discrete measurements of bead particle size vs weight fraction for: reference polystyrene system (▲), and experiments S/NPMI-03-01 (■) and S/NPMI-03-02 (□) (see table 6.3 for operating conditions).

CHAPTER 7

α-METHYLSTYRENE/N-PHENYLMALEIMIDE COPOLYMERS

Throughout this chapter, the synthesis and characterization of high T_g α-Methylstyrene/N-Phenylmaleimide (AMS-NPMI) engineering copolymers, through bulk copolymerization with bifunctional initiators, is described. From the experimental results, information compiled in the previous work with SAMS and S-NPMI copolymers, and literature data, the rate constants and copolymerization parameters, necessary for the simulation of this copolymerization system, are estimated. The experimental results for monomer conversion history, and the development of molecular weight averages, copolymer composition, copolymer glass transition temperature, and copolymer micro-structure, are compared with the model results obtained with the simulation program BICOP, developed in Chapter 4. Under simulation assisted optimized conditions, the feasibility to synthesize suspension copolymers, with the desired characteristics of terminal conversion, molecular weight distribution, and glass transition temperature, was established for α-methylstyrene/N-phenylmaleimide copolymers.

7.1 Introduction

For the last fifteen years, it has been known that the free radical copolymerization of N-substituted maleimides with various electron donors leads to the formation of alternating copolymers. The participation of donor-acceptor complexes, the so called charge-transfer complexes (CTC), in these copolymerization systems has been proposed and fully demonstrated [Barrales-Rienda et.al.(1977), Olson and Butler (1983), Mohamed et.al.(1986)].

However, until very recently, no attempts had been made to copolymerize N-phenylmaleimide (NPMI) with α-methylstyrene (AMS).

Fles et.al. (1989) were the first to study the free radical solution copolymerization of this donor-acceptor pair, above the ceiling temperature of AMS (T_c=61°C [Danton and Ivin (1948)]), using monofunctional initiator (AIBN).

In this study, Fles and coworkers found that the slight deviations from the formation of perfectly alternating copolymer were due to the competitive statistical copolymerization taking place simultaneously with the donor-acceptor propagation mechanism. Based on their experimental data, they derived kinetic expressions to quantify the relative participation of both mechanisms in the observed copolymerization rate, and to evaluate the four reactivity ratios involved in their terminal plus complex participation model, proposed. According to their results at 70°C, statistical addition of free monomer dominates at low monomer concentrations, with complex participation increasing rapidly as the amount of solvent decreases (i.e. higher initial monomer concentrations). In addition, they found that the T_g of the AMS-NPMI copolymer synthesized at equimolar feed composition was about 266°C (see Chapter 2 for details of this work).

Since, in the present study, the interest is set on bulk rather than solution copolymerization, owing to the final goal of synthesizing suspension copolymers, the results of Fles and coworkers suggest that complex propagation will be the dominant copolymerization mechanism in bulk AMS-NPMI free radical copolymerization. Their results also offer clear prove that very high glass transition temperature copolymers can be obtained with this copolymer system.

Unfortunately, the methodology for the evaluation of the relative participation of both mechanisms and the reactivity ratios involved, developed by these authors, cannot be directly extrapolated to higher initial monomer concentrations or adapted to the model proposed in this work, owing to the different definitions used in both models of the

pseudo-kinetic propagation rate constant, and the unique features of bifunctionally initiated copolymerization, described in Chapter 4. The experimental data reported, however, has proven to be very valuable for the understanding and interpretation of the results of this work, as well for the parameter estimation (see below).

If complex participation dominates the propagation reactions, as expected, very high initial polymerization rates yielding highly alternating copolymers should be observed in the early stages of the polymerization, due to the high propagation rates exhibited by donor-acceptor complexes. As the contribution from complex participation decreases, a sharp reduction in polymerization rate should be observed, owing to the very low homo-propagation rates exhibited by both monomers (see Chapters 5 and 6). As a result it is expected that this system behaves almost exclusively as a donor-acceptor copolymerization, with the rate and terminal conversion mainly determined by the equilibrium of donor-acceptor complex formation. Moreover, the low homopropagation rates of both monomers in this system, may lower both the rates and the molecular weights of the final products.

The kinetic and micro-structure models for simultaneous and competitive statistical/donor-acceptor copolymerization, proposed in Chapter 4, will be, then, tested for this primarily donor-acceptor system, as they have been successfully tested for pure statistical SAMS copolymerization (Chapter 5) and simultaneous statistical/donor-acceptor S-NPMI copolymerization (Chapter 6).

7.2 Design of Experiments

Similarly to the previous SAMS and S-NPMI copolymerization studies, and according to the main objectives of this research project, the experimental program was divided in three phases. The first one is an exploratory research to evaluate the effect of monomer feed composition (f) on copolymerization rate (R_p), molecular weight distribution (MWD),

copolymer composition (F), and copolymer glass transition temperature (T_g), at terminal conversion, through isothermal bulk copolymerization at the optimal suspension polystyrene conditions (i.e. T_p=105°C, [TBPCC]=0.01 M/L, Villalobos et.al.(1991)]). The experimental design AMS/NPMI-01 for this exploratory phase, is shown below in Table 7.1.

Table 7.1

Experimental Design AMS/NPMI-01 for the Exploratory Research

RUN AMS/NPMI-01	f_{1o} (mol)	T_p (°C)	[TBPCC]o (Mol/L)	POLYM. TIME (hrs)
1	0.90	105	0.01	2.0
2	0.80	105	0.01	2.0
3	0.70	105	0.01	2.0
4	0.60	105	0.01	2.0
5	0.50	105	0.01	2.0

From the results of the exploratory phase, an optimization research phase was planned and carried out for a narrow range of experimental variables, in order to evaluate the effects of comonomer feed composition, polymerization temperature, and bifunctional initiator concentration, on monomer conversion history, and the development with conversion of molecular weight averages, copolymer composition, copolymer glass transition temperature and micro-structure.

Since temperatures in the range of 130 to 160°C, were used in this experimental phase, owing to reasons explained below, the bifunctional initiator selected was 1,1-di(tertbutyl peroxy)cyclohexane (TPC). This initiator has proven to be effective in temperature applications within this range, owing to its higher mean life time than that of TBPCC. The experimental design AMS/NPMI-02 for this experimental phase is shown below in Table 7.2.

Table 7.2

Experimental Design AMS/NPMI-02 for the Optimization Research

Run AMS/NPMI-02	f_{1o} (mol)	T_p (°C)	[TPC]o (Mol/L)	POLYM. TIME (min)
1	0.5	160	0.010	60
2	0.5	130	0.010	60
3	0.6	160	0.010	60
4	0.6	130	0.010	60
5	0.5	130	0.005	60

The sum of the experimental results of phases one and two, allowed for the complete model parameter estimation of the simulation program BICOP. Simulation of all the experimental runs of the first two experimental stages were performed to evaluate the goodness of the fit and the ability of the simulation program to predict the copolymer properties aforementioned.

In the third experimental stage, suspension copolymerizations were carried out, at the simulation assisted optimal conditions selected, to evaluate the effect of the imposed R_p on suspension stability, mean particle size (MPS), and particle size distribution (PSD), under the previously described reactor scaled-down conditions for optimal suspension polystyrene (see chapters 3, 5 and 6).

The initial design for this experimental phase, comprised two suspension polymerization runs. However, every time that suspension set-up was the result of the runs of the design, two more runs were designed and carried out until the full eight runs of the experimental design were completed.

The design AMS/NPMI-03, is shown below in table 7.3.

Table 7.3

Experimental Design AMS/NPMI-03, Suspension Copolymerization[a]

RUN AMS/ NPMI-03	f_{10} (mol)	T_p (°C)	[TPC][b] (M/L_{org})	[TCP][c] (g/L_{aq})	ϕ[d]	NPMI added as
1	0.5	130	0.0030	7.5	0.4	solid
2	0.5	130	0.0035	7.5	0.4	solid
3	0.5	130	0.0030	15.0	0.2	solid
4	0.5	130	0.0035	15.0	0.2	solid
5	0.5	130	0.0030	15.0	0.2	liquid
6	0.5	130	0.0035	15.0	0.2	liquid
7	0.5	130	0.0030	10.0*	0.1	liquid
8	0.5	130	0.0035	10.0*	0.1	liquid

a) Reactor arrangement and operating conditions as in Tables 5.3 and 6.3.
b) TPC=bifunctional initiator 1,1-di(tertbutyl peroxy)cyclohexane.
c) TCP=tricalcium phosphate, suspending agent.
d) ϕ=disperse phase hold-up (V_{org}/V_{tot})
e) Hydroxyethyl cellulose (HEC) used as steric stabiliser.

7.3 Experimental

7.3.1 Materials

The purification and treatment procedures for the two monomers of this study, AMS and NPMI, as well as solvent, chloroform, non-solvent, methanol, T_g depressor, toluene, and bifunctional initiator TBPCC, have been described in Chapters 5, and 6.

The only alternative material employed in this study was the bifunctional initiator 1,1-di(tertbutyl peroxy)cyclohexane, (TPC), supplied by Pennwalt-Lucidol (now Atochem) as Lupersol-331, which was used without any further purification.

7.3.2 Techniques

For the exploratory research phase, isothermal bulk copolymerization in DSC cells, and ampoules, was carried out following the procedures described in Chapter 5.

Due to the low solubility of NPMI in AMS observed (~5 wt% @ 25°C), master batch copolymerization mixtures for the DSC experiments, as well as for the ampoule samples, were prepared through the same procedures described for S/NPMI copolymers (see Chapter 6).

With the antecedent of the high copolymerization rates observed for S/NPMI copolymers, DSC cell copolymerizations were carried out for 2 hours, and ampoule runs were sampled at 0.5 and 120 minutes, at the conditions prescribed by the experimental design AMS/NPMI-01 (Table 7.1).

Characterization of the ampoule copolymer samples, for conversion (mass basis), terminal conversion (Xt), MWD at terminal conversion, initial (instantaneous) and final (accumulated) copolymer composition, and glass transition temperature at final conversion, were performed through the same procedures described in Chapters 3 and 5.

For the optimization experimental phase, isothermal bulk copolymerizations in ampoules, were carried out at the conditions prescribed by the experimental design AMS/NPMI-02 (Table 7.2).

Ampoule preparation, polymerization, purification, and treatment of the ampoule contents, for each sample taken at previously determined copolymerization times, were performed following the procedures outlined in Chapter 6.

Characterization of each sample (ampoule), to determine monomer conversion history, and the development with conversion of molecular weight averages, copolymer composition, and copolymer glass transition temperature were performed through the same procedures described in Chapter 5.

Due to the impossibility of obtaining stable suspensions at all the conditions prescribed by the experimental design AMS/NPMI-03 (see below), no copolymer beads were obtained for this copolymerization system. As a result characterization of the suspension copolymers particle size distributions and extrusion and copolymer degradation experiments were not carried out.

In what follows, all the experimental and model results are shown and discussed in detail.

7.4 Results and Discussion

7.4.1 Exploratory Research

According to the experimental design AMS/NPMI-01, the effect of the monomer feed composition on copolymerization rate (R_p), was studied first. Figure 7.1 shows the DSC (translated) experimental results for monomer conversion history as a function of monomer feed composition (AMS/NPMI mol%).

Direct translation of the integrated heat of reaction for each run, normalized with the terminal conversion obtained through ampoule copolymerization at the same conditions, was possible owing to both the negligible compositional drift experienced by this systems (see below), and the lack of other thermal event occurring during the allotted copolymerization time. In this figure, the enlarged area shows the first five minutes of copolymerization, were most of the changes occur.

For the conversion curves shown, it is quite obvious that the initial copolymerization rate increases as the concentration of NPMI in the feed increases. This is due to the increasing amounts of donor-acceptor complex being formed in the system, thus demonstrating that the early stages of the reaction are dominated by complex propagation.

As complex participation becomes less important, the very slow statistical addition of free monomer takes place over the remainder of the copolymerization, and the reaction rate decays by two to three orders of

magnitude depending on the initial rate. As a result, the conversion increases extremely slowly except at high NPMI concentrations where the conversion seems to overpass the onset of the gel effect, and auto-acceleration is observed.

The terminal conversion of about 60 %, reached at the equimolar feed composition, seems to be the limiting conversion for this high T_g copolymer system at this relatively low polymerization temperature.

It is worth noting that for all of these systems, most of the observed monomer conversion takes place within the first two minutes of reaction. This results in very high heat generation rates. In large scale production, if a system were designed to control this polymerization isothermally, the capacity of the heat removal system required would exceed the heat generated, after the first two minutes, by more than two orders of magnitude. This, obviously, is an impractical manufacturing process.

Alternative manufacturing processes might be: i) polymerize adiabatically, starting at lower temperatures; ii) employ dilute solution copolymerization to reduce the copolymerization rate; iii) reduce the disperse phase fraction in suspension copolymerization to transfer the heat to a larger amount of water thus minimizing the overheating across the particles; and iv) adopt a starving semicontinuous NPMI feed policy to control the propagation rate. In this study, as shown below, the third alternative has been investigated.

In figure 7.2, the experimental and model results for terminal conversion, in bulk AMS/NPMI copolymerization with bifunctional initiator [TBPCC]=0.01 M/L, at 105°C, after 2 hours of polymerization, are shown. Note, again, that the terminal conversion seems to reach its limiting value as the concentration of NPMI in the feed exceeds 40 mol%. Lower NPMI feed concentrations, cause lower terminal conversions due to the excess of slow-propagating AMS monomer in the mix, with its consequent higher participation in free monomer addition.

The model predictions closely follow the observed behaviour for the entire feed composition range studied.

Figure 7.3 shows the experimental and model results for initial copolymerization rate as a function of the monomer feed composition, at the conditions given. In this figure it is quite noticeable the extraordinary increase in R_{p0}, as the concentration of NPMI in the feed increases. At equimolar composition, the system does not seem to have reached its maximum value, which means that higher concentrations of NPMI in the feed will lead to lesser amounts of free AMS monomer, with the consequent higher initial copolymerization rates. Then, it follows that the reversible nature of the AMS homopropagation reactions at this temperature level is mainly responsible for the sharp decrease in polymerization rate as the statistical monomer addition increases and more so when the reaction becomes free monomer controlled.

It is interesting to compare the results for R_{p0} shown in this figure with those of the S/NPMI system at the same conditions (see figure 6.5). The observed R_{p0} for AMS/NPMI is only slightly lower than for the former system, throughout the entire feed composition range studied. Considering the higher electron-donor character of AMS than that of styrene, it should be expected that complex formation occurs more readily in the AMS/NPMI system. If this actually occurs, the reactivity of both complexes must be similar, with the differences in the observed initial copolymerization rates mainly due to the slower addition of free AMS monomer in this system.

The experimental and model results for the AMS/NPMI copolymer molecular weight averages, obtained at terminal conversion at the conditions given, as a function of the monomer feed composition, is shown in figure 7.4.

Two things are worth noting in this figure. The first one is the nearly exponential increase in M_w as the concentration of NPMI in the mix increases from 0 to 60 mol%, followed by a very small increase at higher NPMI feed concentrations, thus corroborating the idea that complex

propagation is mainly responsible for the molecular weight build-up in the system.

The second one is that even though the complex propagation rates may be similar for this system and for the S/NPMI one at the same conditions, the observed M_w for the AMS/NPMI system is 150,000 to 200,000 units smaller than that of the former.

From the behaviour of the molecular weight development of S/NPMI copolymers it could be thought that an extremely sharp decrease in molecular weight with conversion occurs for this system. However, as it will be shown below, the development of the molecular weight for this copolymer does not show such a sharp decrease. Therefore, the very low molecular weights exhibited by this copolymer, especially at low NPMI feed concentrations are mainly due to the low propagation rates after free monomer addition. In addition, more chain transfer to AMS (methyl hydrogens) than to styrene, is likely to occur, which also contributes to the observed decreases in AMS/NPMI copolymer molecular weight.

To understand this more clearly, let us picture the behaviour of a growing chain. Let us assume that the formation of a sequence of alternating copolymer by complex propagation is suddenly interrupted by the addition of a unit of free monomer, mainly AMS since it is in higher concentration. After this addition, the propagation rate of such growing chain will instantaneously decrease at least one order of magnitude, thus virtually preventing the chain from further growth given the high termination rate exhibited by these monomers (see Chapters 5 and 6). If, in addition, diads of AMS units form, either through termination by combination or through free monomer propagation, such chain will be prone to be broken down into smaller chains through further depropagation of such diads [O'Driscoll and Dickson (1968)].

Consequently, a large amount of short copolymer chains will be produced, thus decreasing substantially the average molecular weights observed.

Considering that the pseudo-kinetic rate constant method provides the model only with a means to approach the overall behaviour of the system when comprised by long copolymer chains, rather than with a description of the individual molecular behaviour, it is no wonder that the system cannot capture this microscopical effect even when some features of the macroscopic behaviour are well represented.

Owing to this limitation, it was decided to fit the model to approach the behaviour of the weight average molecular weight, with the consequent large over-estimation in M_n observed. Therefore, in what follows, comparison is made only between experimental and model results for M_w.

Figure 7.5, shows the experimental and model results for the effect of the monomer feed composition on the observed compositional drift between the experimental initial (extrapolated from $X_{t=0.5\ min}$) and terminal conversions (Xt), for AMS/NPMI bulk copolymerization with bifunctional initiator [TBPCC]=0.01 M/L, at 105°C. The upper curve in this figure, then, approximates the instantaneous copolymer composition at each monomer feed given, whereas the bottom curve represents the copolymer composition accumulated at terminal conversion. The gap between both curves, therefore, represents the compositional drift experienced by each copolymer system.

As expected, the initial copolymer composition approaches rapidly the perfect alternation, as the concentration of NPMI in the feed increases, crossing the equimolar copolymer composition (dotted curve) at feed compositions above 40 mol% of NPMI. These results are in agreement with the results reported by Fles et.al.(1989), showing that at 70°C, the equimolar copolymer composition is observed at about 30 mol% NPMI in the feed. Considering that the homopropagation rate of AMS units is lower than that of AMS at 70°C, and higher above 90°C, this also demonstrates that the reactivity ratios for free monomer addition vary little with temperature (see experimentally determined values of K_{22} in Chapters 5 and 6).

Note also in figure 7.5, that the compositional drift is very small for all the systems studied. This is mainly due to the fact that early complex dominated propagation leads to the formation of nearly alternating homogeneous copolymer, whereas the free monomer addition dominated late stages of the copolymerization, which could induced larger compositional drift, causes negligible progress in conversion, thus limiting the compositional drift.

In figure 7.6, the aliphatic portion (0 to 4 ppm), of the H-NMR spectra of the AMS/NPMI copolymers obtained at terminal conversions, are shown. In this figure note the small changes in the relative areas of the aliphatic NPMI protons (peak of CH~2.25 ppm) with respect to the combined areas of the aliphatic AMS protons (peaks of CH_2~1.6 ppm, and CH_3~1.25 ppm), thus demonstrating the little variation in copolymer composition observed.

Accordingly, the molar concentration of AMS units in the copolymer was obtained from the H-NMR spectra, by dividing the combined area of the aliphatic CH_2 and CH_3 of AMS by the total area of aliphatic protons ($CH+CH_2+CH_3$). In this work, all the AMS/NPMI copolymer compositions reported were established through this procedure.

Since, as shown above, the AMS/NPMI copolymer synthesized at equimolar feed composition yields a nearly equimolar copolymer composition (F_2=0.486), it was decided to further investigate the micro-structure of this copolymer to assess its degree of alternation. To accomplish this, ^{13}C-NMR characterization was performed. Figure 7.7 shows two different portions of the ^{13}C-NMR spectrum of this copolymer: the aliphatic carbons portion, between 30 and 60 ppm, and a down-field portion, between 135 and 190 ppm, containing the carbonyl peak and some information about triads. The interpretation of this spectrum, based completely on the works of Buchak and Ramey (1976), and Barron et.al.(1984) for styrene/maleic anhydride copolymers, is as follows:

In the aliphatic region, the peaks at ~44 and a small component at ~52 ppm belong to the methine carbons (CH) of NPMI units. The signal at ~35 ppm is identified with the methylene carbons (CH_2) of AMS units, with a small component extending to ~41 ppm. The signal for the CH_3 carbons of AMS units appearing at ~52 ppm is , then, completely overlapped with the small component of the NPMI methine carbons.

From the methylene carbons signal for this copolymer, is estimated that about 95% of the signal at 52 ppm corresponds to the CH_3 carbons of AMS units, with the remainder being due to the signal for methine (CH) carbons of NPMI. Therefore, the combined area for AMS carbons must be close to 6.93 units. This area, when compared with the carbonyl (C=O) area, which peak is clearly identified in the down-field portion of the spectrum at ~172 ppm, yields a mol fraction of NPMI in the copolymer F_2=0.489, which is in excellent agreement with the value of 0.486 obtained for this copolymer using H-NMR.

With respect to the alternating sequences identifiable from the ^{13}C-NMR spectrum, after Barron et.al.(1984), it is established here for this AMS/NPMI system, that the area (somewhat overlapped) between the methine (NPMI) and methylene (AMS) areas in the aliphatic region, with its peak at ~40 ppm, corresponds to a combination of $M_1M_2M_1$, $M_1M_1M_2$, and $M_2M_1M_1$ triads. In addition, Buchak and Ramey (1976), identified the down-field peak at ~137.5 ppm with the $M_2M_1M_2$ triad, and the very small (non integrated) peak at ~143 ppm with the $M_2M_1M_1$ triad.

Therefore, by assigning an area for the $M_1M_2M_1$ triad equal to the area of the $M_2M_1M_2$ triad, it can be established that the copolymer microstructure is comprised at least by ~55 mol% of these triads, and 45 mol% of $M_1M_1M_2$ and $M_2M_1M_1$ triads. Further calculations based on the fact that both of the non alternating triads bear an alternating diad, M_2M_1 or M_1M_2, show that the overall copolymer microstructure is comprised by nearly 90 mol% of alternating sequences, and 10 mol% of statistical M_1M_1 and M_2M_2 sequences (mostly M_1M_1), randomly distributed along the copolymer chains.

These results offer irrefutable evidence for the simultaneous and competitive statistical/donor-acceptor propagation mechanisms occurring in this copolymerization system, inasmuch as the perfectly alternating sequences formed through donor-acceptor propagation reactions are disrupted by statistical addition of non-complexed free monomer, even when the overall copolymer composition approaches the equimolar value.

Figure 7.8, shows the experimental and model results for the effect of copolymer composition on glass transition temperature, at terminal conversion, for bulk AMS/NPMI copolymers. The Fox model [Fox (1956)], was introduced to the simulation program BICOP, as:

$$T_g = 1/(W_1/T_{g1} + W_2/T_{g2}) \qquad (7.1)$$

Where: T_g is the glass transition temperature of the copolymer in °K; W_i is the weight fraction of monomer i units bound in the copolymer, and T_{gi} is the glass transition temperature of the homopolymer i, in °K. The previously determined correlations of T_g with M_n (see Chapters 5 and 6), were introduced as:

$$T_{g1} = 446.15 - 3.6x10^5/M_n \qquad (7.2)$$

and

$$T_{g2} = 621.15 - 1.7x10^5/M_n \qquad (7.3)$$

With these expressions and the model values for copolymer composition, and the over-estimated M_n, the model predictions for copolymer T_g, showed excellent agreement with the experimental glass transition temperatures determined, shown in figure 7.8.

Note also in this figure that for copolymer compositions exceeding 42.5 mol% of NPMI units ($F_2 > 0.425$), AMS/NPMI copolymer with very high glass transition temperatures, between 245 and 260°C, are obtained.

The copolymer T_g=258.6°C, obtained at equimolar feed composition, is in agreement with the value of 266°C, reported by Fles et.al.(1989), for AMS/NPMI copolymer synthesized at similar feed composition, with AIBN, at 70°C. The slight difference being due to the higher NPMI copolymer content obtained at the latter temperature.

The observed AMS/NPMI copolymer T_g range , places this copolymer within the classification of High Performance Polymers (see Chapter 1). This makes it extremely attractive for commercial production, provided the molecular weights can be increased.

The summary of all experimental and model results for this exploratory research phase, is given below in Table 7.4.

Table 7.4

Summary of Experimental and Model Results for the Exploratory Research Phase AMS/NPMI-01

RUN AMS/NPMI-01	f_{20} (mol)	EXP Xt @2 hrs	MODEL Xt @2 hrs	EXP Rpo L/M-m	MODEL Rpo L/M-m	EXP Mn @ Xt	MODEL Mn @ Xt
1	0.10	0.2554	0.2091	0.8391	0.7496	10856	14497
2	0.20	0.3522	0.3532	1.3342	1.3544	12990	27826
3	0.30	0.5130	0.4909	1.7495	1.7848	25702	43650
4	0.40	0.5851	0.5922	2.1191	2.2133	32066	58112
5	0.50	0.5760	0.6001	2.4449	2.4548	38312	68187
RUN AMS/NPMI-01	f_{20} (mol)	EXP Mw @ Xt	MODEL Mw @ Xt	EXP F2 @ Xt	MODEL F2 @ Xt	EXP Tg(°C) @ Xt	MODEL Tg(°C) @ Xt
1	0.10	30026	24028	0.389	0.368	216.93	217.90
2	0.20	43195	45505	0.436	0.442	244.78	241.91
3	0.30	72597	71034	0.455	0.468	249.88	251.09
4	0.40	98346	97776	0.476	0.487	256.14	255.53
5	0.50	105358	113669	0.486	0.496	258.57	257.73

7.4.2 Optimization Research

According to the results of the exploratory research, the following criteria were taken into account to design the optimization research phase:

1. Concentrations of NPMI in the feed below 40 mol%, were not attractive for this system given the low terminal conversions and low weight average molecular weight of the copolymers formed.
2. The ability of the systems with 40 and 50 mol% of NPMI to drive alternating AMS/NPMI units into the copolymer, by complex propagation reactions, thus reducing the amount of statistical AMS diads which are prone to depropagate, were the bases for the selection of these feed compositions.
3. Results for S/NPMI suggest that higher polymerization temperatures at similar initiation rates, will promote the formation of higher molecular weight copolymers due to an increased complex propagation participation, which is mainly responsible for the formation of high molecular weight copolymer chains. In addition, higher limiting conversions can be reached at higher polymerization temperatures.
4. Since bifunctional initiator TBPCC is not effective at temperatures above 120°C, bifunctional initiator 1,1-di(tertbutyl peroxy)cyclohexane (TPC), was chosen owing to its higher mean life times, at high temperatures [Villalobos et.al.(1991)].

From this analysis, the experiments AMS/NPMI-02 were designed to evaluate in a narrow variable range, the effects of feed composition, polymerization temperature, and initiator concentration, on monomer conversion history, and the development of M_w, copolymer composition, and copolymer glass transition temperature with conversion (see Table 7.2).

Figure 7.9, shows the experimental and model results for the effect of monomer feed composition on monomer conversion history, in bulk AMS/NPMI copolymerization with [TPC]=0.01 M/L, at 130°C. The enlarged

area in this figure shows the first ten minutes of copolymerization, where most of the changes take place.

In this figure it is clear that the equimolar AMS/NPMI feed composition yields higher initial copolymerization rates and higher terminal conversions than the 60/40 mol% feed composition. Comparison of these curves, with those obtained in the exploratory research at similar feed compositions, shows slightly lower initial copolymerization rates for the systems at 130°C with TPC, but sustained over a longer period of time than for the systems at 105°C with TBPCC. This leads to higher terminal conversions approaching a limiting value of about 85%. The observed behaviour, is mainly due to the decrease in the equilibrium constant for donor-acceptor complex formation at higher temperatures, which results in lower concentrations of complex in the system accumulating (and therefore being consumed) more slowly.

Note, in the curve at f_{10}=0.6 that after 30 minutes of polymerization, the observed monomer conversion decreases slowly. This may be due to actual depropagation of AMS diads in the copolymer chains, with the formation of AMS monomer [Malhotra et.al. (1978,b)].

Since depropagation was not observed in the system with equimolar feed composition, the fact that very small concentration of AMS diads are formed at these conditions (see above), seems to corroborate that depropagation of AMS diads becomes important for systems which stoichiometric excess of AMS leads to larger participation of this monomer through statistical addition.

In figure 7.10, the experimental and model results for the effect of f_{10} on monomer conversion, in bulk AMS/NPMI with [TPC]=0.01 M/L, at 160°C, is shown. As with the experiments at 130°C, the increase in polymerization rate as the concentration of NPMI in the feed increases, is noticeable. However, at these conditions the difference in initial polymerization rate is not nearly as large as in the former. This means that at 160°C the system approaches its maximum polymerization rate at the equimolar composition.

Opposite to what was expected, these systems reached lower terminal conversions than those at 130°C. This was likely due to a very low value for the equilibrium constant for donor-acceptor complex formation at this temperature, which must promote complex dissociation at a higher rate than it propagates, as the concentration of the monomers decrease substantially. As a result, the extremely slow statistical addition of free monomers takes over the polymerization with the consequent sharp decrease in the copolymerization rates observed.

In addition, the virtual initiator depletion after 30 minutes of polymerization ($t_{1/2}$=6 min at 160°C for TPC) causes dead end polymerization, even though thermal initiation of AMS occurs, owing to the low propagation rates observed under the free monomer addition regime.

Note also in this figure that after 15 minutes of polymerization, a decrease in conversion due to the aforementioned depropagation of the AMS diads, is observed in both systems. This depropagation, however, is more noticeable for the system with f_{10}=0.6, than for the system with equimolar feed composition.

Although model predictions are in good agreement with the experimental results throughout the conversion range, the model does not predict the chain depropagation observed, inasmuch as no reversibility of the AMS homopropagation reaction was considered. This may also be the main cause for the large disagreement between M_n predictions and experimental determinations. The extension of the model to consider reversible propagation steps, however, will not be attempted here.

Figure 7.11, shows the experimental and model results for the effect of bifunctional initiator concentration on monomer conversion history, in bulk AMS/NPMI with equimolar feed composition, at 130°C.

In the enlarged portion of this figure the similarity of the initial copolymerization rates at different initiator concentration levels, is evident. This means that the observed propagation rate is so large that a considerable decrease in the initial radical concentration do not sensibly affect the initial donor-acceptor complex propagation rate.

A large effect of lower initiator concentration on copolymer molecular weights is evident, however (see below). This phenomenon has been reported by Georgiev and Zobov (1978) for the copolymerization of styrene/maleic anhydride, and referred to as "spontaneous initiation" of donor/acceptor copolymerization.

The aforementioned sharp change from a donor-acceptor dominated copolymerization regime to a free monomer statistical addition regime, followed by dead end polymerization, is more noticeable in the system with low initiator concentration. Note also in this system that after 15 minutes of polymerization, the conversion seems to decrease slowly for a period of time, and then little increases in conversion are observed. This is not considered to be an actual trend, but a heat effect in the individual ampoules, brought about by slightly different degree of overheating within each ampoule during the early stages of the polymerization, with the consequent small variations in the terminal conversion observed for each sample.

Figure 7.12 shows the experimental and model results for the effect of monomer feed composition on the development of the weight average molecular weight in bulk AMS/NPMI at 130°C. The experimental results at both feed compositions tested, show a nearly constant M_w about 82,000 for the system with f_{10}=0.5 and about 77,000 for f_{10}=0.6, throughout the conversion range, with the exception of a decrease in M_w at high conversions, for the system with f_{10}=0.6.

This reduction in M_w corroborates the above observations of chain degradation during the statistical copolymerization regime. The model predictions for this property are in poor agreement with experiment, under the conditions studied, inasmuch as an ascending M_w trend is predicted, in spite of the weak function for the decay of K_{tc} with which the model was fit (see below). Therefore, the model predictions for M_w must be only considered as gross estimates of the actual values.

For the systems at 160°C (not shown in the plot), also nearly constant values of M_w about 50,000 (f_{10}=0.5), and 45,000 (f_{10}=0.6), were observed. Thus, invalidating the hypothesis that higher temperatures could produce larger molecular weights, through faster complex propagation. Instead, typical free radical behaviour of higher initiation rates leading to the formation of lower molecular weight chains at high copolymerization rates, was observed.

In figure 7.13, the experimental (SEC) curves for the development of the MWD with conversion, in AMS/NPMI copolymerization with f_{10}=0.6, at 160°C, are shown. Note in this figure that between 45 and 63% conversion the MWD changes are negligible. In this figure, the curve for 60% conversion with the top arrow, represents the MWD after monomer conversion decreased from 63 to 60%. The observed MWD after the decrease in conversion given, demonstrates the formation of a considerable amount of short chains through depropagation of the AMS diads formed.

The observed behaviour clearly indicates, that chain depropagation of AMS/NPMI copolymers can only be prevented by increasing the contents of alternating copolymer in the chains (i.e. by decreasing f_{10}). As a result, equimolar feed compositions are preferred for the synthesis of thermally stable AMS/NPMI copolymers.

The experimental and model results for the effect of bifunctional initiator concentration on the development of M_w in bulk AMS/NPMI with equimolar feed composition, at 130°C, are shown in figure 7.14. Again, little variation with conversion of M_w was observed for the system with low initiation concentration ([TPC]=0.005 M/L).

For this system, M_w of about 125,000 was obtained throughout the conversion range, in accordance to the reduction in bifunctional initiator concentration. This means that even lower bifunctional initiator concentrations are needed in order to increase the M_w to the target value of 200,000. The model M_w prediction for this system, gave only gross approximation to the actual behaviour.

Figure 7.15 shows the experimental and model results for the effect of polymerization temperature on the development of the accumulated copolymer composition with conversion (compositional drift path). The systems chosen for this plot were those with f_{10}=0.6, owing to its relative larger compositional drift with respect to the almost negligible one experienced by the systems at equimolar feed composition.

Note from the scale of this figure, that the small variations with conversion of the copolymer composition observed (largest absolute difference less than 5%) are close to the experimental error of H-NMR determinations. Therefore, the observed compositional drift for these systems may also be considered as negligible. Model predictions yielded values within 2% difference of the experimental determinations, for the different trends observed, which may be considered satisfactory.

In figure 7.16, the experimental and model results for the development of the copolymer glass transition temperature with conversion, are shown. The systems selected for this plot were those showing the largest differences in copolymer composition and molecular weights (i.e. systems AMS/NPMI-02-03 and 05, see table 7.2).

Owing to the small variation with conversion of both copolymer composition and molecular weights in both systems, the experimental and model results showed, as well, negligible variations in copolymer T_g with conversion. However, a difference of about 2°C in average, is observed between these copolymers.

The final value of T_g=265.9°C, for the copolymer synthesized from equimolar feed composition, is in excellent agreement with the value of T_g=266°C, reported by Fles et.al.(1989), at similar feed composition.

For the copolymer synthesized with f_{10}=0.6, the slightly lower content of NPMI units in the copolymer, along with its lower molecular weight, led to the formation of a copolymer with T_g=262.5°C. The difference in T_g between both products being less than 1.5%, which shows a strong dependence of AMS/NPMI copolymer T_g on copolymer composition, and a weak dependence on molecular weight, as suggested by the T_g model

introduced in the simulation program (see above).

As mentioned above, the extremely high T_g observed for AMS/NPMI copolymers, is within the range of High Performance Polymers, which makes these systems, very attractive for commercial production, especially at equimolar feed compositions and low initiator concentrations.

Figure 7.17, shows the model results for the effect of the synthesis conditions on the development with conversion of the copolymer multi-block structure, characterized by the number average number of segments per copolymer chain. The systems selected to be shown in this plot, were the same as in figure 7.16.

In this figure, note for the system with f_{10}=0.6, at 160°C, the sharp increase in S_n before approaching its maximum value of 2, during the free monomer addition controlled copolymerization regime. This means, that even though conversion does not increase substantially during the statistical copolymerization regime, recombination of chains previously formed, through macro-initiator reactions, is important. This should result in an M_w increase as predicted by the model. However, the effect of AMS diads depropagation with consequent chain degradation, seems to counteract the expected molecular weight build-up, thus resulting in the nearly constant molecular weights exhibited by these systems, throughout the conversion range.

For the system with equimolar feed composition at 130°C, and low initiator concentration, a lower degree of coupling between macroradicals is predicted, owing to the lower initiator and macro-initiator decomposition rates at this temperature.

Since for all the systems studied in this experimental phase the observed compositional drift is negligible, the number average number of segments per copolymer chain (S_n), as an indicator of the reduction in the effective compositional drift of the system, becomes irrelevant.

7.4.3 Model Parameter Estimation

From the model parameter estimation performed during the studies for S/AMS and S/NPMI copolymers, all the values for the parameters involving homopropagation, homotermination by combination, and transfer to monomer reactions, as well as physical properties and glassy effect parameters for both monomers were already established.

This greatly simplified the model parameter estimation for the copolymerization of AMS/NPMI with bifunctional initiators TBPCC and TPC, which was performed as follows.

The decomposition rate constants for both peroxide groups of the bifunctional initiators (TBPCC and TPC) used in this study, were taken from Villalobos et.al.(1991).

Initiator and macro-initiator efficiencies were set to 0.8 and 0.7, respectively, as before (see Chapters 5 and 6).

All the parameters and physical properties known for AMS and NPMI, from the two previous studies of this thesis, were used in the simulation program BICOP.

The cross termination rate constant was set to the value found for the system S/NPMI which follows the temperature dependency:

$$K_{tc12} = 1.00 \times 10^{12} \exp(-1667/RT) \qquad \text{(L/M-min)}$$

Since a negligible effect of temperature on the reactivity ratios during the statistical free monomer addition regime, was experimentally established in the optimization research phase, the values of r_1=0.03 (AMS), and r_2=0.21 (NPMI), reported by Fles et.al.(1989), were employed in all the simulations.

With all these parameters known, BICOP simulations were run interactively with the non-linear parameter estimation subroutine UWHAUS, in order to find the complex formation and propagation rate constants (K_c, K_{pq}, β_1 and β_2) and the gel effect parameters (K, and A), that best fit the

experimental data for monomer conversion history and molecular weights development.

The values reported by Fles and coworkers for the complex formation and propagation parameters, and the gel effect parameters for S/NPMI determined in Chapter 6, were used as initial guesses.

The minimum variance results for these parameters, in their exponential temperature dependence form, were:

$$K_c = 8.29 \times 10^{3} \exp(-6795/RT) \qquad \text{(L/M-min)}$$

$$K_{eq} = 5.90 \times 10^{-2} \exp(1195/T)$$

$$\beta_1 = 2.73 \times 10^{-1} \exp(1006/T)$$

$$\beta_2 = 3.04 \times 10^{-4} \exp(4138/T)$$

$$A = 0.218;\ K = 8.86 \exp(1929/T)$$

The summary of all these parameter values used in every BICOP simulation reported in this study, is shown below in table 7.5.

7.4.4 AMS/NPMI Suspension Copolymerization

According to the results of the optimization phase discussed above, it was decided to carry out the suspension AMS/NPMI copolymerizations under equimolar feed composition conditions, at 130°C, using bifunctional initiator 1,1-di(tertbutyl peroxy)cyclohexane (TPC), in order to obtain thermally stable-high T_g suspension copolymers.

The same scaled-down reactor settings and recipes used in the previous studies of this project, were initially used, to assess the results for suspension stability and particle size distribution, with respect to the reference polystyrene system (see Chapters 3, 5 and 7).

Table 7.5

Values of the Parameters Used in the Simulations

Initiation Chemical (TPC) and Thermal[a]	
$K_{d1} = 1.269 \times 10^{18} \exp(-35662/RT)$; $f_1 = 0.8$	Min^{-1}
$K_{d2} = 1.090 \times 10^{21} \exp(-42445/RT)$; $f_2 = 0.7$	Min^{-1}
Propagation	
$K_{11} = 1.588 \times 10^{10} \exp(-9992/RT)$	L/mol-min
$K_{22} = 4.301 \times 10^{5} \exp(-2290/RT)$	L/mol-min
$r_1 = K_{11}/K_{12} = 0.03$; $r_2 = K_{22}/K_{21} = 0.21$	70 - 160°C
$\beta_1 = K_{1C}/K_{12} = 2.73 \times 10^{-1} \exp(1006/T)$	105 - 160°C
$\beta_2 = K_{2C}/K_{21} = 3.04 \times 10^{-4} \exp(4138/T)$	105 - 160°C
$K_c = 8.294 \times 10^{3} \exp(-6795/RT)$	L/mol-min
$K_{eq} = 5.90 \times 10^{-2} \exp(1195/T)$	105 - 160°C
Termination	
$K_{tc11} = 7.55 \times 10^{12} \exp(-1677/RT)$	L/mol-min
$K_{tc12} = 1.00 \times 10^{12} \exp(-1677/RT)$	L/mol-min
$K_{tc22} = 7.55 \times 10^{10} \exp(-1677/RT)$	L/mol-min
Transfer to Monomer	
$K_{fm11} = K_{fm21} = 6.128 \times 10^{9} \exp(-13450/RT)$	L/mol-min
$K_{fm22} = K_{fm12} = 1.225 \times 10^{10} \exp(-13450/RT)$	L/mol-min
Free Volume Variables (T_g in °K, α in 1/°K, d in Kg/L)	
$T_g = 192.15$; $\alpha = 0.001$; $d = 0.925 - 0.0009*T(°C)$	AMS
$T_g = 201.15$; $\alpha = 0.001$; $d = 1.310 - 0.0011*T(°C)$	NPMI
T_g (see text); $\alpha = 0.00048$; $d = 1.145 - 0.000905*T(°C)$	Copolymer
Gel and Glassy Effect Parameters	
$K = 8.86\exp(1929/T)$; $\delta = 0$; $A = 0.218$; $M = 0.5$; $N = 1.75$ (gel effect)	
$VF_{crAMS} = 0.0475$; $VF_{crNPMI} = 0.0453$; $B_1 = 1.0$; $B_2 = 0.6$ (glassy effect)	

a) Values for TBPCC and thermal initiation as in Tables 5.3, and 6.3.

The required initial concentration of bifunctional initiator, to produce copolymers with M_w around the target value of 200,000, was established by running BICOP simulations within the range of [TPC] from

0.0025 to 0.0045 M/L, at .0005 M/L intervals, and considering the model M_n results as gross estimates for the final product.

The use of toluene as a T_g depressor for the reaction mix, was discouraged by the experimental findings that the low terminal conversions reached were due to low propagation rates in the statistical free monomer addition regime, and not to limiting conversions due to glass transition of the reacting mix.

Accordingly, the first two suspension AMS/NPMI copolymerization runs of the experimental design AMS/NPMI-03, shown in Table 7.3, were carried out.

The results of both experiments were suspension set-up (massive particle coagulation) and suspension loss, with much of the bulk polymer sticking to the reactor walls. The exact time of suspension set-up, could not be established since no changes in agitation speed were detected.

Even though, similarly high initial copolymerization rates led to stable suspensions in S/NPMI copolymerization (see Chapter 6), the causes for the observed suspension set up were attributed to a combination of high polymerization rates and enhanced particle coalescence due to monomer-induced plasticization of the polymer/monomer particles.

Accordingly, the next two runs of the experiment AMS/NPMI-03, were designed to enhance suspension stability by decreasing the disperse phase volume fraction (ϕ) from 0.4 to 0.2, and increase the stabiliser concentration (TCP), from 7.5 g/L-water to 15.0 g/L-water. These conditions represent a highly over-stabilized operation point, for the reference polystyrene system (see Chapter 3).

With these modifications, the experiments AMS/NPMI-03-03 and 04, were carried out. To monitor the stability of the system, samples were taken from the reactor, at 3 minutes intervals from t=0. The results for both runs were again, total suspension set-up between 3 and 6 minutes of polymerization.

Characterization of the copolymer of run 03, recovered from the sample taken after 3 minutes, showed a conversion of 35%, low molecular weights, M_w < 30,000, and low contents of NPMI in the copolymer, F_2=0.22. Thus suggesting that most of the NPMI was either forming a separate phase in the suspension or sticking to the walls upon addition.

The second hypothesis was proven to be the cause of the copolymer characteristics observed, after repeating the loading sequence and heating cycle in a 1 L, glass reactor. After loading the water, TCP, initiator, and monomers at room temperature, the NPMI precipitated to the bottom of the reactor. Upon agitation and heating, all the NPMI readily formed a very solid aggregate stuck to the bottom of the reactor at about 50°C. When the temperature of the reactor approached the melting point of NPMI (87°C), slow and gradual melting of the NPMI aggregate was observed, with the molten fraction readily incorporating into the AMS rich dispersed phase. As a result, the above suspension copolymerizations took place under a large excess of AMS in the particles, thus producing low molecular weight copolymers which seem to be so sticky that coalesced almost immediately, even before the NPMI aggregate had completely melted.

It is important to point out here that this behaviour was not observed during S/NPMI copolymerization owing to the high content of styrene in the optimal systems (f_{10}=0.8, ~70 wt%), which seems to effectively dissolve the NPMI at temperatures below its melting point. In the copolymerization at hand, the system contains nearly 60 wt% of NPMI and the AMS present cannot dissolve it during the heating cycle.

As an attempted solution to this problem, runs 05 and 06 were carried out at the same conditions as 03 and 04 (see design), but introducing in batch fashion molten NPMI at 90°C, when the temperature of the reactor, containing water, TCP, and AMS, was also kept at this temperature. After allowing 15 minutes for bead formation and stabilization, the initiator, dissolved in a small amount of AMS, was introduced to the reactor, the dome was closed, and the polymerization was heated to 130°C.

After 9 minutes of stable polymerization at 130°C, suddenly, total suspension set-up occurred before 12 minutes. Characterization of the copolymer (05) recovered from the last sample taken, showed 64% conversion, M_w=145000 with a long low molecular weight tail, and a copolymer composition F_2=0.496. With the addition of the NPMI controlled, the failure to achieve a stable suspension with this system was attributed to the residual AMS and oligomer-induced enhanced particle coalescence, due to copolymer plasticization.

From the above results, then, it is clear that the main problem preventing the attainment of stable suspensions for these systems, is caused by the extremely sticky character of the plasticized beads, therefore, more efficient stabilisers than TCP must be employed, as an attempt to control the particle coalescence.

Results reported for suspension polystyrene at high temperatures and reaction rates by Villalobos (1989), showed that steric stabilization of the suspension with hydroxyethyl cellulose (HEC) led to negligible particle coalescence when [HEC] exceeded 5 g/L-water, at ϕ=0.4.

Accordingly, runs 07 and 08, were designed by setting ϕ=0.1, and [HEC]=10 g/L-water, maintaining the loading sequence of the previous two experiments. It is obvious that under these conditions, the particle coalescence rate exhibited by suspension polystyrene would be virtually zero. In spite of this, and after only 6 and 9 minutes of polymerization for runs 07 and 08, respectively, total suspension set-up, with the copolymer completely stuck to the reactor walls, was observed.

In light of these results, it is concluded here that the extraordinarily high coalescence rates exhibited by the monomer/polymer particles, during AMS/NPMI copolymerization, even for very dilute systems and high stabiliser concentrations, makes the production of this copolymer by suspension copolymerization infeasible, at the conditions (and with the stabilisers) tested.

The extremely sticky character of the beads, due to large particle plasticization by the residual monomer at the low terminal conversions reached, has been identified as the main cause of the observed high particle coalescence. Since, terminal conversions could not be increased, through polymerizations at higher temperatures, it follows that bifunctionally initiated AMS/NPMI high T_g copolymers, at the conditions tested, can only be synthesized to high conversions and high molecular weights, through bulk and solution processes.

7.5 Conclusions

Throughout this study it has been demonstrated that AMS/NPMI engineering copolymers having glass transition temperatures above 250°C, can be synthesized to relatively high conversions and high molecular weights through bifunctionally initiated bulk free radical copolymerization.

The copolymers synthesized at equimolar feed compositions, offered the best balance of conversion-molecular weight-T_g, from all the conditions tested. In addition, the copolymers synthesized under these conditions, showed a highly alternating structure bearing nearly 90% of perfectly alternating sequences and only 10% of statistical sequences.

Copolymers synthesized from higher concentrations of AMS in the feed, showed lower terminal conversions and lower molecular weights, as well as poor thermal stability, due to depropagation of the more abundant AMS diads. These diads are formed through free monomer statistical addition to the growing copolymer chains.

The extraordinarily high particle coalescence exhibited by the monomers/copolymer particles in suspension polymerization, due to monomer-induced particle plasticization, could not be overcome even in very dilute suspensions with high stabiliser concentrations. Therefore, it is concluded that AMS/NPMI copolymers cannot be produced by suspension polymerization, in the range of conditions tested.

The simultaneous and competitive participation of donor-acceptor and statistical propagation mechanisms, in this copolymerizing system, has been proven. It has also been shown that the early stages of the copolymerization are dominated by donor-acceptor complex propagation reactions, whereas the late stages are dominated by statistical free monomer addition.

The kinetic and microstructure models proposed, showed good agreement for the predictions of monomer conversion history, and the development with conversion of copolymer composition and copolymer glass transition temperature. However, very poor predictions of M_n, and only gross estimates of M_w, were achieved with the model.

Since the main source for deviations between model predictions of molecular weight averages and the actual molecular weights observed were brought about by AMS depropagation reactions, further model refinements can be introduced by considering reversibility of the AMS homopropagation reactions.

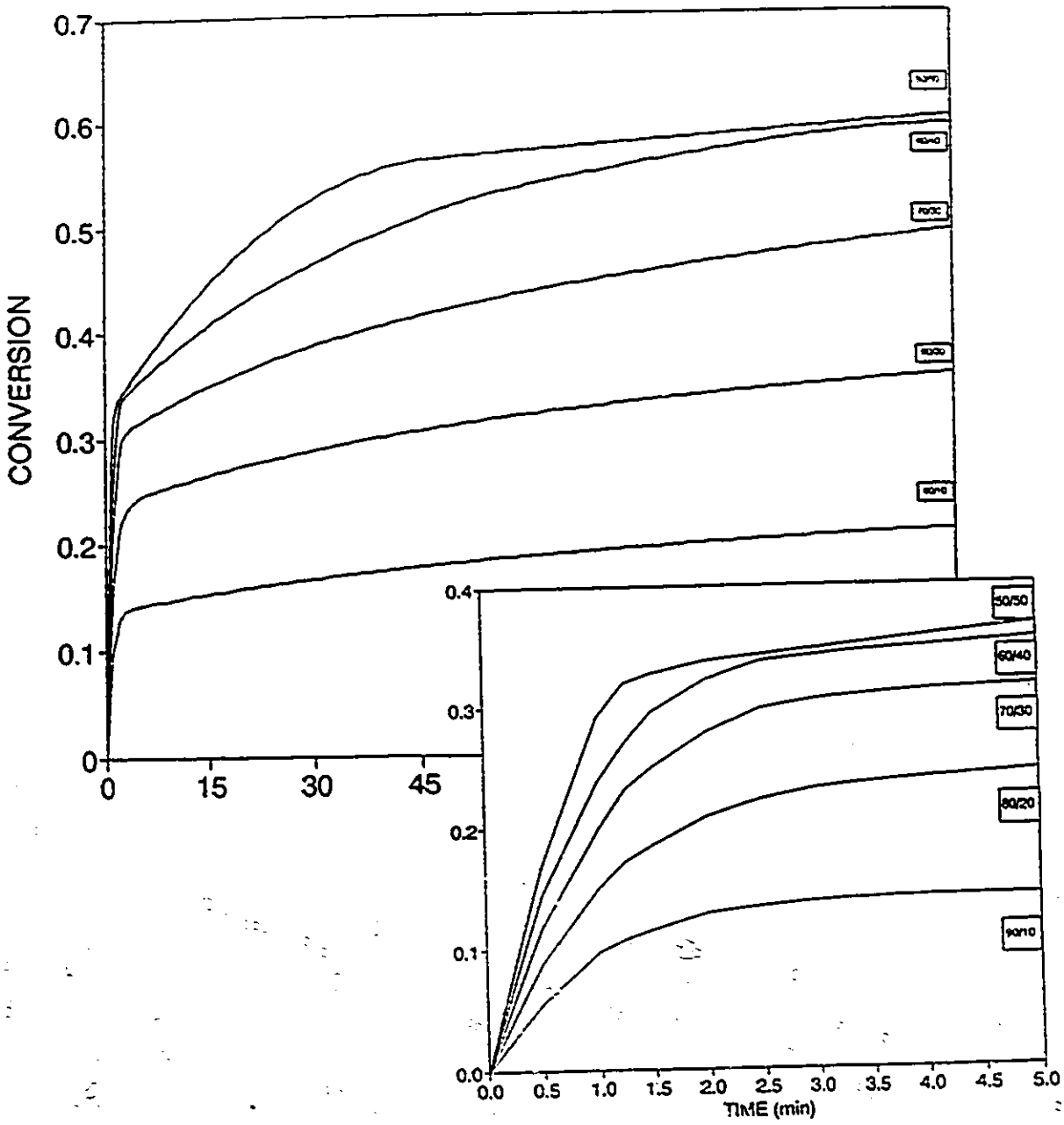

Fig. 7.1. Effect of comonomer feed composition on monomer conversion history for AMS/NPMI bulk copolymerization with bifunctional initiator [TBPCC]=0.01 M/L, at 105°C. Parameter monomer feed composition mol% S/AMS.

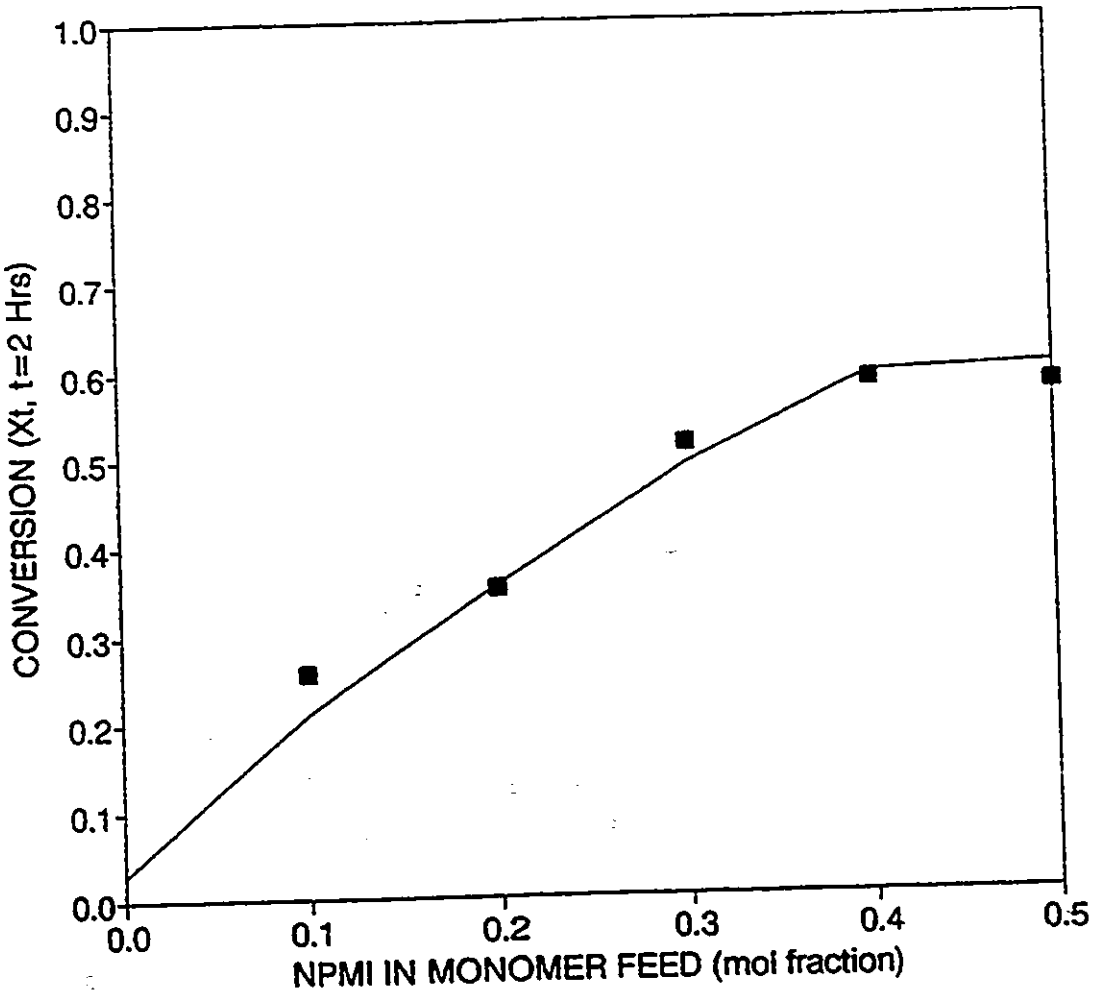

Fig. 7.2. Effect of comonomer feed composition on terminal conversion reached after 2 hours of AMS/NPMI bulk copolymerization with bifunctional initiator [TBPCC]=0.01 M/L, at 105 °C. Experimental results (■). Model predictions (——).

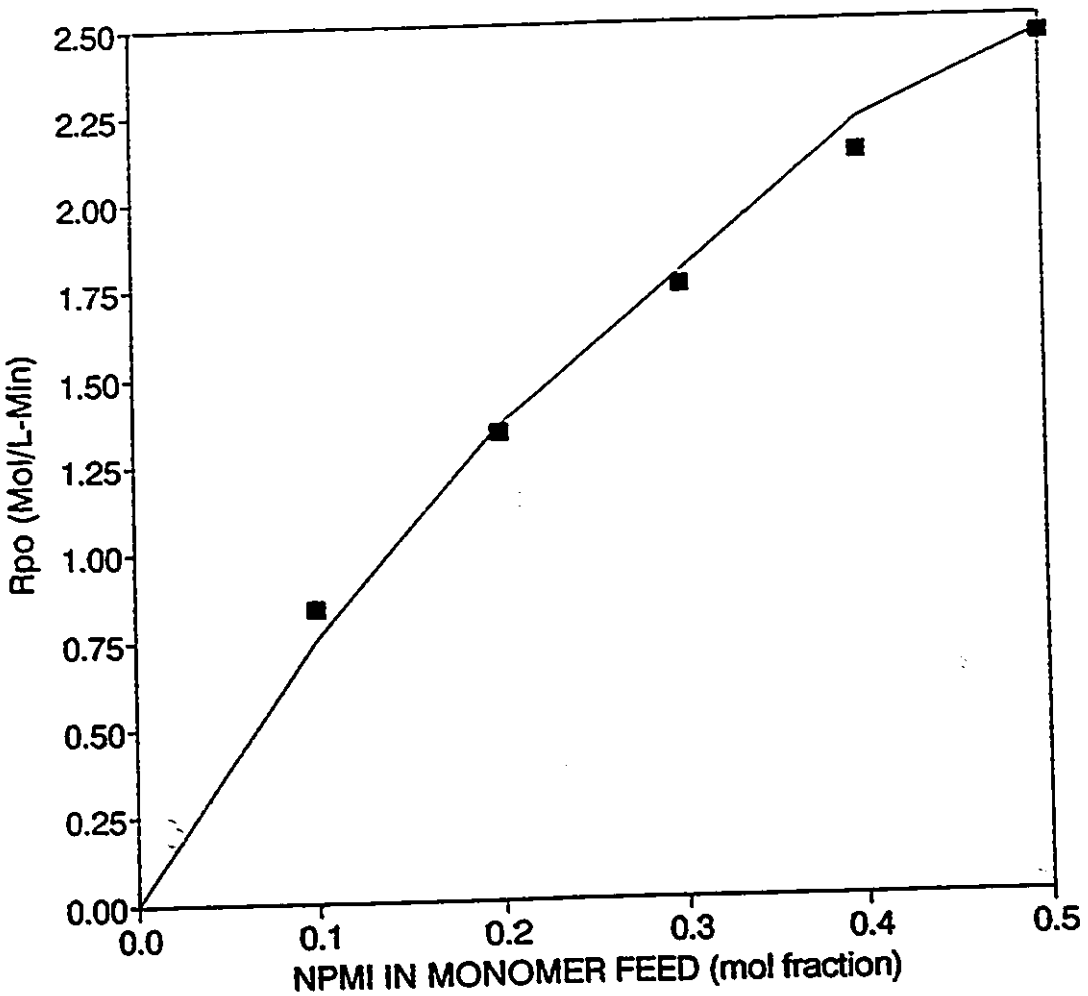

Fig. 7.3. Effect of comonomer feed composition on initial copolymerization rate for AMS/NPMI bulk copolymerization with bifunctional initiator [TBPCC]=0.01 M/L, at 105°C. Experimental results (▪). Model predictions (——).

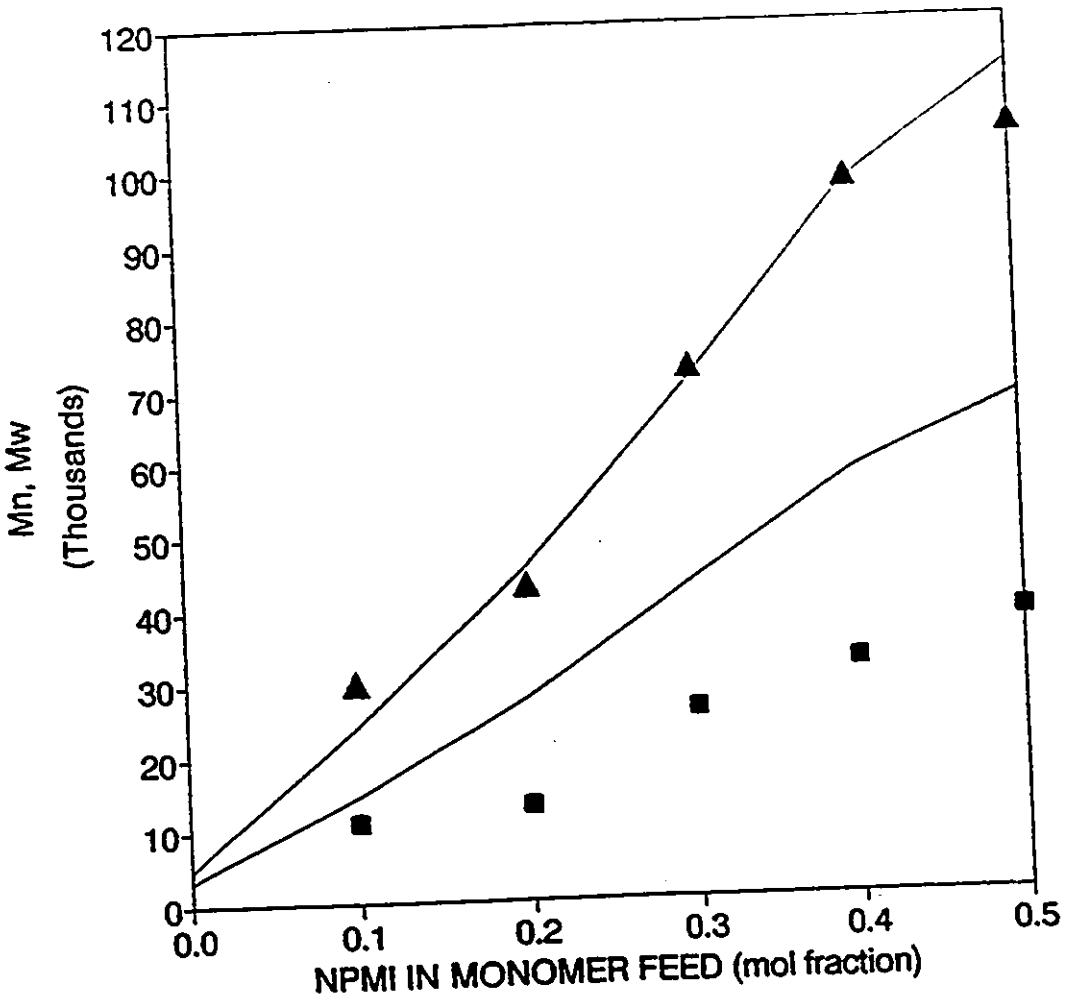

Fig. 7.4. Effect of comonomer feed composition on molecular weight averages of AMS/NPMI copolymer at terminal conversion. Bulk copolymerization with bifunctional initiator [TBPCC]=0.001 M/L, at 105°C. Experimental M_n (■), and M_w (▲). Model predictions (——).

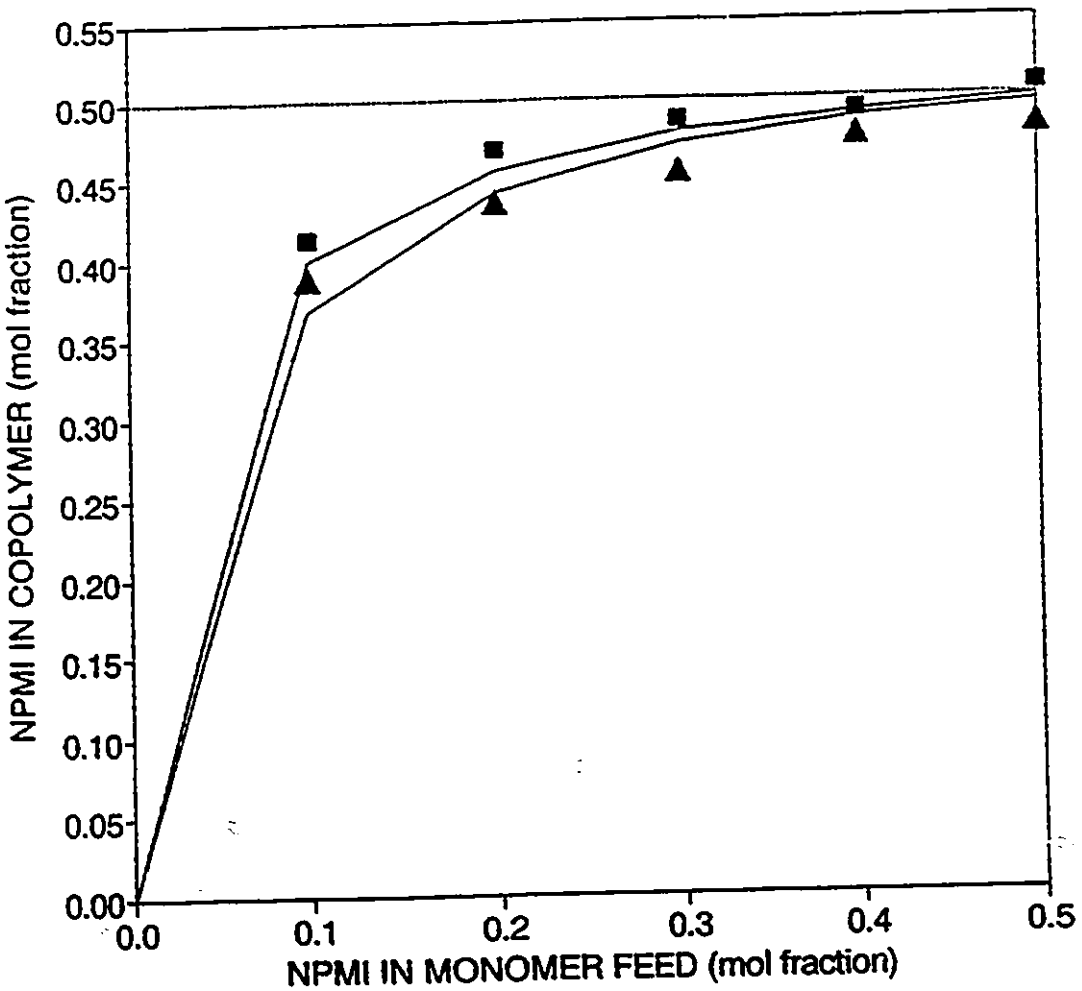

Fig. 7.5. Effect of comonomer feed composition on the observed compositional drift of AMS/NPMI copolymers. Bulk copolymerization with bifunctional initiator [TBPCC]=0.01 M/L, at 105°C. Experimental instantaneous (X=0) (■), and accumulated (X=Xt) copolymer composition (▲). Model predictions (——).

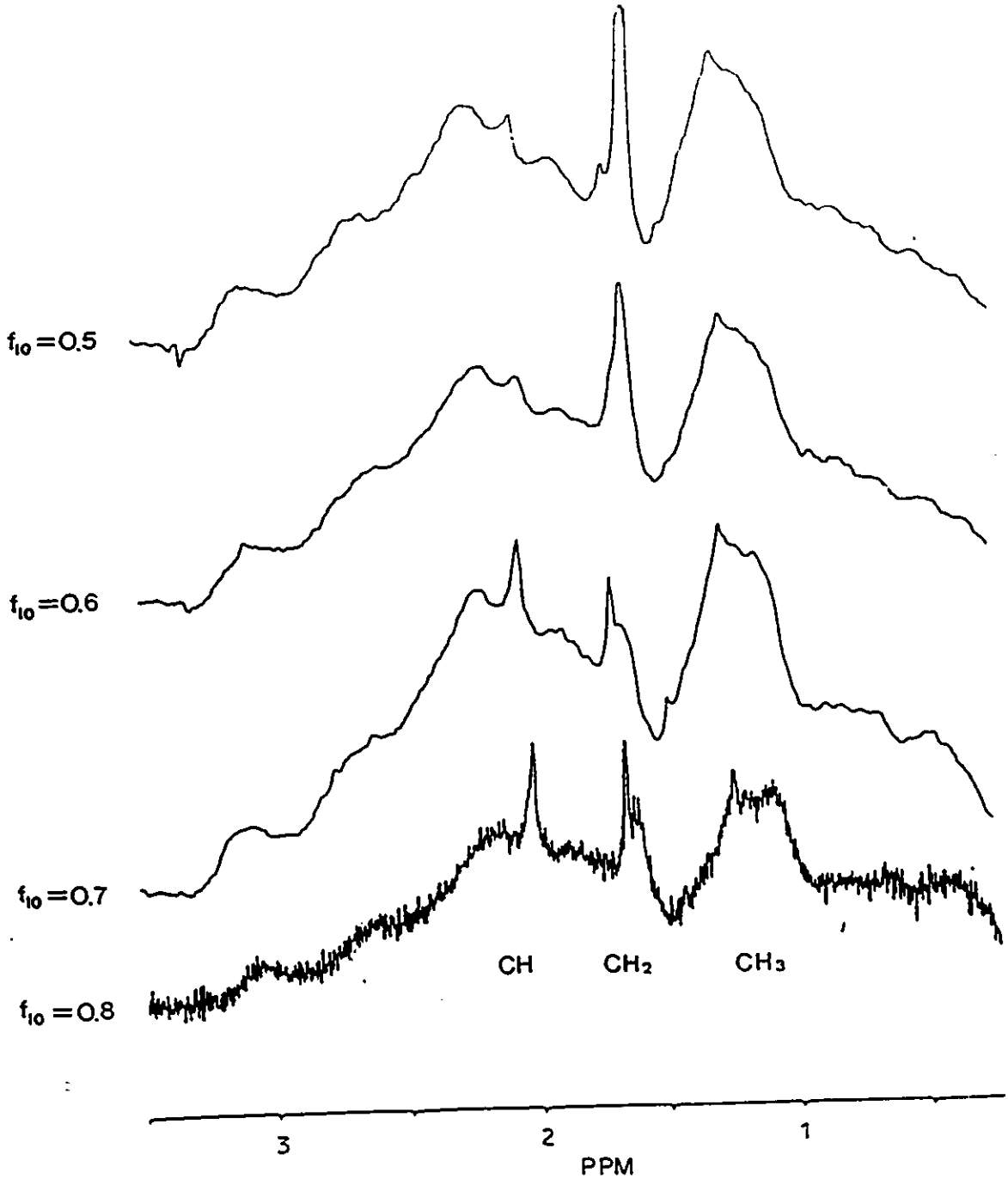

Fig. 7.6. Evolution of the H-NMR spectrum (portion between 0 and 3 ppm) with monomer fed composition for AMS/NPMI copolymers at terminal conversion. Bulk copolymerization with bifunctional initiator [TBPCC]=0.01 M/L, at 105°C.

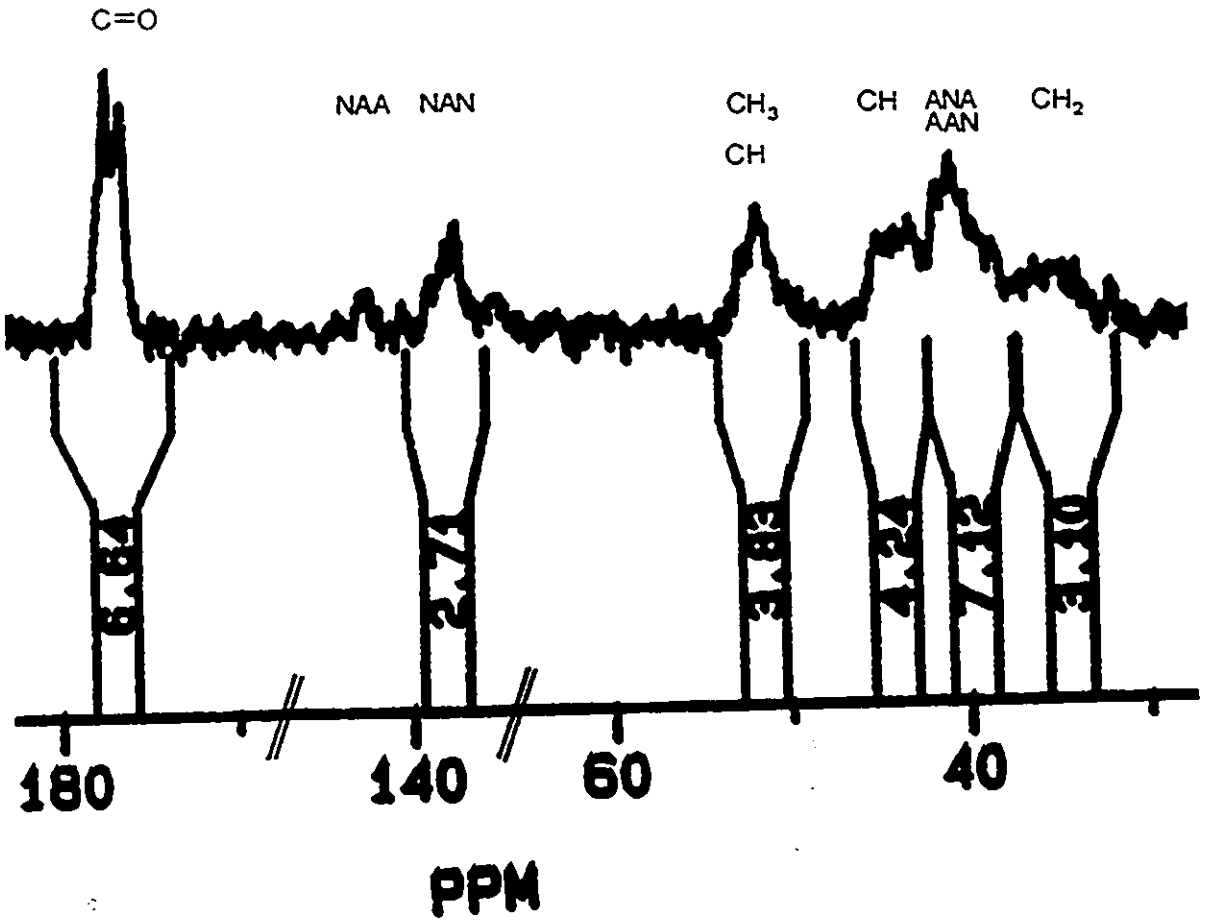

Fig. 7.7. Aliphatic (30 to 60 ppm), and down-field (140 to 180 ppm) portions of the ^{13}C-NMR spectrum of AMS/NPMI copolymer at terminal conversion. Bulk copolymer synthesized at equimolar feed composition with [TBPCC]=0.01 M/L, at 105°C. A refers to AMS units, and N to NPMI units.

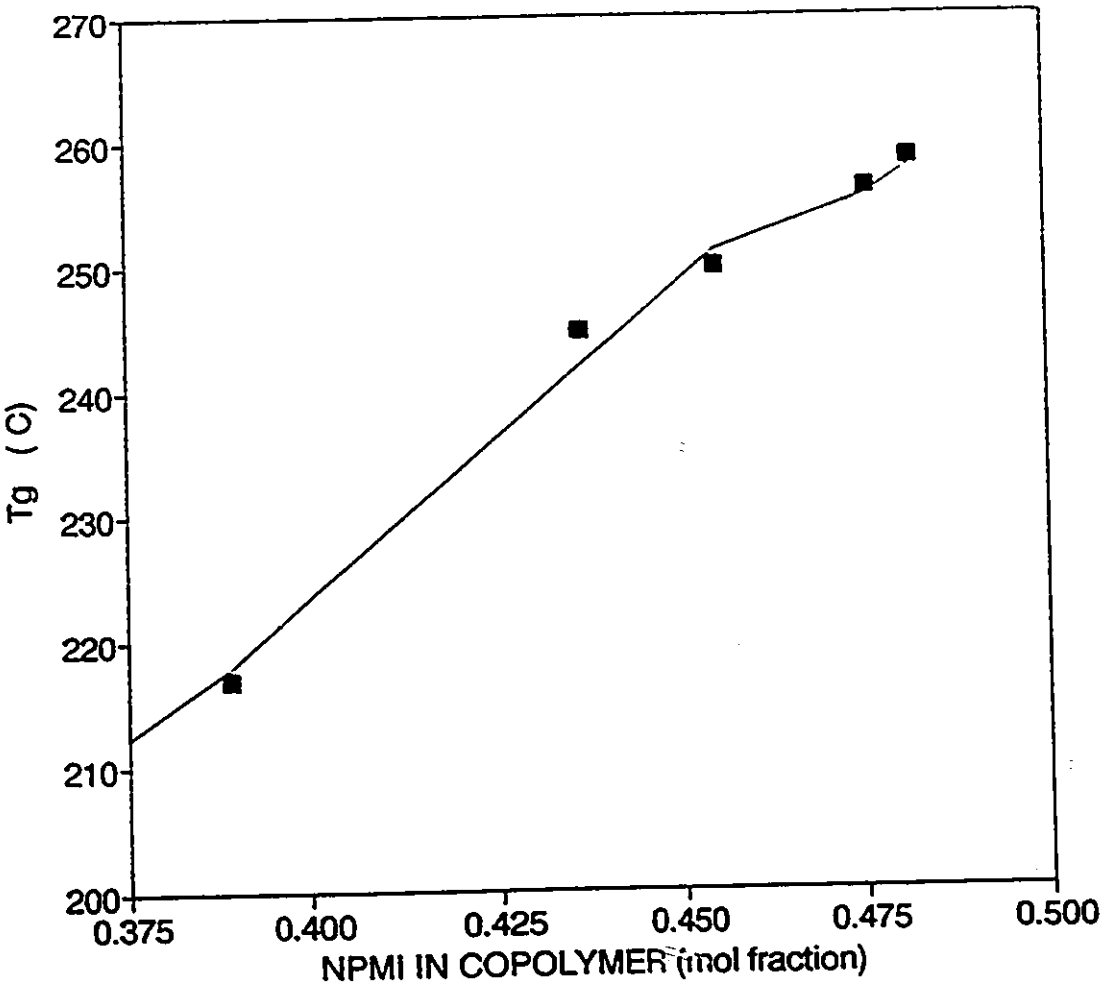

Fig. 7.8. Effect of AMS/NPMI copolymer composition at Xt, on glass transition temperature. Bulk copolymerization with bifunctional initiator [TBPCC]=0.01 M/L, at 105°C. Experimental results (■). Model prediction (——).

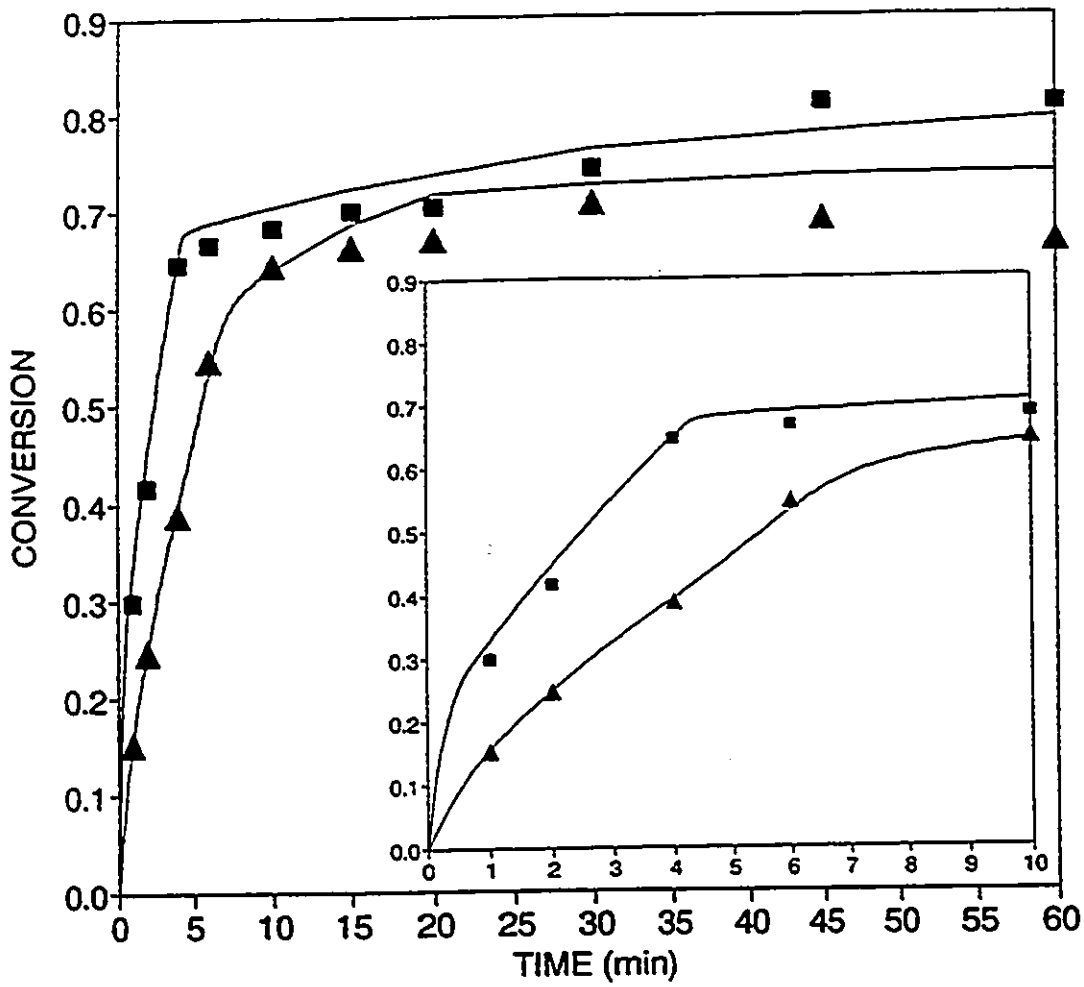

Fig. 7.9. Effect of monomer feed composition on monomer conversion history in AMS/NPMI bulk copolymerization with [TPC]=0.01 M/L, at 130°C. Experimental results for f_{10}=0.6 (▲), and f_{10}=0.5 (■). Model predictions (——).

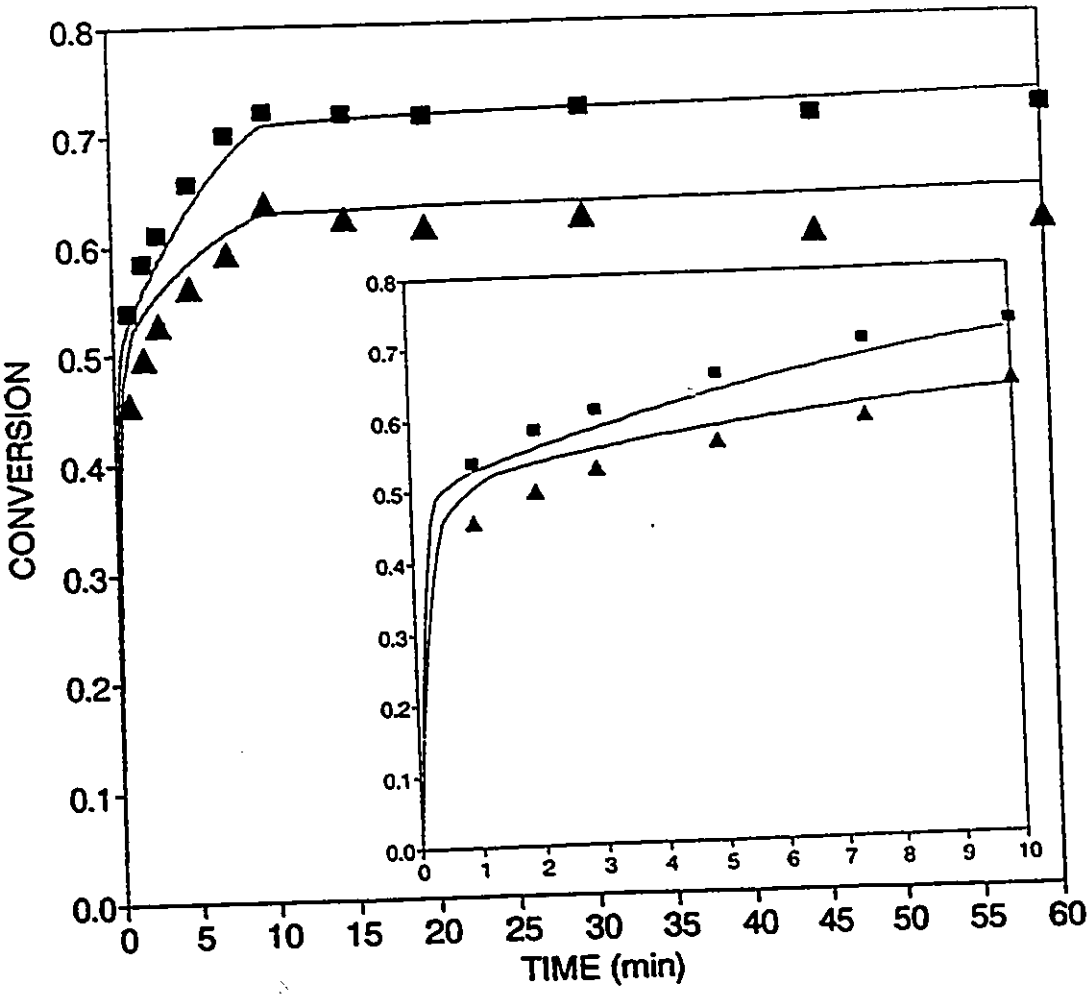

Fig. 7.10. Effect of monomer feed composition on monomer conversion history in AMS/NPMI bulk copolymerization with [TPC]=0.01 M/L, at 160°C. Experimental results for f_{10}=0.6 (▲), and f_{10}=0.5 (■). Model predictions (——).

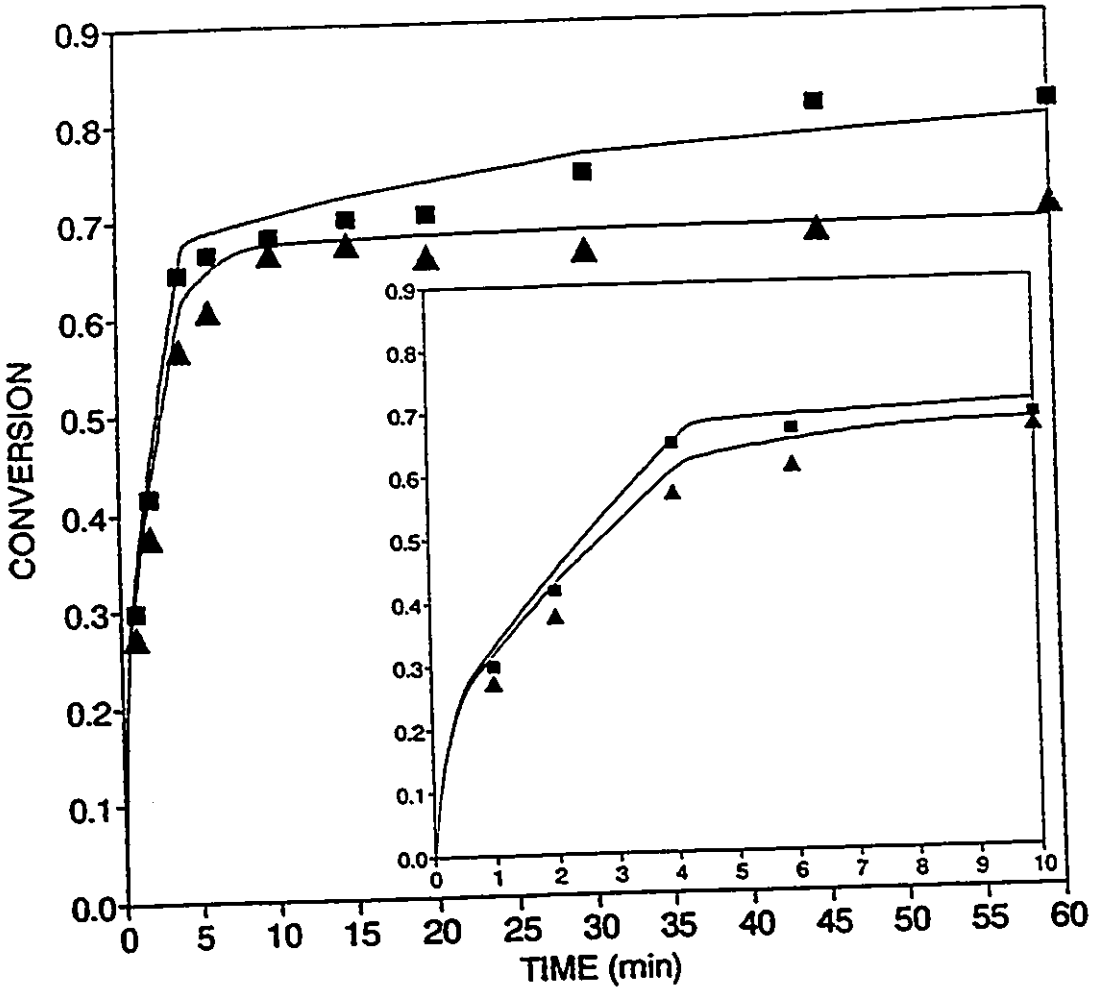

Fig. 7.11. Effect of bifunctional initiator concentration on monomer conversion history in AMS/NPMI bulk copolymerization with f_{10}=0.5, at 130°C. Experimental results for [TPC]=0.005 M/L (▲), and [TPC]=0.01 M/L (■). Model predictions (——).

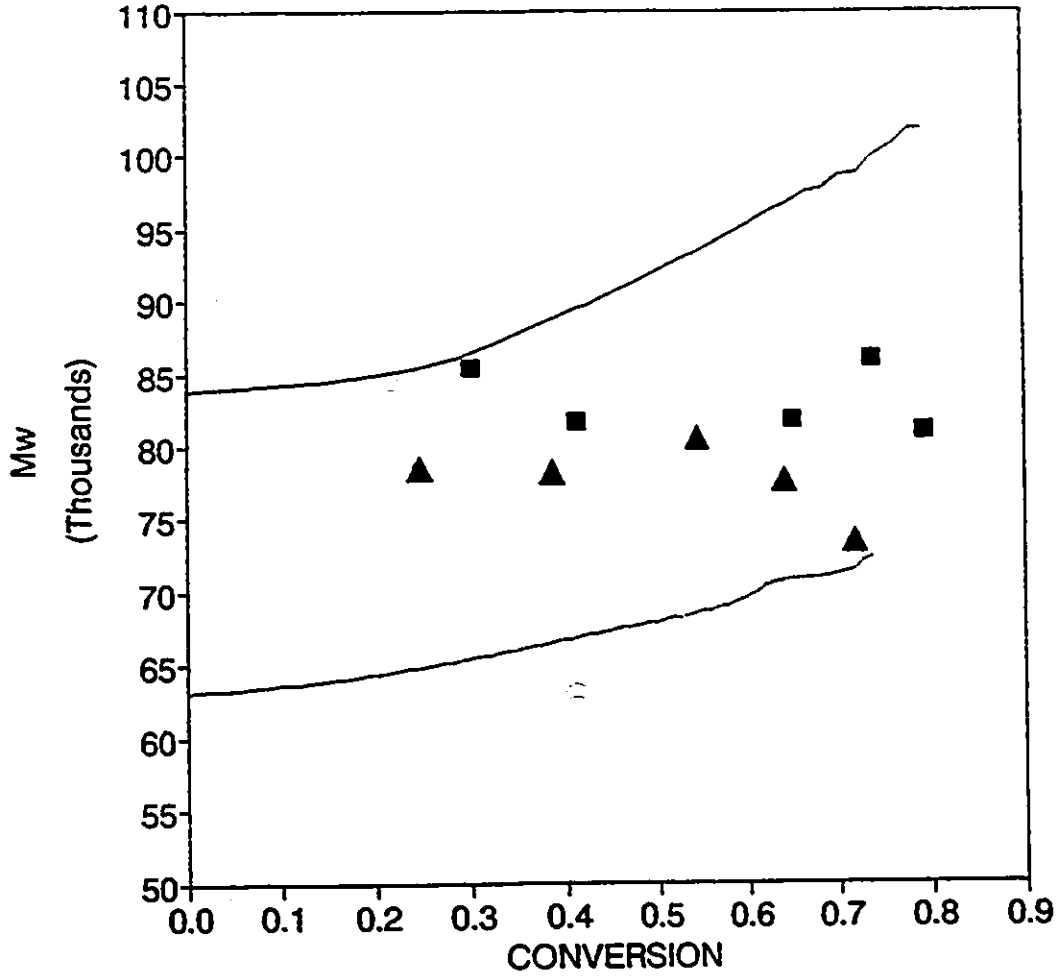

Fig. 7.12. Effect of monomer feed composition on weight average molecular weight development in AMS/NPMI bulk copolymerization with [TPC]=0.01 M/L, at 130°C. Experimental M_w for f_{10}=0.6 (▲), and f_{10}=0.5 (■). Model predictions for f_{10}=0.6 (···), and f_{10}=0.5 (——).

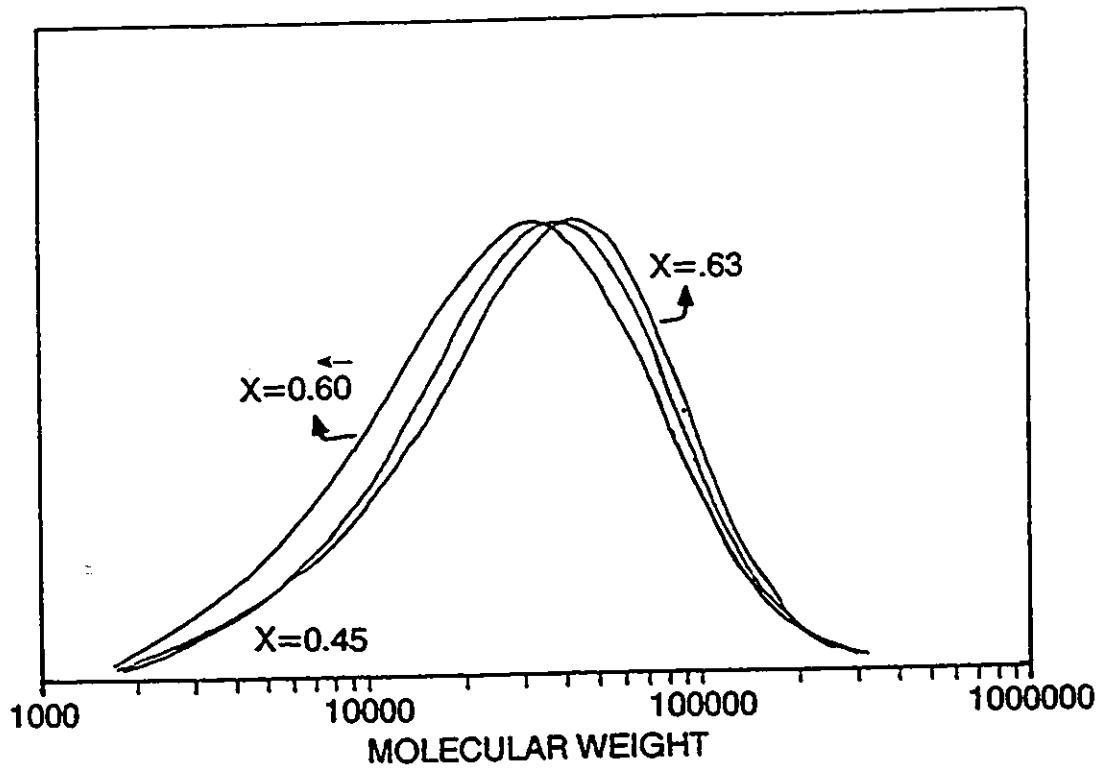

Fig. 7.13. Evolution of the MWD with conversion in AMS/NPMI bulk copolymerization (f_{10}=0.6) with bifunctional initiator [TPC]=0.01 M/L, at 160°C. Curve for X=0.6 shows the MWD after depolymerization from 63% conversion.

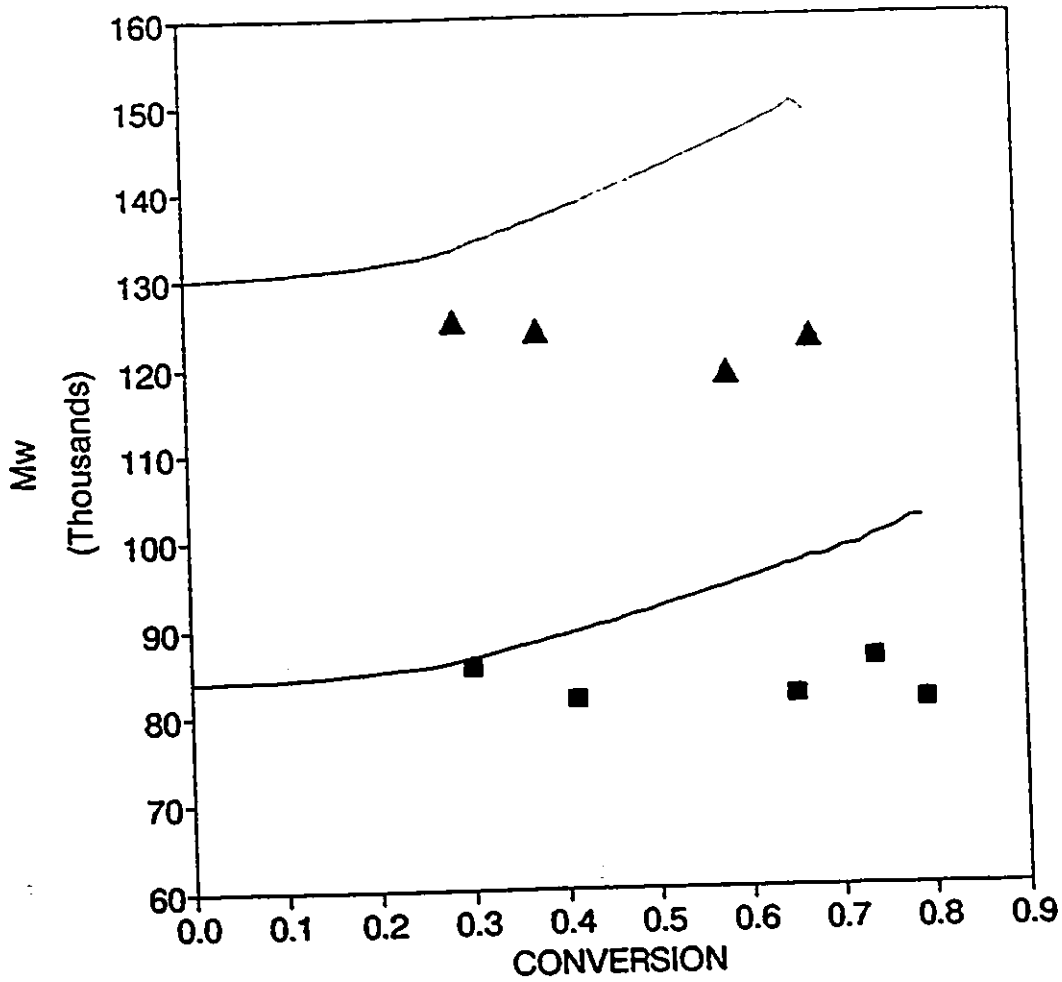

Fig. 7.14. Effect of bifunctional initiator concentration on weight average molecular weight development, in AMS/NPMI bulk copolymerization with f_{10}=0.5, at 130°C. Experimental M_w for [TPC]=0.005 M/L (▲), and [TPC]=0.01 M/L (■). Model predictions for [TPC]=0.005 (···), and 0.01 M/L (——).

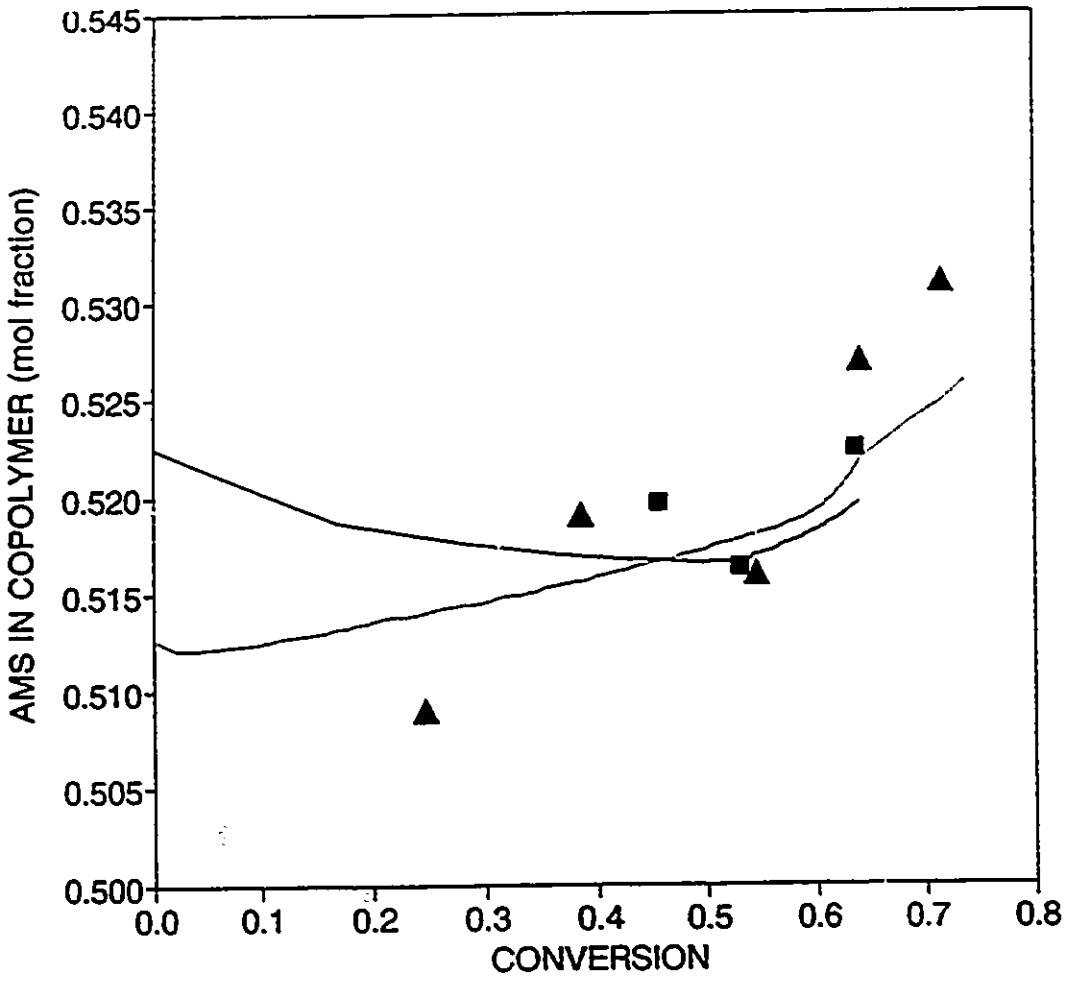

Fig. 7.15. Effect of polymerization temperature on copolymer composition development in AMS/NPMI bulk copolymerization with f_{10}=0.6, [TPC]=0.01 M/L. Experimental results for T_p=130°C (▲), and 160°C (■). Model predictions for T_p=130°C (···), and 160°C (——).

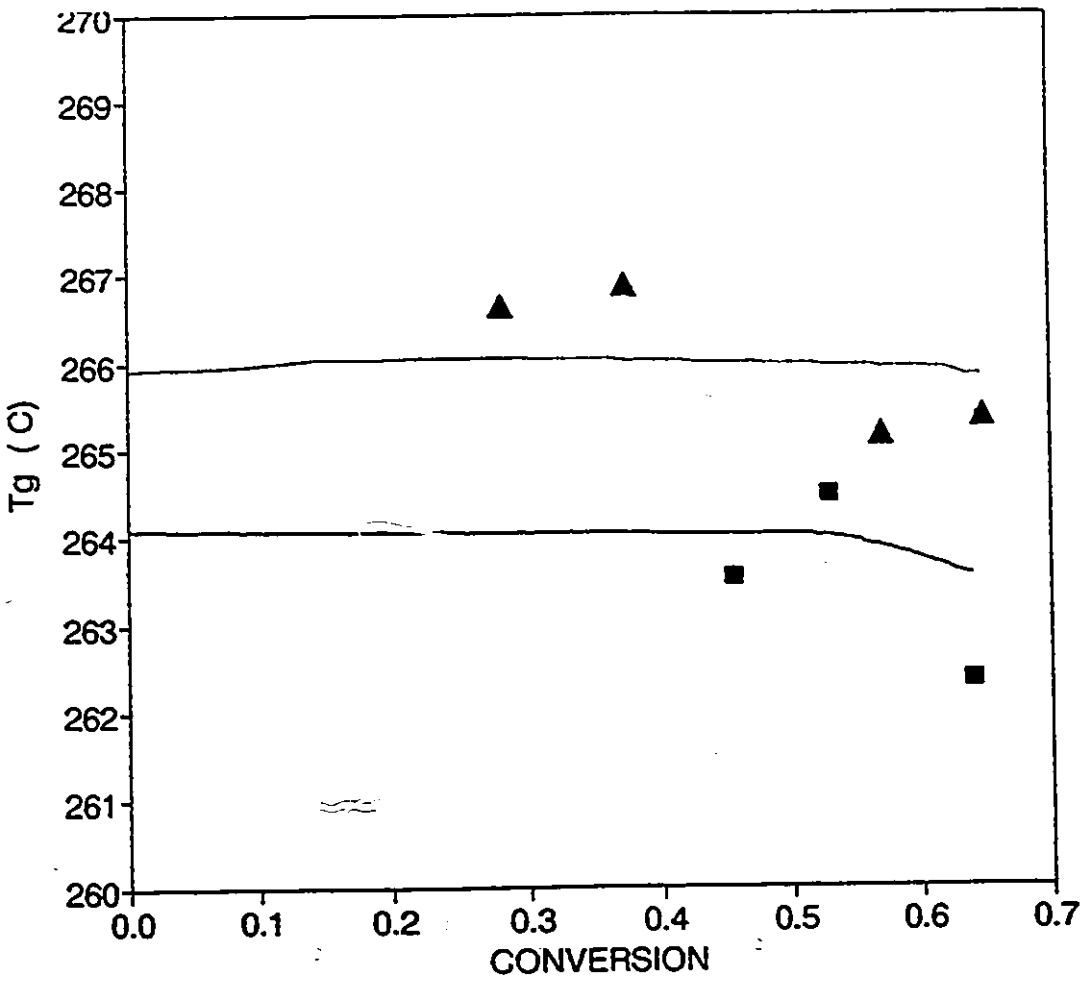

Fig. 7.16. Effect of copolymerization conditions on AMS/NPMI copolymer glass transition temperature development with conversion. Experimental results for f_{10}=0.5, T_p=130°C, [TPC]=0.005 M/L (▲); and f_{10}=0.6, T_p=160°C, [TPC]=0.01 M/L (■). Model predictions (···), and (——), at the same conditions, respectively.

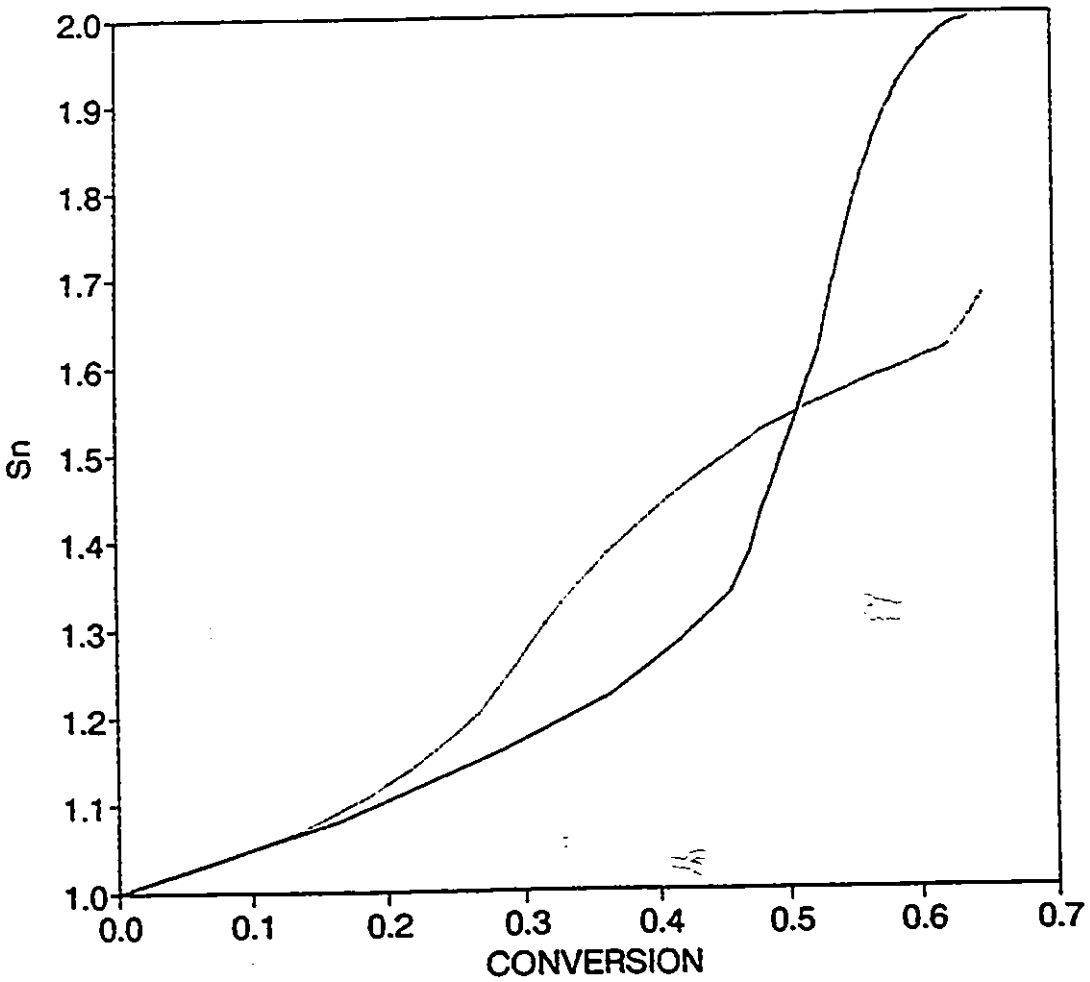

Fig. 7.17. Effect of copolymerization conditions on the development of number average number of segments per copolymer chain for AMS/NPMI copolymers. Experimental results for f_{10}=0.5, T_p=130°C, [TPC]=0.005 M/L (▲); and f_{10}=0.6, T_p=160°C, [TPC]=0.01 M/L (■). Model predictions (···), and (——), at the same conditions, respectively.

CHAPTER 8

TERPOLYMERS OF STYRENE/α-METHYLSTYRENE/N-PHENYLMALEIMIDE

As a complementary part of this research project, in this chapter, an experimental investigation of the synthesis and characterization of styrene/α-methylstyrene/N-phenylmaleimide terpolymers, through bifunctionally initiated free radical polymerization, is performed. Based on the results obtained for the individual binary systems (SAMS, S/NPMI, and AMS/NPMI), conditions were established to synthesize high glass transition temperature terpolymers up to high conversions and high molecular weights. Suspension polymerizations were carried out to evaluate the feasibility to synthesize these terpolymers through bifunctionally initiated free radical suspension polymerization.

8.1 Introduction

Although, free radical SAMS copolymers have been widely studied for more than three decades, and AMS/NPMI copolymers have been recently studied (see Chapter 2), no information has been published as yet on terpolymerization of S/AMS/NPMI (here referred to as SAMS-N).

In the previous three chapters of this thesis, the synthesis, characterization and modelling of binary copolymerization of styrene/α-methylstyrene (SAMS), styrene/N-phenylmaleimide (S/NPMI), and α-methylstyrene/N-phenylmaleimide (AMS/NPMI), with bifunctional initiators, has been described in detail. In these studies, it has been found, that under certain conditions of feed composition, polymerization temperature, and bifunctional initiator concentration, high T_g copolymers can be synthesized up to high conversions and high molecular weights.

Binary SAMS copolymers bearing T_g-115°C, showed that only low concentrations of AMS (-15 mol%) can be bound in the copolymer, in order to achieve high conversions and molecular weights in a reasonable batch time. Binary AMS/NPMI copolymers, bearing T_g-260°C, on the other hand, showed that high AMS concentrations (-50 mol%) can be driven at high rates into the copolymer, through donor-acceptor complex propagation, up to intermediate conversions and molecular weights. The AMS units bound to the copolymer in this way, were unable of depropagate when the statistical formation of AMS diads in the copolymer chains was minimized.

In addition, extremely high copolymerization rates, leading to the formation of very high T_g copolymers (T_g-212°C) up to high conversions and molecular weights, were found when NPMI was introduced in low concentrations (-20 mol%) as comonomer for styrene.

Consequently, it follows that bifunctionally initiated free radical SAMS-N terpolymers, bearing glass transition temperatures between 212 and 260°C, can be synthesized up to high conversions and molecular weights if the following conditions for the comonomer feed composition are followed

a) The concentration of NPMI in the feed must be kept about 20 mol%, in order to provide the necessary stiffness to the copolymer chains, for high T_g products.

b) AMS must be introduced in the feed in lower concentrations than NPMI in order to promote very high complexation of this monomer, thus reducing its participation through free monomer addition, which is responsible for low polymerization rates and low molecular weights.

When these conditions are met, the mechanism of bifunctionally initiated free radical terpolymerization of S/AMS/NPMI can be explained as follows:

At zero conversion, competition of both electron-donor monomers (styrene and AMS) to form the respective donor-acceptor complexes with NPMI will determine the relative amount of both complexes and the three

free monomers in the copolymerization mix. Given that AMS is a stronger electron-donor than styrene, owing to the inductive effect of its CH_3 group, it is thought that the AMS-NPMI complex should form more readily than the S-NPMI one. As a result, the initial mix should comprise, in decreasing molar concentration:

$$[S] > [AMS\text{-}NPMI] > [S\text{-}NPMI] > [NPMI] > [AMS]$$

Since it has been established before that the propagation rate of both complexes is similar (see Chapter 6), upon polymerization, rapid propagation of both complexes must dominate the early stages of the reaction. However, given the relatively large amounts of free styrene in the system, long complex sequences must be frequently interrupted by styrene-rich statistical sequences.

As concentrations of complexes and free monomer decrease, the participation of free monomer addition must become important, thus sharply reducing the observed copolymerization rate. Further decreases in monomer concentration (i.e. higher conversions), will promote negligible complex formation and, therefore, a low rate styrene-rich statistical addition regime of the three free monomers.

8.2 Terpolymerization Mechanism

Little, if anything, is known about terpolymerization when two different donor-acceptor complexes compete in propagation with statistical terpolymerization.

The terminal terpolymerization model has been successfully employed when only one binary pair forms a donor-acceptor complex, by using binary reactivity ratios, calculated through the terminal copolymerization model, to simulate the high alternation experimentally found for the complexing pair [Schmidt-Naake et.al.(1990,a,b)].

Nevertheless, it is stated here that such a model cannot be successfully employed for the case at hand owing to the lack of knowledge on complex formation and propagation behaviour when two different donor-acceptor complexes co-exist in the same reaction mix.

Extension of the binary copolymerization model developed in Chapter 4, for simultaneous binary statistical/donor-acceptor copolymerization, shows that the following complex formation and propagation reactions must be considered when dealing with terpolymerization with the formation of two distinct complexes (M_1 = styrene, M_2 = AMS, M_3 = NPMI):

Formation of Donor-Acceptor Complexes

M_1	+	M_3	$\leftrightarrow$	C_1	(K_{C1}, K_{eq1})
M_2	+	M_3	$\leftrightarrow$	C_2	(K_{C2}, K_{eq2})

Propagation

$R^{\bullet}_{r,1}$	+	M_1	$\rightarrow$	$R^{\bullet}_{r+1,1}$	(K_{11})
$R^{\bullet}_{r,2}$	+	M_1	$\rightarrow$	$R^{\bullet}_{r+1,1}$	(K_{21})
$R^{\bullet}_{r,3}$	+	M_1	$\rightarrow$	$R^{\bullet}_{r+1,1}$	(K_{31})
$R^{\bullet}_{r,1}$	+	M_2	$\rightarrow$	$R^{\bullet}_{r+1,2}$	(K_{12})
$R^{\bullet}_{r,2}$	+	M_2	$\rightarrow$	$R^{\bullet}_{r+1,2}$	(K_{22})
$R^{\bullet}_{r,3}$	+	M_2	$\rightarrow$	$R^{\bullet}_{r+1,2}$	(K_{32})
$R^{\bullet}_{r,1}$	+	M_3	$\rightarrow$	$R^{\bullet}_{r+1,3}$	(K_{13})
$R^{\bullet}_{r,2}$	+	M_3	$\rightarrow$	$R^{\bullet}_{r+1,3}$	(K_{23})
$R^{\bullet}_{r,3}$	+	M_3	$\rightarrow$	$R^{\bullet}_{r+1,3}$	(K_{33})
$R^{\bullet}_{r,1}$	+	C_1	$\rightarrow$	$R^{\bullet}_{r+2,1}$	(K_{1C1})
$R^{\bullet}_{r,2}$	+	C_1	$\rightarrow$	$R^{\bullet}_{r+2,1}$	(K_{2C1})
$R^{\bullet}_{r,3}$	+	C_1	$\rightarrow$	$R^{\bullet}_{r+2,3}$	(K_{3C1})
$R^{\bullet}_{r,1}$	+	C_2	$\rightarrow$	$R^{\bullet}_{r+2,2}$	(K_{1C2})
$R^{\bullet}_{r,2}$	+	C_2	$\rightarrow$	$R^{\bullet}_{r+2,2}$	(K_{2C2})
$R^{\bullet}_{r,3}$	+	C_2	$\rightarrow$	$R^{\bullet}_{r+2,3}$	(K_{3C2})

The extreme complexity of a model involving 15 propagation reactions for monofunctional initiation and 30 for bifunctional initiation (the above propagation reactions take place also with the radicals with one undecomposed peroxide group), makes the development of a comprehensive kinetic model equally complex.

Since the development of such a model is beyond the scope of this thesis (and would very likely represent a complete thesis work by itself), the terpolymerization model will not be developed here. Consequently, this chapter gives account only of the experimental results for the bifunctionally initiated free radical terpolymerization of S/AMS/NPMI.

8.3 Design of Experiments

Following the conditions set above according to the objectives of this project, the exploratory experiments SAMS-N-01, shown in Table 8.1 below, were designed in order to evaluate the effect of the comonomer feed composition, and type of bifunctional initiator, on monomer conversion history, and the development of molecular weights, terpolymer composition, and glass transition temperature, in free radical bulk terpolymerization of S/AMS/NPMI.

Table 8.1

Experimental Design SAMS-N-01 for the Exploratory Research

RUN SAMS-N-01	$f_{10}/f_{20}/f_{30}$ (mol %)	T_p (°C)	[I]o (Mol/L)	POLYM. TIME (hrs)
1	70/10/20	105	0.010[a]	2.0
2	75/10/15	105	0.010[a]	2.0
3	70/10/20	130	0.005[b]	2.0
4	75/10/15	130	0.005[b]	2.0

a) Runs with bifunctional initiator TBPCC.
b) Runs with bifunctional initiator TPC.

The polymerization temperatures and initiator concentrations were set according to the best results obtained during the previous studies for binary copolymerization of S/NPMI and AMS/NPMI, respectively, as; T_p=105°C when [TBPCC]=0.01 M/L was employed, and T_p=130°C when [TPC]=0.005 M/L was employed.

In this study, no optimization research phase was carried out given the narrow set of conditions studied in the exploratory research, established as viable for the synthesis of these terpolymers (see above).

From the results of the exploratory phase, then, two suspension terpolymerization runs, under the conditions given in the experimental design SAMS-N-02 shown in Table 8.2, were carried out to evaluate the effect of the imposed terpolymerization rate on suspension stability mean particle size (MPS), and particle size distribution (PSD).

Table 8.2

Experimental Design SAMS-N-02, Suspension Terpolymerization[a]

RUN SAMS-N-02	$f_{10}/f_{20}/f_{30}$ (mol %)	[I]o (Mol/L) (org. phase)	T_p (°C)	TIME @ T_p (min)
REFERENCE	100/0/0	0.010[b]	105	240
1	70/10/20	0.010[b]	105	120
2	70/10/20	0.005[c]	130	120

a) Scaled reactor arrangement, recipes, and operating conditions as for S/AMS, and S/NPMI suspension copolymerization (see Tables 5.3 and 6.3).
b) Run with bifunctional initiator TBPCC
c) Run with bifunctional initiator TPC.

The beads obtained were characterized, extruded, and exposed to high temperatures, to evaluate the feasibility of these products to commercial use.

8.4 Experimental

8.4.1 Materials

The treatment of styrene, α-methylstyrene, N-phenylmaleimide, bifunctional initiators TBPCC and TPC, as well as solvent (chloroform) and non-solvent (methanol), has been described in detail in Chapters 5 to 7.

8.4.2 Techniques

For the exploratory research, isothermal ampoule bulk polymerizations of SAMS-N, were carried out under the conditions prescribed by the experimental design SAMS-N-01. Ampoule preparation, polymerization, sampling, and characterization of the terpolymers recovered from the samples to determine conversion history, and the development with conversion of molecular weight distribution, terpolymer composition, and terpolymer glass transition temperature, was performed according to the procedures described in Chapters 6 and 7.

For the suspension polymerization runs, the scaled-down reactor internal arrangement, operating conditions and recipes, were used in order to evaluate the results by comparison with the reference polystyrene system. Details of the operation procedures as well as conditions of the reference polystyrene system have been given in Chapters 3 and 5.

Characterization of the beads, to determine MPS, PSD, terminal conversion, molecular weight distribution, terpolymer composition and terpolymer glass transition temperature, were performed according to the procedures described in Chapter 5.

Owing to the high residual monomer content in the terpolymer suspension beads, samples of the beads were devolatilized by exposing them to 200°C for 12 hrs, in vacuo, before extrusion.

Extrusion of the devolatilized beads, and high temperature exposure of the extrudates, to evaluate the processability of the suspension terpolymers, were performed at the same conditions established for S/NPMI copolymers in Chapter 6.

8.5 Results and Discussion

8.5.1 Exploratory Research

According to the experimental design SAMS-N-01, the effects of the feed composition, and bifunctional initiator type (at their respective optimal temperature and concentration conditions), on monomer conversion history, and the development of the molecular weight distribution, terpolymer composition, and glass transition temperature were studied.

Figure 8.1 shows the experimental results for monomer conversion history for the four runs of the experimental design SAMS-N-01. The enlarged area of this figure shows the first ten minutes of polymerization where the largest changes in conversion occur.

In this figure it is noticeable that the systems with 20 mol% of NPMI in the feed reached higher terminal conversions (above 70%) than those with 15 mol%. Also note that the systems with TPC at 130°C show a much higher initial polymerization rate than those with TBPCC at 105°C. In addition, the sharper decrease in polymerization rate exhibited at lower conversions by the systems with 15 mol% of NPMI, demonstrates that the transition from a complex propagation dominated regime to a statistical free monomer addition regime occurs rapidly after the NPMI decreases to levels where complex formation is not extensive.

The limiting conversions exhibited by the systems with 20 mol% of NPMI in the feed, indicate that the continuing propagation in the soft polymer domains after glass transition of the polymerization mix, observed in S/NPMI copolymerization, does not occur in this system. This may be due to the inclusion of AMS units in the statistical styrene rich chains formed at high conversions, which reduces the mobility of these chains, thus preventing them from forming soft domains.

From the enlarged section of this figure, it is evident that the initial polymerization rate of all four systems, is lower than the initial polymerization rates of S/NPMI, and AMS/NPMI copolymers, at similar conditions.

This indicates higher participation of free monomer addition in the early stages of the reaction, during the terpolymerization, than that observed during the copolymerizations mentioned.

In figure 8.2, the effect of monomer feed composition on molecular weight averages development, in bulk S/AMS/NPMI terpolymerization with [TBPCC]=0.01 M/L, at 105°C, is shown.

Similarly as for S/NPMI copolymerization, a decrease in the average molecular weights with conversion is observed for this terpolymer system. This is due to the high propagation rates during the complex propagation dominated early stages of the reaction, followed by the low propagation rates during the statistical free monomer addition regime, at high conversions. As expected, the system with 15 mol% NPMI in the feed, produces lower molecular weight copolymer than the system with 20 mol%. This, again, is due to the lesser formation, and in turn participation, of donor-acceptor complexes at lower NPMI concentrations.

Note that the M_w of the final product synthesized from 20 mol% NPMI in the feed about 155,000, can be considered as close to the target value of 200,000 (see Chapter 5), whereas a lower value of M_w~125,000 was obtained for the system with 15 mol% of NPMI.

The effect of monomer feed composition on molecular weight distribution development in bulk S/AMS/NPMI terpolymerization with [TPC]=0.005 M/L, at 130°C, is shown in figure 8.3.

In this figure it is clear that similar decreasing trends in molecular weights, as for the above conditions, were observed. However, the combined effect of higher temperature and lower initiator concentration for these systems, resulted in higher molecular weight averages.

The system with 20 mol% NPMI in the feed showed a terminal M_w~190,000, very close to the target value (see above), whereas the system with 15 mol% NPMI yielded M_w~115,000. These results show that the extent of complex participation in the propagation reactions is mainly responsible for the molecular weight development of these terpolymers.

Figure 8.4 shows the evolution of the complete MWD with conversion, obtained through SEC, for the system with 15 mol% NPMI in the feed at 105°C. Note how the distributions broadens slightly with conversion towards low molecular weights, to yield the observed polydispersities, PD=M_w/M_n, about 3.1.

Figure 8.5 shows the terpolymer composition development in bulk S/AMS/NPMI terpolymerization with [TBPCC]=0.01 M/L, at 105°C. In this figure, note that the extrapolated initial terpolymer composition approaches 53/12/35, and 57/17/26 (S/AMS/NPMI mol%) for the initial feed compositions 70/10/20, and 75/10/15, respectively. This clearly indicates that at these conditions, the AMS/NPMI complex forms in higher concentrations than the S/NPMI complex. As a result AMS units are readily driven into the copolymer by its complex propagation, thus preventing the system from forming long statistical sequences of AMS which may be prone to depropagate [O'Driscoll and Dickson (1968)].

In addition, the relatively low initial concentrations of NPMI in the terpolymer indicates that its preferable complexation with AMS prevents the formation of larger amounts of S/NPMI complex, thus increasing the participation of free styrene addition, which reduces the initial terpolymerization rates, as discussed in figure 8.1, above.

At terminal conversion, the final terpolymer compositions about 64/9/27 and 71/7/22 (S/AMS/NPMI mol%) for the initial feed compositions 70/10/20, and 75/10/15, respectively, show that AMS units are driven into the copolymer almost exclusively during the early stages of the polymerization. At high conversions, therefore, styrene-rich chains formed through statistical addition, dominate the polymerization owing to the fact that free NPMI must be in extremely low concentration, given that it has been driven into the copolymer through complex propagation with both other monomers. As a result, the styrene contents in the terpolymer increases rapidly during this stage.

For the systems polymerized with [TPC]=0.005 M/L, at 130°C, figure 8.6 shows a substantially different terpolymer composition development.

In this figure, the extrapolated initial terpolymer compositions about 51/6/43, and 52/8/40 (S/AMS/NPMI mol%), obtained from feed compositions 70/10/20, and 75/10/15, respectively, indicate that at these conditions NPMI forms complex preferably with styrene than with AMS. As a result nearly equimolar S/NPMI copolymer is formed, with some participation of AMS/NPMI complex in lesser concentration.

Since lower amounts of free styrene monomer are present at these conditions than at 105°C, higher initial polymerization rates, and higher molecular weights, are achieved. The somewhat larger amounts of free AMS in these systems with the consequent larger participation of this monomer through free addition in the styrene-rich chains formed at high conversions, are, then, responsible for the sharp decrease in polymerization rates and molecular weights observed after the concentration of the complexes in the system becomes negligible.

The terpolymer compositions observed at terminal conversions about 64/7/29, and 68/10/22 (S/AMS/NPMI mol%), from feed compositions 70/10/20 and 75/10/15, corroborate the larger participation of free AMS in the terpolymerization at 130°C than at 105°C.he

Figure 8.7 shows the evolution with conversion of the aliphatic portion of the H-NMR spectrum (0 to 4 ppm) for S/AMS/NPMI terpolymers, synthesized at 105°C, with [TBPCC]=0.01 M/L, from a 70/10/20 feed composition. Note in this figure the increase with conversion of the area of CH protons of styrene and NPMI units (peak -2.25 ppm) mostly due to styrene increases in concentration, as well as the increase in the areas of CH_2 protons of styrene and AMS units (peak -1.75 ppm) also due to the increase in styrene concentration. On the other hand, the relative area of CH_3 protons of AMS units (peak -0.5 ppm) decreases slightly with conversion, as expected from the increase in styrene units bound to the copolymer.

Since the synthesis and characterization of this terpolymer has never been published before (as far as the author knows), the interpretation of these spectra was carried out by quantifying the molar contributions of the styrene and NPMI units to the area of CH protons. In turn, the concentration of styrene units was established by quantifying its molar contribution to the CH_2 areas of the spectra (S + AMS), subtracted from the area of CH_3 protons (AMS). By following this procedure, all terpolymer compositions reported in this study were established.

In figure 8.8, the development of T_g with conversion for the four terpolymer systems given in the experimental design SAMS-N-01, are shown.

From the curves in this figures it is easy to see that terpolymers with high initial glass transition temperatures (extrapolated from the initial experimental values shown), in the range of 220 to 224°C, are formed in the early stages of the reaction. This is undoubtedly due to the highly alternating chain structures formed through the propagation of both complexes, with limited free monomer addition.

As conversion increases, the T_g of both systems synthesized with [TPC]=0.005 M/L, at 130°C, sharply decreases to their values at terminal conversion about 212°C ($f_{10}/f_{20}/f_{30}$ = 70/10/20), and 202°C (75/10/15), with the latter system exhibiting a second lower glass transition, $T_{g soft}$=123°C, with a soft fraction of about 12 mol%. This is undoubtedly due to the larger free styrene participation throughout the reaction coordinate which leads to the production of lower T_g chains as its concentration in the terpolymer increases (see discussion of figure 8.1).

On the other hand, both terpolymers synthesized with [TBPCC]=0.01 M/L, at 105°C, experience only a slight decrease in T_g throughout the reaction coordinate. This moderate decrease is brought about by the larger participation of AMS during the late stages of the polymerization. The values of T_g=217°C (system with 70/10/20 molar feed composition), and T_g=218°C, observed for these terpolymers, are similar to those obtained for S/NPMI copolymers (T_g 212 to 217°C see Chapter 6).

The large extent of chain recombination caused by the multiple macro-initiation/propagation/termination cycles in bifunctionally initiated free radical polymerization, is evident in these systems from the fact that only a single high T_g, was observed for systems comprised by 70 to 75 mol% styrene, and only 15 to 20% NPMI.

The high glass transition temperatures exhibited by these S/AMS/NPMI terpolymers, makes them very attractive as engineering copolymers for high temperature applications (see Chapter 1).

8.5.2 S/AMS/NPMI Suspension Terpolymerization

From the results of the exploratory phase, it is clear that the best balance of terminal conversion-molecular weight-glass transition temperature, of the terpolymers studied, was obtained when the monomer feed compositions of 70/10/20 (S/AMS/NPMI mol%), were employed.

Accordingly, the terpolymers systems SAMS-N-01, and SAMS-N-03, were chosen to carry out suspension S/AMS/NPMI terpolymerizations. The conditions of these runs correspond to the initial feed composition of 70/10/20 (mol%) with [TBPCC]=0.01 M/L at 105°C (01), and [TPC]=0.005 M/l, at 130°C (03).

The suspension copolymerizations were carried out under the scaled-down reactor conditions and recipes, prescribed by the experimental design SAMS-N-02 (see Table 8.2).

Both suspension terpolymerization runs were successfully completed. In both cases stable suspensions leading to the formation of non-aggregated spherical beads, opaque, with a slight beige coloration, were obtained.

Figure 8.9, shows the particle size distribution (PSD) of the two suspension terpolymers, along with the PSD for the reference polystyrene system ([TBPCC]=0.01 M/L, T_p=105°C).

For the terpolymer beads synthesized at 105°C, using TBPCC as bifunctional initiator, a mean particle size, MPS=0.76 mm was calculated from the discrete PSD measurements, with a coefficient of variation, CV=σ/MPS=0.435.

Comparison with the reference suspension polystyrene system (MPS=0.542 mm, CV=0.361), shows that this terpolymer system presents higher particle coalescence leading to larger particle growth during the sticky stage. This may be due to a combination of the high polymerization rates and a more sticky character of the beads containing large amounts of residual monomer. Nevertheless, the suspension can be qualified as stable inasmuch as suspension set-up is a possibility only when the beads grow rapidly to sizes larger than 3 mm [Villalobos (1989)].

A terminal conversion X_t=80.3%, determined for the terpolymer recovered from the beads, was about 8% larger than that observed during the exploratory research for the same system in bulk ampoule polymerization. The high stirring rate in the suspension polymerization reactor, along with the multiple fragmentation of the particles during breakage and the subsequent coalescence, must have led to a much better mixing of the reacting species with the consequent higher conversions observed.

The molecular weight averages M_n=53000, and M_w=163000, as well as the terpolymer glass transition temperature, T_g=219.25°C, and terpolymer composition, 66/09/25 (S/AMS/NPMI mol%), for the S/AMS/NPMI terpolymer recovered from the beads, were very similar to those observed during the exploratory phase for this system (see above).

For the beads synthesized at 130°C, with TPC as bifunctional initiator, the same MPS=0.76 mm was observed. The PSD, however, was slightly narrower for this terpolymer system, CV=0.427 (vs 0.435 for run 01), with the peak of this distribution at a PS=0.66 mm being more defined than for the former system.

Characterization of the terpolymer recovered from the beads, also showed higher terminal conversions than for the bulk system at the same conditions, X_t=86.3% (X_t=76% for bulk). The reasons being the same as explained before. The molecular weight averages, M_n=59000, and M_w=182000, as well as the terpolymer glass transition, T_g=215.22°C, and composition, 68/9/23 (mol%), were all in good agreement with the values found for this system during the exploratory research (see above).

The summary of the bifunctionally initiated S/AMS/NPMI suspension terpolymerization results, is given below in Table 8.3.

Table 8.3

Summary of Suspension Terpolymerization Results

RUN → VARIABLE	REFERENCE POLYSTYRENE(*)	SAMS-N-02 01	SAMS-N-02 02
MPS (mm)	0.542	0.760	0.760
σ (mm)	0.196	0.330	0.325
CV=σ/MPS	0.361	0.435	0.427
CONVERSION	0.999	0.803	0.863
Mn	83870	53432	58973
Mw	203011	163248	182437
F_1 (mol)	1.000	0.663	0.679
F_2 (mol)	0.000	0.083	0.089
F_3 (mol)	0.000	0.254	0.232
T_g (°C)	98.60	219.25	215.22

* See Chapter 3 for reference system results.

Samples of the beads obtained in both runs were devolatilized through the procedures described in section 8.4, and extruded in a RandleCastle Minitruder, at 275°C, and 50 rpm, following the procedures described in chapter 5. The residence time of the terpolymer in the extruder was 1.16 min, and 1.25 min, for samples SAMS-N-02-01, and 02, respectively.

Opaque, continuous extrudates, with appreciable swelling at the die exit, D/d~2.35, were obtained in both cases. A single glass transition temperature, T_g=218.54°C, and T_g=216.36°C, for extrudates 01 and 02, respectively, were determined. The slight variations observed with respect to the T_g of the devolatilized beads, before extrusion, is within the error limits of DSC determinations, and showed that annealing or degradation of the products during extrusion, did not occur.

Exposure of samples of the extrudates to 300°C during 5 and 10 hours, showed no appreciable mass losses for any of the products. This means that the products are thermally stable at the conditions tested, in spite of the content of AMS in the polymer chains. This verifies the hypothesis that AMS units are only able to depropagate when they form sequences equal or larger than two units. The summary of the terpolymer degradation tests is given below in Table 8.4.

Table 8.4

Terpolymer Extrusion and Degradation Results

SAMPLE SAMS-N -02-	BEADS T_g (°C)	EXTRUD T_g (°C)	MASS LOSS(%)* 5 hrs @300°C	MASS LOSS(%)* 10 hrs @300°C	BEADS Mw
1	219.25	218.54	0.000	0.000	163248
2	215.22	216.36	0.000	0.000	182437

* Results of sample characterization after exposure to the prescribed conditions (variations observed were only within the limit of precision of the analytical balance used).

These products, in almost every regard, were similar to the S/NPMI copolymers studied in Chapter 6. An advantage of the terpolymer over the copolymer, however, resides in its more moderated polymerization rate which may be more controllable in large scale reactors, even though the terpolymer particles showed larger coalescence rates than those observed during S/NPMI suspension copolymerization.

8.6 Conclusions

Styrene/α-methylstyrene/N-phenylmaleimide engineering terpolymers, bearing glass transition temperatures between 215 and 220°C, can be synthesized up to high conversions and high molecular weights through bifunctionally initiated free radical suspension polymerization.

Two synthesis routes yielding a good balance of terpolymer properties, polymerization rates, and terminal conversions, have been identified as feasible for scaling-up.

The first route involves a feed composition of 70/10/20 (S/AMS/NPMI mol%), polymerized in batch for 2 hours at 105°C, using 1,4-bis(tertbutyl peroxycarbo)cyclohexane as bifunctional initiator, in a concentration of 0.01 M/L.

The second route involves the same feed composition (70/10/20), polymerized in batch for 2 hours at 130°C, using 1,1-di(tertbutyl peroxy)cyclohexane as bifunctional initiator, in a concentration of 0.005 M/L.

Both suspension terpolymerization systems were equally stable, even under the high copolymerization rates exhibited by these systems, and led to the formation of spherical beads, without the formation of aggregates.

Since both systems were found to be stable under the scaled-down reactor conditions for suspension polystyrene, it follows that these suspension terpolymer systems could be produced in larger reactors, provided that the larger particle coalescence rates exhibited by these terpolymers with respect to those observed for polystyrene, be more strictly controlled through higher stabiliser concentrations.

The high T_g suspension terpolymers synthesized, were processable through extrusion at moderate temperatures (275°C), and thermally stable for at least 10 hours at 300°C. Therefore, these terpolymers may find use in engineering applications to temperatures up to 200°C.

The incorporation of up to 10 mol% of AMS units in the terpolymer, seems to be beneficial to the synthesis of these products inasmuch as more controllable polymerization rates and unimodal molecular weight distributions are achieved, differently from S/NPMI copolymers in which very high initial polymerization rates and broad molecular weight distributions are obtained. In this sense, the inclusion of small amounts of AMS into the S/NPMI copolymerization formulations, seems to improve the quality of the product.

Although, the development of a kinetic model for the simultaneous and competitive statistical/donor-acceptor terpolymerization, with two complexing donor-acceptor pairs, was not pursued here, a set of elementary propagation reactions on which such model can be based, has been proposed in this work.

Finally, in addition to the suspension terpolymers synthesized, this study gives good experimental bases for the synthesis of S/AMS/NPMI terpolymers, through bulk free radical polymerization with bifunctional initiators.

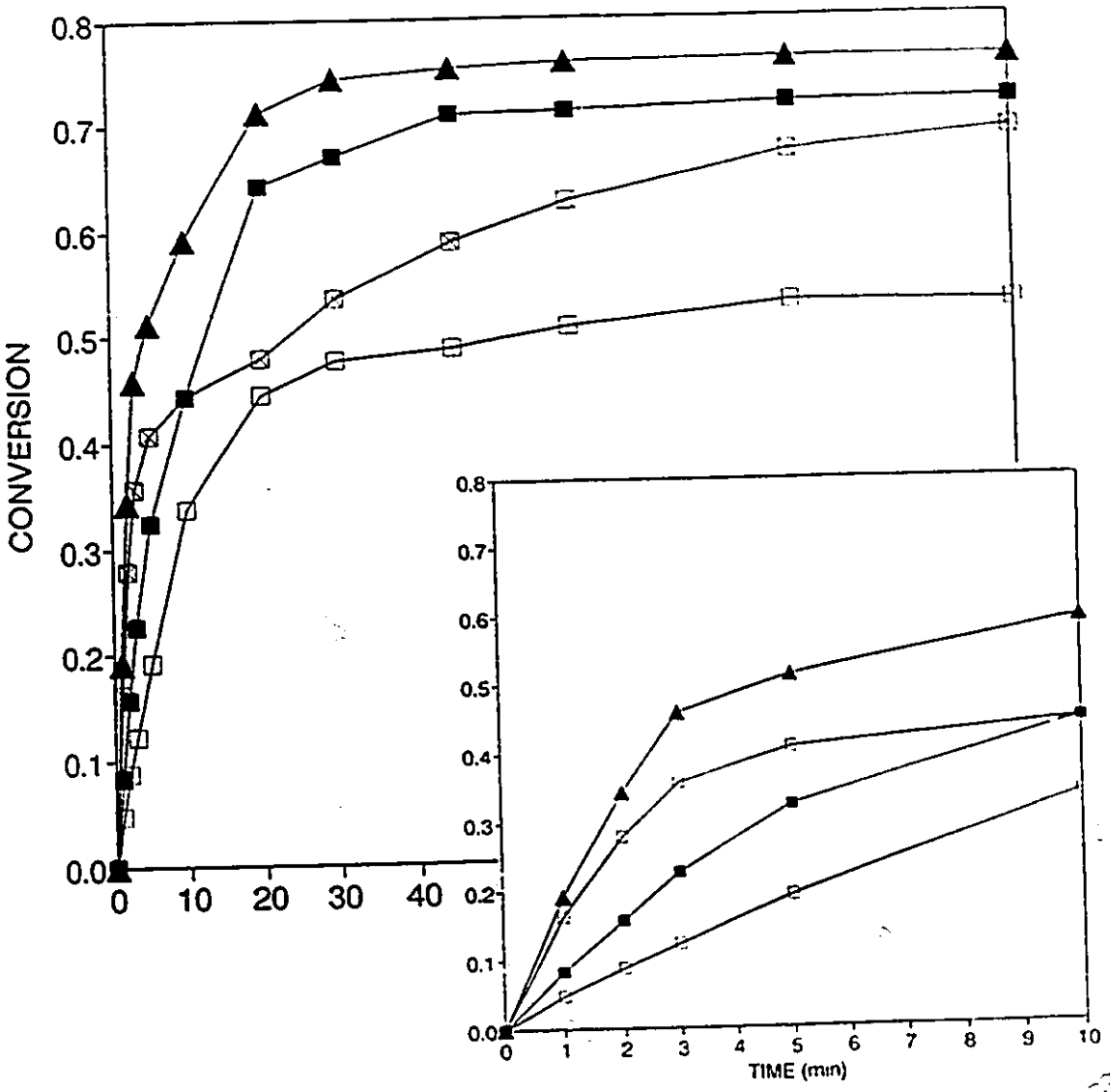

Fig. 8.1. Effect of monomer feed composition and polymerization conditions on monomer conversion history in bifunctionally initiated bulk S/AMS/NPMI terpolymerization. Results for feed composition 70/10/20 mol% at: T_p=105°C, [TBPCC]=0.01 M/L (▲), and T_p=130°C, [TPC]=0.005 M/L (■); and feed composition 75/10/15 mol% at; T_p=105°C, [TBPCC]=0.01 M/L (□), and T_p=130°C, [TPC]=0.005 M/L (▣).

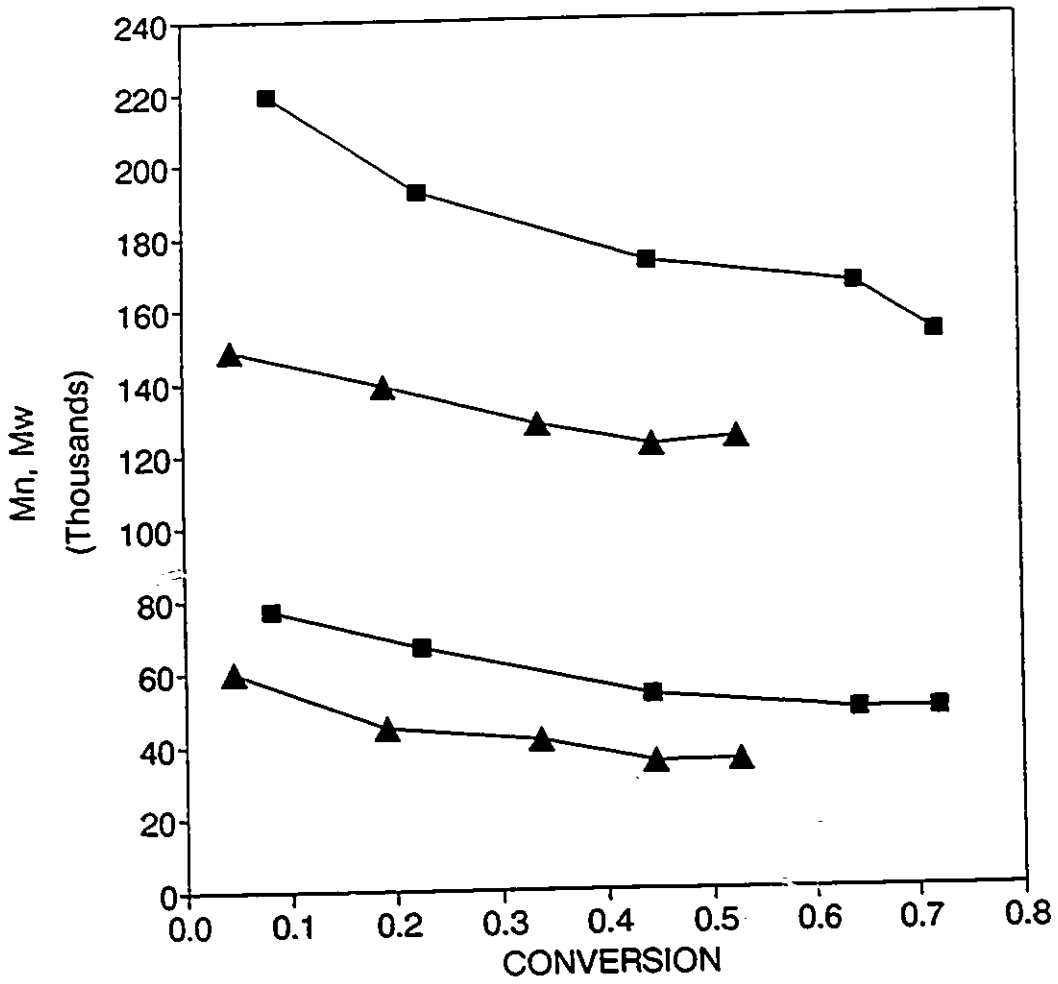

Fig. 8.2. Effect of monomer feed composition on molecular weight averages development in bulk S/AMS/NPMI terpolymerization with [TBPCC]=0.01 M/L, at 105°C. M_n and M_w results for 70/10/20 mol% (■), and 75/10/15 (▲).

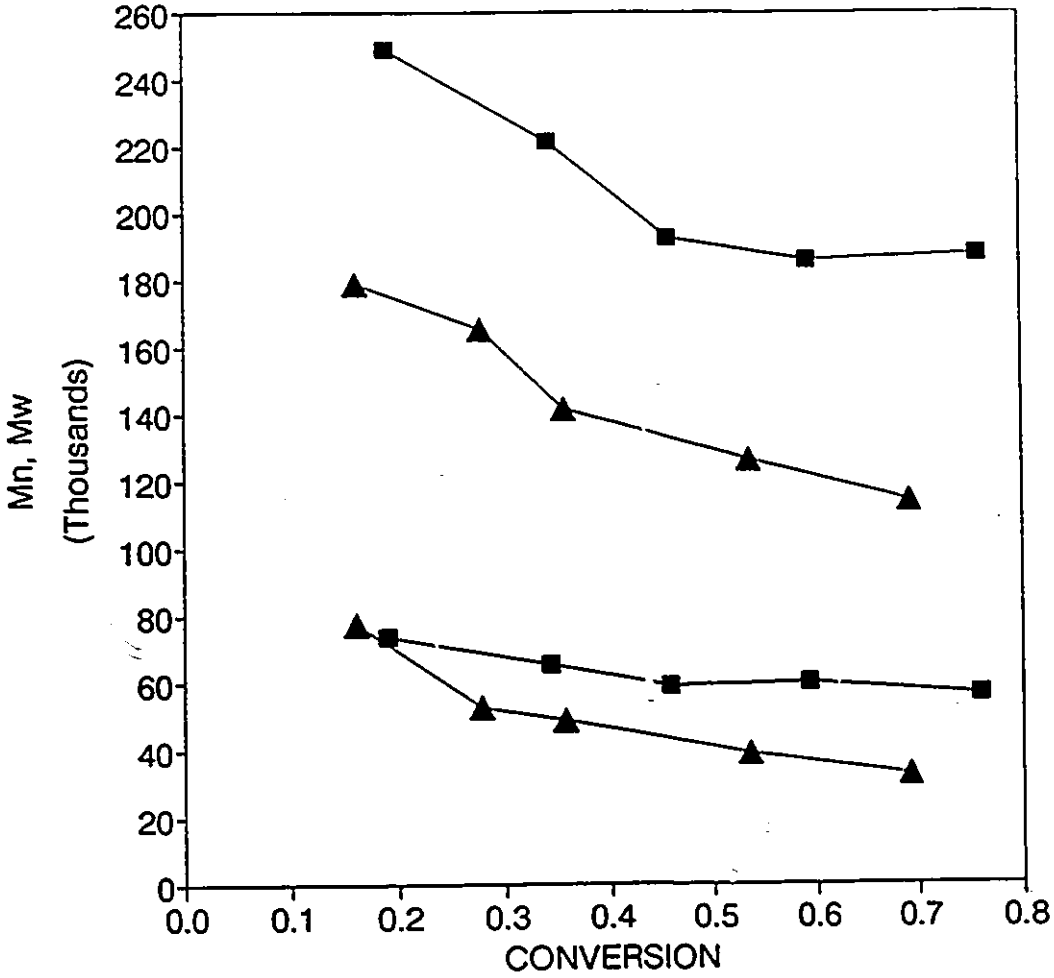

Fig. 8.3. Effect of monomer feed composition on molecular weight averages development in bulk S/AMS/NPMI terpolymerization with [TPC]=0.005 M/L, at 130°C. M_n and M_w results for 70/10/20 mol% (■), and 75/10/15 (▲).

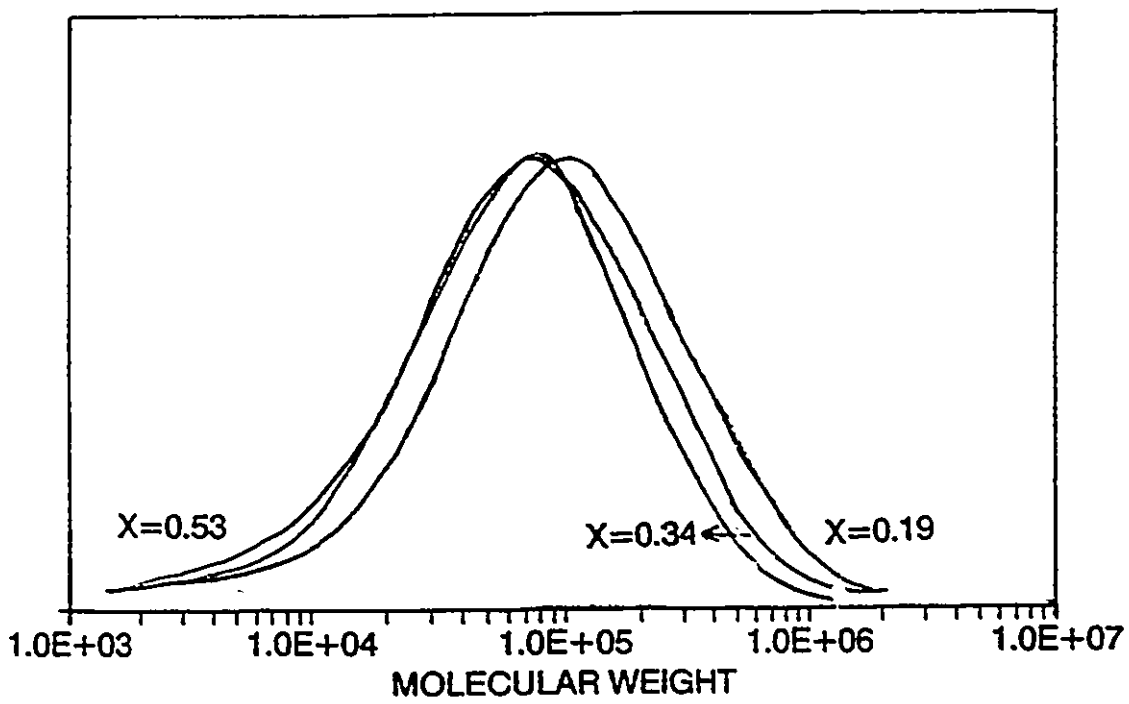

Fig. 8.4. Evolution of the molecular weight distribution with conversion during bulk S/AMS/NPMI terpolymerization at 105°C with [TBPCC]=0.01 M/L. Feed composition 75/10/15 mol%.

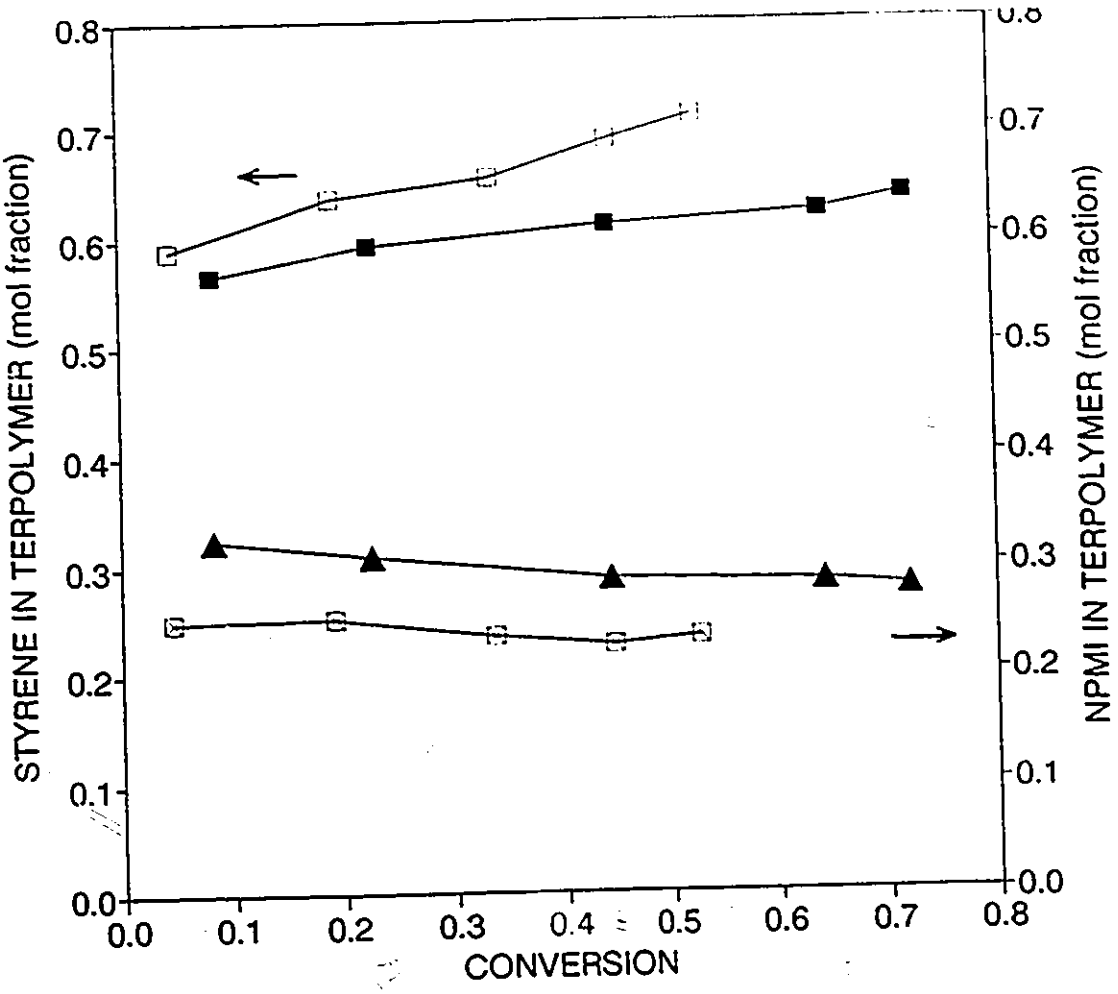

Fig. 8.5. Effect of monomer feed composition on S/AMS/NPMI terpolymer composition development. Bulk terpolymerization with [TBPCC]=0.01 M/L, at 105°C. Results for feed composition 70/10/20 mol%: F_1 (■), F_2 (▲); and 75/10/15 mol%: F_1 (□), F_2 (Ø).

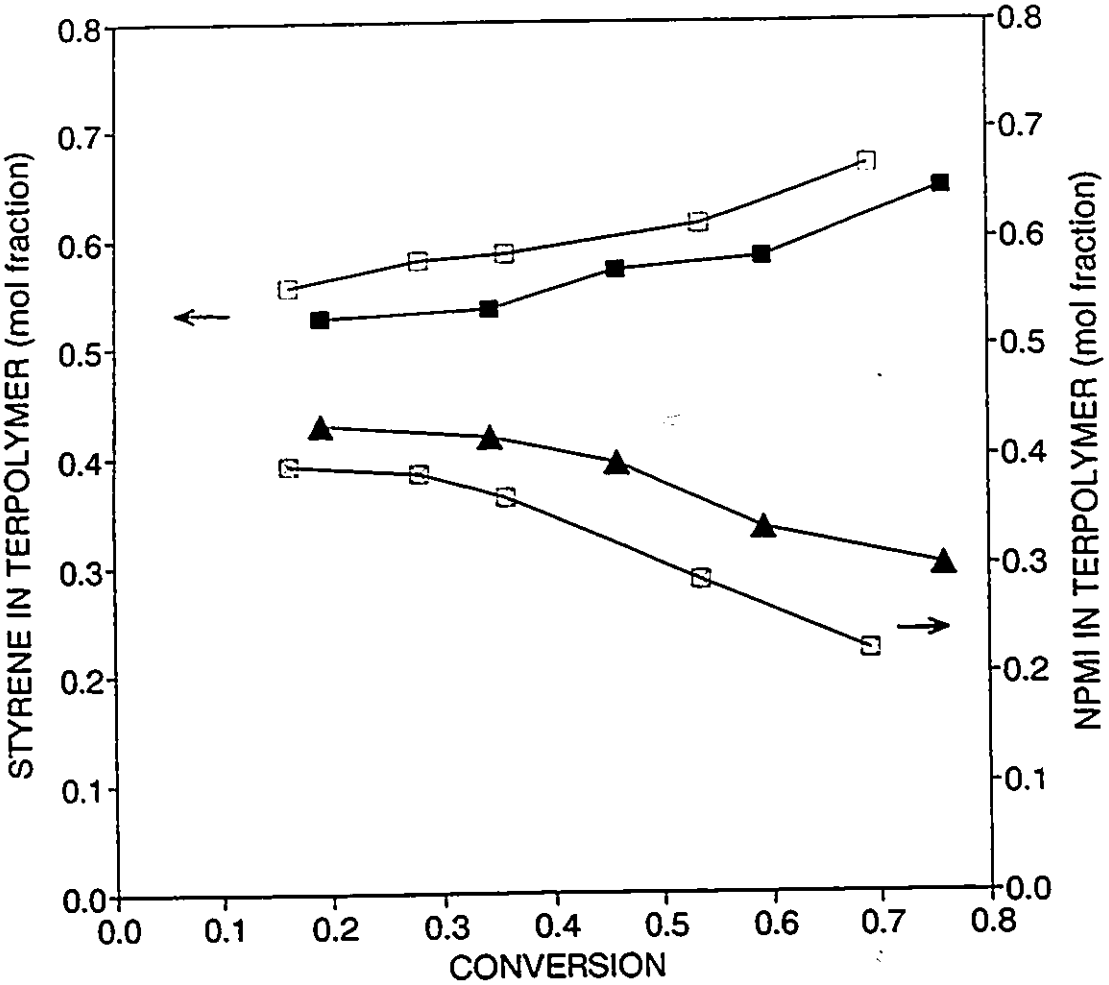

Fig. 8.6. Effect of monomer feed composition on S/AMS/NPMI terpolymer composition development. Bulk terpolymerization with [TPC]=0.005 M/L, at 130°C. Results for feed composition 70/10/20 mol%: F_1 (■), F_3 (▲); and 75/10/15 mol%: F_1 (□), F_3 (▣).

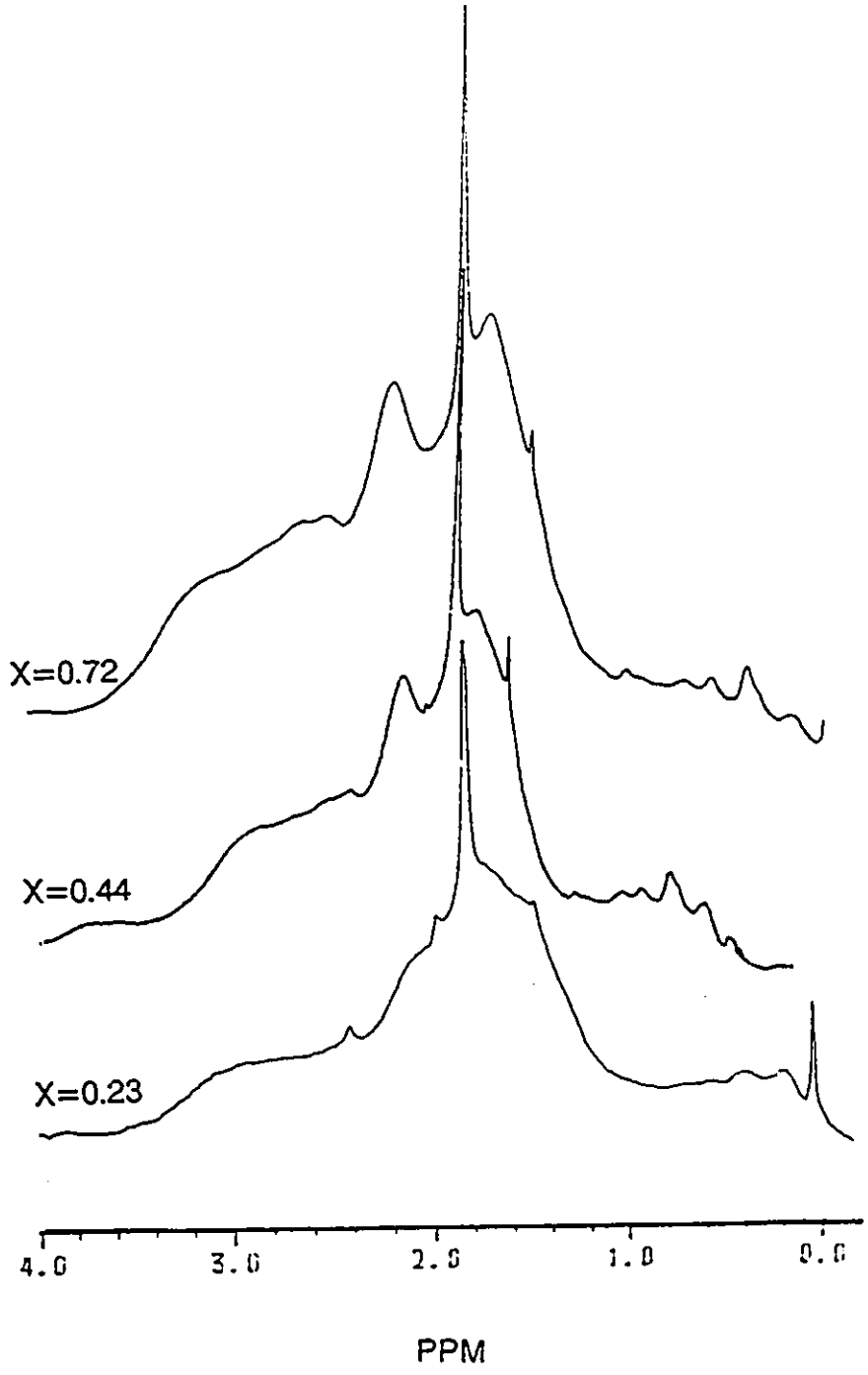

Fig. 8.7. Evolution of the aliphatic portion (0 to 4 ppm) of the H-NMR spectrum of S/AMS/NPMI terpolymers, during bulk copolymerization at 105°C with [TBPCC]=0.01 M/L. Feed composition 70/10/20 mol%.

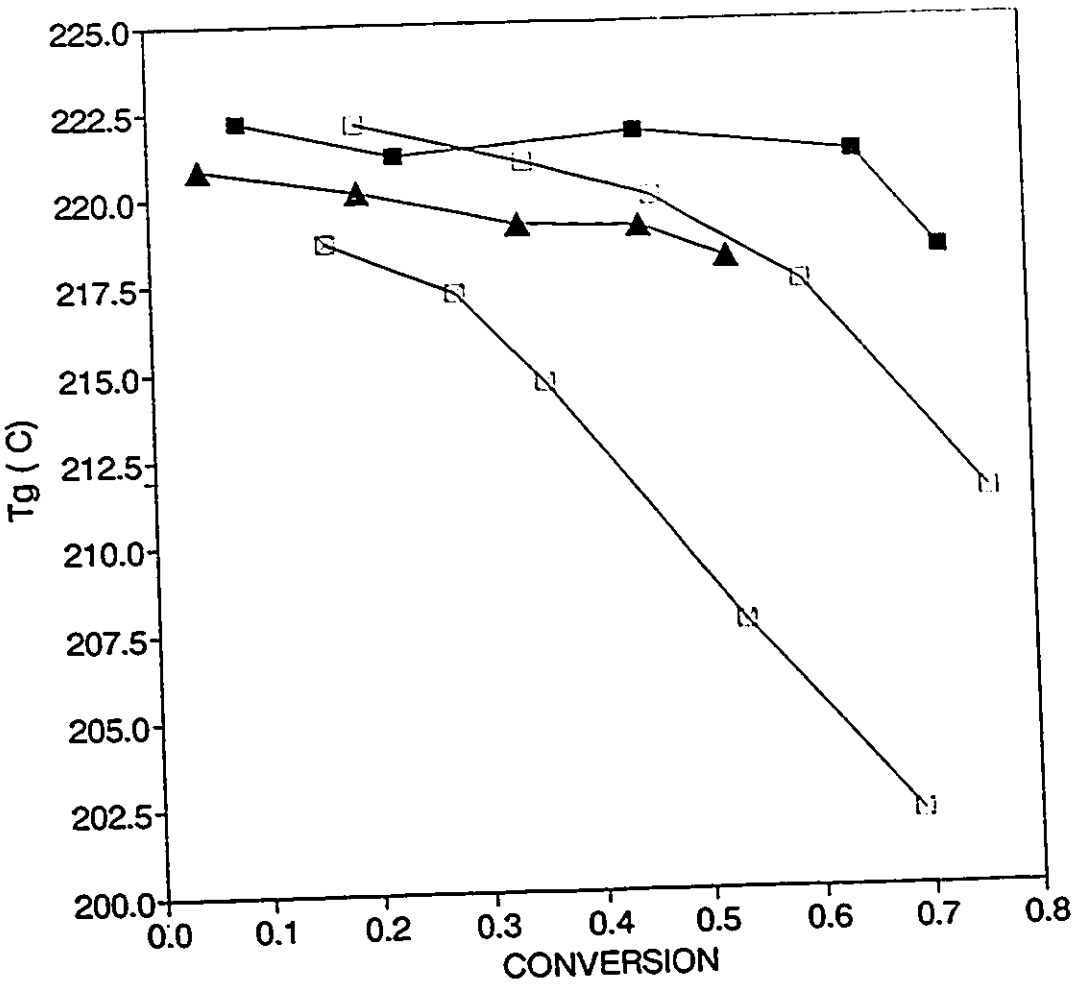

Fig. 8.8. Effect of monomer feed composition and polymerization conditions on terpolymer glass transition temperature development in bulk S/AMS/NPMI terpolymerization. Results for feed composition 70/10/20 mol% at: T_p=105°C, [TBPCC]=0.01 M/L (■), and T_p=130°C, [TPC]=0.005 M/L (□); and feed composition 75/10/15 mol% at: T_p=105°C, [TBPCC]=0.01 M/L (▲), and T_p=130°C, [TPC]=0.005 M/L (⊠).

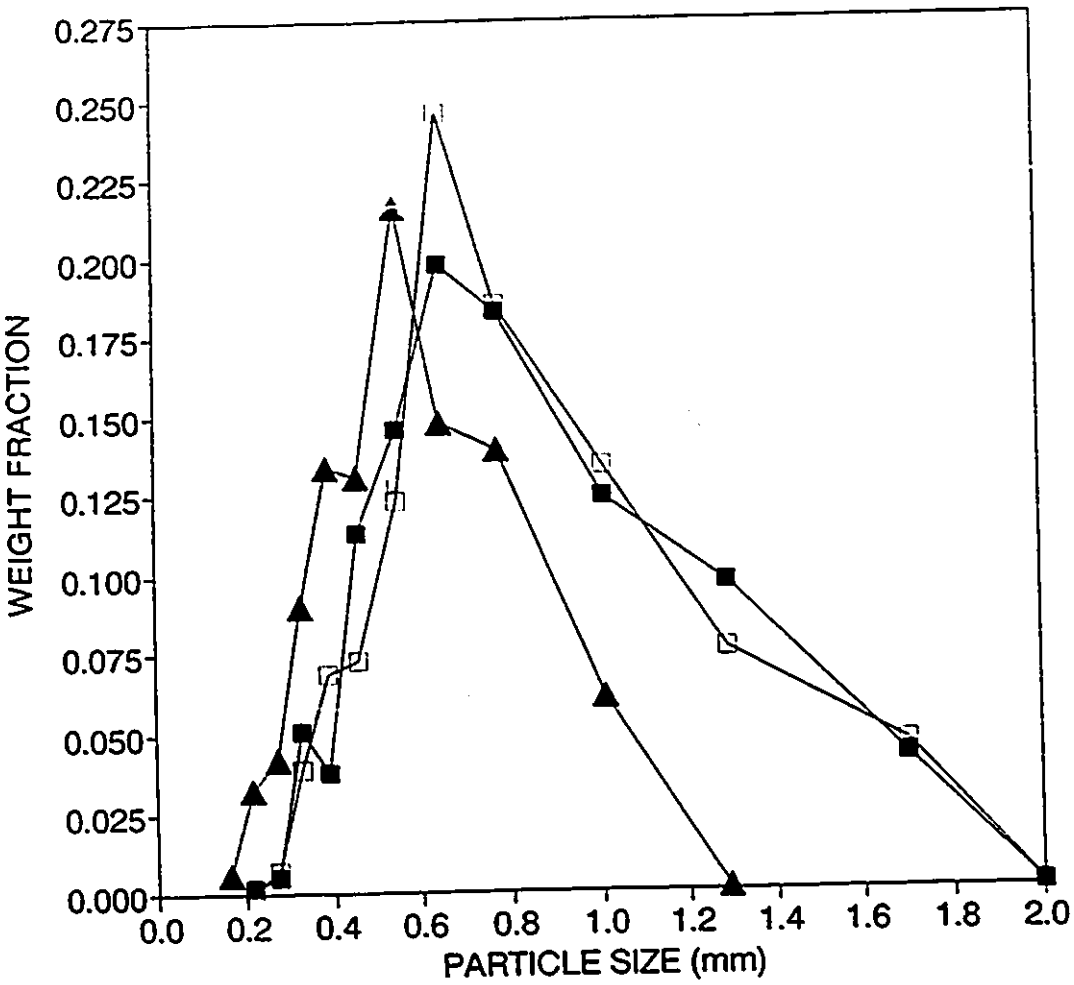

Fig. 8.9. Particle size distribution for S/AMS/NPMI suspension terpolymers, feed composition 70/10/20 mol%. Results for T_p=105°C, [TBPCC]=0.01 M/L (■); T_p=130°C, [TPC]=0.005 M/L (□); and reference polystyrene system T_p=105°C, [TBPCC]=0.01 M/L (▲) (see Table 8.2 for reactor operating conditions).

CHAPTER 9

CONCLUDING REMARKS AND RECOMMENDATIONS

In what follows a summary of the most important results of this research project, along with its main contributions to the field, and recommendations for future work in this area, are given.

A comprehensive kinetic model describing the most important features of bifunctionally initiated free radical homo and copolymerization processes has been developed, along with a statistical model describing the molecular events which define the micro-structural characteristics of polymers formed when bifunctional initiators are employed.

The kinetic and micro-structure models developed considering simultaneous and competitive statistical/donor-acceptor copolymerization with bifunctional initiators, have been integrated into the simulation program BICOP.

This program has proven to successfully simulate monomer conversion history, and the development of molecular weight distribution, copolymer composition, copolymer glass transition temperature, and copolymer multi-block formation, for binary statistical copolymerization, binary donor-acceptor copolymerization, and simultaneous statistical/donor-acceptor copolymerization. This program has also been successfully used to simulate homopolymerization.

It is recommended here, however, that further refinements be introduced into the models, by considering reversible propagation reactions for one of the monomers, inasmuch as model disagreement with experimental molecular weight distribution development, has been important in copolymer systems exhibiting considerable depropagation.

Throughout this thesis five experimental studies on free radical homopolymerization, and copolymerization with bifunctional initiators have been carried out.

The first study carried out in this work, has demonstrated that suspension expandable polystyrene (EPS) can be synthesized in a single stage process comprising the up to now separated polymerization and impregnation stages. In this process, suspension polymerization of styrene is carried out with addition of the blowing agent in the early stages of the polymerization, employing bifunctional initiation at polymerization temperatures above the glass transition temperature of polystyrene.

The novel resulting combined polymerization/impregnation process is completed in a batch time of less than 6 hours, which represents an increase in productivity of nearly 100%, since current EPS manufacturing processes require between 11 and 12 hours to complete the separated polymerization/impregnation stages. In addition, the scale-up of this novel process to commercial production is considered as highly feasible, inasmuch as more stable suspensions leading to smaller particle sizes and narrower distributions, than those obtained with the current monofunctionally initiated process, were obtained.

Comparison between monofunctional and bifunctional initiation in these processes of early impregnation of suspension polystyrene, has shown that the single stage process cannot be carried out in monofunctionally initiated systems due to extended particle growth stages which lead to eventual suspension set-up.

The understanding and modelling of the multiple initiation/propagation/termination cycles experienced by the polymer chains which leads to the formation of multi-block structures during bifunctionally initiated free radical polymerization, has been instrumental in the design of high glass transition temperature engineering copolymers in this work.

These multiple chain recombination phenomena, have been comprehensively described through the effective instantaneous copolymer composition theory, proposed in Chapter 4, and modelled through the definition of the distribution of the number of segments (blocks) per copolymer chain, developed in this thesis.

By taking advantage of this multiple chain recombination to modify polystyrene through the introduction of small amounts of α-methylstyrene and N-phenylmaleimide, as comonomers, two different engineering copolymers have been designed and synthesized through bulk and suspension copolymerization with bifunctional initiators.

Styrene/α-methylstyrene (SAMS) bulk and suspension statistical copolymers, bearing glass transition temperatures about 115°C, have been optimally synthesized from feed compositions of 85/15 mol%, up to high conversions and high molecular weights, with bifunctional initiator TBPCC, at 105°C.

The resulting SAMS suspension copolymers have been evaluated as feasible for scaling-up to commercial production, for extrusion applications at temperatures below 115°C.

Styrene/N-phenylmaleimide (S/NPMI) bulk and suspension copolymers, bearing glass transition temperatures about 212°C, have been optimally synthesized from feed compositions of 80/20 mol%, up to high conversions and high molecular weights, with bifunctional initiator TBPCC, at 105°C.

Characterization of the micro-structure of these copolymers has shown that the re-combination of highly alternating chains with styrene-rich statistical chains in multi-segment structures is mainly responsible for the outstanding thermal properties of this copolymers.

The resulting suspension copolymers have also been evaluated as feasible for scaling-up to large scale production. The high glass transition temperature, high thermal stability and processability of these copolymers make them extremely attractive for engineering applications at temperatures up to 200°C.

In addition, considering the extremely high polymerization rates exhibited by this S/NPMI donor-acceptor system, especially at equimolar feed compositions and high temperatures where the reaction is completed in about 2 minutes, it is suggested here that under such conditions this copolymer could be produced through Reaction Injection Molding (RIM) processes.

The ability of N-phenylmaleimide to form a donor-acceptor complex with α-methylstyrene (AMS/NPMI), has been exploited to produce thermally stable copolymers with large contents of AMS.

Copolymers of AMS/NPMI, bearing glass transition temperatures about 260°C, have been optimally synthesized from equimolar feed composition, up to 80% conversion and weight average molecular weights about 120,000, through bulk copolymerization with bifunctional initiator TPC, at 130°C.

Characterization of the microstructure of these copolymers, has shown a very high degree of alternation, nearly independent of the feed composition. this demonstrates that AMS/NPMI copolymerization proceeds almost exclusively through donor-acceptor propagation reactions.

The high residual monomer contents of these copolymers, which plasticizes the suspension particles, along with their highly "sticky" character, promotes extensive particle coalescence in suspension polymerization, which cannot be controlled even with high stabiliser concentrations and low disperse phase volume fractions.

Consequently, AMS/NPMI cannot be synthesized through bifunctionally initiated suspension polymerization processes, in the range of conditions tested.

Accordingly, bifunctionally initiated free radical solution copolymerization of AMS/NPMI, is recommended here as an alternative process for the production of these extremely attractive copolymers, bearing T_g within the limits of High Performance Polymers.

The selection of a suitable solvent for this system must be made on the bases of displacing the equilibrium of donor-acceptor complex formation toward more complex production, with which higher terminal conversions should be reached.

Combining the best characteristics of the three individual copolymers studied, styrene/α-methylstyrene/N-phenylmaleimide bulk and suspension terpolymers, bearing glass transition temperatures above 215°C, have been synthesized.

Feed compositions of 70/10/20, and the use of bifunctional initiators TBPCC and TPC, at 105 and 130°C, respectively, yielded a good balance of terminal conversion and molecular weights for these S/AMS/NPMI terpolymers.

Stable suspensions and high thermal stability during and after extrusion of the resulting suspension terpolymers, make these terpolymers feasible for production in large reactors and attractive for engineering applications up to 200°C.

Finally, it is recommended here to extend the kinetic model developed for binary copolymerization, to terpolymerization when two pairs of donor-acceptor complexes are formed, from the propagation reaction scheme proposed.

Accordingly, the main contributions of this research project to the polymer field, can be listed as follows:

1. The copolymerization theory has been extended to consider the unique features of bifunctional initiation, in simultaneous statistical/donor-acceptor copolymerization.
2. The concepts of effective instantaneous copolymer composition and average number of segments per copolymer chain, have been introduced to the copolymerization theory.
3. The instantaneous copolymer composition equation has been generalized for simultaneous statistical/donor-acceptor copolymerization, from the terminal plus complex participation model developed in this thesis.

4. Comprehensive kinetic and micro-structure models, comprising the above additions to the copolymerization theory, have been integrated in a program that simulates the most important features of bifunctionally initiated statistical/donor-acceptor copolymerization.

5. A novel, highly productive process for the manufacture of expandable polystyrene beads, through a single simultaneous polymerization/impregnation stage, with bifunctional initiators, has been developed and proven out on pilot plant scale.

6. The synthesis of bulk and suspension S/AMS copolymers has been optimized at pilot plant scale, to produce SAMS engineering copolymers with T_g~115°C, through bifunctional initiation.

7. The synthesis of bifunctionally initiated bulk and suspension S/NPMI copolymers has been optimized at pilot plant scale, to produce engineering copolymers with T_g~212°C.

8. The synthesis of bulk AMS/NPMI copolymers has been optimized at laboratory scale, to produce engineering copolymers with T_g~260°C, through bifunctional initiation.

9. The synthesis of bulk and suspension S/AMS/NPMI terpolymers, has been successful at pilot plant scale to produce engineering terpolymers with T_g~215-220°C, through bifunctional initiation.

REFERENCES

REFERENCES

Numbered References

[1] European Plastics News, Material Trends, 17,1, 9 (1990).

[2] European Plastics News, The Month, 17, 5, 3 (1990).

[3] Encyclopedia Reprint Series; High performance Polymers and Composites, John Wiley & Sons, Inc., (1991).

[4] European Plastics News, Engineering Polymers, 16, 12, 22 (1989).

Author's References

Alfrey, T., and Goldfinger, G.; J. Chem. Phys., 12, 205 (1944).

Alfrey, T., and Goldfinger, G.; J. Chem. Phys., 14, 115 (1946).

Alfrey, T., and Price, C.C.; J. Polym. Sci., 2, 101 (1947).

Allegra, G.; Die Makrom. Chem., 117, 12 (1968).

Allegra, G.; J. Chem. Phys., 68, 3600 (1978).

Allegra, G., and Immirzi, A.; Die Makrom. Chem.; 124, 70 (1969).

Allegra, G., Bignotti, F., Gargani, L., and Cociani, M.; Macromolecules, 23, 5326 (1990).

Arai, K., Konno, M., Matunaga, Y., and Saito, S.; J. Chem. Eng. Jpn., 10, 325 (1977).

Baldwin, M.G., and Reed, S.F.; J. Polym. Sci. Part A-1, 6, 2627 (1968).

Bamford, C.H., and Tompa, H.; J. Polym. Sci., 10, 345 (1953).

Bamford, C.H., Barb, W.G., Jenkins, A.D., and Onyon, P.F.; The Kinetics of Vinyl Polymerization by Radical Mechanism, Butterworths, London (1958).

Barrales-Rienda, J., Gonzalez-Ramos, J., and Sanchez-Chaves, M.; Eur. Polym. J.; 13, 129 (1977).

Barron, P.F., Hill, D.J.T., O'Donnell, J.H., and O'Sullivan, P.W.; Macromolecules, 17, 1967 (1984).

Bartlett, P.D., and Nozaki, K.; J. Am. Chem. Soc., 68, 1495 (1946).

Barton, J.; J. Polym. Sci. Part C, 30, 573 (1970).

Benesi, H.A., and Hildebrand, J.H., J. Am. Chem. Soc., 71, 2703 (1949).

Bhattacharya, D., and Hamielec, A.E.; Polymer, 27, 611 (1986).

Bishop, R.B.; Practical Polymerization for Polystyrene, Cahners, Boston MA (1971).

Brown, A.S., Fujimori, K., and Craven, I.E.; J. Polym. Sci., Part A Polym. Chem., 27, 3315 (1989).

Bruckner, S.; Macromolecules, 14, 449 (1981).

Buchak, B.E., and Ramey, K.C.; J. Polym. Sci., Polym. Lett. Ed., 14, 401 (1976).

Carter, S., Murrell, J.N., and Rosch, E.J.; J. Am. Chem. Soc., 2048 (1965).

Caze, C., and Loucheux, C.; J. Macrom. Sci. (Chem), A12(10), 1501 (1978).

Choi, K.Y., and Lei, J.C.; AIChE J., 33(12), 2067 (1987).

Choi, K.Y., Liang, W.R., and Lei, G.D.; J. Appl. Polym. Sci., 35, 1547 (1988).

Church, J.M.; Chem. Eng., 73, 79 (1966).

Cohen, M/H., and Turnbull, D.; J. Chem. Phys., 31, 1164 (1959).

Couchman, P.R.; Macromolecules, 11, 1156 (1978).

Couchman, P.R.; J. Appl. Phys., 50, 6043 (1979).

Couchman, P.R.; Macromolecules, 15, 770 (1982).

Couchman, P.R., and Karasz, F.E.; Macromolecules, 11, 117 (1978).

Dainton, F.S., and Ivin, K.J.; Nature, 162, 705 (1948).

Doolittle, A.K., J. Appl. Phys., 22, 1471 (1951).

Ebdon, J.R., Towns, C.R., and Dodgson, K.; JMS-Rev. Macrom. Chem. Phys., C26, 523 (1986).

Estes, G.M., Cooper, S.L., and Tobolsky, A.V.; JMS-Rev. Macrom. Chem., C4, 313 (1970).

Fischer, J.P.; Die Makrom. Chem., 155, 211 (1972).

Fles, D.D., Vukovic, R., and Ranogajec, F.; J. Polym. Sci. Part A Polym. Chem., 27, 3227 (1989).

Flory, P.J.; Statistical Mechanics of Chain Molecules, Interscience, New York, N.Y. (1969).

Flory, P.J., Orwoll, R.A., and Vrij, A.; J. Am. Chem. Soc., 86, 3507 (1964).

Fox, G.T.; Bull. Am. Phys. Soc., 1, 123 (1956).

Fox, G.T., and Flory, P.J.; J. Am. Chem. Soc., 70, 2384 (1948).

Fox, G.T., and Flory, P.J.; J. Appl. Phys., 21, 581 (1950).

Fox, G.T., and Flory, P.J.; J. Polym. Sci., 14, 315 (1954).

Fox, G.T., and Loshaek S.; J. Polym. Sci., 15, 371 (1955).

Friis, N., and Hamielec, A.E.; J. Appl. Polym. Sci., 19, 97 (1975).

Fryd, M.; Structure Tg Relationship in Polyimides, in Polyimides, K.L. Mittal, Ed., Plenum, 1, 377 (1984).

Gaylord, N.G., and Deshpande, A.B.; J. Macrom. Sci. (Chem), A11(10), 1795 (1977).

Georgiev, G.S., and Zubov, V.P.; Eur. Polym. J., 14, 93 (1978).

Gibbs, J.H., and DiMarzio, E.A.; J. Chem. Phys., 28 (3), 373 (1958).

Gloor, P., and Hamielec, A.E.; Reactive Extrusion of Polyolefins, Lecture at Polymer Colloquium Series, McMaster University, Canada (1991).

Gordon, M., and Taylor. J.S.; J. Appl. Chem., 2, 492 (1952).

Grulke, E.A., Suspension Polymerization, in Encyclopedia of Polymer Science and Technology, 2nd. Ed., Wiley, N.Y., 16, 443 (1985).

Guillot, J.; Macrom. Chem., Macrom. Symp., 35/36, 269 (1990).

Gunesin, B.Z., and Piirma, I.; J. Appl. Polym. Sci., 26, 3103 (1981).

Gutmann, V.; Pure and Appl. Chem., 51, 2197 (1979).

Ham, G.E.; J. Polym. Sci., 45, 169 (1960).

Ham, G.E.; J. Polym. Sci., 45, 183 (1960).

Ham, G.E.; J. Macrom. Chem., 1, 93 (1966).

Ham, G.E.; J. Macrom. Sci. (Chem), A19(5), 693 (1983).

Ham, G.E.; J. Macrom. Sci. (Chem), A19(5), 699 (1983).

Hamielec, A.E., and MacGregor, J.F.; Polymer Reaction Engineering, Reichert, K.H., and Geiseler, W., Eds., 21 (1983).

Hamielec, A.E., MacGregor, J.F., and Penlidis, A.; Makrom. Chem., Makrom. Symp., 10/11, 521 (1987).

Hamielec, A.E., Hodgins, J.W., and Tebbens, K.; AIChE J., 13, 1087 (1967).

Haward, R.N.; J. Macrom. Sci.-Revs. Macrom. Chem., C4 (2), 191 (1970).

Hergenrother, P.M.; Heat Resistant Polymers, in "High Performance Polymers and Composites", John Wiley & Sons, N.Y. (1991).

Hiemenz, P.C.; Polymer Chemistry, Marcel Dekker, Inc., New York, N.Y. (1984).

Hill, D.J.T., O'Donnell, J.H., and O'Sullivan, P.W.; Macromolecules, 18, 9 (1985).

Horie, K., Mita, I., and Kambe, H.; J. Polym. Sci., Part A-1, 6, 2663 (1989).

Hui, A.W., and Hamielec, A.E.; J. Appl. Polym. Sci., 16, 749 (1972).

Illers, K.H.; Kolloid-Z & Z fur Polymere, 190, 16 (1963).

Ivanechev, S.S.; Polym. Sci. USSR., 20, 2157 (1979).

Ivin, K.J., and Spensley, R.H.; J. Macrom. Sci. (Chem), A1(4), 653 (1967).

Javni, I., Fles, D., and Vukovic, R.; J. Polym. Sci., Polym. Chem. Ed., 20, 977 (1982).

Johnson, R.N.; Polysulfones, in "High Performance Polymers and Composites", John Wiley & Sons, N.Y. (1991).

Johnston, H.K., and Rudin, A.; Macromolecules, 4, 661 (1971).

Johnston, N.; Amer. Chem. Polym. Prepr., 14, 46 (1973).

Kanig, G.; Kolloid-Z & Z fur Polymere, 190, 1 (1963).

Kang, B.K., O'Driscoll, K.F., and Howell, J.A.; J. Polym. Sci. Part A-1, 10, 2349 (1972).

Kelen, T., and Tudos, F.; J. Macrom. Sci (Chem), A9(1), 1 (1975).

Kelly, F.N., and Bueche, F.; J. Polym. Sci., 50, 549 (1961).

Kim, L.F., Stotskaya, L.L., Krentsel, B.A., Zubov, V.P., Golubev, V.B., and Stoyachenko, I.L.; J. Macrom. Sci. (Chem), A12(8), 1197 (1978).

Kim, K.J., Liang, W., and Choi, K.Y.,; Ind. Eng. Chem. Res., 28, 131 (1989).

Konno, M., Arai, K., and Saito, S.; J. Chem. Eng. Jpn., 15, 31 (1982).

Konno, M., Muto, T., and Saito, S.; J. Chem. Eng. Jpn., 21, 335 (1988).

Lee, C.J.; JMS-Rev. Macrom. Chem. Phys., C29, 431 (1989).

Leonard, J., and Malhotra, S.L.; J. Macrom. Sci. (Chem), A10(7), 1279 (1976).

Leonard, J., and Malhotra, S.L.; J. Macrom. Sci. (Chem), A11(10), 1867 (1977).

Li, T., Cao, W.X., and DeFeng, X.; JMS-Rev. Macrom. Chem. Phys., C29, 153 (1989).

Lowry, G.G.; J. Polym. Sci., 42, 463 (1960).

Mahabadi, H.K., and O'Driscoll, K.F.; Macromolecules, 10, 55 (1977).

Malhotra, S.L., and Leonard, J.; J. Macrom. Sci. (Chem), A11(10), 1907 (1977).

Malhotra, S.L., Leonard, J., and Thomas, M.; J. Macrom. Sci. (Chem), A11(12), 2213 (1977).

Malhotra, S.L.; J. Macrom. Sci. (Chem), A12(1), 73 (1978).

Malhotra, S.L., Baillet, C., Minh, L., and Blanchard, L.P.; J. Macrom. Sci. (Chem), A12(1), 129 (1978).

Malhotra, S.L., Minh, L., and Blanchard, L.P.; J. Macrom. Sci. (Chem), A12(1), 167 (1978).

Marten, F.L., and Hamielec, A.E.; J. Appl. Polym. Sci., 27, 489 (1982).

Mayo, F.R., and Lewis, F.M.; J. Am. Chem. Soc., 66, 1594 (1944).

McCormick, H.W.; J. Polym. Sci., 25, 488 (1957).

Meyer, V.E., and Lowry, G.G.; J. Polym. Sci. Part A., 3, 2843 (1965).

Mita, I., and Horie, K.; JMS-Rev. Macrom. Chem. Phys., C27, 91 (1987).

Mohamed, A.A., and Hildebrand, J.H., J. Am. Chem. Soc., 71, 2703 (1949).

Odian, G.; Principles of Polymerization, Wiley-Interscience, N.Y. (1981).

O'Donnell, J.H., and Sothman, R.D.; J. Polym. Sci., Part B, 7, 129 (1969).

O'Driscoll, K.F., and Gasparro, F.P.; J. Macrom. Sci. (Chem), A1(4), 643 (1967).

O'Driscoll, K.F., and Dickson, J.R.; J. Macrom. Sci. (Chem), A2(3), 449 (1968).

O'Driscoll, K.F., and Bevington, J.C.; Eur. Polym. J., 21, 1039 (1985).

Okufi, S., Perez, E.S., and Sawistowski, H.; Can. J. Chem. Eng., 68, 400 (1990).

Olson, K.G., and Butler, G.B., Macromolecules, 16, 710 (1983).

Onen, A., and Yagci, Y.; J. Macrom. Sci. (Chem), A27(6), 743 (1990).

Onen, A., and Yagci, Y.; Die Angew. Makrom. Chem., 181, 191 (1990).

O'Reilly, J.M.; J. Polym. Sci., 57, 429 (1962).

Piirma, I., and Chou, L.H.; J. Appl. Polym. Sci., 24, 2051 (1979).

Price, C.C., and Alfrey, T.; J. Polym. Sci., 1, 83 (1946).

Priddy, D.B., Traugott, T.D., and Seiss, R.H.; J. Appl. Polym. Sci., 41, 383 (1990).

Prisyazhnyuk, A.I., and Ivanechev, S.S.; Polym. Sci. USSR., 12, 514 (1970).

Regel, W., and Canessa, G.; Makrom. Chem., 181, 1703 (1980).

Richardson, M.J., and Davill, N.G.; Polymer, 18, 3 (1977).

Ring, W.; Die Makrom. Chem., 101, 145 (1967).

Rudin, A., and Chiang, S.S.M.; J. Polym. Sci.: Polym. Chem. Ed., 12, 2235 (1974).

Ryong-Joon, R., and Tonelli, A.E.; Macromolecules, 11, 114 (1978).

Schmidt, H., Schimdt-Naake, G., and Berger, W.; Makrom. Chem., 191, 2957 (1990).

Schmidt-Naake, G., Schmidt, H., Litauszki, B., and Bieger, W.; Makrom. Chem., 191, 2963 (1990).

Schmidt-Naake, G., Schmidt, H., Litauszki, B., and Berger, W.; Makrom. Chem., 191, 3033 (1990).

Scheflan, L., and Jacobs, M.B.; Handbook of Solvents, D. Van Nostrand Co. Inc. (1953).

Sears, K.J., and Darby, J.R.; The Technology of Plasticizers, John Wiley & Sons, N.Y. (1982).

Shirota, Y., Yoshimura, M., Matsumoto, A., and Mikawa, H.; Macromolecules, 7, 4 (1974).

Simionescu, C.I., Sik, K.G., Comanita, E., and Dumitriu, S.; Eur. Polym. J., 20, 467 (1984).

Simionescu, C.I., Comanita, E., Pastravanu, M., and Dumitriu, S., Prog. Polym. Sci., 12, 1 (1986).

Tanaka, H., and Otsu, T.; J. Macrom. Sci. (Chem), A11(9), 1663 (1977).

Tobita, H., and Hamielec, A.E.; Macromolecules, 22, 3098 (1989).

Tobita, H.; Ph.D. Thesis, McMaster University, Hamilton, Ontario, Canada (1990).

Tsuchida, E., and Tomono, T.; Die Makrom. Chem., 141, 265 (1971).

Tsuchida, E., Tomono, T., and Sano, H.; Die Makrom. Chem., 151, 245 (1972).

Ueberreiter, K., and Kanig, G.; J. Coll. Sci., 7, 569 (1952).

Verbicky, J.W.; Polyimides, in "High Performance Polymers and Composites", John Wiley & Sons, N.Y. (1991).

Villalobos, M.A.; M. of Eng. Thesis, McMaster University, Hamilton, Ontario, Canada (1989).

Villalobos, M.A.; Global Optimization of Suspension Expandable Polystyrene, Short Course Notes, MIPPT-McMaster University, Canada (1990).

Villalobos, M.A., Hamielec, A.E., and Wood, P.E.; J. Appl. Polym. Sci., 42, 629 (1991).

Villalobos, M.A.; Diffusion of Blowing Agent into PS Beads, Report EPR-01 to PlastiFab LTD, Calgary, Alberta, Canada (1991).

Villalobos, M.A., Hamielec, A.E., and Wood, P.E.; Accepted for Publication in Polymer (1992 a,b).

Walling, C., Briggs, E.R., Wolfstirn, K.B., and Mayo, F.R.; J. Am. Chem. Soc., 70, 1537 (1948).

Waltz, R., and Heitz, W.; J. Polym. Sci. Polym. Chem. Ed., 16, 1807 (1978).

Williams, M.L., Landel, R.F., and Ferry, J.D.; J. Am. Chem. Soc., 77, 3701 (1955).

Williams, A.D., and Flory, P.J.; J. Am. Chem. Soc., 91, 3111 (1969).

Wittmer, P.; Die Angew. Makrom. Chem., 170, 1 (1989).

Worsfold, D.J., and Bywater, S.; J. Polym. Sci., 26, 299 (1957).

Yagci, Y., and Onen, A.; J. Macrom. Sci. (Chem), A28(1), 129 (1991).

Yoon, D.Y., Sundararajan, P.R., and Flory, P.J.; Macromolecules, 8, 776 (1975).

Yuan, H.G., Kalfas, G., and Ray, W.H.; JMS-Rev. Macrom. Chem. Phys., C31, 215 (1991).

Zeng, W., and Shirota, X.; Macromolecules, 22, 4204 (1989).

Zhu, S., and Hamielec, A.E.; Macromolecules, 22, 3039 (1989).

Zhu, S., Tian, Y., Hamielec, A.E., and Eaton, D.R.; Polymer, 31, 154 (1990).

Zhu, S., Tian, Y., Hamielec, A.E., nad Eaton, D.R.; Macromolecules, 23, 1144 (1990).

Zhu, S.; Ph.D. Thesis, McMaster University, Hamilton, Ontario, Canada (1991).

Zott, H., and Heusinger, H.; Eur. Polym. J., 14, 89 (1978).

APPENDICES

APPENDIX A

A.1 Derivation of Pseudo-Kinetic Rate Constants:

As an example let us consider the mass balance equation for radicals of chain length r (r≥3) without undecomposed peroxide groups, given by eq. (4.72) in the text. From the reaction scheme:

$R^{\bullet}_{r,\cdot}$ (r≥3): (A-1)

$$\begin{aligned}
\frac{1}{V}\frac{d([R^{\bullet}_{r,\cdot}]V)}{dt} &= f_2 K_{d2}[\widetilde{P}_n] + (K_{11}[M_1] + K_{12}[M_2] + K_{1c}[C])[R^{\bullet}_{r-1,1}] \\
&+ (K_{21}[M_1] + K_{22}[M_2] + K_{2c}[C])[R^{\bullet}_{r-1,2}] \\
&+ (K_{1c}[R_{1,1}] + K_{2c}[R^{\bullet}_{1,2}])[C] \\
&- (K_{11}[M_1] + K_{12}[M_2] + K_{1c}[C])[R^{\bullet}_{r,1}] \\
&- (K_{21}[M_1] + K_{22}[M_2] + K_{2c}[C])[R^{\bullet}_{r,2}] \\
&- ((K_{tc11}[R^{\bullet}_1] + K_{tc12}[R^{\bullet}_2])[R^{\bullet}_{r,1}] + (K_{tc21}[R^{\bullet}_1] + K_{tc22}[R^{\bullet}_2])[R^{\bullet}_{r,2}]) \\
&- ((\widetilde{K}_{tc11}[\widetilde{R}^{\bullet}_1] + \widetilde{K}_{tc12}[\widetilde{R}^{\bullet}_2])[R^{\bullet}_{r,1}] + (\widetilde{K}_{tc21}[\widetilde{R}^{\bullet}_1] + \widetilde{K}_{tc22}[\widetilde{R}^{\bullet}_2])[R^{\bullet}_{r,2}]) \\
&- ((K_{td11}[R^{\bullet}_1] + K_{td12}[R^{\bullet}_2])[R^{\bullet}_{r,1}] + (K_{td21}[R^{\bullet}_1] + K_{td22}[R^{\bullet}_2])[R^{\bullet}_{r,2}]) \\
&- ((\widetilde{K}_{td11}[\widetilde{R}^{\bullet}_1] + \widetilde{K}_{td12}[\widetilde{R}^{\bullet}_2])[R^{\bullet}_{r,1}] + (\widetilde{K}_{td21}[\widetilde{R}^{\bullet}_1] + \widetilde{K}_{td22}[\widetilde{R}^{\bullet}_2])[R^{\bullet}_{r,2}]) \\
&- (K_{tc1}[R^{\bullet}_{r,1}] + K_{tc2}[R^{\bullet}_{r,2}])[T] \\
&- ((K_{t11}[M_1] + K_{t12}[M_2])[R^{\bullet}_{r,1}] + (K_{t21}[M_1] + K_{t22}[M_2])[R^{\bullet}_{r,2}])
\end{aligned}$$

Applying the definitions for f_1, Φ_1, and $\Phi_{r,1}$ given in the text (see Chapter 4), equation (A-1) becomes:

(A-2)

$R^{\bullet}_{r,\bullet}$ $(r \geq 3)$:

$$\frac{1}{V}\frac{d([R^{\bullet}_{r,\bullet}]V)}{dt} = f_2 K_{tr}[\widetilde{P}_r] + ((K_{11}f_1 + K_{12}f_2 + K_{1c}f_c)\Phi_{r-1,1})[M][R^{\bullet}_{r-1,\bullet}]$$

$$+ ((K_{21}f_1 + K_{22}f_2 + K_{2c}f_c)\Phi_{r-1,2})[M][R^{\bullet}_{r-1,\bullet}]$$

$$+ ((K_{1c}\Phi_{1,1} + K_{2c}\Phi_{1,2})f_c)[M][R^{\bullet}_{1,\bullet}]$$

$$- ((K_{11}f_1 + K_{12}f_2 + K_{1c}f_c)\Phi_{r,1})[M][R^{\bullet}_{r,\bullet}]$$

$$- ((K_{21}f_1 + K_{22}f_2 + K_{2c}f_c)\Phi_{r,2})[M][R^{\bullet}_{r,\bullet}]$$

$$- ((K_{tc11}\Phi_1 + K_{tc12}\Phi_2)\Phi_{r,1} + (K_{tc21}\Phi_1 + K_{tc22}\Phi_2)\Phi_{r,2})Y_0[R^{\bullet}_{r,\bullet}]$$

$$- ((\widetilde{K}_{tc11}\widetilde{\Phi}_1 + \widetilde{K}_{tc12}\widetilde{\Phi}_2)\Phi_{r,1} + (\widetilde{K}_{tc21}\widetilde{\Phi}_1 + \widetilde{K}_{tc22}\widetilde{\Phi}_2)\Phi_{r,2})\widetilde{Y}_0[R^{\bullet}_{r,\bullet}]$$

$$- ((K_{td11}\Phi_1 + K_{td12}\Phi_2)\Phi_{r,1} + (K_{td21}\Phi_1 + K_{td22}\Phi_2)\Phi_{r,2})Y_0[R^{\bullet}_{r,\bullet}]$$

$$- ((\widetilde{K}_{td11}\widetilde{\Phi}_1 + \widetilde{K}_{td12}\widetilde{\Phi}_2)\Phi_{r,1} + (\widetilde{K}_{td21}\widetilde{\Phi}_1 + \widetilde{K}_{td22}\widetilde{\Phi}_2)\Phi_{r,2})\widetilde{Y}_0[R^{\bullet}_{r,\bullet}]$$

$$- (K_{tt1}\Phi_{r,1} + K_{tt2}\Phi_{r,2})[T][R^{\bullet}_{r,\bullet}]$$

$$- ((K_{t11}f_1 + K_{t12}f_2)\Phi_{r,1} + (K_{t21}f_1 + K_{t22}f_2)\Phi_{r,2})[M][R^{\bullet}_{r,\bullet}]$$

If the mole fraction of each radical type is independent of its chain length, namely

$$\Phi_1 = \Phi_{1,1} = \Phi_{2,1} = \Phi_{3,1} = \cdots\cdots = \Phi_{r,1} \tag{A-3}$$

$$\widetilde{\Phi}_1 = \widetilde{\Phi}_{1,1} = \widetilde{\Phi}_{2,1} = \widetilde{\Phi}_{3,1} = \cdots\cdots = \widetilde{\Phi}_{r,1} \tag{A-4}$$

$$\Phi_2 = \Phi_{1,2} = \Phi_{2,2} = \Phi_{3,2} = \cdots\cdots = \Phi_{r,2} \tag{A-5}$$

$$\widetilde{\Phi}_2 = \widetilde{\Phi}_{1,2} = \widetilde{\Phi}_{2,2} = \widetilde{\Phi}_{3,2} = \cdots\cdots = \widetilde{\Phi}_{r,2} \tag{A-6}$$

and the equalities given in the text by eqs. (4.57) and (4.58) are valid (i.e. for number-average chain length greater than a few hundred), equation (A-2) reduces to:

$R^{\bullet}_{r,\cdot}$ $(r \geq 3)$: (A-7)

$$\frac{1}{V}\frac{d([R^{\bullet}_{r,\cdot}]V)}{dt} = f_2 K_{tc}[\widetilde{P_r}] + K_p[M][R^{\bullet}_{r-1,\cdot}] + (K_{1c}\Phi_1 + K_{2c}\Phi_2) f_c[M][R^{\bullet}_{1,\cdot}] - (K_p[M] + (K_{tc} + K_{td})Y_{T0} + K_{ft}[T] + K_{fm}[M])[R^{\bullet}_{r,\cdot}]$$

If the definitions for K_p, K_{tc}, K_{td}, K_{ft}, and K_{fm} are given by eqs. (4.59) to (4.63), in the text. Note that eqs. (A-7) and (4.72) are exactly the same.

Applying the same procedure, the rest of the equations involving pseudo-kinetic rate constants were derived.

A.2 Equality of Φi and $\widetilde{\Phi i}$

Commonly the fraction of polymer radicals of type i, Φ_i, is obtained by using the stationary state hypothesis for each type of radical, in the form:

$$\sum R_{ji} = \sum R_{ij} \qquad \text{(A-8)}$$

In Eq. (A-8), above, R_{ji} is the rate of propagation in which M_i follows M_j. It is evident that for long chains eq. (A-8) is statistically correct and leads to the expression given by eq. (4.58). For long chains equalities given by eqs. (4.57) also apply and therefore the equality of Φ_i and $\widetilde{\Phi_i}$ is correct.

More rigorously, if eqs. (4.57) are valid, the application of the stationary state hypothesis to the mass balance of radicals of chain length r with active centre in monomer unit 1, with and without undecomposed peroxide, ($[R_{r,1}]$), leads to the following expressions:

$$\Phi_1 = \frac{f_1[M]\,(K_{21}\Phi_2 + K_{t21}(\Phi_2 + \widetilde{\Phi}_2\widetilde{Y}_0/Y_0) + K_{t11}\widetilde{\Phi}_1\widetilde{Y}_0/Y_0)}{(K_{12}f_2[M] + (K_{tc11}+K_{td11})\,(\Phi_1Y_0+\widetilde{\Phi}_1\widetilde{Y}_0) + (K_{tc12}+K_{td12})\,(\Phi_2Y_0+\widetilde{\Phi}_2\widetilde{Y}_0) + K_{t12}f_2[M] + K_{tc1}[T])}$$

and (A-9)

$$\widetilde{\Phi}_1 = \frac{f_1[M]\,(K_{21}\widetilde{\Phi}_2)}{(K_{12}f_2[M] + (K_{tc11}+K_{td11})\,(\Phi_1Y_0+\widetilde{\Phi}_1\widetilde{Y}_0) + (K_{tc12}+K_{td12})\,(\Phi_2Y_0+\widetilde{\Phi}_2\widetilde{Y}_0) + (K_{t11}f_1+K_{t12}f_2)\,[M] + K_{tc1}[T])}$$

Order of magnitude estimates show that the transfer terms in the above equations are at least five orders of magnitude smaller than the propagation terms all throughout the conversion range and therefore, completely negligible. Thus, equations (A-9) reduce to:

$$\Phi_1 = \frac{K_{21}[M]\,f_1\Phi_2}{K_{12}f_2[M] + (K_{tc11}+K_{td11})\,(\Phi_1Y_0+\widetilde{\Phi}_1\widetilde{Y}_0) + (K_{tc12}+K_{td12})\,(\Phi_2Y_0+\widetilde{\Phi}_2\widetilde{Y}_0)}$$

and (A-10)

$$\widetilde{\Phi}_1 = \frac{K_{21}[M]\,f_1\widetilde{\Phi}_2}{K_{12}f_2[M] + (K_{tc11}+K_{td11})\,(\Phi_1Y_0+\widetilde{\Phi}_1\widetilde{Y}_0) + (K_{tc12}+K_{td12})\,(\Phi_2Y_0+\widetilde{\Phi}_2\widetilde{Y}_0)}$$

It is easy to see in the above equations that the right hand sides are equal and therefore the fractions of radicals of each type with and without peroxide groups are equal (i.e. $\Phi_1 = \Phi_1$).

Let us now analyze the participation of the termination terms. If the termination terms in eqs. (A-10) are negligible then this equations reduce to eq. (4.58). In typical linear copolymerization at low monomer conversion the termination terms are three to four orders of magnitude smaller than the propagation terms.

As monomer concentration decreases one order of magnitude (i.e. high conversion), the termination rate becomes diffusion controlled and the rate constant decreases several orders of magnitude, while the radical concentration increases less than one order of magnitude [Zhu and Hamielec (1989), Zhu et.al.(1990)].

As a result, the termination terms quickly become more than four orders of magnitude smaller than the propagation terms. Only at very high conversions, and with the system approaching its glassy state, where the propagation rates drop to nearly zero, the termination terms will be of similar magnitude to the propagation ones.

In the worst case, the error introduced by neglecting the participation of the termination terms in determining the value of Φ_i is likely to be less than 0.1 %. This error is smaller than those commonly involved in the evaluation of the rate constants themselves.

In conclusion eq. (4.58) is valid for linear copolymers of number average chain-length greater than a few hundred, which is in perfect agreement with the rest of the mathematical derivation of the model.

APPENDIX B

B.1 Distribution of Copolymer Species

The following derivation of the equations defining the distribution of copolymer species in bifunctionally initiated free radical copolymerization, is totally based on the work by Wittmer (1989). Some of the concepts and nomenclature, however, have been adapted to the case at hand (see text in Chapter 4).

In the instantaneous state of the polymerizing system, p peroxide groups decompose to form 2p radicals. Therefore, it is assumed that

$$1 \leq p \leq N_t \tag{B-1}$$

Since the peroxide groups decompose with the same probability, the corresponding radicals are formed proportionately to the mol fractions of the peroxide groups, each copolymer species form as:

$$N_{ia} = N_i b - p\gamma_{ib} + pW_i \tag{B-2}$$

where, γ is the mol fraction of the peroxide groups of the individual species, and the subindexes b and a, denote the state of the system before and after, the free radical decomposition and subsequent combination, respectively, and W_i is the individual probability of formation of the corresponding copolymer specie.

From the text note that decomposition of any peroxide group during the course of the polymerization gives always a radical $R_{in}^{\bullet}$ along with a radical $R\text{-}O\text{-}O\text{-}(Q)_i^{\bullet}$, or $R\text{-}(Q)_i^{\bullet}$ (i=1,2,..).

The number Z of all possible combinations of 2p radicals is given by:

$$Z = p(2p - 1) \qquad \text{(B-3)}$$

In what follows:

n_{oi} = number of radicals $R\text{-}O\text{-}O\text{-}(Q)_i^{\bullet}$

n_{di} = number of radicals $R\text{-}(Q)_i^{\bullet}$

n_p = number of radicals $R_{in}^{\bullet} = p$

It can be shown that the probabilities of formation for each copolymer species are given by:

(B-4)

$$\widetilde{\widetilde{W}}_i = (1/p(2p-1))[\Sigma n_{oj} \cdot n_{o(i-j)}] \qquad \text{(from j=1 to (i-1)/2)}$$

$$\widetilde{W}_i = (1/p(2p-1))[n_{oi} \cdot p + \Sigma n_{oj} \cdot n_{d(i-j)}] \qquad \text{(from j=1 to i-1)}$$

$$W_i = (1/p(2p-1))[n_{di} \cdot p + \Sigma n_{dj} \cdot n_{d(i-j)}] \qquad \text{(from j=1 to (i-1)/2)}$$

Radicals R_r° are formed by decomposition of P_r molecules, always with the formation of a R_{in}° radical.

$$n_{oi} = 2p(\widetilde{\widetilde{N}}_{ib}/N_t) \qquad \text{(B-5)}$$

Radicals R_r° are formed by decomposition of P_r molecules, also with the formation of a R_{in}° radical.

$$n_{di} = p(\widetilde{N}_{ib}/N_t) \qquad \text{(B-6)}$$

Simplifying equations B-4 by introducing the definitions given in B-5 and B-6, we get:

(B-7)

$$\overset{\approx\approx}{W_i} = (2/N_t^2)\,[\Sigma \overset{\approx\approx}{N_{jb}} \cdot \overset{\approx\approx}{N_{(i-j)b}}]$$

$$\overset{\sim}{W_i} = (\overset{\approx\approx}{N_{ib}}/N_t + 1/N_t^2)\,[\Sigma \overset{\sim}{N_{jb}} \cdot \overset{\approx\approx}{N_{(i-j)b}}]$$

$$W_i = (\overset{\sim}{N_{ib}}/2N_t^2 + 1/2N_t^2)\,[\Sigma \overset{\sim}{N_{jb}} \cdot \overset{\sim}{N_{(i-j)b}}]$$

where the summations are within the same limits shown above.

Introducing equation B-2 (for each specie) and the definitions for the mol fractions as $\gamma_i = 2N_i/N_t$ and $\gamma_i = N_i/N_t$, equations B-7 become:

(B-8)

$$\overset{\approx\approx}{N_{ia}} = (\overset{\approx\approx}{N_{ib}}(1-2p/N_t) + 2p/N_t^2)\,[\Sigma \overset{\approx\approx}{N_{jb}} \cdot \overset{\approx\approx}{N_{(i-j)b}}]$$

$$\overset{\sim}{N_{ia}} = (\overset{\sim}{N_{ib}}(1-p/N_t) + p/N_t^2 + p\overset{\approx\approx}{N_{ib}}/N_t)\,[\Sigma \overset{\sim}{N_{jb}} \cdot \overset{\approx\approx}{N_{(i-j)b}}]$$

$$N_{ia} = (N_{ib} + p/2N_t^2 + p\overset{\sim}{N_{ib}}/N_t)\,[\Sigma \overset{\sim}{N_{jb}} \cdot \overset{\sim}{N_{(i-j)b}}]$$

The number of undecomposed peroxide groups present at any moment during the polymerization is given by:

$$N_t = 2N_0 - A \qquad \text{(B-9)}$$

where N_0 is the initial number of bifunctional initiator molecules, 2A is the total number of radicals formed, and A is the total number of all previous combinations.

Since p is a small difference of successive A (i.E. dA) and assuming that $N_{ib} = N_i$, equations B-8, become:

B-10

$$d\tilde{\tilde{N}}_i = (-2\tilde{\tilde{N}}_i/(2N_0-A) + 2/(2N_0-A)^2 \cdot [\tilde{\tilde{\Sigma}}N_j \cdot \tilde{\tilde{N}}_{(i-j)}])dA$$

$$d\tilde{N}_i = ((\tilde{\tilde{N}}_i-\tilde{N}_i)/(2N_0-A) + 1/(2N_0-A)^2 \cdot [\tilde{\Sigma}N_j \cdot \tilde{\tilde{N}}_{(i-j)}])dA$$

$$dN_i = (\tilde{N}_i/2(2N_0-A) + 1/2(2N_0-A)^2 \cdot [\tilde{\Sigma}N_j \cdot \tilde{N}_{(i-j)}])dA$$

Finally, when the system of equations B-10, is integrated stepwise with the marginal conditions:

(B-11)

$$\lim_{A\to 0} \tilde{\tilde{N}}_i = N_0$$

$$\lim_{A\to 0} \tilde{\tilde{N}}_i = 0 \qquad (i\neq 1)$$

$$\lim_{A\to 0} N_j = 0 \qquad \text{(other 2 species)}$$

Equations 4.128 to 4.130 (in the text) are obtained, respectively.